Methods in Molecular Biology 1684

Springer Protocols

Show-Ling Shyng
Francis I. Valiyaveetil
Matt Whorton *Editors*

Potassium Channels

Methods and Protocols

EXTRAS ONLINE

Humana Press

METHODS IN MOLECULAR BIOLOGY

Series Editor
John M. Walker
School of Life and Medical Sciences
University of Hertfordshire
Hatfield, Hertfordshire, AL10 9AB, UK

For further volumes:
http://www.springer.com/series/7651

Potassium Channels

Methods and Protocols

Edited by

Show-Ling Shyng
and Francis I. Valiyaveetil

Department of Physiology and Pharmacology, Oregon Health and Science University, Portland, OR, USA

Matt Whorton

The Vollum Institute, Oregon Health and Science University, Portland, OR, USA

Humana Press

Editors
Show-Ling Shyng
Department of Physiology and Pharmacology
Oregon Health and Science University
Portland, OR, USA

Francis I. Valiyaveetil
Department of Physiology and Pharmacology
Oregon Health and Science University
Portland, OR, USA

Matt Whorton
The Vollum Institute
Oregon Health and Science University
Portland, OR, USA

ISSN 1064-3745 ISSN 1940-6029 (electronic)
Methods in Molecular Biology
ISBN 978-1-4939-7361-3 ISBN 978-1-4939-7362-0 (eBook)
DOI 10.1007/978-1-4939-7362-0

Library of Congress Control Number: 2017954932

Printed on acid-free paper

This Humana Press imprint is published by Springer Nature
The registered company is Springer Science+Business Media LLC
The registered company address is: 233 Spring Street, New York, NY 10013, U.S.A.

Foreword

The past 70 years have witnessed unprecedented advances in our knowledge of ion channels. In 1952, Hodgkin and Huxley derived a mathematical model to describe how action potentials are initiated and propagated in the squid giant axon. This conductance-based model required only voltage-gated Na^+ and K^+ channels, leak channels, and ion pumps, and did not require an understanding of the molecules themselves or how they function. Yet, even in the absence of molecular knowledge of the channels, there were remarkably accurate depictions of how the channels function. For example, in 1973 Armstrong proposed a model of the Na^+ channel in which ion permeation through an aqueous pore was regulated by a "ball and chain" in which the ball portion of the ion channel protein occluded the pore from the inside of the cell. Indeed, using protease treatment he showed that the ball could be "cut off" and leave the channel continuously open. Then, with the discovery of the patch clamp by Sakmann and Neher in the early 1980s, the activities of single ion channels could be studied and suggested a much wider array of individual ion channels than had been previously considered. In 1982, the recombinant DNA revolution, started in the 1970s, allowed Noda and colleagues to present the first predicted amino acid sequence of an ion channel protein, the Na^+ channel from the electric ray, Torpedo. They had biochemically purified channel protein from the electric organ where it is very highly expressed. This purified protein was used to generate antibodies. In addition, the amino acid sequences of tryptic digest peptides were determined. Immunological screening of a cDNA library identified several candidate clones that were rescreened with degenerate oligonucleotide pools containing all possible coding combinations of the tryptic peptide sequences. Using clones that contained the coding sequences of the tryptic peptides, and subsequently, larger cDNA probes, they deduced the entire predicted coding sequence of the Na^+ channel protein. These studies marked the dawn of the cloning era of ion channel proteins.

Studies of native K^+ channels had indicated a more diverse molecular family than for Na^+ channels. Yet no highly enriched tissue source was available to facilitate biochemical purification. However, Jan and colleagues devised an alternative strategy using *Drosophila* genetics. Electrophysiological studies of larval muscle showed that *Shaker* mutants, flies that shake their legs when anesthetized with ether, selectively affect an A-type K^+ current. Therefore, based on cytological localization they used a chromosomal walk and then fine structure gene mapping to isolate clones encoding portions of the *Shaker* protein. These were used, in turn, to isolate cDNA clones that ultimately yielded the entire predicted protein coding sequence of a K^+ channel. Notably, they identified several alternatively spliced variants. Finally, they expressed the *Shaker* cDNA clones in *Xenopus* oocytes and used two-electrode voltage clamp recordings to present the first heterologous expression of functional K^+ channels. They showed that *Shaker* encoded an A-type current and that the alternatively spliced mRNAs gave rise to functionally distinct K^+ channels. Importantly, a single mRNA species directed expression of functional K^+ channels.

These pioneering studies opened the "gates". Low stringency homology screens of cDNA libraries captured an unexpected expanse of voltage-gated K^+ channels from flies and mammals that presented subtle yet important functional distinctions when expressed in heterologous systems such as oocytes or transfected cell lines.

While homology screens were capable of identifying the members of the Kv families, other strategies were required to isolate clones encoding different K^+ channel families. Thus, the Hebert and Jan groups independently fractionated mRNA isolated from two different sources—outer medulla of rat kidney and a mouse macrophage cell line, respectively—and identified fractions that directed expression of a K^+ current following injection into *Xenopus* oocytes. Expression screening the corresponding cDNA libraries yielded the first two inward rectifier clones, ROMK1 and IRK1. Once again, low stringency homology screens identified a large family of related but distinct inward rectifier channels. Among these, in addition to a host of classic inward rectifiers, were the G-protein coupled inward rectifier channels (GIRKs) and the K_{ATP} channels.

The availability of the primary amino acid sequences for multiple subfamilies of K^+ channels focused attention on the question of what structural components mediate the universal properties of exquisite ion selectivity and permeation. Based upon sequence conservation and mutagenesis studies, and the nascent sequence databases, the selectivity sequence within the pore of the channels was identified. Lazdunski and colleagues then searched the databases for predicted proteins with the K^+ channel signature sequence and identified a yeast protein with a tandem of inward rectifier like motifs, the first K2P channel, YORK1, and then a mammalian counterpart, TWIK1. Once again, low stringency screens revealed a large family of K2P channels that vary particularly in their sensitivities to modulatory effectors.

Ganetsky and colleagues used *Slowpoke* mutant flies, lacking a Ca^{2+}-activated K^+ current in larval muscle, and a molecular genetic strategy similar to that used for *Shaker* to isolate genomic and cDNA clones encoding the BK large conductance voltage and Ca^{2+}-activated K^+ channels, *Slo* channels. Slo2.1 (*Slack*), a Na^+ and voltage activated K^+ channel, was identified using a pore sequence as an in silico probe, and Slo2.2 (*Slick*), a Na^+ and Cl^- activated K^+ channel, was isolated based on homology to *Slack*. We used an anchored PCR strategy and degenerate pools of oligonucleotides based upon the K^+ channel selectivity sequence, to isolate the SK, small conductance Ca^{2+} activated K^+ channels.

The number of K^+ channel genes was far more than had been anticipated; the mammalian genome harbors over 80. Yet the molecular—and functional—diversity goes much farther. First, unlike Na^+ or Ca^{2+} channels for which a single polypeptide with four homologous repeat units comprises a functional channel, K^+ channels assemble from four (or two; K2P) independent subunits, such that the functional channel always contains four pore domains. Within a given subfamily these subunits may be the same or different, dramatically expanding channel diversity. Second, each of the K^+ channel genes undergoes alternative splicing to further expand functional diversity. Indeed, the single BK channel gene can generate more than 1000 possible exon combinations. Third, channel activity and/or subcellular trafficking and localization are modulated by nonhomologous subunits that may co-assemble with the channels. Thus, the combinatorial K^+ channel repertoire is the most diverse among the ion channel families.

The cloning of the K^+ channel superfamily permitted detailed investigations into the structure and function of individual K^+ channels. Cloned channels could be functionally expressed and their activities, in virtual purity and isolation, could be measured accurately. This was combined with site-directed mutagenesis to reveal the molecular bases of essential attributes including gating, permeation, and pharmacology. With the historic presentation of the crystal structure of KCSA, a new level of resolution was obtained that revealed the chemistry of K^+ selectivity and permeation.

Today, structure-function studies that incorporate a diverse toolbox of approaches continue to yield profound insights into the molecular mechanisms underlying potassium channel function. This book, edited by Show-Ling Shyng, Francis Valiyaveetil, and Matt Whorton, provides a timely update on techniques and approaches used to study these channels, with a wide range of topics including channel structure, gating, cell biology, pharmacology, physiological functions, and channelopathies. This volume will be a welcome addition to the Methods in Molecular Biology book series collection and serve those who are interested in studying potassium channels.

Portland, OR, USA *John P. Adelman*

Preface

Potassium is nature's ion of choice for regulating cellular excitability. This is underscored by the fact that potassium channels are the most widely expressed type of ion channel and are found in virtually all organisms. In fact, there are over 90 K^+ channel genes in humans, which is more than the number of Na^+, Ca^{2+}, and Cl– channel genes combined. Potassium channel diversity is further expanded by differential splicing, heterotetrameric channel assembly, and association with accessory proteins. This breadth of diversity allows K^+ channels to respond to and integrate a variety of chemical, electrical, and mechanical signals. This has necessitated the development of a wide range of methods to study K^+ channels and their roles in physiology and disease.

Over the past few decades, advances in structural biology have produced atomic-resolution structures of many representative examples of K^+ channels. While these structures have offered unprecedented insight into the mechanisms of ion selectivity, gating, and ligand regulation, many questions remain regarding channel dynamics which are best addressed through other methods. These complementary approaches are covered in this book and include the use of NMR, EPR, single-molecule FRET, and molecular dynamics simulations.

As new modalities of K^+ channel regulation are discovered, increasingly sophisticated methods are needed to characterize the biophysical properties of certain K^+ channels. Several such methods are presented in this book, including photo-crosslinking, patch clamp and mechanical manipulation of channels reconstituted into lipid vesicles, stopped-flow spectroscopy, and incorporation of unnatural amino acids.

The identification and cloning of K^+ channels was only the beginning in understanding their roles in physiology and disease. This book includes a number of chapters dedicated to this topic, including ways to modulate and monitor protein expression levels in vivo, real-time correlation of channel activity and physiology, as well as optogenetic control of K^+ channel activity. As K^+ channels have so many important physiological roles, it is no surprise that they have great potential as therapeutic drug targets which is addressed in this book with a chapter describing a thallium-based high-throughput drug screen.

The methods used to study K^+ channels continue to improve and expand. This book is intended to provide an update on techniques and approaches that have been developed since the last Methods in Molecular Biology book on Potassium Channels published in 2009. With the wide range of topics covered including channel structure, gating, cell biology, pharmacology, physiological functions, and channelopathies, it is our hope that this book will serve as a practical guide for investigators wishing to study potassium channels.

Portland, OR, USA

Show-Ling Shyng
Francis I. Valiyaveetil
Matt Whorton

Contents

Contributors

Olaf S. Andersen • *Department of Physiology and Biophysics, Weill Cornell Medical College, New York, NY, USA*

Joshua B. Brettmann • *Department of Cell Biology and Physiology, Center for the Investigation of Membrane Excitability Diseases, Washington University School of Medicine, St. Louis, MO, USA*

Stephen G. Brohawn • *Department of Molecular and Cell Biology, University of California – Berkeley, Berkeley, CA, USA; The Helen Wills Neuroscience Institute, University of California – Berkeley, Berkeley, CA, USA*

Pei-Chun Chen • *Department of Physiology, College of Medicine, National Cheng Kung University, Tainan, Taiwan*

Xu Chen • *College of Life Sciences, Shaanxi Normal University, Xi'an, Shaanxi, China*

Jinke Cheng • *Department of Biochemistry and Molecular Cell Biology, Shanghai Jiao Tong University School of Medicine, Shanghai, China*

Roger D. Cone • *Life Sciences Institute, University of Michigan, Ann Arbor, MI, USA*

D. Marien Cortes • *Texas Tech University Health Science Center, Lubbock, TX, USA*

Luis G. Cuello • *Texas Tech University health Science Center, Lubbock, TX, USA*

Lucie Delemotte • *Structure et Réactivité des Systèmes Moléculaires Complexes, CNRS, Université de Lorraine, Nancy, France*

Prasanna Devaraneni • *Department of Biochemistry and Molecular Biology, Oregon Health & Science University, Portland, OR, USA*

Audrey Deyawe • *Structure et Réactivité des Systèmes Moléculaires Complexes, CNRS, Université de Lorraine, Nancy, France*

Matthew T. Dickerson • *Department of Molecular Physiology and Biophysics, Vanderbilt University, Nashville, TN, USA*

Wanying Dong • *College of Life Sciences, Shaanxi Normal University, Xi'an, Shaanxi, China*

Benjamin W. Elberson • *Texas Tech University health Science Center, Lubbock, TX, USA*

Masoud Ghamari-Langroudi • *Department of Molecular Physiology and Biophysics, Vanderbilt University Medical Center, Nashville, TN, USA*

Qiuming Gong • *Knight Cardiovascular Institute, Oregon Health & Science University, Portland, OR, USA*

Jui-Yi Hsieh • *Department of Physiology, David Geffen School of Medicine at UCLA, Los Angeles, CA, USA*

Jifang Huang • *College of Life Sciences, Shaanxi Normal University, Xi'an, Shaanxi, China*

David A. Jacobson • *Department of Molecular Physiology and Biophysics, Vanderbilt University, Nashville, TN, USA*

Balamurugan Kandasamy • *Department of Biochemistry and Molecular Biology, Oregon Health & Science University, Portland, OR, USA*

Hanaho Kano • *Graduate School of Pharmaceutical Sciences, The University of Tokyo, Bunkyo-ku, Tokyo, Japan*

Marina A. Kasimova • *Structure et Réactivité des Systèmes Moléculaires Complexes, CNRS, Université de Lorraine, Nancy, France*

Robin Y. Kim • *Department of Pharmacology, University of Alberta, Edmonton, AB, Canada*
Harley T. Kurata • *Department of Pharmacology, University of Alberta, Edmonton, AB, Canada*
Michael J. Litt • *Department of Molecular Physiology & Biophysics, Vanderbilt University Medical Center, Nashville, TN, USA*
Shian Liu • *Department of Biology, Texas A&M University, College Station, TX, USA; Janelia Research Campus, Howard Hughes Medical Institute, Ashburn, VA, USA*
Zhenfeng Liu • *National Heart Research Institute Singapore, National Heart Centre Singapore, Singapore, Republic of Singapore*
Steve W. Lockless • *Department of Biology, Texas A&M University, College Station, TX, USA*
Gildas Loussouarn • *L'institut du thorax, INSERM, CNRS, Université de Nantes, Nantes, France*
Josefina del Mármol • *Department of Molecular and Cell Biology, University of California – Berkeley, Berkeley, CA, USA; The Helen Wills Neuroscience Institute, University of California – Berkeley, Berkeley, CA, USA*
Olfat A. Malak • *I'institut du thorax, INSERM, CNRS, Université de Nantes, Nantes, France*
Yoko Mase • *Graduate School of Pharmaceutical Sciences, The University of Tokyo, Bunkyo-ku, Tokyo, Japan*
Kimberly Matulef • *Program in Chemical Biology, Department of Physiology and Pharmacology, Oregon Health & Science University, Portland, OR, USA*
David Nedrud • *Department of Biochemistry, Molecular Biology and Biophysics, University of Minnesota–Twin Cities, Minneapolis, MN, USA*
Colin G. Nichols • *Department of Cell Biology and Physiology, Center for the Investigation of Membrane Excitability Diseases, Washington University School of Medicine, St. Louis, MO, USA*
Crina M. Nimigean • *Department of Anesthesiology, Weill Cornell Medical College, New York, NY, USA; Department of Physiology & Biophysics, Weill Cornell Medical College, New York, NY, USA; Department of Biochemistry, Weill Cornell Medical College, New York, NY, USA*
Valery Novoseletsky • *Moscow M. V. Lomonosov State University, Moscow, Russia*
Masanori Osawa • *Graduate School of Pharmaceutical Sciences, The University of Tokyo, Hongo, Bunkyo-ku, Tokyo, Japan; Faculty of Pharmacy, Keio University, Minato-ku, Tokyo, Japan*
Diane M. Papazian • *Department of Physiology, David Geffen School of Medicine at UCLA, Los Angeles, CA, USA*
Louis H. Philipson • *Department of Medicine, Kovler Diabetes Center, The University of Chicago, Chicago, IL, USA; Department of Pediatrics, The University of Chicago, Chicago, IL, USA*
David J. Posson • *Department of Anesthesiology, Weill Cornell Medical College, New York, NY, USA; Department of Physiology and Biophysics, Weill Cornell Medical College, New York, NY, USA; Vertex Pharmaceuticals Inc., Boston, MA, USA*
Yitao Qi • *College of Life Sciences, Shaanxi Normal University, Xi'an, Shaanxi, China*

Emily A. Rex • *Department of Biochemistry & Molecular Biology, Oregon Health & Science University, Portland, OR, USA*
Robert A. Rietmeijer • *Biophysics Graduate Group, University of California, Berkeley, CA, USA*
Jing-Syuna Ruan • *Department of Physiology, College of Medicine, National Cheng Kung University, Tainan, Taiwan*
Radda Rusinova • *Department of Physiology and Biophysics, Weill Cornell Medical College, New York, NY, USA*
Daniel Schmidt • *Department of Genetics, Cell Biology & Development, University of Minnesota – Twin Cities, Minneapolis, MN, USA*
Huanjie Shao • *College of Life Sciences, Shaanxi Normal University, Xi'an, Shaanxi, China*
Ichio Shimada • *Graduate School of Pharmaceutical Sciences, The University of Tokyo, Bunkyo-ku, Tokyo, Japan*
Show-Ling Shyng • *Department of Physiology and Pharmacology, Oregon Health and Science University, Portland, OR, USA*
Olga S. Sokolova • *Moscow M. V. Lomonosov State University, Moscow, Russia*
Mounir Tarek • *Structure et Réactivité des Systèmes Moléculaires Complexes, CNRS, Université de Lorraine, Nancy, France; CNRS, Unité Mixte de Recherches 7565, Université de Lorraine, Boulevard des Aiguillettes, Vandoeuvre-lès-Nancy, France*
Cholpon Tilegenova • *Texas Tech University Health Science Center, Lubbock, TX, USA*
Yuki Toyama • *Graduate School of Pharmaceutical Sciences, The University of Tokyo, Bunkyo-ku, Tokyo, Japan; Japan Biological Informatics Consortium (JBiC), Koto-ku, Tokyo, Japan*
Francis I. Valiyaveetil • *Department of Physiology and Pharmacology, Oregon Health and Science University, Portland, OR, USA*
Nicholas C. Vierra • *Department of Molecular Physiology and Biophysics, Vanderbilt University, Nashville, TN, USA*
Kang Wang • *Department of Obstetrics and Gynecology, Oregon Health and Science University, Portland, OR, USA*
Liguo Wang • *Department of Biological Structure, University of Washington, Seattle, WA, USA*
Shizhen Wang • *Department of Cell Biology and Physiology, Center for the Investigation of Membrane Excitability Diseases, Washington University School of Medicine, St. Louis, MO, USA*
C. David Weaver • *Department of Pharmacology, Institute of Chemical Biology, Vanderbilt University School of Medicine, Nashville, TN, USA*
Heming Wei • *National Heart Research Institute Singapore, National Heart Centre Singapore, Singapore, Republic of Singapore*
Hongmei Wu • *College of Life Sciences, Shaanxi Normal University, Xi'an, Shaanxi, China*
Jianjun Wu • *National Heart Research Institute Singapore, National Heart Centre Singapore, Singapore, Republic of Singapore*
Hui Xiao • *College of Life Sciences, Shaanxi Normal University, Xi'an, Shaanxi, China*
Huaiyu Yang • *Shanghai Key Laboratory of Regulatory Biology, Institute of Biomedical Sciences and School of Life Sciences, East China Normal University, Shanghai, China*
Mariko Yokogawa • *Graduate School of Pharmaceutical Sciences, The University of Tokyo, Hongo, Bunkyo-ku, Tokyo, Japan; Faculty of Pharmacy, Keio University, Minato-ku, Tokyo, Japan*
Qiansen Zhang • *Shanghai Key Laboratory of Regulatory Biology, Institute of Biomedical Sciences and School of Life Sciences, East China Normal University, Shanghai, China*

SHANSHAN ZHANG • *College of Life Sciences, Shaanxi Normal University, Xi'an, Shaanxi, China*

ZHENGFENG ZHOU • *Knight Cardiovascular Institute, Oregon Health & Science University, Portland, OR, USA*

Chapter 1

Manipulating Potassium Channel Expression and Function in Hippocampal Neurons by In Utero Electroporation

Kang Wang

Abstract

In utero electroporation (IUE) of plasmid DNA into specific brain regions such as hippocampus and cortex has made it possible to reduce protein expression levels or even replace the endogenous protein with site-directed mutant proteins to reveal important physiological consequences. For example, shRNA can mediate targeted knockdown, and can be complemented by simultaneously expressing the shRNA immune wild-type protein to validate on-target effects, or by expression of an shRNA-immune protein harboring site-specific mutations. More recently, IUE has been adapted to express CRISPR/Cas9 components for targeted gene editing that abolishes protein expression. Utilizing these approaches via IUE results in transfected neurons that are interspersed with non-transfected control neurons in the same brain slices, allowing for direct comparisons. Because IUE is performed late in embryonic development and is confined to a relatively small percentage of neurons, developmental compensatory mechanisms that may compromise gene targeting via germ line transmission are minimized. Thus, IUE presents a powerful opportunity to rapidly and cost-effectively dissect molecular and cellular physiology in the context of the intact brain.

Key words Potassium channel, In utero electroporation, Hippocampus, Neurons, shRNA, Animal model

1 Introduction

The cloning of the K channel superfamily and the ensuing structure-function studies that incorporate a diverse toolbox of approaches have yielded profound insights into the molecular mechanisms of function of individual K channels. Now, it is necessary to use the molecular knowledge of the K channels to gain insights and understanding of their physiological roles. One method that has been successfully used is to manipulate the K channel genes using a transgenic approach. Until recently, this was best accomplished in mice by homologous recombination in ES cells followed by introduction into blastocysts and ultimately germ line transmission. This has enabled the creation of null lines that may be targeted to specific tissues and developmental time

Show-Ling Shyng et al. (eds.), *Potassium Channels: Methods and Protocols,* Methods in Molecular Biology, vol. 1684,
DOI 10.1007/978-1-4939-7362-0_1,

points as well as gene modifications that introduce point mutations or fluorescent tags. However, these experiments are time consuming and quite costly, not conducive to testing multiple structure-function hypotheses or creating multiple different modified genes to investigate physiological roles.

Since in utero electroporation was introduced in 2001 [1, 2], it has become a widely used standard tool to fast and efficiently manipulate various genes expression in rodent central nervous system. The application of electroporation in rodent embryos in utero allows injected DNA plasmid to be delivered to specific area of the brain, therefore accomplishing the goal of transfection of neurons. Since DNA is negatively charged, during the electric pulse, the injected plasmid migrates toward the positive pole of the electrode. Therefore, by varying the positions and angles of the positive electrode, IUE can be used to target specific brain areas, including the cortical area, hippocampus, lateral septal nucleus and striatum, thalamus, and hypothalamus.

In this protocol, I describe the details of the in utero electroporation method in targeting pyramidal neurons in the hippocampus. The examples of fluorescent protein expression in hippocampal pyramidal neurons are shown in Fig. 1 (low magnification) and Fig. 2 (high magnification). Briefly, pregnant mice at E16 (or rats at E18) are anesthetized with isofluorane, their abdominal cavity is cut open, and the uterine horns are exposed. DNA plasmids are injected to the lateral ventricle through the uterine wall by using a glass micropipette pulled from thin-walled capillary glass. The head of each embryo within its uterine sac is positioned between tweezer-type electrodes, and five square electric pulses (40–50 mV; 100 ms; 1 s intervals) are passed using an electroporator. After electroporation, the wall and skin of the abdominal cavity of the pregnant mice/rats are sutured closed and embryos are allowed to develop normally [3].

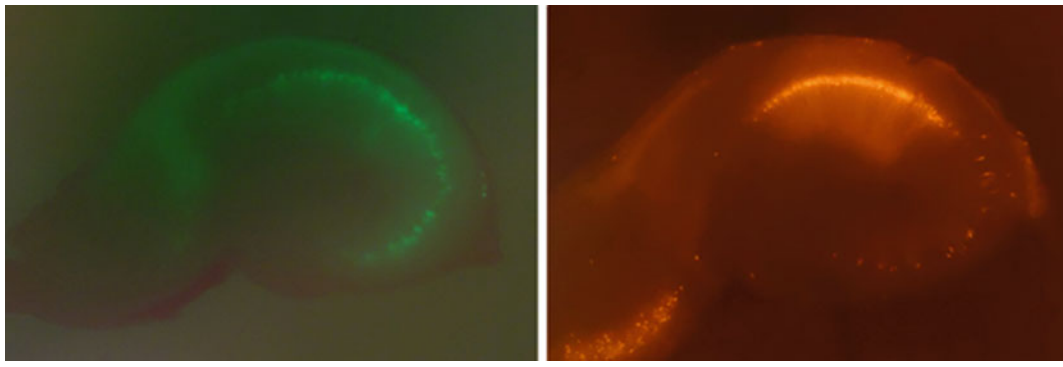

Fig. 1 Expression of green or red fluorescent proteins in pyramidal neurons of different hippocampal slices (10× ocular × 4× objective Lens)

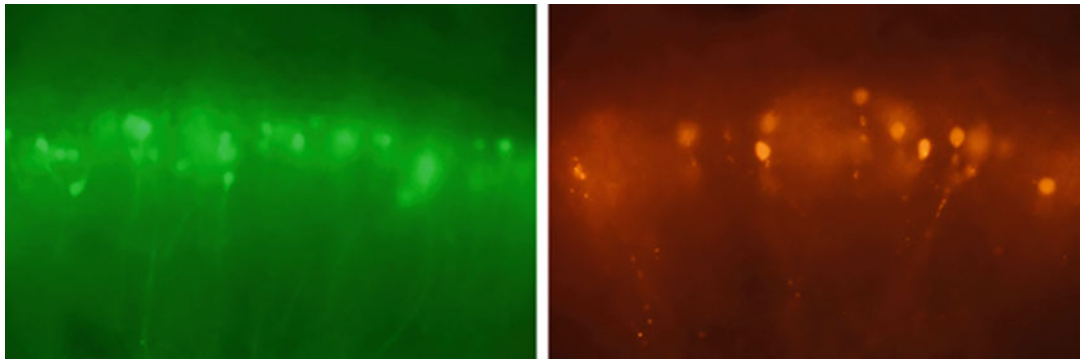

Fig. 2 Expression of green or red fluorescent proteins in pyramidal neurons of different hippocampal slices (10× ocular × 40× objective Lens)

2 Materials

1. Timed-pregnant C57BL/6 mice at embryonic day (E) 16 or pregnant Wistar rats at E18 are proper choices for targeting hippocampal neurons.
2. 2 μg/μl DNA plasmid with ~2% fast green.
3. Surgical instruments: straight and curved forceps with blunt ends, ring forceps (4.8 mm ID/6 mm OD) for holding embryos, scalpel and scissors with different sizes, suturing needle holder with lock-tungsten carbide, and wound clip applier for rats if needed. All instruments should be sterilized before performing animal surgery.
4. Vaporizer with attached oxygen tank for animal anesthesia.
5. Isofluorane for anesthetizing the animal.
6. Borosilicate glass capillaries (0.86 mm ID/1.5 mm OD).
7. Microloader tips for loading DNA solution into pipette.
8. Microinjector with foot control and capillary holder.
9. Electroporator with foot control.
10. Paddle-type electrodes (5 mm for mice embryos and 8–10 mm for rats embryos) (*see* **Note 1**).
11. Heating pads.
12. Alcohol and iodine swabs.
13. Sterilized gauze.
14. Pre-warmed saline.
15. Carprofen for pain relief.

3 Methods

3.1 Preparation of the Surgery

1. Turn on the heating pads and all IUE equipment, set five square electric pulses (40–50 mV; 100 ms; 1 s intervals) for electroporator (*see* **Note 2**).
2. Fill the micropipette with DNA solution using a microloader tip, connect the pipette to the capillary holder.

3.2 Surgery Procedures

1. Induce anesthesia of the animal in a chamber with isofluorane at 4.5% flow rate mixed with oxygen.
2. Transfer the animal to surgical area with isofluorane at 2% flow rate mixed with oxygen and maintain the same rate for the rest of surgery.
3. Shave the abdominal skin to remove the fur, apply pain relief pre- and post-surgery.
4. Clean the shaved area for at least three times with iodine and alcohol.
5. Use a scalpel to make a vertical incision along the midline through the skin for about 2 cm in length, use scissors to make a similar incision underneath the skin along the linea alba. Make sure the animal is fully anesthetized before making incision; this could be checked by the disappearance of toe pinch reflex.
6. Cover the shaved skin by 5–6 sterilized gauze with a hole of 4–5 cm in the middle over the incision. Drop pre-warmed saline in the cutting area and apply saline when necessary to keep the embryos hydrated all through the surgery.
7. Place the ring forceps between two most accessible embryos and gently pull the uterine horns out of the abdominal cavity.
8. Hold one embryo with ring forceps and slowly inject 2 μl colored DNA solution into the lateral ventricle, start one embryo after another, and complete DNA injection for the rest of embryos.
9. Place the electrodes on the side of the embryo head and apply the appropriate voltage to individual embryos.

3.3 Post Electroporation/ Postoperative Care

1. Carefully replace the uterine horns back to the abdominal cavity, start with one side of the uterine horn, and then the other side (*see* **Note 3**).
2. Suture the muscular and skin walls separately with 4–0 silk suture. Apply clips to the skin of rats if necessary (*see* **Note 4**).
3. Transfer the animal to a recovery chamber placed on a heating pad, and supervise the animal during recovery.
4. Put the animal back to the cage and to the animal room. Check the behavior of the animal regularly after the surgery.

4 Notes

1. Choose paddle size of the electrodes properly, 5 mm works well for mice E16 embryos and 10 mm works well for rats E18 embryos. It is a balance between efficiency and specificity.
2. Apply appropriate voltage for electroporation, high voltages could result in decreased embryonic survival rates while low voltages lead to reduced transfection efficiency. Always monitor the size of current during electroporation, which should remain constant among embryos. Big variation of current for certain embryos indicates the misplacement of electrode paddle or loss of voltage application during electroporation.
3. After electroporation, replace the embryonic chain carefully and sequentially back to the abdominal cavity, avoid twisting the uterine horns when inserted back to the abdomen, which could result in a difficult delivery for the mom or ingestion of the embryos before delivery.
4. Keep the surgical length within 40 min for each pregnant animal.

References

1. Saito T, Nakatsuji N (2001) Efficient gene transfer into the embryonic mouse brain using in vivo electroporation. Dev Biol 240:237–246
2. Tabata H, Nakajima K (2001) Efficient in utero gene transfer system to the developing mouse brain using electroporation: visualization of neuronal migration in the developing cortex. Neuroscience 103:865–872
3. Wang K, Lin MT, Adelman JP, Maylie J (2014) Distinct Ca^{2+} sources in dendritic spines of hippocampal CA1 neuron couple to SK and Kv4 channels. Neuron 81(2):379–387

Chapter 2

Studying *KCNQ1* Mutation and Drug Response in Type 1 Long QT Syndrome Using Patient-Specific Induced Pluripotent Stem Cell-Derived Cardiomyocytes

Heming Wei, Jianjun Wu, and Zhenfeng Liu

Abstract

Patient-specific human induced pluripotent stem cell (hiPSC)-derived cardiomyocytes (hiPSC-CMs) are becoming a valuable model for studying inherited cardiac arrhythmias. Type 1 long-QT syndrome is associated with the genetic variants of *KCNQ1* gene that encodes Kv7.1, the α-subunit of the voltage-gated potassium channel QKT subfamily member 1 that channels the slow component of the outwardly rectifying K^+ channel current in cardiac myocytes. Patient- or disease-specific hiPSC-CM model could facilitate the characterization of the genotype-phenotype relationships and testing of individualized drug responses.

Here, we describe the methods in the generation of hiPSC-CMs, molecular and electrophysiological characterizations of their cellular phenotypes associated with *KCNQ1*/Kv7.1 defects, and evaluation of the effects of K^+ channel-specific drugs.

Key words Human-induced pluripotent stem cells, Cardiomyocytes, Inherited cardiac arrhythmias, Long-QT Syndrome, *KCNQ1*, Kv7.1

1 Introduction

Human-induced pluripotent stem cells (hiPSC) are embryonic stem cell-like that can be derived from postnatal somatic cells [1, 2]. hiPSCs are capable of differentiating into functional cardiomyocytes (hiPSC-CMs) [3]. Such cardiomyocytes carry the basic characteristics of the native cardiac myocytes from the heart [3, 4].

Inherited cardiac arrhythmias, such as the long-QT syndromes (LQTS), are associated with complicated genetic defects in a number of critical cardiac ion channels [5, 6] with various penetrance and expressivity. To date, studies on the disease mechanisms and ion channel-targeted drug therapies have been hampered by a lack of proper cellular models particularly cardiomyocytes from the patients with favourable genetic backgrounds. Patient-specific hiPSC-CMs, as a source of cardiomyocytes derived from patients of inherited

Show-Ling Shyng et al. (eds.), *Potassium Channels: Methods and Protocols,* Methods in Molecular Biology, vol. 1684,
DOI 10.1007/978-1-4939-7362-0_2,

cardiac arrhythmias, are being recognized as a valuable and unique model for studying various neuronal and cardiac diseases, particularly of those associated with single-gene variations [7–10].

Type 1 LQTS (LQT1) is the most common subtype of LQTS which contributes to ~40% of all LQTS. Variations in the *KCNQ1* gene have been identified in LQT1 patients. *KCNQ1* encodes Kv7.1 proteins, a voltage-activated potassium channel alpha-subunit, which forms a homotetrameric channel and facilitates a voltage-dependent slow delayed rectifier K(+) current (I_{Ks}). In the human heart, *KCNQ1* associates with the auxiliary β-subunit *KCNE1* to give rise to I_{Ks}, characterized by slow activation and deactivation kinetics, contributes to cardiac action potential repolarization. To date, nearly 100 different *KCNQ1* mutations, including alternative splicing mutations [11–15], have been reported responsible for the defects in I_{Ks} current associated with prolonged QT-intervals on the electrocardiogram (ECG) of patients. Prolonged QT interval could lead to a polymorphic ventricular tachycardia or torsade de pointes (TdP), syncopes, and sudden death [16]. At cellular level, *KCNQ1* mutations could compromise the functions of the Kv7.1 channels via reducing their protein synthesis, attenuating their intracellular trafficking and disturbing their gating properties [15, 17, 18].

Patient-specific hiPSC-CM model, with different *KCNQ1* mutations and favourable genetic backgrounds that may harbor potential genetic modifiers, could be ideal for validating the defects in Kv7.1. Application of the hiPSC-CMs model could facilitate not only the characterization of the genotype-phenotype relationships, but also the testing of patient- or disease-specific, individualized drug responses [19, 20]. To date, hiPSC-CMs from patients of inherited cardiac arrhythmias, such as LQTS, have been successfully adopted for disease modeling [7–10]. With a LQT1 patient with in-frame heterozygous deletion of exon 7 (C.922 ~ 1032 del; P.308 ~ 344 del) in *KCNQ1* gene, we have generated patient-specific hiPSC-CMs and successfully tested the impacts of the *KCNQ1* mutation on Kv7.1 channels as well as therapeutic potential of an I_{Ks} channel opener [20].

In this chapter, the methods in the generation of hiPSC-CMs, molecular and electrophysiological characterization of the cellular phenotypes associated with *KCNQ1*/Kv7.1 defects, and testing of the cellular responses to ion channel-specific drugs are described while the focus is on the key procedures for molecular and electrophysiological characterizations of hiPSC-CMs.

2 Materials

2.1 Materials for Cell Culture-Related Studies

Unless specified, all materials are from Life Technologies-Thermo Fisher Scientific.

2.1.1 Basal Media

1. Dulbecco's Modified Eagle Medium, high glucose (DMEM-HG) (Cat. No. 11965092). Store at 4 °C.
2. RPMI1640 basal medium (Cat. No. 11875119). Store at 4 °C.
3. RPMI1640 medium without D-glucose (Cat. No. 11879). Store at 4 °C.
4. B-27 Supplement (50×), serum free (Cat. No. 17504044). Store at −20 °C.

2.1.2 Supplements (Store at −20 °C to −30 °C)

1. Fetal Bovine Serum (FBS), heat inactivated (Cat. No. 10082147). *See* **Note 1**.
2. Penicillin-Streptomycin-Glutamine (100×) (Cat. No. 10378016).
3. Sodium Pyruvate Solution 100 mM (100×), liquid (Cat. No. 11360070).
4. Non-Essential Amino Acids (NEAA) Solution, 10 mM (100×) (Cat. No. 11140).
5. β-Mercaptoethanol, 1000× liquid, 50 ml (Cat. No. 21985023). *See* **Note 2**.
6. L-Ascorbic acid 2-phosphate sesquimagnesium salt hydrate (Sigma-Aldrich, A8960).
7. *O. sativa*-derived recombinant human albumin (Sigma-Aldrich, A9731).
8. Sodium DL-lactate (Sigma-Aldrich, L4263).

2.1.3 Other Materials

1. Hanks' Balanced Salt Solution (HBSS) without calcium and magnesium (Cat. No. 14170112). *See* **Note 3**.
2. Gelatin (Sigma-Aldrich, G1890). To prepare 0.1% (w/v) gelatin, add 0.5 g gelatin to MilliQ water to 500 ml and autoclave the solution. Store at room temperature and use within 12 months.
3. Trypsin-EDTA (0.25%), phenol red, liquid (Cat. No. 25200056). To prepare 0.05% Trypsin-EDTA, dilution 0.25% Trypsin-EDTA (1:5) in HBSS. Store at −30 °C.
4. TrypLE™ Select Enzyme (1×), no phenol red (Cat. No. 12563011).

2.1.4 Human Dermal Fibroblasts Medium

1. DMEM-HG Medium contains (final concentrations): 82% DMEM-HG supplemented with 15% FBS, 1% Penicillin-Streptomycin-Glutamine (1×), 1% NEAA and 1% Sodium Pyruvate.

2.1.5 hiPSC-CM Maintaining Medium

1. RPMI + B27 Medium. Prepare 50 ml medium containing 49 ml of RPMI and 1 ml of B27 supplement. Store at 4 °C and use within 1 month.

2.1.6 Equipment

1. Level II Biological Safety Cabinet.
2. CO_2 incubator.
3. Centrifuge for cell culture.

2.2 Materials for Molecular Biology Assays

2.2.1 For DNA and RNA Work

1. PureLink® Genomic DNA Mini Kit for genomic DNA extraction (Invitrogen™-Thermo Fisher Scientific, Cat. No. K182001).
2. RNeasy Mini kit (QIAGEN, Germany, Cat. No. 74106).
3. RNase-Free DNase Set for total RNA isolation (QIAGEN, Germany, Cat. No. 79254).
4. SuperScript® III First-Strand Synthesis System for reverse transcription (RT) reaction (Life Technologies-Thermo Fisher Scientific, Cat. No. 18080051).
5. PCR Master Mix (2×) for PCR (Thermo Fisher Scientific, Cat. No. K0171).
6. QIAquick PCR Purification Kit for gel extraction of PCR products (QIAGEN, Cat. No. 28104).

2.2.2 For Western Blotting

1. Cell scraper (Greiner Bio-One GmbH, Frickenhausen, Germany).
2. Dulbecco's phosphate-buffered saline (DPBS), no calcium, no magnesium (Life Technologies-Thermo Fisher Scientific, Cat. No. 14190144). *See* **Note 4**.
3. RIPA Lysis and Extraction Buffer (Pierce Biotechnology-Thermo Fisher Scientific, Cat. No. 89900) containing 20 mM Tris–HCl, pH 7.4; 150 mM NaCl; 40 mM NaF; 5 mM EDTA; 1% Triton X-100; 1 mM sodium orthovanadate; 1% (vol/vol) Nonidet P-40, 0.1% (wt/vol) sodium deoxycholate; 0.1% (wt/vol) SDS; 1 mM phenylmethylsulfonyl fluoride; and 10 ng/ml aprotinin.
4. 2D Quant kit for protein quantification (Amersham-GE Healthcare Life Sciences, Cat. No. 80-6483-56).
5. TGX™ FastCast™ Acrylamide Solutions (Bio-Rad Laboratories).
6. Polyvinylidine fluoride membrane (PVDF) membrane (0.22 μm) (Amersham-GE Healthcare Life Sciences, Cat. No. 10600021).
7. Transferring Buffer containing 25 mM Tris, 190 mM glycine, 20% methanol, and 0.01% (wt/vol) SDS.

8. Methanol (Sigma-Aldrich, M1775 Sigma). To prepare 90% methanol, add 5 ml MilliQ water to 45 ml pure methanol. Store at −20 °C.
9. Tris-buffered saline (TBS), 20× (Pierce-Thermo Fisher Scientific, Cat. No. 28358). Store at 4 °C. To prepare 1× TBS working solution, dilute 20× TBS (20:1) in MilliQ water.
10. TBS-T (1×): 1× TBS solution containing 0.1% Tween-20.
11. Bovine Serum Albumin or BSA (Sigma-Aldrich, A9418 Sigma). To prepare 5% BSA, dilute 5 g BSA in 100 ml 1× TBS-T. Store at 4 °C and use within 6 months.
12. ECL plus Western blot Detection Reagent (Pierce-Thermo Fisher Scientific, Cat. No. 32132).
13. WesternBright HRP substrate (Advansta, Cat. No. K-12045).
14. Restore™ Western Blot stripping solution (Pierce-Thermo Fisher Scientific, Cat. No. 21059).

2.2.3 For Immunofluorescence

1. 5% BSA in DPBS: dilute 5 g BSA in 100 ml in 1× DPBS. Store at 4 °C and use within 6 months.
2. 16% Paraformaldehyde (PFA) (Electron Microscopy Sciences, Hatfield, PA, USA). To prepare 4% PFA, diluted 16% PFA in 1× DPBS. Use a freshly prepared solution.
3. Triton X-100 (Sigma-Aldrich, T8532) . To prepare 10% Triton X-100 solution (50 ml), add 5 ml Triton X-100 into 45 ml 1× DPBS. Store at 4 °C and use within 6 months.
4. ProLong® Gold Antifade Mountant with DAPI (Life Technologies-Thermo Fisher Scientific, Cat. No. P36935).
5. Nail polish (colorless).
6. 8-mm round coverslips.
7. Glass slides.

2.2.4 Antibodies

Primary Antibodies

1. Anti-KV7.1 rabbit polyclonal antibody (Alomone Labs, Jerusalem, Israel, Cat. No. APC-022). Use 1:500 dilution for Western blotting and 1:200 dilution for immunofluorescent imaging.
2. Anti-Golgi apparatus monoclonal antibody (Life Technologies-Thermo Fisher Scientific, Cat. No. A-21270). Use 1:200 dilutions for immunofluorescence imaging.
3. Anti-α-actinin monoclonal antibody (Sigma-Aldrich, clone EA-35). Use 1:500 dilutions for immunofluorescence imaging.
4. Anti-β-actin polyclonal antibody (abcam, ab8229). Use 1/2000 dilution for Western blotting.
5. Dilute the primary Abs in 1× TBS-T (for Western blotting) or DPBS (for immunofluorescence) containing 2% BSA.

Secondary Antibody

1. Horseradish peroxidase (HRP)-conjugated secondary antibody. Use 1:5000 dilutions (in 1× TBS-T) for Western blotting.
2. Fluorochrome-conjugated secondary antibodies. Use 1:500 dilutions (in 1× DPBS) for immunofluorescence staining.

2.2.5 Equipment

1. Sonic Dismembrator (Fisher Scientific™ Model 705 Sonic Dismembrator).
2. Bench-top microcentrifuge (temperature controlled, with speed capacity up to 10,000 × *g*).
3. ELISA reader (SpectraMax® M3 Multi-Mode Microplate Reader, Molecular Devices).
4. PCR machine.
5. NanoDrop Spectrophotometer for DAN/RNA quantification (Thermo Fisher Scientific).
6. Mini-PROTEAN® Electrophoresis System (Bio-Rad Laboratories). Including glass plates, medium binder clips (1¼ in.) and plastic container.
7. Trans-Blot® SD Semi-Dry Transfer Cell (Bio-Rad Laboratories).
8. The PowerPac™ Basic power supply (Bio-Red Laboratories) for submerged horizontal and mini vertical gel electrophoresis. Applies for nucleic acid gel and protein gel electrophoresis.
9. Gel Doc™ XR+ Gel Documentation System (Bio-Rad Laboratories).
10. GS-800 Calibrated Densitometer and Quantity One quantification analysis software version 4.5.2 (Bio-Rad Laboratories).
11. Confocal microscope.

2.3 Materials for Electrophysiology Assays

1. Glass capillaries: Capillary Glass & Filaments (O.D. 1.5 mm, I. D. 0.86 mm, 10 cm length). From Sutter Instrument (Item#: BF 150-86-10), Novato, CA, USA.

2.3.1 Consumables

2.3.2 Solutions

Unless specified, chemicals are from Sigma-Aldrich Corp (St. Louis, USA).

1. Solutions for action potential (AP) recording.
   (a) Pipette solution contained (in mM): KCl 140, NaCl 5, $MgCl_2$ 1, MgATP 3, EGTA 10, and HEPES 10, adjusted to pH 7.2 with KOH.
   (b) Extracellular solution (Tyrode's solution) contained (in mM): NaCl 140, KCl 5.4, $CaCl_2$ 1.8, $MgCl_2$ 1, glucose 10 and HEPES 10, adjusted to pH 7.4 with NaOH.

2. Solutions for I_{Ks} recording.
   (a) Pipette solution contained (in mM): potassium aspartate 110, KCl 20, $MgCl_2$ 1, EGTA 10, Na_2ATP 5 and HEPES 10, adjusted to pH 7.2 with KOH.
   (b) Extracellular solution (Na^+-free) contained (in mM): Choline chloride 140, KCl 5.4, $MgCl_2$ 1, $CaCl_2$ 1.8, glucose 10 and HEPES 10, adjusted to pH 7.4 with Tris base. Add $CdCl_2$ (0.3 mM) to block the L-type Ca^{2+} current.

2.3.3 Ion Channel Openers/Blockers

1. Chromanol 293B (Sigma-Aldrich, C2615 Sigma).
2. E-4031 (Sigma-Aldrich, M5060 Sigma).
3. ML277 or (R)-N-(4-(4-methoxyphenyl)thiazol-2-yl)-1-tosylpiperidine-2-carboxamide (Sigma-Aldrich, SML0524 Sigma).

2.3.4 Equipment and Software

1. Axopatch 700B and Axopatch 200B amplifiers (Axon Instrument-Molecular Devices, Sunnyvale, USA).
2. Digidata 1440A (Axon Instrument).
3. pCLAMP10.7 Software (Axon Instrument).
4. Origin 7.0 software (Origin Lab Corporation, Northampton, USA).
5. Sutter P-97 microelectrode puller (Novato, CA, USA).
6. Microforge (NARISHIGE MF-900, Japan).
7. Temperature controller (Warner Instruments, Hamden, USA).
8. A Cybercyte System (Cytocybernetics, Buffalo, USA).

3 Methods

3.1 Generation of hiPSC-CMs (Only the Key Procedures Are Described in Brief)

3.1.1 Derivate Somatic Cells from Human for Reprogramming

1. Perform skin biopsy on patients and sibling controls to obtain dermis tissue. Manually separate and mince the dermis tissue. Plate the tissue fractions onto a 0.1% (w/v) gelatin-coated petri dish, culture in DMEM-HG Medium. To subculture the fibroblasts that migrated out of the dermis tissue, wash cells two times with HBSS and incubate cells with 0.05% trypsin at 37 °C for 5 min. Then replate the cells with a split ratio of 1:3. Use passage 2 or younger cells for reprogramming.
2. Alternatively, derive peripheral blood cells, such as activated T cells, and use them as an alternative source for reprogramming [21]. This less-invasive way for deriving somatic cells is becoming the top choice.

3.1.2 Reprogram Somatic Cells into hiPSCs

Reprogram the somatic cells via ectopic expression of *OCT-4*, *SOX-2*, *KIF-4*, and *c-Myc* [1, 2, 20, 21]. One of the latest and mostly adopted protocols is the Sendai virus transduction method [21]. *See* **Note 5**.

3.1.3 Characterize the Pluripotency of hiPSCs

The pluripotency of hiPSCs can be confirmed by their expression of pluripotent stem cell markers in vitro and their capability of teratoma formation in immunodeficient mice in vivo, as previously described [1, 2].

3.1.4 Differentiate hiPSCs into Cardiomyocytes

Use the latest and mostly adopted protocols including that by Lian et al. [22] and Zhang et al. [23] for higher cardiomyogenic differentiation efficiency ($\geq$80%).

In brief, prepare confluent monolayer of single hiPSC dissociated from hiPSC colonies and initiate the direct cardiomyogenic differentiation process. The differentiation can be carried out in a serum-free defined system by temporal modulation of canonical Wnt signaling (appropriate temporal application of Gsk3 inhibitor followed by chemical Wnt inhibitors) [22]. Alternatively, hiPSC-CMs can be generated with high efficiency by combining the extracellular matrix sandwich with sequential application of growth factors (Activin A, bone morphogenetic protein 4 and basic fibroblast growth factor) [23].

3.1.5 Dissociate hiPSC-CMs into Single Cells

1. Wash the hiPSC-CMs (sometimes in clusters or clumps) twice with 1× HBSS and leave the cells covered by HBSS for 10 min at room temperature.
2. Remove the HBSS and add TrypLE™ Select Enzyme and incubate the cells in a 37 °C CO_2 incubator for 5–8 min. Pipetting up-and-down to further dissociate the cells.
3. Transfer the detached cells to a 15 ml centrifuge tube. Centrifuge at 300 rpm for 5 min.
4. Replete the cells on 0.1% gelatin-coated cultural plastic or glass surface and continually culture in RPMI + B27 Medium.

3.1.6 Purify and Enrich hiPSC-CMs by Metabolic Selection (See Note 6)

1. hiPSC-CMs can be further purified and enriched by metabolic selection. Change the RPMI + B27 Medium of hiPSC-CMs 10–20 days post differentiation to a variant RPMI1640 medium (without D-glucose) supplemented with l-ascorbic acid 2-phosphate, *O. sativa*-derived recombinant human albumin, and sodium DL-lactate [24]. Such chemically defined metabolic selection favours the survival of hiPSC-CMs and they can therefore be enriched over 90%.

3.1.7 Maintaining of hiPSC-CMs

1. Maintain hiPSC-CMs in RPMI + B27 Medium at 37 °C in a humid CO_2 incubators supplemented with 5% CO_2. Change the cultural medium every three days. The cells can be maintained with spontaneously beating phenotype for more than 6 months [3, 22]. Cells can be used 48 h post platting.

3.2 Molecular and Cellular Characterization of the KCNQ1 Defects

3.2.1 Characterization of the KCNQ1 Gene Defects in hiPSC-CMs

Determine Genomic Variations

1. Isolate genomic DNA from the peripheral blood, somatic cells, and hiPSC-CMs of control and patient.
2. Quantify DNA with a NanoDrop Spectrophotometer.
3. Sequence the *KCNQ1* gene and compare to the reference sequence. *See* **Note 7**.

Assess Gene Transcription by Reverse Transcription-Polymerase Chain Reaction Assay

1. Isolate total RNA from hiPSC-CMs using the RNeasy Mini kit and RNase-Free DNase Set following the recommended protocols.
2. Quantify the total RNA with a NanoDrop Spectrophotometer.
3. Synthesize the first-strand cDNA by Reverse Transcription (RT) using SuperScript® III First-Strand Synthesis System. Use oligo dTs as the primer for RT reaction.
4. Perform Polymerase Chain Reaction (PCR) assay to quantify the level of gene transcription.
5. Prepare PCR reaction mix containing cDNA and primers for the gene of interest.
6. Amplify the *KCNQ1* for 42 cycles of the following: denaturing at 94 °C for 30 s, annealing at 60 °C for 30 s and extension at 72 °C for 60 s.
7. Amplify the Glyceraldehyde-3-Phosphate Dehydrogenase (*GAPDH*) PCR for 29 cycles.
8. PCR Primers are shown in Table 1.
9. Human left ventricular tissue mRNA could be used as reference.
10. Separate the PCR products in a 1.5% agarose gel by horizontal gel electrophoresis.
11. Quantify the PCR bands of *KCNQ1* and *GAPDH* by Gel Doc™ XR+ Gel Documentation System. Normalize *KCNQ1* to *GAPDH* and plot the results as relative expression levels.
12. Purify the *KCNQ1* PCR products from the agarose gel (full length and potential isoforms with various sizes) and send for Sanger sequencing to confirm the specific sequences of *KCNQ1*.

Figure 1 serves as an example of the RT-PCR assays.

Table 1
PCR primers

Gene access #	Gene	SEQUENCE (5′–3′) of PCR primers	
NM_000218.2	*KCNQ1*	F	GTA CCT GGC TGA GAA GGA CG
		R	AGA CTT CTT GGG TTT GGG GC
NM_002046.5	*GAPDH*	F	
		R	

Reproduced from ref. 20 with modifications.
KCNQ1 PCR covers a region from exon 6 to exon 9 of the cDNA

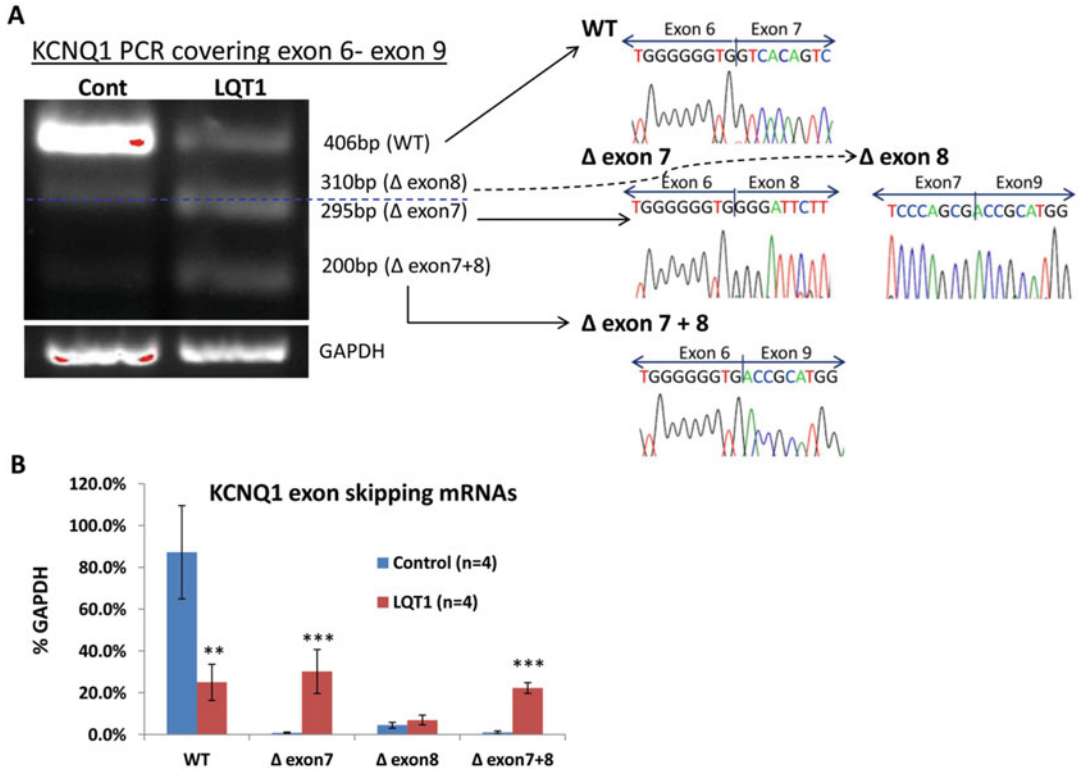

Fig. 1 Expression of *KCNQ1* gene in control and LQT1 patient hiPSC-CMs. (**A**) Representative agarose gel images show the *KCNQ1* and *GAPDH* PCR products amplified from the cDNA of control and patient hiPSC-CMs (*left*). *KCNQ1* PCR covers a fragment from exon 6 to exon 9. The *blue dashed line* separates the PCR products of Δexon8 (above) and Δexon7 (below). The sequences of the corresponding PCR products are presented on the *right*. The full length (WT) and exon-skipping (with deletion of exon 7, exon 8, or both exon 7 and exon 8) *KCNQ1* cDNA are identified in control and patient hiPSC-CMs. (**B**) A bar-graph shows the quantitative comparisons of the full length (WT) and exon-skipping cDNA identified in control and patient hiPSC-CMs. Values are given as mean ± SD. $^{**}p < 0.01$, $^{***}p < 0.001$, vs. control (Reproduced from ref. 20)

3.2.2 Determine the Levels and Sizes of Kv7.1 Protein in hiPSC-CMs by SDS-PAGE and Western blotting

Preparation of Cell Lysate and Extraction of Protein

1. Harvest the adherent hiPSC-CMs using a cell scraper. Collect the detached cells into a 15 ml centrifuge tube (BD Falcon, BD Biosciences) and centrifuge at 500 × *g* at 4 °C for 5 min.
2. Wash twice with 1× ice-cold DPBS.
3. Add lysis buffer (RIPA buffer) to cells and resuspend the pellet with pipetting up and down for 30 times followed by 20 s sonication on ice.
4. Centrifuge the cell lysate at 10,000 × *g* at 4 °C for 10 min. Collect the supernatant that contains the protein extract. Use immediately or store at −80 °C for further analysis.
5. Quantify the protein in samples with a 2D Quant kit with at least two independent replicates. Use BSA as a standard for protein quantification.

SDS-PAGE and Western Blotting

1. Case polyacrylamide (8–12%) mini-gels (~9 × 7 cm) with TGX™ FastCast™ Acrylamide Solutions using the gel-casing apparatus from the Mini-PROTEAN® Electrophoresis System.
2. Use Mini-PROTEAN® Electrophoresis System to separate proteins on resolving SDS-PAGE under denaturing conditions at 20 mA constant current.
3. Transfer the proteins from the gel to PVDF membrane by applying the "semi-dry" transfer method for 60 min at 120 mA in Transferring Buffer.
4. Block the membrane with 5% BSA in 1× TBS-T for 2 h at room temperature, wash three times in 1× TBS-T (10 min each).
5. Incubate the membrane with primary antibodies (such as anti-KV7.1/*KCNQ1* diluted 1:500 in PBS-T plus 2% BSA) overnight at 4 °C.
6. Wash the membranes with 1× TBS-T and incubate with HRP-conjugated secondary antibody for 1 h at room temperature.
7. Develop the membranes with ECL plus Western blot Detection Reagent.
8. Expose the membranes and obtain images using a Bio-Rad Gel Doc machine.
9. To reprobe the same membrane with another primary antibody (such as anti-β-actin Ab), strip the membrane with stripping solution and incubate with anti-β-actin followed by a corresponding secondary antibody. β-Actin serves as reference protein for normalizing the equal sample loading. Develop and expose the membrane as above-mentioned.
10. Perform densitometric quantification of the protein bands. Values = relative protein expression normalized to β-actin.

Figure 2 serves as an example of the Western blotting assay.

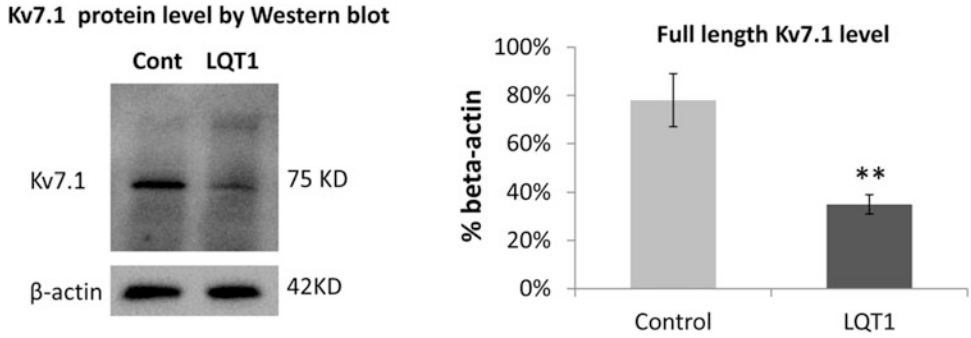

Fig. 2 Kv7.1 protein expression in control and LQT1 patient hiPSC-CMs. (*Left*) Representative Western blotting images of Kv7.1 and β-actin. A ~75 kDa band is identified as Kv7.1. The membrane was stripped and reprobed with anti-β-actin antibody. (*Right*) A bar graft shows the levels of Kv7.1 plotted against β-actin. Only the full length Kv7.1 is clearly presented and it is markedly reduced in LQT1 patient hiPSC-CMs. $^{**}p < 0.01$, vs. control (Reproduced from ref. 20 with modifications)

3.2.3 Immunofluorescence Assay to Determine the Intracellular Localization of Kv7.1

Fix and Permeabilize the Cells

1. Plate hiPSC-CMs on 0.1% (w/v) gelatin-coated 8 mm round coverslips in a 24-well plate in RPMI + B27 Medium. Continue culturing for 48–72 h.
2. Fix cells with 4% paraformaldehyde at room temperature for 10 min.
3. Permeabilize cells with 0.1% Triton X-100 at room temperature for 10 min.
4. Wash cells three times with 1× DPBS and block cells with 5% BSA in 1× DPBS for 1 h.

Immunostaining (*See* **Note 8**)

1. Incubate cells with a mix of two primary antibodies, such as an anti-Kv7.1 polyclonal Ab combined with an anti-α-actinin monoclonal Ab, or an anti-Kv7.1 polyclonal Ab combined with an anti-Golgi monoclonal Ab, at 4 °C overnight.
2. Wash the cells five to seven times with 1× DPBS.
3. Incubated cells with a mix of corresponding secondary antibodies conjugated with different fluorochromes at room temperature for 1 h.
4. Mount the coverslips on glass slides using Mount Gold (with DAPI) medium, seal with nail-polish.

Image the Cells and Quantify the Kv7.1 Signals

1. View and image the cells with confocal microscopy.
2. Quantify the immunofluorescent signals and intensity of Kv7.1 with ImageJ software.
3. Determine the intracellular localization of Kv7.1 by measuring the distance of Kv7.1 staining to nucleus.

Figure 3 serves as an example of the immunofluorescence assay.

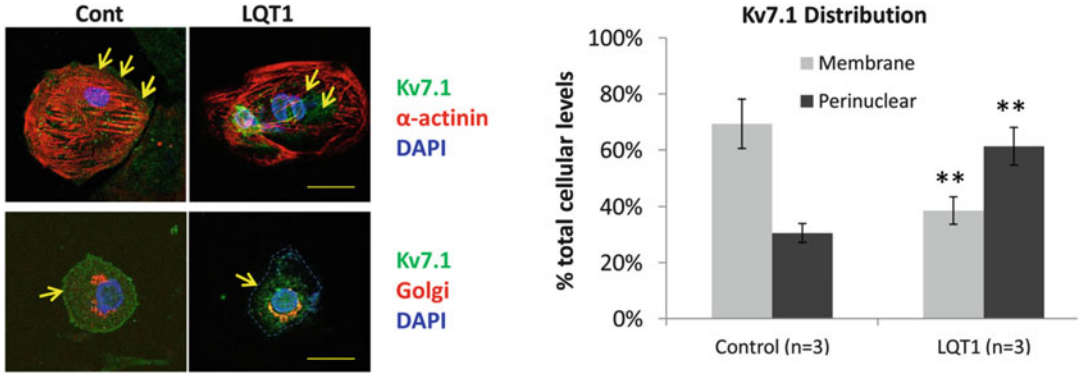

Fig. 3 Intracellular distributions of Kv7.1 in control and LQT1 patient hiPSC-CMs. (*Left*). Representative co-immunofluorescent images of Kv7.1 (*green*) and α-actinin (*red*) (*top panel*), or Kv7.1 (*green*) and Golgi apparatus (*red*) (*bottom panel*), of control and patient hiPSC-CMs are presented. Cell nuclei were stained with DAPI (*blue*). *Arrows* indicate Kv7.1. Magnitude: 63×. Scale bar: 20 μM. (*Right*) A bar graph presents the ratio of membranous and peri-nuclear distributions of Kv7.1 quantified in cells costained with Kv7.1 and Golgi apparatus (distance less than half of radius is considered as perinuclear whereas distance over half of radius is considered membranous). $^{**}p < 0.01$, vs. control (Reproduced from ref. 20 with modifications)

3.3 Electrophysiology Characterization of the Kv7.1 Defects in hiPSC-CMs

3.3.1 Prepare hiPSC-CMs for Patch-Clamp Recording

1. Plate single hiPSC-CMs into 3.5 cm petri dishes precoated with 0.1% (w/v) gelatin to 30–40% confluency.
2. Maintain the hiPSC-CMs at 37 °C in RPMI + B27 Medium in a humidified CO_2 (5%) incubator. Use hiPSC-CMs 5–6 weeks post hiPSCs differentiation. *See* **Note 9**.

3.3.2 Set Up the Patch-Clamp Systems

1. Use conventional whole cell patch-clamp recording protocols to record K^+ currents and action potentials (AP) in hiPSC-CMs.
2. Use Axopatch 700B amplifiers to amplify the signals.
3. Use Digidata 1440 acquisition system and pClamp10.7 software (Axon Instruments) for data acquisition.
4. Prepare the patch pipettes by fabricating the glass capillaries using a microelectrode puller and heat polish the tips with a microforge to gain a resistance of 3–5 MΩ when filled with internal solution.
5. Form the gigaseal and achieve whole-cell configuration by applying gentle suction.
6. Select cells with series resistance below 6 MΩ before compensation (70% to 80%). Up to 75% series resistance compensation could be achieved.

3.3.3 Record I_{ks} by Voltage-Clamping

Set Up the Voltage-Clamping Protocols [7, 20]

1. Determine cell membrane capacitance of hiPSC-CMs automatically by the Patch-Clamp sampling software (pClamp10.7 software) after compensation.
2. Low-pass filter the currents at 5 kHz and digitize at a sampling rate of 5 kHz by Digidata 1440 (Axon Instruments).
3. Superfuse the cells with a Na^+-free extracellular solution as above-mentioned, add $CdCl_2$ to perfusate to block L-type Ca^{2+} current.
4. Record the I_{Ks} currents at room temperature.

Record Step and Tail I_{Ks} Currents

1. Elicit the outwardly rectifying K^+ channel (I_K) currents (*see* **Note 10**) by 4 s depolarization steps from a holding of −80 mV to potentials ranging from −40 to +60 mV in 10 mV increments, followed by a 4 s repolarization phase to −40 mV to elicit the tail current.
2. Record step and tail I_K currents at baseline.
3. To isolate I_{Ks} from I_K, perform either of the following actions:
4. Apply Chromanol 293B (10 μM), a I_{Ks} blocker, to the superfusate to block I_{Ks}. Next, calculate the I_{Ks} currents by subtracting the effect of Chromanol 293B from that of baseline [7, 20]. Figure 4 serves as an example of the I_{Ks} recording.
5. Apply 5 μM E-4031, a blocker of $I_{Kr,}$ to the superfusate to block I_{Kr}. The remaining outward currents are I_{Ks} [25] as they can be completely suppressed by 10 μM Chromanol 293B.

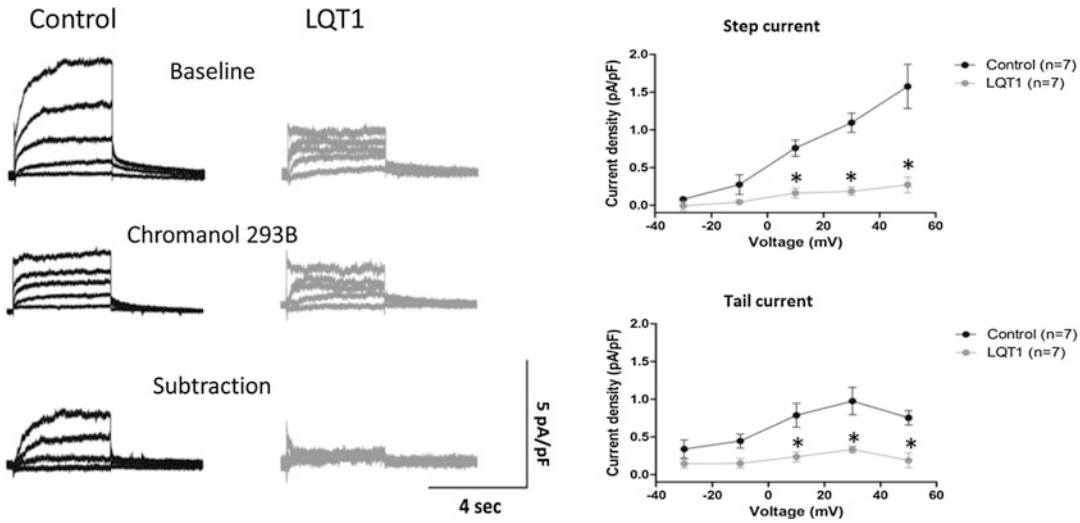

Fig. 4 I_{ks} recorded from control and LQT1 patient hiPSC-CMs. (*Left*) I_{ks} currents are validated as Chromanol 293B-sensitive (after subtraction) I_K currents. (*Right*) The averaged peak and tail current density (pA/pF) in control and patient hiPSC-CMs is presented. Values given are mean ± SEM ($n = 7$ for both patient and control). *$p < 0.05$, vs. control (Reproduced from ref. 20)

6. Calculate the I_{Ks} current density by normalizing the I_{Ks} current (pA) to the cell capacitance (pF) and express the current density as pA/pF.

Determine the Voltage Dependence of Activation

1. Calculate the voltage dependence of activation (evaluated from normalized tail current amplitudes) by fitting with Boltzmann equation, $y = I_{max}/(1 + \exp.((V/_{1/2} - V)/\kappa))$ to determine the membrane potential for half-maximal activation ($V_{1/2}$) and the slope factor (κ).

Measuring the Deactivation of I_{Ks}

1. Hold the cells at −80 mV followed by a depolarized prepulse to +60 mV for 4 s. Elicit the tail currents by various repolarized potential from −120 to −20 mV in 10 mV increments [26].
2. Calculate the time course of deactivation by fitting with a single-exponential function, $y = A \times (1 - \exp.(-t/\tau))$, where A is amplitude and τ is time constant.

Measuring the Inactivation of I_{Ks}

1. Use a triple-pulse protocol. Pulse the cells to a series of test potential from +40 to +100 mV in 10 mV increments before applying a 20 ms interpulse to −130 mV. Return the membrane potential to the test potential to measure the degree of activation [27].
2. Calculate the inactivation: Following the triple-pulse protocol, count the percentage of current reduced over the corresponding current tested in the first pulse [27]. Degree of inactivation of Kv7.1 channels at each potential is indirectly revealed by the hooked tail currents.

3.3.4 Record Action Potentials (APs) by Current-Clamping

Set Up the Current-Clamping [7, 20]

1. Record APs of hiPSC-CMs with pipette and extracellular (Tyrode's) solution above-mentioned.
2. Low-pass filter the electrical signals at 2 kHz and sample the signals at 20 kHz.
3. Maintain cells at 35 °C during the recording by a temperature controller.

Record APs

1. Record APs in spontaneous contracting hiPSC-CMs.
2. Record APs in paced hiPSC-CMs. Intracellularly elicit (evoke), through the patch pipette, at 1 Hz by 1 ms depolarizing current pulse of ~1.5× of the stimulation threshold at a cycle length of 1 s.
   - Analyze the average AP duration (APD) at 90%, 70%, 50%, and 20% of repolarization (APD90, APD70, APD50, and APD20), AP amplitude (APA), maximal upstroke velocity (dV/dt_{max}), resting membrane potential (BMP) or maximal diastolic potential (MDP) and beating frequency [1, 19, 20].

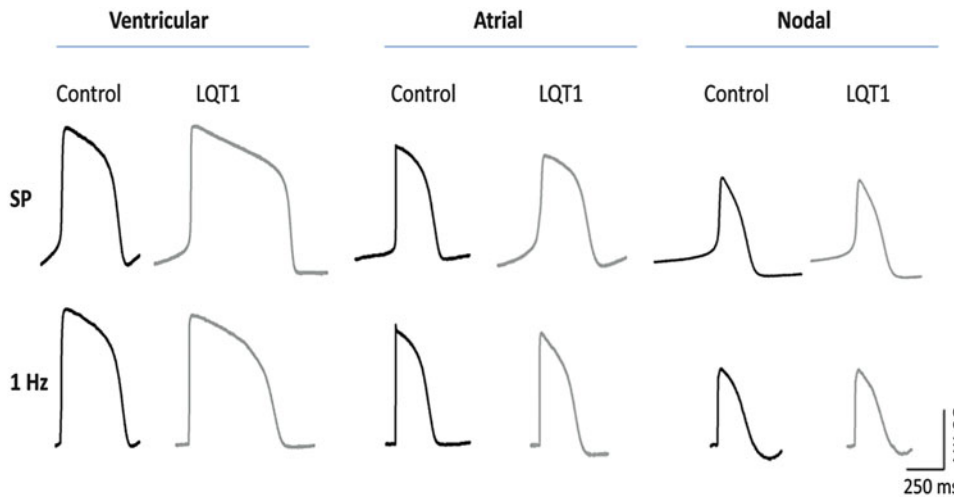

Fig. 5 Action potentials recorded from control and LQT1 patient hiPSC-CMs. Representative traces of spontaneous (SP, *upper panel*) and paced (1 Hz, *bottom panel*) APs recorded from V-like, A-like, and N-like hiPSC-CMs of control and LQT1 patient are presented. Prolonged APDs are observed with the V- and A-like hiPSC-CMs of LQT1 patient (Reproduced from ref. 20)

The APDs of spontaneous APs can be corrected by heart rates following the Fridericia's formula for correcting the QT intervals (APDc = APD/interspike interval$^{1/3}$) [28].

3. Identify the ventricular-like (V), atrial-like (A), and nodal-like (N) subtypes of hiPSC-CMs by their characteristic AP parameters including APA, APD, and dV/dt_{max} [7, 20]. Figure 5 serves as an example of the AP recording.

3.3.5 Determine the Effects of Drugs on I_{Ks} and APs

1. Record baseline I_{Ks} and APs as above mentioned.
2. Apply ML277 [29] or other drugs of interest. *See* **Note 11**.
3. Determine the effects of ML277 or the drugs of interest on I_{Ks} and APs. Figures 6 and 7 show I_{Ks} and APs recorded from hiPSC-CMs responded to ML277 treatment, respectively.

3.3.6 Recording Adult Cardiac Myocyte-Like APs in hiPSC-CMs by the Dynamic Action Potential Clamp (DAPC) Technique

Background: Although hiPSC-CMs share many important similarities with native human cardiac myocytes, a limitation is the lack of the inward rectifier K^+ current (I_{K1}) that leads to a more depolarized MDP (−50 to −65 mV) [30] and spontaneous APs (*see* **Note 12**). In contrast, adult ventricular and atrial myocytes from the heart which have a MDP of ~90 mV are quiescent [30]. A more positive MDP in hiPSC-CMs could alter the AP characteristics of hiPSC-CMs, such as compromising the I_{Na} during phase-0 depolarization [30], and therefore downplays the significance of the hiPSC-CM model. Such a drawback could be fixed by the dynamic action potential clamp (DAPC) technique.

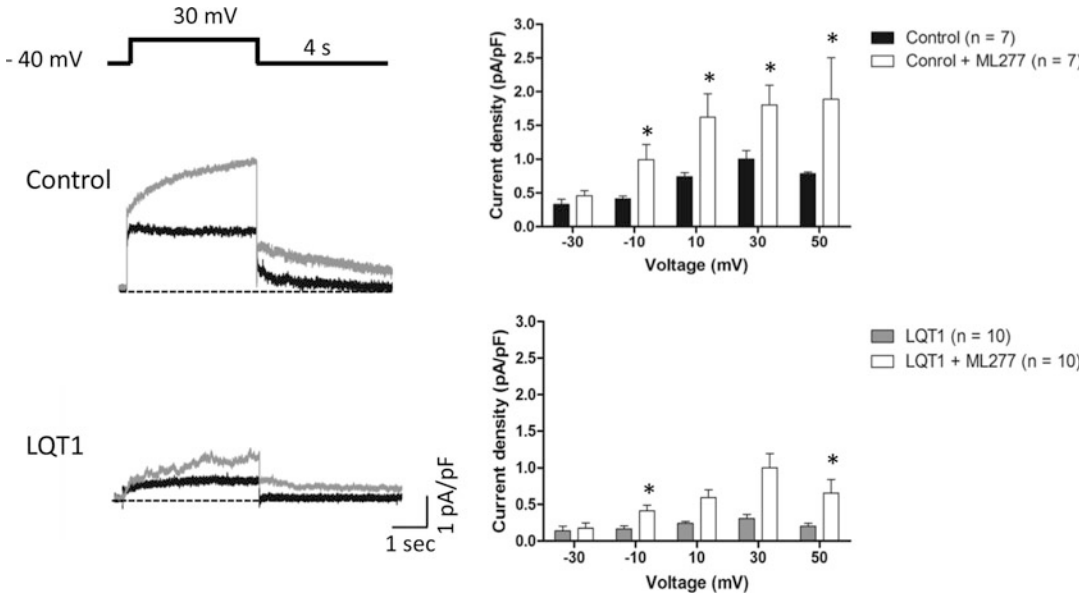

Fig. 6 I_{Ks} recorded from control and LQT1 patient hiPSC-CMs treated with ML277. (*Left*) I_{Ks} recorded from control and patient hiPSC-CMs at baseline (*black lines*) and post ML277 treatment (*gray lines*). (*Right*) Bar-graphs show the averaged tail current density (pA/pF). Values given are mean ± SEM. $*p < 0.05$, vs. untreated baseline. ML277 enhanced the step and tail currents in both control and LQT1 hiPSC-CMs (Reproduced from ref. 20 with modifications)

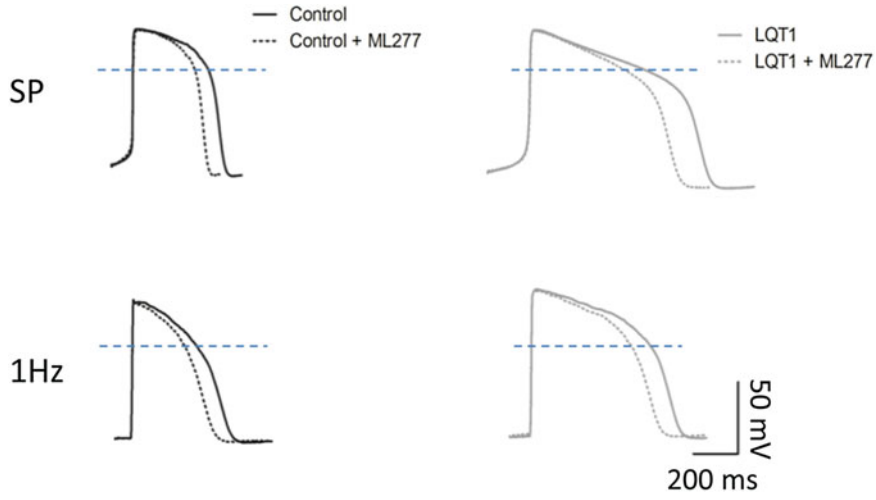

Fig. 7 Action potentials recorded from control and LQT1 patient hiPSC-CMs responded to ML277 treatment. Representative traces of spontaneous (SP, *upper panel*) and paced (1 Hz, *lower panel*) action potentials recorded from control (*left*) and LQT1 patient (*right*) V-like hiPSC-CMs at baseline (*solid lines*) and post ML277 treatment (*dotted lines*) are presented. ML277 reduced the APDs in both control and LQT1 hiPSC-CMs (Reproduced from ref. 20 with modifications)

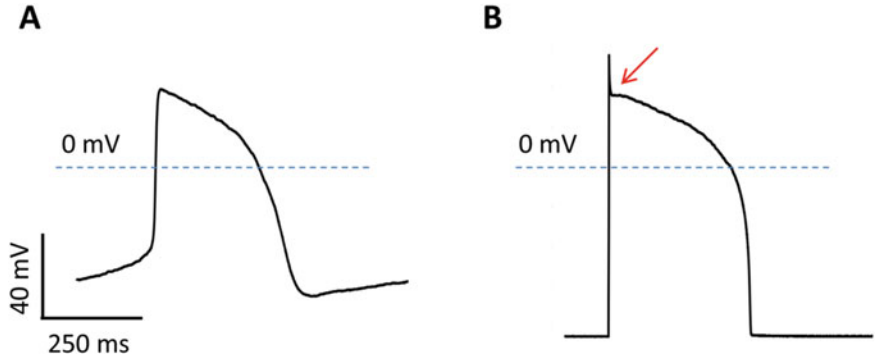

Fig. 8 APs measured without or with the DAPC technique. (**A**) A representative AP waveform recorded from a normal V-like hiPSC-CM without I_{K1} injection. (**B**) The AP waveform recorded from the same cell after I_{K1} injection by the DAPC technique. The *arrow* indicates a phase-1 repolarization. Compared to hiPSC-CMs ($I_{K1}-$), the AP morphology from hiPSC-CMs ($I_{K1}+$) clearly resembles that of the native human ventricular myocytes with markedly increases of dV/dt_{Max} and APA/overshoot

Carry out the DAPC technique as follows.

Configure the DAPC System with Patch-Clamp Amplifier

1. Configure the Cybercyte System with a patch-clamp amplifier (Use Axopatch 200B amplifiers or Axopatch-1D) [30].

Convert hiPSC-CMs ($I_{K1}-$) to hiPSC-CMs ($I_{K1}+$)

1. Inject a real-time voltage dependent in silico I_{K1} (peaked at 150 pA per cell) in hiPSC-CMs to bring the MDP down to ~ −85 mV which is more physiological and is close to that of adult ventricular and atrial myocytes [30].

Record the APs in V-like hiPSC-CMs ($I_{K1}+$)

1. Record APs in V-like hiPSC-CMs ($I_{K1}-$) following the conventional current-clamp protocol. APs are clearly rounded pattern (Fig. 8A).
2. Record APs in the same cell following the DAPC technique [30]. A phase-1 repolarization AP morphology can be recorded (Fig. 8B) and APs recorded from such V-like hiPSC-CMs ($I_{K1}+$) are characterized by increased dV/dt_{Max}, APA and overshoot that resemble normal human ventricular myocytes [30].

3.3.7 Verify the Results from hiPSC-CMs with Simulation Model of Human Ventricular Cardiac Myocytes

Background: As hiPSC-CMs are relatively immature compared with the native myocytes from the adult heart, the findings from hiPSC-CMs may not fully or preciously reflect that of human cardiac myocytes. While it is highly challengeable to obtain human ventricular myocytes from the patients and controls for testing, computer simulation models (*see* **Note 13**), such as the O'Hara–Rudy (ORd) human ventricular cardiac myocytes model [31], could be helpful for validating the results from hiPSC-CMs.

The followings are the brief procedures for using the ORd model:

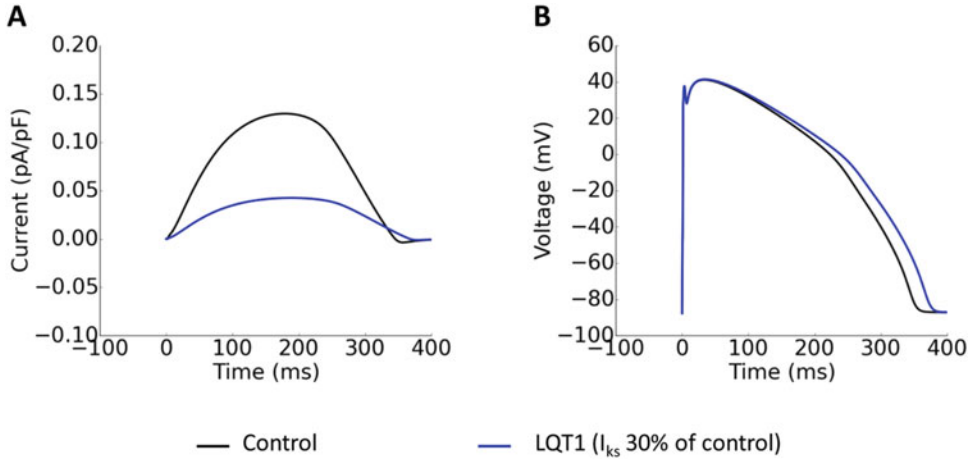

Fig. 9 Simulated APs of human ventricular myocytes. (**A**) Simulated voltage-dependent I_{Ks} in human ventricular myocytes. The I_{ks} of 30% of the control level is denoted as LQT1 (simulating the case of LQT1 in ref. 20). (**B**) Simulated APs in the ventricular myocytes (midmyocardial cells) of control and LQT1. The cycle length is 1 s. Note that the magnitude of APD prolongation is moderate compared with the change in hiPSC-CMs of LQT1

1. Download the Matlab code or C++ code of the ORd original human ventricular model 2011 from the website of Rudy Laboratory (http://rudylab.wustl.edu), Washington University in St. Louis, MO, USA.
2. Run the Matlab source code with Matlab 2013 software. The program automatically generates figures of action potentials and ion currents.
3. Alternatively, compile the c++ source code and run the compiled program to generate the result. Software like Origin or Python can be used to generate data for plotting.
4. Convert the I_{Ks} value (experimentally recorded from heterologous *KCNQ1* expressing cell lines or hiPSC-CMs) as % of control and integrate it in the ORd model to simulate the corresponding APs.
5. Verify the simulated AP parameters for the hallmark of LQT1 AP characteristics (Fig. 9).
6. Evaluate the effects of I_{Ks} channel openers on APs.

4 Notes

1. The batch-to-batch variations of FBS could be overcome by testing a few batches of FBS and selecting a better one. Using the same batch of FBS throughout the study could help to minimize variations and inconsistency in cell culture.

2. Cautions should be excised while handling β-mercaptoethanol as it is combustible, corrosive, and toxic. Avoid ingestion and direct skin contact.
3. Hanks' Balanced Salt Solution (HBSS) without calcium and magnesium is required for rinsing chelators from the culture before.
4. Dulbecco's phosphate-buffered saline (DPBS) is a balanced salt solution used for a variety of cell culture applications. Formulations without calcium and magnesium are required for rinsing chelators from the culture before.
5. Sendai virus-mediated transduction for hiPSC reprogramming represents one of the latest and most preferred strategies for ectopic expression of the transcription factors.
6. Cardiac differentiation of hiPSCs will generate other undesired cell lineages in addition to hiPSC-CMs. Purification and enrichment of hiPSC-CMs are necessary in some cases to facilitate their various applications.
7. Send DNA samples to creditable sequencing facilities for sequencing and consultation. As the derivation of hiPSC-CMs takes multiple procedures associated with risks of mutagenesis and contaminations from other sources of cells, it would be important to sequence the genomic DNA from hiPSC-CMs to confirm the results obtained from genomic DNA of blood cells.
8. Dual immunostaining of cells, in combination with DAPI nuclear staining, is commonly performed to reveal the intracellular localizations of a protein.
9. After differentiation, hiPSC-CMs undergo a period (~4 weeks) of rapid maturation during which the expressions of major ion channels increase rapidly to the levels close to that of native cardiac myocytes.
10. In a ventricular myocyte, the total tail currents of the voltage-gated, outwardly rectifying K^+ channel currents (I_K) consist of I_{Kr} and $I_{Ks,}$ which are sensitive to selective blockers, such as E-4031 and Chromanol 293B, respectively.
11. ML277 is a potent activator/opener of KCNQ1 (Kv7.1) channels and is the first selective and potent activator found, with an EC50 of 260 nM. With >100-fold selectivity versus KCNQ2 and KCNQ4 and no activity against the hERG potassium channel (up to 30 μM), activators of KCNQ1 channels like ML277 could have potential use in treatment of LQT1.
12. Compared with adult ventricular and atrial myocytes that are quiescent and have a maximum diastolic potential (MDP) of ~90 mV, hiPSC-CMs demonstrate a spontaneous firing activity with a more depolarized MDP of −50 to −65 mV, which could

alter the electrophysiology of hiPSC-CMs. For example, a MDP of −60 mV could compromise the I_{Na} activation during phase-0 depolarization. The depolarized MDP with hiPSC-CMs has been associated with the lack of the inward rectifier K^+ current (I_{K1}) in those cells.

13. Simulation models of the electrophysiology of cardiac myocytes have been developed over the years and undergone continuous improvements. Available models range from rodent to canine and human, with more ion channels, ion transporters, and regulators included. The O'Hara–Rudy [31] model represents the latest and more comprehensive models of human ventricular myocytes. Yet, its applicable value on faithfully reproducing the correct pathophysiological situations or drug responses is still being evaluated.

Acknowledgment

This work is supported by National Medical Research Council of Singapore (NMRC CG12Aug09).

References

1. Takahashi K, Tanabe K, Ohnuki M, Narita M, Ichisaka T, Tomoda K et al (2007) Induction of pluripotent stem cells from adult human fibroblasts by defined factors. Cell 131:861–872
2. Yu J, Vodyanik MA, Smuga-Otto K, Antosiewicz-Bourget J, Frane JL, Tian S et al (2007) Induced pluripotent stem cell lines derived from human somatic cells. Science 318:1917–1920
3. Zhang J, Wilson GF, Soerens AG, Koonce CH, Yu J, Palecek SP et al (2009) Functional cardiomyocytes derived from human induced pluripotent stem cells. Circ Res 104:e30–e41
4. Priori SG, Napolitano C, Di Pasquale E, Condorelli G (2013) Induced pluripotent stem cell-derived cardiomyocytes in studies of inherited arrhythmias. J Clin Invest 123:84–91
5. Spoonamore KG, Ware SM (2016) Genetic testing and genetic counseling in patients with sudden death risk due to heritable arrhythmias. Heart Rhythm 13:789–797
6. Roden DM (2008) Clinical practice. Long-QT syndrome. N Engl J Med 358:169–176
7. Moretti A, Bellin M, Welling A, Jung CB, Lam JT, Bott-Flugel L et al (2010) Patient-specific induced pluripotent stem-cell models for long-QT syndrome. N Engl J Med 363:1397–1409
8. Itzhaki I, Maizels L, Huber I, Zwi-Dantsis L, Caspi O, Winterstern A et al (2011) Modelling the long QT syndrome with induced pluripotent stem cells. Nature 471:225–229
9. Yazawa M, Hsueh B, Jia X, Pasca AM, Bernstein JA, Hallmayer J et al (2011) Using induced pluripotent stem cells to investigate cardiac phenotypes in Timothy syndrome. Nature 471:230–234
10. Ma D, Wei H, Zhao Y, Lu J, Li G, Sahib NB et al (2013) Modeling type 3 long QT syndrome with cardiomyocytes derived from patient-specific induced pluripotent stem cells. Int J Cardiol 168:5277–5286
11. Li H, Chen Q, Moss AJ, Robinson J, Goytia V, Perry JC et al (1998) New mutations in the KVLQT1 potassium channel that cause long-QT syndrome. Circulation 97:1264–1269
12. Murray A, Donger C, Fenske C, Spillman I, Richard P, Dong YB et al (1999) Splicing mutations in KCNQ1: a mutation hot spot at codon 344 that produces in frame transcripts. Circulation 100:1077–1084
13. Tsuji-Wakisaka K, Akao M, Ishii TM, Ashihara T, Makiyama T, Ohno S et al (2011) Identification and functional characterization of KCNQ1 mutations around the exon 7-intron 7 junction affecting the splicing process. Biochim Biophys Acta 1812:1452–1459
14. Tsuji K, Akao M, Ishii TM, Ohno S, Makiyama T, Takenaka K et al (2007) Mechanistic basis for

the pathogenesis of long QT syndrome associated with a common splicing mutation in KCNQ1 gene. J Mol Cell Cardiol 42:662–669

15. Loussouarn G, Baró I, Escande D (2006) KCNQ1 K+ channel-mediated cardiac channelopathies. Methods Mol Biol 337:167–183
16. Dessertenne F (1966) Ventricular tachycardia with 2 variable opposing foci. Arch Mal Coeur Vaiss 59:263–272
17. Bohnen MS, Peng G, Robey SH, Terrenoire C, Iyer V, Sampson KJ et al (2017) Molecular pathophysiology of congenital long QT syndrome. Physiol Rev 97:89–134
18. Wilson AJ, Quinn KV, Graves FM, Bitner-Glindzicz M, Tinker A (2005) Abnormal KCNQ1 trafficking influences disease pathogenesis in hereditary long QT syndromes. Cardiovasc Res 67:476–486
19. Matsa E, Burridge PW, Yu KH, Ahrens JH, Termglinchan V, Wu H et al (2016) Transcriptome profiling of patient-specific human iPSC-cardiomyocytes predicts individual drug safety and efficacy responses in vitro. Cell Stem Cell 19:311–325
20. Ma D, Wei H, Lu J, Huang D, Liu Z, Loh LJ et al (2015) Characterization of a novel KCNQ1 mutation for type 1 long QT syndrome and assessment of the therapeutic potential of a novel I_{Ks} activator using patient-specific induced pluripotent stem cell-derived cardiomyocytes. Stem Cell Res Ther 6:39
21. Seki T, Yuasa S, Fukuda K (2012) Generation of induced pluripotent stem cells from a small amount of human peripheral blood using a combination of activated T cells and Sendai virus. Nat Protoc 7:718–728
22. Lian X, Zhang J, Azarin SM, Zhu K, Hazeltine LB, Bao X et al (2013) Directed cardiomyocyte differentiation from human pluripotent stem cells by modulating Wnt/β-catenin signaling under fully defined conditions. Nat Protoc 8:162–175
23. Zhang J, Klos M, Wilson GF, Herman AM, Lian X, Raval KK et al (2012) Extracellular matrix promotes highly efficient cardiac differentiation of human pluripotent stem cells: the matrix sandwich method. Circ Res 111:1125–1136
24. Tohyama S, Hattori F, Sano M, Hishiki T, Nagahata Y, Matsuura T et al (2013) Distinct metabolic flow enables large-scale purification of mouse and human pluripotent stem cell-derived cardiomyocytes. Cell Stem Cell 12:127–137
25. Yu H, Lin Z, Mattmann ME, Zou B, Terrenoire C, Zhang H et al (2013) Dynamic subunit stoichiometry confers a progressive continuum of pharmacological sensitivity by KCNQ potassium channels. Proc Natl Acad Sci U S A 110:8732–8737
26. Spätjens RL, Bébarová M, Seyen SR, Lentink V, Jongbloed RJ, Arens YH et al (2014) Long-QTmutation p.K557E-Kv7.1: dominant-negative suppression of I_{Ks}, but preserved cAMP-dependent up-regulation. Cardiovasc Res 104:216–225
27. Moreno C, Oliveras A, de la Cruz A, Bartolucci C, Muñoz C, Salar E et al (2015) A new KCNQ1 mutation at the S5 segment that impairs its association with KCNE1 is responsible for short QT syndrome. Cardiovasc Res 107:613–623
28. Clements M, Thomas N (2014) High-throughput multi-parameter profiling of electrophysiological drug effects in human embryonic stem cell derived cardiomyocytes using multi-electrode arrays. Toxicol Sci 140:445–461
29. Mattmann ME, Yu H, Lin Z, Xu K, Huang X, Long S et al (2012) Identification of (R)-N-(4-(4-methoxyphenyl)thiazol-2-yl)-1-tosylpiperidine-2-carboxamide, ML277, as a novel, potent and selective K(v)7.1 (KCNQ1) potassium channel activator. Bioorg Med Chem Lett 22:5936–5941
30. Bett GC, Kaplan AD, Lis A, Cimato TR, Tzanakakis ES, Zhou Q et al (2013) Electronic "expression" of the inward rectifier in cardiocytes derived from human-induced pluripotent stem cells. Heart Rhythm 10:1903–1910
31. O'Hara T, Virág L, Varró A, Rudy Y (2011) Simulation of the undiseased human cardiac ventricular action potential: model formulation and experimental validation. PLoS Comput Biol 7:e1002061

Chapter 3

Monitoring Changes in the Abundance of Endogenously Expressed ATP-Sensitive Potassium (K_{ATP}) Channels in the Plasma Membrane Using Surface Biotinylation

Jing-Syuna Ruan and Pei-Chun Chen

Abstract

The conductance of K_{ATP} channel activity can be regulated by gating and/or surface expression. Gating analysis is usually performed by electrophysiological recording. Analysis of surface K_{ATP} channel expression levels requires cell fractionation, protein separation, and quantification. Cell fractionation involves time-consuming high-speed centrifugation steps and skilled techniques for taking out specific layers. Moreover, contamination of intracellular membranes can confound results. Although commercial kits have been developed to make it easier for scientists, qualities of these kits vary which can give rise to variable results. Detection of membrane proteins using surface biotinylation technique consists of labeling cell surface proteins with a biotin reagent before lysing the cells, and isolating these tagged proteins by NeutrAvidin pulldown. Then, the samples are subjected to SDS-PAGE separation, transferred to PVDF membranes, and probed with specific antibodies. Quantification of cell surface expression is accomplished by densitometric measurement of the bands corresponding to the protein of interest and subsequent normalization by a membrane protein (as control). This alternative method for detecting expression of surface protein is relatively easy in steps and more economical in comparison to other methods such as cell fractionation.

Key words ATP-sensitive potassium channels, Immunoblotting, Biotin, NeutraAvidin beads, Glycosylation, INS-1 cell, Glycine

1 Introduction

Plasma membrane (PM) of a cell not only serves as the boundary between extracellular environment and intracellular content, but also carries out distinctive activities via multiple proteins [1]. There is growing evidence that dynamic expression of PM proteins also plays a crucial role in regulation of physiological functions and pathological conditions [2, 3].

ATP-sensitive potassium channels (K_{ATP} channel) play an important role in the regulation of insulin release in pancreatic β-cells. The pancreatic β-cell K_{ATP} channel is an octameric complex containing four pore-forming Kir6.2 subunits and four regulatory

Show-Ling Shyng et al. (eds.), *Potassium Channels: Methods and Protocols,* Methods in Molecular Biology, vol. 1684,
DOI 10.1007/978-1-4939-7362-0_3,

sulfonylurea receptor (SUR1) subunits [4–7]. Regulation of channel activity is mediated by cytosolic nucleotides: when cells are in the state of high glucose, high ATP-to-ADP ratio closes K_{ATP} channels resulting in membrane potential depolarization, opening of voltage-dependent Ca^{2+} channels (VDCC), Ca^{2+} influx, and insulin secretion [4–7]. In addition to gating, previous studies have shown that surface expression of K_{ATP} channels affects electrical activity as well as insulin release in pancreatic β-cells [8–11]. For example, leptin, a peptide produced by adipocytes, stimulates trafficking of K_{ATP} channels from cytosolic vesicles to the plasma membrane of β-cells via a CaMKK/AMPK/PKA pathway. This transient increase of surface K_{ATP} channel expression hyperpolarizes membrane potential and reduces insulin secretion [12, 13].

Biotinylation is the process of attaching biotin to proteins and other macromolecules. Biotinylation reagents are available for targeting specific functional groups or residues and for distinguishing substrates inside or outside cells based on membrane permeability of the reagent. Cleavable or reversible biotinylation reagents enable the specific elution of biotinylated molecules from biotin-binding proteins (e.g., NeutrAvidin). In order to measure endogenous K_{ATP} channel expression at the cell surface, we choose non-membrane permeable EZ-link Sulfo-NHS-SS-biotin to label lysine residues in the extracellular region of SUR1. Kir6.2 subunit lacks extracellular lysine residues; hence, surface SUR1 is the indicator for the expression of K_{ATP} channel in the plasma membrane. SUR1 is a glycoprotein with two N-linked glycosylation sites that are core-glycosylated in the endoplasmic reticulum (ER). As the channel complex travels through the medial Golgi, the glycosylation pattern is further modified to give rise to the complex-glycosylated form, referred to as the "upper band" that migrates slower on the SDS gel than the core-glycosylated "lower band." The appearance of the upper band is therefore diagnostic of SUR1 having exited the ER and reached the medial Golgi; accordingly, only the upper band is detected at the cell surface using rabbit SUR1 antiserum generated with the last 13 amino acids of hamster SUR1 (KDSVFASFVRADK) as the antigen [14–16]. Note this biotinylation reagent has a cleavable disulfide spacer allowing recovery of biotinylated protein from immobilized streptavidin. We have employed this technique to investigate effects of leptin on trafficking of K_{ATP} channels to the cell surface as shown in Fig. 1, [12, 13]. In this chapter, we will detail the protocols regarding this technique and further applications using leptin treatment as an example.

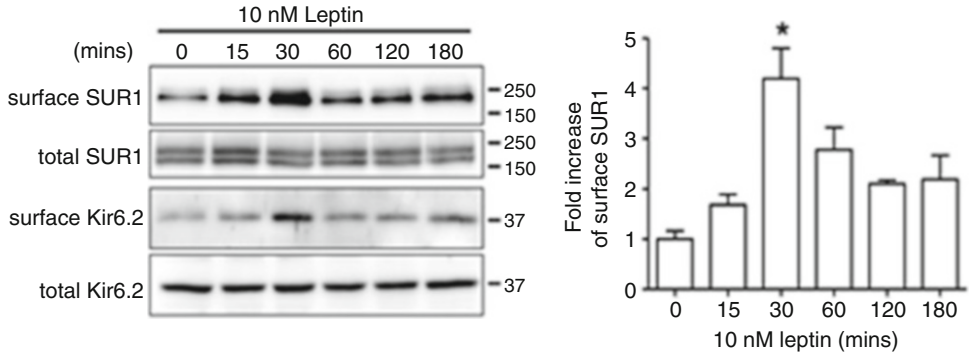

Fig. 1 INS-1 cells were treated with 10 nM leptin for the times indicated and subjected to surface biotinylation. *Left*: Representative western blots showing surface biotinylated SUR1 pulled down with NeutrAvidin beads and total SUR1 in the cell lysate. Note only the upper band corresponding to the complex-glycosylated SUR1 and not the lower band corresponding to the ER-core glycosylated SUR1, was detected at the cell surface. Molecular weight markers in this and subsequent figures are in kDa. *Right*: Bar graph showing the fold increase in surface SUR1 relative to the upper band of total SUR1 and normalized to time zero ($n = 4$, $^*p < 0.05$ by one-way ANOVA and Dunnett's *post-hoc* test) (Reproduced from ref. 12 with permission from authors)

2 Materials

1. Freshly prepare all reagents at 4 °C and place them on ice. We use a single well from a 6-well tissue culture plate to indicate the amounts of reagents we use during this experiment.
2. The rat insulinoma cell INS-1 clone 823/13 [17] (*see* **Note 1**).
3. Culture medium: RPMI 1640 medium with 11.1 mM D-glucose supplemented with 10% fetal bovine serum (FBS), 100 units/ml penicillin, 100 μg/ml streptomycin, 10 mM HEPES, 2 mM glutamine, 1 mM sodium pyruvate, and 50 μM β-mercaptoethanol [18].
4. Serum-free RPMI medium.
5. Dulbecco's phosphate-buffered saline (DPBS) with calcium and magnesium, prechilled on ice or at 4 °C (*see* **Note 2**).
6. Biotin labeling solution (1 mg/ml): Dissolve 6 mg of NHS-Sulfo-SS-biotin in 6 ml DPBS (*see* **Note 3**).
7. 50 mM Glycine solution: dissolve 91 mg of Glycine in 24 ml DPBS.
8. Cell lysis buffer: 20 mM HEPES, 150 mM NaCl, 4 mM EDTA, 1 mM EGTA, 1% Igepal (NP-40), 0.1% SDS, 0.04% Deoxycholic Acid and 1× Protease inhibitors (PIs) (*see* **Note 4**).
9. NeutrAvidin agarose beads: 50% slurry in cell lysis buffer.
10. Elution buffer: 2× Laemmli sample buffer.

11. Mini protein gel casting, electrophoresis, and Western blot system.
12. Western blot transfer buffer (for 1 l): 0.32 g of Na_2CO_3, 0.84 g of $NaHCO_3$, 100 ml methanol, add ddH_2O to 1 l.
13. Tris-buffered-saline with TWEEN 20 (TBST): 50 mM Tris–Cl, 150 mM NaCl, pH 7.5, with 0.1% TWEEN 20.
14. Blocking solution for Western blot: TTBS with 5% (w/v) nonfat dry milk.
15. Anti-SUR1 serum raised in rabbit (*see* Subheading 1 and **Note 5**).
16. Anti-rabbit secondary antibody conjugated to horseradish peroxidase (HRP).
17. Enhanced chemiluminescent substrate (ECL substrate) for the detection of the secondary antibody-conjugated HRP activity (*see* **Note 6**).
18. Gel imaging system for visualizing immunoblots.
19. ImageJ software (available at http://rsb.info.nih.gov/ij) (National Institute of Health, NIH).

3 Methods

3.1 Biotinylation

1. Plate INS-1 cells onto 6-well tissue culture plates and perform the surface biotinylation experiment when cells have reached 80–90% confluency.
2. Replace the culture medium with 2 ml warm serum-free RPMI medium per well and incubate in a 37 °C incubator for 30 min (*see* **Note 7**).
3. Add 2 μl of 10 μM Leptin to each well such that the final concentration of leptin is 10 nM. Incubate further in a 37 °C incubator for 0, 15, 30, 60, 120, or 180 min to follow the time course of the effect of leptin on surface K_{ATP} channel abundance (*see* **Note 8**).
4. Place cells on ice and carry out all subsequent steps in this section at 4 °C or on ice (*see* **Note 9**).
5. Remove leptin and RPMI by suctioning, and wash cells gently four times with ice-cold DPBS (*see* **Note 10**).
6. Add 1 ml per well of ice-cold biotin labeling solution and incubate on ice for 30 min (*see* **Note 11**).
7. Quench unreacted biotin by washing two times with 50 mM glycine solution. For each wash, keep the glycine solution on cells for 5 min.
8. Wash cells with DPBS two times as in **step 5**.

9. Add 250 μl of prechilled cell lysis buffer to each well.
10. Scrape cells from each well of a 6-well plate using a cell scraper, and transfer cell lysate to six chilled 1.5 ml Eppendorf tubes. Place tubes on the rotator and rotate for 20 min at 4 °C.
11. Centrifuge tubes in a microcentrifuge at 15,000 × *g* at 4 °C for 20 min.
12. Transfer the supernatant to a new 1.5 ml Eppendorf tube and discard pellets.
13. Determine protein concentrations using the Lowry assay (*see* **Note 12**).
14. Adjust protein concentrations using cell lysis buffer so that all tubes have the same protein concentration.
15. Transfer the amount of cell lysate to a new tube, which will be used for affinity purification using NeurtrAvidin beads. Save the remainder to set up a separate Western blot as input control for later quantification (*see* **Note 13**).

3.2 Affinity Purification of Biotinylated Proteins Using NeutrAvidin Agarose Beads

1. Take 300 μl (50 μl × 6) of NeutrAvidin agarose beads out of the bottle into a 1.5 ml tube (*see* **Note 14**).
2. Spin down using a table top centrifuge for 30 s.
3. Aspirate out the supernatant and leave the beads pellet.
4. Add 500 μl cell lysis buffer into the tube and vortex lightly.
5. Repeat the wash **steps 2–5** for a total of three times.
6. Add 600 μl cell lysis buffer into the tube after the final wash and mix gently.
7. Add 100 μl of the above washed NeutrAvidin beads to each of the 1.5 ml tubes containing the cell lysate.
8. Place tubes on a rotator and rotate at 4 °C overnight.
9. Wash the NeutrAvidin beads three times with cold cell lysis buffer (500 μl/tube/wash).
10. Elute proteins bound to the beads with 40 μl 2× Laemmli sample buffer for 30 min at room temperature (*see* **Note 15**).

3.3 SDS-PAGE and Western Blotting

1. Cast 7.5% mini-protein gels (*see* **Note 16**).
2. Load 30 μl of eluent from each tube. Be careful not to pipet up any NeutrAvidin beads. On a separate gel, load 30 μl of the original cell lysate sample to be used as input controls.
3. Run gel until the 25 kDa marker reaches the bottom of the gel (35 mA for ~1–2 h).
4. Transfer at 50 mV at 4 °C for 135 min.
5. Block the membrane with blocking solution for 1 h.

6. Dilute primary antibody for SUR1 in a blocking solution (1:500) and incubate the membrane in a primary antibody solution at 4 °C overnight with constant shaking.
7. Wash three times with the TTBS solution, each for 10 min.
8. Incubate with Donkey-anti-rabbit HRP (1:4000) in 5% nonfat dry milk in TTBS for 1 h at room temperature.
9. Wash three times with the TTBS solution, each for 10 min.
10. Develop the blot using the enhanced chemiluminescence substrate and view the signal immediately using a gel imaging system.
11. Quantify signals by dividing the surface SUR1 band intensity (only the complex-glycosylated or "upper" band is observed because this is the mature SUR1 form found at the cell surface) by the upper SUR1 band intensity observed in the input blot (which represents mature SUR1 in the secretory pathway beyond the endoplasmic reticulum in the total cell lysate) using ImageJ (*see* **Note 17**).

4 Notes

1. The rat insulinoma cell INS-1 clone 823/13 is used as a model system here because the cell expresses endogenous K_{ATP} channels and leptin receptors [17].
2. In this procedure, there are many washing steps that may result in loss of cells. DPBS containing calcium and magnesium helps to keep cells attached to the tissue culture plate. This DPBS reduces cell loss during the experiment and maximizes biotinylated protein signals.
3. Biotin labeling solution must be prepared quickly and used fresh as it will precipitate over time. Before preparing the solution, the reagent powder needs to be warmed to room temperature to avoid moisture buildup.
4. We used the cOmplete™, EDTA-free protease inhibitor cocktail tablets from SigmaAldrich. However, other protease inhibitors can also be used.
5. The rabbit antiserum against SUR1 we use is not commercially available. While other commercially available SUR1 antibodies can be used, in our experience they do not work as well.
6. We use ECL to detect protein signals in Western blots; however, other methods of detection such as fluorescently labeled secondary antibodies are also suitable.
7. Preincubation of cells in serum-free medium for 30 min minimizes signaling events through growth factors present in the

serum, which may interfere with the effects of leptin on K_{ATP} channel surface density. At this time, drugs that target-specific molecules in the leptin signaling pathway can be added to study how they impact surface expression of K_{ATP} channels.

8. If testing the effects of drugs that interfere with leptin signaling, these drugs are co-administered with leptin during this incubation period. If testing the effects of compounds that mimic the effect of leptin, substitute leptin with these compounds for the desired durations.
9. It is very important to keep the cells cold to arrest membrane trafficking events such as endocytosis. Membrane endocytosis could allow the membrane-impermeable biotinylation reagent to enter the cell and biotinylating intracellular proteins to confound the results.
10. The washing steps prior to the biotinylation reaction are important as it removes unhealthy or dead cells that may have damaged plasma membranes and can lead to biotinylation of intracellular proteins. When aspirating off culture medium or washing solution, tilt the plate slightly and apply suction on a corner to minimize tearing of the cell layer.
11. Make sure the plate is on a flat surface so that all the cells are well covered by the solution.
12. We use the Bio-Rad DC protein assay kit, which is similar to Lowry assay.
13. We typically use ~500 μg of proteins of each sample for affinity purification. If you do not have enough proteins for affinity purification, it may be necessary to combine two wells (6-well plate) of cells.
14. When taking out the NeutrAvidin beads slurry, use a 1 ml pipette tip and cut the tip so it is easier to pipet. Mix the slurry well before pipetting.
15. Do not boil the sample as SUR1 becomes aggregated at high temperature.
16. A gradient gel (4–20%) also works well and allows simultaneous detection of surface Kir6.2 (~40 kDa) co-purified with the biotinylated SUR1.
17. Treatment with 10 nM of leptin for 30 min in INS-1 cells has been shown to increase endogenous surface K_{ATP} channels by ~2.5-fold as compared to control.

Acknowledgment

This work received financial support from the Ministry of Science and Technology (MOST103-2320-B-006-005-MY2 and MOST105-2628-B-006-006-MY3) to P.C.C.

References

1. Hormann K et al (2016) A surface biotinylation strategy for reproducible plasma membrane protein purification and tracking of genetic and drug-induced alterations. J Proteome Res 15(2):647–658
2. Elia G (2012) Cell surface protein biotinylation for SDS-PAGE analysis. Methods Mol Biol 869:361–372
3. Li A et al (2016) Surface biotinylation of cytotoxic T lymphocytes for in vivo tracking of tumor immunotherapy in murine models. Cancer Immunol Immunother 65(12):1545–1554
4. Clement JP et al (1997) Association and stoichiometry of K(ATP) channel subunits. Neuron 18(5):827–838
5. Inagaki N, Gonoi T, Seino S (1997) Subunit stoichiometry of the pancreatic beta-cell ATP-sensitive K+ channel. FEBS Lett 409 (2):232–236
6. Mikhailov MV et al (2005) 3-D structural and functional characterization of the purified KATP channel complex Kir6.2-SUR1. EMBO J 24(23):4166–4175
7. Shyng S, Nichols CG (1997) Octameric stoichiometry of the KATP channel complex. J Gen Physiol 110(6):655–664
8. Cartier EA et al (2001) Defective trafficking and function of KATP channels caused by a sulfonylurea receptor 1 mutation associated with persistent hyperinsulinemic hypoglycemia of infancy. Proc Natl Acad Sci U S A 98 (5):2882–2887
9. Crane A, Aguilar-Bryan L (2004) Assembly, maturation, and turnover of K(ATP) channel subunits. J Biol Chem 279(10):9080–9090
10. Lin CW et al (2006) Kir6.2 mutations associated with neonatal diabetes reduce expression of ATP-sensitive K+ channels: implications in disease mechanism and sulfonylurea therapy. Diabetes 55(6):1738–1746
11. Yan F et al (2004) Sulfonylureas correct trafficking defects of ATP-sensitive potassium channels caused by mutations in the sulfonylurea receptor. J Biol Chem 279 (12):11096–11105
12. Chen PC, Kryukova YN, Shyng SL (2013) Leptin regulates KATP channel trafficking in pancreatic beta-cells by a signaling mechanism involving AMP-activated protein kinase (AMPK) and cAMP-dependent protein kinase (PKA). J Biol Chem 288(47):34098–34109
13. Wu Y, Shyng SL, Chen PC (2015) Concerted trafficking regulation of Kv2.1 and KATP channels by leptin in pancreatic beta-cells. J Biol Chem 290(50):29676–29690
14. Chen PC et al (2011) Syntaxin 1A regulates surface expression of beta-cell ATP-sensitive potassium channels. Am J Physiol Cell Physiol 300(3):C506–C516
15. Chen PC et al (2013) Carbamazepine as a novel small molecule corrector of trafficking-impaired ATP-sensitive potassium channels identified in congenital hyperinsulinism. J Biol Chem 288(29):20942–20954
16. Yan FF et al (2010) Role of Hsp90 in biogenesis of the beta-cell ATP-sensitive potassium channel complex. Mol Biol Cell 21 (12):1945–1954
17. Hohmeier HE et al (2000) Isolation of INS-1-derived cell lines with robust ATP-sensitive K+ channel-dependent and -independent glucose-stimulated insulin secretion. Diabetes 49 (3):424–430
18. Zhou Q et al (2010) Neonatal diabetes caused by mutations in sulfonylurea receptor 1: interplay between expression and Mg-nucleotide gating defects of ATP-sensitive potassium channels. J Clin Endocrinol Metab 95(12): E473–E478

Chapter 4

Nonsense-Mediated mRNA Decay of hERG Mutations in Long QT Syndrome

Qiuming Gong and Zhengfeng Zhou

Abstract

Long QT syndrome type 2 (LQT2) is caused by mutations in the human ether-à-go-go related gene (hERG), which encodes the Kv11.1 potassium channel in the heart. Over 30% of identified LQT2 mutations are nonsense or frameshift mutations that introduce premature termination codons (PTCs). Contrary to intuition, the predominant consequence of LQT2 nonsense and frameshift mutations is not the production of truncated proteins, but rather the degradation of mutant mRNA by nonsense-mediated mRNA decay (NMD), an RNA surveillance mechanism that selectively eliminates the mRNA transcripts that contain PTCs. In this chapter, we describe methods to study NMD of hERG nonsense and frameshift mutations in long QT syndrome.

Key words Nonsense-mediated mRNA decay, KCNH2, Potassium channel, Long QT syndrome

1 Introduction

The human ether-à-go-go related gene (hERG or KCNH2) encodes the Kv11.1 potassium channel that conducts the rapidly activating delayed rectifier current (I_{Kr}) in the heart [1–4]. I_{Kr} plays an important role in controlling cardiac action potential repolarization. Mutations in hERG cause long QT syndrome type 2 (LQT2) and more than 500 mutations have been identified in patients with LQT2 [5–7]. Over 30% of identified LQT2 mutations are nonsense or frameshift mutations that introduce premature termination codons (PTCs). These PTC mutations are generally assumed to result in truncated dysfunctional channel proteins. However, our recent studies indicate that most LQT2 nonsense and frameshift mutations result in the degradation of PTC-containing hERG mRNAs by nonsense-mediated mRNA decay (NMD) rather than the production of truncated proteins [7–13]. NMD is an evolutionarily conserved mRNA quality control mechanism that detects and eliminates PTC-containing mRNA transcripts [14].

Show-Ling Shyng et al. (eds.), *Potassium Channels: Methods and Protocols*, Methods in Molecular Biology, vol. 1684,
DOI 10.1007/978-1-4939-7362-0_4,

The identification of NMD as a disease-causing mechanism of hERG PTC mutations has important implications in genotype-phenotype correlations in LQT2. NMD eliminates abnormal mRNA transcripts harboring PTCs, thereby preventing the production of truncated proteins that often have dominant-negative effects. Thus, NMD protects against severe disease phenotypes by converting dominant-negative effects to haploinsufficiency [8, 15]. On the other hand, NMD could be detrimental if it prevents the production of truncated proteins that are fully or partially functional. This is exemplified in the LQT2 Q1070X mutation in which the degradation of mutant mRNA by NMD precludes the formation of functional truncated channels, causing profound QT prolongation and severe ventricular arrhythmias in homozygous subjects [9].

Our studies have shown that downstream intron splicing is required for the degradation of hERG transcripts containing PTCs by the NMD pathway [7, 10]. Pre-mRNA splicing results in the deposition of a multi-protein complex, known as the exon-junction-complex (EJC), 20–24 nt upstream of each exon-exon junction [14]. The EJCs are displaced by the ribosome during the pioneer round of translation. If translation terminates at a PTC that is located 50–55 nt upstream of an exon–exon junction, the downstream EJC serves as a binding platform for NMD factors (such as UPF1 and UPF2) that trigger NMD. Many LQT2 nonsense and frameshift mutations have been studied using hERG cDNA constructs under the assumption that PTC mutations would generate truncated hERG channels [16–25]. Because NMD of hERG mRNA transcripts bearing PTCs requires splicing of a downstream intron, the effect of NMD could not be observed in the context of cDNA constructs. Therefore, in studies of hERG nonsense and frameshift mutations it is important to analyze the endogenously expressed hERG mRNA from LQT2 patients or use a splicing-competent hERG construct expressed in mammalian cells.

Here, we describe methods to study NMD of LQT2 nonsense and frameshift mutations identified in patients with long QT syndrome. The first approach for studying NMD of LQT2 nonsense and frameshift mutations is to analyze the endogenously expressed hERG mRNA from LQT2 patients [8]. Because heart tissue from mutation carriers is not usually available, hERG mRNA transcripts isolated from peripheral blood lymphocytes of patients can be analyzed. For allele-specific quantification, hot-stop PCR is used to distinguish between WT and mutant (R1014X) alleles [8, 26, 27]. The WT allele contains a *Taq*I restriction site, which is destroyed by the R1014X mutation. Following hot-stop PCR and digestion of the PCR products with *Taq*I, WT and 1014X alleles can be distinguished and quantified. Genomic DNA from patients

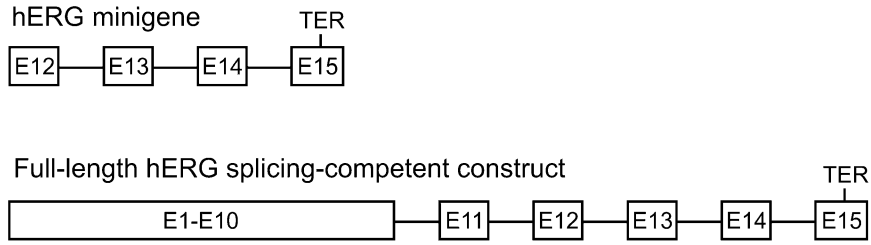

Fig. 1 Diagram of the hERG minigene and the full-length hERG splicing-competent structure. The position of normal termination codon (TER) is indicated

can be used as a control for WT and R1014X alleles. One limitation of the hot-stop PCR method is the requirement of disruption or creation of a unique restriction site by the disease-causing mutation. Thus, the hot-stop PCR approach can only be used in a small number of LQT2 mutations.

The second approach for studying NMD of LQT2 nonsense and frameshift mutations is to use the hERG minigene or the full-length hERG splicing-competent construct. The hERG minigene contains the hERG genomic sequence spanning from exon 12 to exon 15 (Fig. 1) [8]. The full-length hERG splicing-competent construct is composed of hERG cDNA exons 1–10 and hERG genomic DNA from intron 10 to the poly(A) site (Fig. 1) [7]. The hERG minigene and the full-length hERG splicing-competent construct are stably transfected into HEK293 cells and expressed mRNAs are analyzed by RNase protection assay (RPA). The hERG channel protein can be analyzed by immunoblot in the context of the full-length hERG splicing-competent construct. The reduction of mutant mRNAs and proteins has been shown in several LQT2 nonsense and frameshift mutations [7–13]. To test the role of NMD in the reduction of LQT2 mutant mRNA expression, we use a translation inhibitor cycloheximide or the RNA interference method to knock down UPF1, which is a key protein in the core machinery of NMD. Inhibition of protein synthesis by cycloheximide or knockdown of UPF1 by RNA interference results in the restoration of the mutant mRNA, suggesting that the mutant mRNA is degraded by NMD [7–13]. Using these approaches we have defined the positional requirements for the susceptibility of LQT2 mutations to NMD and suggested that the majority of reported LQT2 nonsense and frameshift mutations are potential targets of NMD [7]. Given that nonsense and frameshift mutations account for more than 30% of reported LQT2 mutations, the degradation of mutant mRNA by NMD is an important disease-causing mechanism in the pathogenesis of LQT2.

2 Materials

2.1 Isolations of RNA and Genomic DNA from Lymphocytes

1. Blood collection tubes containing anticoagulant.
2. RiboPure-Blood Kit for RNA Stabilization and Isolation from Whole Blood (Ambion).
3. RNAlater solution (Ambion).
4. Gentra Puregene Blood Core Kit (Qiagen).

2.2 Hot-Stop-PCR Analysis of RNA and Genomic DNA

1. SuperScript III First-Strand Synthesis System for RT-PCR (Life Technologies).
2. Forward primer in exon 13 (E13-F: 5′-GCCTTCTCAGGA GTGTCCAA-3′), reverse primer in exon 14 (E14-R: 5′-GAAAGCGAGTCCAAGGTGAG-3′) and reverse primer in intron 13 (I13-R, 5′-CTCCGCGCTAGAGGTGTG-3′).
3. Advantage 2 PCR Kit (TaKaRa).
4. Radioisotope [^{32}P]-dCTP at a specific activity of 3000 Ci/mmol.
5. *Taq*I restriction enzyme.
6. 40% Acrylamide gel (acryl:bis-acryl = 19:1).
7. 10× TBE (0.9 M Tris Base, 0.9 M Boric Acid and 20 mM EDTA).

2.3 Cell Line, Culture Medium, and Transfection

1. Flp-in 293 cells (Life Technologies). The Flp-In HEK293 cells contain the FRT site at a single genomic locus, allowing stable integration and expression of a single copy of the hERG constructs via Flp recombinase-mediated DNA recombination at a specific genomic location in all cell clones.
2. Flp recombinase expression vector pOG44 (Life Technologies).
3. The hERG minigene spanning exons 12–15 and the full-length hERG splicing-competent construct composed of hERG cDNA exons 1–10 and hERG genomic DNA from intron 10 to poly(A) site are used (Fig. 1) [7, 8]. Both the hERG minigene and the full-length hERG splicing-competent construct are in pcDNA5/FRT vector (Life Technologies).
4. LQT2 mutations in the hERG minigene and the full-length hERG splicing-competent construct are generated using the pAlter in vitro site-directed mutagenesis system (Promega).
5. Culture medium: Dulbecco's Modified Eagle Medium (DMEM) supplemented with 10% fetal bovine serum, 100 units/ml penicillin, and 100 μg/ml streptomycin.
6. Effectene Transfection Reagent (Qiagen).
7. Hygromycin.
8. Cycloheximide.

2.4 RNA Interference

1. Two plasmids, pSUPERpuro-hUPF1/I and pSUPERpuro-hUPF1/II (obtained from Dr. Oliver Mühlemann) [28], are used to inhibit expression of UPF1. These plasmids contain short hairpin RNAs targeting two sequences of human UPF1 (5′-GAGAATCGCCTACTTCACT-3′ for pSUPERpuro-hUPF1/I and 5′-GATGCAGTTCCGCTCCATT-3′ for pSUPERpuro-hUPF1/II). A plasmid, pSUPERpuro with a scrambled sequence of hUPF1/I, is used as a control.
2. LipofectAmine 2000 (Invitrogen).
3. Puromycin.

2.5 RNA Extraction

1. RNeasy Mini Kit from Qiagen.
2. RLN solution: 50 mM Tris–HCl, pH 8.0, 140 mM NaCl, 1.5 mM $MgCl_2$, 0.5% (v/v) Noidet P-40. Just before use, add 1 mM DTT and precool to 4 °C.

2.6 RNase Protection Assay

1. pCRII vector (Life Technologies).
2. pGEM vector (Promega).
3. Dual Promoter TA Cloning Kit (Life Technologies).
4. MAXIscriptIII in vitro Transcription Kit from Ambion for labeling probes.
5. Biotin-14-CTP.
6. RPA III Ribonuclease Protection Assay Kit from Ambion.
7. 40% Acrylamide gel (acryl:bis-acryl = 19:1).
8. Urea.
9. 10× TBE (0.9 M Tris Base, 0.9 M Boric Acid and 20 mM EDTA).
10. Positively Charged Nylon membrane.
11. UV crosslinker.
12. BrightStar BioDetect Kit from Ambion for the detection of biotin-labeled probes.

2.7 SDS-Polyacrylamide Gel Electrophoresis and Western Blot

1. Bio-Rad Mini-Protein Electrophoresis system.
2. Bio-Rad Mini-Protein Transfer unit.
3. Cell lysis buffer: 50 mM Tris–HCl, pH 7.4, 150 mM NaCl, 10 mM EDTA and 1% Triton x 100 (v/v) with proteinase inhibitor cocktail (Roche).
4. Bio-Rad DC Protein Assay Kit.
5. 40% Acrylamide (acryl:bis-acryl =29:1).
6. 4× running gel buffer: 1.5 M Tris–HCl, pH 8.8, 0.4% SDS.
7. 4× stacking gel buffer: 1 M Tris–HCl, pH 6.8, 0.4% SDS.
8. *N*,*N*,*N*′,*N*′-Tetramethylethylenediamine (TEMED).

9. 10% (w/v) ammonium persulfate.
10. 10× Tris-glycine electrophoresis buffer: 0.25 M Tris Base, 1.92 M glycine, 1% (w/v) SDS.
11. 6× loading buffer: 375 mM Tris–HCl pH 6.8, 10% SDS, 30% glycerol, 9% 2-Mercaptoethanol, and 0.03% bromophenol blue.
12. Prestained protein size marker.
13. Transfer buffer: 20 mM Tris Base, 192 mM glycine and 10% methanol.
14. PBS-T buffer: PBS containing 0.2% Tween 20.
15. Blocking buffer: 5% nonfat dry milk in PBS-T.
16. Antibodies: Anti-hERG (H175, Santa Cruz), Anti-UPF1 (obtained from Dr. Jens Lykke-Andersen) [29], Anti-hygromycin B phosphotransferase (HPT) [30] and horseradish peroxidase (HRP)-conjugated anti-rabbit IgG.
17. ECL reagent.

3 Methods

3.1 Isolation of Genomic DNA from Lymphocytes

1. Collect 5–10 ml blood samples in tubes containing anticoagulant.
2. Continue genomic DNA isolation by following the instructions of the Gentra Puregene Blood Core Kit provided by the manufacturer.
3. Measure DNA concentration by a NanoDrop UV spectrophotometer.

3.2 Isolation of RNA from Lymphocytes and Reverse Transcription (RT)

1. Collect 5–10 ml blood samples in tubes containing anticoagulant.
2. Centrifuge at 2000 × *g* for 15 min at room temperature to separate plasma, red blood cells, and white blood cells.
3. Use a disposable transfer pipette to remove the upper layer plasma to expose a thin layer of white blood cells, and then carefully transfer the white blood cells in a volume of about 0.5 ml or less into a 2 ml tube containing RNAlater solution.
4. Continue RNA isolation by following the instructions of the RiboPure-Blood Kit provided by the manufacturer.
5. Measure RNA concentration by a NanoDrop UV spectrophotometer.
6. Use 4 μg RNA for the RT reaction with Random hexamers following the instructions of the SuperScript III First-Strand Synthesis System for RT-PCR provided by the manufacturer.

3.3 Allele-Specific Quantification of RNA and Genomic DNA by Hot Stop PCR

1. Use 4 μl of the RT reaction or about 200 ng of genomic DNA to perform PCR in a final volume of 50 μl according to the instructions of the Advantage 2 PCR Kit provided by the manufacturer using primers E13-F and E14-R for RT-PCR and primers E13-F and I13-R for genomic DNA PCR.
2. Amplify as follows: incubate at 94 °C for 5 min followed by 35 cycles of 30 s at 94 °C, 30 s at 58 °C and 30 s at 72 °C, and a final incubation of 7 min at 72 °C.
3. Mix 15 μl of PCR product from above with 10 μl of labeling mixture containing 1 μl of 10× PCR buffer, 0.2 μl of 10 μM of E13-F forward primer, 0.2 μl of 10 μM of E14-R or I13-R reverse primer, 0.2 μl of 10 mM dNTP, 0.3 μl of [^{32}P]-dCTP, 0.1 μl of *Taq* DNA polymerase and 8 μl of nuclease-free water.
4. Run a single cycle of PCR as follows: incubate at 94 °C for 5 min, 58 °C for 30 s, and 72 °C for 7 min (*see* **Note 1**).
5. Digest 25 μl of [^{32}P] labeled PCR product with *Taq*I for RT-PCR or genomic DNA PCR in a total volume of 50 μl (*see* **Note 2**).
6. Analyze the digested PCR products by 5% polyacrylamide gel electrophoresis in 1× TBE buffer and autoradiography on x-ray film.

3.4 Cell Cultures, Transfection, and Treatment with Cycloheximide

1. In order to study NMD of LQT2 PTC mutations, the hERG minigene and the full-length hERG splicing-competent construct are stably transfected into Flp-in 293 cells that contain a single FRT genomic locus, allowing the integration of a single copy of hERG minigene or the full-length hERG splicing-competent construct.
2. Flp-in 293 cells are grown in culture medium. When approaching ~80–90% confluency, cells are passed with 0.25% Trypsin.
3. To establish stable transfected cell lines, cells are seeded in a 60 mm dish one day prior to transfection. Transfection is performed at ~60% confluency using Effectene Transfection Reagent with the hERG minigene or the full-length hERG splicing-competent construct (0.1 μg) and the Flp recombinase expression vector pOG44 (0.9 μg). After two days of transfection, the cells are split into two 100 mm culture dishes and culture medium is replaced with hygromycin B containing medium at 100 μg/ml. The medium is changed every three days until foci can be identified and 5–20 hygromycin B-resistant foci are picked for expansion (*see* **Note 3**).
4. For inhibition of NMD by protein synthesis inhibitor cycloheximide, cells stably expressing the hERG minigene or the full-length hERG splicing-competent construct are treated with cycloheximide (100 μg/ml) for three hours before RNA isolation.
5. For RNA extraction and Western blot analysis experiments, the 2–3 × 10^5 cells are seeded in 60 mm culture dishes.

3.5 RNA Interference of hUPF1

1. For RNA interference experiments, cells stably expressing the hERG minigene or the full-length hERG splicing-competent construct are seeded in a 100 mm dish one day prior to transfection. Transfection is performed at ~60% confluency using LipofectAmine 2000 (Invitrogen) with a mixture of 1 μg pSUPERpuro-hUPF1/I and 1 μg pSUPERpuro-hUPF1/II, or 2 μg pSUPERpuro with a scrambled sequence of hUPF1/I as a control.
2. At 24 h post-transfection, add puromycin in cell culture at the final concentration of 1.5 μg/ml for 48 h to eliminate the untransfected cells. Before analysis, culture the cells without puromycin for 24 h to avoid the potential effects of puromycin on NMD.
3. Analyze the knockdown of the UPF1 protein by Western blot.

3.6 RNA Extraction from HEK293 Cells

1. Completely aspirate cell-culture medium.
2. Add 175 μl of ice-cold RLN solution directly to the cell culture dish.
3. Detach cells gently using a rubber policeman, and transfer to a microcentrifuge tube. Incubate on ice for 5 min.
4. Centrifuge lysate at 4 °C for 2 min at 300 × *g*. Transfer the supernatant to a new tube and discard the pellet.
5. Add 600 μl Buffer RLT to the supernatant and mix.
6. Add 430 μl 100% ethanol to the lysate.
7. Continue the RNA isolation following the instructions of the RNeasy Mini Kit provided by the manufacturer (*see* **Note 4**).
8. Measure the RNA concentration using a NanoDrop UV spectrophotometer.

3.7 RNase Protection Assay

1. The RNA probe spanning the region of hERG exons 13 and 14 is amplified by PCR and cloned into the pCRII vector using the Dual Promoter TA cloning Kit. The RNA probe for the hygromycin B resistance gene is amplified by PCR and cloned into the pGEM vector.
2. The pCRII vector containing the hERG probe and the pGEM vector containing the hygromycin B resistance gene probe are linearized by restriction enzymes *Xba*I and *Hind*III, respectively, and then used as the templates for antisense probe synthesis (*see* **Note 5**).
3. The antisense probes are transcribed and labeled nonisotopically with SP6 RNA polymerase for the hERG probe or T7 RNA polymerase for the hygromycin B resistance gene probe in the presence of biotin-CTP using the MAXIscriptIII in vitro Transcription Kit. The total length of the probe for hERG is 408 nt, containing 278 nt of hERG sequence and 130 nt from

the pCRII vector at both the ends. The probe for the hygromycin B resistance gene is 228 nt, containing 158 nt of the gene and 70 nt from the pGEM vector (*see* **Note 6**).

4. Following the instructions of the RPA III Ribonuclease Protection Assay Kit, 20 μg RNA is precipitated by adding 1/10 volume of 5 M NH_4OAc and 2.5 volume of 100% ethanol, and incubated on ice for 30 min (*see* **Note 7**).
5. The RNA is pelleted by centrifuging at 10,000 × *g* for 20 min at 4 °C, and washed with 70% ethanol. Let pellet air dry for 5 min.
6. Add 600 pg of probe to the pellets, and resuspend the pellets in 10 μl of Hybridization buffer III (*see* **Note 8**).
7. Heat samples to 90–95 °C for 3 min to denature the RNA.
8. Incubate tubes at 42 °C overnight for hybridization.
9. Add 150 μl of 1:200 diluted RNase solution and incubate for 30 min at 37 °C.
10. Add 225 μl of RNase inactivation solution and incubate for 15 min at −20 °C.
11. Centrifuge for 15 min in a microcentrifuge at maximum speed to pellet the precipitated products.
12. Remove all supernatant and wash the pellets with 70% ethanol.
13. Resuspend the pellets in 8 μl of loading buffer and incubate 3 min at 95 °C to denature the RNA.
14. Continue to follow the manufacturer's instructions to prepare a 5% acrylamide and 8 M urea gel with 40% Acrylamide (acryl: bis-acryl = 19:1) and 10× TBE buffer using the Bio-Rad Mini-Protein Electrophoresis system.
15. Load samples on the gel and run the gel in 1 x TBE buffer.
16. Transfer the gel to a positively charged nylon membrane by electroblotting using the Bio-Rad Mini-Protein transfer unit, and UV crosslink nucleic acids to the membrane.
17. Detect the biotin labeled probe by following the instructions of the BrightStar BioDetect Kit (Ambion).

3.8 SDS-Polyacrylamide Gel Electrophoresis and Western Blot

1. Wash cells with PBS.
2. Add 100–200 μl of ice-cold lysis buffer.
3. Scrape cells and transfer to a microcentrifuge tube.
4. Incubate on ice for 30 min.
5. Centrifuge at 10,000 × *g* for 20 min at 4 °C.
6. Collect the supernatant and measure the protein concentration with the Bio-Rad DC Protein assay kit.

7. Prepare 7.5% separation gel and 4% stacking gel with 4× running gel buffer and 4× stacking gel buffer, respectively, and 40% Acrylamide (acryl:bis-acry = 29:1), using the Bio-Rad Mini-Protein Electrophoresis system.
8. Prepare the cell lysates containing 30–50 μg protein by adding 6× loading buffer.
9. Denature the cell lysates for 5 min at 85 °C.
10. Load the samples on the gel and load a well with a prestained protein size marker.
11. Run the gel at 30 mA (two gels at 60 mA) in 1× Tris-glycine electrophoresis buffer.
12. Prepare the PVDF membrane by wetting it in 100% methanol for 5 s, transferring into distilled H_2O for 2 min, and then equilibrating in transfer buffer for 5 min.
13. Set up "transfer sandwich" by following the Bio-Rad Mini Transfer instructions.
14. Insert the sandwich into the transfer tank.
15. Run at 100 V for 1 h in transfer buffer.
16. Incubate the membrane blot in blocking buffer for 1 h at room temperature.
17. Incubate with primary antibody (Anti-hERG, H175, Anti-UPF1, or Anti-HPT) in blocking buffer overnight at 4 °C (*see* **Note 9**).
18. Wash the membrane four times, 10 min each time at room temperature with PBS-T buffer.
19. Incubate the blot with secondary antibody (HRP-anti-rabbit-IgG) in blocking buffer for 1 h at room temperature.
20. Wash the membrane four times, 10 min each time at room temperature with PBS-T buffer.
21. Prepare the ECL reagent following the manufacturer's instructions.
22. Expose the membrane to a chemiluninescence detection film.

4 Notes

1. In hot-stop PCR, a single cycle of PCR is performed in the presence of [^{32}P]-dCTP. This ensures that only homoduplexes incorporate ^{32}P-labels, and any heteroduplexes formed during previous cycles are unlabeled. Thus, hot-stop PCR prevents detection of WT/mutant heteroduplexes, which are resistant to restriction enzyme digestion.
2. *Taq*I is specific for the analysis of the R1014X mutation. It digests the WT allele, but not the mutant allele. For other

mutations, a unique restriction enzyme that can distinguish between the WT and mutant alleles should be used.

3. Transfection condition can be optimized to achieve the highest efficiency and lowest toxicity by adjusting the cell density and varying the amount or ratio of transfection reagent and DNAs.
4. We recommend isolating cytoplasmic RNA with the RNeasy Mini Kit.
5. The orientation of the probes in the pCRII and pGEM vectors needs to be checked by sequencing to ensure that antisense probes are synthesized.
6. Since the prematurely terminated transcription products in probes may cause background bands in RPA, we recommend performing denaturing polyacrylamide gel electrophoresis to purify the full-length probe.
7. The signal-to-noise ratio in the RPA should be optimized by varying the dilution of RNase, and the amounts of probe and RNA used. For the quantitative detection of mRNA, it is essential that the probe is present in molar excess over the target mRNA. Yeast RNA is used as a control for the complete digestion of the probes by RNase.
8. The hERG probe and the control hygromycin B probe can be added to the same RNA sample for hybridization. The hERG probe protects a 278 nt fragment and the control hygromycin B probe protects a 158 nt fragment. The relative abundance of the mRNA levels of wild-type and LQT2 mutants can be quantified using Scion Image or ImageJ software.
9. Different dilutions of antibodies can be tested for optimal condition. Incubation of primary antibody in Western blot can also be done for 1.5 h at room temperature. Because the H-175 anti-hERG antibody recognizes an epitope in the N-terminus of hERG protein, detection of full-length and C-terminally truncated hERG proteins can be ensured. The relative protein levels of wild-type and LQT2 mutants can be quantified using Scion Image or ImageJ software.

Acknowledgments

This work was supported in part by NIH grant HL68854.

References

1. Warmke JW, Ganetzky B (1994) A family of potassium channel genes related to eag in Drosophila and mammals. Proc Natl Acad Sci U S A 91:3438–3442
2. Sanguinetti MC, Jiang C, Curran ME, Keating MT (1995) A mechanistic link between an inherited and an acquired cardiac arrhythmia: HERG encodes the IKr potassium channel. Cell 81:299–307

3. Trudeau MC, Warmke JW, Ganetzky B, Robertson GA (1995) HERG, a human inward rectifier in the voltage-gated potassium channel family. Science 269:92–95
4. Zhou Z, Gong Q, Ye B, Fan Z, Makielski JC, Robertson GA, January CT (1998) Properties of HERG channels stably expressed in HEK 293 cells studied at physiological temperature. Biophys J 74:230–241
5. Curran ME, Splawski I, Timothy KW, Vincent GM, Green ED, Keating MT (1995) A molecular basis for cardiac arrhythmia: HERG mutations cause long QT syndrome. Cell 80:795–803
6. Splawski I, Shen J, Timothy KW, Lehmann MH, Priori S, Robinson JL, Moss AJ, Schwartz PJ, Towbin JA, Vincent GM, Keating MT (2000) Spectrum of mutations in long-QT syndrome genes. KVLQT1, HERG, SCN5A, KCNE1, and KCNE2. Circulation 102:1178–1185
7. Gong Q, Stump MR, Zhou Z (2014) Position of premature temination codons determines susceptibility of hERG mutations to nonsense mediated mRNA decay in long QT syndrome. Gene 529:190–197
8. Gong Q, Zhang L, Vincent GM, Horne BD, Zhou Z (2007) Nonsense mutations in hERG cause a decrease in mutant mRNA transcripts by nonsense-mediated mRNA decay in human long-QT syndrome. Circulation 116:17–24
9. Bhuiyan ZA, Momenah TS, Gong Q, Amin AS, Ghamdi SA, Carvalho JS, Homfray T, Mannens MM, Zhou Z, Wilde AA (2008) Recurrent intrauterine fetal loss due to near absence of HERG: clinical and functional characterization of a homozygous nonsense HERG Q1070X mutation. Heart Rhythm 5:553–561
10. Gong Q, Stump MR, Zhou Z (2011) Inhibition of nonsense-mediated mRNA decay by antisense morpholino oligonucleotides restores functional expression of hERG nonsense and frameshift mutations in long-QT syndrome. J Mol Cell Cardiol 50:223–229
11. Zarraga IG, Zhang L, Stump MR, Gong Q, Vincent GM, Zhou Z (2011) Nonsense-mediated mRNA decay caused by a frameshift mutation in a large kindred of type 2 long QT syndrome. Heart Rhythm 8:1200–1206
12. Stump MR, Gong Q, Packer JD, Zhou Z (2012) Early LQT2 nonsense mutation generates N-terminally truncated hERG channels with altered gating properties by the reinitiation of translation. J Mol Cell Cardiol 53:725–733
13. Stump MR, Gong Q, Zhou Z (2013) LQT2 nonsense mutations generate trafficking defective NH2-terminally truncated channels by the reinitiation of translation. Am J Physiol Heart Circ Physiol 305:H1397–H1404
14. Kuzmiak HA, Maquat LE (2006) Applying nonsense-mediated mRNA decay research to the clinic: progress and challenges. Trends Mol Med 12:306–316
15. Khajavi M, Inoue K, Lupski JR (2006) Nonsense-mediated mRNA decay modulates clinical outcome of genetic disease. Eur J Hum Genet 14:1074–1081
16. Li X, Xu J, Li M (1997) The human delta1261 mutation of the HERG potassium channel results in a truncated protein that contains a subunit interaction domain and decreases the channel expression. J Biol Chem 272:705–708
17. Paulussen A, Yang P, Pangalos M, Verhasselt P, Marrannes R, Verfaille C, Vandenberk I, Crabbe R, Konings F, Luyten W, Armstrong M (2000) Analysis of the human KCNH2 (HERG) gene: identification and characterization of a novel mutation Y667X associated with long QT syndrome and a non-pathological 9 bp insertion. Hum Mut 15:483
18. Kupershmidt S, Yang T, Chanthaphaychith S, Wang Z, Towbin JA, Roden DM (2002) Defective human Ether-a-go-go-related gene trafficking linked to an endoplasmic reticulum retention signal in the C terminus. J Biol Chem 277:27442–27448
19. Gong Q, Keeney DR, Robinson JC, Zhou Z (2004) Defective assembly and trafficking of mutant HERG channels with C-terminal truncations in long QT syndrome. J Mol Cell Cardiol 37:1225–1233
20. Teng S, Ma L, Dong Y, Lin C, Ye J, Bahring R, Vardanyan V, Yang Y, Lin Z, Pongs O, Hui R (2005) Clinical and electrophysiological characterization of a novel mutation R863X in HERG C-terminus associated with long QT syndrome. J Mol Med 82:189–196
21. Paulussen AD, Raes A, Jongbloed RJ, Gilissen RA, Wilde AA, Snyders DJ, Smeets HJ, Aerssens J (2005) HERG mutation predicts short QT based on channel kinetics but causes long QT by heterotetrameric trafficking deficiency. Cardiovasc Res 67:467–475
22. Choe CU, Schulze-Bahr E, Neu A, Xu J, Zhu ZI, Sauter K, Bahring R, Priori S, Guicheney P, Monnig G, Neapolitano C, Heidemann J, Clancy CE, Pongs O, Isbrandt D (2006) C-terminal HERG (LQT2) mutations disrupt IKr channel regulation through 14-3-3ε. Hum Mol Genet 15:2888–2902
23. Christé G, Thériault O, Chahine M, Millat G, Rodriguez-Lafrasse C, Rousson R, Deschênes I, Ficker E, Chevalier P (2008) A new C-

terminal hERG mutation A915fs+47X associated with symptomatic LQT2 and auditory-trigger syncope. Heart Rhythm 5:1577–1586

24. Nof E, Cordeiro JM, Pérez GJ, Scornik FS, Calloe K, Love B, Burashnikov E, Caceres G, Gunsburg M, Antzelevitch C (2010) A common single nucleotide polymorphism can exacerbate long-QT type 2 syndrome leading to sudden infant death. Circ Cardiovasc Genet 3:199–206
25. Trudeau MC, Leung LM, Roti ER, Robertson GA (2011) hERG1a N-terminal eag domain-containing polypeptides regulate homomeric hERG1b and heteromeric hERG1a/hERG1b channels: a possible mechanism for long QT syndrome. J Gen Physiol 138:581–592
26. Uejima H, Lee MP, Cui H, Feinberg AP (2000) Hot-stop PCR: a simple and general assay for linear quantitation of allele ratios. Nat Genet 25:375–376
27. Kurreeman FA, Schonkeren JJ, Heijmans BT, Toes RE, Huizinga TW (2004) Transcription of the IL10 gene reveals allele-specific regulation at the mRNA level. Hum Mol Genet 13:1755–1762
28. Paillusson A, Hirschi N, Vallan C, Azzalin CM, Muhlemann O (2005) A GFP-based reporter system to monitor nonsense-mediated mRNA decay. Nucleic Acids Res 33:e54
29. Lykke-Andersen J, Shu MD, Steitz JA (2000) Human Upf proteins target an mRNA for nonsense-mediated decay when bound downstream of a termination codon. Cell 103:1121–1131
30. Gong Q, Stump MR, Dunn AR, Deng V, Zhou Z (2010) Alternative splicing and polyadenylation contribute to the generation of hERG1 C-terminal isoforms. J Biol Chem 285:32233–32241

Chapter 5

Probing Subunits Interactions in K_{ATP} Channels Using Photo-Crosslinking via Genetically Encoded *p*-Azido-L-phenylalanine

Prasanna Devaraneni, Emily A. Rex, and Show-Ling Shyng

Abstract

Potassium channels are multimeric protein complexes regulated by diverse physiological and pharmacological ligands. The key to understanding mechanisms of channel regulation is the ability to detect structural changes associated with ligand binding. While high-resolution structural methods such as X-ray crystallography and single-particle cryo-electron microscopy offer direct visualization of channel structures, these methods do have limitations and may not be suitable for the question of interest. In this chapter, we describe the use of a photo-cross-linker unnatural amino acid, *p*-azido-L-phenylalanine, to probe interactions between two proteins, the sulfonylurea receptor 1 and the inwardly rectifying potassium channel Kir6.2, that form the ATP-sensitive potassium (K_{ATP}) channel complex in the absence or presence of ligands. The difference in the extent of crosslinking between a liganded state and unliganded state can be used as a readout of ligand-induced structural changes. We anticipate that the protocol described here will also be applicable for other potassium channels and protein complexes.

Key words Sulfonylurea receptor, Kir6.2, Azidophenylalanine, Glibenclamide, Carbamazepine, Membrane protein, Pharmacological chaperone

1 Introduction

Potassium channels are multimeric protein complexes that contain two or four pore-forming potassium channel subunits and often also contain regulatory subunits that are important for channel trafficking and gating. Physiological and pharmacological ligands may interact with the pore subunit, the regulatory subunit, or both to induce conformational changes that result in changes in channel behavior. To understand the mechanism of channel regulation, it is important to understand structural changes associated with ligand binding. The most direct way to detect conformational changes is to obtain high-resolution channel structures in the absence or presence of ligands, such as using X-ray crystallography or single-particle cryo-electron microscopy. However, these methods require

Show-Ling Shyng et al. (eds.), *Potassium Channels: Methods and Protocols*, Methods in Molecular Biology, vol. 1684,
DOI 10.1007/978-1-4939-7362-0_5,

substantial resources that are not available to many researchers. Moreover, channel proteins may need to be placed in non-physiological environment or be mutated for stability or crystallization. Even in cases where high-resolution structures are available, protein regions critical for regulation may be disordered and poorly resolved. Thus, there is a need to develop other methods to probe structural changes in response to ligand binding.

The ATP-sensitive potassium (K_{ATP}) channel is a hetero-octamer of four pore-forming inwardly rectifying potassium channel Kir6.2 subunits and four regulatory sulfonylurea receptor 1 (SUR1) subunits [1–5]. K_{ATP} channels are molecular sensors that link cellular energetics to membrane excitability and are crucial for coupling glucose metabolism to insulin secretion in pancreatic β-cells [6]. Mutations that disrupt folding or assembly of Kir6.2 or SUR1 impair channel expression at the cell surface, leading to loss of channel function and the insulin secretion disorder congenital hyperinsulinism [7]. Sulfonylureas such as glibenclamide are anti-diabetic medications that bind and inhibit β-cell K_{ATP} channel thereby increasing insulin secretion [6]. It has been shown that these drugs also act as pharmacological chaperones to rescue mutations that impair channel folding and assembly thereby restoring surface expression of mutant channels [8–10]. However, it was not well understood how binding of sulfonylureas to mutant channel proteins restores complex formation and trafficking to the cell surface. Interestingly, sulfonylureas only rescue trafficking defects caused by mutations in the first transmembrane domain (TMD0) of SUR1 and that the rescue effect of glibenclamide requires Kir6.2. These observations led us to hypothesize that sulfonylureas alter the interactions between the mutant SUR1 and Kir6.2 to overcome mutation-induced folding or assembly defects.

One approach to probing structural changes in proteins is to monitor crosslinking between two protein regions in the absence or presence of a ligand. A change in the extent of crosslinking would serve as evidence for ligand-induced structural changes. Crosslinking can occur between pairs of cysteine residues that are in close proximity [11, 12], or by using chemical crosslinkers that target specific functional groups in amino acids. The former method can work well when there is existing knowledge of the cysteine residue pairs available. The latter method needs to be coupled with quantitative mass spectrometry to identify peptides that are differentially crosslinked in the absence or presence of ligands [13, 14]. Recent advances in the ability to co-translationally incorporate photo-crosslinker unnatural amino acids into proteins expressed in mammalian cells offer a new strategy to probe protein-protein interactions. In this case, the position of the photo-crosslinker unnatural amino acid can be specified using the amber stop codon suppression methodology [15], by mutating the naturally occurring codon into an amber stop codon (also *see* Chapter 19

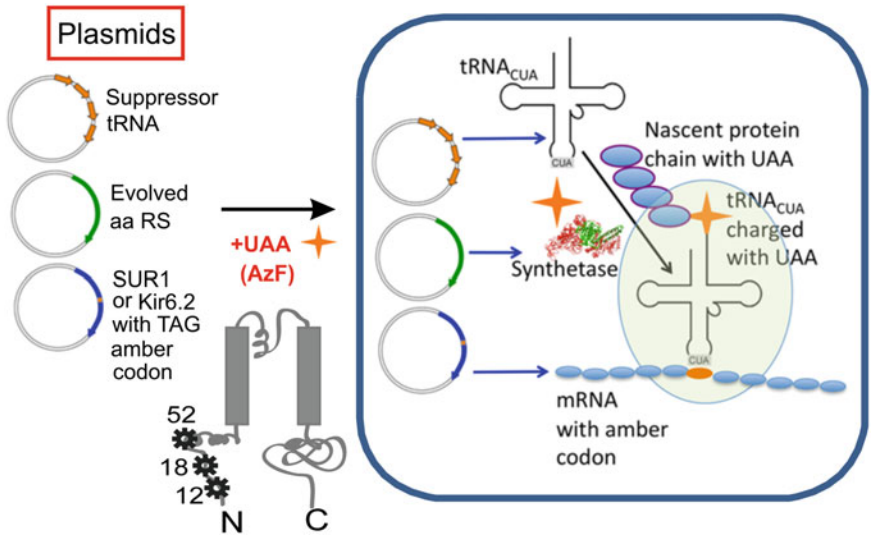

Fig. 1 Cartoon depicting the amber stop codon suppression technology used to incorporate AzF into Kir6.2 at specified amino acid position. For our study, we engineered the TAG stop codon into amino acid positions 12, 18, or 52

by Kim and Kurata), affording the capability to interrogate interactions between regions of interest (*see* Fig. 1).

The use of genetically encoded photo-crosslinker amino acids, *p*-azido-L-phenylalanine (AzF) and *p*-banzoyl-L-phenylalanine, was pioneered by Dr. Thomas Sakmar's group and has been used extensively to study ligand binding as well as conformational and functional dynamics of G-protein coupled receptors (GPCRs) and other membrane proteins [16–23]. Several excellent review articles and method papers have been published on this topic [18, 24, 25]. In this chapter, we share our protocol of adapting the use of *p*-azido-L-phenylalanine to monitor changes in interactions between SUR1 and Kir6.2 upon exposure to a high affinity sulfonylurea drug glibenclamide or another K_{ATP} channel pharmacological chaperone carbamazepine.

2 Materials

Mutagenesis studies showed that deletion of the N-terminal thirty amino acids of Kir6.2 diminished the ability of glibenclamide or carbamazepine to rescue K_{ATP} channel trafficking mutants harboring mutations in the TMD0 of SUR1, suggesting that this region may be involved in ligand binding or ligand-induced structural changes in the channel complex. Therefore, we introduced the amber stop codon in the distal N-terminus of Kir6.2 and monitored crosslinking to SUR1 in the absence or presence of

glibenclamide or carbamazepine. The protocol described below uses Kir6.2 with a TAG stop codon introduced at the amino acid 12 position to replace the codon for tyrosine (referred to as Kir6.2-Tyr12TAG hereinafter).

2.1 Tissue Culture

1. 4-Azido-L-phenylalanine (AzF) (e.g., from Chem-Impex, Wood Dale, IL).
2. Glibenclamide and carbamazepine for pharmacological treatment of cells.
3. COS cell Growth Media: High glucose (4.5 g/L) + L-Glutamine DMEM, 10% Fetal Bovine Serum, 100 U/ml penicillin/streptomycin.
4. Trypsin-EDTA 0.05%.
5. Phosphate-buffered-saline (PBS): 137 mM NaCl, 2.7 mM KCl, 8 mM Na_2HPO_4, 1.5 mM KH_2PO_4, adjust pH to 7.4 and filter sterilize (0.22 μM) into a sterile bottle. Store at 4 °C and warm to 37 °C before use.
6. Sterile serological pipettes.
7. Sterile 35 mm tissue culture grade dishes.
8. 37 °C tissue culture incubator, 5.0% CO_2.

2.2 Transfection

1. Plasmids encoding Kir6.2 Tyr12TAG and wild-type SUR1 in mammalian expression vectors (*see* **Note 1**).
2. TPS136 (encodes unnatural suppressor tRNA) and TPS192 (encodes amino acyl tRNA synthetase specific for AzF) (*see* **Note 2**).
3. OptiMEM®: reduced serum media.
4. FuGENE®6 transfection reagent.
5. COS cells plated in 35 mm dish (*see* **Note 3**).

2.3 Harvesting Cells

1. PBS containing Mg^{2+} and Ca^{2+}, stored at 4 °C.
2. Cell scraper.
3. UV lamp (365 nm) (*see* **Note 4**).
4. Tabletop centrifuge prechilled to 4 °C.

2.4 Cell Lysis

1. Lysis Buffer: 50 mM Tris–HCl, 150 mM NaCl, 1 mM EDTA, 1% TRITON X-100, pH 7.4, 0.22 μM filter sterilized and stored at 4 °C.
2. Mini-Protease Inhibitor (P.I.) Cocktail, EDTA.
3. Carousel tube mixer.

2.5 FLAG Pulldown

1. ANTI-FLAG M2 Affinity Gel.
2. Tris-buffered saline (TBS): 50 mM Tris–HCl, 150 mM NaCl, pH 7.4 and filter sterilized (0.22 μM).
3. [2×] SDS-PAGE Sample Buffer: 10 mM DTT, 200 mM SDS, 20% glycerol, 25% 4× upper gel buffer, 0.375 mM bromophenol blue.
4. Lysis Buffer, same as above.

3 Methods

3.1 Preparing [2×] AzF Growth Media

Prepare AzF containing growth media 16 h prior to cell transfection by weighing 4 mM worth of AzF into an adequate volume (1 ml—half of working volume—per 35 mm dish for a final concentration of 2 mM AzF) of pre-warmed growth media in a sterile 50 ml conical tube and rocking the tube gently at room temperature overnight to dissolve AzF (*see* **Note 5**).

3.2 Plating Cells

All tissue culture media is stored at 4 °C and preheated to 37 °C prior to any tissue culture work. All solutions and materials must be pre-sterilized and remain so before coming in contact with cells to avoid contamination.

1. Culture COS cells in DMEM, 10% FBS, 100 U/ml penicillin/streptomycin in T-25 tissue culture flasks at 37 °C, 5.0% CO_2. Grow to ~70% confluency and passage (*see* **Note 6**).
2. Plate ~2.5 × 10^5 COS cells into each 35 mm dish in half the working volume of vessel (1 ml) 16 h before transfection, or enough cells to reach approximately 80% confluency the next morning.

3.3 Transfection and Adding AzF Supplement to Transfected Cells

The following transfection procedure is adapted from Promega's transfection protocol, and routinely used in the lab. The listed quantities represent volumes for one 35 mm dish; scale volumes as necessary for varying vessel sizes or total sample amounts. When possible, make a master mix to ensure equal exposure to transfection complexes per sample. Both the FuGENE6® and DNA are diluted in pre-warmed serum-reduced media, OptiMEM, and prepared under sterile conditions at room temperature.

In the absence of any TPS plasmids or AzF, Kir6.2 is truncated with only 11 N-terminal amino acids translated. A successful read-through results in expression of full-length Kir6.2 (*see* Fig. 2). Before supplementing the cells with the AzF media, allow a minimum incubation of 5 h for the transfection to take place. This ensures adequate read-through of the genetically engineered amber stop codon, and the orthogonal pair of tRNA and aminoacyl

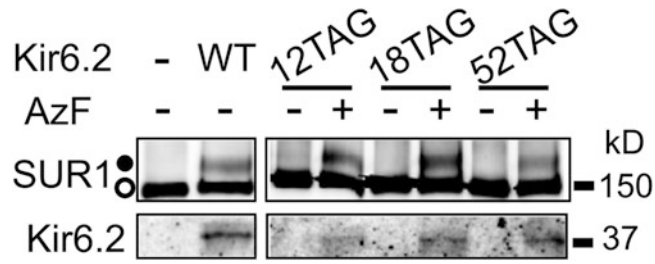

Fig. 2 Western blots showing complete translation of the Kir6.2-TAG cDNAs in the presence of AzF. Correct channel assembly is indicated by the upper, complex-glycosylated band of co-expressed SUR1 (*solid circle*; the lower, core-glycosylated band is indicated by the *open circle*). Western blots of wild-type Kir6.2 and SUR1 co-expressed in COS cells are shown on the *left* as controls. Adapted from Devaraneni et al. [26]

tRNA synthetase specific for AzF. Again, limit light exposure to the cells and media upon AzF supplementation.

1. The following morning, prepare 50 μl of OptiMEM and dilute the FuGENE®6 transfection reagent for approximately a 1:2 DNA-to-FuGENE®6 mixture (6 μl per 35 mm dish). Thoroughly mix and incubate at RT for at least 5 min.
2. Separately, prepare another 50 μl of OptiMEM and add 1 μg of the Kir6.2 Tyr12TAG DNA, 0.5 μg of SUR1 DNA, 1 μg of TPS136, and 0.2 μg of TPS192. Mix well and incubate for at least 5 minutes at room temperature (*see* **Note 6**).
3. Combine dilutions and thoroughly mix. Incubate for 20 min at room temperature.
4. Add mixture dropwise to cells, rocking the plate gently to ensure equal distribution of transfection mixture, and incubate at 37 °C, 5.0% CO_2 for 5–7 h.
5. After the preliminary incubation, add the additional half working volume of media supplemented with [2×] AzF into the dish. With the volume now adjusted to its working standard, the final concentration of AzF is 2 mM.
6. Rock media gently to blend the media together.
7. Continue the incubation at 37 °C, 5.0% CO_2. Harvest cells 48 h post transfection.

3.4 Pharmacological Treatments

COS cells are exposed to various pharmacological treatments 16–20 h prior to harvesting (*see* **Note 7**). In this case, we treat cells with 5 μM glibenclamide (diluted from 5 mM stock in DMSO) or 10 μM carbamazepine (diluted from 10 mM stock in DMSO); both glibenclamide and carbamazepine are K_{ATP} channel pharmacological chaperones that can increase the biogenesis efficiency of wild-type channels and also correct channel-processing defects

caused by mutations in TMD0 of SUR1 [8, 9]. Reserve two dishes as vehicle-treated samples (e.g., 0.1% DMSO)—one undergoes UV exposure while the other serves as a control.

3.5 Harvesting Cells for UV Exposure

If so desired, the pharmacological compounds may be included throughout the harvesting procedure to continually expose the protein to the chemical agents. All the subsequent steps hereafter are performed on ice or at 4 °C, unless noted otherwise.

When exposing the cells to UV light, arrange each vessel equidistantly under the UV lamp to ensure every dish has uniform UV exposure. Keep cells on ice and perform photo-crosslinking at 4 °C if possible to reduce heating up samples. If necessary, create a chamber enclosing the lamp and the samples to limit any contaminating light.

1. Aspirate media.
2. Rinse cells twice in 1 ml of ice-cold PBS to remove media and aspirate.
3. Scrape cells in 1 ml of PBS and gently pipette to make uniform cell suspension (*see* **Note 8**).
4. Leave on ice (with or without compound) for 10 min to equilibrate.
5. Set up the vessel under UV and expose the cells for 20 min in 4 °C (*see* **Note 9**).
6. Carefully transfer the cells after UV exposure into prechilled 1.3 ml Eppendorf tube. Gently centrifuge at low speed ($<1000 \times g$) for 5 min at 4 °C.
7. Aspirate PBS.

STOPPING POINT: Flash freeze pellet and store at −80 °C, thaw on ice when ready to use. For immediate use, keep on ice and continue protocol.

3.6 Cell Lysis

1. Resuspend cell pellet in 150 μl of lysis buffer + complete P.I.
2. Lyse cells by performing end-over-end mixing at 4 °C for 30 min.
3. Spin at 14,000 rpm (~9,000 × *g*) in a table top centrifuge for 20 min 4 °C.
4. Transfer lysate into a fresh prechilled 1.5 ml Eppendorf tube.

3.7 FLAG Pulldown

The FLAG octapeptide (Asp-Tyr-Lys-Asp-Asp-Asp-Asp-Lys) is located on the N-terminal region of the sulfonylurea protein (SUR1) (*see* **Note 10**). The anti-FLAG M2 affinity resin is stored at −20 °C and supplied in a 50% glycerol suspension. This protocol elutes the immunoprecipitated protein directly off the beads at room temperature using [2×] SDS-PAGE sample buffer in the

presence of a reducing agent; therefore, the resin is disposed of after a single use.

1. Invert the anti-FLAG M2 affinity resin bottle to uniformly distribute beads in slurry.
2. Extract appropriate aliquot with a wide-mouthed pipette tip (~10 μl of packed gel volume, ~20 μl slurry, binds >1 μg FLAG-tagged protein).
3. Rinse resin aliquot in 20× the volume with TBS and spin for 30 s at 14,000 rpm (~9,000 × *g*) to remove glycerol. Let beads settle for 30 s and then aspirate. Repeat washes 3×.
4. Thoroughly resuspend packed gel beads in lysis buffer.
5. Add equal volumes of thoroughly resuspended gel beads to each sample of cell lysate.
6. End-over-end mix samples for 5 h or overnight at 4 °C.
7. Centrifuge the sample for 30 s at 14,000 rpm (~9,000 × *g*) in a tabletop microfuge. Carefully remove the supernatant with a narrow-tip pipette to avoid discarding any beads.
8. Wash resin three times in Lysis Buffer in 20× the bead volume.
9. Remove all supernatants.
10. Elute protein in [2×] SDS-PAGE sample buffer in a volume equal to the resin. Incubate at room temperature for 10 min, agitating samples every few minutes.
11. Centrifuge the sample for 30 s at 14,000 rpm (~9,000 × *g*) to settle beads.
12. Transfer elution to a new tube, and samples are ready for loading on a SDS-PAGE gel. Analyze by immunoblotting against the FLAG peptide or Kir6.2.
13. One should observe a crosslinked SUR1-Kir6.2 band that is recognized by anti-FLAG antibody and anti-Kir6.2 antibody and that the intensity of the crosslinked band is higher in glibenclamide or carbamazepine-treated samples than in control sample treated with 0.1% DMSO (*see* Fig. 3).

4 Notes

1. For expression of K_{ATP} channels, both Kir6.2 and SUR1 are needed. Successful assembly and maturation of the channel complex can be discerned by the presence of the complex-glycosylated SUR1 band on SDS-PAGE (*see* Fig. 2).
2. TPS136 (encodes unnatural suppressor tRNA) and TPS192 (encodes amino acyl tRNA synthetase for AzF) are generous

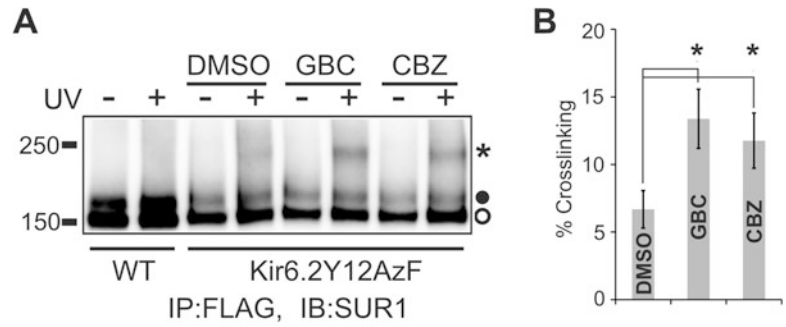

Fig. 3 Glibenclamide (GBC; 5 μM) and carbamazepine (CBZ; 10 μM) overnight treatment significantly increased photocrosslinking of Kir6.2Y12AzF to SUR1 upon UV exposure. Right: Quantification of crosslinked SUR1 as a percentage of total SUR1 signal. *$p < 0.001$, $n = 4$. Adapted from Devaraneni et al. [26]

gifts from Dr. Thomas Sakmar. These plasmids are essential for the experiments.

3. The adherent COS cell line, a derivative of African Green Monkey Kidney cells, requires passage every 2–3 days upon reaching ~70% confluency (from a 1:10 dilution). Ensure the cells are well maintained and frequently passaged to optimize experimental results. Other mammalian cell lines that do not express channels of interest can be used as alternative expression systems.
4. AzF is activated by 365 nm light. UV lamps with different wavelengths may affect the efficiency of crosslinking.
5. Ensure the 4-azido-L-phenylalanine (AzF) is shielded from direct light at all times and apply the sterile technique when preparing the solution. We found that rocking the solution overnight at room temperature is the easiest way to dissolve AzF.
6. To express amber stop codon containing K_{ATP} channel, we need to co-transfect four different plasmids, two for the channel subunits and two for the orthogonal pair of tRNA and tRNA synthetase. The amount of FuGENE®6 (or other comparable transfection reagents) and plasmids used need to be systematically tested for optimal expression of AzF-containing channels without sacrificing cell viability.
7. Depending on the induction rate of the pharmacological chemical in question, treat cells according to the predetermined concentration and exposure duration. For our purposes, select dishes are often treated with a predetermined concentration of an agonist (channel activator), an antagonist (channel blocker), or is vehicle-treated to observe the crosslinking responses to the various agents. The addition of such compounds is done under sterile conditions and with limited exposure to light.

8. UV light exposure is done with cells scraped off from the bottom of the culture dish. This likely maximizes exposure and improves crosslinking efficiency.
9. The duration of UV light exposure should be tested for optimal results. Exposure for too long may increase background while too short may decrease signal.
10. In our study, the stop codon is placed in Kir6.2 and channels affinity purified via the FLAG-tag at the N-terminus of SUR1 after cell lysis for detection. Because there is also FLAG-tagged SUR1 that is not complexed with Kir6.2, the cross-linked SUR1-Kir6.2 species is only a fraction of the affinity purified SUR1, thus the signal of the crosslinked band tends to be weaker than if the stop codon is introduced in SUR1. This should be taken into consideration when designing experiments for channels containing different protein subunits.

Acknowledgments

We are grateful to Dr. Thomas Sakmar for the suppressor tRNA plasmid and the plasmid of tRNA synthetase specific for *p*-azido-L-phenylalanine, and for valuable advice. This work was supported by National Institutes of Health grant R01DK066485.

References

1. Clement JP, Kunjilwar K, Gonzalez G, Schwanstecher M, Panten U, Aguilar-Bryan L, Bryan J (1997) Association and stoichiometry of K(ATP) channel subunits. Neuron 18 (5):827–838
2. Inagaki N, Gonoi T, Clement JP, Namba N, Inazawa J, Gonzalez G, Aguilar-Bryan L, Seino S, Bryan J (1995) Reconstitution of IKATP: an inward rectifier subunit plus the sulfonylurea receptor. Science 270(5239):1166–1170
3. Inagaki N, Gonoi T, Seino S (1997) Subunit stoichiometry of the pancreatic beta-cell ATP-sensitive K+ channel. FEBS Lett 409 (2):232–236
4. Martin GM, Yoshioka C, Rex EA, Fay JF, Xie Q, Whorton MR, Chen JZ, Shyng SL (2017) Cryo-EM structure of the ATP-sensitive potassium channel illuminates mechanisms of assembly and gating. eLife 6. doi:10.7554/eLife.24149
5. Shyng S, Nichols CG (1997) Octameric stoichiometry of the KATP channel complex. J Gen Physiol 110(6):655–664
6. Aguilar-Bryan L, Bryan J (1999) Molecular biology of adenosine triphosphate-sensitive potassium channels. Endocr Rev 20 (2):101–135. doi:10.1210/edrv.20.2.0361
7. Martin GM, Chen PC, Devaraneni P, Shyng SL (2013) Pharmacological rescue of trafficking-impaired ATP-sensitive potassium channels. Front Physiol 4:386. doi:10.3389/fphys.2013.00386
8. Martin GM, Rex EA, Devaraneni P, Denton JS, Boodhansingh KE, DeLeon DD, Stanley CA, Shyng SL (2016) Pharmacological correction of trafficking defects in ATP-sensitive potassium channels caused by sulfonylurea receptor 1 mutations. J Biol Chem 291 (42):21971–21983. doi:10.1074/jbc.M116.749366
9. Yan F, Lin CW, Weisiger E, Cartier EA, Taschenberger G, Shyng SL (2004) Sulfonylureas correct trafficking defects of ATP-sensitive potassium channels caused by mutations in the sulfonylurea receptor. J Biol Chem 279 (12):11096–11105. doi:10.1074/jbc.M312810200
10. Yan FF, Lin YW, MacMullen C, Ganguly A, Stanley CA, Shyng SL (2007) Congenital hyperinsulinism associated ABCC8 mutations

that cause defective trafficking of ATP-sensitive K+ channels: identification and rescue. Diabetes 56(9):2339–2348. doi:10.2337/db07-0150

11. Lin YW, Jia T, Weinsoft AM, Shyng SL (2003) Stabilization of the activity of ATP-sensitive potassium channels by ion pairs formed between adjacent Kir6.2 subunits. J Gen Physiol 122(2):225–237. doi:10.1085/jgp.200308822
12. Pratt EB, Zhou Q, Gay JW, Shyng SL (2012) Engineered interaction between SUR1 and Kir6.2 that enhances ATP sensitivity in KATP channels. J Gen Physiol 140(2):175–187. doi:10.1085/jgp.201210803
13. Rappsilber J (2011) The beginning of a beautiful friendship: cross-linking/mass spectrometry and modelling of proteins and multi-protein complexes. J Struct Biol 173 (3):530–540. doi:10.1016/j.jsb.2010.10.014
14. Weisbrod CR, Chavez JD, Eng JK, Yang L, Zheng C, Bruce JE (2013) In vivo protein interaction network identified with a novel real-time cross-linked peptide identification strategy. J Proteome Res 12(4):1569–1579. doi:10.1021/pr3011638
15. Huber T, Naganathan S, Tian H, Ye S, Sakmar TP (2013) Unnatural amino acid mutagenesis of GPCRs using amber codon suppression and bioorthogonal labeling. Methods Enzymol 520:281–305. doi:10.1016/B978-0-12-391861-1.00013-7
16. Grunbeck A, Huber T, Abrol R, Trzaskowski B, Goddard WA 3rd, Sakmar TP (2012) Genetically encoded photo-cross-linkers map the binding site of an allosteric drug on a G protein-coupled receptor. ACS Chem Biol 7 (6):967–972. doi:10.1021/cb300059z
17. Grunbeck A, Huber T, Sachdev P, Sakmar TP (2011) Mapping the ligand-binding site on a G protein-coupled receptor (GPCR) using genetically encoded photocrosslinkers. Biochemistry 50(17):3411–3413. doi:10.1021/bi200214r
18. Grunbeck A, Sakmar TP (2013) Probing G protein-coupled receptor-ligand interactions with targeted photoactivatable cross-linkers. Biochemistry 52(48):8625–8632. doi:10.1021/bi401300y
19. Koole C, Reynolds CA, Mobarec JC, Hick C, Sexton PM, Sakmar TP (2017) Genetically-encoded photocrosslinkers determine the biological binding site of exendin-4 in the N-terminal domain of the intact human glucagon-like peptide-1 receptor (GLP-1R). J Biol Chem. doi:10.1074/jbc.M117.779496
20. Park M, Sivertsen BB, Els-Heindl S, Huber T, Holst B, Beck-Sickinger AG, Schwartz TW, Sakmar TP (2015) Bioorthogonal labeling of ghrelin receptor to facilitate studies of ligand-dependent conformational dynamics. Chem Biol 22(11):1431–1436. doi:10.1016/j.chembiol.2015.09.014
21. Periole X, Knepp AM, Sakmar TP, Marrink SJ, Huber T (2012) Structural determinants of the supramolecular organization of G protein-coupled receptors in bilayers. J Am Chem Soc 134(26):10959–10965. doi:10.1021/ja303286e
22. Rannversson H, Andersen J, Sorensen L, Bang-Andersen B, Park M, Huber T, Sakmar TP, Stromgaard K (2016) Genetically encoded photocrosslinkers locate the high-affinity binding site of antidepressant drugs in the human serotonin transporter. Nat Commun 7:11261. doi:10.1038/ncomms11261
23. Valentin-Hansen L, Park M, Huber T, Grunbeck A, Naganathan S, Schwartz TW, Sakmar TP (2014) Mapping substance P binding sites on the neurokinin-1 receptor using genetic incorporation of a photoreactive amino acid. J Biol Chem 289(26):18045–18054. doi:10.1074/jbc.M113.527085
24. Grunbeck A, Huber T, Sakmar TP (2013) Mapping a ligand binding site using genetically encoded photoactivatable crosslinkers. Methods Enzymol 520:307–322. doi:10.1016/B978-0-12-391861-1.00014-9
25. Naganathan S, Grunbeck A, Tian H, Huber T, Sakmar TP (2013) Genetically-encoded molecular probes to study G protein-coupled receptors. J Vis Exp:79. doi:10.3791/50588
26. Devaraneni PK, Martin GM, Olson EM, Zhou Q, Shyng SL (2015) Structurally distinct ligands rescue biogenesis defects of the KATP channel complex via a converging mechanism. J Biol Chem 290(12):7980–7991. doi:10.1074/jbc.M114.634576

Chapter 6

Hyper-SUMOylation of K^+ Channels in Sudden Unexplained Death in Epilepsy: Isolation and Primary Culture of Dissociated Hippocampal Neurons from Newborn Mice for Subcellular Localization

Xu Chen, Shanshan Zhang, Jifang Huang, Wanying Dong, Hui Xiao, Huanjie Shao, Jinke Cheng, Hongmei Wu, and Yitao Qi

Abstract

The physiological characteristics of rat and murine hippocampal neurons are widely studied, especially because of the involvement of the hippocampus in learning, memory, and neurological functions. Primary cultures of hippocampal neurons are commonly used to discover cellular and molecular mechanisms in neurobiology. By isolating and culturing individual hippocampal neurons, neuroscientists are able to investigate the activity of neurons at the individual cell and single synapse level, and to analyze properties related to cellular structure, cellular trafficking, and individual protein subcellular localization or protein-protein interaction using a variety of biochemical techniques. Conclusions addressed from such research are critical for testing theories related to memory, learning, and neurological functions. Here, we will describe how to isolate and culture primary hippocampal cells from newborn mice. The hippocampus may be isolated from newborn mice in as short as 2 min, and the cell cultures can be maintained for up to 2 weeks, and then ready for investigation of subcellular localization of K^+ channel proteins and interaction with SUMO-specific protease 2 (SENP2). The protocol provides a fast and efficient technique for the culture of neuronal cells from mouce hippocampal tissue, and will ensure the immunocytochemistry detection of subcellular localization or protein-protein interactions in neurological research.

Key words Hippocampal neuron, Newborn mice, Isolation, Primary culture, Channel protein, Sudden unexplained death in epilepsy (SUDEP), Small ubiquitin-like modifier (SUMO), SUMO-specific protease 2 (SENP2)

1 Introduction

It has been estimated that the rate of sudden death is 20-fold higher in epilepsy patients than in the general population, and sudden unexplained death in epilepsy (SUDEP) represents the most common epilepsy-related cause of death [1]. Among those epileptic conditions linked to channelopathies, mutations in potassium channel subunits represent the largest category [2]. Small

Show-Ling Shyng et al. (eds.), *Potassium Channels: Methods and Protocols*, Methods in Molecular Biology, vol. 1684,
DOI 10.1007/978-1-4939-7362-0_6,

ubiquitin-like modifier (SUMO) covalently modifies a large number of cellular proteins, and can be reversed by a family of SUMO-specific proteases (SENPs) [3]. SENP2 is involved in embryonic development [4] and myogenesis [5], as well as regulation of M-current and that reversing SUMOylation of potassium channels may present a new approach for treating patients with SUDEP [6].

Hippocampal neuron cultures have been applied in neurobiology for many years, and have proven to be the most popular method due to the relatively simple architecture of the nerve cell population in the hippocampus [7]. The hippocampus has been implicated in both spatial and contextual learning [8] and memory [9]. Growth of primary cultures from the hippocampus can allow a correlation between subcellular biological events and their effects on learning and memory. The ability to isolate and culture primary hippocampal neurons under serum-free conditions facilitates tighter control of neuronal studies, including protein localization and interaction. Some serum-free media and supplements allow for the low-density neuronal cultures, which in turn enables the study of individual neurons and synapses [10]. We applied this method to obtain specific mouse hippocampal neurons for the detection of protein subcellular localization and protein-protein interactions [6]. This chapter details the isolation and culture of hippocampal neural cells from newborn mice in serum-free media and supplements. This technique has the potential to bridge the gap between in vivo and in vitro studies in adult mice, and could be a much needed tool for studying adult mouse neuronal regeneration, aging, and cell patterning, as well as in vitro drug-screening.

2 Materials

Prepare all solutions with ultrapure water and analytical grade reagents. Prepare and store all reagents at room temperature unless indicated otherwise. Diligently follow all waste disposal regulations when disposing waste materials.

1. CMF-HBSS buffered with 10 mM HEPES: To prepare 1000 mL, add 100 mL 10× CMF-HBSS into 900 mL water. Then add 2.383 g HEPES and titrate pH to 7.1 with NaOH.
2. 2.5% (weight/volume) papain, prepare just before use (*see* **Note 1**).
3. Borate buffer: To prepare 40 mL of 0.1 M borate buffer at pH 8.5, mix 124 mg boric acid and 190 mg sodium tetraborate in 40 mL water.
4. Poly-D-lysine solution, 1 mg/mL, dilute in borate buffer to a final concentration of 50 μg/mL. To prepare 50 mL of 50 μg/mL poly-D-lysine, add 2.5 mL of 1 mg/mL poly-D-lysine to

47.5 mL borate buffer, then filter sterilize and store in a 15 mL conical tube.

5. Laminin solution, 1 mg/mL, dilute in water to a final concentration of 5 μg/mL. To prepare 5 mL of 5 μg/mL laminin, add 25 μL of 1 mg/mL laminin into 4.975 mL sterile water, then filter sterilize and store in a 15 mL conical tube.
6. Neurobasal A/B27/Glutamax-I media: To prepare 250 mL, pour 242.5 mL Neurobasal A media into a filter-sterilizing apparatus, add 5 mL 50× B27 solution, 2.5 mL 100× Glutamax-I solution (just before use, unstable), add penicillin/streptomycin (half of normal, because no serum), then filter sterilize (*see* **Note 2**).
7. Formaldehyde: 16%, methanol free, Dilute 1 in 4 in 1× PBS to make a 4% formaldehyde solution (*see* **Note 3**).
8. Blocking Buffer: (1× PBS/5% normal serum/0.3% Triton X-100): To prepare 10 mL, add 0.5 mL normal serum from the same species as the secondary antibody and mix well. While stirring, add 30 μL Triton X-100.
9. Antibody Dilution Buffer: (1× PBS/1% BSA/0.3% Triton X-100): To prepare 10 mL, add 30 μL Triton X-100 to 10 mL 1× PBS. Mix well and then add 0.1 g BSA, mix.

3 Methods

3.1 Preparation of Coverslips

1. Rinse coverslips serially in water, 70%, 95% and then 100% ethanol alcohol three times each (*see* **Note 4**).
2. Two days before dissection, remove any remaining droplets by rinsing in 100% ethanol, then air-dry individually in 6-well dish.
3. At least 2 days before dissection, coat coverslips with 100 μL poly-D-lysine. When properly cleaned, the coverslips are very hydrophilic and this small volume will spread evenly over the entire surface. The hydrophobicity of the bacteriological plate will prevent the solution from spreading onto the dish. Let it stand for 12–24 h at room temperature, covered to protect the dishes from evaporation.
4. Remove the poly-D-lysine solution and rinse with sterile water for 2 h (*see* **Note 5**).
5. Remove the rinse solution and add 100 μL laminin with a concentration of 5 μg/mL. Let it sit for 2 h. Rinse once with sterile water for 2 h.
6. Remove the rinse solution and add 2 mL Neurobasal A/B27 medium. Place the dishes in a CO_2 incubator (*see* **Note 6**).

3.2 Preparation for Dissection

1. Thaw Fetal Bovine Serum (FBS) and papain, place in hood with a 15 mL conical tube.
2. Pour 10 mL 95% ethanol in 60 mm Falcon dish next to the dissecting microscope.
3. Make sure proper tools are next to the dissecting microscope.
4. Ensure 4 °C filtered and HEPES buffered CMF-HBSS is available at the dissecting microscope and in the hood. Prepare 60 mm Falcon dishes next to the dissecting microscope.
5. Prepare a 15 mL conical tube, P1000 and P200 pipettes in hood.
6. Set temperature of water bath incubator to 37 °C.
7. Prepare 1.5 mL eppendorf tubes for collecting tails for genotyping if needed.
8. Prepare bag for disposal of mouse fetus after dissection.

3.3 Isolation of Cerebral Cortex and Hippocampus

1. Place a single-mouse pup on P0 in 60 mm dish with 95% ethanol for 2–3 s, and then place on ice for 5–10 s until movements slow (*see* **Note 7**).
2. Use long scissors to decapitate, and place the head in ice-cold CMF-HBSS in 60 mm Falcon dish. Cut tail if genotyping is needed.
3. Dissect the brain and place in fresh CMF-HBSS in 60 mm Falcon dish (*see* **Note 8**).
4. Transfer to fresh CMF-HBSS in 60 mm Falcon dish to dissect out the entire cerebral cortex.
5. Hippocampus were removed rapidly under stereomicroscopic observation, and cut it into small pieces.
6. Move to laminar flow hood, and transfer each set of hippocampus to a separate 15 mL conical tube.
7. Bring volume to 4.5 mL level with fresh ice-cold CMF-HBSS.

3.4 Digestion (Divide Reagents by Total Number of Animals Being Dissected)

1. Add 0.5 mL of 2.5% papain and incubate for 15 min in a water bath at 37 °C.
2. Add 0.5 mL FBS to neutralize papain.
3. Gently remove papain/FBS solution, leaving cells at the bottom of the tube.
4. Add 5 mL CMF-HBSS and let it stand for 5 min at room temperature.
5. Repeat steps 2–4 twice, but bring the final volume to 2–3 mL.
6. Dissociate with a fire-polished Pasteur pipette in the presence of DNase I until there are no chunks of tissue left (*see* **Note 9**).

3.5 Plating Cells

1. Count cells with hemocytometer and adjust the density to about 1–1.5 million cells/mL.
2. The cells were plated at a density of 2×10^4 cells on 12 mm glass coverslips previously coated with poly-D-lysine and laminin and maintained in Neurobasal A medium (*see* **Note 10**).
3. Incubate for 1 h at 37 °C and 5% CO_2 (*see* **Note 11**).
4. Transfer coverslip to a well containing 0.4 mL Neurobasal A/B27 media.
5. Rinse coverslips twice with Neurobasal A/B27 media.
6. Two hours after plating, the medium was removed and a fresh Neurobasal A/B27 medium was added. The hippocampal neurons were cultured in Neurobasal A supplemented with 2% B27 and 1% Glutamax-I in a humidified atmosphere containing 5% CO_2 at 37 °C. Add 0.4 mL of growth medium (Neurobasal A/B27 medium with 5 ng/mL FGF2, *see* **Note 12**).
7. Incubate at 37 °C and 5% CO_2 for up to 14 days.
8. If incubating for more than 4 days, subsequent feeding occurred twice weekly, half the medium should be replaced with B27/Neurobasal A with 10 ng/mL FGF2 and 5 μM AraC every 4 days (*see* **Note 13**). The neurons will be ready for further experiments at DIV (days in vitro) 14.

3.6 Immunofluorescence Staining

1. Aspirate cell culture media, then cover cells to a depth of 2–3 mm with 4% formaldehyde diluted in warm PBS (*see* **Note 14**).
2. Allow cells to fix for 15 min at room temperature.
3. Aspirate fixative, rinse three times in 1× PBS for 5 min each.
4. Block specimen in blocking buffer for 60 min (*see* **Note 15**).
5. While blocking, prepare primary antibody by diluting as indicated on datasheet in antibody dilution buffer.
6. Aspirate blocking solution, apply diluted primary antibody, and Incubate overnight at 4 °C.
7. Rinse three times in 1× PBS for 5 min each.
8. Incubate specimen in fluorochrome-conjugated secondary antibody diluted in antibody dilution buffer for 1 h at room temperature in the dark.
9. Rinse three times in 1× PBS for 5 min each.
10. Incubate cells with DAPI (DNA stain) for 1 min, and then rinse with PBS.
11. Mount coverslip with a drop of mounting medium.
12. Seal coverslip with nail polish to prevent drying and movement under a microscope (*see* **Note 16**), and then examine by confocal laser scanning microscopy (Fig. 1).

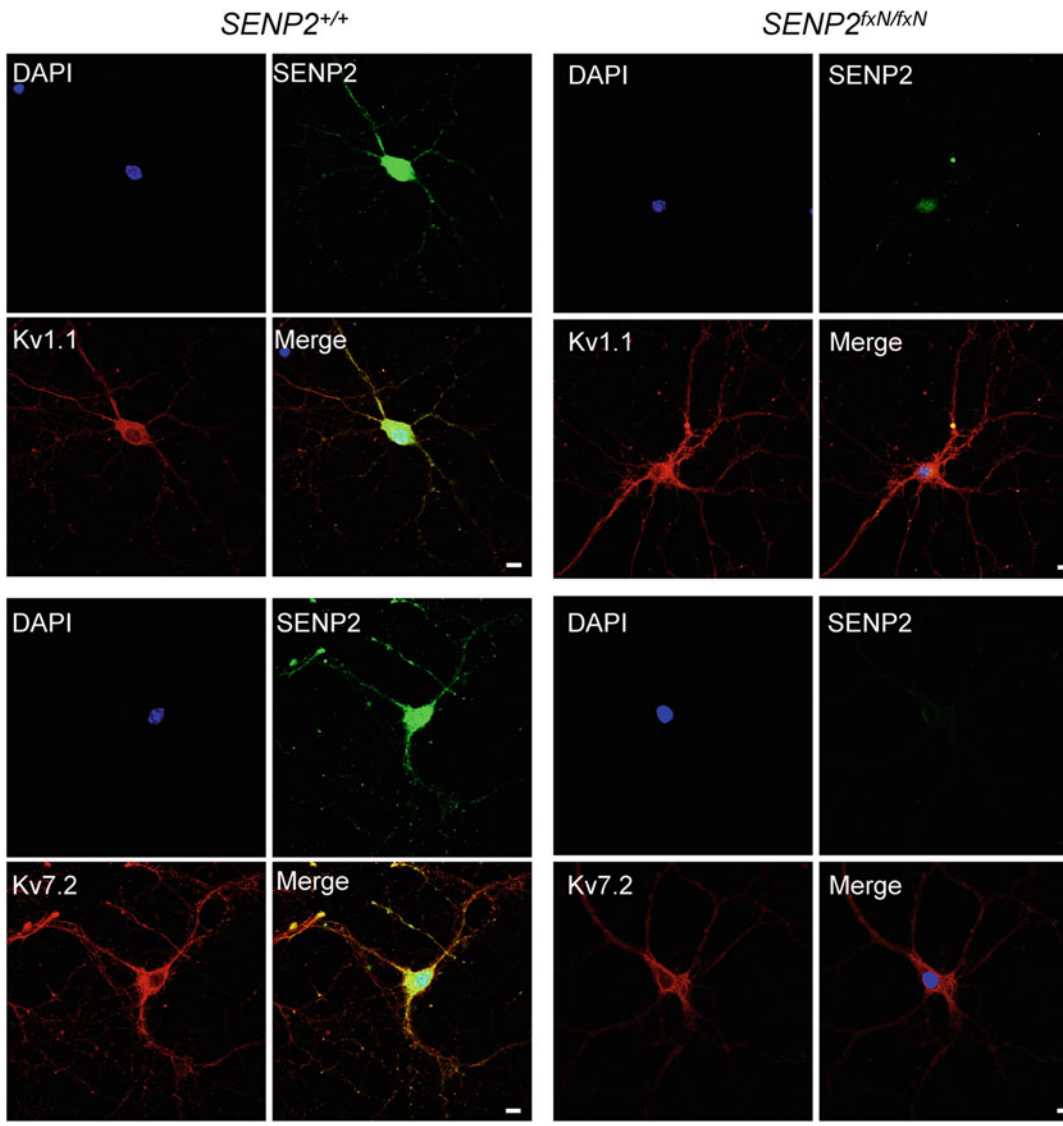

Fig. 1 SENP2 colocalizes with Kv1.1 and Kv7.2 in hippocampal neurons. Neurons from the brains of *SENP2*$^{+/+}$ and *SENP2*$^{fxN/fxN}$ mice were cultured for immunocytochemistry with SENP2 (*green*) and Kv1.1- (*red*) or Kv7.2 (*red*)-specific antibodies. DAPI (*blue*) was used to show nuclei. Bars in all panels are 5 mm

4 Notes

1. Once harvested, hippocampal tissue usually will be treated with a dilute trypsin solution to dissociate adherent cells. However, prolonged exposure to higher concentrations of trypsin can be detrimental to cell subculture. In the current protocol, we used papain as an alternative enzyme, because it has been proven to

be more effective and less destructive with certain tissues such as retinal neurons [11]. Once hippocampal tissue is isolated, gentle dissociation of neuronal cells is achieved with a dilute concentration of papain and mechanical disruption designed to separate cells from connective tissue while providing minimum damage to individual cell. Papain need to be prepared just before use.

2. The concentration of penicillin/streptomycin should be half of normal usage, because there is no serum in the culturing media.
3. The formaldehyde needs to prepare fresh and store in opened vials at 4 °C in the dark.
4. It is easier to handle coverslips using fine forceps, for example, Dumont No. 5.
5. The poly-D-lysine-treated coverslips should not dry during these steps.
6. The dishes with coverslips can be stored in a CO_2 incubator for several days before use.
7. Hippocampal neuronal cultures were prepared from 1-day-old mouse pups.
8. The tissue should remain submerged at all times, and the whole process should be done once.
9. Cell dissociation is followed by trituration of the tissue, and this has proven to be the most important step in consistent neuronal culture. We used fire-polished Pasteur pipette with a smoother surface to reduce mechanical damage to cells as they pass through. The speed and force of trituration through the pipette is of major importance. Appropriate number of times to pass the tissue through the pipette will result in sufficient numbers of neurons without resulting in gross damage to the population.
10. Optimal plating densities need to be optimized to maximize successful cell culture. If neuron density is too low at plating, cell growth will likely not be sufficient as plating density is an important variable in the propagation of the cell population [12].
11. We recommend using a 6-well plate for neuron plating.
12. In serum-supplemented media, glial cells continue to multiply, necessitating the use of cytotoxic mitotic inhibitors. Serum also contains unknown and variable levels of growth factors, hormones, vitamins, and proteins. In this protocol, we use Neurobasal media with B27 supplement for growth of neurons in a serum-free environment. It is advantageous to optimize growth of healthy neurons and minimize the growth of non-desired cell types, such as astrocytes and glial cells.

13. As mentioned, glial cells contamination may still occur during hippocampal neuron isolation. It is possible to reduce glial cell contamination by treatment with cytosine arabinoside (AraC) at early time points in the culture [13, 14]. AraC can be used as an anti-mitotic agent to reduce the population of non-neuronal cells capable of DNA synthesis. However, to avoid possible toxic effects of treatment on neurons, it should be used at its lowest effective dose (5 μM) and not added until 4 days of culture [15]. Another option would be the use of 5-fluoro-2′-deoxyuridine (FUdR) treatment to decrease the proportion of fibroblastic-reactive microglial cells [11].
14. Formaldehyde is toxic, use only in a fume hood.
15. All subsequent incubations should be carried out at room temperature unless otherwise noted in a humid light-tight box or covered dish/plate to prevent drying and fluorochrome fading.
16. For best results, allow mountant to cure overnight at room temperature. For long-term storage, store slides flat at 4 °C protected from light.

Acknowledgment

This work was supported by the National Natural Science Foundation of China (81671294 to Y.T.Q. and 81502531 to H.M.W.), the Natural Science Foundation of Shaanxi Province, China (2017JM3013 to Y.T.Q.), and the Fundamental Research Funds for the Central Universities (GK201603061 to Y.T.Q., GK201603064 to H.M.W., GK201603062 to H.J.S., GK201701005 to H.X., and 2016CSY014 to X.C.).

References

1. Sillanpaa M, Shinnar S (2010) Long-term mortality in childhood-onset epilepsy. N Engl J Med 363(26):2522–2529
2. Brenner R, Wilcox KS (2012) Potassium channelopathies of epilepsy. In: Noebels JL et al (eds) Jasper's basic mechanisms of the epilepsies. National Center for Biotechnology Information, Bethesda, MD
3. Yeh ET, Gong L, Kamitani T (2000) Ubiquitin-like proteins: new wines in new bottles. Gene 248(1-2):1–14
4. Kang X et al (2010) SUMO-specific protease 2 is essential for suppression of polycomb group protein-mediated gene silencing during embryonic development. Mol Cell 38 (2):191–201
5. Qi Y et al (2014) An essential role of small ubiquitin-like modifier (SUMO)-specific Protease 2 in myostatin expression and myogenesis. J Biol Chem 289(6):3288–3293
6. Qi Y et al (2014) Hyper-SUMOylation of the Kv7 potassium channel diminishes the M-current leading to seizures and sudden death. Neuron 83(5):1159–1171
7. Kaech S, Banker G (2006) Culturing hippocampal neurons. Nat Protoc 1(5):2406–2415
8. Burwell RD et al (2004) Corticohippocampal contributions to spatial and contextual learning. J Neurosci 24(15):3826–3836
9. Gluck MA, Myers C, Meeter M (2005) Cortico-hippocampal interaction and adaptive stimulus representation: a neurocomputational

theory of associative learning and memory. Neural Netw 18(9):1265–1279

10. Varghese K et al (2009) Regeneration and characterization of adult mouse hippocampal neurons in a defined in vitro system. J Neurosci Methods 177(1):51–59
11. Oorschot DE (1989) Effect of fluorodeoxyuridine on neurons and non-neuronal cells in cerebral explants. Exp Brain Res 78 (1):132–138
12. Brewer GJ (1995) Serum-free B27/neurobasal medium supports differentiated growth of neurons from the striatum, substantia nigra, septum, cerebral cortex, cerebellum, and dentate gyrus. J Neurosci Res 42(5):674–683
13. Mao L, Wang JQ (2001) Gliogenesis in the striatum of the adult rat: alteration in neural progenitor population after psychostimulant exposure. Brain Res Dev Brain Res 130(1):41–51
14. Mao L, Wang JQ (2001) Upregulation of preprodynorphin and preproenkephalin mRNA expression by selective activation of group I metabotropic glutamate receptors in characterized primary cultures of rat striatal neurons. Brain Res Mol Brain Res 86(1-2):125–137
15. Schwieger J et al (2016) Establishment of a long-term spiral ganglion neuron culture with reduced glial cell number: effects of AraC on cell composition and neurons. J Neurosci Methods 268:106–116

Chapter 7

Simultaneous Real-Time Measurement of the β-Cell Membrane Potential and Ca^{2+} Influx to Assess the Role of Potassium Channels on β-Cell Function

Nicholas C. Vierra, Matthew T. Dickerson, Louis H. Philipson, and David A. Jacobson

Abstract

Stimulus-secretion coupling in pancreatic β-cells requires Ca^{2+} influx through voltage-dependent Ca^{2+} channels, whose activity is controlled by the plasma membrane potential (V_m). Here, we present a method of measuring fluctuations in the β-cell V_m and Ca^{2+} influx simultaneously, which provides valuable information about the ionic signaling mechanisms that underlie insulin secretion. This chapter describes the use of perforated patch clamp electrophysiology on cells loaded with a fluorescent intracellular Ca^{2+} indicator, which permits the stable recording conditions needed to monitor the V_m and Ca^{2+} influx in β-cells. Moreover, this chapter describes the protocols necessary for the preparation of mouse and human islet cells for the simultaneous recording of V_m and Ca^{2+} as well as determining the specific islet cell type assessed in each experiment.

Key words Calcium imaging, Pancreatic β-cell, Membrane potential, Potassium channels, Fluo-4 AM

1 Introduction

In electrically excitable insulin-secreting β-cells, Ca^{2+} influx through voltage-dependent Ca^{2+} channels (VDCCs) initiates stimulus-secretion coupling. Elevations in blood glucose and other nutrients accelerate β-cell metabolism, increasing the ATP:ADP ratio. This results in K_{ATP} channel inhibition and V_m depolarization, which triggers VDCC opening and action potential firing [1]. Thus, β-cells transduce nutrient metabolism into an electrical signal that stimulates Ca^{2+} influx and insulin secretion. Electrical excitability of human β-cells is modulated by the orchestrated function of several ion channels, which include VDCCs, voltage-gated Na^+ channels, as well as a number of K^+ channels (e.g., voltage-gated K^+ (K_v) [2], Ca^{2+}-activated K^+ (K_{Ca}^{2+}) [3], and two-pore domain (K2P) [4, 5] channels). K^+ channels regulate

Show-Ling Shyng et al. (eds.), *Potassium Channels: Methods and Protocols*, Methods in Molecular Biology, vol. 1684,
DOI 10.1007/978-1-4939-7362-0_7,

the frequency and amplitude of glucose-stimulated oscillations in β-cell electrical activity and cytosolic Ca^{2+} (Ca^{2+}_c), which are important determinants of insulin secretion. Because electrical excitability stimulates activation of VDCCs, simultaneous measurement of Ca^{2+}_c and β-cell V_m allows us to correlate how electrical activity influences Ca^{2+} influx in single cells as well as across intact whole islets. Here, we describe the use of Ca^{2+} indicators to examine rapid changes in Ca^{2+}_c concurrently with measurements of the V_m. As demonstrated in Fig. 1, this technique allows the investigator to assess how changes in factors which regulate action potential firing (e.g., in response to manipulation of K^+ channel function) affect β-cell Ca^{2+} influx.

Live-cell imaging of intracellular Ca^{2+} has contributed enormously to understanding basic cellular processes in a broad range of tissues. By using the appropriate Ca^{2+} indicator and detection methods, it is possible to define how individual cells or groups of cells tune Ca^{2+} signals to modulate physiological outputs. Since their introduction more than 30 years ago [6], synthetic Ca^{2+}-sensitive fluorescent indicator dyes have been widely used to investigate the molecular mechanisms that control cellular Ca^{2+} signals. Based on the spectral and Ca^{2+}-buffering characteristics of these dyes, investigators can measure fast changes in Ca^{2+} (e.g., action potentials), or use time-lapse imaging to determine changes in absolute Ca^{2+} levels. More recently, genetically encoded Ca^{2+} indicators (GECIs) have enabled measurement of Ca^{2+} signals in specific organelles such as the endoplasmic reticulum (ER) and mitochondria [1, 7], as well as Ca^{2+}_c changes of specific cells within a heterogeneous population (e.g., α-cells of the pancreatic islet [8]). Although we focus here on the use of dyes for these types of experiments, the described approaches are amenable to use with GECIs.

Accurate measurement of the V_m using patch clamp electrophysiology in β-cells requires intact cytosolic components that are lost using traditional whole-cell ruptured patch techniques. Therefore, it is necessary to use the perforated patch configuration, which preserves cytosolic elements required for regenerative action potential firing in β-cells. For this purpose, we include the pore-forming antifungal agent, amphotericin B [9], in the patch pipette solution, which causes perforations in the cellular membrane within the patch pipette tip. These perforations allow monovalent cations to equilibrate across the patch, permitting excellent recordings of β-cell electrical activity. In combination with Ca^{2+}_c measurements, it is possible to assess how changes in the β-cell V_m affect Ca^{2+} influx. For example, with pharmacological inhibitors of K^+ channels, it is possible to resolve Ca^{2+} influx due to single-action potentials [3]. These data allow the investigator to dissect the ion channels that coordinate β-cell action potential firing. Although VDCC activity is required for insulin secretion, β-cell Ca^{2+}_c levels

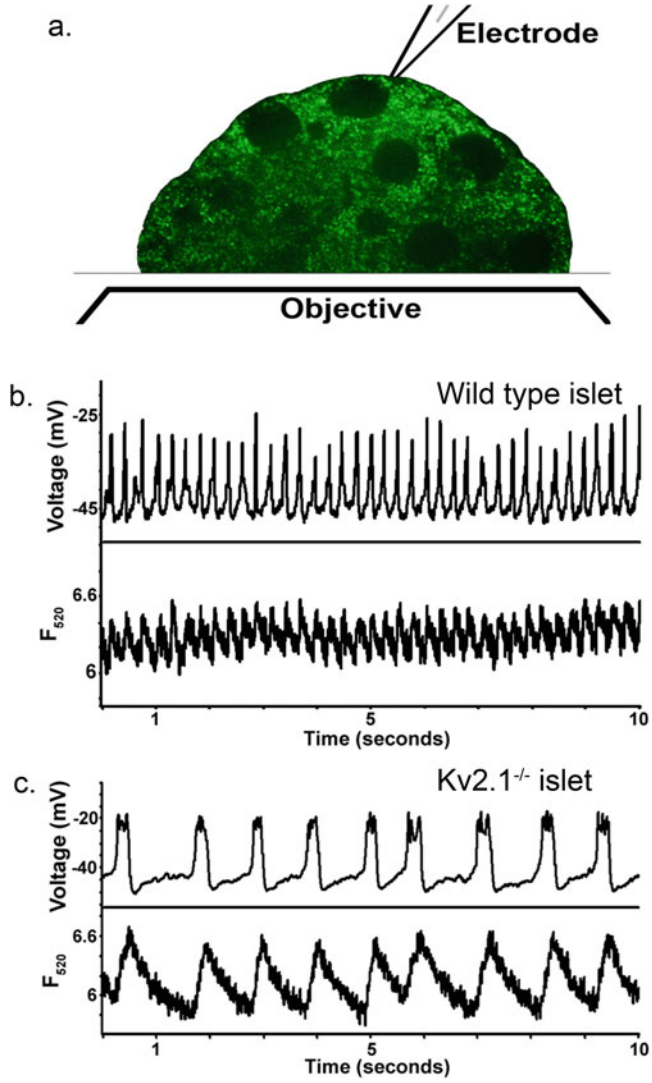

Fig. 1 Simultaneous monitoring of β-cell electrical activity and islet Ca^{2+} influx. (**a**) Representation of a Fluo-4-loaded islet attached to a glass coverslip, with an electrode recording the V_m of an islet cell in perforated-patch whole cell current clamp mode. The islet is exposed to constant 488 nm light through a 20× objective and the emission signal at 520 nm is monitored with a PMT and sampled at 10 kHz. The electrode is used to monitor electrical activity in whole cell perforated-patch current clamp mode at 20 kHz. (**b**) Representative recording of Ca^{2+} influx measured from the bottom of an intact C57Bl6 mouse islet simultaneously with a V_m recording of a β-cell on the top of the islet in response to the indicated glucose stimulation. (**c**) Representative recording of Ca^{2+} and V_m from a Kv2.1 knockout C57Bl6 mouse islet in response to the indicated glucose stimulation

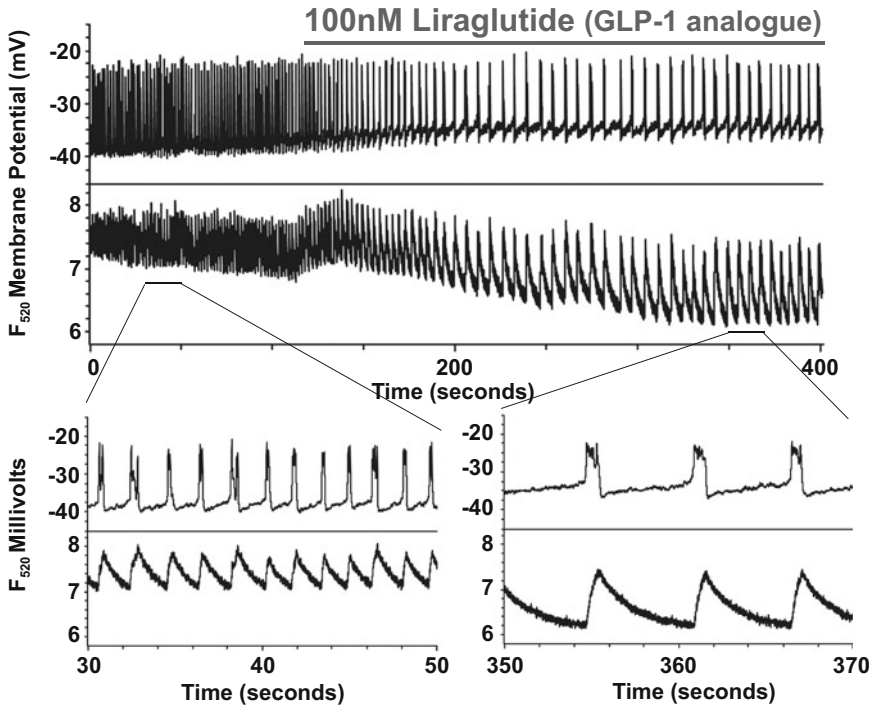

Fig. 2 Simultaneous monitoring of islet Ca^{2+} and V_m in response to GLP-1 receptor activation. Simultaneous monitoring of β-cell electrical activity (*top portion* of each panel) recorded from an intact whole islet in response to 200 μM tolbutamide and 2 mM glucose with (*black line*) and without 100 nM liraglutide (GLP-1 analogue), with fast-acquisition Ca^{2+} traces recorded from the entire islet (*lower portion* of each panel). The islets were loaded with Fluo-4AM and imaged at 10 kHz. *Inset lines* represent the section of the top tracings expanded below

are also influenced by Ca^{2+} release from intracellular stores, primarily the ER. Thus, simultaneous measurement of the V_m and $Ca^{2+}{}_c$ has also revealed important information about the mechanisms of β-cell Ca^{2+} influx [10]. Therefore, this technique permits examination of various stimuli that impact β-cell $Ca^{2+}{}_c$ with concomitant assessment of their effects on the V_m (*see* Figs. 1 and 2).

2 Materials

2.1 Islet Isolation

1. Islet isolation buffer (500 mL): 1× HBSS, divalent-free, 10 mM HEPES, 1 mM $MgCl_2$ (pH 7.4 with NaOH), (sterilize by autoclave); prior to use, add 1.25 mM $CaCl_2$, 5 mM glucose, and 0.2 mg/mL BSA (this forms modified islet buffer, MIB); MIB supplemented with 10% fetal bovine serum, 7.5 mL per pancreas.
2. Collagenase P solution: prepare 0.25–0.5 mg/mL collagenase P (collagenase strength varies by lot, thus optimal concentration must be determined experimentally) in cold MIB (without FBS), 10 mL per pancreas.

3. 5 mL syringe and needle (30 G × ½ in.).
4. Histopaque-1077, warmed to room temperature.
5. Serological pipettes (2 and 5 mL) and pipettor.
6. 15- and 50 mL conical centrifuge tubes.
7. Glass Pasteur pipettes, 230 mm (e.g., Wheaton #357335).
8. Water bath set to 37 °C.
9. Wrist-action shaker (e.g., Burrell Model 75).
10. Centrifuge capable of accommodating 15- and 50 mL Falcon-style centrifuge tubes (e.g., Eppendorf 5810R).
11. Falcon 60 mm petri dishes.
12. Inverted tissue culture microscope (e.g., Olympus CK2).
13. Adjustable volume micropipettes capable of pipetting 20, 200, and 1000 µL (e.g., Gilson Pipetman P20, P200, P1000).

2.2 Islet Culture

1. Poly-D-lysine coated 35 mm glass-bottom dishes (CellVis #D35–14-1.5-N).
2. 0.05% Trypsin-EDTA.
3. Versene solution.
4. 1.5 mL Eppendorf tubes.
5. Islet culture medium: RPMI 1640 supplemented with 15% fetal bovine serum (FBS), 100 IU/mL penicillin, and 100 mg/mL streptomycin.
6. Cell culture incubator (37 °C, 5% CO_2).

2.3 Imaging and Electrophysiology: Solutions

1. Krebs-Ringer-based buffer containing (in mM): 119 NaCl, 2.5 $CaCl_2$, 4.7 KCl, 25 HEPES, 1.2 $MgSO_4$, 1.2 KH_2PO_4, (pH 7.35 with NaOH); glucose added as needed.
2. Fluo-4AM (Molecular Probes), dissolved in DMSO (1 µg/µL).
3. Intracellular recording solution containing (in mM): 140 KCl, 5 HEPES, 1 EGTA, 0.5 $CaCl_2$, (pH 7.22 with KOH); supplemented with ~0.025 mg/mL amphotericin B.

2.4 Imaging and Electrophysiology: Equipment

1. An inverted microscope equipped with at least a 20× objective (e.g., Nikon Eclipse TE2000-U).
2. An object marker (e.g., Nikon MBW10020).
3. Borosilicate glass capillaries (e.g., World Precision Instruments #1B150F-4).
4. Micropipette puller (e.g., Sutter P-97).
5. 1 mL syringe (e.g., BD #309659).
6. Needle for filling patch pipettes (e.g., WPI #MF28).
7. Micromanipulator (e.g., Burleigh PCS-5000).

8. Patch clamp amplifier (e.g., Axon 200B).
9. Analog signal digitizer (e.g., Axon Digidata 1440).
10. Waveform generator (e.g., BK Precision Model 4045).
11. Wide-field fluorescence light source (e.g., Excelitas X-Cite 120Q).
12. Appropriate excitation/emission bandpass filters (e.g., 485/530 nm for Fluo-4).
13. Photomultiplier tube (PMT) equipped with apertures (e.g., PTI D-104 microscope photometer).
14. Data acquisition and analysis software (e.g., pCLAMP suite of software, GraphPad Prism).

2.5 Post-staining of Islet Cells

1. 1× Phosphate-buffered saline (PBS).
2. Paraformaldehyde, 4% in PBS.
3. Bovine serum albumin (BSA).
4. Normal donkey serum (NDS).
5. Triton X-100.
6. Primary antibodies: anti-insulin (e.g., Dako #A0564), anti-glucagon (e.g., Proteintech #15954), anti-somatostatin (e.g., Santa Cruz #D-20).
7. Secondary antibodies (e.g., Alexa Fluor 594-conjugated anti-guinea pig, Alexa Fluor 488-conjugated anti-rabbit, Alexa Fluor 647-conjugated anti-goat).

3 Methods

3.1 Islet Isolation

1. Distend pancreas from 6 to 10 week old mouse with 4 mL cold collagenase P solution [11].
2. Transfer pancreas into 6 mL of cold collagenase P solution in a 15 mL conical tube and shake at 37 °C for 10 min (*see* **Note 1**) followed by 2–5 vigorous shakes by hand.
3. Transfer digested pancreas suspension into a 50 mL conical tube filled with approximately 25 mL cold MIB.
4. Add cold MIB to bring the total volume to 50 mL and gently mix by inverting several times (*see* **Note 2**).
5. Centrifuge for 2 min at 150 × *g*, 25 °C.
6. Aspirate MIB, being careful not to disturb the pelleted tissue.
7. Repeat **steps 4–6**.
8. Suspend the digested pancreas pellet in 15 mL of cold MIB by triturating with a 5 mL serological pipette, and transfer to a 15 mL conical tube.

9. Centrifuge 2 min at 150 × *g*, 25 °C.
10. Aspirate MIB, being careful not to disturb the pelleted tissue.
11. Suspend the digested pancreas pellet in 7.5 mL of MIB supplemented with 10% FBS.
12. Carefully underlay the digested pancreas/MIB suspension with 5 mL of Histopaque-1077 (*see* **Note 3**) and centrifuge for 15 min at 450 × *g*, 25 °C.
13. Transfer Histopaque-1077 layer containing islets to a 50 mL conical tube.
14. Add 40 mL of cold MIB and gently mix by inverting several times.
15. Centrifuge for 1 min at 450 × *g*, 25 °C.
16. Aspirate MIB, being careful not to disturb the pelleted tissue.
17. Repeat **steps 14–16**.
18. Resuspend islets in 8 mL cold islet culture media and transfer to a 60 mm petri dish (*see* **Note 4**).
19. Transfer islets into a second 60 mm petri dish containing 8 mL islet culture media on ice using a P200 pipette and an inverted tissue culture microscope.
20. Disperse islets by gently rocking the petri dish then incubate at 37 °C, 5% CO_2 until ready to plate (*see* **Note 4**).

3.2 Islet Plating and Culture (Mouse or Human Islets)

3.2.1 Whole Islets

1. Under aseptic conditions, dilute 2 mg/mL poly-D-lysine stock to 80 μg/mL with sterile deionized H_2O (diH_2O) and add 100 μL to each 35 mm glass-bottom dish and incubate at room temperature for at least 2 h.
2. Wash glass-bottom dishes twice with diH_2O and keep dishes open in hood until dry.
3. Add 3 mL of pre-warmed (37 °C) islet culture media to each glass-bottom dish and transfer the desired number of islets into each dish using a P20 pipette (*see* **Note 5**).
4. Incubate islets at 37 °C, 5% CO_2 for 24–48 h prior to experimentation.

3.2.2 Islet Clusters and Single Cells

1. Prepare poly-D-lysine-coated 35 mm glass-bottom dishes as detailed in Subheading 3.2.1.
2. Transfer islets from the petri dish to a sterile 1.5 mL Eppendorf tube on ice using a P20 pipette.
3. Allow islets to settle to the bottom of the Eppendorf tube and carefully remove islet culture media.
4. Add 850 μL of Versene to the Eppendorf tube followed by 150 μL of 0.05% trypsin-EDTA.

5. Triturate islet suspension by pipetting up and down with a P1000 pipette approximately 20× to prepare islet clusters, or 30× to prepare single cells.
6. Centrifuge islet cell suspension 1.5 min at 250 × *g*, 25 °C.
7. Remove Versene/trypsin-EDTA solution and resuspend islet clusters/single cells in pre-warmed islet culture media.
8. Pipette 100–125 μL cell suspension into the middle of the glass-bottom dishes forming a liquid "bubble."
9. Incubate islet clusters/single cells at 37 °C, 5% CO_2 for 6–18 h to allow them to adhere to poly-D-lysine-coated surfaces.
10. Supplement with 3 mL of pre-warmed islet culture media and incubate at 37 °C, 5% CO_2.

3.3 Measurement of V_m and Intracellular Ca^{2+}: Loading with Ca^{2+} Dye

1. Load cells with 5 μM Fluo-4AM in 1 mL of islet culture media and incubate for 25 min at 37 °C, 5% CO_2 (*see* **Note 6**).
2. Wash twice with KRB supplemented with the desired glucose concentration (*see* **Note 7**).
3. After washing the cells, add approximately 2 mL of KRB to the plate.
4. Load the plate onto the microscope, and identify the desired cell(s) to record. Position the bath electrode, any perfusion lines, vacuum line, and PMT apertures (if equipped) to capture fluorescence signal from cell(s) to be recorded.
5. Proceed to patch clamp setup.

3.4 Patch Clamp Setup

1. Use a 1 mL syringe and MicroFil filament (WPI) to fill patch pipette with intracellular recording solution. Ensure there are no bubbles present in the pipette by grasping it between the thumb and forefinger and gently "flicking" the patch pipette.
2. Place the filled patch pipette in the electrode holder.
3. Apply positive pressure using an air-filled syringe attached to the pipette holder to minimize debris entering the patch pipette. Lower the patch pipette into the KRB bath and position over the cell to be recorded using the micromanipulator.
4. Adjust offset potential to zero.
5. Apply a test potential (e.g., a 5 mV voltage step at 10 Hz) to monitor the resistance of the patch pipette.
6. Using the micromanipulator, slowly guide the patch pipette toward the cell until contact is made with the plasma membrane, which is indicated by a sudden reduction in the amplitude of the square wave produced by the voltage step.
7. Rapidly release positive pressure on patch pipette and apply light negative pressure to facilitate seal formation. As the seal

between the patch pipette and the plasma membrane improves, the amplitude of the square wave will decrease.

8. Activate the external command function of the patch clamp amplifier to hold the command voltage at −80 mV and turn off the waveform generator used to apply the test potential.
9. Release negative pressure on patch electrode and monitor leak current until less than −15 pA.
10. Allow perforations to form for ~10 min.
11. Turn off the external command function and switch to current clamp mode to monitor cell V_m.
12. To assess the role of potassium channels on V_m and intracellular Ca^{2+} (see below), apply pharmacological agents targeting specific potassium channels in the bath solution by perfusion during the recording. Alternatively, the role of a specific potassium channel can be assessed by comparing islets from wild-type mice and islets from mice lacking the channel, overexpressing the channel, or expressing a mutant form of the channel.

3.5 Simultaneous Measurement of V_m and Intracellular Ca^{2+}

1. After successfully patching an electrically excitable cell, activate the fluorescence light source. If necessary, change the optical path on the microscope to direct the emitted fluorescence to the PMT.
2. Optimize the fluorescence light source and microscope apertures as well as PMT sensitivity to produce detectable signals with the minimal amount of fluorescence excitation light intensity required.
3. Begin recording protocol. Exemplary data that were obtained using this approach are provided in Fig. 2.

3.6 Post-staining of Islet Cells

1. After the completion of the experiment mark the region of the dish containing recorded cell(s) using a microscope object marker.
2. Add approximately 1 mL of ice-cold 4% PFA. Incubate for 30 min on ice.
3. Remove PFA, then wash cells twice with PBS (*see* **Note 8**).
4. Prepare protein blocking solution in PBS: 0.2% w/v BSA, 2% v/v NDS, 0.05% v/v Triton X-100.
5. Remove any remaining PBS and then apply the blocking solution to the cells and incubate for at least 1 h at room temperature. No wash step is necessary after blocking.
6. Prepare primary antibody solution in PBS: 0.2% w/v BSA, 1% v/v NDS, 0.1% Triton X-100 with primary antibodies diluted as follows (insulin: 1:400, glucagon: 1:400, somatostatin: 1:250).

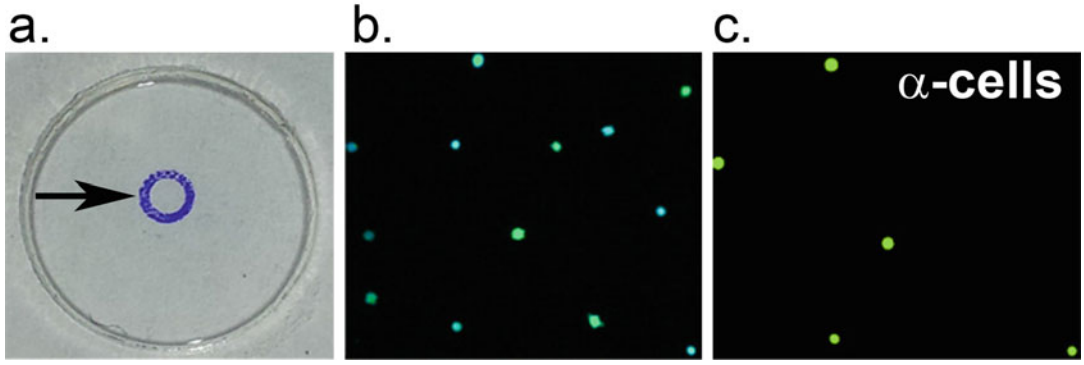

Fig. 3 Identification of the human islet cell type recorded or imaged. The data show a typical experiment where the plate is marked and stained for glucagon to identify imaged alpha-cells. (**a**) The MatTek plate is marked with a Nikon Object Marker leaving a *purple ink circle* on the dish representing the field of view (*arrow*), marks are also placed on one side of the *X* and *Y* axes for orientation. (**b**) The cells (Fura-2 fluorescence) are fixed in 4% paraformaldehyde and stained for islet hormones, panel (**c**) shows glucagon staining of the cells in panel (**b**)

7. Remove the blocking solution and then apply the primary antibody solution to the cells. Incubate in a humidity chamber overnight at 4 °C.
8. Remove the primary antibody solution and then wash with PBS. Leave PBS on cells for 10 min. Aspirate PBS and repeat this wash step.
9. Remove PBS and add the secondary antibody solution to the cells: 1% v/v NDS, with 1:500 dilutions of secondary antibodies (e.g., Alexa Fluor 594-conjugated anti-guinea pig, Alexa Fluor 488-conjugated anti-rabbit, Alexa Fluor 647-conjugated anti-goat); incubate between one and two hours at room temperature.
10. Remove the secondary antibody solution and wash with PBS. Leave PBS on cells for 10 min. Aspirate PBS and repeat this wash step. While not required, further incubation of the cells overnight in PBS at 4 °C helps to reduce nonspecific staining.
11. Proceed to imaging/identification of stained cells. Representative staining is shown in Fig. 3.

4 Notes

1. Shaking can be performed by hand; however, using a wrist-action shaker provides more consistency in islet preparations. At the end of shaking, 2–5 vigorous shakes by hand are usually needed to dissociate any remaining pieces of pancreas.
2. Connective tissue and fat are resistant to collagenase P digestion, and have a tendency to "catch" islets and acinar cells

during the isolation process. To improve yield and purity of islet preparations, it is helpful to remove floating fat from the suspension with clean forceps.

3. Histopaque-1077 and islet isolation buffer with 10% FBS should be at room temperature. Underlay Histopaque-1077 by placing a glass Pasteur pipette into the digested pancreas suspension and adding Histopaque-1077 through the Pasteur pipette with a 2 mL serological pipette. Sometimes, it is necessary to briefly lift the Pasteur pipette to liberate air bubbles that prevent the Histopaque from flowing. Ensure that the MIB/Histopaque interface is minimally disrupted when removing the Pasteur pipette and transferring to the centrifuge.
4. "Picking" islets in cold culture media will minimize clustering of islets and acinar tissue, improving cleanliness of the preparation. Islets should not be stored under these conditions for more than a few hours as they will begin to aggregate. If the islets must be stored for a longer period of time supplement islet culture media with 0.5 mg/mL bovine serum albumin to minimize aggregation.
5. Slowly drop islets into the dish with a P20 pipette to ensure that they form a tight cluster.
6. Transfer 1 mL of islet culture media from dish to a 1.5 mL Eppendorf tube, add 5 μL 1 mM Fluo-4 AM stock to media, remove the remaining media from the dish, and replace with media containing Fluo-4AM.
7. The glucose concentration present in the KRB wash will change depending on the type of experiment being performed. However, for β-cells, incubation and starting experiments in a stimulatory glucose concentration (e.g., 11 mM glucose) facilitates obtaining a GΩ seal.
8. Be very gentle when exchanging liquids in the plate, as cells have a tendency to detach from or relocate on the coverslip if fluid exchange is too forceful. Another important point is to avoid exposing the cells to air during the staining process— a small amount of liquid should remain on the cells when exchanging solutions.

Acknowledgments

Work in the laboratory of D.A.J. has been supported by National Institutes of Health Grants K01DK081666, R01DK097392, Vanderbilt DRTC Pilot and Feasibility Grant P60DK20593, ADA grant 1-17-IBS-024 (D.A.J.).; Vanderbilt METP grant 5T32DK07563, National Institutes of Health Grant 1F31DK109625 (N.C.V.); Vanderbilt ITED grant

T32DK101003 (M.T.D.). Previous work in the Philipson lab was also supported by R01DK092616-01A1 (P.I.M.W. Roe) and P30DK020595 (G.I. Bell) and R01DK48494 (L.H. Philipson).

References

1. Gilon P, Chae HY, Rutter GA, Ravier MA (2014) Calcium signaling in pancreatic beta-cells in health and in Type 2 diabetes. Cell Calcium 56(5):340–361. doi:10.1016/j.ceca.2014.09.001
2. Jacobson DA, Kuznetsov A, Lopez JP, Kash S, Ammala CE, Philipson LH (2007) Kv2.1 ablation alters glucose-induced islet electrical activity, enhancing insulin secretion. Cell Metab 6 (3):229–235. doi:10.1016/j.cmet.2007.07.010
3. Jacobson DA, Mendez F, Thompson M, Torres J, Cochet O, Philipson LH (2010) Calcium-activated and voltage-gated potassium channels of the pancreatic islet impart distinct and complementary roles during secretagogue induced electrical responses. J Physiol 588(Pt 18):3525–3537. doi:10.1113/jphysiol.2010.190207
4. Dadi PK, Vierra NC, Jacobson DA (2014) Pancreatic beta-cell-specific ablation of TASK-1 channels augments glucose-stimulated calcium entry and insulin secretion, improving glucose tolerance. Endocrinology 155 (10):3757–3768. doi:10.1210/en.2013-2051
5. Vierra NC, Dadi PK, Jeong I, Dickerson M, Powell DR, Jacobson DA (2015) The type-2-diabetes-associated K+ channel TALK-1 modulates beta-cell electrical excitability, 2nd-phase insulin secretion, and glucose homeostasis. Diabetes. doi:10.2337/db15-0280
6. Tsien RY, Pozzan T, Rink TJ (1982) T-Cell mitogens cause early changes in cytoplasmic free Ca2+ and membrane potential in lymphocytes. Nature 295(5844):68–71
7. Suzuki J, Kanemaru K, Ishii K, Ohkura M, Okubo Y, Iino M (2014) Imaging intraorganellar Ca2+ at subcellular resolution using CEPIA. Nat Commun 5:4153. doi:10.1038/ncomms5153
8. Dadi PK, Luo B, Vierra NC, Jacobson DA (2015) TASK-1 potassium channels limit pancreatic alpha-cell calcium influx and glucagon secretion. Mol Endocrinol:me20141321. doi:10.1210/me.2014-1321
9. Rae J, Cooper K, Gates P, Watsky M (1991) Low access resistance perforated patch recordings using amphotericin B. J Neurosci Methods 37(1):15–26
10. Beauvois MC, Merezak C, Jonas JC, Ravier MA, Henquin JC, Gilon P (2006) Glucose-induced mixed [Ca2+]c oscillations in mouse beta-cells are controlled by the membrane potential and the SERCA3 Ca2+−ATPase of the endoplasmic reticulum. Am J Physiol Cell Physiol 290(6):C1503–C1511. doi:10.1152/ajpcell.00400.2005
11. Roe MW, Philipson LH, Frangakis CJ, Kuznetsov A, Mertz RJ, Lancaster ME, Spencer B, Worley JF 3rd, Dukes ID (1994) Defective glucose-dependent endoplasmic reticulum Ca2+ sequestration in diabetic mouse islets of Langerhans. J Biol Chem 269 (28):18279–18282

Chapter 8

Methods for Characterizing Disease-Associated ATP-Sensitive Potassium Channel Mutations

Balamurugan Kandasamy and Show-Ling Shyng

Abstract

The ATP-sensitive potassium (K_{ATP}) channel formed by the inwardly rectifying potassium channel Kir6.2 and the sulfonylurea receptor 1 (SUR1) plays a key role in regulating insulin secretion. Genetic mutations in *KCNJ11* or *ABCC8* which encode Kir6.2 and SUR1 respectively are major causes of insulin secretion disorders: those causing loss of channel function lead to congenital hyperinsulinism, whereas those causing gain of channel function result in neonatal diabetes and in some cases developmental delay, epilepsy, and neonatal diabetes, referred to as the DEND syndrome. Understanding how disease mutations disrupt channel expression and function is important for disease diagnosis and for devising effective therapeutic strategies. Here, we describe a workflow including several biochemical and functional assays to assess the effects of mutations on channel expression and function.

Key words K_{ATP} channel, Sulfonylurea receptor 1, Inwardly rectifying potassium channel Kir6.2, Congenital hyperinsulinism, Neonatal diabetes, DEND syndrome, Channelopathy

1 Introduction

Pancreatic β-cells secrete insulin in response to increased plasma glucose concentrations to maintain glucose homeostasis. A central player in this process is a potassium channel called the ATP-sensitive potassium (K_{ATP}) channel which couples glucose metabolism to β-cell membrane potential [1]. When glucose levels rise, the increased glucose metabolism in β-cells leads to an increased intracellular ATP to ADP ratio [1–3]. As ATP inhibits while MgADP stimulates K_{ATP} channels, the increased ATP to ADP ratio favors channel closure, resulting in membrane depolarization. Membrane depolarization then activates voltage-gated calcium channels, allowing for Ca^{2+} influx to trigger exocytosis of insulin granules. Conversely, when glucose levels fall, the reduced ATP to ADP ratio favors K_{ATP} channel opening, which keeps β-cell membrane potential in a hyperpolarized resting state to prevent insulin secretion.

Show-Ling Shyng et al. (eds.), *Potassium Channels: Methods and Protocols*, Methods in Molecular Biology, vol. 1684,
DOI 10.1007/978-1-4939-7362-0_8,

The K_{ATP} channel is an octameric complex composed of four inwardly rectifying potassium channel Kir6.2 subunits and four sulfonylurea receptor 1 (SUR1) subunits [4–6]. Kir6.2 and SUR1 are encoded by the *KCNJ11* and *ABCC8* genes, respectively [7]. Loss-of-function (or inactivating) mutations in *KCNJ11* or *ABCC8* underlie congenital hyperinsulinism, an infant/childhood disease characterized by persistent insulin secretion despite severe hypoglycemia [1, 8, 9]. In mild cases with residual channel function, patients may be successfully treated with diazoxide—a K_{ATP} channel opener. However, in severe cases patients require surgical removal of the pancreas to prevent life-threatening hypoglycemia. By contrast, gain-of-function (or activating) mutations in *KCNJ11* or *ABCC8* cause neonatal diabetes, characterized by insufficient insulin secretion and hyperglycemia [8, 10]. Some activating mutations also cause *d*evelopmental delay and *e*pilepsy in addition to *n*eonatal *d*iabetes, known as the DEND syndrome because these channels are also expressed in the central nervous system [8]. Sulfonylureas, drugs that bind and inhibit K_{ATP} channels to stimulate insulin secretion, can be used to treat patients with activating mutations [8, 11]. In patients harboring mutations that cause severe channel defects, however, sulfonylureas are ineffective. Biochemical and functional studies of disease-associated K_{ATP} mutations are crucial for patients and clinicians as these studies yield information that is important for disease diagnosis and clinical management. Currently, clinical endocrinologists worldwide who directly care for patients with K_{ATP} channel mutations can only acquire such information by collaborating with a few academic laboratories that carry out K_{ATP} channel studies. Given the continuous demand for such studies, it is important to make the methods easily accessible. These methods are also useful for those interested in K_{ATP} channel structure-function and may be applied to study disease mutations in other potassium channels.

To study K_{ATP} channel defects caused by disease mutations, recombinant mutant channels are expressed in mammalian cell lines such as COS or HEK293 by transient transfection. These heterologous expression systems afford a convenient experimental platform for genetic manipulations; moreover, they are devoid of endogenous channels that might confound data interpretation. Mutant channel proteins can be expressed either as a homogeneous population to mimic the homozygous state or co-expressed with the wild-type protein at 1:1 ratio to simulate the heterozygous state.

Mutations can disrupt channel function by causing abnormal channel expression, gating, or both. Several methods have been developed to study mutant channel function and expression. Figure 1 presents a workflow we use to study disease mutations identified in patients with congenital hyperinsulinism or neonatal diabetes/DEND syndrome. The first step involves s tracer ion

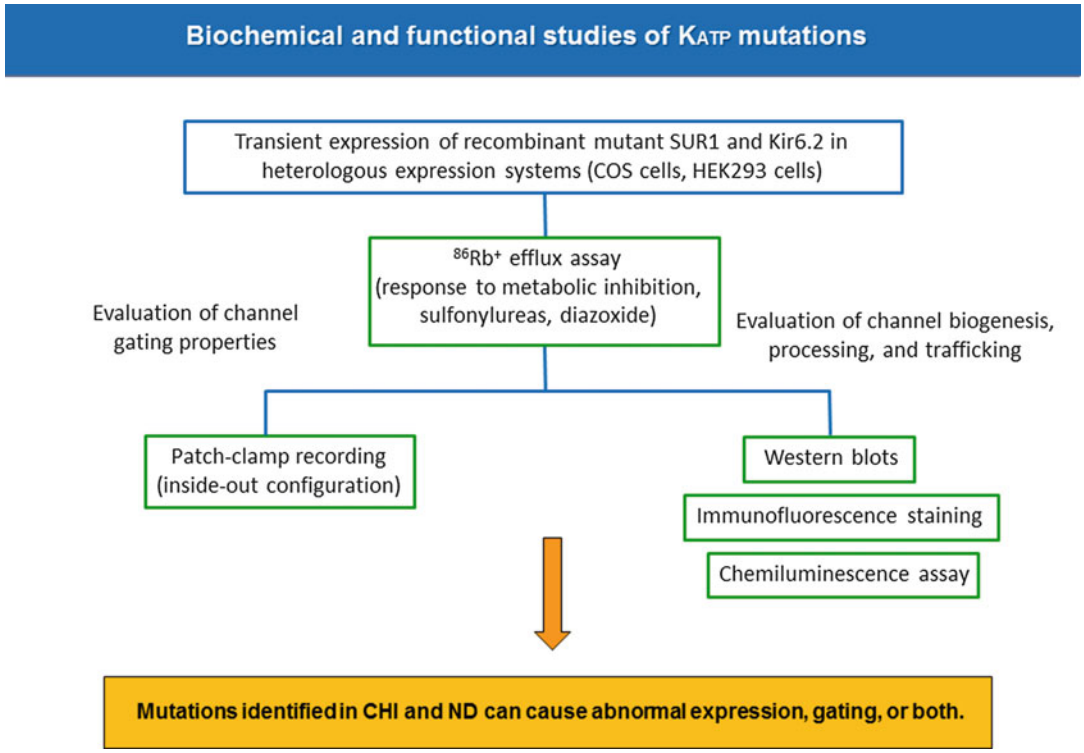

Fig. 1 Workflow of studying the effects of disease mutations on K_{ATP} channel expression and function

efflux assay (using $^{86}Rb^+$ as a substitute for the physiological conduction ion K^+) which is suitable for assessing mutant channel activity in intact cells [12, 13]. For congenital hyperinsulinism mutations, we look for channel activity in response to metabolic inhibition. Metabolic inhibition lowers the intracellular ATP/ADP ratio and activates K_{ATP} channels. Reduced $^{86}Rb^+$ efflux therefore indicates loss of channel function and a causal role of a mutation in congenital hyperinsulinism. For neonatal diabetes/DEND mutations, we look for basal channel activity without metabolic inhibition. Increased basal $^{86}Rb^+$ efflux is indicative of a gain-of-function mutation. This assay is also used to test whether mutant channels respond to pharmacological agents such as the K_{ATP} channel opener diazoxide or the inhibitors sulfonylureas such as tolbutamide or glibenclamide. The responsiveness of a given mutation to pharmacological agents will suggest effective treatments for patients carrying the mutation.

Once it is determined that a mutation causes loss or gain of channel function, three complementary methods are used to evaluate whether a mutation affects channel maturation and surface expression. Western blots of SUR1 and Kir6.2 inform steady-state levels of the two proteins [14]. Reduced protein levels suggest possible rapid degradation due to misfolding. SUR1 contains two

N-linked glycosylation sites and manifests as two bands in Western blots: a core-glycosylated lower band that corresponds to the immature SUR1 in the endoplasmic reticulum (ER), and a complex-glycosylated upper band corresponding to the mature SUR1 that has exited the ER and reached medial Golgi where complex glycosylation occurs. Since the ability of SUR1 to exit the ER is dependent on successful assembly with Kir6.2 into a channel complex [15], the relative abundance of the mature and immature SUR1 bands can be used as a readout for channel biogenesis efficiency. The abundance of the upper band, in general, correlates with surface channel expression; however, it is not a direct measure as mature SUR1 is present not only in the plasma membrane but also in other post-*Golgi* intracellular secretory and endocytic membrane compartments. To directly visualize surface expression, immunofluorescent staining experiments are performed. Currently, there are no antibodies for SUR1 or Kir6.2 that recognize extracellular epitopes to allow for staining of K_{ATP} channels present in the plasma membrane. We therefore use a SUR1 variant in which a FLAG-epitope (DYKDDDDK) is inserted at the extracellular N-terminus of SUR1 [14]. By staining for the FLAG-epitope using commercially available anti-FLAG antibodies in non-permeabilized cells, surface SUR1, hence surface channels can be visualized. Although immunofluorescence staining allows visualization of surface channels in individual cells, it is not suitable for quantitative measurements of channel surface expression levels considering that in transient transfection experiments protein expression can vary widely from cell to cell. To quantify surface expression of K_{ATP} channels, we use a chemiluminescence assay whereby the FLAG-epitope of surface SUR1 is labeled by anti-FLAG antibodies followed by a secondary antibody conjugated to the enzyme horseradish peroxidase which when incubated with the luminol substrate gives out chemiluminescence signals that can be quantified using a liminometer [14].

For mutants that are expressed at the cell surface, electrophysiological recordings are performed to assess how mutations impact channel response to physiological and pharmacological ligands using the inside-out patch configuration [14]. Using this configuration, solutions bathing the cytosolic face of the channel can be precisely controlled and channel response to various ligands easily monitored and quantified. Typically, channel response to ATP and MgADP is monitored. For congenital hyperinsulinism-associated mutations, diazoxide response is tested which will help determine whether a patient will respond to diazoxide treatment. For neonatal diabetes-associated mutations, glibenclamide response will be tested to determine whether sulfonylurea therapy will be effective.

In the following sections, we provide detailed protocols for the methods outlined above, including the ^{86}Rb efflux assay, Western blot of K_{ATP} channel proteins, immunofluorescence staining of surface K_{ATP} channels, surface chemiluminescence assay, and inside-out patch-clamp recording.

2 Materials

Materials for cell culture and transfection are the same for all the methods. They are described at the beginning of this section.

2.1 Cell Culture

1. COSm6 cells (*see* **Note 1**).
2. Dulbecco's Modified Eagles Medium (DMEM, high glucose) supplemented with 10% fetal bovine serum and 100 U/mL penicillin/streptomycin.
3. 0.25% trypsin-EDTA.
4. Tissue culture ware: T25 culture flasks, 6-well or 12-well tissue culture plates, 35 mm tissue culture dishes for chemiluminescence assays, glass coverslips (22 × 22 mm or 18 mm circular) for plating cells for immunofluorescence staining and patch-clamp recording (*see* **Note 2**).

2.2 Transfection

1. Plasmids for transfection: Kir6.2 and SUR1 cDNAs in mammalian expression vectors (*see* **Note 3**). For patch-clamp recording, a plasmid for expressing enhanced green fluorescent protein (EGFP) is also needed.
2. Transfection reagents: Opti-MEM, FuGENE®6 (Promega) (*see* **Note 4**).

2.3 $^{86}Rb^{+}$ Efflux Assay

1. Ringer's solution: 118 mM NaCl, 2.5 mM $CaCl_2$, 1.2 mM KH_2PO_4, 4.7 mM KCl, 25 mM $NaHCO_3$, 1.2 mM $MgSO_4$, 10 mM HEPES (sodium salt), pH 7.4.
2. Metabolic inhibitors: 2-deoxy-D-glucose, oligomycin (25 mg/mL stock in DMSO).
3. ^{86}RbCl (*see* **Note 5**).
4. Cell lysis solution: Ringer's solution + 1% sodium dodecyl sulfate (SDS).
5. Scintillation counting: scintillation vials, scintillation cocktail, liquid scintillation counter.

2.4 Western Blotting

1. Cell lysis buffer: 50 mM Tris-HCl, 2 mM EDTA, 2 mM EGTA, 100 mM NaCl, 1% Triton-X-100, pH 7.4, with protease inhibitors (e.g., cOmplete™ EDTA-free protease inhibitor cocktail tablets from Roche).

2. Polyacrylamide gels (8% for SUR1 and 12% for Kir6.2; alternatively use 8–12% gradient gels) for protein electrophoresis.
3. 10× Gel running buffer: 248 mM Tris-base, 1.91 M glycine, and 1% SDS.
4. 4× Sample loading buffer: 200 mM dithiothreitol, 12% (w/v) SDS, 40% glycerol (100%), 250 mM Tris-base (pH 6.8), and 0.05% Bromophenol blue (w/v). Aliquot and store at −20 °C. Add 10% 2-mercaptoethanol just before use.
5. Nitrocellulose membrane.
6. Western blot transfer buffer: 3 mM Na_2CO_3, 1 mM $NaHCO_3$, 10% methanol.
7. Tris-buffered saline (TBS): 50 mM Tris-Cl, 150 mM NaCl, pH 7.5.
8. Tween TBS (TTBS): 0.1% Tween in TBS.
9. Blocking buffer: 5% nonfat dry milk in TBS.
10. Primary antibody diluted to desired concentrations in the blocking buffer (*see* **Note 6**).
11. Secondary antibody: HRP (horseradish peroxidase)-conjugated secondary antibodies of appropriate species diluted to desired concentrations in the blocking buffer.
12. SuperSignal West Femto Maximum Sensitivity substrate from Thermo scientific.

2.5 Surface Immunofluorescence Staining of K_{ATP} Channels

1. Ice-cold PBS.
2. Anti-FLAG antibody 1:500 dilution in Opti-MEM (~10 μg/mL) for staining FLAG-tagged SUR1 (*see* **Note 7**).
3. Washing solution (0.1% BSA in ice-cold PBS).
4. Methanol (−20 °C) for fixing cells.
5. Blocking buffer (0.1% BSA in PBS with 1% normal goat serum).
6. Secondary antibody (fluorophore-conjugated goat anti-mouse IgG) diluted to desired concentrations in the blocking buffer.
7. Mounting medium containing DAPI to counterstain the nuclei.
8. Glass slides for mounting coverslips.
9. Confocal microscope or regular fluorescence microscope.

2.6 Chemiluminescence Assays

1. Freshly prepared 2% paraformaldehyde (*see* **Note 8**).
2. Phosphate-buffered saline (PBS): 137 mM NaCl, 2.7 mM KCl, 10 mM Na_2HPO_4, 1.8 mM KH_2PO_4, pH 7.4.
3. Blocking solution: 0.1% bovine serum albumin (BSA) in PBS.

4. M2 anti-FLAG primary antibody diluted in blocking solution to a final concentration of 10 μg/mL.
5. HRP-conjugated goat anti mouse IgG secondary antibody (1:1000).
6. Wash solution: 0.1% bovine serum albumin (BSA) in PBS.
7. Luminometer that can accommodate a 35 mm tissue culture dish (e.g., from Turner BioSystem TD-20/20).

2.7 Inside-Out Patch-Clamp Recording

1. Kint solution: 140 mM KCl, 10 mM K-HEPES, and 1 mM K-EGTA adjust pH to ~7.2 using 5 N KOH (*see* **Note 9**).
2. 100 mM ATP (potassium salt) and ADP (potassium salt) stock solution in Kint (*see* **Note 10**).
3. 300 mM diazoxide stock solution in DMSO.
4. 300 mM tolbutamide stock solution in DMSO.
5. 1 mM glibenclamide stock solution in DMSO.
6. Glass pipettes for patch-clamp recording (*see* **Note 11**).
7. Pipette puller (e.g., P-97 Flaming/Brown micropipette puller from Sutter Instrument).
8. Electrophysiology rig: air table, inverted fluorescent microscope, perfusion system, micromanipulator, amplifier, data digitizer, and a computer.

3 Methods

The procedures for cell culture and transfection are similar for all methods (also *see* Chapter 5 by Devaraneni et al.) and will be described at the beginning of this section.
All tissue culture media and solutions are pre-sterilized, stored at 4 °C, and pre-warmed to 37 °C prior to use.

3.1 Cell Culture

1. Culture COSm6 cells in DMEM, 10% FBS, 100 U/mL penicillin/streptomycin in T25 tissue culture flasks at 37 °C, 5.0% CO_2. Passage cells every 3–4 days at ~1:10 dilution from a confluent flask for routine maintenance.
2. Seed cells onto 35 mm dishes (for chemiluminescence assays), or 6- or 12-well plates (for Rb efflux, immunofluorescence staining, or electrophysiology) at ~1:8–1:10 dilution from a confluent T25 flask such that the cells will be ~70% confluent the next day ready for transfection.

3.2 Transfection

1. For each 35 mm dish or 6-well plate well, set up a sterile Eppendorf tube, add 50 μL of Opti-MEM and 3 μL FuGENE®6 and mix by pipetting up and down a few times, set aside.

2. Set up another tube and add 50 μL OptiMEM plus ~1 μg total of SUR1 and Kir6.2 plasmids at ~1:1 molar ratio, mix (*see* **Note 12**). To transfect cells for patch-clamp recording, add ~0.1 μg EGFP plasmid to the DNA mixture.
3. Combine the FuGENE®6 mixture and the DNA mixture, mix well by pipetting up and down a few times, and incubate at room temperature (RT) for 20–30 min. If using a 12-well plate, cut down the reagents in **steps 1** and **2** by half for each well.
4. Add mixture dropwise to cells, rocking the plate gently to ensure equal distribution of transfection mixture, and incubate at 37 °C, 5.0% CO_2 until cells are ready for experiments.

3.3 Rb^{86} Efflux Assay

The volumes of various solutions stated in the steps below are for 12-well plates. If using 6-well plates, double the volume.

1. Twenty-four to 36 h post transfection, load cells with radioactive ^{86}Rb. First, add ^{86}Rb to the tube of pre-warmed medium (~0.05 μCi ^{86}Rb in 1 mL medium/well) and mix. Then aspirate off the medium from the cells, and replace with the ^{86}Rb-containing medium. Incubate cells overnight in a tissue culture incubator that has a lead shield and place cells behind the shield (*see* **Note 13**).
2. Next day, prepare Ringer solution containing metabolic inhibitors (1 mM 2-deoxy-D-glucose and 2.5 μg/mL oligomycin, referred to as "MI"). For each well, prepare ~8 mL Ringers with metabolic inhibitors, so make enough for the entire experiment.
3. Pipette Ringer's + MI into a tube (1 mL/well), and add ^{86}Rb to the tube (~0.05 μCi/well).
4. Remove the radioactive ^{86}Rb-containing medium in the well, and rinse once with Ringer's solution, then add fresh Ringer's + MI + ^{86}Rb, and let it sit at room temperature behind a lead shield for 30 min (*see* **Note 14**). This will be the MI preincubation.
5. At the end of the 30 min incubation, remove the radioactive medium, rinse cells quickly 2× with Ringer's + MI.
6. Carefully remove all wash solution, and add 0.5 mL Ringer's + MI to each well for efflux measurement. Remove efflux solutions at time points 2.5, 5, 7.5, 15, 25, 40 min (these are cumulative time points) and place into a scintillation vial and add fresh 0.5 mL Ringer's + MI for the next time point (*see* **Note 15**).
7. After collecting the 40 min time point efflux solution, add 0.5 mL Ringer's + 1% SDS to lyse cells.
8. Collect cell lysate and place in a scintillation vial (*see* **Note 16**).

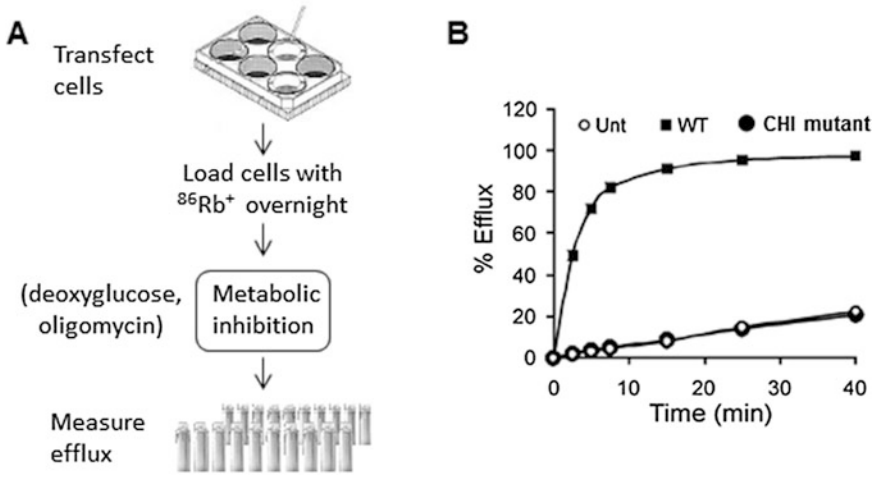

Fig. 2 The ^{86}Rb efflux assay. (**a**) Schematic showing the main steps involved in the ^{86}Rb efflux assay. (**b**) An example of ^{86}Rb efflux plot showing % efflux over a period of 40 min (min) from untransfected cells (Unt), which serves as a negative control; cells transfected with WT K_{ATP} channels (WT), which serves as a positive control; and cells transfected with a mutant channel identified in congenital hyperinsulinism (CHI mutant). The CHI mutant shows efflux levels similar to untransfected cells (note the *large black circles* for the CHI mutant are behind the Unt *open circles*). The loss of function indicates a causal role of the mutation in the disease

9. To each vial, add 3 mL scintillation counting cocktail, put the cap on tight, shake well to mix, and count in a scintillation counter.
10. To plot the results, add all the counts from all time points plus the counts from the cell lysate. This is the total ^{86}Rb present at the start of the efflux experiment. Divide the counts from the first time point by the total counts times 100%, this gives you the percent efflux for the first time point. For subsequent time points, add counts from a time point to earlier time points and divide that by the total counts and times 100%. This gives you the cumulative percent efflux up to that time point. For wild-type channels, we typically observe 80–90% efflux at the end of the 40-min time point, in contrast to ~10–15% efflux in untransfected control cells (*see* Fig. 2). The experimental conditions can be modified to measure efflux through channels under different metabolic conditions or in response to drugs (*see* Subheading 1).

3.4 Western Blotting

Western blotting protocols for SUR1 and Kir6.2 are similar to those described in Chapter 3 by Ruan and Chen. The steps described below use cells transfected in 12-well plates.

1. Harvest cells 36–48 h post-transfection by washing cells 2× with cold PBS and lyse in 125 μL lysis buffer on ice.
2. Mix ~15–30 μg of protein sample with 4× sample loading buffer such that the final sample loading buffer concentration is 1× and

place in 37 °C heat block for 10 min (*see* **Note 17**). Load protein samples along with a prestained standard protein marker.

3. Electrophorese at 15 mA until samples entered into the separating gel and then increase current to 20 mA until the dye front reaches the bottom of the gel.
4. Carefully cut and remove the stacking gel and rinse the gel with deionized water and transfer to a container with transfer buffer.
5. Equilibrate the nitrocellulose membrane, filter paper, and fiber pads in transfer buffer for 10–15 min before preparing the gel sandwich.
6. Place the cassette with the gray side down and assemble prewetted fiber pad, filter paper, equilibrated gel, nitrocellulose membrane, filter paper, and final fiber pad following standard Western blot assembly steps for protein transfer.
7. Close the cassette firmly, being careful not to move or slide the gel and filter paper sandwich. Place the cassette in a module.
8. Put ice pack and add a stir bar to help maintain even buffer temperature and ion distribution in the tank.
9. Put on the lid and start transfer at 50 V for 135 min or overnight at 15 V in a 4 °C cold room.
10. After transfer carefully disassemble the cassette and wash membrane 2× with TBS (5 min each) to remove all residual methanol in the transfer buffer.
11. Block membrane in 5% nonfat dry milk in TBS for 1–2 h at room temperature on a shaker.
12. Incubate with appropriate primary antibody solutions (*see* **Note 6**) on a shaker overnight at 4 °C or 1 h at room temperature.
13. Wash the membrane 3× with TTBS (10 min each).
14. Incubate with appropriate HRP-conjugated secondary antibody solutions for 1 h at room temperature on a shaker.
15. Wash the membrane 3× with TTBS (10 min each).
16. Mix 1:1 dilution of ECL A and B solution and develop the membrane for at least 30 s.
17. Detect bands in chemiluminescence setting on Fluorchem E (from ProteinSimple) or equivalent gel documentation imaging systems. Examples of Western blots of wild-type and congenital hyperinsulinism-causing mutant SUR1 or Kir6.2 are shown in Fig. 3.

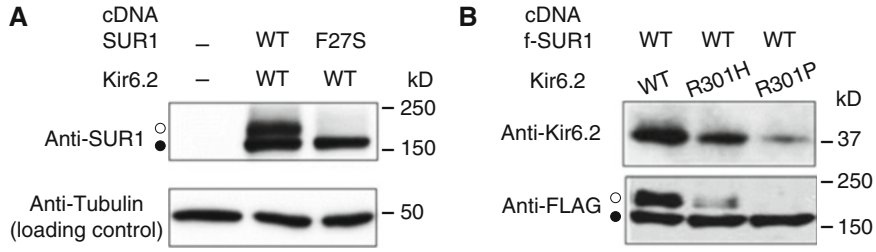

Fig. 3 Western blotting of K_{ATP} channel proteins. (**a**) COSm6 cells were transfected with human SUR1 and Kir6.2 cDNAs and subjected to Western blotting analysis. The *top blot* shows SUR1 protein probed with antibody raised against the C-terminus of hamster SUR1 (*see* **Note 6**). The *open circle* indicates the complex-glycosylated, mature band and the *solid circle* indicates the core-glycosylated immature band. The *lower blot* shows tubulin signals probed with anti-tubulin antibody and serves as loading controls. (**b**) An example of cells transfected with cDNAs encoding WT or mutant Kir6.2 identified in congenital hyperinsulinism (R301H or R301P) along with WT SUR1 that carries a FLAG-tag at the N-terminus of SUR1 (f-SUR1). Kir6.2 (*top blot*) and f-SUR1 (*bottom blot*) were detected using anti-Kir6.2 and anti-FLAG antibodies respectively (*see* **Note 6**). Both R301H and R301P mutant Kir6.2 show reduced protein levels and also reduced maturation of co-transfected f-SUR1, indicative of channel processing and trafficking defects. Figure panels **a** and **b** are modified from [18] and [19], with permission from authors

3.5 Surface Immunofluorescence Staining

The following steps are for cells transfected in 12-well plates and staining performed on cells replated onto 18 mm circular coverslips (*see* **Note 2**).

1. Clean and sterilize 18 mm circular coverslips for replating cells for staining.
   - Place coverslips one by one into a beaker and rinse with distilled water by swirling.
   - Pour out water and replace with 70% ethanol, swirl a few times, and let it sit for ~1 h.
   - Pour out 70% ethanol and replace with 100% ethanol, enough to cover all coverslips.
   - Flame each coverslip using a Benson burner briefly in a tissue culture hood and place dried coverslips into a well of a 12-well plate.
   - Leave the plates containing the coverslips under UV with the covers off for 30 min to sterilize.
2. Split transfected cells onto coverslips ~24 h post transfection at ~1:4 dilution (*see* **Note 18**). Place cells on ice and wash twice with ice-cold PBS.
3. Incubate with 10 μg/mL (~1:500 dilution) anti-FLAG antibody in OptiMEM supplemented with 0.1% BSA at 4 °C for 1 h (*see* **Note 19**).
4. Wash the cells 2× with ice-cold PBS/0.1%BSA.

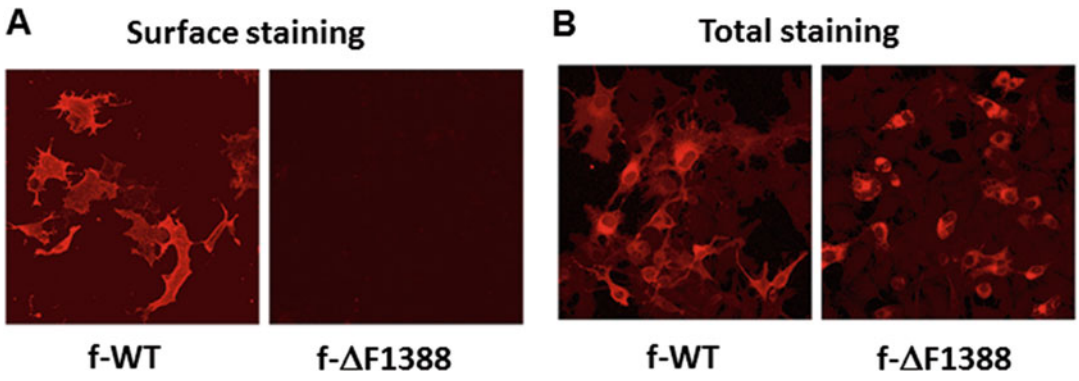

Fig. 4 Immunofluorescence staining of surface and total K_{ATP} channel proteins. Surface (**a**) and total (**b**) staining of COSm6 cells transfected with WT or ΔF1388 mutant f-SUR1 along with WT Kir6.2 cDNAs. Primary antibody used was anti-FLAG and secondary antibody used was conjugated to Cy-3 (*red*). Note the ΔF1388 mutant showed no signal in surface staining and intense peri-nuclear signal in total staining, indicating ER retention and trafficking defects [14]

5. Fix the cells with −20 °C Methanol for 10 min on ice (alternatively, fix the cells with 2–4% paraformaldehyde in PBS).
6. Wash the cells 3× with ice-cold PBS.
7. Incubate the cells in blocking buffer (PBS + 0.1% BSA + 1% normal goat serum) for 1 h at room temperature.
8. Incubate the cells with a fluorophore-conjugated anti-mouse IgG secondary antibody diluted to appropriate concentrations in blocking buffer for 1 h at room temperature in the dark (e.g., by covering with aluminum foil).
9. Wash the cells 3× with PBS + 0.1% BSA (20 min each).
10. Wash the cells once with PBS for 10 min.
11. Dip coverslips briefly in distilled water before mounting. This will prevent crystallization of the salt in the PBS when the coverslips dry out.
12. Mount coverslips using mounting medium containing DAPI (to stain nuclei) on slides.
13. If doing total staining as a control, fix the cells with −20 °C methanol for 10 min on ice first, then proceed with the staining protocol. Examples of surface and total staining of FLAG-tagged WT or mutant SUR1 are shown in Fig. 4.

3.6 Chemiluminescence Assays

For these assays, cells are plated onto 35 mm culture dishes for transfection. Duplicates (or triplicates) of dishes are prepared for each mutant or condition for averaging out cell plating or transfection efficiency variations (*see* **Note 20**).

1. Thirty-six to 48 h post-transfection, cells were placed on ice and washed 2× with cold PBS (2 mL/dish).

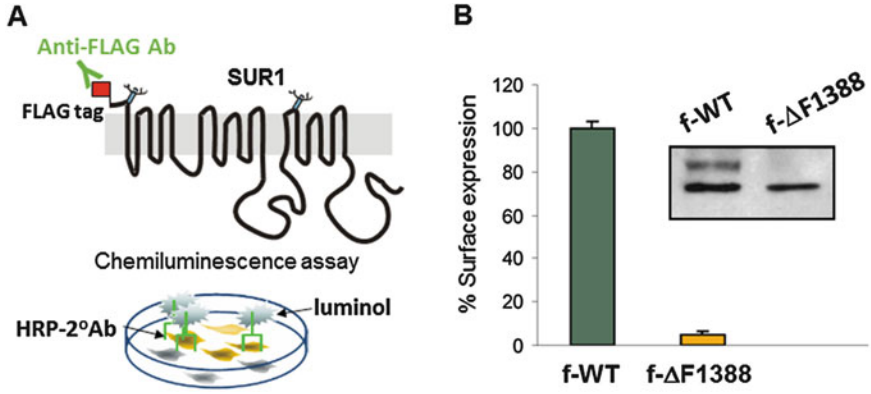

Fig. 5 The chemiluminescence assay. (**a**) Cartoon illustrating the chemiluminescence method. It uses a SUR1 construct containing an extracellular N-terminal FLAG-tag to allow for quantification of surface K_{ATP} channels. The *blue rods* with branches in the SUR1 topology model represent the two N-linked glycosylation sites. Addition of luminol that reacts with the HRP conjugated to 2°Ab for the anti-FLAG primary antibody generates chemiluminescence signals that can be detected using a luminometer. (**b**) The SUR1-ΔF1388 mutation is again used as an example. The mutation exhibits almost no surface expression, which is consistent with the lack of mature SUR1 *upper band* in Western blots (blotted with the M2 anti-FLAG antibody)

2. Cells were then fixed with cold 2% paraformaldehyde for 30 min on ice (*see* **Notes 7** and **21**).
3. Rinse cells 3× with PBS.
4. Place cells in PBS + 1 mg/mL BSA and preblock on a rotator set at low speed for 30 min at room temperature.
5. Incubate the cells with anti-FLAG antibody (~10 μg/mL) in PBS-BSA and place on the rotator with low speed rotation for 1 h.
6. Wash the cells in PBS-BSA 4× 30 min with gentle shaking.
7. Incubate the cells with HRP-conjugated anti-mouse IgG (in PBS-BSA at appropriate dilution) for 30 min.
8. Wash the cells in PBS-BSA 4× 30 min with gentle shaking and final wash once with plain PBS for 10 min.
9. Prepare the Super Signal ELISA solution according to the manufacturer's instructions.
10. Aspirate PBS from each well/dish and add 650 μL luminol solution. Rock the dish back and forth for 10 s, place in the luminometer, and record the luminescence reading on the luminometer. Examples of chemiluminescence results using FLAG-tagged WT or mutant SUR1 are shown in Fig. 5.

3.7 Inside-Out Patch Voltage-Clamp Recording

For these experiments, an electrophysiology setup with the equipment items listed in Subheading 2.7, **item 8** needs to be in place. Researchers performing these experiments should be familiar with the patch-clamp recording technique. For making seals, please also *see* Subheading 3.4 in Chapter 7 by Vierra et al.

1. Transfect the cells in a 12-well plate as described above for immunofluorescence staining (*see* Subheading 3.5). Remember to include the EGFP plasmid to facilitate identification of transfected cells under the fluorescence microscope (*see* Subheading 3.2, **step 2** and **Note 12**).
2. The next day, replate the cells onto cleaned and sterilized glass coverslips and incubate overnight to allow the cells to adhere to the coverslips (*see* **Note 22**). The cells are ready for recording the following day and the day after.
3. Before recording, pull glass electrodes, float the air table, turn on the fluorescence as well as the transmission light sources, and prepare solutions. We typically set up four different solutions to test channel response to ATP and MgADP (or diazoxide). The solutions are: (1) Kint, (2) Kint + 1 mM ATP + 1.4 mM $MgCl_2$, (3) Kint + 0.1 mM ATP + 1.1 mM $MgCl_2$, (4) Kint + 0.1 mM ATP + 0.5 mM ADP (or 0.2 mM diazoxide) + 1.3 mM $MgCl_2$ (*see* **Note 23**). The solutions can be modified to test channel response to other ligands [16, 17]. The solutions are perfused into the recording chamber by gravity (flow rate can be set using a dial-a-flow regulator) and removed by vacuum or a pump such that the solution level is kept relatively constant.
4. Take cells plated on coverslips out of the incubator. Use a diamond pen and press hard on the coverslip to break free a shard of coverslip that will fit in the recording chamber. Carefully transfer the coverslip piece into the recording chamber with Kint solution (*see* **Note 24**) using a pair of forceps. Place the remaining cells back into the incubator. There is no need to worry about keeping the cells sterile. One coverslip will last for the entire day of recording.
5. Fill an electrode with Kint solution by first immersing the tip of the electrode in an Eppendorf tube containing Kint for a few seconds, then filling the electrode ~halfway with Kint using a 1 mL syringe with a microfil needle (note a syringe filter is placed between the syringe and the needle to make sure that nothing clogs up the electrode). Tap the electrode to get rid of any air bubbles, especially near the very tip. Mount the electrode onto the electrode holder and apply positive pressure before lowering the electrode into the bath solution to prevent any debris from blocking the electrode.
6. Find a green cell under the fluorescence microscope and move the electrode close to the cell using the micromanipulator, changing the magnification of the objective lens and the coarse/fine control of the micromanipulator as needed. Always start with cells expressing wild-type K_{ATP} channels to make sure all the solutions are working properly.

7. Slowly lower the electrode onto the cell while monitoring the seal using the amplifier (by applying a test voltage pulse and watching the amount of currents that goes through the electrode). Once the electrode touches the cell, turn off the positive pressure and apply negative pressure until a gigaohm seal is formed, which is indicated by nearly 0 currents going through the electrode (and often shown numerically on the seal test display screen on the computer program, for example Clampex from pClamp, connected to the amplifier).
8. Once a tight seal is made, turn off the test pulse and apply a command potential (usually +50 mV). To make an inside-out patch, change the micromanipulator setting to coarse control and lift the electrode abruptly away from the cell into the Kint bath solution. In voltage-clamp mode, you should *see* currents if there are K_{ATP} channels (*see* **Note 25**).
9. Start recording using a gap-free recording protocol.
10. Now expose the patch to Kint with 1 mM ATP (solution 2) and you should see immediate inhibition of currents. This inhibition is a signature of K_{ATP} channels. Next, expose the patch to Kint with 0.1 mM ATP and 1.1 mM $MgCl_2$ (solution 3). In isolated patches, the IC_{50} of ATP for the channel is ~10 μM so at 0.1 mM ATP you should see a small current that is significantly below half of the current observed in Kint (solution 1). Finally, expose channels to Kint containing 0.1 mM ATP, 0.5 mM ADP, and 1.3 mM $MgCl_2$. You should see a gradual rise in current amplitude relative to currents seen in solution 3 due to the stimulatory effect of MgADP acting through SUR1. An example of activities of WT channels in the different solutions is shown in Fig. 6.

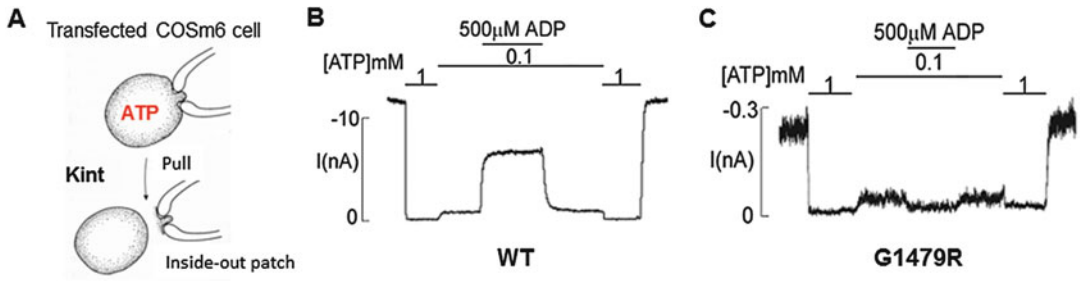

Fig. 6 Inside-out patch-clamp recording. (**a**) Cartoon showing the inside-out patch-clamp recording technique. (**b**) Representative current trace (50 mV in symmetrical Kint) of WT K_{ATP} channels showing current inhibition by 1 and 0.1 mM ATP and current stimulation by 500 μM ADP (in the presence of 0.1 mM ATP and ~1 mM free Mg^{2+}; *see* **Note 23**). (**c**) Representative current trace of mutant channels containing a congenital hyperinsulinism-associated mutation G1479R in SUR1. In contrast to WT channels, mutant channels failed to be stimulated by MgADP, a gating defect that renders K_{ATP} channels unable to open in response to hypoglycemia and is commonly observed in mutants associated with congenital hyperinsulinism [20]. Inward currents are shown as upward deflections in both (**b**) and (**c**).

4 Notes

1. We use COSm6, a clonal cell line derived from African green monkey COS cells for our experiments, but other COS cell clones are also adequate. Sometimes, we tend to see a nonspecific band close to the SUR1 bands that could obscure or interfere with the SUR1 band signals in Western blots, but this can be circumvented by trying different percentage gel or running the gel longer to separate the bands. Also, some researchers use *Xenopus* oocyte for expressing mutant channels. Although this expression system is good for electrophysiology studies, it is not a good system to study channel biogenesis and trafficking because the oocytes, being cultured at a lower temperature and having different protein quality control mechanisms, will permit surface expression of misfolded or misassembled channel proteins that would normally be retained in the ER in mammalian cells cultured at 37 °C.
2. We usually use T25 flasks to maintain the cells and use the plates for transfection and experiments. The choice of the size of the multi-well tissue culture plates and coverslips is dependent on the researcher's preference and consideration of reagent costs.
3. We usually use mammalian expression vectors containing the CMV promotor. Vectors such as the pCDNA series work well.
4. We use FuGENE®6 from Promega for transfection, but other transfection reagents also work.
5. We usually purchase 1 mCi of ^{86}RbCl (e.g., from PerkinElmer LAS), which is enough for numerous experiments. Because the half-life of ^{86}Rb is 19 days, it is a good idea to conduct Rb efflux experiments in a reasonable period of time before the radioactivity becomes too low.
6. The primary antibody we used for SUR1 was generated in rabbit against the C-terminus of hamster SUR1 (KDSVFASFVRADK), which also recognizes human SUR1. Anti-Kir6.2 was generated in rabbit using the C-terminal domain of rat Kir6.2 (amino acids 170–390) fused to the bacterial protein glutathione-S-transferase (GST) and also recognizes human Kir6.2. Other commercial antibodies will also work but working concentrations will need to be tested empirically. If antibodies against SUR1 or Kir6.2 proteins are not available, one can use tagged construct (for example, a FLAG-tagged SUR1 as shown in Fig. 4b).
7. Because there are currently no good antibodies against the extracellular domains of SUR1 or Kir6.2, we use a SUR1 construct that contains an engineered extracellular N-terminal FLAG tag to allow us to perform surface staining.

8. We use 2% paraformaldehyde to fix cells. At this concentration, anti-FLAG antibody binds mostly to the cell surface FLAG-SUR1. Higher concentrations of paraformaldehyde tend to give higher background likely because more antibodies can access the cell interior.
9. Use KOH instead of NaOH to adjust pH to avoid introducing Na^+ in the recording solution.
10. Prepare 5–10 mL of 100 mM ATP and ADP stock solutions in Kint and freeze them in 1 mL aliquots. Again, purchase potassium salts of ATP and ADP to avoid having Na^+ in the solution. ATP and ADP are acidic so the stock solutions will need to be titrated to bring the pH to ~7. We usually dissolve ATP or ADP in Kint at a volume ~1 mL less than the final volume. To monitor pH, add some phenol red just enough to see color. Gradually add KOH until the color of the solution is bright red which indicates pH is ~7. Then top off the solution with Kint to the final desired volume.
11. We use Kimble Chase non-heparinized capillary glass tubes (can purchase from Amazon) to make patch-clamp pipettes. This is relatively cheap and works very well for macroscopic current recordings in our hands.
12. When transfecting more than one plasmid, it is important to mix the plasmids in a separate tube before mixing with FuGENE®6. This will ensure uptake of multiple plasmids into a cell needed for K_{ATP} channel expression or GFP expression.
13. Take necessary precautions when working with ^{86}Rb. Proper shielding will minimize exposure. During overnight incubation in ^{86}Rb containing medium, place a label on the incubator door to alert others especially if using a shared incubator.
14. For preincubation in Ringer's + MI, it is necessary to include ^{86}Rb. This is because MI will activate channels and deplete ^{86}Rb present in the cell from the overnight incubation such that there would not be any ^{86}Rb left for efflux measurement. Continuous presence of ^{86}Rb in the extracellular solution during MI will ensure sufficient radioactivity inside the cell for subsequent efflux experiments.
15. It is important to remove any residual wash solution prior to efflux measurements as it contains residual ^{86}Rb that could contaminate the subsequent first timed measurement of ^{86}Rb efflux, which will confound experimental results. Likewise, it is a good idea to remove the efflux solution completely to avoid carryover to the next time point. A 1 mL pipetman (p-1000) works well for these steps.

16. Cells lysed in 1% SDS will be very viscous. Use p-1000 pipetman to pipet up and down a few times to ensure all lysate is collected.
17. SUR1 tends to aggregate at high temperature so it is very important not to boil the protein samples. Instead, incubate samples at 37 °C for 10 min before running on SDS-PAGE.
18. If desired, one can plate multiple coverslips for each transfected well and use for surface staining or total cellular staining.
19. This is most easily done by placing the coverslips on a sheet of parafilm in the cold room. Only ~100–150 μL antibody solution is needed for each coverslip due to surface tension. This will help conserve antibody. A similar setup can be used for secondary antibody incubation at room temperature. Washing and fixation steps are more easily done in the wells by transferring coverslips back to the 12-well tissue culture plates.
20. In our experience, the chemiluminescence signals from dish to dish only vary slightly if precautions are taken to ensure equal cell plating and transfection. Therefore, we do not correct for cell numbers but simply average the signals from duplicates or triplicates dishes.
21. Paraformaldehyde is a potential carcinogen. Collect the paraformaldehyde waste in a 50 mL Falcon tube and add a few drops of Formalex in a chemical hood to inactivate before disposal.
22. The cell density for patching should be lower than that used for other experiments. When cells are too dense and growing on top of one another, it is more difficult to select green cells and make seals. We typically replate one well of transfected cells onto multiple coverslips at 1:4–1:6 dilutions. Usually, cells are good for patching for 2 days so plate the cells at a slightly higher density for Day 1 of patching than Day 2 of patching.
23. Sometimes K_{ATP} channel activity can run down very quickly, making it challenging for later currents quantification. This is usually because there are cations such as Mg^{2+} which may induce hydrolysis of membrane PIP_2. To minimize rundown, 1 mM EDTA (pH 7.4) can be included in solution 1 (Kint). Using HPLC grade H_2O will also help reduce rundown. Note channel stimulation by ADP (as well as diazoxide) requires Mg^{2+}. The $MgCl_2$ concentrations used in solution 2–4 are calculated to give ~1 mM free Mg^{2+} (i.e., Mg^{2+} not in complex with ATP or ADP).
24. We put the cells in the Kint solution such that when patch is pulled the channels are exposed to symmetrical $[K^+]$, as the electrode is also filled with Kint. Because the concentration of K^+ in Kint is 140 mM which is greater than tenfold higher than physiological external $[K^+]$, the cells will not stay healthy for

long. We typically record 2–3 cells before switching to a new coverslip piece.

25. Because the intracellular ATP concentrations are very high (1–5 mM range, which is >100-fold higher than the ATP concentration needed to achieve half maximal inhibition of the channel measured in inside-out patches), K_{ATP} channels are mostly closed when in cell-attached mode. Once an inside-out patch is formed, the cytoplasmic face of the channels is exposed to Kint solution devoid of ATP and the channels will open (with the +50 mV command potential in symmetrical $[K^+]$). If you do not observe any currents, there are two possibilities: one is that there are no channels expressed, the other is that a vesicle has formed while you pull the electrode off the cell. In the latter case, the membrane is sealed such that the channels are not exposed to Kint. To break the vesicle, try to lift the electrode out of the solution and back in again. Alternatively, use an empty syringe with a microfil needle and push an air bubble in the solution near the electrode to help break the vesicle. However, these manipulations can damage the seal. Start over again when this happens.

Acknowledgments

This work was supported by National Institutes of Health grants R01DK057699 and R01DK066485 to S.L.S.

References

1. Aguilar-Bryan L, Bryan J (1999) Molecular biology of adenosine triphosphate-sensitive potassium channels. Endocr Rev 20 (2):101–135. doi:10.1210/edrv.20.2.0361
2. Ashcroft FM (2006) K(ATP) channels and insulin secretion: a key role in health and disease. Biochem Soc Trans 34(Pt 2):243–246. doi:10.1042/BST20060243
3. Nichols CG (2006) KATP channels as molecular sensors of cellular metabolism. Nature 440 (7083):470–476. doi:10.1038/nature04711
4. Clement JP, Kunjilwar K, Gonzalez G, Schwanstecher M, Panten U, Aguilar-Bryan L, Bryan J (1997) Association and stoichiometry of K(ATP) channel subunits. Neuron 18 (5):827–838
5. Shyng S, Nichols CG (1997) Octameric stoichiometry of the KATP channel complex. J Gen Physiol 110(6):655–664
6. Inagaki N, Gonoi T, Seino S (1997) Subunit stoichiometry of the pancreatic beta-cell ATP-sensitive K+ channel. FEBS Lett 409 (2):232–236
7. Inagaki N, Gonoi T, Clement JP, Namba N, Inazawa J, Gonzalez G, Aguilar-Bryan L, Seino S, Bryan J (1995) Reconstitution of IKATP: an inward rectifier subunit plus the sulfonylurea receptor. Science 270(5239):1166–1170
8. Ashcroft FM (2005) ATP-sensitive potassium channelopathies: focus on insulin secretion. J Clin Invest 115(8):2047–2058. doi:10.1172/JCI25495
9. Stanley CA (2016) Perspective on the genetics and diagnosis of congenital hyperinsulinism disorders. J Clin Endocrinol Metab 101 (3):815–826. doi:10.1210/jc.2015-3651
10. Gloyn AL, Pearson ER, Antcliff JF, Proks P, Bruining GJ, Slingerland AS, Howard N, Srinivasan S, Silva JM, Molnes J, Edghill EL, Frayling TM, Temple IK, Mackay D, Shield JP, Sumnik Z, van Rhijn A, Wales JK, Clark P, Gorman S, Aisenberg J, Ellard S, Njolstad PR, Ashcroft FM, Hattersley AT (2004) Activating mutations in the gene encoding the ATP-sensitive potassium-channel subunit Kir6.2 and permanent neonatal diabetes. N Engl J

Med 350(18):1838–1849. doi:10.1056/NEJMoa032922

11. Ashcroft FM (2007) The Walter B. Cannon physiology in perspective lecture, 2007. ATP-sensitive K+ channels and disease: from molecule to malady. Am J Physiol Endocrinol Metab 293(4):E880–E889. doi:10.1152/ajpendo.00348.2007
12. Yan FF, Lin YW, MacMullen C, Ganguly A, Stanley CA, Shyng SL (2007) Congenital hyperinsulinism associated ABCC8 mutations that cause defective trafficking of ATP-sensitive K+ channels: identification and rescue. Diabetes 56(9):2339–2348. doi:10.2337/db07-0150
13. Zhou Q, Garin I, Castano L, Argente J, Munoz-Calvo MT, Perez de Nanclares G, Shyng SL (2010) Neonatal diabetes caused by mutations in sulfonylurea receptor 1: interplay between expression and Mg-nucleotide gating defects of ATP-sensitive potassium channels. J Clin Endocrinol Metab 95(12):E473–E478. doi:10.1210/jc.2010-1231
14. Cartier EA, Conti LR, Vandenberg CA, Shyng SL (2001) Defective trafficking and function of KATP channels caused by a sulfonylurea receptor 1 mutation associated with persistent hyperinsulinemic hypoglycemia of infancy. Proc Natl Acad Sci U S A 98(5):2882–2887. doi:10.1073/pnas.051499698
15. Zerangue N, Schwappach B, Jan YN, Jan LY (1999) A new ER trafficking signal regulates the subunit stoichiometry of plasma membrane K(ATP) channels. Neuron 22(3):537–548
16. Cartier EA, Shen S, Shyng SL (2003) Modulation of the trafficking efficiency and functional properties of ATP-sensitive potassium channels through a single amino acid in the sulfonylurea receptor. J Biol Chem 278(9):7081–7090. doi:10.1074/jbc.M211395200
17. Shyng SL, Nichols CG (1998) Membrane phospholipid control of nucleotide sensitivity of KATP channels. Science 282(5391):1138–1141
18. Chen PC, Olson EM, Zhou Q, Kryukova Y, Sampson HM, Thomas DY, Shyng SL (2013) Carbamazepine as a novel small molecule corrector of trafficking-impaired ATP-sensitive potassium channels identified in congenital hyperinsulinism. J Biol Chem 288(29):20942–20954. doi:10.1074/jbc.M113.470948
19. Lin YW, Bushman JD, Yan FF, Haidar S, MacMullen C, Ganguly A, Stanley CA, Shyng SL (2008) Destabilization of ATP-sensitive potassium channel activity by novel KCNJ11 mutations identified in congenital hyperinsulinism. J Biol Chem 283(14):9146–9156. doi:10.1074/jbc.M708798200
20. Shyng SL, Ferrigni T, Shepard JB, Nestorowicz A, Glaser B, Permutt MA, Nichols CG (1998) Functional analyses of novel mutations in the sulfonylurea receptor 1 associated with persistent hyperinsulinemic hypoglycemia of infancy. Diabetes 47(7):1145–1151

Chapter 9

Thallium Flux Assay for Measuring the Activity of Monovalent Cation Channels and Transporters

C. David Weaver

Abstract

Monovalent cation channels are critically important for physiological processes ranging from the control of neuronal excitability to the maintenance of solute balance. Mutations in these channels are associated with a multiplicity of diseases and monovalent cation channel-modulating drugs are used as therapeutics. Techniques that allow the measurement of the activity of these ion channels are useful for exploring their many biological roles as well as enabling the discovery and characterization of ion channel modulators for the purposes of drug discovery. Although there are numerous techniques for measuring the activity of monovalent cation channels, the thallium flux assay technique is a widely used fluorescence-based approach. Described herein is a method for using the thallium-flux technique for detecting and quantifying the activity of small-molecule potassium channel modulators in 384-well plates.

Key words Ion channel, Potassium channel, Sodium channel, Drug discovery, High-throughput screening, Fluorescent dye, Thallium

1 Introduction

Ion channels are critical for life. Many ion channels are capable of conducting monovalent cations, most commonly sodium and potassium. Voltage-clamp electrophysiology is often the method of choice for measuring the activity of ion channels. However, traditional micromanipulator-based techniques are slow and laborious while more rapid automated planar techniques are not useful for studying complex cell preparations such as brain slices. In the 1980s, the emergence of fluorescent dyes like Fura-2 and Fluo-3 made possible the fluorescence-based measurements of divalent cation channels [1, 2]. Sodium and potassium-sensitive dyes followed closely behind the divalent cation-sensitive ones [3]. Unfortunately, these dyes had issues that severely limited their utility, including poor sensitivity and poor selectivity under normal intracellular sodium and potassium concentrations. Because monovalent cation channels make up the majority of all ion channels, new

Show-Ling Shyng et al. (eds.), *Potassium Channels: Methods and Protocols*, Methods in Molecular Biology, vol. 1684,
DOI 10.1007/978-1-4939-7362-0_9,

approaches to measuring their activity were desperately needed. One such approach, voltage-sensitive fluorescent dyes, takes advantage of the potential difference across cell membranes. However, these dyes suffer limitations for quantitative measurement of ion channel activity because of the relationship of membrane potential, current, and resistance described by Ohms law, $V = IR$. The facts that sodium [4], potassium [5], and other monovalent cation channels are capable of conducting thallium and that thallium is not normally present in physiological solutions, set the stage for the use of thallium flux to measure the activity of these channels. The potential utility of thallium flux for measuring the activity of monovalent cation channels led to a search for and discovery of the thallium-sensitive fluorescent dyes and subsequent development of the thallium flux assay technique [6].

The thallium flux technique was first applied to enable high-throughput screening of potassium channels. Since then it has been used for measuring the activity of a wide variety of channels and transporters including voltage-gated potassium channels, two-pore-domain potassium channels, cation-coupled chloride co-transporters, sodium channels, sodium/potassium ATPases, and others [7–16]. Described below is a specific example of the use of the thallium flux technique to measure the activity of an inward-rectifying potassium channel. The specific example provided here describes the use of the thallium flux assay in 384-well plates. However, the technique may also be used for microscope-based assays in ways similar to calcium-sensitive fluorescent dye-based approaches. In each case systematic determination of the optimal assay conditions is required.

2 Materials

Prepare all solutions in ultrapure water. All chemicals should be obtained from a reputable supplier and should be of reagent grade or higher quality unless otherwise specified. Dimethyl sulfoxide (DMSO) should be free of water (*see* **Note 1**). All solutions and reagents can be stored at room temperature unless otherwise noted. Thallium is toxic. Wear appropriate personal protective equipment. Dispose of all thallium-contaminated solutions and labwear in accordance with your institution's policies.

1. Assay buffer: Hanks Balanced Salt Solution, 10 mM HEPES, sodium salt, pH 7.2.
2. Thallium-stimulus base buffer: 145 mM sodium gluconate (*see* **Note 2**), 1.3 mM $CaSO_4$ 0.9 mM $MgSO_4$, 5 mM Glucose, 10 mM HEPES, sodium salt, pH 7.2.
3. Thallium sulfate solution: 100 mM Tl_2SO_4 in water (*see* **Note 3**).

4. Dimethyl sulfoxide (DMSO): water-free DMSO.
5. 20% Pluronic F-127 solution (*see* **Note 4**): 20% (w/v) Pluronic F-127 in DMSO.
6. Thallium-sensitive fluorescent dye: there are a number of commercially available thallium-sensitive fluorescent dyes. Most of these dyes are available in the form of assay kits sold under various names: ThaLux Green (WaveFront Biosciences) FluxOR, FluxOR II (Thermo Fisher Scientific), FLIPR Potassium Assay Kit (Molecular Devices) while others are also available as dye alone: ThaLux Green AM (WaveFront Biosciences) (*see* **Note 5**), FluoZin-2 AM (Thermo Fisher Scientific), BTC AM (Thermo Fisher, AAT Bioquest). Regardless of the thallium-sensitive dye provider, the dye should be stored desiccated at −20 °C.
7. Ion channel-expressing cells: HEK-293 cells (ATCC) (*see* **Note 6**) stably overexpressing $K_{ir}3.1$ (GIRK1) and $K_{ir}3.2$ (GIRK2).
8. Extracellular-masking solution (*see* **Note 7**): 100 mM allura red AC in assay buffer.
9. Dye retention solution (*see* **Note 8**): 250 mM sodium probenecid in assay buffer.
10. Ion channel modulator: 10 mM ML297 in DMSO (*see* **Note 9**).
11. Cell culture medium: α-Minimum Essential Medium (α-MEM) plus 10% (v/v) fetal bovine serum and 1× glutagro (Corning) or GlutaMax (Thermo Fisher Scientific), 3 μg/mL puromycin sulfate and 5 μg/mL blasticidin. Filter sterilize using a 0.2 μm filter and store at 4 °C.
12. Cell dislodging solution: TrypLE Express (Thermo Fisher Scientific) (*see* **Note 10**).
13. Assay Plates (*see* **Note 11**): 384-well, black-wall, clear-bottom, PureCoat Amine plates (Corning).
14. Compound and thallium-stimulus additions plates: 384-well, polypropylene, conical-bottom plates (Greiner).
15. Fluorescent plate reader: any fluorescent plate reader that is able to acquire signals from cells in plates can be used for thallium flux assays. However, kinetic imaging plate readers including Panoptic (WaveFront Biosciences), FDSS (Hamamatsu Photonic Systems), FLIPR (Molecular Devices), or FlexStation (Molecular Devices) are strongly preferred. For the thallium-sensitive dyes listed above, the nominal excitation and emission wavelengths are 490 nm and 520 nm, respectively.

3 Methods

All the procedures are carried out at room temperature. Thallium is toxic. Wear appropriate personal protective equipment.

3.1 Cell Culture and Plating

1. Cultivate the cells in a cell-culture medium at 37 °C in a humidified 5% CO_2-containing atmosphere to ~80–90% confluence in a T75 or other appropriate cell culture vessels.
2. Transfer the cell culture vessel to a biocontainment cabinet.
3. Remove the cell-culture medium and add 3 mL TrypLE Express and incubate for ~5 min.
4. Dislodge the cells from cell culture vessel by tapping the vessel sharply on the side and/or pipetting the TrypLE Express up and down on the inside bottom surface of the vessel using a serological pipette.
5. After the cells are dislodged add 7 mL of tissue culture medium.
6. Place the serological pipette tip in the bottom corner of the cell culture vessel and pipette the cell suspension up and down for five strokes to achieve a single-cell suspension.
7. Quantify the number of live cells in the cell suspension using a hemocytometer.
8. Dilute the cell suspension with the cell-culture medium (*see* **Note 12**) to achieve a concentration of ~500 cells/μL (*see* **Note 13**).
9. Add 20 μL/well of cell suspension to one or more cell plates.
10. Transfer the cell plates to the 37 °C, 5% CO_2, cell culture incubator and incubate until the cells are well adhered to the bottom of the plate (6 h—overnight).

3.2 Thallium Flux Assay (See Note 14)

1. Prepare a dye-loading solution by dissolving 12 μg of dye in 25 μL DMSO plus 25 μL 20% Pluronic F-127 solution with vigorous vortexing. Add the 50 μL of dissolved dye to 10 mL of assay buffer with gentle vortexing.
2. Prepare 2×-test compound solution by diluting ML297 to twofold over the desired final concentration in assay buffer and transfer 30 μL/well to a 384-well polypropylene plate.
3. Remove the cell plate from the cell culture incubator.
4. Remove the cell-culture medium (*see* **Note 15**).
5. Add 20 μL/well dye-loading solution (*see* **Note 16**).
6. Incubate for 30 min–2 h at room temperature.
7. While the dye is loading, prepare a 5×-thallium-stimulus plate by adding an appropriate volume of 100 mM Tl_2SO_4 solution (*see* **Note 17**) to 15 mL of thallium-stimulus base buffer and

mix well. Transfer 30 μL/well to a 384-well polypropylene plate.

8. Remove the dye-loading solution (*see* **Note 18**).
9. Add 20 μL/well assay buffer.
10. Transfer the plates to the plate reader.
11. Using the manufacturer's instructions, set up the plate reader to run an experiment where 10 time points of baseline data are collected (1 Hz) followed by the addition of 20 μL/well from the 2×-test compound plate with constant data collection. After 90 s of incubation (*see* **Note 19**), add 10 μL/well of 5×-thallium-stimulus solution and collect data for another 90 s.

3.3 Analysis of Results

1. Open the raw data file exported from the plate reader (Fig. 1a) in Excel (Microsoft).
2. Normalize the data to account for well-to-well variability caused by nonuniform optics of the plate reader and/or by uneven cell plating (*see* **Note 20** and Fig. 1b).
3. Select wells that have not been treated with test compound and average each data point from those waves to yield an average, untreated control waveform. Subtract the untreated control wave from the data for each of the untreated and untreated wells (*see* **Note 21** and Fig. 1c).
4. Reduce data by fitting the slope of ten data points beginning 5 s after thallium addition (*see* **Note 22** and Fig. 1c).
5. Fit the slopes values calculated above using XLfit (IDBS), Prism (GraphPad), or other appropriate nonlinear curve-fitting application(Fig. 1d).

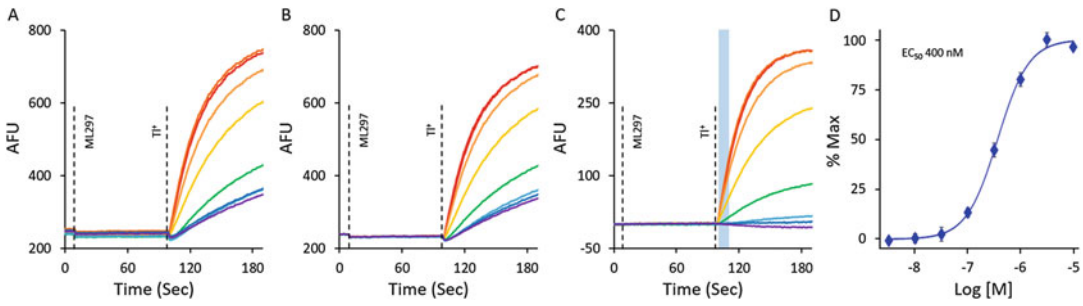

Fig. 1 Data normalization and analysis of a thallium flux assay. Shown are varying concentrations of ML297 added to HEK-293 cells expressing GIRK channels comprised of GIRK1 and GIRK2 subunits. (**a**) Raw data from kinetic imaging plate reader. (**b**) Normalized data (F/F_0 multiplied by the average of F_0 for of all wells). (**c**) Untreated control wave-subtracted data (**d**) fit to slope of each ML297 concentration normalized to the maximally effective concentration of ML297. *Dotted lines* show the point of addition of ML297 and Tl^+. *Light blue box* shows the time window for fitting of slopes used in (**d**). Error bars are standard error of the mean of three replicate samples

4 Notes

1. DMSO is hygroscopic and will absorb up to 30% (w/w) water from the atmosphere. Many test compounds and the acetate/acetoxymethyl esters of thallium-sensitive fluorescent dyes will be less soluble and less stable in water-contaminated DMSO. Therefore, care should be taken to use water-free DMSO.
2. Some thallium salts are very poorly soluble in water. Thallium chloride, for instance, has a solubility of about 5 mM at room temperature. Therefore, depending on the expression levels and the degree to which a channel is able to flux thallium, other sodium salts in the thallium-stimulus buffer may be required to achieve the desired thallium concentration. Useful sodium salts include sodium gluconate, sodium bicarbonate, sodium fluoride, and when consistent with the desired thallium concentration, sodium chloride. In addition, sometimes it is desirable to substitute some or all of the sodium in thallium-stimulus buffer with other cations most often, potassium. It is highly recommended that at the beginning of assay development for a given channel that thallium concentration and buffer composition is systematically evaluated to produce optimal results. Care should be taken if sodium bicarbonate and/or potassium bicarbonate is chosen for the thallium-stimulus buffer due to the fact that the pH of these solutions is unstable. Bicarbonate-based thallium-stimulus solutions should be made fresh and containers should be kept tightly closed until ready for use.
3. A mole of thallium sulfate contains 2 moles of thallium and thus, 100 mM Tl_2SO_4 is 200 mM in thallium.
4. Pluronic F-127 is a detergent that is often used to aid dissolution of hydrophobic esters of thallium-sensitive fluorescent pro-dyes. Although the use of Pluronic F-127 or similar detergents is not absolutely required, it does facilitate dye loading.
5. ThaLux Green AM is the same dye once sold by TEFlabs under the name "Thallos AM."
6. A wide variety of cell lines in addition to HEK-293 cells may be used for thallium flux assays. These cell types include but are not limited to CHO, HeLa, and COS-7 as well as tissue-derived primary cell preparations.
7. A variety of optional membrane impermeant dyes including allura red AC, amaranth, and others can be used as agents to mask assay background contributed by buffer components, fluorescent compounds, or extracellular thallium-sensitive dye. While useful, these dyes may also have unanticipated effects on the target of interest and care must be taken to

make sure that these masking dyes are not causing undesired effects such as activation, inhibition, or other modulation of the activity of the target. Final masking agent concentrations typically range between 1 and 0.1 mM. These concentrations should be determined empirically as part of assay optimization.

8. The sodium salt of probenecid as well as sulfinpyrazone can be optionally included in assay buffer to inhibit the activity of membrane transporters that can promote intracellular compartmentalization and extrusion of thallium-sensitive dyes from cells [17]. These compounds are particularly useful when performing thallium flux assays in cells such as CHO cells that are very effective at extruding thallium-sensitive dyes. As is the case with extracellular masking dyes, care should be taken when using probenecid and sulfinpyrazone as they may also result in changes in the activity of the target. Typical final concentrations of probenecid and sulfinpyrazone range from 0.5 to 2.5 mM and from 10 to 200 μM, respectively.
9. ML297 is offered as an example for the purposes of this chapter. Any one of a host of compounds capable of directly or indirectly modulating the activity of the ion channel of interest may be chosen. An important consideration, however, is that ion channels are often sensitive to DMSO. Therefore, DMSO effects on the target should be evaluated as part of assay development in cases where DMSO may be present in solutions.
10. Any one of a number of protease-containing and non-protease-containing cell dislodging solutions can be used based on cell type and user preference.
11. Different cell types perform differently depending on the surface coating of multi-well assay plates. Coating types vary widely and include tissue culture (TC) treated, poly-D-lysine, synthetic amine, fibronectin, collagen, and others. The optimal assay plate surface should be determined empirically as part of assay optimization.
12. Some cell types will allow the use of serum-free medium at this step. This can be advantageous if there is a desire to remove the cell-culture medium prior to the addition of thallium-sensitive dye in a later step. If this is desired, phenol red-free cell-culture medium should be used.
13. The concentration of cells may vary depending on cell type. The effects of cell plating concentration should be evaluated as part of assay optimization.
14. If you are using one of the thallium flux assay kits, you may follow the kit manufacturer's instructions from this step forward.

15. In some instances removal of cell-culture medium may be omitted including when the serum-free cell-culture medium is used for cell plating or when the presence of serum-containing medium is desired. If the serum-containing medium is allowed to remain in the wells for the duration of the assay, it may affect dye loading as well as compound potency determinations.
16. In cases where there is a desire to avoid removal of cell-culture medium, an extracellular-masking solution may be added to the dye-loading solution. The extracellular-masking solution may also be added to the dye-loading solution in instances when the cell-culture medium is removed but when post-dye loading washing is undesirable.
17. The amount of 100 mM Tl_2SO_4 solution will vary depending on the cell line and channel being assayed. The optimal amount should be determined as part of assay optimization. If sodium chloride-containing thallium-stimulus base buffer is used, the maximum thallium concentration in the 5×-stimulus buffer is ~4.5 mM. For non-chloride-containing thallium-stimulus base buffers, the maximum thallium concentration in 5X-stimulus buffer is 22.5 mM. Using higher thallium concentrations than recommended may result in thallium chloride precipitation.
18. In cases where the extracellular-masking solution has been added to the dye-loading solution, this step may be omitted.
19. Test compound incubation times and post-thallium addition data acquisition times may be varied based on assay-specific goals and parameters. In some cases, it may be preferable to perform test compound addition and thallium addition simultaneously. The optimal times of test compound addition and thallium addition should be determined empirically.
20. Typically, this operation is performed by averaging the first five data points from each well in a plate and dividing each of the data points by this initial average. The function is applied to each well of the plate and is often referred to as static ratio or more commonly, F/F_0. At this stage users may choose to multiply F/F_0 by the average initial fluorescence value for each well in the plate to yield normalized fluorescence values (Fig. 1b).
21. This is an optional step that is often useful to visually compare subtle effects under different assay conditions including treatment with test compounds (Fig. 1c).
22. In some cases users may choose to measure a change in fluorescent amplitude at a discrete time point or a maximum change in fluorescent amplitude instead of the initial slope of the change in fluorescence evoked by the addition of thallium. Regardless of the method chosen, these values may be used to

compare differences between experimental treatments for use in the selection of active compounds in high-throughput screening or determination of the potency and efficacy of ion channel modulators.

Acknowledgment

This work was supported by the Vanderbilt Department of Pharmacology and the Vanderbilt Institute of Chemical Biology.
Conflict of Interest: CDW receives royalties from the sales of the Panoptic kinetic imaging plate reader, ThaLux Green, and the FLIPR Potassium Assay Kit. CDW is an owner of WaveFront Biosciences.

References

1. Grynkiewicz G, Poenie M, Tsien RY (1984) A new generation of Ca^{2+} indicators with greatly improved fluorescence properties. J Biol Chem 260:3440–3450
2. Minta A, Kao JPY, Tsien RY (1988) Fluorescent indicators for cytosolic calcium based on rhodamine and fluorescein chromophores. J Biol Chem 264:8171–8178
3. Minta A, Tsien RY (1989) Fluorescent indicators for cytosolic sodium. J Biol Chem 264:19449–19457
4. Hille B (1972) The permeability of the sodium channel to metal cations in myelinated nerve. J Gen Physiol 59:637–658
5. Hille B (1973) Potassium channels in myelinated nerve. Selective permeability to small cations. J Gen Physiol 61:669–686
6. Weaver CD, Harden D, Dworetzky SI, Robertson B, Knox RJ (2004) A thallium-sensitive, fluorescence-based assay for detecting and characterizing potassium channel modulators in mammalian cells. J Biomol Screen 9:671–677
7. Niswender CM, Myers KA, Lou Q, Ayala J, Kim C, Conn PJ, Weaver CD (2008) Development of a novel and direct assay for high-throughput screening of Gi/o-linked GPCRs using thallium flux through GIRK channels. J Mol Pharm 73:1213–1224
8. Raphemot R, Lonergan DF, Nguyen TT, Utley T, Lewis LM, Kadakia R, Weaver CD, Gogliotti R, Hopkins C, Lindsley CW, Denton JS (2011) Discovery, characterization, and structure-activity relationships of an inhibitor of inward rectifier potassium (Kir) channels with preference for Kir2.3, Kir3.x, and Kir7.1. Front Pharmacol 2:75
9. Yu H, Wu M, Townsend SD, Zou B, Long S, Daniels JS, McManus OB, Li M, Lindsley CW, Hopkins CR (2011) Discovery, synthesis, and structure activity relationship of a series of N-Aryl- bicyclo[2.2.1]heptane-2-carboxamides: characterization of ML213 as a novel KCNQ2 and KCNQ4 potassium channel opener. ACS Chem Nerosci 2:572–577
10. Lewis M, Bhave G, Chauder BA, Banerjee S, Lornsen K, Redha R, Fallen K, Lindsley CW, Weaver CD, Denton JS (2009) High-throughput screening reveals a small-molecule inhibitor of ROMK and Kir7.1. Mol Pharmacol 76:1094–1103
11. Bhave G, Chauder BA, Liu W, Dawson ES, Kadakia R, Nguyen TT, Lewis LM, Meiler J, Weaver CD, Satlin LM, Lindsley CW, Denton JS (2010) Development of a selective small-molecule inhibitor of Kir1.1, the Renal Outer Medullary Potassium Channel. Mol Pharmacol 79:42–50
12. Potet F, Lorinc AN, Chaigne S, Hopkins CR, Venkataraman R, Stepanovic SZ, Lewis LM, Days E, Sidorov VY, Engers DW, Zou B, Afshartous D, George AL Jr, Campbell CM, Balser JR, Li M, Baudenbacher FJ, Lindsley CW, Weaver CD, Kupershmidt S (2012) Identification and characterization of a compound that protects cardiac tissue from human ether-a-go-go-related gene (hERG)-related, drug-induced Arrhythmias. J Biol Chem 287:39613–39625
13. Li Q, Rottländer M, Xu M, Christoffersen CT, Frederiksen K, Wang MW, Jensen HS (2011) Identification of novel KCNQ4 openers by a high-throughput fluorescence-based thallium flux assay. Anal Biochem 418:66–72

14. Schmalhofer WA, Swensen AM, Thomas BS, Felix JP, Haedo RJ, Solly K, Kiss L, Kaczorowski GJ, Garcia ML (2010) A pharmacologically validated, high-capacity, functional thallium flux assay for the human Ether-à-go-go related gene potassium channel. Assay Drug Dev Technol 8:714–726
15. Delpire EJ, Days E, Lewis M, Mi D, Lindsley C, Weaver CD (2009) Small molecule screen identifies novel inhibitors of the neuronal K-Cl cotransporter KCC2. Proc Natl Acad Sci U S A 106:5383–5388
16. Carmosino M, Rizzo F, Torretta S, Procino G, Svelto M (2013) High-throughput fluorescent-based NKCC functional assay in adherent epithelial cells. BMC Cell Biol 14:16
17. Di Virgilio F, Steinberg TH, Swanson JA, Silverstein SC (1988) J Immunol 140:915–920

Chapter 10

Nuclear Magnetic Resonance Approaches for Characterizing Protein-Protein Interactions

Yuki Toyama, Yoko Mase, Hanaho Kano, Mariko Yokogawa, Masanori Osawa, and Ichio Shimada

Abstract

The gating of potassium ion (K^+) channels is regulated by various kinds of protein-protein interactions (PPIs). Structural investigations of these PPIs provide useful information not only for understanding the gating mechanisms of K^+ channels, but also for developing the pharmaceutical compounds targeting K^+ channels. Here, we describe a nuclear magnetic resonance spectroscopic method, termed the cross saturation (CS) method, to accurately determine the binding surfaces of protein complexes, and its application to the investigation of the interaction between a G protein-coupled inwardly rectifying K^+ channel and a G protein α subunit.

Key words NMR, Protein-protein interaction, Cross saturation, GIRK, G protein

1 Introduction

1.1 Nuclear Magnetic Resonance Spectroscopy for Characterizing Protein-Protein Interactions

The gating of potassium ion (K^+) channels is regulated by numerous protein-protein interactions (PPIs). For example, voltage sensing K^+ channels are regulated by accessory subunits [1, 2], and G protein-coupled inwardly rectifying K^+ channels (GIRKs) are regulated by G proteins [3]. The structural characterization of these PPIs provides valuable information for understanding biological processes, and for developing pharmaceutical compounds targeting K^+ channels. Solution nuclear magnetic resonance (NMR) spectroscopy is a powerful method for the structural characterizations of PPIs. A major advantage of NMR is that proteins under physiologically relevant conditions (proteins in solution, membrane proteins in lipid bilayers [4, 5], proteins in cellular environments [6], and so on) can be characterized. Therefore, the information obtained from NMR can provide structural insights that are deeply related to physiological functions, and precisely complement other methods for high-resolution structural determination, such as

Show-Ling Shyng et al. (eds.), *Potassium Channels: Methods and Protocols,* Methods in Molecular Biology, vol. 1684,
DOI 10.1007/978-1-4939-7362-0_10,

X-ray crystallography and cryo-electron microscopy, which require crystallized or frozen samples.

One of the most widely used NMR methods for studying PPIs is a chemical shift perturbation (CSP) experiment, in which the chemical shift differences (i.e., differences in peak positions in an NMR spectrum) induced by the binding are monitored. Since chemical shift differences occur not only for the residues forming a binding surface, but also for the residues in areas with significant structural changes, the information obtained from the CSP experiment is ambiguous. To overcome this difficulty, we have developed an NMR method for accurately determining the binding surface of PPIs, the cross saturation (CS) experiment, which utilizes the dipolar cross relaxation phenomenon between ^{1}H nuclei in an optimally isotopically labeled system [7–9]. By combining the results from the CSP and CS experiments, the primary effects of the direct intermolecular contacts and the secondary effects induced by conformational changes can be separated, providing solid structural insights into the mechanisms underlying protein functions. The method has been successfully applied to the PPIs of K^{+} channels, i.e., the KcsA-agitoxin [10], KvAP-VSTx1 [11], and GIRK-G proteins [12, 13].

1.2 Principle of the CS Method

The CS method is schematically represented in Fig. 1a. In the CS method, the complex of the non-labeled protein (donor protein) and the uniformly ^{2}H, ^{15}N-labeled protein (acceptor protein) is formed in a solvent with a low H_2O/D_2O ratio. When irradiated with a radio frequency (RF) pulse at the frequency corresponding to the aliphatic ^{1}H resonances, the ^{1}H nuclei incorporated in the donor protein are efficiently saturated. Although the ^{1}H nuclei incorporated in the acceptor protein are not directly saturated by the applied RF pulses, the saturation is transferred from the donor protein through the binding interface, by dipolar cross relaxation. Since the ^{1}H density of the acceptor protein is sufficiently low, the saturation transfer occurs selectively to the ^{1}H nuclei located on a binding surface (*see* **Note 1**). We call this phenomenon cross saturation (CS). The effect of CS can be detected as the intensity reduction of the NMR signals of the acceptor protein, which can be measured by recording a ^{1}H-^{15}N transverse relaxation-optimized spectroscopy (TROSY) spectrum [14]. Therefore, by investigating the signal intensity reductions induced by the application of RF pulses, the binding surface can be accurately determined.

The CS experiment can be applied to a system where the complex is exchanging between free- and bound-states. In this situation, the binding surface can be determined from the cross saturation effects that are transferred to the NMR signals originating from the free-state (Fig. 1b) (*see* **Note 2**). We call this modified experiment a transferred CS (TCS) experiment [15]. The TCS experiment is advantageous to investigate the interactions of

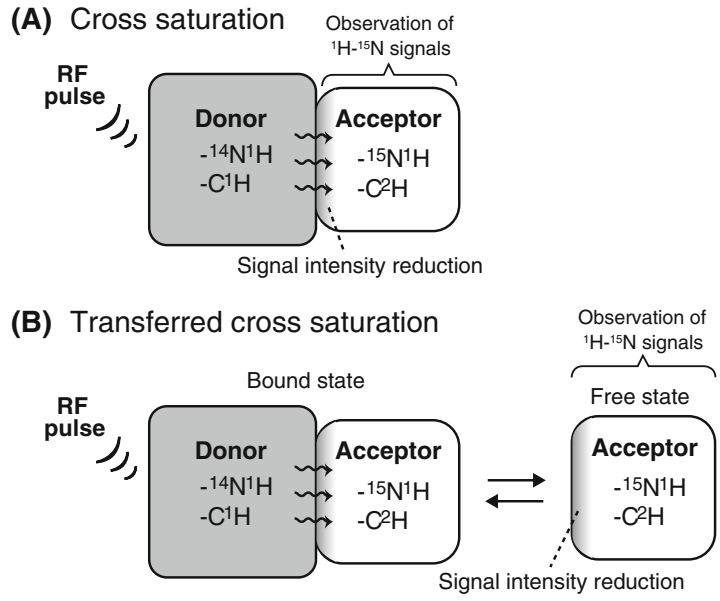

Fig. 1 (**a**) Schematic diagram of the CS experiment. The RF pulse causes saturation of the ^{1}H nuclei incorporated in the donor protein, as shown in *gray*. In contrast, the acceptor protein, which has no aliphatic ^{1}H nuclei, is not affected by the RF irradiation directly, but the saturation is transferred selectively to ^{1}H nuclei located on a binding surface. The effect of cross saturation can be detected as the intensity reduction of the NMR signals of the acceptor protein. (**b**) Schematic diagram of the TCS experiment. In systems where a free- and a bound-states are exchanging, the cross saturation effects are transferred to the NMR signals originating from the free state

extremely large and/or heterogeneous molecules, such as membrane proteins reconstituted in lipid bilayers [4], because the NMR signals in the bound-state are not directly observable.

In this chapter, we describe the experimental details of the TCS experiment, highlighting the interaction between the cytoplasmic domain of GIRK (residues 41–63 and 190–386, $GIRK_{CP\text{-}L}$) and a G protein α subunit ($G\alpha_{i3}$) bound to GTPγS, which reportedly plays critical roles in the efficient activation and deactivation of GIRK [13].

2 Materials

1. $G\alpha_{i3}$ pET-24d plasmid.
2. $GIRK_{CP\text{-}L}$ pET-24d plasmid.
3. *E. coli* BL21(DE3) CodonPlusRP competent cells (Agilent Technologies).

4. Luria-Bertani (LB) medium (H_2O): 10 g/L tryptone, 5.0 g/L yeast extract, and 5.0 g/L NaCl dissolved in Milli-Q water. Adjust the pH to 7.4. Autoclave at 121 °C for 15 min.
5. Luria-Bertani (LB) medium (D_2O): 10 g/L tryptone, 5.0 g/L yeast extract, and 5.0 g/L NaCl dissolved in 99.9% D_2O. Adjust the pH to 7.4. Sterilize with a 0.22 μm filter.
6. M9 medium (D_2O) (*see* **Note 3**): dissolve 12.9 g Na_2HPO_4, 3.0 g KH_2PO_4, 1.0 g $^{15}NH_4Cl$, 0.5 g NaCl, 2.0 g ^{2}H glucose, and 1.0 g ^{2}H, ^{15}N CELTONE® base powder in 1.0 L of 99.9% D_2O, and add the following stock solutions: 2.0 mL of 1 M $MgSO_4$, 100 μL of 10 mM $FeCl_3$, 1.0 mL of 1 mg/mL biotin, 100 μL of 50 mg/mL thiamine, 1 mL of 0.1 M $CaCl_2$, 100 μL of 0.5 M $ZnSO_4$, 100 μL of 10 mg/mL choline chloride, 100 μL of 10 mg/mL folic acid, 100 μL of 10 mg/mL niacin, 100 μL of 1 mg/mL riboflavin, and 1.0 mL of 40 mg/mL kanamycin sulfate. Adjust the pH to 7.4. Sterilize with a 0.22 μm filter. For the purification of [u-^{2}H] $GIKR_{CP\text{-}L}$, use non-labeled NH_4Cl and ^{2}H CELTONE® base powder, instead of $^{15}NH_4Cl$ and ^{2}H, ^{15}N CELTONE® base powder.
7. 1.0 M Isopropyl β-D-1-thiogalactopyranoside (IPTG) stock solution, dissolved in D_2O.
8. Purification buffer: 50 mM Tris-HCl (pH 8.0), 200 mM NaCl, 100 mM KCl, 1 mM DTT. Add 20 μM GDP for the purification of [u-^{2}H, ^{15}N] $G\alpha_{i3}$.
9. HIS-Select® Nickel Affinity Gel (Sigma).
10. PreScission™ protease (GE Healthcare).
11. Spectra/Por® 7 MWCO 10K (Spectrum® Laboratories).
12. Glutathione Sepharose™ 4B (GE Healthcare).
13. Amicon® Ultra Centrifuge Filter Unit NMWL 10 kDa (Merck Millipore).
14. Gel filtration buffer: 20 mM NaPi (pH 8.0), 100 mM NaCl, 50 mM KCl, 1 mM DTT.
15. HiLoad™ 26/60 Superdex™ 200 pg column (GE Healthcare).
16. NMR buffer (*see* **Note 4**): 10 mM HEPES-NaOH (pH 6.5), 10 mM $MgCl_2$, 0.8 mM GTPγS, 5 mM DTT, 1 mM sodium 4,4-dimethyl-4-silapentane-1-sulfonate in 80% D_2O.

3 Methods

3.1 Preparation of the Deuterated Acceptor Protein, [u-^{2}H, ^{15}N] $G\alpha_{i3}$

1. Transform the *E. coli* BL21 (DE3) CodonPlusRP cells with the $G\alpha_{i3}$ pET-24d plasmid.
2. Inoculate 5.0 mL of LB medium (10% D_2O) containing 50 mg/L of kanamycin sulfate with a single colony from a

freshly plated transformation. Grow overnight in a 37 °C shaker incubator.

3. Centrifuge 1.0 mL of the culture at 4000 × *g* for 5 min and remove the supernatant thoroughly, resuspend, and transfer into 10 mL of LB medium (D_2O) containing 50 mg/L of kanamycin sulfate. Grow overnight in a 37 °C shaker incubator (*see* **Note 5**).
4. Centrifuge the culture at 3000 × *g* for 10 min and remove the supernatant thoroughly, resuspend, and transfer into 100 mL of M9 medium (D_2O). Grow overnight in a 37 °C shaker incubator.
5. Centrifuge the culture at 4000 × *g* for 5 min and remove the supernatant thoroughly, resuspend, and transfer into 900 mL of M9 medium (D_2O). Grow in a 37 °C shaker incubator.
6. When the OD_{600nm} reaches 0.5, decrease the incubation temperature to 25 °C and grow for 30 min in a shaker incubator.
7. Induce protein expression by adding 1.0 mM of IPTG from an IPTG stock solution. Grow for 8 h in a 25 °C shaker incubator. The final OD_{600nm} is typically between 1.8 and 2.0.
8. Harvest the cells by centrifugation at 7000 × *g* for 15 min at 4 °C. Resuspend the cell pellets in 50 mL of purification buffer per liter of cell culture. If you do not proceed to purification immediately, flash-freeze the cells in liquid N_2 and store at −80 °C.
9. Lyse the cell suspension by sonication (on ice, with short bursts to avoid excessive heating). Centrifuge the cell lysate at 100,000 × *g* for 30 min, and collect the supernatant.
10. Load the clarified cell lysate onto a 5.0 mL HIS-Select® Nickel Affinity Gel column equilibrated with purification buffer containing 30 mM imidazole. Wash the column successively with 5 column volume (CV) of purification buffer containing 20 mM imidazole, 5 CV of purification buffer containing 30 mM imidazole. Elute the $G\alpha_{i3}$ protein with 5 CV of purification buffer containing 100 mM imidazole, and 3 CV of purification buffer containing 300 mM imidazole.
11. Pool the elution fractions and quantify the amount of the $G\alpha_{i3}$ protein by absorbance at 280 nm ($\varepsilon = 38{,}850\ cm^{-1}M^{-1}$). Add 5.0 U/mg protein PreScission™ protease. Dialyze against 30-fold volume of purification buffer with a Spectra/Por® 7 MWCO 10K membrane at 4 °C for 12 h.
12. Load the protein solution subsequently onto a 2.5 mL Glutathione Sepharose™ 4B column and a 2.5 mL HIS-Select® Nickel Affinity Gel column to remove the protease and the cleaved His-tag. Collect the flow-through and the wash fractions. Typical yield of the protein is 5–7 mg/L culture.

13. Concentrate the protein to 5–10 μM with an Amicon® Ultra Centrifuge Filter Unit. Add 100 μM GTPγS and incubate at room temperature for 1 h.
14. Exchange the solvent to NMR buffer by sequential dilution and concentration with an Amicon® Ultra Centrifuge Filter Unit.

3.2 Preparation of the Non-labeled Donor Protein, $GIRK_{CP-L}$

1. Transform the *E. coli* BL21(DE3) CodonPlusRP cells with the $GIRK_{CP-L}$ pET-24d plasmid.
2. Inoculate 5.0 mL of LB medium containing 50 mg/L of kanamycin sulfate with a single colony from a freshly plated transformation. Grow overnight in a 37 °C shaker incubator.
3. Transfer the cell culture into 1.0 L of LB medium. Grow in a 37 °C shaker incubator. When the OD_{600nm} reaches 0.5, decrease the incubation temperature to 25 °C and grow for 30 min in a shaker incubator.
4. Induce protein expression by adding 1.0 mM of IPTG from a stock of 1 M IPTG solution. Grow for 8 h in a 25 °C shaker incubator. The final OD_{600nm} is typically between 1.8 and 2.0.
5. Harvest the cells by centrifugation at 7000 × *g* for 15 min at 4 °C. Resuspend the cell pellets in 30 mL of purification buffer per liter of cell culture. If you do not proceed to purification immediately, flash-freeze the cells in liquid N_2 and store at −80 °C.
6. Load the clarified cell lysate onto a 5 mL HIS-Select® Nickel Affinity Gel column equilibrated with purification buffer containing 30 mM imidazole. Wash the column successively with 5 CV of purification buffer containing 20 mM imidazole, 5 CV of purification buffer containing 30 mM imidazole. Elute the $GIRK_{CP-L}$ protein with 5 CV of purification buffer containing 100 mM imidazole, and 3 CV of purification buffer containing 300 mM imidazole.
7. Pool the elution fractions and quantify the amount of the $GIRK_{CP-L}$ protein by absorbance at 280 nm (ε = 11,460 $cm^{-1}M^{-1}$). Add 5.0 U/mg protein PreScission™ protease. Dialyze against 30-fold volume of purification buffer with a Spectra/Por® 7 MWCO 10K membrane at 4 °C for 12 h.
8. Load the protein solution subsequently onto a 2.5 mL Glutathione Sepharose™ 4B column and a 2.5 mL HIS-Select® Nickel Affinity Gel column to remove the protease and the cleaved His-tag. Collect the flow-through and the wash fractions.
9. Concentrate the protein solution to ~10 mL. Filter the concentrated solution with a 0.22 μm filter unit.

10. Load onto the HiLoad™ 26/60 Superdex™ 200 pg column equilibrated with gel-filtration buffer. Collect the fractions containing $GIRK_{CP\text{-}L}$ tetramer (typically 180–200 mL).
11. Exchange the solvent to NMR buffer by sequential dilution and concentration with an Amicon® Ultra Centrifuge Filter Unit.

3.3 Preparation of the ^{2}H-Labeled Donor Protein for a Control Experiment, [u-^{2}H] $GIRK_{CP\text{-}L}$

1. Transform the *E. coli* BL21 (DE3) CodonPlusRP cells with the plasmid pET24d-$GIRK_{CP\text{-}L}$.
2. Inoculate 5.0 mL of LB medium (10% D_2O) containing 50 mg/L of kanamycin sulfate with a single colony from a freshly plated transformation. Grow overnight in a 37 °C shaker incubator.
3. Centrifuge 1.0 mL of the culture at 4000 × *g* for 5 min and remove the supernatant thoroughly, resuspend, and transfer into 10 mL of LB medium (D_2O) containing 50 mg/L of kanamycin sulfate. Grow overnight in a 37 °C shaker incubator.
4. Centrifuge the culture at 3000 × *g* for 10 min and remove the supernatant thoroughly, resuspend, and transfer into 100 mL of M9 medium (D_2O). Grow overnight in a 37 °C shaker incubator.
5. Centrifuge the culture at 4000 × *g* for 5 min and remove the supernatant thoroughly, resuspend, and transfer into 900 mL of M9 medium (D_2O). Grow in a 37 °C shaker incubator.
6. When the OD_{600nm} reaches 0.5, decrease the incubation temperature to 25 °C and grow for 30 min in a shaker incubator.
7. Induce protein expression by adding 1.0 mM of IPTG from a stock of 1 M IPTG solution. Grow for 8 h in a 25 °C shaker incubator.
8. Harvest the cells and proceed to the purification as described in Subheading 3.2, **steps 5–11**.

3.4 TCS Experiments

1. Mix the purified [^{2}H, ^{15}N] $G\alpha_{i3}$ (final concentration 300 μM) and non-labeled $GIRK_{CP\text{-}L}$ (final concentration 250 μM as a tetramer). Centrifuge the mixed sample at 17,800 × *g* for 15 min at 25 °C to remove insoluble matters. Transfer the sample to the NMR tube.
2. Determine an optimum ^{1}H *90°* pulse power, a water resonance frequency, and a receiver gain. Check a ^{1}H 1D spectrum and a ^{1}H-^{15}N TROSY spectrum to confirm sample homogeneity and purity (*see* **Note 6**).
3. The pulse scheme for the TCS experiment is shown in Fig. 2. The pulse scheme consists of a band selective RF irradiation period, followed by a ^{1}H-^{15}N TROSY scheme. During the RF irradiation period, the carrier frequency is set to 0.83 ppm, and

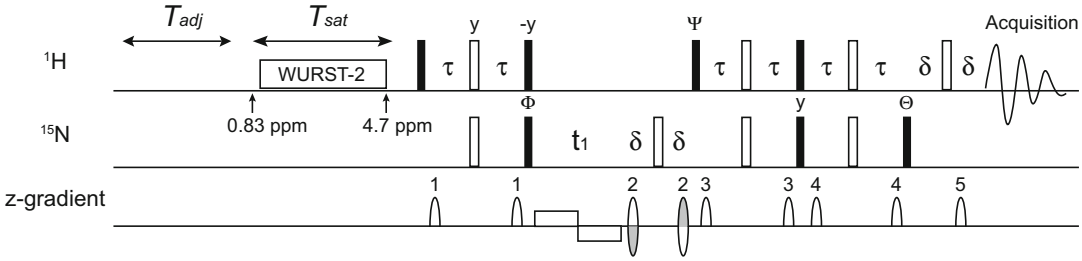

Fig. 2 Pulse scheme for the TCS experiment. Unless otherwise specified, pulse phases are along the *x*-axis. *Filled* and *open rectangles* represent 90° and 180° pulses, respectively. The duration and the amplitude of the sine-shaped pulsed magnetic field gradient applied along the *z*-axis: G1 = (1 ms, 15 G/cm); G2 = (0.6 ms, 40 G/cm); G3 = (1 ms, 22.5 G/cm); G4 = (1 ms, 25 G/cm); G5 = (0.6 ms, 8.1 G/cm). The bipolar gradient (0.5 G/cm) is applied during the t_1 period. The delay τ is set to 2.25 ms, and the delay δ is set to 0.8 ms. The following phase cycling scheme was used: $\Phi = \{y, -y, -x, x\}$; $\Psi = \{y\}$; $\Theta = \{x\}$; receiver = $\{x, -x, -y, y\}$. In the ^{15}N (t_1) dimension, a phase-sensitive spectrum is obtained by recording a second free induction decay (FID) for each increment of t_1, with $\Phi = \{-y, y, -x, x\}$; $\Psi = \{-y\}$; $\Theta = \{-x\}$; receiver = $\{x, -x, -y, y\}$, and inverting the sign of the G2. To measure a spectrum with RF irradiation of an aliphatic region, a band-selective WURST-2 saturation scheme is applied during the T_{sat} period prior to the TROSY scheme. In this case, the carrier frequency is switched to that for the irradiation (0.83 ppm) before the WURST-2 saturation period (T_{sat}) and back to the water frequency (4.7 ppm) just before the TROSY scheme. The adjusting delay (T_{adj}) can be set to an appropriate value for obtaining a sufficient signal-to-noise ratio. The scheme presented here is modified from a basic TROSY experiment implemented in a TopSpin2.1 software (Bruker) as "trosyetf3gpsi," which is based on the scheme proposed by Zhu and coworkers [25]

the WURST-2 (the adiabatic factor $Q_0 = 1.0$) pulses with the maximum amplitude of 0.17 kHz are successively applied in a MLEV-16 phase cycling scheme [16]. Following the RF irradiation period, the carrier frequency is switched to the water frequency (4.7 ppm). Two spectra, with and without RF irradiation, are recorded alternatively for each ^{15}N increment. The length of the RF irradiation period for saturation (T_{sat}) and the adjusting delay (T_{adj}) are set to 1.5 s and 2.5 s, respectively, and the number of scans for each increment is set to 80. A total measurement time is 43 h (*see* **Notes 7** and **8**).

4. Perform a 2D Fourier transform of the time domain data to obtain the frequency domain spectrum.
5. Measure the peak intensities of ^{1}H-^{15}N cross peaks with the RF irradiation (I_{sat}), and those without the RF irradiation (I_{ref}) (Fig. 3a).
6. To evaluate the effect of the residual aliphatic ^{1}H nuclei within $G\alpha_{i3}$, a control experiment is also performed with the same procedures as described in **steps 1–5**, using the sample containing [^{2}H,^{15}N] $G\alpha_{i3}$ (final concentration 300 μM) and [u-^{2}H] $GIRK_{CP\text{-}L}$ (final concentration 250 μM as a tetramer). Record the TCS experiments and measure the peak intensities of ^{1}H-^{15}N cross peaks with the RF irradiation ($I_{sat(control)}$), and

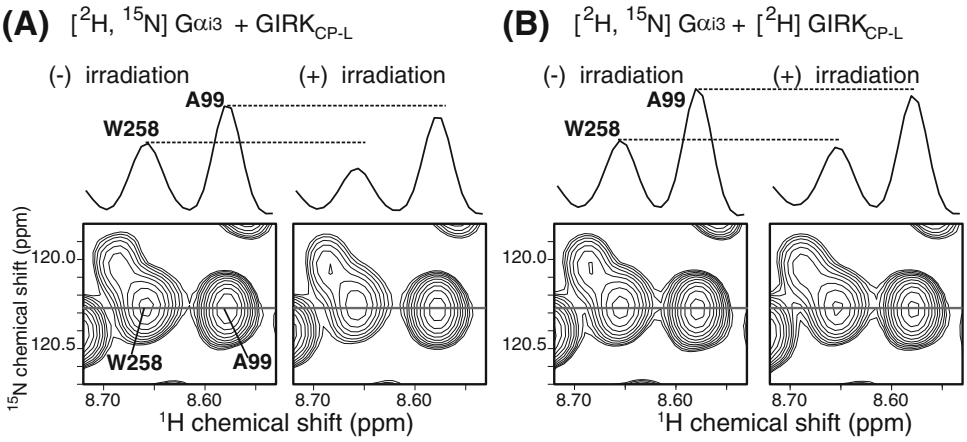

Fig. 3 TCS from $GIRK_{CP-L}$ to $G\alpha_{i3}$. (**a**) A selected portion of the ^{1}H-^{15}N TROSY spectra of the [u-^{2}H, ^{15}N] $G\alpha_{i3}$ (300 μM) in the presence of non-labeled $GIRK_{CP-L}$ (250 μM as a tetramer), which was recorded without (*left*) and with (*right*) RF irradiation. Cross-sections are also shown for the signals from Ala99 and Trp258. (**b**) Procedures were the same as (**a**), except that [u-^{2}H] $GIRK_{CP-L}$ was used instead of non-labeled $GIRK_{CP-L}$, as a control. The figures were originally published in the Journal of Biological Chemistry vol. 287, No.23, pp. 19537–19549, June 1, 2012. © 2012 by The American Society for Biochemistry and Molecular Biology, Inc.

those without the RF irradiation ($I_{ref(control)}$) (Fig. 3b) (*see* **Notes 9** and **10**).

7. Calculate the difference in the signal intensity reduction ratios (ΔRR) using an equation below. The ΔRR value represents the cross-saturation effect from $GIRK_{CP-L}$ on $G\alpha_{i3}$. Calculate the errors based on the signal-to-noise ratios.

$$\Delta RR = \left(1 - \frac{I_{sat}}{I_{ref}}\right) - \left(1 - \frac{I_{sat(control)}}{I_{ref(control)}}\right) = \frac{I_{sat(control)}}{I_{ref(control)}} - \frac{I_{sat}}{I_{ref}}$$

8. Plot the ΔRR values according to the residue number (Fig. 4a), and map the residues showing a significant ΔRR value (ΔRR > 0.08, including errors) on the structure of the Gα (Fig. 4b, c). These residues are located on the helical domain (G89 in the αA helix; G112 and A114 in the αB helix) and the GTPase domain (R208, K209, W211, I212, H213, E216, and G217 in the α2 helix and the following loop; M240, K248, L249, I253, N256, and W258 in the α3 helix and the flanking loops; E186 in the β2 strand). The mapping of these residues on the structure of Gα revealed that the residues identified on the GTPase domain of $G\alpha_{i3}$ were clustered, indicating that this site mainly contributes to the $GIRK_{CP-L}$ binding (*see* **Notes 11–13**).

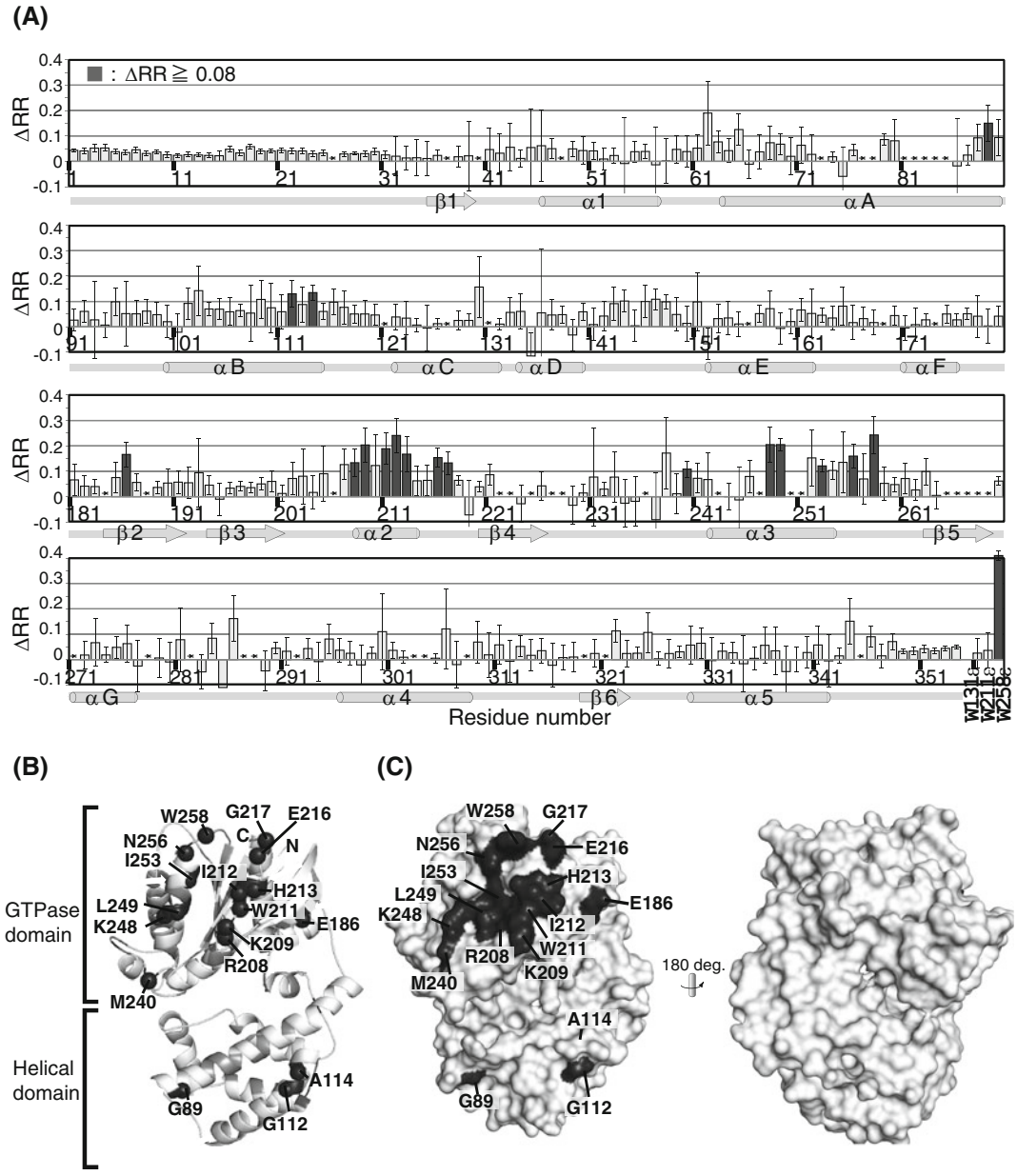

Fig. 4 (**a**) A plot of the difference in the reduction ratios (ΔRR) originating from the backbone amide groups with and without irradiation in the presence of non-labeled $GIRK_{CP-L}$ and [u-^{2}H] $GIRK_{CP-L}$. The residues indicated by *asterisks* are those with no data mostly due to overlapping of the resonances or insufficient signal-to-noise ratio. The error bars were calculated based on the signal-to-noise ratios. Bars corresponding to the residues with significant intensity reductions ($\Delta RR \geq 0.08$, including errors) are colored *black*. The secondary structure elements of $G\alpha_{i3}$ are depicted in *gray* below the sequence. (**b**) Mapping of the affected residues in the TCS experiment on the Gα structure (PDB code: 1GIA) is shown. The backbone nitrogen atoms of the affected residues are shown as *black balls* in the *ribbon* diagram of the Gα structure, whereas the residues with no data, including proline residues, are colored *gray* (*left*). The affected residues are colored *black* on the surface representations of the Gα structure (*center* and *right*). The figures were originally published in the Journal of Biological Chemistry vol. 287, No.23, pp. 19537–19549, June 1, 2012. © 2012 by The American Society for Biochemistry and Molecular Biology, Inc.

4 Notes

1. In the acceptor protein, all hydrogens are replaced with ^{2}H, except for the solvent-exchangeable amide hydrogens. And the fraction of ^{1}H for the exchangeable hydrogens is low in a solvent with a low H_2O/D_2O ratio. In this situation, the spin diffusion (dipolar cross relaxation between ^{1}H within the acceptor protein) is effectively suppressed.
2. The lower bound of the dissociation rate constant is estimated to be about 0.1 s^{-1} from the simulation using a model spin system [17].
3. The ^{2}H labeling efficiency of the acceptor protein is critical for suppressing the spin diffusion effects from residual ^{1}H nuclei. Use thoroughly dried beakers and culture flasks, and anhydride phosphate when preparing the M9 (D_2O) media.
4. In the CS and TCS experiments, a solvent with a low H_2O/D_2O ratio is essential for suppressing the spin diffusion within the acceptor protein. However, the low H_2O/D_2O ratio also reduces the observable magnetization by decreasing the ^{1}H occupancies of amide groups in the acceptor protein. Calculations using a model spin system showed that the H_2O/D_2O ratio between 10% and 30% is desirable [17].
5. To improve ^{2}H labeling efficiency, preculture is prepared in a multi-stage process.
6. The resonance assignment of the amide signals on the ^{1}H-^{15}N TROSY spectrum needs to be established before conducting the TCS experiment [18].
7. The length of the T_{sat} and T_{adj} should be optimized according to the systems. The use of the long T_{sat} enhances the observed cross saturation effect; however, the spin diffusion effects also tend to be strong. The total repetition period, which mainly depends on the sum of T_{sat} and T_{adj}, should be long enough to obtain a sufficient signal-to-noise ratio. The short repetition period results in signal attenuations, because the observable magnetization has not returned to the equilibrated value at the start of the sequence, due to a long longitudinal relaxation time (T_1) of amide ^{1}H nuclei in a buffer with a low H_2O/D_2O ratio. The short repetition period can also lead to artifacts originating from the site-to-site variance of the T_1.
8. The TCS experiments usually require a long measurement time due to the setting of a long repetition delay and the low observable magnetization in a buffer with a low H_2O/D_2O ratio. To overcome this difficulty, we have developed the method to reconstruct 2D NMR spectra from the limited number of data points utilizing the chemical shift information,

"conservation of experimental data in analysis of Fourier (Co-ANAFOR)," which can shorten the measurement time to one-half or one-quarter without the loss of the accuracy of signal intensities [19]. The use of co-ANAFOR is particularly beneficial, when the protein complexes are not stable and cannot tolerate a long measurement time [20].

9. It is usually sufficient to perform a control experiment using the sample containing only the acceptor protein. In the case of the TCS experiment of $G\alpha_{i3}$ and $GIRK_{CP\text{-}L}$, the sample with high protein concentration (total 550 μM) is needed to increase the fraction of $G\alpha_{i3}$ bound to $GIRK_{CP\text{-}L}$. The high protein concentration causes an increase in solvent viscosity, which leads to enhanced spin diffusion effects caused by the slowing of the overall tumbling motion. Therefore, we used the control sample containing [u-^{2}H] $GIRK_{CP\text{-}L}$ to correct the effects of solvent viscosity.
10. When the spin diffusion effects from the residual ^{1}H severely hamper the analysis, the use of selective RF pulses (I-BURP [21] or continuous wave) would be effective. The use of selective RF irradiations reduces the direct saturation of the residual ^{1}H nuclei and the exchangeable ^{1}H nuclei in the hydroxyl and thiol groups, alleviating the spin diffusion effects.
11. A CS experiment utilizing side chain methyl ^{1}H-^{13}C signals is an alternative approach for the identification of a binding surface [22]. Since the side chain methyl groups usually have direct contacts with the interacting proteins, the efficiency of the cross saturation is expected to be higher than that for main chain amide groups. The combined use of the methyl-utilizing CS experiment and the amide-based CS experiment would be recommended for highly accurate determinations of the binding surfaces.
12. The binding surface of the donor protein can be identified from several approaches. The simplest approach is to conduct the experiment, in which the donor and the acceptor proteins are swapped. This approach is effective when the both donor and acceptor proteins can be isotopically labeled and observed by NMR. Alternatively, amino acid selective cross saturation (ASCS) experiment can be conducted [23]. The ASCS experiment uses a donor protein, in which only one amino acid is selectively ^{1}H-labeled in a ^{2}H-background, and an acceptor protein with uniformly ^{2}H, ^{15}N labeled. Using the three-dimensional structure of each protein, the combinatorial analysis of multiple ASCS results can specify the CS-source residues, based on the spatial complementarity between the CS-source residues on the CS donor and the amide protons on the acceptor protein.

13. The complex model structure can be obtained with the HADDOCK (High Ambiguity Driven protein-protein DOCKing) software [24]. The residues identified from the TCS experiments are specified as the "active residues" in the program, so that they form the interface of the complex. Then, models of the complex satisfying the TCS results are generated by the rigid body docking procedures.

Acknowledgments

This work was supported in part by grants from the Japan New Energy and Industrial Technology Development Organization (NEDO) and the Ministry of Economy, Trade, and Industry (METI) (to I.S.), a Grant-in-Aid for Scientific Research on Priority Areas from the Japanese Ministry of Education, Culture, Sports, Science, and Technology (MEXT) (to I.S.), the Development of core technologies for innovative drug development based upon IT from Japan Agency for Medical Research and development, AMED (to I.S.), JSPS KAKENHI Grant Number JP16H01368 (to M.O.), a grant from The Vehicle Racing Commemorative Foundation (to M.O.), and a grant from Nagase Science Technology Foundation (to M.O.).

References

1. Barhanin J, Lesage F, Guillemare E et al (1996) K_VLQT1 and IsK (minK) proteins associate to form the I_{KS} cardiac potassium current. Nature 384:78–80
2. Sanguinetti MC, Curran ME, Zou A et al (1996) Coassembly of K_VLQT1 and minK (IsK) proteins to form cardiac I_{KS} potassium channel. Nature 384:80–83
3. Logothetis DE, Kurachi Y, Galper J et al (1987) The βγ subunits of GTP-binding proteins activate the muscarinic K^+ channel in heart. Nature 325:321–326
4. Yokogawa M, Takeuchi K, Shimada I (2005) Bead-linked proteoliposomes: a reconstitution method for NMR analyses of membrane protein–ligand interactions. J Am Chem Soc 127:12021–12027
5. Yoshiura C, Kofuku Y, Ueda T et al (2010) NMR analyses of the interaction between CCR5 and its ligand using functional reconstitution of CCR5 in lipid bilayers. J Am Chem Soc 132:6768–6777
6. Kubo S, Nishida N, Udagawa Y et al (2013) A gel-encapsulated bioreactor system for NMR studies of protein-protein interactions in living mammalian cells. Angew Chem Int Ed Engl 52:1208–1211
7. Takahashi H, Nakanishi T, Kami K et al (2000) A novel NMR method for determining the interfaces of large protein-protein complexes. Nat Struct Biol 7:220–223
8. Shimada I, Ueda T, Matsumoto M et al (2009) Cross-saturation and transferred cross-saturation experiments. Prog NMR Spect 54:123–140
9. Ueda T, Takeuchi K, Nishida N et al (2014) Cross-saturation and transferred cross-saturation experiments. Q Rev Biophys 47:143–187
10. Takeuchi K, Yokogawa M, Matsuda T et al (2003) Structural basis of the KcsA K^+ channel and agitoxin2 pore-blocking toxin interaction by using the transferred cross-saturation method. Structure 11:1381–1392
11. Ozawa S, Kimura T, Nozaki T et al (2015) Structural basis for the inhibition of voltage-dependent K^+ channel by gating modifier toxin. Sci Rep 5:14226
12. Yokogawa M, Osawa M, Takeuchi K et al (2011) NMR analyses of the Gβγ binding and conformational rearrangements of the

cytoplasmic pore of G protein-activated inwardly rectifying potassium channel 1 (GIRK1). J Biol Chem 286:2215–2223

13. Mase Y, Yokogawa M, Osawa M et al (2012) Structural basis for modulation of gating property of G protein-gated inwardly rectifying potassium ion channel (GIRK) by i/o-family G protein α subunit ($G\alpha_{i/o}$). J Biol Chem 287:19537–19549
14. Pervushin K, Riek R, Wider G et al (1997) Attenuated T_2 relaxation by mutual cancellation of dipole-dipole coupling and chemical shift anisotropy indicates an avenue to NMR structures of very large biological macromolecules in solution. Proc Natl Acad Sci U S A 94:12366–12371
15. Nakanishi T, Miyazawa M, Sakakura M et al (2002) Determination of the interface of a large protein complex by transferred cross-saturation measurements. J Mol Biol 318:245–249
16. Kupce E, Wagner G (1995) Wideband homonuclear decoupling in protein spectra. J Magn Reson 109:329–333
17. Matsumoto M, Ueda T, Shimada I (2010) Theoretical analyses of the transferred cross-saturation method. J Magn Reson 205:114–124
18. Mase Y, Yokogawa M, Osawa M et al (2012) Backbone resonance assignments for G protein α_{i3} subunit in the GTP-bound state. Biomol NMR Assign 6:217–220
19. Ueda T, Yoshiura C, Matsumoto M et al (2015) Development of a method for reconstruction of crowded NMR spectra from undersampled time-domain data. J Biomol NMR 62:31–41
20. Yoshiura C, Ueda T, Kofuku Y et al (2015) Elucidation of the CCR1- and CCR5-binding modes of MIP-1α by application of an NMR spectra reconstruction method to the transferred cross-saturation experiments. J Biomol NMR 63:333–340
21. Geen H, Freeman R (1991) Band-selective radiofrequency pulses. J Magn Reson 93:93–141
22. Takahashi H, Miyazawa M, Ina Y et al (2006) Utilization of methyl proton resonances in cross-saturation measurement for determining the interfaces of large protein–protein complexes. J Biomol NMR 34:167–177
23. Igarashi S, Osawa M, Takeuchi K et al (2008) Amino acid selective cross-saturation method for identification of proximal residue pairs in a protein−protein complex. J Am Chem Soc 130:12168–12176
24. de Vries SJ, van Dijk M, Bonvin AMJJ (2010) The HADDOCK web server for data-driven biomolecular docking. Nat Protoc 5:883–897
25. Zhu G, Kong XM, Sze KH (1999) Gradient and sensitivity enhancement of 2D TROSY with water flip-back, 3D NOESY-TROSY and TOCSY-TROSY experiments. J Biomol NMR 13:77–81

Chapter 11

Studying Mechanosensitivity of Two-Pore Domain K^+ Channels in Cellular and Reconstituted Proteoliposome Membranes

Josefina del Mármol, Robert A. Rietmeijer, and Stephen G. Brohawn

Abstract

Mechanical force sensation is fundamental to a wide breadth of biology from the classic senses of touch, pain, hearing, and balance to less conspicuous sensations of proprioception, blood pressure, and osmolarity and basic aspects of cell growth, differentiation, and development. These diverse and essential systems use force-gated (or mechanosensitive) ion channels that convert mechanical stimuli into cellular electrical signals. TRAAK, TREK1, and TREK2 are K^+-selective ion channels of the two-pore domain K^+ (K2P) family that are mechanosensitive: they are gated open by increasing membrane tension. TRAAK and TREK channels are thought to play roles in somatosensory and other mechanosensory processes in neuronal and non-neuronal tissues. Here, we present protocols for three assays to study mechanical activation of these channels in cell membranes: (1) cell swelling, (2) cell poking, and (3) patched membrane stretching. Patched membrane stretching is also applicable to the study of mechanosensitive K2P channel activity in a cell-free system and a procedure for proteoliposome reconstitution and patching is also presented. These approaches are also readily applicable to the study of other mechanosensitive ion channels.

Key words K2P ion channel, TREK1, TREK2, TRAAK, Mechanosensitive ion channel, Membrane tension gating, Patch clamp, Cell poking, Cell swelling, Patch inflation, Proteoliposome reconstitution

1 Introduction

Mechanosensitive ion channels transduce mechanical forces into electrical currents. They underlie force sensation in hearing, balance, touch, and an increasingly appreciated repertoire of less conspicuous force sensations. In fact, mechanosensitive ion channel activity is almost ubiquitous in cells, although the biological function of the currents in many contexts is unknown [1–5]. Cationic depolarizing, anionic depolarizing, and K^+-selective hyperpolarizing mechanosensitive currents have been recorded from different underlying ion channels. The K^+-selective mechanosensitive

Josefina del Mármol and Robert A. Rietmeijer contributed equally to this work.

Show-Ling Shyng et al. (eds.), *Potassium Channels: Methods and Protocols,* Methods in Molecular Biology, vol. 1684,
DOI 10.1007/978-1-4939-7362-0_11,

currents are of two types: one is carried by a subset of voltage-gated K^+-selective (K_v) channels [6, 7] and the second is carried by a subset of two pore domain K^+-selective (K2P) channels [8, 9]. The three related mechanosensitive K2P channels TRAAK, TREK1, and TREK2 are intrinsically and remarkably mechanosensitive: they are activated by membrane tension over essentially the entire range of their accessible open probability [10, 11].

Here we present three robust and complementary assays we routinely use for studying the mechanical activation of TRAAK and TREK K2P channels: cell swelling, cell poking, and patched membrane stretching. All three assays are applicable to recording channel activity in cells. Patched membrane stretching is also applicable to studying mechanical activation of K2Ps in a fully reconstituted system and a procedure for purification and reconstitution of mechanosensitive K2Ps into proteoliposomes for this purpose is also presented.

Cell swelling involves changing the osmolarity of the solution surrounding cells. Hypo-osmotic bath solution causes water influx into cells and the resulting volume change generates stress on the plasma membrane. Depending on the physiology of the cell under study, different cascades of downstream events can follow, but the initial swelling is thought to generate tension in the plasma membrane that can open mechanosensitive ion channels including TRAAK and TREK channels. Their activation can be assessed by electrophysiology. The advantages of this technique include simplicity and adaptability to most recording setups and experimental preparations. There are two major disadvantages of this technique. First, although solution composition can be controlled precisely, the assay is not perfectly quantitative because the mechanical response of different cells to the same osmotic stimulus can vary. Second, swelling is a slow process (typically on the order of seconds depending on the solution exchange system) compared to channel activation (which can occur on milli- to micro-second time scale). As a result, a number of intracellular signaling events are initiated in parallel with the increase in membrane tension. It is difficult to then distinguish whether changes in channel activity are due to tension changes or intracellular signaling events. Channel activation from hypo-osmotic shock thus may or may not be due to membrane tension sensitivity.

Cell poking involves mechanically stimulating an individual cell by depressing a blunt probe against its plasma membrane. The probe is mounted on a stacked piezo actuator to control displacement and the cell is simultaneously recorded with an electrode through a distal region of the membrane [12, 13]. Compared to swelling, poking stimuli can be delivered more rapidly (milliseconds). This permits kinetic aspects of channel activation to be reliably studied. Solution changes are not necessary and cells can be studied in a more physiological context. However, it is still a

challenge to quantify mechanical activation that results from the membrane tension created by poking. While the position of the probe can be precisely controlled, the tension created by probe depression of the same distance will vary between cells as a result of their different volumes and morphologies and poking different parts of the same cell often generates different responses. Despite these caveats, cell poking is in many ways the best approach for studying mechanical activation of channels in a cellular context.

Patched membrane stretching involves applying steps of positive or negative pressure through the recording pipette to a patch of membrane under study. The membrane is stretched by the pressure change to create tension in the bilayer. Using a high-speed pressure clamp allows for rapid (milliseconds) and precise changes in the applied pressure [14]. There are several advantages to this approach compared to cell swelling and poking. First, it permits quantification of membrane tension. According to the Young-Laplace relationship, tension in the membrane is related to its radius of curvature and the pressure difference across the bilayer. These can be measured and tension calculated during patched membrane stretching [15]. Despite some caveats to this approach including a relatively high (~0.5–4 mN/m) and nonuniform basal tension in the patched membrane [16, 17], it has been instrumental in characterizing mechanosensitive channels [18–22]. Second, membrane stretching is applicable to patches from cells in any configuration (inside-out, outside-out, or cell-attached) and to patches from proteoliposomes containing purified channels reconstituted into fully defined lipid membranes [23]. The ability to study channel mechanosensitivity in the absence of all other cellular components is invaluable for understanding mechanisms of channel mechanosensitivity: it is the only rigorous way to exclude roles of other macromolecules in sensing and transmitting force to a mechanosensitive channel [24]. Without a reductionist approach, whether mechanical force opens the channel through tension in the surrounding membrane or by other means cannot be unequivocally determined. Reconstitution furthermore permits the chemical and physical properties of the surrounding lipid bilayer to be systematically varied so that their effects on channel activity can be determined.

Below we present procedures for studying mechanosensitivity of K2P ion channels using these complementary approaches: expression of mechanosensitive K2P channels in (1) cultured cells for study with cell swelling, cell poking, and patched membrane stretching assays and (2) in *Pichia pastoris* for purification, reconstitution into proteoliposomes, and study with patched membrane stretching.

2 Materials

2.1 Expression of Mechanosensitive K2Ps in Cultured Cells

1. Host cells: HEK293T, CHO-K1, or SF9 cells (*see* **Notes 1** and **2**).
2. Growth media and reagents. HEK293T cell media: DMEM with 10% Fetal bovine serum (FBS), 1% Glutamax, and 1% nonessential amino acids. CHO-K1 cell media: DMEM:F12 with 10% FBS, and 1% nonessential amino acids. Trypsin, Dulbecco's phosphate-buffered saline (DPBS), 35 mm plastic tissue culture-treated dishes, and poly-D-lysine (PDL)-coated coverslips.
3. Transfection media and reagents: Fugene HD, Optimem (*see* **Note 3**).
4. Mechanosensitive K2P cloned into a suitable mammalian cell expression vector (e.g., human TRAAK in pCEH [21]).

2.2 Expression of Mechanosensitive K2Ps in Pichia pastoris

2.2.1 Transformation of Pichia pastoris

1. Host cells: *Pichia pastoris* strain (e.g., SMD1163) stored as glycerol stock.
2. Mechanosensitive K2P cloned into suitable *Pichia* expression vector to generate a protease cleavable, EGFP and His-tagged fusion protein (e.g., human TRAAK-EGFP-10×His in pPICZ [21]).
3. Solutions for transformation: 3 M Sodium Acetate pH 5.2, 100% Ethanol, 70% Ethanol, ice-cold 1 M Sorbitol (0.22 μm filtered), 1 M HEPES-KOH pH 8.0, 1 M DTT, YPD (1% w/v yeast extract, 2% peptone, 2% dextrose, *see* **Note 4**), 100 mg/mL Zeocin in H_2O.
4. Selection plates: YPD with 1 M sorbitol, 2% w/v agar, and 0.5 mg/mL Zeocin (final concentrations).
5. Equipment for transformation: electroporator, electroporation cuvettes, 250 mL baffled flask, glass plating beads.

2.2.2 Growth and Expression of Pichia pastoris

1. Media components: 10× YNB (per liter: 100 g $(NH_4)_2SO_4$ and 34 g yeast nitrogen base without amino acids and without ammonium sulfate), 10× Glycerol (10% v/v), 10× Potassium Phosphate (KP_i) pH 6 (per liter: 52.26 g K_2HPO_4 and 95.26 g KH_2PO_4), 250× Biotin (0.1 mg/mL in H_2O), Methanol (*see* **Note 5**).
2. Prepared media: Glycerol growth media (BMGY: 1× YNB, 1× Glycerol, 1× Biotin, 1× KP_i pH 6) and Methanol expression media (BMMY: 1× YNB, 1× Biotin, 1× KP_i pH 6, 0.5% v/v Methanol).
3. Materials to freeze cells: Liquid nitrogen, silicone kitchen spatulas, metal strainer, plastic bags.

2.3 Purification of Mechanosensitive K2Ps from Pichia

2.3.1 Materials Common to Large and Small-Scale Procedures

1. Cryogenic mixer mill and liquid nitrogen.
2. Lysis Buffer (*see* **Note 6**, all final concentrations): 50 mM Tris-HCl pH 8.0, 150 mM KCl, 1 mM EDTA pH 8.0, DNAse (50 μg/mL), protease inhibitors (Leupeptin (1 μg/mL), Pepstatin A (1 μg/mL), Soy Trypsin Inhibitor (10 μg/mL), Aprotinin (1 μg/mL), Benzamidine (1 mM), PMSF (1 mM), *see* **Note 7**).
3. Dodecyl maltoside (DDM) (*see* **Note 8**).
4. Size-exclusion chromatography (SEC) buffer (all final concentrations): 20 mM Tris-HCl pH 8.0, 150 mM KCl, 1 mM EDTA, 1 mM DDM.
5. Liquid chromatography instrument and Superose 200 10/300 size-exclusion column (*see* **Note 9**).

2.3.2 Materials for Small-Scale Lysis and Extraction Testing

1. Eppendorf tube adapter for mixer mill.
2. 0.1–0.25 mm glass beads.
3. 8× DDM: 320 mM DDM in Lysis Buffer (163 mg DDM added to 900 μL Lysis Buffer).

2.3.3 Materials for Large-Scale Lysis and Purification

1. 50 mL grinding jars, 25 mm diameter ball bearings, O-rings, Styrofoam box for chilling grinding jars in liquid nitrogen.
2. Fritted glass column, peristaltic pump, column flow adapter, UV monitor, flatbed recorder.
3. Cobalt immobilized metal chromatography (IMAC) resin (e.g., Talon).
4. Lysis Buffer with 40 mM DDM.
5. PreScission protease.
6. IMAC buffers (volumes are for a purification from ~25 g *Pichia* cells): TK (40 mL, 50 mM Tris-HCl pH 8.0, 150 mM KCl), TKD (10 mL, TK + 6 mM DDM), TKDI10 (50 mL, TKD + 10 mM imidazole), TKDI30 (25 mL, TKD + 30 mM imidazole), TKDI300 (25 mL, TKD + 300 mM imidazole).

2.4 Reconstitution of Mechanosensitive K2Ps into Proteoliposomes

1. Lipids (e.g., L-α-phosphatidylcholine from soybean or pure lipids).
2. Chloroform, Pentane.
3. Argon gas stream supplied through a glass Pasteur pipette.
4. De/Rehydration (DR) Buffer (100 mL/sample, 200 mM KCl, 5 mM HEPES-KOH pH to 7.2, 0.2 μm filtered).
5. Vacuum chamber with Drierite desiccant.
6. Purified mechanosensitive K2P.
7. Bio-Beads SM-2 absorbent washed according to the manufacturer's instructions followed by one wash into DR buffer.

8. Ultracentrifuge.
9. 35 mm glass-bottom petri dishes.

2.5 Electrophysiology

2.5.1 Materials Common to All Techniques

1. Electrophysiology rig: inverted microscope (*see* **Note 10**) with two high-resolution micromanipulators (<1 μm step size) on an air table to minimize vibration, amplifier with head stage, digitizer, computer, and computer interface.
2. Electrode preparation: bleach, 1.5 mL Eppendorf tubes, silver wire.
3. Pipettes: pipette puller, 10 cm Borosilicate glass with filament O.D.: 1.5 mm, I.D.: 1.17 mm, microforge, 10× Eyepiece with protractor, 2 mL syringes, 0.22 μm filters and fine injection needles or microfil tips for filling.

2.5.2 Cell Swelling

1. Pipette solution: 10 mM HEPES, 150 mM KCl, 3 mM $MgCl_2$, 5 mM EGTA, pH 7.2 (adjusted with KOH). Filter to 0.22 μm.
2. Bath solution, iso-osmotic: 10 mM HEPES, 100 mM NaCl, 15 mM KCl, 3 mM $MgCl_2$, 1 mM $CaCl_2$, 60 mM Sucrose or Sorbitol. pH 7.3 (adjusted with NaOH), 315 mOsm/kg.
3. Bath solution, hypo-osmotic: 10 mM HEPES, 100 mM NaCl, 15 mM KCl, 3 mM $MgCl_2$, 1 mM $CaCl_2$, 60 mM Sucrose or Sorbitol. pH 7.3 (adjusted with NaOH), 250 mOsm/kg.
4. Grounding reservoir solution: 150 mM KCl.
5. Diamond-shape perfusion chamber compatible with coverslips with a small accessory reservoir for the grounding electrode (*see* **Note 11**).
6. Gravity-fed perfusion: 60 mL syringes, luer valve assortment kit and tubing, 18 or 20 G needles, tubing.
7. Salt bridges: 2–5% (w/v) agar in 1 M KCl, 10 cm Borosilicate glass with filament O.D.: 1.5 mm, I.D.: 1.17 mm, microforge.

2.5.3 Cell Poking

1. Pipette solution: 10 mM HEPES, 150 mM KCl, 3 mM $MgCl_2$, 5 mM EGTA, pH 7.2 (adjusted with KOH), 0.22 μm filtered.
2. Bath solution: 10 mM HEPES, 15 mM KCl, 135 mM NaCl, 3 mM $MgCl_2$, 1 mM $CaCl_2$, pH 7.3 (adjusted with NaOH), 0.22 μm filtered.
3. Piezo-driven actuator driven by a controller/amplifier controlled through the electrophysiology software.
4. Glass probes: pipette puller, 10 cm Borosilicate glass with filament O.D.: 1.5 mm, I.D.: 1.17 mm, microforge.

2.5.4 Patched Membrane Stretching

1. High-Speed Pressure Clamp (HSPC), pump, and tubing.
2. Proteoliposome Bath Solution (*see* **Note 12**): 5 mM HEPES, 200 mM KCl, 40 mM $MgCl_2$, pH 7.2 (adjust with KOH), 0.22 μm filtered.

3. Proteoliposome Pipette Solution: 5 mM HEPES, 20 mM KCl, 180 mM NaCl, pH 7.2 (adjust with NaOH), 0.22 μm filtered.
4. High magnification, high NA DIC objective (e.g., 100× 1.4 NA oil immersion) and image analysis software if calculating membrane tension from patch radius of curvature.

3 Methods

3.1 Expression of Mechanosensitive K2Ps in Cultured Cells

1. HEK 293 or CHO cells should be kept using standard sterile technique in an appropriate cell culture environment. Cells should be routinely passaged before reaching 100% confluency.
2. Plate cells in 35 mm plastic dishes (for poking) or poly-D-lysine-coated coverslips (for cell swelling or best optics) 3 days before the experiment day at 0.2–0.5 × 10^6 cells per dish.
3. One day later, transfect cells using Fugene HD following recommended protocol (*see* **Note 13**). Cells will be optimal for recording 36–72 h after transfection (*see* **Note 14**).

3.2 Expression of Mechanosensitive K2Ps in Pichia pastoris

3.2.1 Transformation of Pichia pastoris

1. Purify pPICZ *Pichia* plasmid DNA with cloned mechanosensitive K2P.
2. Linearize 7.5 μg plasmid DNA with 2 μL PmeI at 37 °C for 1.5 h in the appropriate buffer in 50 μL total volume (*see* **Note 15**).
3. Ethanol-precipitate the DNA: Add 5 μL 3 M Sodium Acetate pH 5.2 and 225 μL 100% Ethanol and precipitate at −80 °C for at least 1 h. Centrifuge ≥13,000 × *g* at 4 °C for 20 min. Decant the supernatant carefully and wash the small clear pellet at least once with 1 mL 70% Ethanol. Dry the DNA at room temperature for at least 1 h. Dissolve the dried DNA pellet in 10 μL 0.22 μm filtered H_2O (*see* **Note 16**).
4. Inoculate 40 mL YPD in a 250 mL baffled flask with 600 μL of a SMD1163 *Pichia pastoris* glycerol stock.
5. Grow overnight (~18 h) at 30 °C with shaking at 250 RPM to an OD_{600} ~ 10.
6. Transfer to a 50 mL tube and centrifuge 4000 × *g* at 4 °C for 5 min. Resuspend cell pellet with gentle vortexing in 30 mL YPD and 6 mL 1 M HEPES-KOH pH 8.0.
7. Add 1 mL sterile 1 M DTT and incubate at 30 °C for ≥15 min.
8. Centrifuge 4000 × *g* at 4 °C for 5 min and wash the pellet twice with 50 mL ice-cold 1 M Sorbitol.
9. Resuspend cell pellet with gentle vortexing in 300 μL ice-cold 1 M Sorbitol. This suspension of competent *Pichia* cells should be stored on ice and is suitable for use for several hours.

10. Add 40 μL competent Pichia cells to the linearized DNA resuspended in H_2O and mix.
11. Transfer cells and DNA to the bottom corner of prechilled electroporation cuvette. Gently tap to remove bubbles and small droplets bridging the electrodes (*see* **Note 17**).
12. Incubate on ice for ≥5 min.
13. Electroporate cells with voltage set to 2 kV. The decay time constant should be ~5 ms.
14. Add 1.0 mL ice-cold 1 M Sorbitol, transfer to a culture tube, and incubate at 30 °C ≥1 h.
15. Add 0.5 mL YPD and incubate at 30 °C ≥1 h with shaking at 250 RPM.
16. Plate 300 μL on YPDS plates with 500 μg/mL Zeocin.
17. Grow plates at 30 °C for 3–4 days or until colonies are visible.

3.2.2 Growth and Expression of Pichia pastoris

Because growth and expression conditions that maximize the yield of purified mechanosensitive K2Ps can vary based on the exact construct, strain, and growth environment, a procedure for optimization using a small-scale lysis and extraction test followed by fluorescence size-exclusion chromatography is presented. Large-scale purification can then be performed using the optimal conditions.

Small-Scale Growth

1. Inoculate 2.6 mL of BMGY + 0.5 mg/mL Zeocin in a culture tube with a single colony from a YPDS plate and grow at 30 °C with shaking at 250 RPM overnight or until OD_{600} ~ 10–20.
2. Prepare glycerol stock by adding 600 μL cells to 300 μL 50% v/v sterile glycerol.
3. Centrifuge 4000 × *g* for 5 min, resuspend cells in 2 mL BMMY + 0.5 mg/mL Zeocin, and grow at 27 °C with shaking at 250 RPM for 24 h (*see* **Note 18**).
4. Centrifuge 4000 × *g* for 5 min, remove the supernatant, and snap-freeze cells in liquid nitrogen. Store cell pellets at −80 °C.

Large-Scale Growth

1. Prepare starter culture: Inoculate 10 mL BMGY + 0.5 mg/mL Zeocin in a 50 mL baffled flask with ~100 μL of frozen glycerol stock and grow at 30 °C with shaking at 250 RPM overnight ($OD_{600} \geq 10$).
2. Prepare large-scale culture: Inoculate 1 L BMGY + 25 μg/mL Zeocin in a 2.8 L baffled flask with 10 mL starter culture and grow at 30 °C with shaking at 250 RPM until OD_{600} ~ 20 (*see* **Note 18**).
3. Transfer culture to a 1 L centrifuge bottle and centrifuge 8000 × *g* at 4 °C for 10 min. Resuspend cells in 1 L

BMMY + 25 μg/mL Zeocin, transfer to a clean 2.8 L baffled flask, and grow at 27 °C with shaking at 250 RPM for 24 h (*see* **Note 19**).

4. Transfer culture to a 1 L centrifuge bottle, centrifuge 8000 × *g* at 4 °C for 10 min, and discard the supernatant. Scoop out the pellet with an ethanol rinsed silicone spatula and scrape into a metal strainer submerged in liquid nitrogen to snap-freeze the cells. Transfer the frozen cells to a plastic bag, record cell mass, and store cell pellets at −80 °C.

3.3 Purification of Mechanosensitive K2Ps from Pichia pastoris

3.3.1 Small-Scale Lysis and Extraction Testing

1. Resuspend cells from small-scale growth (or ~50 mg of frozen cells) in 750 μL of Lysis Buffer in a 1.5 mL tube.
2. Add ~0.75 mL glass beads.
3. Mill 3 cycles at 30 Hz for 1.5 min per cycle. Incubate on ice for 2 min between cycles.
4. Taking care to avoid glass beads, transfer the supernatant to a new 1.5 mL tube on ice, wait for a minute to allow any transferred beads to settle, and transfer 490 μL of supernatant to a second new 1.5 mL tube.
5. Add 70 μL 8× DDM to lysate, mix gently, and extract at 4 °C with rocking for ≥1 h.
6. Centrifuge ≥13,000 × *g* at 4 °C for 1 h to pellet insoluble material.
7. Load 100 μL onto SEC column equilibrated in SEC buffer and monitor fluorescence using HPLC/FPLC to assess expression level and biochemical stability.

3.3.2 Large-Scale Purification of Mechanosensitive K2Ps

1. Fit two 50 mL grinding jars with ball bearing and o-rings, seal tightly, and submerge in liquid nitrogen in a styrofoam box to cool.
2. Transfer 12.5 g of frozen cells into each chamber (*see* **Note 20**).
3. Mill 5 cycles at 30 Hz for 3 min per cycle. Submerge chambers in liquid nitrogen between cycles.
4. Use a spatula to transfer milled cell powder into stirring extraction buffer at 4 °C, cover, and stir gently at 4 °C for 3 h. Check pH periodically (typically after 30 and 90 min) and adjust pH to 8 as needed with KOH.
5. Transfer lysate to centrifuge tubes and pellet insoluble material by centrifuging 30,000 × *g* at 4 °C for 45 min.
6. Transfer 4 mL bed volume IMAC resin to a 15 mL falcon tube and wash sequentially with H_2O, TK, and TKD buffers by mixing and centrifuging at 2000 × *g* at 4 °C for 3 min.
7. Collect the soluble cell extract in a plastic beaker and add washed IMAC resin. Stir gently at 4 °C for 3 h.

8. Collect resin in a fritted glass column.
9. Wash peristaltic pump, tubing, and UV monitor with H_2O and a small amount of detergent-containing buffer (TKDI10). Blank the UV monitor. Connect the column and chart recorder to the UV monitor and the peristaltic pump to the column adapter and a buffer inlet line.
10. Wash the IMAC resin sequentially with TKDI10 and TKDI30 buffers until absorbance at 280 nm falls to baseline (*see* **Note 21**).
11. Elute the channel from the IMAC resin with TKDI300 buffer. Collect the peak fraction in a 15 mL falcon tube on ice. Immediately after elution, add EDTA pH 8.0 to 1 mM final concentration.
12. Add PreScission protease at a 1:50–1:500 molar ratio and incubate overnight at 4 °C with gentle inversion to cleave the fused EGFP-10×His tag.
13. Wash a spin concentrator (15 mL, 50 kDa MWCO) in TKDI300 or SEC buffer by centrifuging 1500 × *g* at 4 °C for 2 min.
14. Pellet any insoluble material in the elution fraction by centrifuging 5000 × *g* at 4 °C for 5 min.
15. Concentrate the elution fraction containing mechanosensitive K2P by applying to the washed spin concentrator and sequentially centrifuging at 3000 × *g* at 4 °C for 5 min and mixing until the volume is ≤500 μL.
16. Load onto SEC column equilibrated in SEC buffer and monitor absorbance at 280 nm using HPLC/FPLC. Fractionate mechanosensitive K2P containing peak that elutes at ~15 mL.
17. Assess purity of SEC fractions by SDS-PAGE and pool fractions with pure channel. Quantify concentration of purified channel and store at 4 °C until use in reconstitution.

3.4 Reconstitution of Mechanosensitive K2Ps into Proteoliposomes

3.4.1 Lipid Preparation

1. Transfer 4 mg of lipid per sample to a clean 15 mL glass test tube flushed with argon and fitted with a plastic screw cap with Teflon plug. Add 2 mL chloroform and dissolve solid lipids by gently rotating or inverting the tube.
2. Dry lipids to a thin film at the bottom of the tube under an argon stream inside a chemical hood. Submerge the tube in a beaker of water during evaporation to keep from cooling excessively. Pop any lipid bubbles at the bottom of the tube with the tip of the glass pipette and keep under argon stream 5 min after last visible traces of chloroform have evaporated to promote drying.
3. Add 2 mL pentane and dissolve lipids by gently rotating or inverting the tube.

4. Repeat drying process under argon stream, transfer to tube vacuum chamber with desiccant, and remove all solvent under vacuum for at least 2 h in the dark.
5. Remove from vacuum and layer dried lipids with argon.
6. Add DR buffer (1 mL/10 mg lipid) and bath sonicate until the solution is transparent to ensure complete formation of small liposomes.

3.4.2 Channel Reconstitution

1. Prepare reconstitutions in 15 mL centrifuge tubes. Each reconstitution consists of 0.4 mg of prepared lipids (0.4 mL of 10 mg/mL solution), a variable amount of channel in SEC buffer (*see* **Note 22**), additional SEC buffer to ensure the final concentration of detergent remains above its critical micelle concentration, and DR buffer to make a final volume of 4 mL. The channel should be added last.
2. Layer with argon gas and rock at 4 °C for ≥1 h.
3. Add ~500 mg prepared Bio-Beads and rock at 4 °C for ≥3 h.
4. Transfer the supernatant to an ultracentrifuge tube. Avoid transferring the beads.
5. Centrifuge ≥130,000 × *g* at 4 °C for 1 h.
6. Remove the supernatant, resuspend the pellet in 80 μL DR buffer, aliquot 20 μL samples into microcentrifuge tubes, snap-freeze in liquid nitrogen, and store at −80 °C until use.

3.5 Electrophysiology

Most electrophysiology rigs can be easily adjusted to perform these experiments. An inverted microscope most easily accommodates the patching electrode and poking probe above the cells. The patching electrode should be mounted on the headstage, which is attached to a micromanipulator positioned on one side of the sample.

3.5.1 Setup Common to All Techniques

1. Prepare electrodes: chlorinate the test and bath silver wire electrodes to replenish the active AgCl coating by immersing in fresh bleach in a 1.5 mL microcentrifuge tube for 10–20 min. Rinse with water before using (*see* **Note 23**).
2. Prepare salt bridges (*see* **Note 24**): bend the shaft of a borosilicate glass tube under a flame to obtain a U-shaped cylinder and break to an appropriate size for bridging solutions in the recording chamber and grounding well. Fill the glass with agar by dipping the ends in 2% agar dissolved in 3 M KCl, dry bridges, and store in 3 M KCl at 4 °C.
3. Prepare recording pipettes: Follow the pipette puller's recommended settings to pull pipettes of 2.5–4.0 MΩ access resistance when filled with the pipette solution. Lightly polish with a microforge. Fill pipettes with a microneedle attached to a 3 mL syringe with a 0.22 μm filter immediately before use.

3.5.2 Cell Swelling

1. Prepare the gravity-assisted perfusion device: place two 60 mL syringes 30–40 cm above the microscope stage to serve as solution reservoirs. Connect their outlets through plastic tubing to a Y-shape connector and connect a needle at the end of the single output tube to deliver solution to the perfusion chamber. Place a roller or slider clamp on the single output tube and pinch clamp valves on the tubes of both solution reservoirs to control flow rate (*see* **Note 25**).
2. Prepare the solution collection system: Connect a second needle to a vacuum source through a fluid trap placed inside the Faraday cage. The tip of the collection needle will be placed on the side of the recoding chamber opposite to the perfusion delivery needle ~5 mm from the bottom of the chamber to keep the height of the solution constant without drying the dish.
3. Fill the solution reservoirs with iso- and hypo-osmotic bath solutions. Flush air from the tubes by opening all pinch clamps, turning the flow to high, and collecting the solution in a waste container. Once cleared of air bubbles, adjust the flow to 2–3 mL/min and close pinch clamps. Fill tubing with iso-osmotic bath solution by flowing for 1–2 min.
4. Rinse the cells with iso-osmotic bath solution and place one coverslip in the recording chamber in the 0.5 mL iso-osmotic bath solution.
5. Place the chamber on the microscope stage. Fill the grounding reservoir with 150 mM KCl solution. Connect the grounding well to the perfusion chamber through the salt bridge. Place inlet and vacuum needles at the opposing ends of the recording chamber.
6. Open the iso-osmotic solution reservoir first, and then the vacuum line, to establish the initial flow and liquid level.
7. Localize the cells on the microscope's field of view using the 20× objective and adjust the microscope's settings to achieve the best possible contrast.
8. Find a cell of interest and achieve a high resistance seal in whole cell mode.
9. Record families of currents evoked by holding voltages varied from −100 mV to 100 mV in 20 mV steps until stable currents are obtained (Fig. 1a).
10. Swell cells by opening the clamp for the hypo-osmotic solution and closing the clamp for the iso-osmotic solution. Within a few seconds, the cell should be visibly swollen (*see* **Note 26**). Record families of currents at varying holding voltage using the same protocol. It is convenient to simultaneously record a movie of the process. The cell can be returned to the iso-osmotic solution to study reversibility of the process (*see* **Notes 27** and **28**).

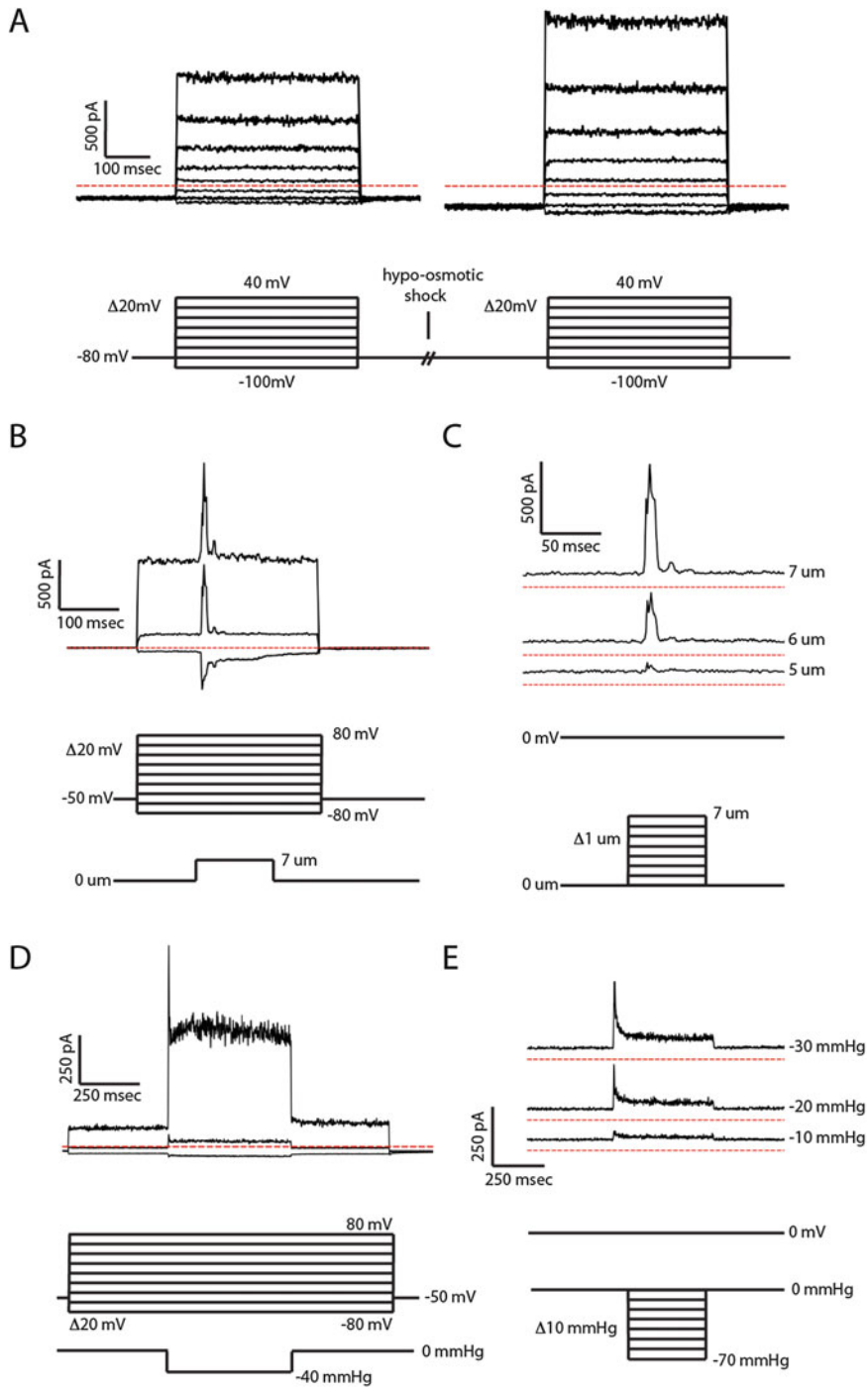

Fig. 1 Protocols for electrical recording and mechanical stimulation for (**a**) cell swelling, (**b**, **c**) cell poking, and (**d**, **e**) patched membrane stretching (*see* **Note 40**). Example current recordings from human TRAAK expressed in CHO cells are presented above the protocol diagrams and were obtained using the bath and pipette solutions described in the text. (**a**) Two voltage family protocols are separated by a solution exchange to induce hypo-osmotic swelling. Each voltage family consists of steps to test voltages ranging from −100 mV to

3.5.3 Cell Poking

1. Prepare poking apparatus: add a second micromanipulator opposite to the one holding the recording electrode and mount the poking apparatus onto it. The recording electrode and poking probe should each approach the sample ~45° from the horizontal surface.
2. Prepare poking probes: pull pipettes from borosilicate glass using a similar program as for patching. Immediately after pulling, use a microforge to seal the tips by holding the tip close to heat source until the opening appears rounded and closed. The tips should be smooth and ~2–3 μm in diameter.
3. Rinse cells with bath solution and add 2 mL bath solution or enough volume to obtain a depth of ~0.5 cm in the recording chamber.
4. Localize the cells on the microscope's field of view using the 20× objective and adjust the microscope's settings to achieve the best possible contrast.
5. Place a poking probe in its holder and position its tip near the region of interest ~200 μm above the cells in a corner of the field of view. Avoid crashing the tip against the glass surface (*see* **Note 29**).
6. Find a cell of interest and achieve a high resistance seal in whole cell mode. Optimal cells for this experiment are relatively large (~15 μm in one dimension) and minimally flat against the surface. Choose a corner of the cell to establish the gigaseal to leave most of the cell surface open for mechanical stimulation.
7. Record families of currents evoked by voltage from −100 mV to 100 mV in 20 mV steps until stable currents are obtained. Ensure the cell is healthy, the seal is tight, the access resistance is not too high, and the cell displays the expected currents.
8. Choose a bulky area of the cell for poking. Bring the tip of poking probe to within 2 μm from the surface of the cell (*see* **Note 30**). Record families of currents at varying holding

Fig. 1 (continued) +40 mV in 20 mV increments for 400 ms from a holding voltage of −80 mV. (**b**) A variable voltage, fixed probe depression family. The voltage family is analogous to (**a**) with the addition of a 150 ms probe depression of a set distance during each voltage step. Only currents from sweeps at −80 mV, 0 mV, and 80 mV are shown. (**c**) A fixed voltage, variable probe depression family. Sweeps are performed from a holding voltage of 0 mV. During each sweep, the probe is depressed for 100 ms. The depth of depression is increased by 1 μm in successive sweeps. Only currents from sweeps of 5, 6, and 7 μm depression are shown. (**d**) A variable voltage, fixed pressure application family. The voltage family is analogous to (**a**, **c**) with the addition of a 500 ms pressure pulse of a set value during each voltage step. (**e**) A fixed voltage, variable pressure family. Sweeps lasting one second each are performed from a holding voltage of 0 mV. During each sweep, pressure is applied for 250 ms. The amount of pressure applied is increased by 10 mmHg in successive sweeps. Only currents from −10, −20, and −30 mmHg are shown

voltage with a fixed depth probe stimulation or families of currents at a fixed holding voltage with varying depth probe stimulations. It is convenient to simultaneously record a movie of the process (*see* **Notes 31** and **32**) (Fig. 1b, c).

3.5.4 Patched Membrane Stretching

Membrane patches from cells or from proteoliposomes can be stretched to activate embedded mechanosensitive K2Ps. Cell preparations are as described above. Considerations for bending pipettes to enable patch imaging and membrane tension calculation, preparation of proteoliposomes for patching, and setup of the recording rig for patched membrane stretching are described below.

Bending Pipette Tips

If desired, pipette tips can be bent to observe changes in the radius of curvature of the patched membrane so that resulting changes in membrane tension can be calculated.

1. Place polished 2.5–4 MΩ tip in the microforge, center and align the pipette tip along the vertical axis of the eyepiece protractor, and orient the heating filament in the plane of the tip on the side of the eyepiece protractor (Fig. 2b, c).
2. Heat the shank of the tip where the horizontal and vertical axes of the eyepiece protractor cross. The tip will bend toward the filament. Match the angle between the micromanipulator and the sample plane such that when the bent tips are loaded in the pipette holder, the tip shank is approximately parallel to the sample plane (*see* **Note 33**).

Preparing Proteoliposomes for Patching

1. Thaw an aliquot of proteoliposomes and dispense in several drops on a 35 mm glass-bottom dish.
2. Dry ≥3 h in a vacuum chamber in the dark to dehydrate the proteoliposomes.

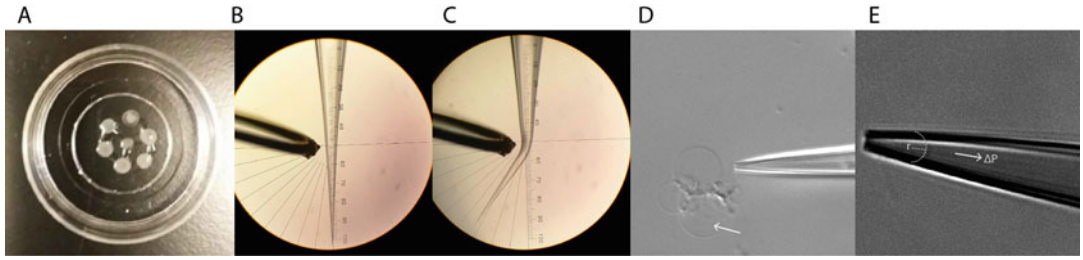

Fig. 2 Proteoliposome reconstitution and patched membrane stretching. (**a**) Photograph of dehydrated/rehydrated proteoliposomes in a 35 mm glass-bottom dish prior to addition of bath solution. Seven, 3 μL drops of proteoliposomes were dehydrated prior to rehydration overnight with 20 μL DR buffer. (**b**) A pipette tip positioned next to the filament of a microforge (*left*) prior to and (*right*) after application of heat to bend the tip to a ~35° angle (**c**). (**d**) A bent pipette tip positioned adjacent to a group of unilamellar proteoliposomes to be patched. (**e**) A bent pipette tip with patched membrane. The radius of curvature of the membrane can be fit and used with the recorded pressure difference to calculate tension within the membrane

3. Rehydrate the proteoliposomes with 20 μL DR buffer. The dry lipids spots should not be touching. Add DR buffer such that each lipid cake is covered and drag the solution between the cakes to connect as many as possible. Place rehydrating proteoliposomes within a humid chamber at 4 °C overnight (Fig. 2a).
4. Move the sample to the microscope stage and gently add ~5 mL of proteoliposome bath solution to the dish. Avoid letting solution rush over the proteoliposomes to limit floating debris that can clog pipettes and inhibit seal formation.
5. Localize a suitable unilamellar proteoliposome in the microscope's field of view using the 20× or 40× objective and adjust the microscope's settings to achieve the best possible contrast (Fig. 2d, *see* **Note 34**).

Patched Membrane Stretching and Analysis

1. Prepare pressure clamp: connect a pressure clamp headstage to the port of the recording electrode holder with a short piece of tubing. Stable connections are important to minimize pipette drift (*see* **Note 35**). Connect the pressure clamp headstage to a vacuum and pressure pump and controller such that pressure can be controlled through the digitizer and recording software.
2. Load a pipette and achieve a high resistance seal in the appropriate configuration. Cell-attached, inside-out, or outside-out patches can be studied from cells. Proteoliposome patches form in the inside-out configuration (*see* **Notes 36** and **37**).
3. Record families of currents evoked by voltage from −100 mV to 100 mV in 20 mV steps until stable currents are obtained and to ensure good seal formation.
4. Record families of currents at varying holding voltage with a fixed pressure pulse or families of currents at a fixed holding voltage with varying pressure stimulations (Fig. 1d, e, *see* **Note 38**).
5. If using bent pipette tips, a movie can be simultaneously recorded. Before stimulation, move the pipette to a field of view free from background material. Switch to a high magnification objective (e.g., 100× DIC 1.4NA oil immersion) prior to imaging.
6. Tension (T) may be estimated in each frame by applying the Young-LaPlace equation, $T = \Delta PR/2$, with R equal to the radius of curvature of the patched membrane and ΔP equal to the pressure difference across the membrane (Fig. 2e). Patched membrane radii of curvature can be fit manually in conventional image analysis software (e.g., ImageJ) or automatically with a custom script. Tension changes can then be correlated with the electrophysiological data (*see* **Note 39**).

4 Notes

1. We have found that common cell lines vary greatly in their expression of endogenous currents (both mechanosensitive and otherwise) and ease of transfection, patching, and growth. In our experience, CHO-K1 cells are particularly suitable for studying mechanosensitive channel activity because they are electrically quiet and have only small (or not measurable) mechanically activated currents. A disadvantage of the CHO cells is that they tend to express transfected channels at lower current densities compared to other cells. HEK293T cells are easier to transfect, patch, and tend to grow under most conditions, but typically contain significant endogenous voltage-gated potassium channel activity and Piezo1-dependant mechanosensitive currents [25]. If HEK cells are to be used, endogenous Piezo1 activity can be distinguished from transfected K^+ channels through the reversal potential of the currents evoked. Piezo1 currents reverse around 0 mV under the tenfold potassium concentration gradient used throughout this chapter, while K^+ currents reverse at $E_K = -59$ mV.
2. Cultured insect cells can be used as an alternative to mammalian cells. We have successfully used these techniques with Sf9 cells, which express low levels of endogenous channel activity and are amenable to patching.
3. We prefer Fugene for transfection as it is minimally toxic to cells.
4. Prepare by autoclaving yeast extract and peptone, cooling, and adding 0.22 μm filtered 20% dextrose.
5. YNB, glycerol, and KP_i can be autoclaved and Biotin should be filter sterilized.
6. This general lysis buffer is appropriate for the purification of human TRAAK and zebrafish TREK1 channels. Modifications may be necessary to promote biochemical stability of other channels.
7. Leupeptin, Soy Trypsin Inhibitor, Aprotinin, and Benzamidine (1 mM) are prepared as 1000× stocks in water, aliquoted, and stored at −20 °C. Pepstatin A is prepared as a 1000× stock in 9:1 v/v Methanol:Acetic acid, aliquoted, and stored at −20 °C. PMSF is prepared as a 100× stock in ethanol and stored at room temperature with molecular sieves to keep anhydrous. PMSF should be added immediately prior to addition of cells.
8. Detergents are stored under argon in a desiccator at −20 °C. Prior to use, they are warmed to room temperature before opening to prevent condensation inside the bottle.

9. A single HPLC or FPLC equipped with an absorbance detector (280 nm), fluorescence detector (EGFP fluorescence; 488 nm excitation 508 nm emission), and fraction collector would be sufficient for both small and large-scale procedures. We use a dedicated HPLC with an autosampler for small-scale testing and FPLC for large-scale purifications.
10. Optics should minimally be sufficient to discern features of mammalian cells. A 20× DIC objective is sufficient for most procedures, but 40×–100× DIC objectives are desirable.
11. In our experience, a diamond-shaped chamber gives the best result as it ensures laminar flow across the bath. The recording chamber should be able to easily accommodate coverslips and have a small volume (<500 μL). If the perfusion chamber does not include the reservoir for the grounding electrode, a decapped 1.5 mL tube attached to one side of the chamber can be used.
12. If recording from patched membranes from cells, use the pipette and bath solutions in Subheading 2.5.3.
13. Other transfection reagents require higher cell confluency at the time of transfection.
14. Overgrown cells are not optimal for recording. HEK cells in particular will develop electrical connections between adjacent cells in close proximity, generating very large capacitive peaks and endogenous currents.
15. PmeI linearizes pPICZ within the 5′ AOX1 promotor region. Additional PmeI sites must not be present within the mechanosensitive K2P gene.
16. The presence of residual salts in the linearized DNA reduces the transformation efficiency.
17. Arcing during electroporation will result in a loud popping or cracking sound. Cells may still be plated, but the efficiency will be lower. The two causes of this are high concentrations of residual salts from insufficient washing of DNA and the presence of small bubbles or droplets bridging the cuvette plates.
18. Reducing the concentration of zeocin at this stage to a level sufficient to inhibit bacterial growth is sufficient to prevent contamination and has no negative consequences on expression or yield.
19. Expression times can be varied and optimal expression assessed by small-scale lysis and FSEC. Human TRAAK is optimally expressed ~48 h post methanol induction.
20. In our experience, ~0.5 mg of human TRAAK or zebrafish TREK1 can be purified from 25 g *Pichia* cells which is approximately the amount recovered from a 1 L culture. Volumes are reported for purification from 25 g of cells.

21. The amount of contaminating proteins eluting in TKDI30 will vary and human TRAAK and zebrafish TREK1 will elute almost exclusively in TKDI300.
22. We have found that reconstitution ratios of 1:10 (w/w) channel:lipid give large (nA) currents in patches and ratios of 1:1000 result in a few channels per patch.
23. Electrodes should be routinely chlorinated to recoat with AgCl. Once every 1–3 days of active recording is typically acceptable.
24. The grounding electrode should be placed in a separate grounding well connected to the recording chamber with a salt bridge to avoid offset artifacts from the changes in liquid junction potential during the experiment. This is particularly important for swelling experiments where the bath is constantly perfused. We store prepared salt bridges for months at 4 °C with no contamination, but sodium azide can be added to the storage solution to prevent microbial growth if desired.
25. This simple setup can be extended to deliver more solutions by using manifold valves.
26. Most cells subjected to hypo-osmotic shock will gradually swell and then recover to close to their original size upon switching back to iso-osmotic solution. However, in some cases, we observe a membrane bleb form around the cell during swelling. This may be due to membrane detachment from the underlying cytoskeleton, appears to be irreversible, and accompanies cell death. We do not use recordings from cells in this state.
27. HEK and CHO cells are healthy to record from for 1–3 h after being removed from the incubator. However, we do not record from a single cell for more than ~15 min as cells usually begin showing signs of compromised health after this time.
28. We replace the coverslip after each swelling trial because it is unclear whether multiple rounds of swelling are detrimental to cell health or result in changes to cellular physiology.
29. We use the same poking probe for successive experiments.
30. The probe can be brought down until it just touches the cell to establish the position at which contact occurs and then immediately brought back up by a known distance. It is important to start the recording without stimulation such that the poking probe is not touching the cell.
31. Occasionally, the cell will show a surface indentation at the point of probe contact. In this case, we withdraw the poking probe and reposition it in another part of the cell.
32. We find that different parts of the cell respond with variable magnitude, suggesting that there is a positional aspect to the

experiment. It is unclear whether this is due to nonuniform spatial distribution of channels and/or membrane tension upon poking. Different target regions of the cell can be evaluated to identify the position for recording maximal poking-evoked currents.

33. In practice, angles ~5° shallower than the angle between the micromanipulator and the sample plane are preferred. This prevents tips from being discarded because they are over bent and cannot reach the target.
34. Multilamellar proteoliposomes will appear thicker at their edges and will not form proper high resistance seals. Unilamellar proteoliposomes are typically located at the edges of lipid cakes, or more frequently, loosely tethered to veins of dried proteoliposomes that emerge from and connect the dried lipid cakes. Intact unilamellar proteoliposomes will quiver if the microscope stage is gently tapped.
35. The most common sources of pipette drift in our experience are: (1) over or under-tightened micropipette holder connections and (2) cable forces from the connection between the pipette holder and pressure clamp headstage. Cable forces and drift can be reduced by incorporating a luer connection that is fixed to the microscope stage in the tubing line between the pressure clamp headstage and pipette holder.
36. If patching proteoliposomes, apply positive 5–10 mmHg pressure to keep the pipette tip clean while approaching the target membrane. Upon contacting the proteoliposomes, dropping the pressure to between 0 and −10 mmHg typically results in a rapid GΩ seal in the inside-out configuration. Maintain zero or slightly positive pressure on the patch in between negative pressure pulses to minimize creep during the experiment.
37. Proteoliposome patches containing mechanosensitive K2Ps will immediately show increases in K^+ current upon pressure stimulation. Patches from cells, in contrast, often display only small increases in K^+ current upon pressure stimulation immediately after formation or excision. The magnitude of the response increases over time to a stable regime and can be accelerated by "exercising" the patch with steps of applied pressure. This run-up phenomenon is likely due to the gradual dissolution of cortical cytoskeleton that is initially intact in the patch membrane as inclusion of cytoskeleton disrupting drugs in the bath solution accelerates this process. We exercise patches from cells with steps of moderate pressure until a stable response is observed.
38. While pressure steps in either direction will activate mechanosensitive K2Ps in patches of any configuration, in our experience, cell-attached, inside-out, and proteoliposome patches are

most mechanically stable when stimulated with negative pressure and outside-out patches are most stable when stimulated with positive pressure.

39. A trigger cable can be used to initiate camera acquisition at the onset of electrical recording to facilitate data synching. Alternatively, images and recordings may be synchronized using time stamps in the metadata.
40. Mechanosensitive potassium currents should display a reversal potential of close to the equilibrium potential for K^+ which is approximately −59 mV in the tenfold K^+ concentrations used here. This feature can be used to distinguish mechanically evoked activation of potassium currents from background and leak currents. It is convenient to using a holding voltage of 0 mV in the constant voltage protocols because currents from nonselective mechanosensitive channels (and leak currents) will be zero at this voltage, while K^+-selective currents from mechanosensitive K2Ps will be outward and nonzero.

References

1. Ranade SS, Syeda R, Patapoutian A (2015) Mechanically activated ion channels. Neuron 87:1162–1179. doi:10.1016/j.neuron.2015.08.032
2. Delmas P, Coste B (2013) Mechano-gated ion channels in sensory systems. Cell 155:278–284. doi:10.1016/j.cell.2013.09.026
3. Nilius B, Honore E (2012) Sensing pressure with ion channels. Trends Neurosci 35:477–486. doi:10.1016/j.tins.2012.04.002
4. Anishkin A, Loukin SH, Teng J, Kung C (2014) Feeling the hidden mechanical forces in lipid bilayer is an original sense. Proc Natl Acad Sci U S A 111:7898–7905. doi:10.1073/pnas.1313364111
5. Wu J, Lewis AH, Grandl J (2017) Touch, tension, and transduction – the function and regulation of piezo ion channels. Trends Biochem Sci 42:57–71. doi:10.1016/j.tibs.2016.09.004
6. Hao J, Padilla F, Dandonneau M et al (2013) Kv1.1 channels act as mechanical brake in the senses of touch and pain. Neuron 77:899–914. doi:10.1016/j.neuron.2012.12.035
7. Schmidt D, del Mármol J, Mackinnon R (2012) Mechanistic basis for low threshold mechanosensitivity in voltage-dependent K+ channels. Proc Natl Acad Sci U S A 109:10352–10357. doi:10.1073/pnas.1204700109
8. Enyedi P, Czirják G (2010) Molecular background of leak K+ currents: two-pore domain potassium channels. Physiol Rev 90:559–605. doi:10.1152/physrev.00029.2009
9. Honore E (2007) The neuronal background K2P channels: focus on TREK1. Nat Rev Neurosci 8:251–261. doi:10.1038/nrn2117
10. Brohawn SG (2015) How ion channels sense mechanical force: insights from mechanosensitive K2P channels TRAAK, TREK1, and TREK2. Ann N Y Acad Sci 1352:20–32. doi:10.1111/nyas.12874
11. Brohawn SG, Campbell EB, Mackinnon R (2014) Physical mechanism for gating and mechanosensitivity of the human TRAAK K+ channel. Nature 516:126–130. doi:10.1038/nature14013
12. Hao J, Delmas P (2011) Recording of mechanosensitive currents using piezoelectrically driven mechanostimulator. Nat Protoc 6:979–989. doi:10.1038/nprot.2011.343
13. Coste B, Mathur J, Schmidt M et al (2010) Piezo1 and Piezo2 are essential components of distinct mechanically activated cation channels. Science 330:55–60. doi:10.1126/science.1193270
14. Besch S, Suchyna T, Sachs F (2002) High-speed pressure clamp. Pflugers Arch 445:161–166. doi:10.1007/s00424-002-0903-0
15. Sokabe M, Sachs F, Jing ZQ (1991) Quantitative video microscopy of patch clamped membranes stress, strain, capacitance, and stretch channel activation. Biophys J 59:722–728. doi:10.1016/S0006-3495(91)82285-8

16. Sukharev SI, Sachs F (2012) Molecular force transduction by ion channels - diversity and unifying principles. J Cell Sci 125:3075–3083. doi:10.1242/jcs.092353
17. Opsahl LR, Webb WW (1994) Lipid-glass adhesion in giga-sealed patch-clamped membranes. Biophys J 66:75–79. doi:10.1016/S0006-3495(94)80752-0
18. Moe P, Blount P (2005) Assessment of potential stimuli for mechano-dependent gating of MscL: effects of pressure, tension, and lipid headgroups †. Biochemistry 44:12239–12244. doi:10.1021/bi0509649
19. Lewis AH, Grandl J (2015) Mechanical sensitivity of Piezo1 ion channels can be tuned by cellular membrane tension. eLife 4:143. doi:10.7554/eLife.12088
20. Sukharev SI (2002) Purification of the small mechanosensitive channel of Escherichia coli (MscS): the subunit structure, conduction, and gating characteristics in liposomes. Biophys J 83:290–298. doi:10.1016/S0006-3495(02)75169-2
21. Brohawn SG, Su Z, Mackinnon R (2014) Mechanosensitivity is mediated directly by the lipid membrane in TRAAK and TREK1 K+ channels. Proc Natl Acad Sci U S A 111:3614–3619. doi:10.1073/pnas.1320768111
22. Berrier C, Pozza A, de Lacroix de Lavalette A et al (2013) The purified mechanosensitive channel TREK-1 is directly sensitive to membrane tension. J Biol Chem 288(38):27307. doi:10.1074/jbc.M113.478321
23. Martinac B, Rohde PR, Battle AR et al (2009) Studying mechanosensitive ion channels using liposomes. In: Lipid-protein interactions. Humana Press, Totowa, NJ, pp 31–53
24. Teng J, Loukin S, Anishkin A, Kung C (2015) The force-from-lipid (FFL) principle of mechanosensitivity, at large and in elements. Pflugers Arch 467:27. doi:10.1007/s00424-014-1530-2
25. Dubin AE, Murthy S, Lewis AH et al (2017) Endogenous Piezo1 can confound mechanically activated channel identification and characterization. Neuron 94:266–270.e3. doi:10.1016/j.neuron.2017.03.039

Chapter 12

Migration of PIP_2 on KCNQ2 Surface Revealed by Molecular Dynamics Simulations

Qiansen Zhang and Huaiyu Yang

Abstract

Lipids and membrane proteins are the main components of cell membranes. Lipid-protein interactions are dynamic because these interactions typically occur on shallow protein surface clefts. Molecular dynamics (MD) simulations provide a tool for studying the dynamics of these interactions. Here, we describe the interactions of phosphatidylinositol-4,5-bisphosphate (PIP_2) with both the open and closed states of a KCNQ2 channel. Through these methods, we show that a lipid can migrate between different binding sites in a protein and this migration modulates protein functions.

Key words Potassium channel, Lipid, Molecular dynamics simulation, Migration, PIP_2, Lipid-protein interaction, Lipid-binding site

1 Introduction

A long-standing goal within the field of ion channels is to elucidate the molecular mechanisms of lipid regulations on channel function—from lipid-channel binding to major conformational changes essential to channel function. Important breakthroughs toward this goal have been made by using various experimental techniques, such as electrophysiological techniques [1], X-ray crystallography [2], and electron cryo-microscopy [3]. These techniques are useful as they can provide information about the static structure and lipid binding of channels. However, lipid-channel interactions are usually highly dynamic and lipid motions are critical to channel function [4–7]. Different from these experimental techniques, molecular dynamics (MD) simulations can generate continuous, atomic-resolution trajectories, providing a potentially powerful technique for investigating structure-activity relationships between lipids and channels, including the lipid-binding process and pathways. The MD method was introduced in the 1950s [8], and it is a method that integrates Newton's equations of motion in time to update the positions and velocities of all the atoms by

Show-Ling Shyng et al. (eds.), *Potassium Channels: Methods and Protocols*, Methods in Molecular Biology, vol. 1684,
DOI 10.1007/978-1-4939-7362-0_12,

alternately computing the forces acting on each atom. MD simulations have been a popular tool to study lipids and membrane proteins [5, 9].

Lipid-channel interactions are dynamic because these interactions typically occur on ion channels' shallow surface clefts rather than in deep pockets [10, 11]. MD simulations allow membrane protein structures to be computationally re-embedded into lipid bilayers, and their dynamic interactions with surrounding lipid molecules to be characterized [12]. However, recent simulation studies probing lipid interactions mainly focused on lipid binding to an individual site of the channel, rather than the properties of dynamic lipid interactions with ion channels. In this chapter, we introduce the MD simulation methods and procedures that studied the PIP_2-KCNQ2 interaction. The simulation results show that PIP_2 can dynamically migrate between different binding sites in the KCNQ2 channel with significant impacts on channel gating. A similar procedure has been successfully used to identify the migrations of very small molecules in proteins, such as CO migration in myoglobin [13]. Here, we start from the structural models of the open and closed states of KCNQ2 channels by using computer homology modeling methods. Then we built the simulation systems based on the open and closed states of the KCNQ2 channel models. In these systems, the KCNQ2 channel models are separately embedded into the cell membrane, and PIP_2 molecules are also included in the inner leaflet of the cell membrane and far away from the channel models. We subjected each simulation system to two independent 1-μs MD simulations and observed the PIP_2 molecules dynamic interactions with the KCNQ2 channel models. Our results suggest that MD simulation methods can also be applied as a powerful tool to reveal the migration of lipids on a protein surface [4].

2 Materials

The procedures or servers laid down in this chapter require the availability of several software components, and most of them are freely available for academic purposes. The commands are provided assuming a Unix-like environment (Linux/BSD) and user-level knowledge of such systems.

1. UniProt database (http:/ /www.uniprot.org/): To access protein sequence and functional information.
2. CLUSTALW Web server (www.ebi.ac.uk/Tools/msa/clustalw2): Helps to generate the multiple sequence alignments.

3. SWISS-MODEL repository (https://swissmodel.expasy.org/): A database of annotated 3D protein structure models generated by the SWISS-MODEL homology-modeling pipeline.
4. RCSB Protein Data Bank: A database of experimental macromolecular structures (*see* **Note 1**).
5. MODELLER: A program for protein structure modeling implemented in Discovery Studio 2.6 (*see* **Note 2**).
6. PROCHECK (http://www.ebi.ac.uk/thornton-srv/software/PROCHECK/): A tool for analyzing stereochemical quality of a protein structure, producing a number of PostScript plots analyzing its overall and residue-by-residue geometry (*see* **Note 3**).
7. QMEAN server (http://swissmodel.expasy.org/qmean): A server for protein model quality estimation (*see* **Note 4**).
8. GROMACS (http://www.gromacs.org/): A suite of programs for molecular dynamics simulations (*see* **Note 5**).
9. PyMOL (The PyMOL Molecular Graphics System, Version 1.3, Schrödinger, LLC): A program that is used to visualize the structure models and generate figures.
10. VMD (Visual Molecular Dynamics) (http://www.ks.uiuc.edu/Research/vmd/) program: For visualization of molecular dynamics trajectories and for displaying protein or membrane structures. In addition, it can also be used to create snapshots of the bilayers (*see* **Note 6**).

3 Methods

The preparation work before MD production was done on PC computers or workstations. MD simulation was performed on a mainframe computer, such as Tianhe 1A.

3.1 Homology Modeling of Open- and Closed-State KCNQ2 Channels

1. The amino acid sequence of human KCNQ2 (O43526) was retrieved from the UniProt database.
2. SWISS-MODEL repository was used to search for suitable template structures for homology modeling. Crystal structures such as the rat Kv1.2 (PDB code 2A79), and the Streptomyces lividans open- and closed-state KcsA structures (PDB codes 3PJS and 3EFF) were chosen as suitable templates for homology modeling of the open- and closed-state KCNQ2 channels, respectively. These template structures were downloaded from PDB database. Meanwhile, the closed-state conformation of a Kv1.2/Kv2.1 "paddle chimera" channel [14] was also selected to model the transmembrane segment of the closed-state KCNQ2 channel.

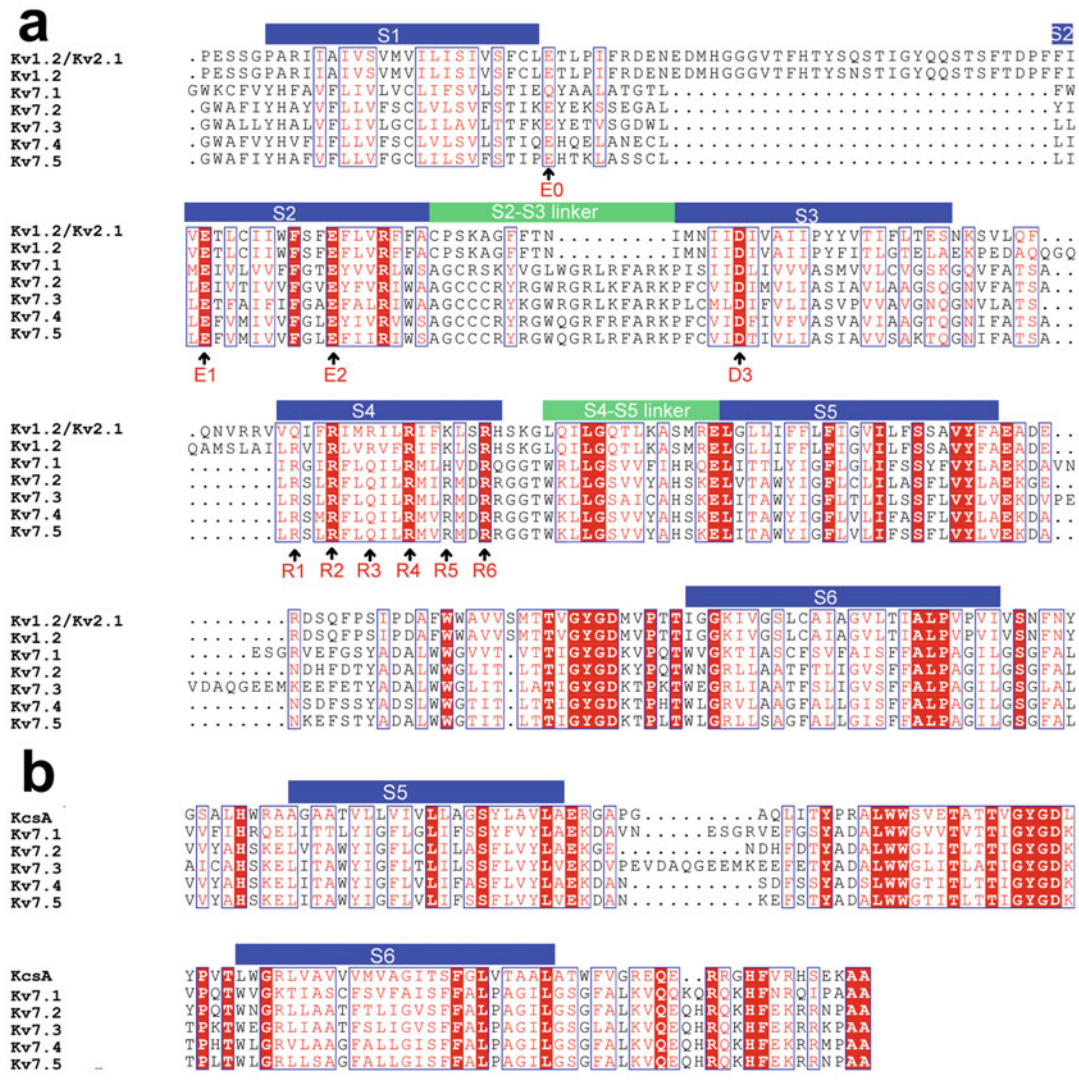

Fig. 1 Multiple sequence alignments. (**a**) Multiple sequence alignment for Kv1.2, Kv1.2/Kv2.1 chimera, and human KCNQ channels. (**b**) Multiple sequence alignment for KcsA and human KCNQ channels

3. Sequence alignment of input model sequences and template structures were carried out using the CLUSTALW Web server (Fig. 1, *see* **Note 7**).
4. MODELLER automodel was used to build homology models of the KCNQ2 channel. We have generated five models for both the open- and closed-state KCNQ2 channels.
5. In the loop refinement procedure for each model, the lowest DOPE score model was selected for loop refinement purposes. The loop refinement was carried out using the MODELLER loop model in Discovery Studio 2.6 (*see* **Note 8**).

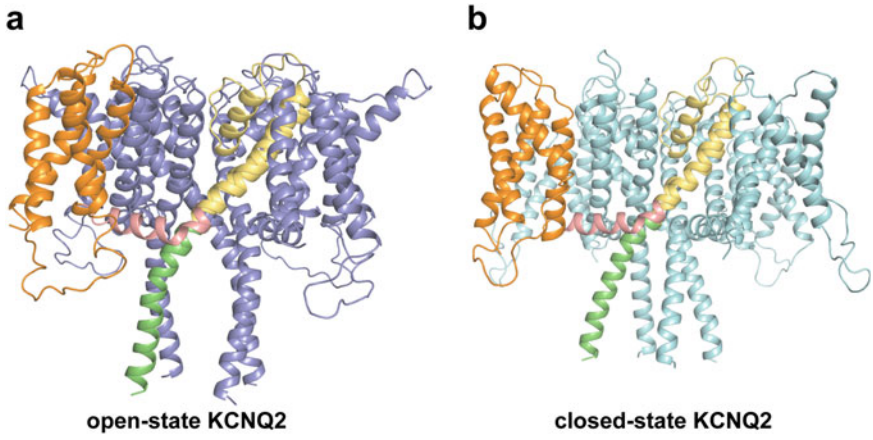

Fig. 2 The homotetramer structure of open- and closed-state KCNQ2 channels

6. The fourfold symmetry structures of the KCNQ2 homotetramer were constructed according to the symmetry matrix of the Kv1.2 crystal structure by using PyMOL (Fig. 2).
7. Structure validation was carried out using PROCHECK and QMEAN software tools by submitting modeled channel structures (*see* **Notes 3** and **4**).
8. The structural models for mutant KCNQ2 channels were built from the open-state KCNQ2 model by mutating R160 or all of the basic residues (R153, R155, R158, R160, K162, R165, and K166) located in the S2-S3 linker to alanines (*see* **Note 9**).

3.2 Simulation Systems

1. Preparing a complete membrane. The VMD Membrane Builder plugin automates this process. In the Membrane window, select the POPC Lipid using Charmm36 force field and change the Membrane X Length and the Membrane Y Length to 140. Then save the membrane without waters (*see* **Note 10**).
2. Aligning proteins in the POPC membrane. The open- and closed-state WT and R160A mutant KCNQ2 channel models were embedded separately into a POPC bilayer by aligning the protein's axis of symmetry with the bilayer normal using VMD. In each system, lipids that were located within 1 Å of the KCNQ2 channel were removed.
3. Inserting the PIP_2 molecule. Four PIP_2 molecules were added manually to the inner leaflet of the POPC bilayer by replacing the overlapped POPC molecules. The initial positions of the PIP_2 molecules were at least 15 or 20 Å away from any atom of the channel, respectively.
4. Solvating systems. Each system was solvated by TIP3P waters with 0.15 M KCl by the follow steps in Gromacs and using VMD to check:

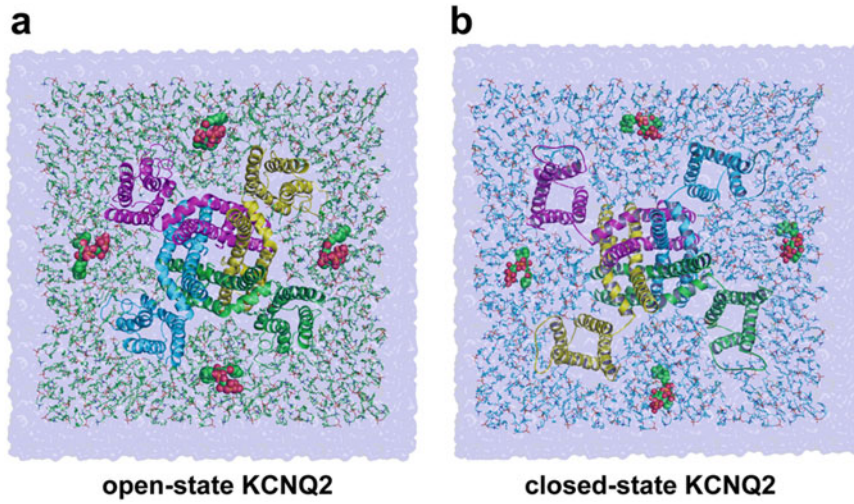

Fig. 3 The simulation systems of open-state (**a**) and closed-state (**b**) KCNQ2 channels. The channels are shown in *cartoon*, viewed from intracellular side. PIP_2 molecules, shown as *spheres*, are placed far from the channel

(a) Building a box. *$ editconf –f channelX-POPC.gro –box 14 14 11 –o channelX-POPC_box.gro* (*see* **Note 11**).

(b) Solvating with water. *$ genbox –cs spc216.gro –cp channelX-POPC_box.gro –p topol.top –o channelX_sol.gro* (*see* **Note 12**).

(c) Adding neutralizing counterions. *$ grompp –f ions.mdp –c channelX_sol.gro –p topol.top –o channelX_ions.tpr* (*see* **Note 13**).
$ genion –s channelX_ions.tpr –o channelX_solv_ions.gro –p topol.top –pname K –nname CL –conc 0.15 –neutral.

5. The coordinate files of the simulation systems (*channelX_solv_ions.gro*) were ready for minimization (Fig. 3) to avoid bad contacts, which often are created during this process. After minimization the systems were ready for simulation.

3.3 Running MD Simulations

1. Running a simulation in Gromacs is a two-step process when all files are ready. The first step is to generate a file (*.tpr) with all the previously gathered information. *$ grommp –f *.mdp –c *.gro –p *.top –o *.tpr.*
2. Once the tpr file is correctly generated the simulation can be performed by using the command: *$ mdrun –v –deffnm *.tpr.*
3. Heating with restraints on the solute. The next stage of the refinement protocol is heating the minimized systems to 300 K. The v-rescale method [15] is used for maintaining and equalizing the system temperature.
4. Equilibration steps. After the systems have been successfully heated up, the equilibration steps were performed with the

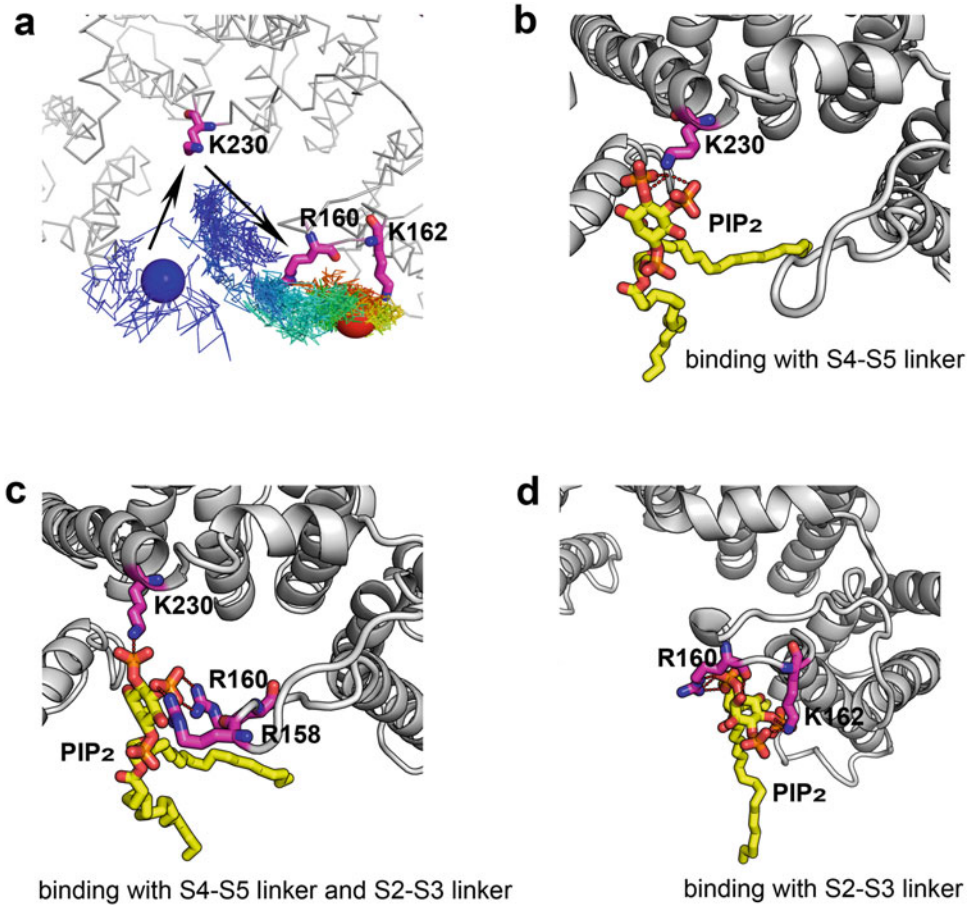

Fig. 4 Analyzing the PIP_2 migration pathway and binding sites at the surface of the KCNQ2 channel. (**a**) One of the migration trajectories of a PIP_2 molecule between the S4–S5 linker and the S2–S3 linker in the simulations of the open-state KCNQ2 channel. (**b**–**d**) Intracellular side view of the three representative binding models of PIP_2 during the migration trajectory: PIP_2 binding with the S4-S5 linker (**b**), PIP_2 binding simultaneously with the S4–S5 linker and S2–S3 linker (**c**), and PIP_2 binding with the S2–S3 linker (**d**)

Isobaric-Isothermal (NPT) ensemble. These phases were run for 27 ns in total to equilibrate the lipid bilayer and the solvent, with restraints on PIP_2 and the main chain of the transmembrane domain (*see* **Note 14**).

5. MD production phase. Two independent 1-μs production runs were performed for each system (*see* **Note 15**). VMD software was used to visualize and analyze the motion trajectories of the PIP_2 molecules, such as in Fig. 4.

4 Notes

1. Homology modeling is a method to predict the 3-D structure of a protein sequence when the crystal structure is not available. The open and closed-state KCNQ2 models were not available in the PDB database. We used the homology modeling method to predict their 3-D structures.
2. MODELLER is a separate program for homology modeling. Note that it requires registration, but it is free for academic use.
3. PROCHECK analysis indicated that stereochemical parameters and side chain packing densities of the two models are within the acceptable range as there are few outlier residues (about 2.8% and 3.7%) (Fig. 5).
4. The QMEAN server provides access to two scoring functions successfully tested at the eighth round of the community-wide blind test experiment CASP. The QMEAN Raw scores of 0.061 and 0.069 (estimated model reliability lies between 0 and 1) and z scores of −7.65 and −7.55 further suggested the eligible quality of the KCNQ2 models.
5. Gromacs is a popular, freely available and relatively user-friendly set of programs for MD simulations. The version we used is 4.6.
6. For the membrane built by VMD, it just supports the POPC and POPE components of the membrane that are based on the charm27 or charmm36 force fields. In our work, we used the POPC bilayer membrane that is based on the charmm36 force field.

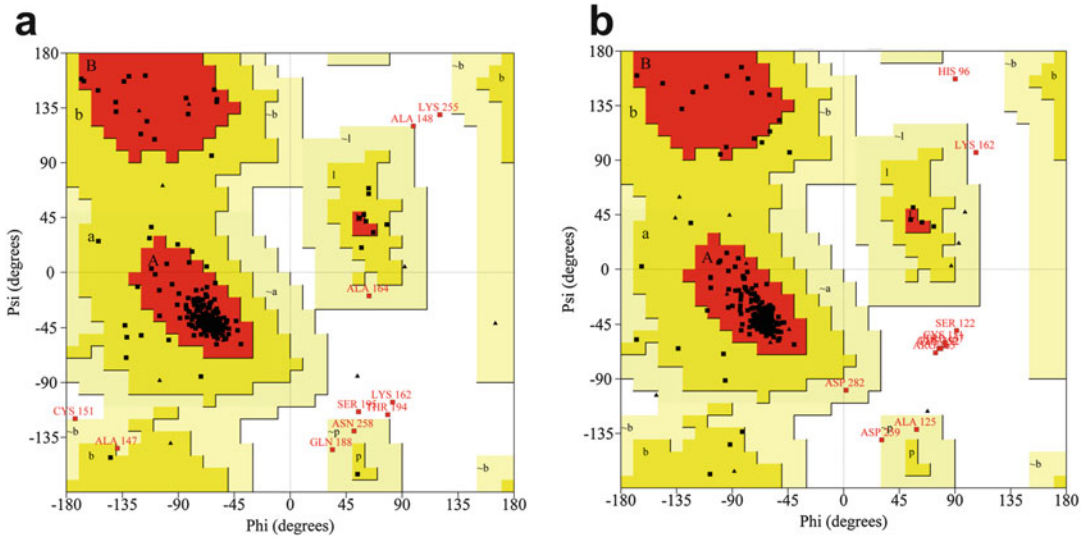

Fig. 5 Ramachandran plot calculations of the psi/phi angle distribution of the open-state (**a**) and closed-state (**b**) KCNQ2 models computed with the program PROCHECK

7. During the homology sequence alignment, the highly conserved residues were used to guide the alignment. The result of the sequence alignment is shown in Fig. 1. The S4–S5 linker, S5, and S6 regions of the Kv channels are highly conserved, which directly provides a reliable basis for mapping the positions of these regions of KCNQ channels based on the structures of the Kv1.2 and Kv1.2/Kv2.1 chimera channels. Although residues are not so highly conserved in S1–S4 segments as in the S5 and S6 segments, the conserved residues, E0, E1, D3, R1, R2, R3, R4, and R5, provided enough information to locate the positions of the S1–S4 segments. The conserved phenylalanine in the S2 segment also helped to map the position of the S2 segment. As a result, the positions of the S1–S4 segments could be accurately mapped.
8. The structures of the loops located in the inside or outside of the membrane are generated randomly, and the reasonable fragment conformations were chosen from the top ten candidates that have the lowest RMS values and considerable geometrical compatibility.
9. In PyMOL, there is a mutagenesis wizard that can be used for rebuilding side chains, by mutating the broken residue to the same type, allowing choosing between different rotamers.
10. For the POPC molecule, the Charmm36 force field allows for MD simulations to be run in the tensionless ensemble (NPT), and is anticipated to be of utility for simulations of pure lipid systems as well as heterogeneous systems including membrane proteins.
11. "*.gro," contains the initial coordinates of each atom present in the simulated system. The X, Y box sizes (14 nm) have to be the same as the x- and y-size in the POPC bilayer above. They can be found in the last line of "channelX-POPC_box.gro" (first two numbers).
12. "*.top" contains the descriptions of the forces between the atoms (molecular topology and force field). In this chapter, the CHARMM36–CAMP force field [16] was applied for the protein and the POPC phospholipids, and Lupyan et al.'s [17] PIP_2 model was used.
13. "*.mdp" contains specification of the algorithms used in the calculation and their parameters. The grompp program may give you some warnings or even errors.
14. During the equilibration steps, we relaxed all of the loops of KCNQ2 models to obtain more reasonable loop conformations.
15. As the KCNQ2 channel contains a large cytoplasmic domain (536 residues) after residue 337, the motions of the C-terminal residues 313–337 should be restrained by the cytoplasmic

domain. Since no similar structure is available in the databank to allow construction of a homology model for this domain, we applied conformational restraints (isotropic force constant $\kappa = 1 \times 103$ kJ/mol/nm^2) to the Cα atoms of residues 313–337 to mimic the effects of the missing cytoplasmic domain on the motion of these residues.

Acknowledgments

The research was supported in part by Ministry of Science and Technology of the People's Republic of China (2013CB910604), National Natural Science Foundation of China (21422208), and Special Program for Applied Research on Super Computation of the NSFC-Guangdong Joint Fund (the second phase). We also thank National Supercomputing Center in Tianjin (Tianhe) for computational resources.

References

1. Sakmann B, Neher E (1984) Patch clamp techniques for studying ionic channels in excitable membranes. Annu Rev Physiol 46:455–472
2. Sheldrick B (1986) Structure determination by X-ray crystallography: by MFC Ladd and RA Palmer. Plenum, New York, NY
3. van Heel M, Gowen B, Matadeen R, Orlova EV, Finn R, Pape T, Cohen D, Stark H, Schmidt R, Schatz M, Patwardhan A (2000) Single-particle electron cryo-microscopy: towards atomic resolution. Q Rev Biophys 33 (4):307–369
4. Chen L, Zhang Q, Qiu Y, Li Z, Chen Z, Jiang H, Li Y, Yang H (2015) Migration of PIP2 lipids on voltage-gated potassium channel surface influences channel deactivation. Sci Rep 5:15079
5. Dror RO, Dirks RM, Grossman JP, Xu H, Shaw DE (2012) Biomolecular simulation: a computational microscope for molecular biology. Annu Rev Biophys 41:429–452
6. Adcock SA, McCammon JA (2006) Molecular dynamics: survey of methods for simulating the activity of proteins. Chem Rev 106 (5):1589–1615
7. Karplus M, Petsko GA (1990) Molecular dynamics simulations in biology. Nature 347 (6294):631–639
8. Haile J (1997) Molecular dynamics simulation: elementary methods, vol 18. Wiley, New York, NY
9. Zhang Q, Zhou P, Chen Z, Li M, Jiang H, Gao Z, Yang H (2013) Dynamic PIP_2 interactions with voltage sensor elements contribute to KCNQ2 channel gating. Proc Natl Acad Sci U S A 110(50):20093–20098
10. Long SB, Tao X, Campbell EB, MacKinnon R (2007) Atomic structure of a voltage-dependent K+ channel in a lipid membrane-like environment. Nature 450(7168):376–382
11. Whorton MR, MacKinnon R (2011) Crystal structure of the mammalian GIRK2 K^+ channel and gating regulation by G proteins, PIP_2, and sodium. Cell 147(1):199–208
12. Stansfeld PJ, Sansom MS (2011) Molecular simulation approaches to membrane proteins. Structure 19(11):1562–1572
13. Ruscio JZ, Kumar D, Shukla M, Prisant MG, Murali TM, Onufriev AV (2008) Atomic level computational identification of ligand migration pathways between solvent and binding site in myoglobin. Proc Natl Acad Sci U S A 105(27):9204–9209
14. Jensen MO, Jogini V, Borhani DW, Leffler AE, Dror RO, Shaw DE (2012) Mechanism of

voltage gating in potassium channels. Science 336(6078):229–233

15. Bussi G, Donadio D, Parrinello M (2007) Canonical sampling through velocity rescaling. J Chem Phys 126(1):014101
16. Klauda JB, Venable RM, Freites JA, O'Connor JW, Tobias DJ, Mondragon-Ramirez C, Vorobyov I, MacKerell AD Jr, Pastor RW (2010) Update of the CHARMM all-atom additive force field for lipids: validation on six lipid types. J Phys Chem B 114(23):7830–7843
17. Lupyan D, Mezei M, Logothetis DE, Osman R (2010) A molecular dynamics investigation of lipid bilayer perturbation by PIP_2. Biophys J 98 (2):240–247

Chapter 13

Studying Structural Dynamics of Potassium Channels by Single-Molecule FRET

Shizhen Wang, Joshua B. Brettmann, and Colin G. Nichols

Abstract

Single-molecule FRET (smFRET) can visualize conformational dynamics of individual ion channels in lipid bilayers of defined composition. Dynamic and distance measurements from smFRET, combined with single channel recordings, can provide previously unattainable direct mechanistic insights into ion channel function and modulation. smFRET measurements require site-specific fluorophore labeling between two distinct sites, which is a major challenge for multimeric ion channels. This chapter aims to provide a step-by-step protocol: (1) to design concatemeric constructs with only two cysteine residues within a homotetrameric channel; (2) to express, purify, label, and reconstitute channel proteins; (3) to perform smFRET imaging on channel proteins in liposomes with an objective-based Total Internal Reflection (TIRF) microscope; and finally (4) to analyze the FRET distributions and dynamics that reflect the dynamic conformational transitions of ion channels in membranes.

Key words Membrane protein, Ion channel, Conformational dynamics, Fluorophore labeling, Single-molecule FRET, TIRF

1 Introduction

Ion channels are integral membrane proteins that selectively conduct ions, thereby controlling many physiological processes [1]. Since gated currents through single-ion channel pores were first observed, over 40 years ago [2], many channels have been recorded and analyzed at the single-channel current level, revealing mechanistic insights to the physical states underlying gating transitions [3]. Over the last 20 years, high-resolution structures of ion channels in different static conformations have informed the structural changes of the gating transitions [4–8]. However, the atomic structures obtained by crystallography or electron-microscopy are typically from protein molecules frozen in stable states and often in environments other than lipid bilayers. Reconstructing the conformational trajectories from these static 'snapshots' and correlating

Show-Ling Shyng et al. (eds.), *Potassium Channels: Methods and Protocols,* Methods in Molecular Biology, vol. 1684,
DOI 10.1007/978-1-4939-7362-0_13,

them with dynamic gating events of ion channels in cell membranes may not always be straightforward, or even apparent.

Fluorescent resonant energy transfer (FRET) can be used to assess intramolecular structures and structural changes in response to physical or chemical stimuli. Single-molecule FRET (smFRET) can report unsynchronized conformational trajectories, reveal structural distributions and transitions, and uncover rare structural states, which are unattainable for ensemble measurements [9, 10]. In recent years, smFRET has been extensively used to examine conformational dynamics of nucleic acids and soluble proteins, but has rarely been applied to membrane proteins [11–15]. Studying ion channels, in particular multimeric ion channels, with smFRET presents significant technical challenges of protein purification, fluorophore labeling, and functional reconstitution.

In this chapter, we provide step-by-step protocols detailing how to prepare smFRET samples for the study of structural dynamics of tetrameric potassium channels. We describe critical controls to help avoid potential artifacts and bias in such measurements. The protocols we describe may also be useful for studying conformational dynamics of other ion channels or transmembrane proteins.

2 Materials

Prepare all the solutions using ultrapure Milli-Q water (resistance >18.2 MΩ). All the chemicals should be of analytic grade purity, except as specified.

2.1 Plasmids and Proteins

KirBac1.1 plasmids, as well as the cysteine configurations of the resulting tetrameric proteins, as shown in Fig. 1, are described in detail in original publications [15, 16], and are available upon request (*see* **Note 1**).

2.2 Protein Purification and Fluorophore Labeling

1. Cell Resuspension Buffer (CSB): 50 mM Tris–HCl, 150 mM KCl, 250 mM Surcose, 10 mM $MgCl_2$, 10 mM imidazole, pH 8.0, containing 2 mM TCEP, 0.02 mg/mL DNase I, 1 EDTA-free Protease Inhibitor Cocktail tablet per 50 mL resuspension (*see* **Note 3**).
2. Washing Buffer (WB): 50 mM Tris–HCl, 150 mM KCl, 5 mM n-Decyl-β-D-Maltopyranoside (DM), 10 mM imidazole, 2 mM TCEP, pH 8.0.
3. Elution Buffer (EB): 50 mM Tris–HCl, 150 mM KCl, 5 mM DM, 400 mM imidazole, 2 mM TCEP, pH 8.0.
4. Labeling Reaction Buffer (LRB): 20 mM Hepes-KOH, 150 mM KCl, 5 mM DM, pH 7.0 (*see* **Note 4**).
5. Gel Filtration Buffer (GFB): 20 mM Hepes-KOH, 150 mM KCl, 5 mM DM, 1 mM TCEP pH 7.5.

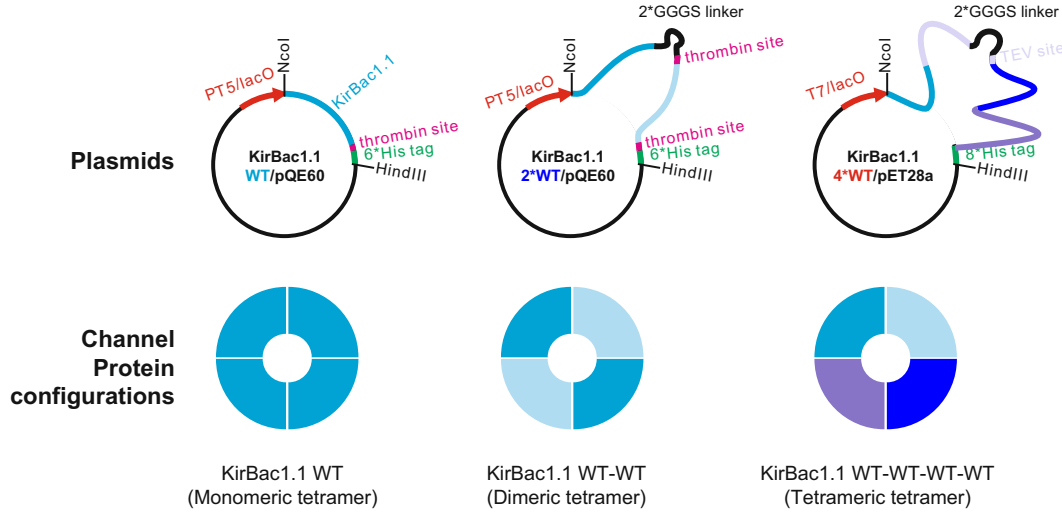

Fig. 1 KirBac1.1 plasmids and the subunit configurations of the resulting proteins for smFRET studies (Wang et al. [15])

2.3 Protein Reconstitution

1. POPE/POPG lipid solution: POPE/POPG/biotinylated-POPE lipid mixer (73:25:2, w/w/w), dissolved in 20 mM Hepes-KOH, 150 mM KCl, 30 mM CHAPS, pH 7.5, with final total lipid concentration as 10 mg/mL (*see* **Note 5**).
2. Reconstitution Buffer (RB): 20 mM Hepes-KOH, 150 mM KCl, pH 7.5.

2.4 PEG/Biotin-PEG Passivation

1. Dremel-3000 with 0.75 mm diamond drill bit.
2. Slides (25 × 75 mm) and coverslips (24 × 60 mm).
3. Glass-staining dishes and 250 mL flask.
4. Propane torch.
5. Nitrogen gas.
6. Methanol.
7. Acetone.
8. 3.0 M KOH.
9. Acetic acid, glacial.
10. N-(2-Aminoethyl)-3-Aminopropyltrimethoxysilane.
11. mPEG-Succinimidyl Carbonate, MW5000.
12. Biotin-PEG-SC-5000.
13. 0.1 M sodium bicarbonate.

2.5 Single-Molecule Imaging

1. Saturated 6-hydroxy-2,5,7,8-tetramethylchroman-2-carboxylic acid (Trolox) solution: Dissolve 30 mg of Trolox in 10 mL of milliQ water, mix gently overnight on a rocker,

then pass through a syringe filter with 0.22 μm pore size, the final concentration is ~3.0 mM.

2. Oxygen scavenging stock (Gloxy, 100×): 1 mg/mL (~160 U/mL) glucose oxidase, and 0.04 mg/mL (~2200 U/mL) catalase in 50 mM Tris–HCl, 50 mM NaCl, pH 8.0. The stock can be stored at −20 °C for up to 6 months.
3. NBA stock (100×): 200 mM NBA (4-nitrobenzyl alcohol) dissolved in DMSO, store at −20 °C.
4. COT stock (100×): 200 mM COT (cyclooctatetraene) dissolved in DMSO, store at −20 °C.
5. Imaging buffer: 20 mM Hepes-KOH, 150 mM KCl, 1 mM EDTA, 1 mM EGTA, pH 7.5, containing 0.8% dextrose, ~3 mM Trolox, degassed by a low vacuum pump for 10 min (*see* **Note 6**).
6. T50: 10 mM Tris–HCl, 50 mM NaCl, pH 8.0.
7. Crimson fluorescent beads (ThermoFisher, CATA#F8806, 0.2 um size with excitation and emission peak at 625 and 645 nm, respectively).

2.6 Customized TIRF Microscope and Software

1. The configuration of the TIRF microscope with a dual-view beam splitter is illustrated schematically in Fig. 2. The customized objective-based TIRF microscope we used was

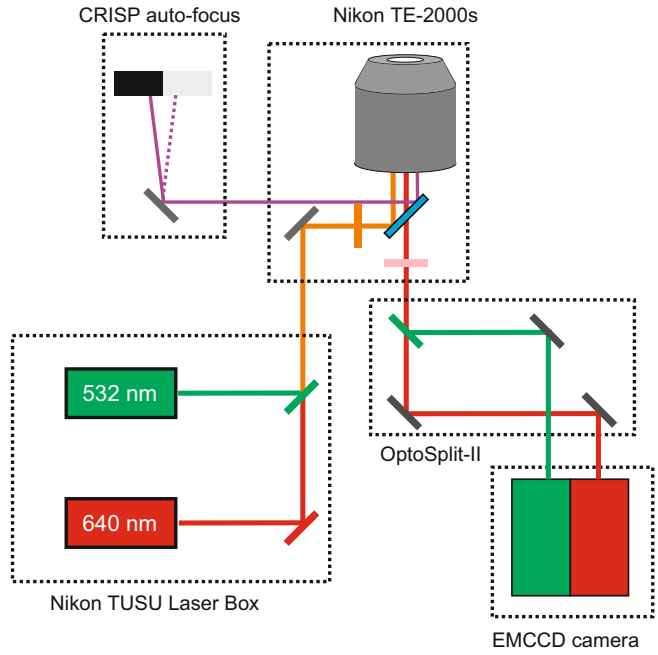

Fig. 2 Schematic of the optical configuration of the TIRF microscope for single-molecule FRET imaging

constructed on a Nikon TE-2000S inverted fluorescence microscope with a 100× 1.49NA Nikon Apo TIRF objective lens. The imaging system is equipped with a Nikon D-Eclipse C1 TIRF illumination system containing a 532 nm (Sapphire 532-LP, 100 mW, Coherent Inc.) and a 640 nm (OBIS 640-LX, 40 mW) laser. A CRISP autofocus system (780 nm, ASI Inc.) is used to compensate for focus drift due to thermal fluctuations or mechanical vibrations that are not avoided by the use of a floating air table. An OptoSplit II LS Image Splitter (Cairn Research Inc) with ZT638RDC-UF2/ET585/65/ET700/75 filter set (Chroma Inc.) is used to split the donor and acceptor emissions, which are imaged by an Evolve 512 delta emCCD camera (Photometrics Inc.).

2. NIS-element AR software is used for collecting images and movies (*see* **Note 6**).
3. IDL8.2 software is used to analyze single-molecule image movies. A set of IDL scripts developed by the group of Dr. Taekjip Ha to align donor and acceptor channels, identify individual molecules, and extract the fluorescence intensity time traces is available for download at https://cplc.illinois.edu/software/.
4. Matlab is used to visualize, select, and analyze these traces interactively. A script set developed by the Ha group is available for download at https://cplc.illinois.edu/software/.

3 Methods

3.1 Protein Purification and Labeling

Perform protein purification and labeling procedures by following the flowchart in Fig. 3, with additional details included in the following protocols.

1. Protein expression and purification.
   (a) Transform KirBac1.1 cysteine mutant constructs into the *E. coli* BL21gold(DE3) host strain, inoculate the transformants in Luria Broth medium, grow at 37 °C until OD600 reaches ~0.6, then induce with 0.1 mM IPTG at 22 °C overnight.
   (b) Harvest *E. coli* expressing KirBac1.1 proteins by centrifugation and then resuspend the cells in CSB, 20 mL/L of culture.
   (c) Break cells by passing through an M-110P Microfluidizer 3×, with an operating pressure of 18,000 psi, cooling with an ice/water mixture.
   (d) Extract KirBac1.1 proteins by adding 30 mM DM and rotate at 4 °C for 3 h.

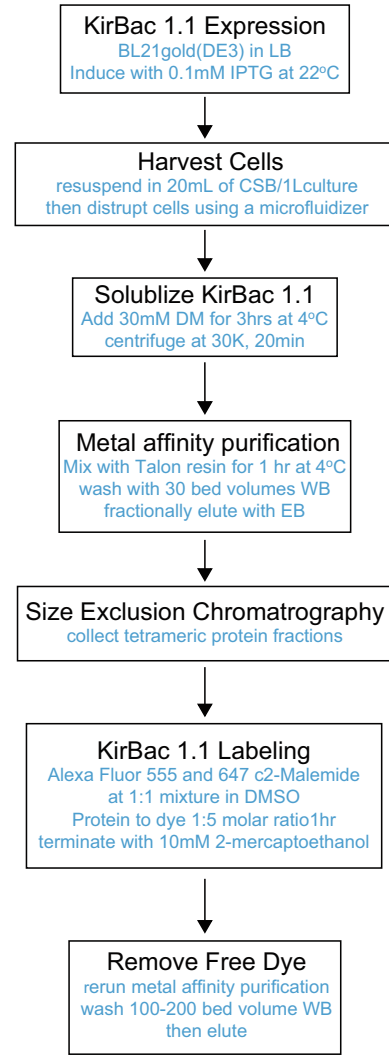

Fig. 3 Flowchart of protein expression, purification, and fluorophore labeling

(e) Spin the cell lysate at 30,000 × *g* for 20 min, mix the supernatant with Talon metal affinity resin (0.4 mL 50% slurry per liter of culture), and gently stir in a rocker for 1 h at 4 °C.

(f) Spin down the resin at 300 × *g*, discard the supernatant and pour the resin into a small column, wash with 30 bed volumes of WB.

(g) Elute the KirBac1.1 proteins with EB (*see* **Note 7**).

2. Protein labeling.

(a) Perform size-exclusion chromatography (SEC) on the purified protein using a Superdex-200 10/300 column

with a flow rate of 0.5 mL/min, collecting 0.5 mL fractions with an AKTA FPLC system. Use LRB as running buffer, collect the KirBac1.1 tetrameric protein fractions, with peak usually at ~12.0 mL, and then concentrate to 2 mg/mL with an Amicon Ultra-4 centrifugal filter (*see* **Note 8**).

(b) Start the fluorophore labeling immediately by adding DMSO-dissolved Alexa Fluor 555 and 647 c2 maleimide (1:1 mixture) to the KirBac1.1 protein solution to a final protein:dye molar ratio of 1:5. Conduct the labeling reaction at room temperature for 1 h, then terminate with 10 mM 2-mercaptoethanol (*see* **Note 9**).

(c) Separate the KirBac1.1 protein conjugated with fluorophores by conducting another metal affinity chromatographic purification as described in **step 1e–g** (*see* **Note 10**).

3.2 Protein Reconstitution

1. Add 10 μg KirBac1.1 protein to 200 μL of POPE/POPG lipid solution (10 mg/mL) to make a final protein:lipid ratio of 1:200 (w/w), and then incubate at room temperature for 20 min.
2. Prepare a Sephadex G-50 column with 2 mL bed volume, equilibrate it with RB, and then centrifuge for 30 s in a swinging bucket centrifuge at 1000 × *g* to dry the column.
3. Load 200 μL lipid-KirBac1.1 protein mixture onto the spin-dried column and then collect KirBac1.1 proteoliposomes by centrifuging at 800 × *g* for 30 s.
4. Immediately before single-molecule imaging experiments, extrude the proteoliposomes 29 times through a polycarbonate membrane with a pore size of 50 nm (*see* **Note 11**).

3.3 Single-Molecule Imaging

1. Prepare sample chamber slide for single-molecule imaging as summarized in the flowchart in Fig. 4.
   (a) Drill a pair of 0.75 mm diameter holes in the glass slide to form each sample chamber; up to five separate sample chambers can be made for each slide of regular size (1 × 3 in.).
   (b) Sonicate the glass slide and coverslips in a glass-staining dish for 30 min in acetone, 30 min in methanol, 30 min in 3 M KOH, rinsing with milliQ water between each solution.
   (c) Rinse the slides and coverslips 6× with MilliQ water.
   (d) Rinse 3× with methanol and then dry the slides and coverslips with nitrogen gas.

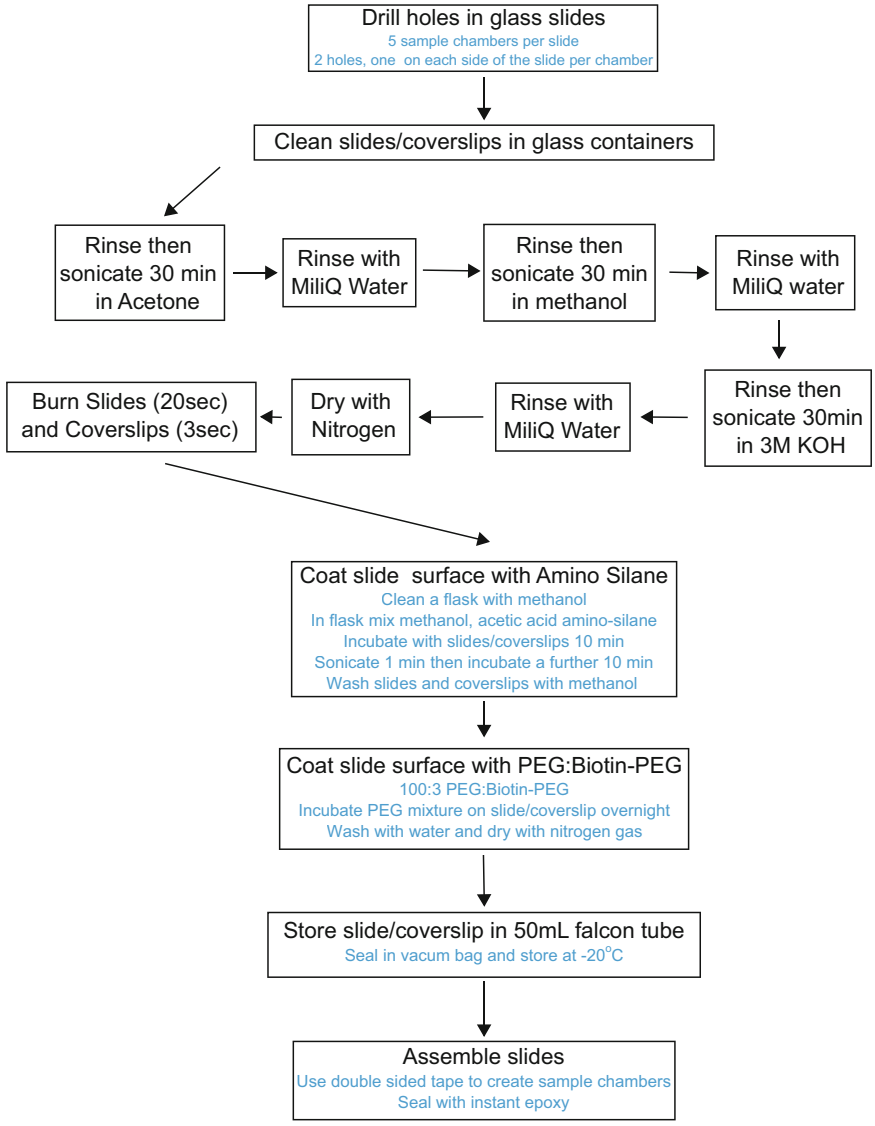

Fig. 4 Flowchart of protocol for preparing slide chamber for single-molecule imaging

(e) Flame slides (<20 s) and coverslips (<3 s) to remove any fluorescent organic molecules and set aside in clean staining jars.

(f) Clean a flask by filling with methanol and sonicating for 5 min, then rinse 3× with methanol.

(g) Add 100 mL methanol to the clean flask, then add 5 mL acetic acid and 1 mL amino-silane using a glass pipette. Mix the solution by gently shaking, then add it into staining jars containing clean glass slides and coverslips, incubate for 10 min, sonicate for 1 min, and then incubate for another 10 min.

(h) Wash the mixture off by rinsing with methanol six times and dry the slides and coverslips using nitrogen gas.

(i) For ten sample chambers, dissolve 100 mg mPEG and 3 mg biotin-PEG in 800 μL 0.1 M sodium bicarbonate (freshly made and filtered through a 0.22 μm filter). Mix with a pipette gently and then spin at 14,000 × *g* for 1 min.

(j) Apply 70 μL PEG mixture on each slide, place coverslip over each slide, and then incubate in a dark and humid box for 4 h or overnight.

(k) Dissemble the slides and coverslips, wash with MilliQ water extensively, then dry with nitrogen gas.

(l) Put each slide/coverslip set in a 50 mL falcon tube with coated surfaces away from each other, seal the tube in a vacuum bag with a regular food saver and then store at −20 °C.

(m) Before smFRET imaging experiments, assemble the slides and coverslip using double-sided tape (~0.1 mm thick) and seal the chamber using instant Epoxy.

(n) A complete video instruction is also available at Journal of Visualized Experiments, demonstrated by Chandradoss et al. [17] (http://www.jove.com/video/50549/surface-passivation-for-single-molecule-protein-studies).

2. Alignment of the OptoSplit II LS Image Splitter.

(a) Prepare a bead slide for aligning the OptoSplit II LS Image Splitter by diluting the crimson fluorescent beads (Invitrogen, Cata#F8806) 50× with 1 M Tris–HCl, pH 8.0. Assemble a clean coverslip and slide with double-sided tape (~0.1 mm thick), add and then seal the diluted beads into the slide chamber by instant Epoxy.

(b) Add a drop of immersion oil to the objective lens and mount the bead slide on the microscope with the coverslip facing the objective lens. Ensure there are no visible air bubbles trapped between the coverslip and the objective lens.

(c) Excite the crimson fluorescent beads with a 532 nm laser, adjust the laser incident angle to set the evanescent field penetration depth, to ensure that only the crimson fluorescent beads on the inner surface of the coverslip are excited.

(d) Adjust the OptoSplit II LS Image Splitter, align the donor (from 545 to 620 nm) and acceptor (from 660 and 750 nm) channels to the left (X[1–256]:Y[1–512]) and right half (X[257–512]:Y[1–512]) of the emCCD camera chip, respectively. In live-acquisition mode, visually inspect the alignment of the donor and acceptor channels pixel by pixel, then acquire a short movie and analyze the

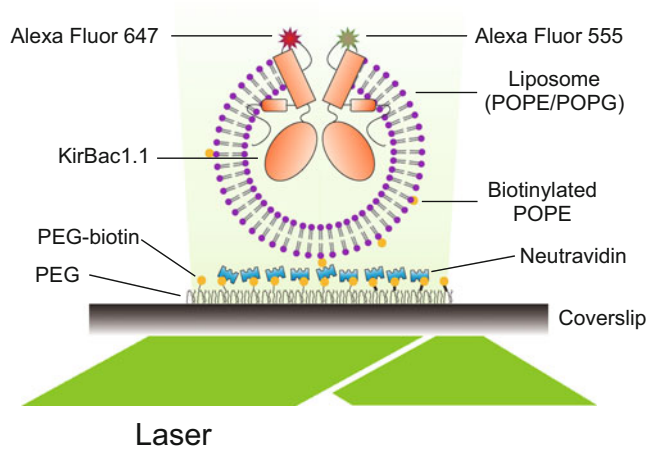

Fig. 5 Objective-based TIRF setup to perform single-molecule imaging on KirBac1.1 reconstituted into liposomes

mapping with the IDL scripts. Iteratively repeat alignment and mapping until fluorescence emissions from the same beads appear at equivalent positions of the donor and acceptor channels with deviations less than 2 pixels for both horizontal and vertical directions.

3. Collect movies on the proteoliposomes.
   (a) Remove the aligning slide and mount a sample chamber on the microscope.
   (b) Hydrate the sample chamber with 50 μL of T50, incubate for ~1–5 min.
   (c) Set the exposure time, focus on the inner surface of the coverslip by looking for fluorescent contaminates or surface scratches, then adjust the laser power, incident angle, and the electronic multiplying (EM) gain to optimize image quality.
   (d) Add 50 μL of neutravidin solution (0.25 mg/mL, in T50), incubate for ~1–5 min.
   (e) Dilute KirBac1.1 proteoliposomes with reconstitution buffer, starting at 1:100,000 dilution, and load the mixture into the slide chamber. The liposomes will immobilize on the surface of the coverslip as illustrated schematically in Fig. 5. Increase the proteoliposome concentration to optimize the number of emission spots in each view, but well separated from each other (*see* **Note 12**).
   (f) Take 100 μL of imaging buffer, add 1 μL COT and 1 μL NBA, then add 1 μL Gloxy and gently mix the imaging buffer with a pipette, flush away the proteoliposome samples with imaging buffer, and collect 5–10 movies for every sample/condition (*see* **Note 13**).

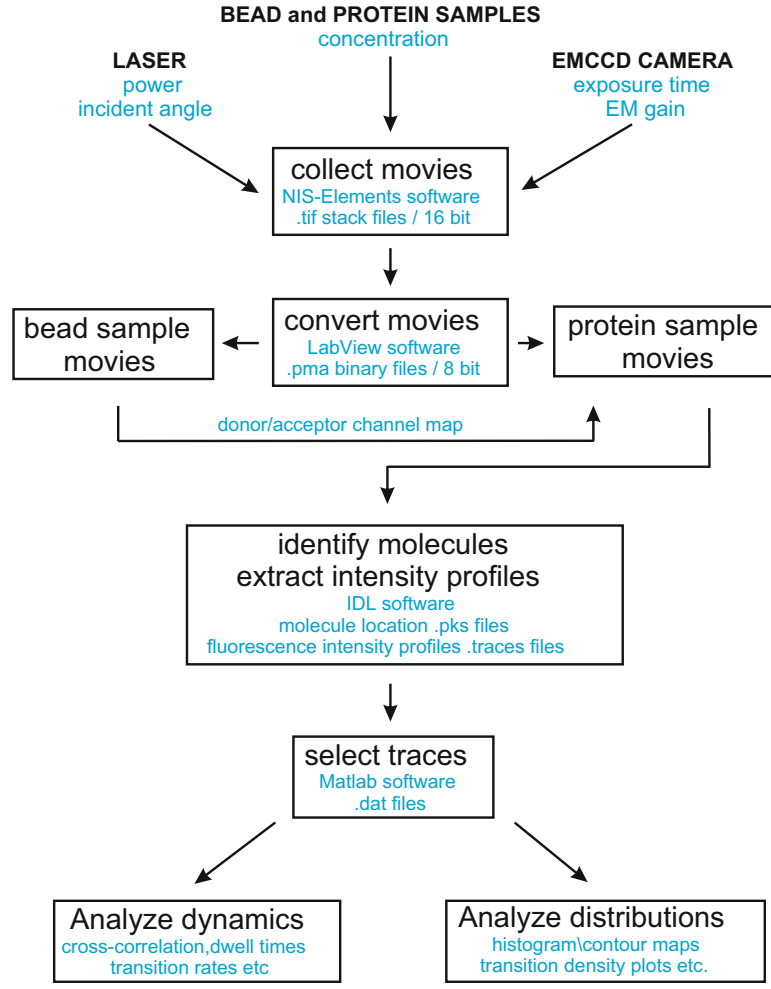

Fig. 6 Flowchart for collection and analysis of smFRET data

3.4 Data Analysis

3.4.1 Data Collection

The overall procedures to collect and analyze imaging data are summarized as a flowchart in Fig. 6. Identify single-molecule spots and extract time intensity profiles using the IDL script set. If the movies are collected by NIS-elements or μManager, export them first as .tif stack files and then convert them into .pma (8-bit binary image stack file format) files, using a Labview script developed in the Nichols lab, available upon request.

3.4.2 Trace Selection

Visualize and manually select the traces using the Matlab script developed by the Ha group, then save them as .dat files, with time, donor, and acceptor intensities in three columns separated by a space. A good practice is to select traces independently by two researchers, at least for part of data, to ensure there is no significant bias in trace selection. The general standards to pick traces are (Fig. 7a, b):

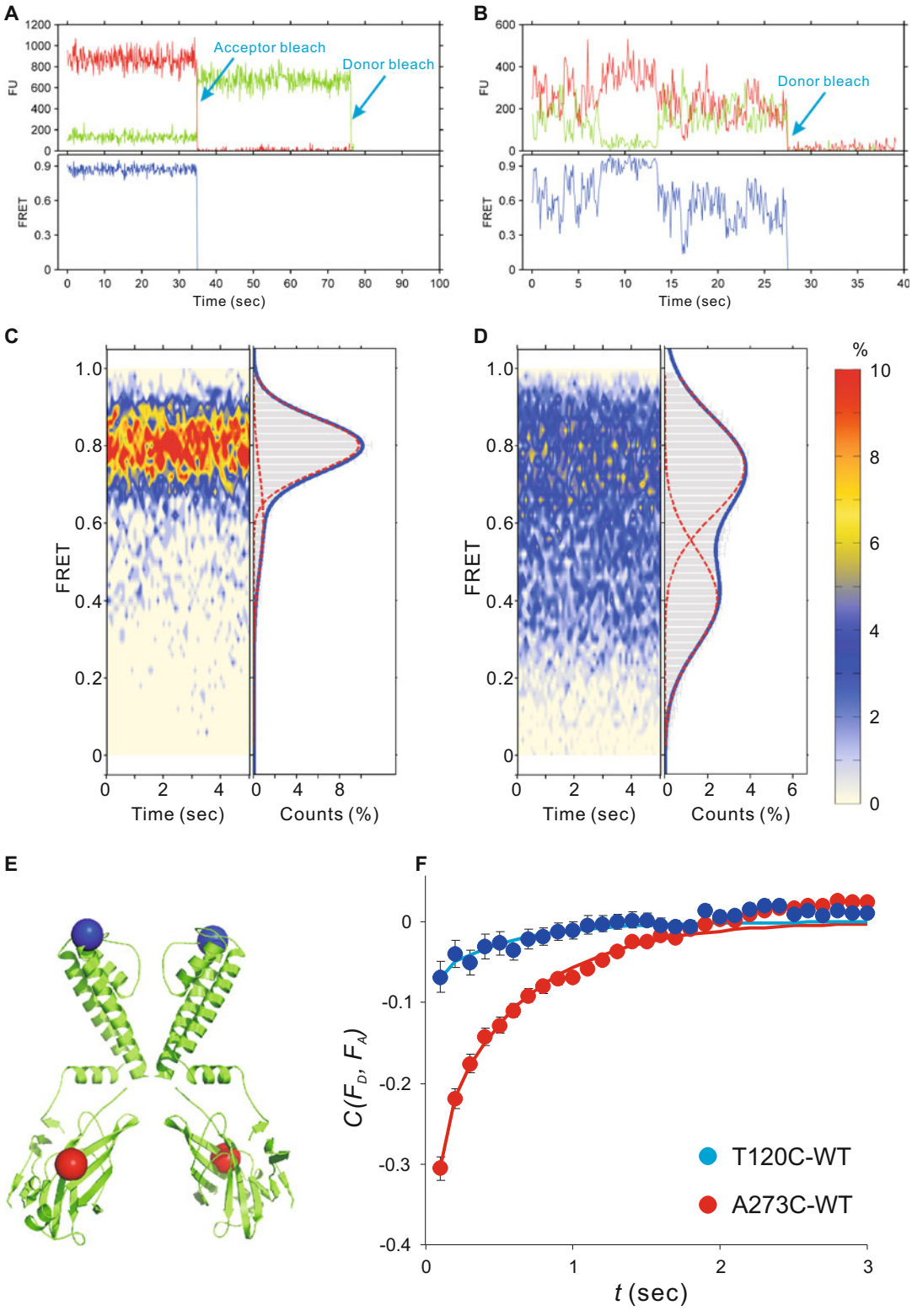

Fig. 7 Studying structural dynamics of KirBac1.1 reconstituted into liposomes by single-molecule FRET. (**a**, **b**) Representative traces from dimeric KirBac1.1, with fluorophore labeling at the T120C and A273C sites. (**c**, **d**)

1. Both donor and acceptor bleach in single steps.
2. The lifetime of the acceptor fluorophore is longer than 5 s.
3. The donor and acceptor intensity traces exhibit a clearly anti-correlated pattern.
4. There is no large variance (usually <20%) in total fluorescence intensities (i.e., the sum of the donor and acceptor fluorescence intensities).
5. The donor or acceptor should not have highly frequent or long-duration blinking events.

3.4.3 Calculate and Correct the FRET Efficiency

1. FRET efficiency is calculated by the following equation:

$$E = \frac{F_A - l \times F_D}{F_A - (F_D \times l) + \gamma \times F_D},$$

where F_A and F_D are fluorescence intensities of the same molecule in the acceptor and donor channels; l is the leakage of the donor fluorescence into the acceptor channel, measured with the samples labeled with donor fluorophore only, on the same TIRF microscope with identical optical elements; γ is the gamma factor resulting from the difference in quantum yields and detection efficiencies between donor and acceptor fluorescence.

2. γ can be calculated by the following equation:

$$\gamma = \frac{{F_A}^b - {F_A}^a}{{F_D}^a - {F_D}^b},$$

where ${F_A}^a$, ${F_A}^b$, ${F_D}^a$ and ${F_D}^b$ are the fluorescence intensities of the same molecule in the acceptor (A) and donor channels (D) before (b) and after (a) acceptor photobleaching (*see* **Note 14**).

3.4.4 Analysis of FRET Signal Distributions

Contour maps and histograms are informative graphical representations of the data. Contour maps (Fig. 7c, d, left panels) show the averaged FRET signals over (in this case) the first 3 or 5 s of all recordings under a given condition and give a visual illustration of the time stability of the FRET signal, and the major FRET levels observed. Fitting the distributions (averaged FRET amplitude over the time segment) with a sum of Gaussian distributions implies discrete amplitudes, reflecting occupancy of distinct physical states with specific discrete distances between the fluorophores.

Fig. 7 (Continued) FRET contour maps (*left*) and histograms (*right*) from KirBac1.1 with fluorophore labeling at the T120C and A273 sites. (**e**) Cartoon showing the KirBac1.1 crystal structure with T120 (*blue*) and A273 (*red*) labeling sites highlighted as *spheres*. (**f**) Cross-correlation analysis of the FRET signals at T120C sites (close to the selectivity filter) and at the A273C sites (in the cytoplasmic domain)

1. Mean FRET histograms can be calculated as the average of FRET histograms from each trace, after pooling all trace data from the same group (Fig. 7c, d).
2. To calculate the FRET contour map, extract the first 3 or 5 s of FRET data of each trace and calculate a histogram from each time point, then plot the contour map with X axis as time, Y axis as FRET, and Z as relative counts, displayed using a customized color map (Fig. 7c, d).

3.4.5 Analysis of FRET Dynamics

Akin to single-ion channel analyses [1] lifetime distributions in discrete states can theoretically be assessed from smFRET traces. However, in practice, multiple FRET states without clearly defined amplitudes have precluded such an analysis of KirBac1.1. For FRET traces without discernable discrete states, dynamics can be quantitatively evaluated by performing autocorrelation analysis on FRET. If the trace data are very noisy, cross-correlation analysis between donor and acceptor fluorescence intensities can be performed. Such an analysis can still be used to infer dynamic flexibility between sites to which the specific fluorophore pair is attached. For instance, there is significant flexibility at residue A273C, reflected in a significant cross-correlation between fluorophore signals, but very little flexibility at residue T120C (Fig. 7e).

1. The autocorrelation of FRET can be analyzed by the following equation:

$$C_{\text{auto}}(t) = \frac{\langle \Delta\text{FRET}_0 \times \Delta\text{FRET}_t \rangle}{\langle \Delta\text{FRET}_0^2 \rangle},$$

where ΔFRET_0 and ΔFRET_t are the variance of FRET at times 0 and t, respectively.

2. The cross-correlation of donor and acceptor fluorescence intensities can be analyzed with the following equation:

$$C_{\text{cross}}(t) = \frac{\langle \Delta F_{\text{D}}^0 \times \Delta F_{\text{A}}^t \rangle}{\langle \Delta F_{\text{D}}^0 \times \Delta F_{\text{A}}^0 \rangle},$$

where ΔF_{D}^0, ΔF_{A}^0, and ΔF_{A}^t are the variances of donor (D) and acceptor (A) fluorescence intensities at times 0 and t, respectively.

3. The lag time (t) vs. coefficients from auto- or cross-correlation analyses can be fitted with exponential functions with 1 or more components (Fig. 7f):

$$f\left(C_{\text{auto/cross}}, t\right) = a_1 \times e^{-\frac{t}{\gamma_1}} + \cdots + a_n \times e^{-\frac{t}{\gamma_n}},$$

where α and T are the amplitudes and time constants of each exponential component.

4 Notes

1. Conjugation of FRET fluorophore pairs with a target protein can specifically be made using cysteine thiol-maleimide chemistry. KirBac1.1 WT has no intrinsic cysteine residues, and thus did not require creation of a cys-less background. For other proteins, creation of a cys-less background is advisable wherever possible. General guidelines for introducing cysteine mutations into target proteins for fluorophore labeling include: (a) The distance between the two target cysteines should be around 4–6 nm, which is close to the R_0 (Förster distance) of the most commonly used FRET pairs, Cy3/Cy5 (~5.5 nm) or Alexa Fluor 555/647 (~5.1 nm); (b) Cysteine mutations should be avoided in loops that are likely to be disordered; (c) Residues with hydrophobic side chains may not be good candidates to mutate into cysteine, since they are often not accessible to the reactive fluorophores; (d) Charged residues may be good candidates for the introduction of cysteine mutations, if they do not interfere with protein function; (e) In designing tandem constructs, a linker consisting of GlyGlyGlySer repeats is flexible and hydrophilic, and therefore an ideal first choice to introduce between monomers; (f) A protease cleavage site can be introduced into the linker if the link interferes with protein function and if removing the link can restore function.
2. If cell resuspensions are going to be stored frozen, then fresh TCEP, DNaseI and protease inhibitor cocktail tablet should be added immediately before purification. Freezing stored cell suspensions is generally a better choice than freezing detergent purified proteins.
3. The pH of the labeling reaction mixture should be between 6.5 and 7.5. Low pH will help to protonate the primary amine group of lysine and arginine side chains and thereby maintain specificity of the thiol-maleimide reaction.
4. (a) Although the detergent CHAPS can be harsh for many membrane proteins, it usually does not denature membrane proteins in the presence of lipids. However, if it does denature the target protein, other relatively mild detergents with high CMC values, such as OG, Cymal-4, and Hega-10, can be used to replace it. (b) KirBac1.1 is functional in POPE/POPG liposomes, but other lipids with different head groups and alkyl chains can also be used for reconstitution to maintain or modulate protein function, or in studies to understand protein-lipid interactions.
5. Imaging buffer should be prepared immediately before use, usually as only a small volume, ~1–2 mL. If a pH meter with

an appropriately small probe is not available, pH strips with a resolution of 0.5 pH units can be used to adjust the pH to the designated value. The pH of the imaging buffer will drop slowly due to the acidic product of the enzymatic oxygen scavenging system, so a good practice is to adjust the imaging buffer pH a little higher (0.2–0.4) than the desired value.

6. The single-molecule imaging could also be performed with μManager (https://www.micro-manager.org/), an open-source software, or smCamera, or a customized software for single-molecule FRET imaging developed by the group of Taekjip Ha, available for download at https://cplc.illinois.edu/software/.
7. A small volume fractional elution can be performed to minimize the elution volume in this step, thereby avoiding concentration before loading onto the size-exclusion chromatography column.
8. TCEP interferes with the cysteine-maleimide reaction, and therefore is not included in the LRB. Hence, it is necessary to start fluorophore labeling immediately after SEC and concentration to avoid oxidation of free cysteine residues.
9. (a) Maleimide groups of the FRET fluorophores are moisture sensitive and should be kept dry. A good practice is to aliquot fluorophores into small quantities, store in vacuumed food bags with desiccators, and try to avoid repetitive exposure to air. (b) FRET fluorophores are also photo-sensitive, therefore all labeling procedures should be conducted in a dark room with minimal light. (c) Labeling conditions may be optimized for a particular protein by adjusting protein:dye ratio, reaction time, and buffer components. For example, sucrose and glycerol, although widely used in the purification of less stable membrane proteins, actually interfere with thiol-maleimide reactions and therefore should be removed in the labeling reaction buffer.
10. (a) Some FRET fluorophores, such as Cy3 and Cy5, are quite hydrophobic and can non-covalently bind to membrane proteins. Nonspecific labeling of protein will severely impact the quality of the collected smFRET data, hence removal of free dye is critical. Wash more extensively if it is necessary, at the metal affinity chromatographic purification step, with 100–200 bed volumes of WB to completely remove these nonspecifically attached fluorophores. (b) It is very important to include a control protein without cysteine in every batch of labeling to evaluate the fraction of fluorophores that do not bind the protein through a cysteine.
11. The proteoliposomes will form after passing through the column. Sometimes, further incubating with 100 mg Bio-Beads

SM2 (wet weight, prewash with methanol and then RB) at room temperature for 4–6 h will help to remove remaining detergent, and also reduce fluorophores nonspecifically attached to the protein.

12. (a) To evaluate contaminants from fluorescent impurities (which should be $<\sim$5%), it is necessary to first collect a few short movies only with T50 and neutravidin. (b) EM gain below 300 will satisfy most single-molecule imaging applications.
13. Due to the enzymatic oxygen scavenging system, the pH of the imaging buffer will drop gradually, so it is a good practice to finish collecting movies within 15–20 min. If more time is needed to collect movies, replace the imaging buffer every 15–20 min.
14. Only traces in which the acceptor bleaches first can be used to calculate γ. Therefore, a good practice is to pick traces with acceptor photobleaching first, then compare FRET with or without correcting γ. If γ correction does not change FRET significantly, then all traces can be included to calculate FRET. Otherwise, an average γ can be calculated from traces with acceptor photobleaching first and then use this to correct all traces.

Acknowledgments

The authors would like to thank Dr. Jonathan Silva for his help at early state in constructing the TIRF microscope for smFRET measurements, and Dr. William Stump for his help in developing the script converting imaging files. The chapter was written by S.W., and edited by J.B. and C.N.

References

1. Hille B (2001) Ion channels of excitable membranes, 3rd edn. Sinauer, Sunderland, MA, xviii. 814 p
2. Neher E, Sakmann B (1976) Single-channel currents recorded from membrane of denervated frog muscle fibres. Nature 260 (5554):799–802
3. Colquhoun D, Sigworth F (1995) Fitting and statistical analysis of single-channel records, in Single-channel recording. Springer, New York, NY, pp 483–587
4. Cao E et al (2013) TRPV1 structures in distinct conformations reveal activation mechanisms. Nature 504(7478):113–118
5. Whorton MR, MacKinnon R (2011) Crystal structure of the mammalian GIRK2 K+ channel and gating regulation by G proteins, PIP2, and sodium. Cell 147(1):199–208
6. Cuello LG et al (2010) Structural mechanism of C-type inactivation in K(+) channels. Nature 466(7303):203–208
7. Cuello LG et al (2010) Structural basis for the coupling between activation and inactivation gates in K(+) channels. Nature 466 (7303):272–275
8. Jiang Y et al (2002) Crystal structure and mechanism of a calcium-gated potassium channel. Nature 417(6888):515–522
9. Ha T et al (1996) Probing the interaction between two single molecules: fluorescence resonance energy transfer between a single

donor and a single acceptor. Proc Natl Acad Sci U S A 93(13):6264–6268

10. Roy R, Hohng S, Ha T (2008) A practical guide to single-molecule FRET. Nat Methods 5(6):507–516
11. Zhao Y et al (2010) Single-molecule dynamics of gating in a neurotransmitter transporter homologue. Nature 465(7295):188–193
12. Akyuz N et al (2013) Transport dynamics in a glutamate transporter homologue. Nature 502 (7469):114–118
13. Erkens GB et al (2013) Unsynchronised subunit motion in single trimeric sodium-coupled aspartate transporters. Nature 502 (7469):119–123
14. Wang Y et al (2014) Single molecule FRET reveals pore size and opening mechanism of a mechano-sensitive ion channel. elife 3:e01834
15. Wang S et al (2016) Structural dynamics of potassium-channel gating revealed by single-molecule FRET. Nat Struct Mol Biol 23 (1):31–36
16. Wang S et al (2009) Differential roles of blocking ions in KirBac1.1 tetramer stability. J Biol Chem 284(5):2854–2860
17. Chandradoss SD et al (2014) Surface passivation for single-molecule protein studies. J Vis Exp 86:PMID:24797261

Chapter 14

Patch-Clamp Recordings of the KcsA K^+ Channel in Unilamellar Blisters

Kimberly Matulef and Francis I. Valiyaveetil

Abstract

Patch-clamp electrophysiology is the standard technique used for the high-resolution functional measurements on ion channels. While studies using patch clamp are commonly carried out following ion channel expression in a heterologous system such as *Xenopus* oocytes or tissue culture cells, these studies can also be carried out using ion channels reconstituted into lipid vesicles. In this chapter, we describe the methodology for reconstituting ion channels into liposomes and the procedure for the generation of unilamellar blisters from these liposomes that are suitable for patch clamp. Here, we focus on the bacterial K^+ channel KcsA, although the methodologies described in this chapter should be applicable for the functional analysis of other ion channels.

Key words GUV recordings, KcsA, Lipid vesicles, Blisters, Patch clamp

1 Introduction

Ion channels are ubiquitously present integral membrane proteins that provide pathways for the movement of ions through biological membranes [1]. Ion channels play essential roles in a number of physiological processes such as neuronal signaling, cardiac excitability, insulin release, and fluid secretion. Functional studies on ion channels are carried out by the electrophysiological techniques of voltage clamp or patch clamp generally following the heterologous expression of the ion channels in *Xenopus* oocytes or HEK cells [2, 3]. Alternately, functional studies on ion channels can be carried out using reconstituted systems, which consist of the purified ion channel proteins incorporated into lipid bilayers [4]. Studies using reconstituted systems are required when the ion channels either do not express or do not properly fold or traffic to the cell membrane in heterologous expression systems. This situation is commonly encountered during heterologous expression of bacterial and archaeal ion channels. Another complication in using a heterologous expression system is that the endogenous proteins or lipids

Show-Ling Shyng et al. (eds.), *Potassium Channels: Methods and Protocols*, Methods in Molecular Biology, vol. 1684,
DOI 10.1007/978-1-4939-7362-0_14,

present may alter the function of the ion channel in a nonnative manner. This complication is not encountered in studies on reconstituted ion channels as all the components present are biochemically defined. A challenge with using reconstituted systems is the requirement for the purified ion channel protein. However, recent advances in membrane protein biochemistry have made overexpression and purification of many ion channel proteins very feasible.

Purification of ion channels requires the use of detergents for extraction from cellular membranes and for stabilizing these proteins during purification. Studies to measure the equilibrium binding of ions, ligands, or inhibitors can be carried out using the purified ion channels in detergent, but the electrophysiological studies to characterize the detailed functional properties require reconstitution of the purified ion channel into a lipid bilayer [4]. Ion channels have been reconstituted into a variety of lipid vesicles that range in size from small unilamellar vesicles (SUVs, tens of nm) [5] to giant unilamellar vesicles (GUVs, 1–100 μm), roughly the size of biological cells [6]. Functional studies on ion channels reconstituted into SUVs are carried out using flux assays, which measure the movement of ions into or out of many vesicles [4]. These flux assays provide the bulk functional properties of the ion channel population but do not allow for easy determination of the single-channel properties such as the conductance or the open probability of the ion channel. These assays also do not allow for rapid control of membrane potential or for rapid exchange of solutions surrounding the membrane without highly specialized stopped-flow equipment. SUVs containing ion channels can also be fused with planar lipid bilayers and electrophysiological methods can be used for measurement of ion channel activity [4]. A limitation of the planar lipid bilayer recording setups that are presently available is that they do not allow for rapid exchange of solutions. Further, the size of the membranes formed in a planar lipid bilayer setup makes them more prone to electrical and mechanical noise that interferes with the ion channel recordings. The membrane size also results in large capacitances that cause a slowing of the voltage response and therefore fast channel events (rapid activation, for example) cannot be investigated.

Ion channels can also be reconstituted into GUVs. GUVs are advantageous compared to SUVs since their large size allows them to be visualized by optical or fluorescence microscopy, thus allowing them to be used for patch-clamp electrophysiological recordings of ion channels. Ion channels that have been functionally characterized in GUVs include the proton-gated K^+ channel KcsA [7–9], the voltage gated K^+ channel KvAP [10], the mechanosensitive ion channels MscS and MscL [11–13], the bacterial porins OmpC and OmpF [14, 15], and the eukaryotic ion channel TrpV1 [16]. In addition to studies on ion channels, GUVs have also been used as model membranes to study characteristics of lipid domains

[17], membrane-protein interactions [18], DNA-membrane interactions [19], and vesicle budding and fission [20, 21].

The techniques commonly used for forming GUVs include spontaneous swelling and electroformation [22–26]. In the spontaneous swelling method, SUVs are dried down, forming a lipid film that consists of the lipid bilayers organized roughly in stacks [27]. Rehydration causes the bilayers to swell as the hydrophilic head groups attract water and results in forming GUVs as water seeps into the interlamellar space. At physiological ionic strength, negatively charged lipids are crucial for the electrostatic repulsion necessary to promote swelling [28]. Neutral lipids may be used in the presence of high concentrations of divalent cations [29], at low ionic strength (<1 mM) [28], or with the addition of non-electrolytic monosaccharides such as glucose, mannose, or fructose [30], which drive water toward the interlamellar space as a result of osmotic pressure. Electroformation works similarly to the spontaneous swelling method, except that an alternating current (AC)-electric field is applied during the rehydration step. The alternating electric field causes the vesicles to become more ordered and also to vibrate, aiding in their ability to fuse and then detach from the surface to form GUVs [31]. While electroformation generally results in a more homogenous GUV population, the drawbacks of electroformation are that it works best under low ionic concentrations that are not physiological, is hampered by the presence of charged lipids, and requires specialized equipment [22].

We have adapted a technique similar to the dehydration/rehydration method for the functional characterization of ion channels. In this method, proteoliposomes containing ion channels are dehydrated on a glass cover slip, and then rehydrated in the presence of magnesium to induce the formation of large unilamellar blisters [32]. We have found it easier to identify these unilamellar blisters and to obtain gigaohm seals from these blisters than compared to the spherical GUVs obtained by electroformation. Further, this method relies on a regular patch clamp setup that is commonly available and therefore provides a relatively easy way for functional studies on reconstituted ion channels. In this chapter, we describe how this approach is used for the functional characterization of the bacterial potassium channel KcsA.

2 Materials

2.1 Reconstitution of the Ion Channel into Liposomes

1. Soybean polar lipid extract in chloroform (Avanti Polar Lipids).
2. Borosilicate glass tubes, 20 × 150 mm with lids (Fisher Scientific).
3. Rotator.

4. Reconstitution buffer: 200 mM KCl, 5 mM MOPS-KOH, pH 7.0 (*see* **Note 1**).
5. Tris(2-carboxyethyl)phosphine (TCEP).
6. High power bath sonicator (Laboratory Supplies, Inc).
7. Liquid nitrogen.
8. n-Dodecyl-β-D-maltopyranoside (DDM).
9. Purified ion channel in detergent.
10. Bio-Beads SM2 (Bio-Rad).
11. Ultracentrifuge and rotor (such as Beckman Optima TLX Ultracentrifuge with rotor TLA 100.4).
12. Ultracentrifuge tubes.
13. Microcentrifuge tube homogenizers.

2.2 Formation of Blisters

1. Glass cover slips.
2. Desiccator at 4 °C.
3. Petri dishes (35 × 10 mm).
4. Phase contrast, DIC, or fluorescent microscope (we use a Nikon Eclipse TS100 with a 40× objective and a 10× eye piece).
5. Rehydration buffer: 200 mM KCl, 10 mM MOPS-KOH, pH 7.0.
6. Blister formation buffer: 200 mM KCl, 40 mM $MgCl_2$, 0.5 mM $CaCl_2$, 10 mM MOPS-KOH pH 7.0.

2.3 Patching of Blisters

1. Patch Amplifier (Molecular Devices).
2. Analog to digital converter (Molecular Devices).
3. Borosilicate glass pipettes (we use Sutter SF150-86-10, OD 1.5 mm, ID 0.86 mm, 10 cm length).
4. Rapid solution changer (BioLogic Science Instruments).
5. Pipette solution: 200 mM KCl, 10 mM succinate-KOH, 0.5 mM $CaCl_2$ pH 4.0 for typical wild-type KcsA recordings.
6. Solutions for rapid solution changer: 200 mM KCl, 10 mM MOPS-KOH pH 8.0 and 200 mM KCl, 10 mM succinate pH 3.0 for typical wild-type KcsA recordings.

3 Methods

3.1 Reconstitution of the Ion Channel into Liposomes

Our protocol is based on the procedure used by Cao et al. for the reconstitution of the TrpV1 channel [16]. In this protocol, lipid vesicles are gently solubilized by detergent, purified ion channel protein is added, and the detergent is slowly removed by Bio-Beads

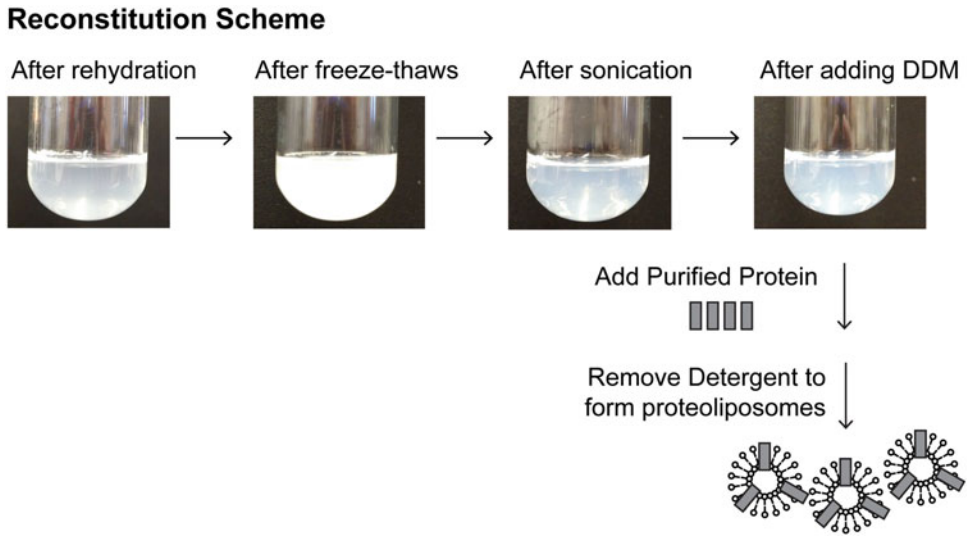

Fig. 1 Reconstitution of the KcsA channel into lipid vesicles. Pictures of lipids at various stages during the preparation of solubilized lipids for ion channel reconstitution, along with a *cartoon* illustrating the incorporation of KcsA channels into the liposomes

for the incorporation of the ion channel proteins into the liposomes (Fig. 1).

1. Dry 2.5–10 mg of soybean polar lipid extract (in a chloroform solution) in a round-bottom glass tube with lid using a gentle stream of argon. During drying, the tube is gently rotated to get a thin layer of lipid. After the chloroform has evaporated, dry under argon for an additional 5 min and then place under vacuum in a desiccator for 2–18 h at room temperature (*see* **Note 2**).
2. Rehydrate lipids at 5 mg/mL in 200 mM KCl, 5 mM MOPS-KOH, 2 mM TCEP pH 7.0. Rotate gently for 30 min at room temperature.
3. Freeze-thaw the lipids ten times, alternating between liquid nitrogen and a warm water bath.
4. Sonicate lipids in a bath sonicator for 3–5 min, until the lipid solution becomes translucent (*see* **Note 3**).
5. Add n-Dodecyl β-D-maltoside (DDM) to 4 mM and rotate lipids for 30 min at room temperature.
6. Add the purified protein to lipids at the desired protein: lipid ratio. We have used a 1:20–200 ratio for macroscopic and a 1:10,000 ratio for single-channel KcsA recordings. Bring total volume to 1 mL with reconstitution buffer. Rotate for 30 min at room temperature (*see* **Note 4**).

7. Remove detergent using Bio-Beads. Add Bio-Beads in four aliquots (30, 30, 50, and 100 mg respectively), one aliquot per hour, while continuing to rotate at room temperature. Add 1 mL of reconstitution buffer along with each of the first three additions of Bio-Beads, thereby diluting the reconstitution solution to a final volume of 4 mL. Following the additions of Bio-Beads, rotate the reconstitution mixture overnight at 4 °C. To ensure complete removal of detergent, add an additional 100 mg of Bio-Beads the following morning and rotate the mixture at room temperature an additional 1–3 h (*see* **Notes 5** and **6**).
8. To harvest the liposomes formed, centrifuge the reconstitution mixture at 100,000 × *g* for 1 h at 4 °C.
9. Resuspend the liposome pellet at ~50 mg/mL of lipid in 200 mM KCl, 10 mM MOPS-KOH pH 8.0. High concentrations of liposomes are necessary to promote GUV formation (*see* **Note 7**).
10. Divide liposomes into ~7 μL aliquots and freeze at −80 °C.

3.2 Formation of Blisters

1. Dry 7 μL of proteoliposomes on a cover slip in a desiccator for 12–36 h at 4 °C (*see* **Note 8**).
2. Rehydrate liposomes by adding 60 μL rehydration buffer directly on the top of the dried liposomes. Incubate overnight at 18 °C or ≥2 h at room temperature. If rehydrating overnight, put the cover slip into a container containing a paper towel soaked in rehydration buffer to prevent the drop from drying out.
3. Using a P2 pipette tip, gently mix the rehydrated liposomes. The solution should contain many small white chunks.
4. Fill 3–4 small petri dishes with 4 mL of the blister formation buffer. Using a P2 pipette, gently distribute very small amounts of rehydrated liposomes around the dish. For this step, pipet up 2 μL of the liposome solution and release in 10–20 small drops around the dish, repeating until the dish contains a total of 15–20 μL of rehydrated liposomes. Mg^{2+} is required for blister formation.
5. After ~1 h in the Mg^{2+}-containing solution, blisters are observed using a phase-contrast, DIC, or fluorescent microscope (Fig. 2). Locating blisters on the dish typically requires much patience, but they are found hanging off of the sides of clumps of lipids and there are typically several blisters per dish.

3.3 Patching of Blisters

1. Use patch pipettes with 1.5–5 MΩ resistance to form gigaohm seals on blisters. Fill pipettes with 200 mM KCl, 0.5 mM $CaCl_2$, 10 mM succinate-KOH, pH 4.0 solution for typical KcsA recordings.

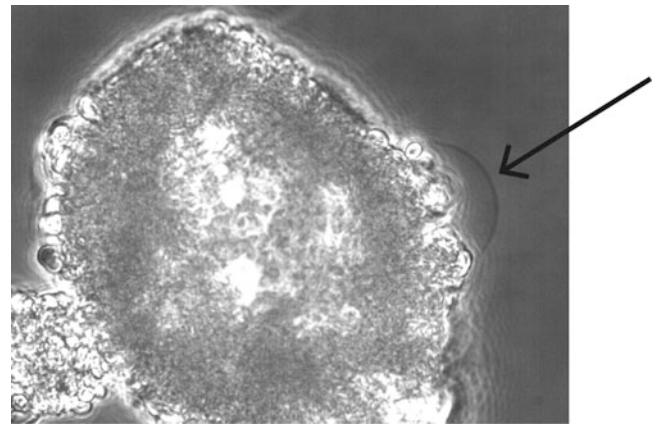

Fig. 2 A unilamellar blister used for patching. A blister attached to a clump of collapsed liposomes observed through a phase contrast microscope is shown. Unilamellar blisters can be recognized from their thin and transparent outline (see *arrow*)

2. Apply slight outward pressure once the pipette is in the solution to prevent the tip of the pipette from getting clogged.
3. As you approach the blister, remove outward pressure just before the tip of the pipette touches the blister. Once the pipette is lightly touching the blister, apply inward pressure to form a gigaohm seal. Typically, seals form quickly and very little inward pressure is required. Once a seal is obtained, slowly pull back the pipette to get an inside-out patch (*see* **Note 9**).
4. To observe activity of the KcsA channel, place the pipette in front of rapid solution changer tube flowing the pH 8.0 solution. Rapidly switch the pipette to the front of low-pH solution tube to observe activation and inactivation of KcsA. Figure 3a shows a single KcsA channel at 100 mV with the bath solution at pH 3.0. Figure 3b shows a macroscopic KcsA recording at 100 mV (*see* **Notes 10** and **11**).

4 Notes

1. In electrophysiological recordings using purified proteins, one must always watch out for contamination by porins. The porins observed either co-purify with the ion channels or originate from small amounts of bacterial contamination in the solutions used. Figure 3c shows an example of a recording showing porin activity. To minimize porin contamination, all the solutions used for protein purification, reconstitution, and recordings should be made fresh starting from powder, stored at 4 °C, and used with one week.

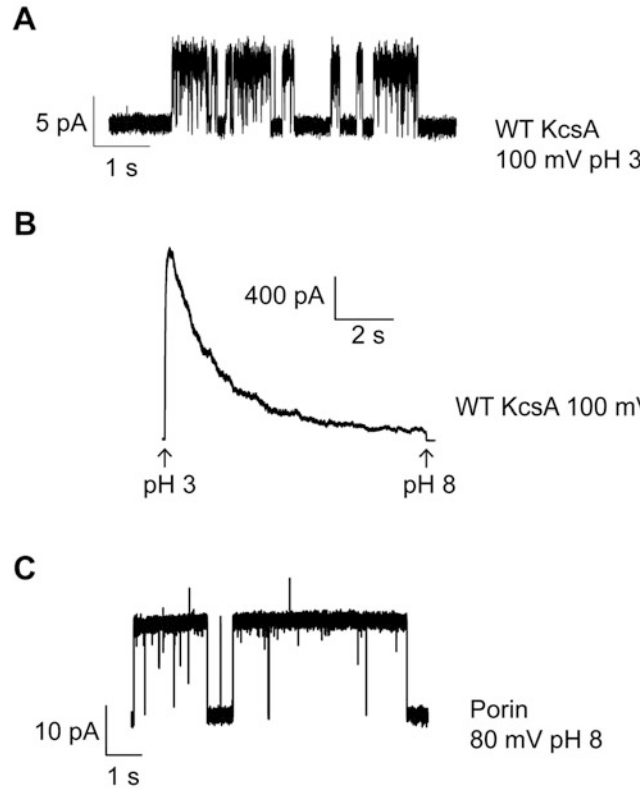

Fig. 3 Electrophysiological recordings of ion channels. (**a**) Single-channel recording of KcsA at 100 mV with 200 mM KCl, 10 mM succinate pH 3.0 in the bath and 200 mM KCl, 40 mM $MgCl_2$, 0.5 mM $CaCl_2$, 10 mM succinate-KOH pH 4.0 in the pipette. (**b**) Macroscopic recording of KcsA at 100 mV. Channels were activated by rapid perfusion of the bath solution from 200 mM KCl, 10 mM MOPS-KOH pH 8.0 to 200 mM KCl, 10 mM succinate pH 3.0. The change in pH causes the channels to rapidly activate and then inactivate. (**c**) Representative porin single-channel activity with 200 mM KCl in the recording solutions. Porins are a common contaminant that can easily incorporate into blisters

2. When drying down the soybean polar lipid solution, it is important for good reconstitutions that the lipid layer formed be as thin as possible. A rotary evaporator can be used for this step but we have found that steady manual rotation under a gentle stream of argon works sufficiently.
3. Formation of unilamellar vesicles is required before protein addition. Vesicle formation is carried out by sonication and the formation of unilamellar vesicles is indicated by the solution turning from cloudy to translucent. If the lipid solution does not look translucent, then additional sonication steps should be used. Care should be taken during the sonication steps to prevent heating as an increase in temperature can cause

spoiling of the lipid vesicles. Sonication is typically done in 30 s intervals with an intervening 30–60 s rest period. The rest period between rounds of sonication allows the lipids to cool to prevent overheating.

4. The protein to lipid ratio used during reconstitution is dependent upon the specific channel being investigated and the desired number of channels in the patch. Too much protein will make blister formation challenging and give leaky patches while too little protein will result in too many patches with no channel activity.
5. Bio-Beads should be washed three times each with methanol, water, and reconstitution buffer before use.
6. The amount of Bio-Beads to use will depend upon the detergent concentration in the purified protein sample. Since proteins are typically concentrated in a manner where the exact detergent concentration in the sample is not known, a trial and error approach has to be used. When detergent present has not been fully removed by the Bio-Beads, we often observe extra bubbles in the rotating protein/lipid mixture. In these cases, an additional aliquot of Bio-Beads is added to remove the excess detergent. If the detergent is not completely removed, then the blisters observed do not give the stable gigaohm seals that are necessary for electrophysiological recordings.
7. To resuspend the liposome pellet obtained following ultracentrifugation, we initially use a pipette tip to break up the pellet into smaller chunks. The solution with the chunks is then transferred into a micro-centrifuge tube and homogenized. Only gentle force must be used during the homogenization step as we have found that using too much force during homogenization can inhibit good blister formation. Gentle homogenization is followed by brief bath sonication to ensure the formation of a uniform solution before the liposomes are aliquoted and frozen.
8. Some ion channels require the addition of sucrose or ethylene glycol to prevent damage during the dehydration step [33–35]. The requirement for these additives has to be determined for the specific protein. We have determined that these additives are not necessary for maintaining the activity of the wild-type KcsA channel during dehydration.
9. Patching the blisters is challenging as they tend to move slightly in the solution along with the lipid chunks that the blisters grow from. Positioning the pipette to touch the moving blister for patching can be done with patience and practice.
10. When recording KcsA currents, rapid perfusion is essential for obtaining accurate rates of activation and inactivation. It is important to make sure the solution lines in the rapid perfusion

setup are free of air bubbles as air bubbles will cause the patch to break.

11. Proteins typically reconstitute into lipid bilayers in both orientations and therefore the patch obtained will contain channels oriented both ways. For the KcsA channel, we use pH 4 in the pipette to fully inactivate and thereby silence the channels that are oriented with their intracellular side facing the pipette. For other channels, a specific blocker can be added, either to the pipette or the bath solution, to silence channel in a specific orientation.

Acknowledgment

This research was supported by a grant from the NIH (GM087546) to F.I.V.

References

1. Hille B (2001) Ion channels of excitable membranes. Sinauer, Sunderland, MA
2. Stuhmer W (1998) Electrophysiologic recordings from Xenopus oocytes. Methods Enzymol 293:280–300
3. Thomas P, Smart TG (2005) HEK293 cell line: a vehicle for the expression of recombinant proteins. J Pharmacol Toxicol Methods 51 (3):187–200
4. Stockbridge RB, Tsai MF (2015) Lipid reconstitution and recording of recombinant ion channels. Methods Enzymol 556:385–404
5. Lin CM et al (2012) Size-dependent properties of small unilamellar vesicles formed by model lipids. Langmuir 28(1):689–700
6. Walde P et al (2010) Giant vesicles: preparations and applications. Chembiochem 11 (7):848–865
7. Yanagisawa M et al (2011) Oriented reconstitution of a membrane protein in a giant unilamellar vesicle: experimental verification with the potassium channel KcsA. J Am Chem Soc 133(30):11774–11779
8. Matulef K et al (2016) Individual ion binding sites in the K(+) channel play distinct roles in C-type inactivation and in recovery from inactivation. Structure 24(5):750–761
9. Chakrapani S, Cordero-Morales JF, Perozo E (2007) A quantitative description of KcsA gating I: macroscopic currents. J Gen Physiol 130 (5):465–478
10. Aimon S et al (2011) Functional reconstitution of a voltage-gated potassium channel in giant unilamellar vesicles. PLoS One 6(10):e25529
11. Martinac B et al (2014) Bacterial mechanosensitive channels: models for studying mechanosensory transduction. Antioxid Redox Signal 20(6):952–969
12. Martinac B et al (2010) Studying mechanosensitive ion channels using liposomes. Methods Mol Biol 606:31–53
13. Battle AR et al (2009) Rapid and improved reconstitution of bacterial mechanosensitive ion channel proteins MscS and MscL into liposomes using a modified sucrose method. FEBS Lett 583(2):407–412
14. Mahendran KR et al (2010) Permeation of antibiotics through Escherichia coli OmpF and OmpC porins: screening for influx on a single-molecule level. J Biomol Screen 15 (3):302–307
15. Kreir M et al (2008) Rapid screening of membrane protein activity: electrophysiological analysis of OmpF reconstituted in proteoliposomes. Lab Chip 8(4):587–595
16. Cao E et al (2013) TRPV1 channels are intrinsically heat sensitive and negatively regulated by phosphoinositide lipids. Neuron 77 (4):667–679
17. Kahya N et al (2003) Probing lipid mobility of raft-exhibiting model membranes by fluorescence correlation spectroscopy. J Biol Chem 278(30):28109–28115
18. Nikolaus J et al (2010) Hemagglutinin of influenza virus partitions into the nonraft domain of model membranes. Biophys J 99(2):489–498
19. Angelova MI, Tsoneva I (1999) Interactions of DNA with giant liposomes. Chem Phys Lipids 101(1):123–137

20. Kovacic J, Bozic B, Svetina S (2010) Budding of giant unilamellar vesicles induced by an amphitropic protein beta2-glycoprotein I. Biophys Chem 152(1-3):46–54
21. Staneva G et al (2005) Detergents induce raft-like domains budding and fission from giant unilamellar heterogeneous vesicles: a direct microscopy observation. Chem Phys Lipids 136(1):55–66
22. Jorgensen IL, Kemmer GC, Pomorski TG (2016) Membrane protein reconstitution into giant unilamellar vesicles: a review on current techniques. Eur Biophys J 46(2):103–119
23. Varnier A et al (2010) A simple method for the reconstitution of membrane proteins into giant unilamellar vesicles. J Membr Biol 233(1-3):85–92
24. Garten M et al (2015) Reconstitution of a transmembrane protein, the voltage-gated ion channel, KvAP, into giant unilamellar vesicles for microscopy and patch clamp studies. J Vis Exp 95:52281
25. Manley S, Gordon VD (2008) Making giant unilamellar vesicles via hydration of a lipid film. Curr Protoc Cell Biol Chapter 24:Unitas 24.3
26. Collins MD, Gordon SE (2013) Giant liposome preparation for imaging and patch-clamp electrophysiology. J Vis Exp 76:PMID: 23851612
27. Reeves JP, Dowben RM (1969) Formation and properties of thin-walled phospholipid vesicles. J Cell Physiol 73(1):49–60
28. Akashi K et al (1996) Preparation of giant liposomes in physiological conditions and their characterization under an optical microscope. Biophys J 71(6):3242–3250
29. Akashi K et al (1998) Formation of giant liposomes promoted by divalent cations: critical role of electrostatic repulsion. Biophys J 74 (6):2973–2982
30. Tsumoto K et al (2009) Efficient formation of giant liposomes through the gentle hydration of phosphatidylcholine films doped with sugar. Colloids Surf B Biointerfaces 68(1):98–105
31. Wesolowska O et al (2009) Giant unilamellar vesicles – a perfect tool to visualize phase separation and lipid rafts in model systems. Acta Biochim Pol 56(1):33–39
32. Delcour AH et al (1989) Modified reconstitution method used in patch-clamp studies of Escherichia coli ion channels. Biophys J 56 (3):631–636
33. Doeven MK et al (2005) Distribution, lateral mobility and function of membrane proteins incorporated into giant unilamellar vesicles. Biophys J 88(2):1134–1142
34. Keller BU et al (1988) Single channel recordings of reconstituted ion channel proteins: an improved technique. Pflugers Arch 411 (1):94–100
35. Riquelme G et al (1990) Giant liposomes: a model system in which to obtain patch-clamp recordings of ionic channels. Biochemistry 29 (51):11215–11222

Chapter 15

Combinatorial Assembly of Lumitoxins

David Nedrud and Daniel Schmidt

Abstract

Ion channels are among the most important proteins in neuroscience and serve as drug targets for many brain disorders. During development, learning, disease progression, and other processes, the activity levels of specific ion channels are tuned in a cell-type specific manner. However, it is difficult to assess how cell-specific changes in ion channel activity alter emergent brain functions. We have developed a protein architecture for fully genetically encoded light-activated modulation of endogenous ion channel activity. Fusing a genetically encoded photoswitch and an ion channel-modulating peptide toxin in a computationally designed fashion, this reagent, which we call Lumitoxins, can mediate light-modulation of specific endogenous ion channel activities in targeted cells. The modular lumitoxin architecture may be useful in a diversity of neuroscience tools. Here, we delineate how to construct lumitoxin genes from synthesized components, and provide a general outline for how to test their function in mammalian cell culture.

Key words Peptide toxin, LOV2, Optogenetic, Ion channel, Electrophysiology, Protein engineering

1 Introduction

A central theme in neuroscience is to understand how individual molecules, ion channels, contribute to brain processes such as cognition, behavior, and—when misregulated—cause disease pathology. On a general level, we appreciate that expression and activity levels of individual ion channel types differ for subsets of neurons, and that they are a critical part of the neuron's *functional identity.* Ion channels form the molecular basis for a neuron's contribution to circuit function and, by extension, network computation. Perhaps not surprisingly then, ion channels represent a significant fraction of the drug targets in the treatment of brain disorders. While previous studies of ion channels have defined their biophysical properties in great detail, their specific roles in different neuronal cell types, different neural circuits, and different developmental stages are much harder to study.

Show-Ling Shyng et al. (eds.), *Potassium Channels: Methods and Protocols,* Methods in Molecular Biology, vol. 1684,
DOI 10.1007/978-1-4939-7362-0_15,

Some methods for precision control of neuronal signaling rely on microbial opsins, which are light-activated membrane proteins from nature, that when illuminated can transport charges [1–4] across the cell membrane to either activate or silence electrically excitable cells . Despite their broad impact, they are exogenous channels or pumps and chiefly useful for analyzing neural circuits at the level of cell types, not individual ion channels.

Other lines of inquiry have yielded chemical modulators that are anchored to mutated ion channels and then agonize or antagonize them in response to light [5–9]. However, the requirement for custom chemical synthesis, and for mutated channels that anchor these chemical modulators, has limited application of these tools. While new methods of precision genome engineering might remove this limitation in the future, it currently precludes their usage to study endogenous ion channels in wild-type model systems.

A third track of molecular engineering has attempted to avoid the need for chemicals to address endogenous channels by expressing fully genetically encoded peptide toxins (which can modulate the activity of diverse classes of potassium-, sodium-, calcium-, and other ion channels) tethered to membranes [10–12]. While they function in mammalian brains in vivo, they are only inducible and reversible over timescales of hours to days. This lack of temporal control complicates usage, precluding the kinds of before versus after comparisons that are expected in the analysis of how ion channel activity levels govern neural dynamics.

We have previously engineered a novel K^+ channel modulator in the form of a synthetic fusion protein that combines a photoswitch (*As*LOV2) and an ion channel-blocking peptide toxin (e.g., alpha-dendrotoxin from eastern green mamba) to actuate the activity of specific endogenous ion channels (Fig. 1) [13]. Channel specificity is contributed by genetically encoded peptide toxins, which have evolved to bind ion channels with extremely high affinity and fidelity [14–18]. Additionally, peptide toxins modulate ion channel function in useful ways (shift voltage-dependence, block ionic current, alter propensity toward channel inactivation or desensitization), and in many cases their mode of action is described by simple first-order binding kinetics captured in quantitative analytical and predictive frameworks, such as one we have previously developed [13].

We demonstrated that lumitoxins change the activities of several endogenous K^+ channels with light in mammalian cells. Lumitoxins allow ion channel activity to be modulated on the order of seconds to minutes, a timescale relevant to many neural processes (*see* **Note 1**) [19–21]. Swapping the encoded peptide toxin, and leaving the non-toxin parts unchanged, readily alters lumitoxin specificity. Based on the latter discovery we put forward the idea that lumitoxins are modular single-chain fusion proteins—a first for fully genetically encoded optogenetic reagents.

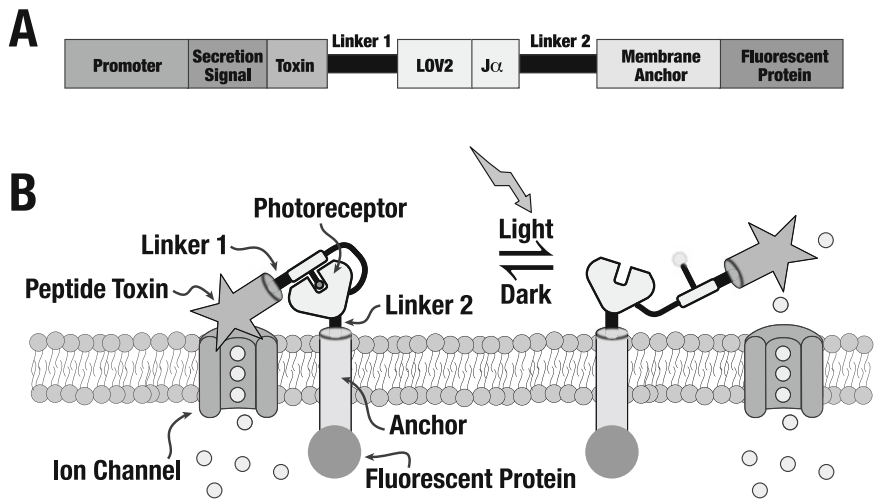

Fig. 1 The lumitoxin architecture: (**a**) Architecture of fusion proteins containing a membrane-anchored peptide neurotoxin linked to photoreceptor AsLOV2/Jα via a flexible linker, optionally equipped with a fluorophore. A secretion signal ensures targeting to the secretory pathway. The choice of promoter determines the overall lumitoxin/target channel ratio, and thus lumitoxin efficacy. (**b**) Upon illumination, the Jα helix reversibly unfolds, serving as a light-operated protein hinge, modulating the local concentration of the peptide toxin, and thus influencing the toxin/channel binding equilibrium

We provide here a protocol for lumitoxin assembly, which consists of these three steps: (1) identify components that will likely endow a lumitoxin with desired features, (2) synthesize and assemble these components into fusion genes encoding the designed lumitoxin, (3) test the designed lumitoxin for function in mammalian cell culture using relevant electrophysiological assays.

2 Materials

2.1 DNA Synthesis

1. Custom-made oligos can be ordered from many commercial vendors (e.g., IDT DNA).
2. Custom-made genes can be ordered from many commercial vendors (e.g., Genscript) in a number of different formats (linear dsDNA, plasmid DNA).

2.2 Cloning

1. Restriction endonuclease BsaI (NEB) (10 U/μL), supplied with 10× CutSmart buffer (500 mM Potassium Acetate, 200 mM Tris-acetate, 100 mM Magnesium Acetate, 1 mg/mL BSA, pH 7.9 at 25 °C).
2. T4 DNA Ligase (NEB) (400 U/μL), supplied with 10× ligation buffer (500 mM Tris–HCl, 100 mM $MgCl_2$, 10 mM ATP, 100 mM DTT, pH 7.5 at 25 °C).

3. NanoDrop, or similar device to determine concentration of DNA.
4. Media to culture *E. coli*, for example Luria-Bertani (LB): Tryptone 10 g/L, NaCl 10 g/L, Yeast Extract 5 g/L.
5. Appropriate Antibiotics, for example Carbenicillin (100 μg/mL), Kanamaycin (50 μg/mL), or Spectinomycin (50 μg/mL).
6. Competent Cells can be ordered from many commercial vendors (e.g., NEB) or can be prepared according to standard protocols.

2.3 Colony PCR

1. OneTaq DNA Polymerase (NEB).

2.4 DNA Gel Electrophoresis

1. 2-Log DNA ladder (NEB).
2. 1× TAE Running Buffer (40 mM Tris, 20 mM Acetic Acid, 1 mM EDTA).
3. 1.5% Agarose gels (prepared with 1× TAE and 1× SYBR Safe (Invitrogen)).

2.5 Plasmid Purification

1. Zyppy Plasmid Miniprep Kit (Zymo Research).

2.6 Sequencing

1. Assembled DNA expression constructs are verified by Sanger sequencing (e.g., McLAB) with appropriate primers.

2.7 Co-expression in Mammalian Cells

1. Cell lines: PC12 adherent (ATCC, CRL-1721.1).
2. Cell culture media: DMEM (Invitrogen) supplemented with 10% FBS (Invitrogen), 100 U/mL Pen/Strep (Invitrogen), 1 mM Sodium Pyruvate (Invitrogen), sterile filtered.
3. Cells are grown on glass coverslip (Carolina, Cat# 633009) coated with growth-factor depleted Matrigel (BD Bioscience).
4. Transfection reagent: Calcium Phosphate.
   (a) Solutions used (Make new solutions every month):
   - 2 M $CaCl_2$ solution in ddH_2O. (Store at −20 °C). For 50 mL volume add 14.7 g $CaCl_2$.
   - 2× HBS—50 mM HEPES-KOH, 280 mM NaCl, 1.5 mM Na_2HPO_4, pH 7.0 precisely. (Store at −20 °C). For 50 mL volume add 0.6 g HEPES, 0.8 g NaCl, 0.02 g $Na_2HPO_4{\cdot}7H_2O$. Since the Na_2HPO_4 concentration is critical, make a 1.5 M stock solution and dilute it to be accurate.
   - DMEM, adjusted to pH 6.8 with Acetic Acid, sterile filtered.

2.8 Optogenetic Stimulation and Electrophysiology

Example optogenetics/electrophysiology rig consisting of these components:

1. Research microscope (preferably inverted, e.g., Nikon TiE) with epi-fluorescent illumination and phase-contrast bright-field illumination, 20× and 40× ELWD objectives.
2. Imaging chamber (custom made, *see* Fig. 3).
3. Light source (e.g., Lumencor Spectra, or custom-built from Thorlabs components, *see* Fig. 3 for assembly diagram (adapted from [22]) and Table 1 for parts list.
4. Three-Axis micromanipulator (e.g., Sutter MP-285).
5. Integrated patch clamp amplifier (e.g., Sutter IPA).
6. Ag/AgCl electrodes (Warner Instrument).
7. For micropipette fabrication: Pipette Puller (e.g., Sutter P-97), Borosilicate Glass (Warner Instrument G150TF-4).
8. Handheld Power Meter (e.g., Thorlabs PM100D).
9. Solutions for electrophysiology:
   (a) Pipette Solution (mM): 125 K-Gluconate, 8 NaCl, 0.1 $CaCl_2$, 0.6 $MgCl_2$, 1 EGTA, 10 HEPES, 4 Mg-ATP, 0.4 Na-GTP, adjusted to pH 7.3 with KOH. Osmolarity was adjusted to 295–300 mOsm/L with sucrose.

Table 1
Parts list to build a custom multi-LED array (modified from [22])

Figure no.	Description	Part no.	Number needed
1	Illumination port adapter	SM1A26 (Thorlabs, for Nikon TiE)	1
2	Mounted LEDs	M455 L3 (Thorlabs, blue) & M565 L3 (Thorlabs, green/yellow)	1 each
–	T-Cube LED driver (1200 mA max)	LEDD1B (Thorlabs)	2
–	15 V power supply for T-cube LED driver	LPS101 (Thorlabs)	2
3	30 mm dichroic mounting cage	CM1-DCH/M (Thorlabs)	1
4	Dichroic filter	FF520-Di02-25x36 (Semrock)	1
5	SM1 end cap	SM1CP (Thorlabs)	1
6	Aspheric condenser lens	ACL2520U-A (Thorlabs)	2
7	SM1 coupler, external threads	SM1T2 (Thorlabs)	3
8	SM1 lens tube, 1/2″ long external thread	SM1V05 (Thorlabs)	2
9	SM1 lens tube, 0.3″	SM1L03 (Thorlabs)	2

(b) Bath Solution (mM): 125 NaCl, 2 KCl, 3 $CaCl_2$, 1 $MgCl_2$, 10 HEPES, 30 glucose, adjusted to pH 7.3 with NaOH. Osmolarity should be about 20 mOsm/L higher than pipette solution.

3 Methods

3.1 Design of Lumitoxins

Lumitoxins are end-to-end fusions of four components: a peptide toxin, linker, membrane anchor, and trafficking signal (*see* Fig. 1), assembled from modules via Golden Gate cloning [23]. Before outlining practical aspects of assembling lumitoxin genes from these individual components, we should consider the degrees of freedom we have for such rationally designed synthetic proteins, and how they influence our design choices.

3.1.1 Peptide Toxins

The choice of the peptide toxin determines the channel-specificity of the resulting lumitoxin. Many publicly accessible databases exist that conveniently collect and curate sequence information of peptide toxins. These include Conoserver [24] and Arachnoserver [25] (Queensland Facility for Advanced Bioinformatics, Australia), the Animal Toxin Database [26] (Hunan Normal University, Chang-Sha, China), the Bioactive Peptide Database [27] (K.U. Leuven, Belgium), and for integrated data, including target channels, the UniProtKB/Swiss-Prot Tox-Prot program [28].

While functional validation is the ultimate arbiter, chemical and biophysical properties of peptide toxins—if known—can help in selecting a peptide toxin. The following points should be considered:

1. Does the peptide toxin have known posttranslational modifications (e.g., amidation, carboxylation, hydroxylation, bromination, glycosylation) that make up a larger percentage of the toxin's primary sequence? Pathways that catalyze these modifications in venom glands might be absent in mammalian expression systems. Additionally, a fusion protein containing these unmodified peptide toxins might not fold properly, or may have altered affinity and/or target specificity.
2. What is the primary sequence length and overall predicted hydrophobicity? While we have not systematically studied the correlation of these parameters with expression and function, we have anecdotal evidence that very short peptide toxins (e.g., μ-conotoxin KIIIA, 16 amino acids), or those that are very hydrophobic (e.g., α-conotoxin PnIB) do not express well at the cell surface.
3. What are the affinity and kinetics of the peptide toxin binding to the target channels? Since lumitoxins switch by changing the

local concentration of a genetically encoded peptide toxin close to the cell membrane in response to light, their function—specifically the achievable dynamic range between the lit and dark state activity of the targeted channel—depends on balancing toxin affinity with target channel abundance. For example, if a high-affinity (nanomolar K_D) peptide toxin is used, and the expression level of the lumitoxin is very large compared to the targeted channel, then no light-induced unblocking of that channel can be achieved. This is due to the high local concentration of the peptide toxin, which when illuminated will not significantly alter how many channel-binding sites are occupied. In another example, if the peptide toxin off-rate is too low, then the refractory period of lumitoxins will increase. That is, how fast after cessation of illumination the system recovers to the ground (dark) state, from where it can be actuated again with another pulse of light. If channel affinity is problematic, mutations can be introduced into many peptide toxins that adjust affinity to a desired range (e.g., [29–31]). We have previously described numerical simulations that assume a simple coupled equilibrium, and can predict efficacy of peptide toxin with different channel affinity over a large range of channel/toxin expression ratios [13].

3.1.2 Protein Linkers

Lumitoxins are synthetic proteins: end-to-end fusion of protein domains from diverse sources that encapsulate specific functions (channel binding, light-sensing, membrane anchoring). The roles of linkers go beyond simply connecting these protein domains. In lumitoxins, their properties (all-helical vs. disordered, short vs. long) determine overall efficacy. Since light induces a conformational change in LOV2 that partially unfolds the bi-stable Jα helix [32, 33], the linker between LOV2 and the membrane anchor determines how much of that free energy change is captured as increased flexibility of the tethered toxin, whose local concentration close to the cell membrane is in turn decreased, thus unblocking the target channel (*see* Fig. 1). Specifically, if the connecting linker is long and flexible, then the additional flexibility and length provided by the unfolded Jα helix will not significantly change the tethered peptide toxin's degrees of freedom, which results in lower lumitoxin efficacy. At the same time, the linker has to be long enough, so the peptide toxin can "reach" its cognate binding site on the channel. Similar constraints apply to the linker connecting the peptide toxin and the LOV2 N-terminus. Here, the linkers need to be as short as possible to keep the peptide toxin's tethered diffusion coupled to the LOV2 conformational state, but long enough to prevent steric clashes between peptide toxin and LOV2. Molecular dynamics simulations capture the length and flexibility-dependent aspect of linker attributes well and can provide some insight to make rational choices [13]. However, these models

cannot predict the effects of the linker on the conformational equilibrium of the domains that they are connected to. Some research suggests that linkers "pre-encode" specific allosteric propagation pathways along which signals are transduced between domains [34, 35]. In other words, linkers themselves affect the equilibrium of domains that they are connected to. For this reason, linkers are thought to be under intense evolutionary optimization pressure in natural proteins, sometimes more so than the connected domains themselves [36]. Intuiting specific linker sequences that are compatible with a desired function of a synthetic fusion protein remains a big challenge. In the end, it is advisable to test a number of linkers with different chemical and physical properties (linker with bulky amino acids, glycine-serine linkers, alpha-helical linkers).

3.1.3 Membrane Anchor

By choosing different membrane anchors, lumitoxins can be generated with different topologies (i.e., N-terminus inside *vs.* outside), and with different trafficking profiles (e.g., to different plasma membrane compartments). The most commonly used designs are derived from single-pass transmembrane domains, such as the platelet-derived growth factor receptor (PDGFR), MHCI, or CD11b to which expression reporters (e.g., fluorescent proteins) can be fused to the intracellular side. The choice of fluorescent reporter ultimately depends on experimental context; however, those excited in the blue spectrum range (400–500 nm) should be avoided so as to prevent overlap with the LOV2 action spectrum [37]. Alternatives for membrane anchoring are motifs that elicit posttranslational modification with a GPI anchor.

3.1.4 Trafficking Signals

Lastly, trafficking signals including those targeting lumitoxins for the secretory pathway are an important choice. Note that our ongoing work suggests that it depends on the peptide toxin context to answer which specific secretion signal yields optimal expression at the cell surface. As before for linker choices, it is advisable to try a few different secretion signals for optimization. One strategy is to retain the native secretion signal of the pre-pro peptide toxin; however, we have found them to work poorly in a mammalian expression context. Surveying existing databases of secretion signals (e.g., www.signalpeptide.de, more than 19,000 mammalian and viral sorting signals) is an option for generating a set of secretion signals common to mammalian membrane proteins.

3.2 Implement the Cloning of Lumitoxins

Golden Gate Assembly is used for the efficient and seamless assembly of multiple components as advised in Subheadings 3.1.2–3.1.4.

3.2.1 Design Lumitoxin Donor Components

Once all component choices are made, the corresponding DNA modules can be obtained by reverse translating the primary amino acid sequence with the appropriate codon usage using one of several available services (e.g., EMBOS Backtranseq [38]). The

resulting nucleotide sequences should be free of internal type IIS restriction enzymes sites, in particular, those for BsaI. Note that stop codons need to be skipped for all but the last module (most often the fluorescent protein reporter). The next step is to add to the reverse translated nucleotide sequences overhangs of four nucleotides plus the desired type IIS restriction site that will be used for the restriction/ligation (Golden Gate) assembly step (*see* Fig. 2a). Most commonly BsaI (NEB) is chosen, but other enzymes (e.g., BpiI or BsmBI) work as well. Refer to Fig. 2 that outlines the overall logic on how specific overhang pairs direct the modules assembly into the correct topologies and consider these additional requirements: Out of 240 possible 4-nucleotide overhangs, avoid the 16 that are palindromic since they can self-ligate. Avoid overhangs that are the same in three out of the four nucleotides (e.g., TAGG and CAGG), since they can ligate spuriously. Finally, ensure that the same overhang (e.g., CAGG and its reverse complement CCTG) is not used twice, since this will result in incorrectly assembled lumitoxin genes, in which some components are deleted. Typical sequences used in previous lumitoxin designs are provided in Fig. 2b. The prepared genes then need to be ordered from a DNA synthesis provider (e.g., Genscript) and subcloned into shuttle vectors.

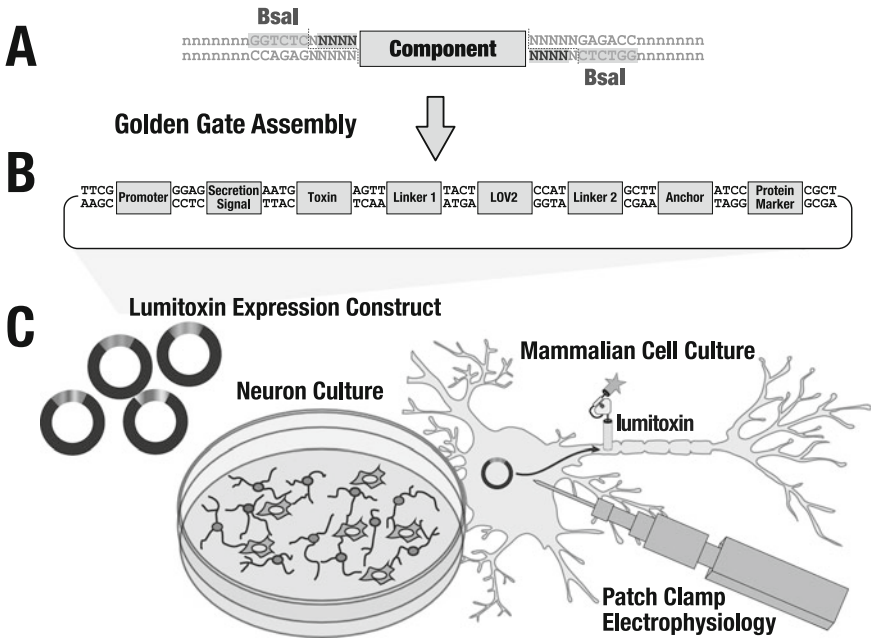

Fig. 2 Lumitoxin Assembly Scheme: (**a**) Individual lumitoxin components are synthesized flanked with two type IIS restriction sites (e.g., BsaI). (**b**) The variable bases of the 5′- and 3′-overhangs are chosen such that they are complementary with the respective overhangs of neighboring components, and mediate Golden Gate Assembly of the lumitoxin gene. (**c**) The resulting lumitoxin expression construct is transfected into mammalian cell culture and assessed for function by patch clamp electrophysiology

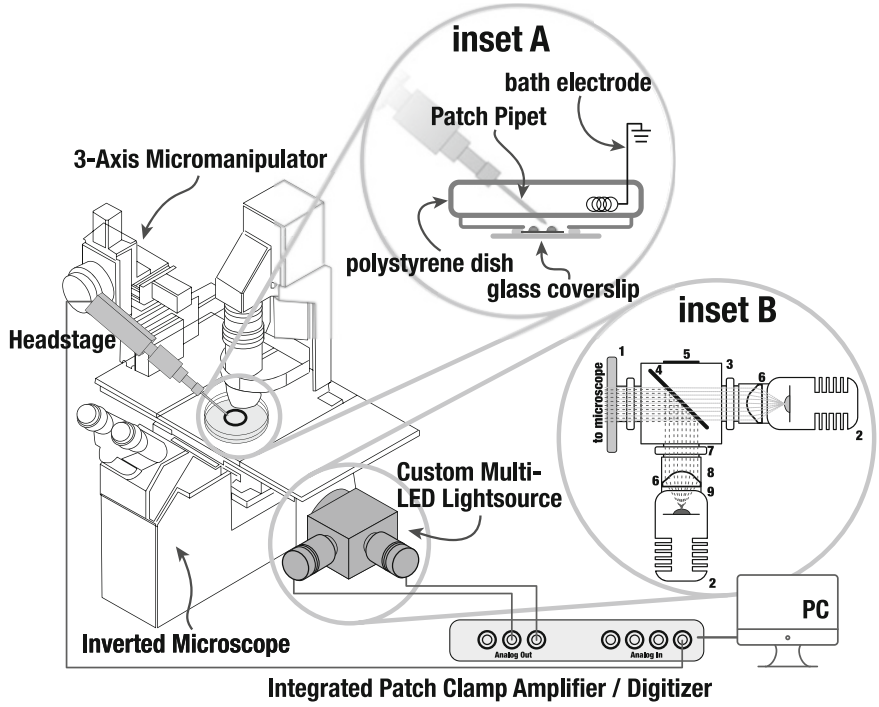

Fig. 3 A typical setup for characterizing lumitoxin function. A patch clamp amplifier headstage is mounted to a 3-axis micromanipulator and enables electrophysiological characterization of ion channels expressed in cultured cells, which are modulated by lumitoxins in response to light. Details on the imaging chamber are provided in the *inset* (**a**). Current and voltage traces are digitized and stored on a computer. A custom multi-LED light source provides epi-illumination for both AsLOV2 (photoswitch) and the fluorescent protein expression reporter. The *inset* (**b**) provides assembly details with parts numbered in accordance with Table 1

3.2.2 Design Lumitoxin Destination Vector

A destination vector that will receive the assembled lumitoxin and supports their expression in the appropriate expression system needs to be generated. Besides the general requirement for it to contain only two type IIS restriction sites (e.g., BsaI) that leave overhangs complementary to those of 5′-end of the first module (secretion signal), and the 3′-end of the last module (membrane anchor plus fluorescent reporter), there are other parameters to consider. What promoter should drive the expression of the lumitoxin? We have found lumitoxin efficacy to be strongly correlated with the relative expression ratio to the targeted channel. Therefore, in some circumstances, it might be desirable to express lumitoxin at lower or higher levels in relation to the target channel level. Ubc, PGK, SV40, EF1α, CMV, CAG have given us graded expression levels from low to high, respectively. Second, what is the mode of gene delivery? For transient expression in cell lines (such as PC12, CHO, or HEK293) many mammalian expression vectors are suitable (e.g., pSF-CMV-Spec, Oxford Genetics). For delivery into primary neuron culture at a later stage, it might be desirable to use a destination vector that supports helper-free packing into the

Adeno-associated virus (AAV), for example, pAAV-Golden (Addgene #51424). Lastly, is the target channel that the lumitoxin acts on expressed endogenously or is heterologous expression required? If the latter is the case, a destination plasmid can be constructed to drive the transcription of the channel gene and the lumitoxin at stoichiometric ratios by using a viral-skipping (P2A) sequence [39], or by using bidirectional promoters [40].

3.2.3 Build Lumitoxin Genes Using Golden Gate Assembly

After the destination vector and lumitoxin components in entry vectors are made and sequence verified, assembling the final lumitoxin gene is only a matter of setting up a one-pot restriction/ligation reaction, aka a Golden Gate assembly [23]. Care should be taken to use equimolar amount for both destination and entry vectors.

1. Set up a Golden Gate reaction with 50 ng (~25 fmol) destination vector, and equimolar amounts of secretion signal, linkers, peptide toxin, and membrane-anchor modules. Add 1.5 μL of 10× T4 DNA Ligase Buffer (with ATP), 1.5 μL of 10× Bovine Serum Albumin (BSA). Add 200 U of T4 DNA Ligase, and 10 U of BsaI. Bring the final volume to 15 μL with ddH_2O.
2. Cycle the reaction in a thermocycler for 45 cycles of: 2 min at 37 °C, followed by 5 min at 16 °C (total time required ~7 h). Then heat-inactivate the reaction by incubating at 80 °C for 10 min. This step is important.
3. As an optional step, the reaction can be treated with 10 U of DNA Exonucleases (Plasmid Safe, EpiCentre) to remove digested but unligated DNA for 30 min at 37 °C, followed by another heat inactivation for 30 min at 70 °C.

3.2.4 Transform into Competent Cells

1. Transform the entire ligation into chemically competent cells (*see* **Note 2**).
2. Pre-warm plates and SOC media at 37 °C.
3. Add the entire restriction/ligation reaction to 50 μL bacteria thawed on ice.
4. Incubate on ice for 20 min.
5. Heat shock at 42 °C for 45 s.
6. Incubate on ice for 2 min.
7. Add 250 μL SOC.
8. Recover the bacteria at 37 °C for 45–60 min, if you are using Kanamycin or Spectinomycin. This step can be skipped for Carbenicillin (*see* **Note 1**).
9. Plate 20 μL of the transformation on appropriate LB-Agar plate and grow overnight at 37 or 30 °C (*see* **Note 2**).

3.2.5 Colony PCR to Identify Lumitoxin Clones

Colony PCR is the easiest way to identify correctly assembled lumitoxin clones. One primer should bind to a region on the destination plasmid upstream the inserted modules, the other should bind in the last module.

1. Using a sterile toothpick or pipet tip, a small amount of bacterial colony is transferred into 95 μL of water.
2. For each colony to be screened, set up the PCR mix: 0.02 μL each of forward and reverse primer (100 μM), 5 μL OneTaq 2× Master Mix (NEB), 2.96 μL ddH_2O.
3. To this add 2 μL of the bacterial suspension, and cycle using the following conditions: 94 °C for 2 min, followed by 30 cycles of 94 °C for 30 s, 52 °C for 60 s, 68 °C for 1 min/kb. Final extension is 5 min at 68 °C.
4. Load the entire PCR reaction into an agarose gel, and analyze by gel electrophoresis that the clone produced a product of the expected size.
5. Bacterial suspensions of clones that are positive are then used to inoculate LB with the appropriate antibiotic and grown overnight. DNA is isolated from these cultures and sent for Sanger sequencing.

3.3 Test Lumitoxin Function in Mammalian Cell Culture

After lumitoxin candidates have been assembled, the final step is to co-express them with their cognate target receptor in mammalian cell culture to validate their function. We routinely use established cell lines (e.g., PC12) or cultured primary hippocampal neurons [41], and below is a versatile transfection protocol applicable to most culture conditions. We have discussed above the need to control relative expression levels of channel target and lumitoxin. In this context, note that with a lipid-based transfection method (e.g., Lipofectamine), it is harder to control the molar ratio of the respective expression plasmids that end up in a given cell. We recommend calcium phosphate transfection, with optimization of recipe and conditions as described previously [42]. Specific parameters to vary for plasmid titration to reduce the multiplicity of transfection are described elsewhere [43].

3.3.1 Transfection

1. Prepare a 24-well plate by placing glass cover slips (Carolina, Cat# 633009) into each well.
2. Coat surfaces with Matrigel (BD, 356230). Dilute Matrigel stock 50-fold in cold DMEM (Gibco). Store at 4 °C. To coat glass coverslips in 24-well plates, add 75 μL of diluted Matrigel. Incubate in a humidified 37 °C incubator for 1 h, and then remove all liquid by aspiration. Let cover slips dry completely; the dried matrigel leaves a white, opaque film behind.

3. Seed the cells at a density of 6×10^4 cells/cm^2 in media with no antibiotics and keep in a humidified incubator (with 5% CO_2) for a period of 12–14 h at 37 °C. The surface area of a well in a 24-well plate is 2 cm^2, so seed 120,000–130,000 cells per well.
4. The next day, pre-warm the ddH_2O, calcium chloride, and 2× HBS to room temperature prior to the procedure. Note: The volumes indicated below are for 24-well plates in which cells have been seeded in 500 μL media.
5. Add the following together to make the transfection mix: 1.25 μg DNA + 3.125 μL 2 M $CaCl_2$ solution + ddH_2O to make a final volume of 25 μL. Add this solution to 25 μL of 2× HBS, mix promptly, and let it stand for 30 s. For low copy transfection (down to one copy per cell on average), dilute plasmid with a dummy plasmid (e.g., pUC19, Agilent Genomics) at a 1:100 mass ratio.
6. Add the transfection mix to the cell media dropwise.
7. Incubate cells for 30 min to 2 h in 5% CO_2 at 37 °C.
8. Remove cell media, and wash cells with successive rounds of DMEM adjusted to pH 6.8 until all calcium phosphate precipitate is removed.
9. Replace complete cell culture media and incubate for 24–48 h in a humidified 37 °C incubator (5% CO_2).

Lumitoxins are very light sensitive, and before the onset of expression the plates need to be shielded from light, for example by wrapping with aluminum foil.

3.3.2 Test for Function

Assaying lumitoxin function combines electrical recording of ion channel function and simultaneous optical stimulation.

The Axon guide can be a good starting point to building electrophysiology rigs in particular patch clamping in general [44]. A general layout for such a system is shown in Fig. 3. Many existing patch clamp electrophysiology systems already contain an (inverted) microscope and high-resolution digitizer with 0–5 V analog outputs, so only minimal modifications are required to include a means to deliver precisely dosed light. Illumination systems range from xenon-arc lamps, solid-state laser, and light-emitting diodes to cover a wide gamut of light spectrum, light power, and speed of light switching. While pre-configured light-sources (Spectra, Sutter HPX) are convenient to use as long as they can be controlled in concert with the patch clamp amplifier, many can come at a considerable upfront cost and are hard to re-configure should experimental needs change. We have found that a customizable LED light source built from standard optomechanical parts (*see* Fig. 3, and Table for parts list adapted from [22])

provides a good balance of cost, versatility, and utility. The LED drivers interface with the digitizer for analog, pulse width, and frequency modulation of the LED light output.

As noted before, many photosystems used in optogenetic reagents are sensitive to even low doses of light. LOV2-containing proteins, for example, are known to be switched by ambient room light. For this reason, precautions need to be taken to block out blue/green light. This is easily accomplished by installing a black-out curtain around the setup and using a film-photography dark-room safelight (red LED, ~640 nm).

Commercial imaging chambers exist that allow patch pipet access, but we have found them too cumbersome for frequent cover slips changes. We have modified a polystyrene petri dish to hold the external cell solution (e.g., Bath Solution, *see* Fig. 3). With the help of vacuum grease, a #1.5 one inch glass coverslip is held in place below a cutout in the plastic. Cell-containing cover slips are placed in this furrow and pushed gently into the grease to prevent movement. In addition to patch pipet access and optical clarity, cover slips can be changed within a few seconds (under safelight conditions).

A typical experimental workflow to assess lumitoxin function is as follows:

1. Obtain whole-cell patch clamp access (monitor access resistance throughout the recording; should be <30 MΩ). *See* **Note 3**.
2. Without illumination, characterize target channel gating under voltage- or current clamp using the appropriate protocol ("before" illumination).
3. Illuminate the patched cell for a specific amount of time (duty cycle and frequency), with a specific dose of light (amplitude: a good starting point is 500 $\mu W/mm^2$), of a specific wavelength (for LOV2: 450 ± 10 nm) and characterize target channel gating under voltage- or current clamp using the same protocol as before ("during" illumination).
4. After holding the system in the dark for 5 minutes, characterize the target channel gating again ("after" illumination).

Figure 4 shows a representative example of how an α-dendrotoxin containing lumitoxin targeting voltage-dependent K^+ channels is unblocking those channels in response to illumination light in a repeated fashion.

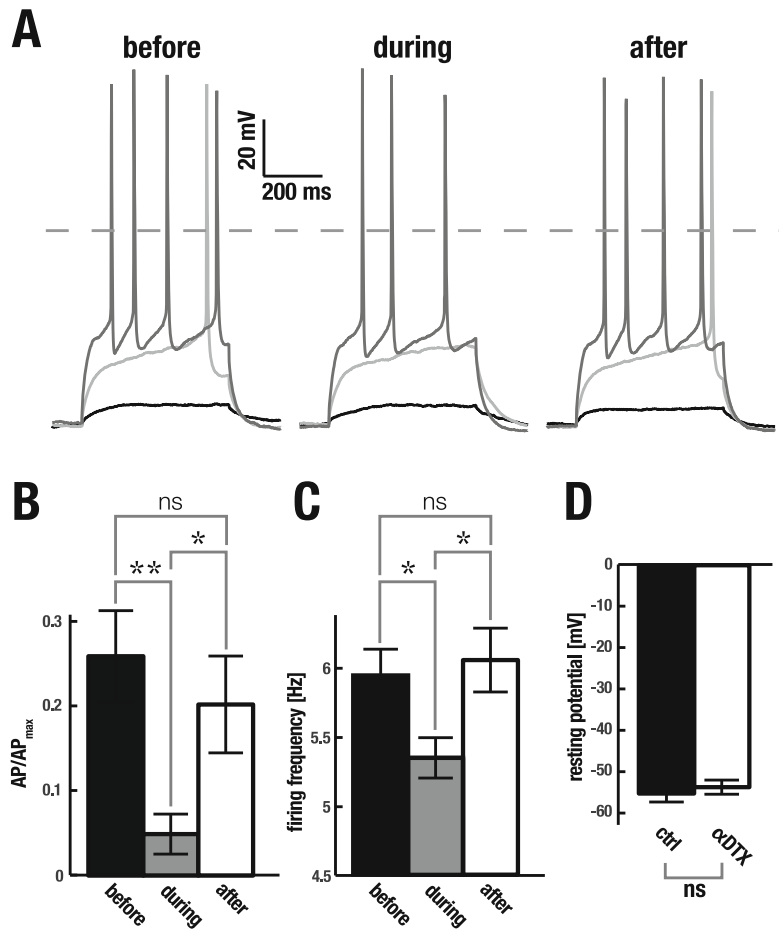

Fig. 4 Lumitoxin modulation of endogenous channels in cultured primary hippocampal neurons. (**a**) Action potentials elicited in cultured neurons under current clamp to −20 pA (*black*), +10 pA (*light gray*), and +50 pA (*medium gray*) before (*left panel*), during illumination (*middle panel*), and after cessation of illumination (*right panel*). *Dashed line*, 0 mV. (**b**) Number of action potentials at rheobase current injection, relative to the maximum number of action potentials elicited, before, during, and after illumination. $n = 11$ neurons. Statistical significance is reported as follows: $^{*}P < 0.05$, $^{**}P < 0.01$, two-tailed Student's *t*-test applied as post hoc test after ANOVA; *ns* not significant. (**c**) Firing frequency under current clamp before (*black*), during (*gray*), and after illumination (*white*), at rheobase current injection. $n = 15$ neurons. (**d**) Resting potential of cultured neurons mock transfected (*black*) and expressing αDTX-lumitoxin (*white*). $n = 6$–15 neurons each bar

4 Notes

1. Temporal resolution of lumitoxins is limited by photokinetics of the photoreceptor, and binding/unbinding kinetics of peptide toxin moiety. Since both are genetically encoded, these

parameters are in principle engineerable and provide experimental inroads into improving switching properties of lumitoxin variants.

2. When using destination vectors that support a helper-free production of AAV, it is advisable to take precautions against possible recombination that plasmids with inverted terminal repeats are prone to. This includes propagating them in *recA1*-negative strains (e.g., NEB Stable), growing bacterial cultures at 30 °C, and using Carbenicillin instead of Ampicillin for antibiotic selection.
3. Avoid patching clumps of cells that share their membranes with each other. While they may look, and be healthier (i.e., less leaky), neighboring cells can be electrically connected through gap junctions. Thus, patching a cell in a large group can lead to space clamp errors [45].
   (a) Pay attention to good trituration of cells during splitting and seeding to avoid clumps.
   (b) Patch healthy looking individual cells or cells at the edges of a larger group.
   (c) Patch within 36–48 h of transfecting. While expression is detectable after 12 h in most cases, it will improve and plateau to "steady state" over time.

References

1. Boyden ES, Zhang F, Bamberg E et al (2005) Millisecond-timescale, genetically targeted optical control of neural activity. Nat Neurosci 8:1263–1268
2. Boyden ES (2011) A history of optogenetics: the development of tools for controlling brain circuits with light. F1000 Biol Rep 3:11
3. Kleinlogel S, Feldbauer K, Dempski RE et al (2011) Ultra light-sensitive and fast neuronal activation with the Ca^2+−permeable channelrhodopsin CatCh. Nat Neurosci 14:513–518
4. Wietek J, Wiegert JS, Adeishvili N et al (2014) Conversion of channelrhodopsin into a light-gated chloride channel. Science 344:409–412
5. Volgraf M, Gorostiza P, Numano R et al (2006) Allosteric control of an ionotropic glutamate receptor with an optical switch. Nat Chem Biol 2:47–52
6. Szobota S, Gorostiza P, Del Bene F et al (2007) Remote control of neuronal activity with a light-gated glutamate receptor. Neuron 54:535–545
7. Zemelman BV, Nesnas N, Lee GA et al (2003) Photochemical gating of heterologous ion channels: remote control over genetically designated populations of neurons. Proc Natl Acad Sci U S A 100:1352–1357
8. Lima SQ, Miesenbock G (2005) Remote control of behavior through genetically targeted photostimulation of neurons. Cell 121:141–152
9. Sandoz G, Levitz J, Kramer RH et al (2012) Optical control of endogenous proteins with a photoswitchable conditional subunit reveals a role for TREK1 in GABA(B) signaling. Neuron 74:1005–1014
10. Ibañez-Tallon I, Wen H, Miwa JM et al (2004) Tethering naturally occurring peptide toxins for cell-autonomous modulation of ion channels and receptors in vivo. Neuron 43:305–311
11. Auer S, Stürzebecher AS, Jüttner R et al (2010) Silencing neurotransmission with membrane-tethered toxins. Nat Methods 7:229–236
12. Choi C, Nitabach MN (2013) Membrane-tethered ligands: tools for cell-autonomous pharmacological manipulation of biological circuits. Physiology (Bethesda) 28:164–171
13. Schmidt D, Tillberg PW, Chen F et al (2014) A fully genetically encoded protein architecture for optical control of peptide ligand concentration. Nat Commun 5:3019
14. Koh DCI, Armugam A, Jeyaseelan K (2006) Snake venom components and their

applications in biomedicine. Cell Mol Life Sci 63:3030–3041
15. Nirthanan S, Gwee MCE (2004) Three-finger alpha-neurotoxins and the nicotinic acetylcholine receptor, forty years on. J Pharmacol Sci 94:1–17
16. Terlau H, Olivera BM (2004) Conus venoms: a rich source of novel ion channel-targeted peptides. Physiol Rev 84:41–68
17. Corzo G, Escoubas P (2003) Pharmacologically active spider peptide toxins. Cell Mol Life Sci 60:2409–2426
18. Blumenthal KM, Seibert AL (2003) Voltage-gated sodium channel toxins: poisons, probes, and future promise. Cell Biochem Biophys 38:215–238
19. Hasson U, Chen J, Honey CJ (2015) Hierarchical process memory: memory as an integral component of information processing. Trends Cogn Sci 19:304–313
20. Kiebel SJ, Daunizeau J, Friston KJ (2008) A hierarchy of time-scales and the brain. PLoS Comput Biol 4:e1000209
21. Kato S, Kaplan HS, Schrödel T et al (2015) Global brain dynamics embed the motor command sequence of Caenorhabditis elegans. Cell 163:656–669
22. Thorlabs–Mounted LEDs. https://www.thorlabs.com/newgrouppage9.cfm?objectgroup_id=2692&tabname=Multi-LED%20Source
23. Engler C, Gruetzner R, Kandzia R et al (2009) Golden gate shuffling: a one-pot DNA shuffling method based on type IIs restriction enzymes. PLoS One 4:e5553
24. conoserver.org, http://conoserver.org
25. arachnoserver.org, http://www.arachnoserver.org
26. protchem.hunnu.edu.cn/toxin/. http://protchem.hunnu.edu.cn/toxin/
27. www.peptides.be, http://www.peptides.be
28. uniprot.org/program/Toxins, http://www.uniprot.org/program/Toxins
29. Gasparini S, Danse JM, Lecoq A et al (1998) Delineation of the functional site of alpha-dendrotoxin. The functional topographies of dendrotoxins are different but share a conserved core with those of other Kv1 potassium channel-blocking toxins. J Biol Chem 273:25393–25403
30. Gui J, Liu B, Cao G et al (2014) A tarantula-venom peptide antagonizes the TRPA1 nociceptor ion channel by binding to the S1–S4 gating domain. Curr Biol 24:473–483
31. Doupnik CA, Parra KC, Guida WC (2015) A computational design approach for virtual screening of peptide interactions across K(+) channel families. Comput Struct Biotechnol J 13:85–94
32. Harper SM, Neil LC, Gardner KH (2003) Structural basis of a phototropin light switch. Science 301:1541–1544
33. Yao X, Rosen MK, Gardner KH (2008) Estimation of the available free energy in a LOV2-J alpha photoswitch. Nat Chem Biol 4:491–497
34. Ma B, Tsai C-J, Haliloğlu T et al (2011) Dynamic allostery: linkers are not merely flexible. Structure (London 1993) 19:907–917
35. Papaleo E, Saladino G, Lambrughi M et al (2016) The role of protein loops and linkers in conformational dynamics and allostery. Chem Rev 116:6391–6423
36. Anantharaman V, Balaji S, Aravind L (2006) The signaling helix: a common functional theme in diverse signaling proteins. Biol Direct 1:25
37. Kennis JTM, Crosson S, Gauden M et al (2003) Primary reactions of the LOV2 domain of phototropin, a plant blue-light photoreceptor. Biochemistry 42:3385–3392
38. EMBOSS Backtranseq. http://www.ebi.ac.uk/Tools/st/emboss_backtranseq/
39. Kim JH, Lee S-R, Li L-H et al (2011) High cleavage efficiency of a 2A peptide derived from porcine teschovirus-1 in human cell lines, zebrafish and mice. PLoS One 6:e18556
40. Bidirectional promoter vectors. http://www.clontech.com/US/Products/Fluorescent_Proteins_and_Reporters/Coexpression/Bidirectional_Promoter
41. Kaech S, Banker G (2006) Culturing hippocampal neurons. Nat Protoc 1:2406–2415
42. Jiang M, Chen G (2006) High Ca2+-phosphate transfection efficiency in low-density neuronal cultures. Nat Protoc 1:695–700
43. Wang S, Cho YK (2016) An optimized calcium-phosphate transfection method for characterizing genetically encoded tools in primary neurons. Meth Mol Biol (Clifton, NJ) 1408:243–249
44. The axon guide. https://www.moleculardevices.com/axon-guide
45. Thomas P, Smart TG (2005) HEK293 cell line: a vehicle for the expression of recombinant proteins. J Pharmacol Toxicol Methods 51:187–200

Chapter 16

Characterization of MC4R Regulation of the Kir7.1 Channel Using the Tl^+ Flux Assay

Michael J. Litt, Roger D. Cone, and Masoud Ghamari-Langroudi

Abstract

The family of inward rectifying potassium channels (Kir channels) plays crucial roles in the regulation of heart rhythms, renal excretion, insulin release, and neuronal activity. Their dysfunction has been attributed to numerous diseases such as cardiac arrhythmia, kidney failure and electrolyte imbalance, diabetes mellitus, epilepsy, retinal degeneration, and other neuronal disorders. We have recently demonstrated that the melanocortin-4 receptor (MC4R), a $G\alpha_s$-coupled GPCR, regulates Kir7.1 activity through a mechanism independent of $G\alpha_s$ and cAMP. In contrast to the many other members of the Kir channel family, less is known about the biophysical properties, regulation, and physiological functions of Kir7.1. In addition to using conventional patch clamp techniques, we have employed a high-throughput Tl^+ flux assay to further investigate the kinetics of MC4R-Kir7.1 signaling in vitro. Here, we discuss the employment of the Tl^+ flux assay to study MC4R -mediated regulation of Kir7.1 activity and to screen compounds for drug discovery.

Key words Melanocortin 4 receptor (MC4R), Inward rectifying K^+ channels (Kir7.1), Thallium flux assay, Intracellular signaling, High-throughput screening

1 Introduction

Inward rectifying K^+ currents (Kir) were first identified more than a half a century ago [1]. Since their discovery, seven subfamilies of Kir channels have been characterized [2]. Kir channels regulate critical cellular parameters including resting membrane potential, action potential duration, and hormone release. Due to their role in regulating these processes, Kir channels are critical for the proper function of cardiac myocytes, neurons, pancreatic β-cells, renal epithelial cells, glia, and epithelial cells. Thus, a better understanding of how Kir channels are regulated holds great potential for future drug discovery.

Invariably, Kir channels are commonly regulated by the signaling lipid PIP_2 that enables channel opening through direct binding [3, 4]. Besides PIP_2, factors that gate Kir channel conductance are unique to each subfamily. For instance, the G protein-coupled

Show-Ling Shyng et al. (eds.), *Potassium Channels: Methods and Protocols*, Methods in Molecular Biology, vol. 1684,
DOI 10.1007/978-1-4939-7362-0_16,

inward-rectifying channels (GIRK, Kir3.x) are opened by the βγ subunits of heterotrimeric G proteins [5], while Kir6.2 (K_{ATP}) is sensitive to intracellular ATP levels [6]. Despite extensive understanding of some Kir channels, the regulatory mechanisms of other Kir channels including Kir7.1 remain largely uncharacterized.

Recently, our group used patch clamp electrophysiology to describe how Kir7.1, a low conductance weakly rectifying Kir subtype, is regulated by the Melanocortin 4 Receptor (MC4R)—a G_s-coupled GPCR [7]. We observed that MC4R activation decreases Kir7.1 opening even in the presence of G_s inhibitors. In order to understand the molecular mechanisms underlying this interaction, we created a heterologous expression system in HEK293 cells and adapted a thallium (Tl^+)-based screening platform for the quantification of channel opening [8].

The use of Tl^+—an equally permeant ion for K^+ channels—and an intracellular Tl^+-sensitive dye enables determination of potassium channel opening in a 384-well format [8]. Cells are loaded with the thallium sensitive dye, exposed to ligands or vehicle for 20 min and given a bolus of thallium Tl^+. The specific techniques below have been employed to characterize MC4R-Kir7.1 signaling and its modulators. However, these techniques can be used to characterize the nature of any Kir-GPCR interaction.

2 Materials

2.1 Assay Buffers

1. Hanks Buffered Salt Solution (HBSS) with Ca^{2+} and Mg^{2+} (Thermo Scientific cat #14025076): 140 mg/L $CaCl_2$, 100 mg/L $MgCl_2{\cdot}6H_2O$, 100 mg/L $MgSO_4{\cdot}7H_2O$, 400 mg/L KCl, 60 mg/L KH_2PO_4, 350 mg/L $NaHCO_3$, 8 g/L NaCl, 48 mg/L Na_2HPO4 (anhydrous), 1 g/L D-Glucose.
2. 1 M HEPES solution: Dissolve 119.15 g HEPES (free acid) in 400 mL ddH_2O. Add 5 M NaOH dropwise to achieve a pH of 7.0. Add ddH_2O until the solution reaches a final volume of 500 mL. Filter sterilize.
3. Assay Buffer: Add 10 mL of a 1 M HEPES solution to 500 mL of HBSS w/ Ca^{2+} & Mg^{2+}. pH solution to 7.4 with 5 M NaOH.
4. 6.7% w/v pluronic acid solution in DMSO: Dilute 200 mL of a 20% Pluronic acid solution (Thermo Scientific cat #P3000MP) with 400 μL anhydrous DMSO to obtain a 6.7% pluronic acid solution.
5. Thallos Stock: Add 60 μL of a 6.7% w/v pluronic acid solution into 100 μg of the cell-permeable Thallos-AM (VU053734-1)

dye (TEFlabs cat # 0901sp, actual MW 841). Thallos-AM stock can be stored in aliquots at −20 °C for 1 month.

6. Dye Buffer: Add 6 μL of the Thallos-AM stock to 10 mL Assay Buffer. This volume is sufficient for one 384-well plate.
7. Thallium Sulfate Stock solution: Prepare 100 mM Thallium sulfate (Tl_2SO_4) solution by dissolving 2.52 g into 50 mL of ddH_2O. CAUTION: Thallium is extremely toxic and should be handled with care. Always wear gloves when handling thallium buffers and ensure proper waste disposal with local environmental health and safety representatives.
8. 5× Thallium Working Solution: Add 0.2 mL of 100 mM Thallium Sulfate to 10 mL Assay Buffer for a final working solution of 2 mM Tl^+. This solution is a 5× concentrated stock that will be added during the assay.
9. Peptide Ligand Buffer: Assay Buffer containing 0.1% w/v Bovine Serum Albumin (BSA). Filter sterilize.
10. Small Molecule Ligand Buffer: Assay Buffer containing 0.1% DMSO.

2.2 Cell Culture Materials

1. Culture Media: 10% FBS supplemented DMEM containing 4.5 g/L Glucose and 50 U/mL Penicillin-Streptomycin.
2. T-REx™ selection media (B-Media): Culture Media containing 0.5 mg/L Blastocidin.
3. Kir channel selection media (BH-Media): B-media containing 200 μg/mL Hygromycin.
4. Double Selection Media (BGH-Media): BH-Media containing 500 μg/mL Geneticin.
5. Plating media: 10% FBS supplemented DMEM containing 4.5 g/L Glucose and 1 μg/mL Tetracycline–HCl.
6. Assay plates: Cell Plate: BD BioCoat Poly-D-Lysine 384-well small volume black microplate.

2.3 Robotics

1. FDSS plate reader with integrated liquid-handling head and kinetic fluorescence detector (Flo3).
2. 384-head automated liquid dispensing platform.
3. Automatic cell plate washer (Optional—*see* **Note 1**).

2.4 Ligands (Peptides)

1. All neuropeptides are diluted in Peptide Ligand Buffer at a 2× final concentration.
2. All small molecules are diluted in Small Molecule Ligand Buffer a 2× final concentration.
3. Compound Plate: Greiner 384-well polypropylene plate, V-bottom (cat. # 781280).

3 Methods

3.1 Generation of Cell Lines Expressing Different Kir Subunits and Melanocortin Receptors

3.1.1 Generation of Polyclonal Cell Lines

1. Tetracycline-Regulated Expression HEK293T cells (T-REx™) expressing a tetracycline regulatory element are transfected (by using Lipofectamine 2000) with a plasmid containing the desired Kir coding sequence (Kir7.1, Kir4.2 etc.) in a pcDNA5/TO plasmid backbone (*see* **Note 2**).
2. Two days following transfection, a polyclonal population of Kir-expressing cells is selected using BH media.
3. After 30 days, stable Kir cells are then transfected with the desired GPCR (MC4R, MC3R, etc.) or a mock vector in a pcDNA3 backbone.
4. Two days following transfection, cells are selected for GPCR expression using BGH media.
5. Thirty days following this second selection, a Kir-GPCR polyclonal cell line is now ready for clonal selection.
6. If characterizing the presence of a Kir-GPCR interaction, polyclonal cell lines can be used. However, if a known Kir-GPCR interaction will be examined in a HTS format, selecting monoclones using the process below is highly recommended.

3.1.2 Generation of Monoclonal Cell Lines (See Notes 3 and 4)

1. Single-cell clones are selected by diluting polyclonal cell lines to 0.8 cells/20 μL in BGH media and then plating them on a poly-D-lysine-coated 384-well culture plate.
2. Wells are examined for the presence of single-cell colonies over the next 30 days. Wells that contain more than one clone are noted and excluded.
3. BGH Media is added weekly until cells become confluent.
4. Once confluent, monoclone cells are transferred to progressively larger culture vessels to ensure sufficient cell number for clonal screening.
5. HEK293T monoclones stably expressing a Kir channel and a GPCR can now be screened for using the protocol described in Subheading 3.2.

3.2 Assay Protocol

3.2.1 Cell Plating

1. Grow cells in BGH media in a 150 mm cell culture dish until 70–90% confluent.
2. Wash cells with DMEM and then disassociate using 5 mL 0.05% trypsin in DMEM.
3. Collect cells in a 15 mL conical tube and add 10 mL plating media.
4. Pellet cells in a swinging bucket centrifuge at 250 × *g* for 5 min.

5. Aspirate the supernatant and resuspend the cell pellet in 10 mL plating media containing Tetracycline to induce channel expression. Tetracycline concentration must be optimized empirically but we have found that 1 μg/mL is sufficient.
6. Count cells on a hemocytometer and dilute to 10^6 cells/mL with plating media containing Tetracycline. A final 75–90% confluency is optimum.
7. Pour the cell suspension into a sterile reservoir. Using an electronic multichannel repeat pipettor, immediately dispense 20 μL into each well of a black-wall, clear-bottom, 384-well poly-D-lysine-coated assay plate (BD Biosciences, Bedford, MA).
8. Lightly tap the corner of the plate to ensure that the cell suspension reaches the bottom of each well. Bubbles should be avoided as they prevent a uniform cell distribution.
9. Place the cell plate in a 37 °C 5% CO_2 incubator for 20–24 h to ensure cell adherence and protein (receptor and channel) expression.
10. If running an assay that requires 24-h incubation with a ligand, add compounds at this time.

3.2.2 Assay Procedure

1. 20–24 h following cell plating, check the assay plate to make sure that the cells are uniformly distributed within each well. If certain wells appear nonuniform, note them in a lab notebook so that they can be excluded from the final analysis.
2. Prior to beginning the assay, prepare all buffers described in Subheading 2.1.
3. Remove the plating media by flicking the plate. Remove any residual media by slamming the plate on a set of clean laboratory napkins (*see* **Note 1**).
4. Add 20 μL of Dye Buffer to each well using an electronic multichannel repeat pipettor (*see* **Note 1**).
5. Incubate cells in the dark for 30–60 min at room temperature. This incubation allows for intracellular esterases to cleave the acetoxymethyl-ester group from the Thallos-AM dye. This ensures intracellular accumulation of the dye and prevents dye efflux.
6. During this incubation, prepare the compound plate. Compound plates containing a ligand compound and the vehicle should be made in a checkerboard pattern (Fig. 1 and *see* **Note 5**). Prepare the ligands at 2× the final desired concentration.
7. Once the incubation is complete, the dye buffer is removed by again flicking the plate and then slamming on a set of clean

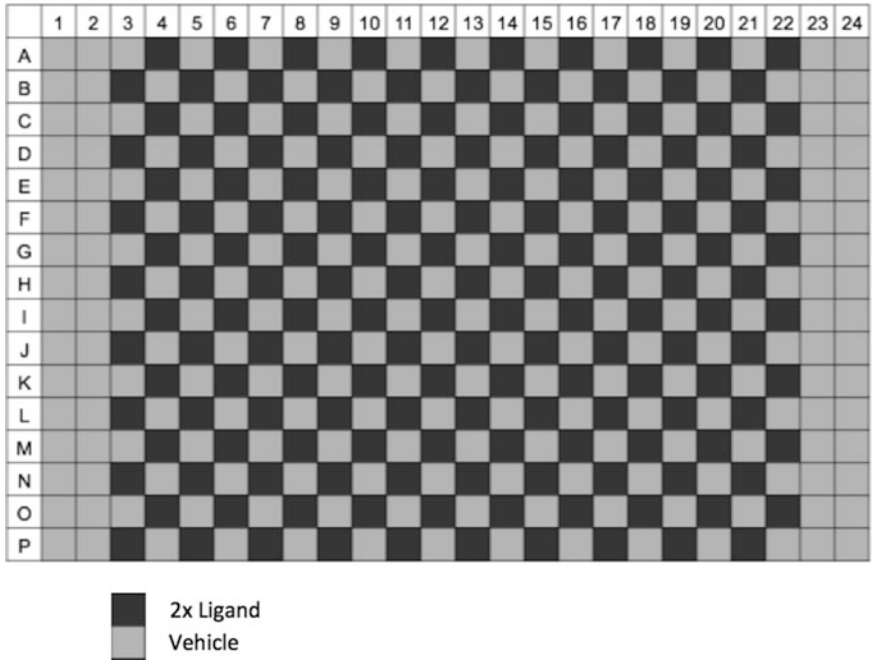

Fig. 1 Sample plate map: calculation of the ΔF_{Ratio} necessitates the use of a checkerboard plate map. F_{Ratio} traces from agonist-treated well traces are subtracted from the vehicle-treated trace directly above (*odd columns*) or below (*even columns*) to obtain ΔF_{Ratio}. We have found that 12–16 compound well/vehicle subtractions, or two columns, are necessary to detect significant differences in Kir7.1 flux

laboratory napkins. Then, add 20 μL of Assay Buffer to each well using an electronic multichannel repeat pipettor.

8. Using a 384-head automated liquid-handling robot, transfer 20 μL of ligand solution from the compound plate to the corresponding well in the assay plate. This step can be done inside the plate reader or on a separate machine depending on the specific assay design.
9. If using α-MSH, incubate the Assay plate for 20 min (Fig. 1 and *see* **Note 6**).
10. During this incubation, prepare a compound plate containing 25 μL of Thallium buffer in every well.
11. Following the ligand incubation, place the assay plate in a 384-well kinetic plate reader with liquid-handling capabilities. Record in the fluorescence mode with an excitation at 470 nm using an argon laser. Emission was filtered using a 530 ± 30 nm bandpass filter. The protocol is as follows:
    (a) 12 min total recording time with sampling at 1–2 Hz.
    (b) While recording, add 10 μL of 5× thallium buffer into all wells using the 384-well liquid-handling module after 2 min of baseline recording.

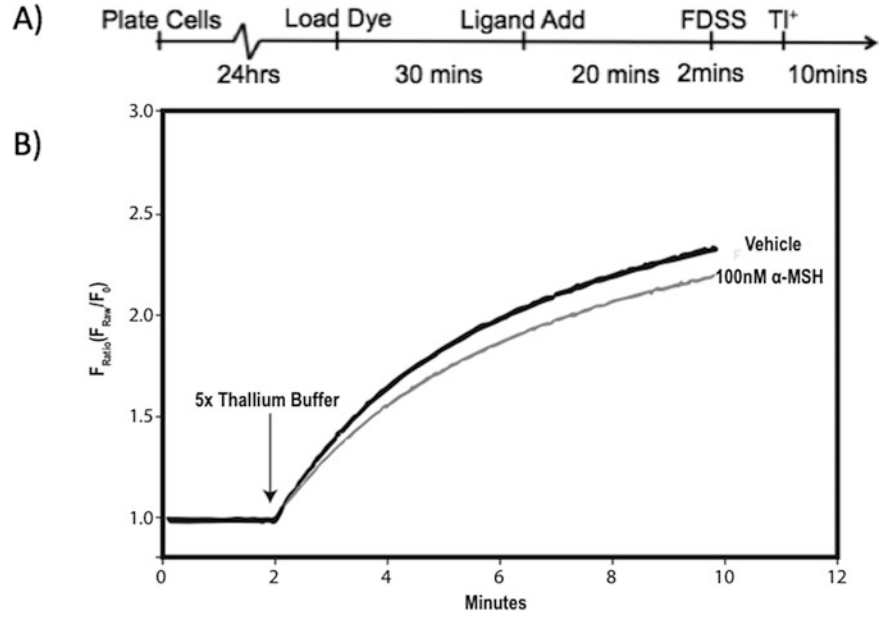

Fig. 2 Experimental protocol and sample traces: (**a**) A cell plate is prepared with 2×10^4 cells/well in a 384-well plate and incubated for 24 h. Cells are then washed with assay buffer, loaded with dye buffer, and incubated for 30 min. After another wash with assay buffer, the ligand is added using a 384-well robotic pipettor to ensure that every well receives agonist at the same time. After 20 min, the plate is now ready to be read in the FDSS kinetic plate reader. (**b**) Once placed in the FDSS reader, a 2 min baseline reading (F_0) is obtained. Using the FDSS automated liquid handler, 10 μL of a 5× Thallium buffer is added to each well of the assay plate. Fluorescence is read for 10 min following this addition. ΔF_{Ratio} is then calculated using the method described in Subheading 3.3

3.3 Data Analysis

1. Data from individual assay wells are exported as normalized fluorescence responses (F_{ratio}), obtained by dividing each data point (F_{raw}) by the average of the fluorescence signal during the two-minute period of baseline recording (F_0) (Fig. 2a):

$$F_{\text{ratio}} = F_{\text{raw}}/F_0.$$

2. Effects of a ligand on Kir channel opening ($F_{\text{Net\_Response}}$) are quantified and displayed by subtracting the fluorescence response of a well treated with the ligand ($F_{\text{ratio\_Compound}}$) from that of a well treated with the vehicle directly below or above ($F_{\text{ratio\_Vehicle}}$). This gives the net effect of a ligand on the channel opening ($F_{\text{Net\_Response}}$) and is also referred to as the "ratio subtracted" measurement (ΔF_{ratio}) (Fig. 2a, b):

$$F_{\text{Net\_Response}} = \Delta F_{\text{Ratio}} = F_{\text{Ratio(Compound)}} - F_{\text{Ratio(Vehicle)}}.$$

3. Once the ΔF_{Ratio} for a ligand has been determined, the maximum or minimum ΔF_{Ratio} ($\Delta F_{\text{Ratio Max}}$) of each replicate can be determined and used to statistically compare between groups.
4. *Z*-Factor, a measure of statistical effect size and variability, is used to investigate the high-throughput screening viability of an assay. A *Z*-factor > 0.5 is considered acceptable for high-throughput screening. The *Z*-factor can be calculated using the following formula:

$$Z\text{-factor} = 1 - \frac{3(\sigma_c + \sigma_v)}{|\mu_c - \mu_v|}.$$

μ_c = Average ΔF_{Ratio} Compound -Vehicle.
μ_v = Average ΔF_{Ratio} Vehicle -Vehicle.
σ_c = Standard Deviation ΔF_{Ratio} Compound−Vehicle.
σ_v = Standard Deviation ΔF_{Ratio} Vehicle−Vehicle.

3.4 Results

We have employed the thallium flux assay to characterize the MC4R-Kir7.1 signaling pathway in HEK293 cells stably expressing MC4R and Kir7.1-M125R. The use of the Kir7.1M125R mutation is critical as wild-type Kir7.1 has an extremely low single-channel conductance (~50 fS) which reduces the assay signal. As reported previously, a 20 min exposure of the MC4R agonist α-MSH reduces Kir7.1-mediated thallium flux by up to 20%, indicating decreases in channel opening (Fig. 3a). Investigating the viability of the α-MSH response for a high-throughput screening using a checkerboard plate format (Fig. 1) and the analysis method described in Subheading 3.3, an assay *Z*-Factor of 0.19 was obtained for 100 nM α-MSH (Fig. 3b). Under these given circumstances, this assay of MC4R-Kir7.1 signaling classifies as "medium throughput" assay.

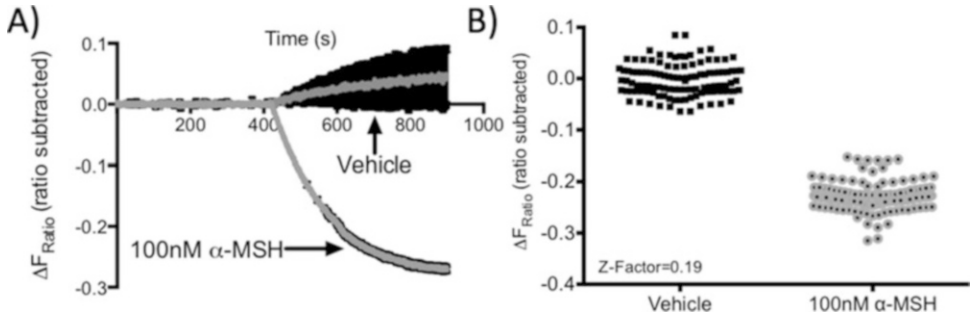

Fig. 3 α-MSH reduces Kir7.1-mediated thallium flux: (**a**) HEK 293 T cells expressing MC4R and Kir7.1 plated in a 384-well plate are exposed to a 20 min incubation of 100 nM α-MSH in a checkerboard pattern. This agonist causes a reduction in ΔF_{Ratio} following the addition of thallium. *Gray* = average of ΔF_{Ratio} measurements, Error bars ± SEM $n = 110$. (**b**) Using the ΔF_{Ratio}, a *Z*-factor of 0.19 was obtained. This indicates a medium throughput assay. $n = 110$

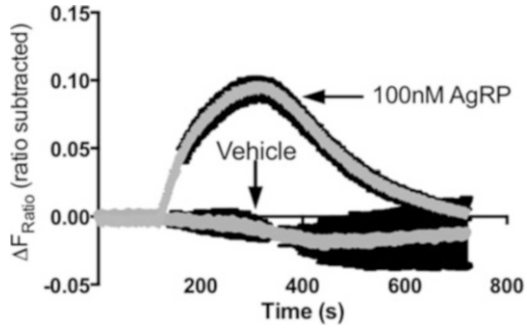

Fig. 4 AgRP increases Kir7.1 mediated thallium flux: 100 nM AgRP increases thallium flux in HEK293 cells expressing MC4R and Kir7.1. *Gray* average of ΔF_{Ratio} measurements, Error bars $\pm$ SEM. $n = 36$

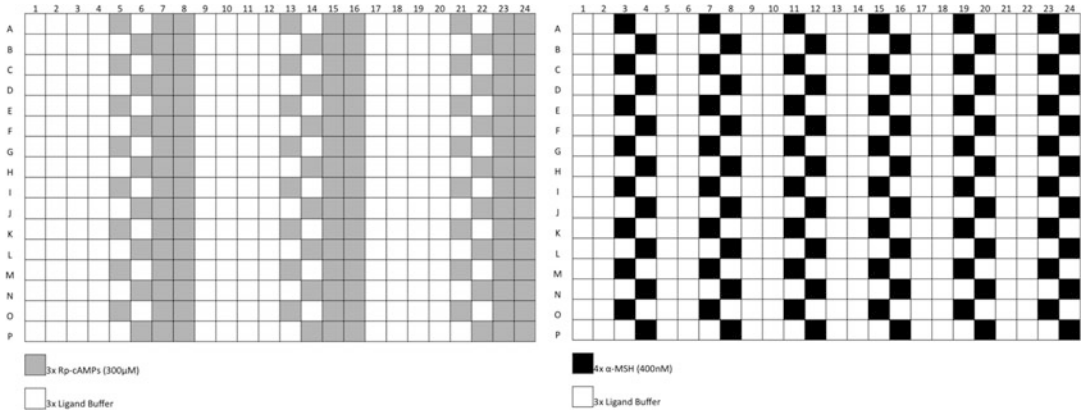

Fig. 5 Plate map strategy for analyzing compounds that modulate MC4R-Kir7.1 signaling: This plate map format allows the study of pharmocological probes in the thallium flux assay. In this example, Rp-cAMPs, a potent competitive inhibitor of the activation of cAMP-dependent protein kinases, is dispensed in a checkerboard format on *columns 5* and *6* but in every well of *columns 7* and *8*. Following a 10 μL addition of this compound to the assay plate, a second 10 μL stimulus of 400 nM (4×) α-MSH is then added. This plate is designed in a checkerboard format on *columns 3* and *4* for a positive control and *columns 7* and *8* to determine the ability of Rp-cAMPs to block the effect of α-MSH

In addition to studying the effects of α-MSH, we have also used the thallium flux assay to characterize the effects of the MC4R inverse agonist AgRP on MC4R-Kir7.1 signaling. Using a checkerboard format as depicted in Fig. 1, 100 nM AgRP was found to increase thallium flux relative to vehicle control indicating increases in channel opening (Fig. 4). Together as previously reported, these results indicate that the thallium assay can be employed to study molecular pathways involved in MC4R-Kir7.1 signaling.

Given the regulation of Kir7.1 by MC4R ligands, we sought to devise an experimental protocol to investigate the molecular signaling pathways that mediate this interaction. Previous electrophysiology experiments have shown that MC4R regulates Kir7.1 through a G-protein-independent manner. Using the strategy outlined in Fig. 5, we first examined a role of cAMP-dependent activation of

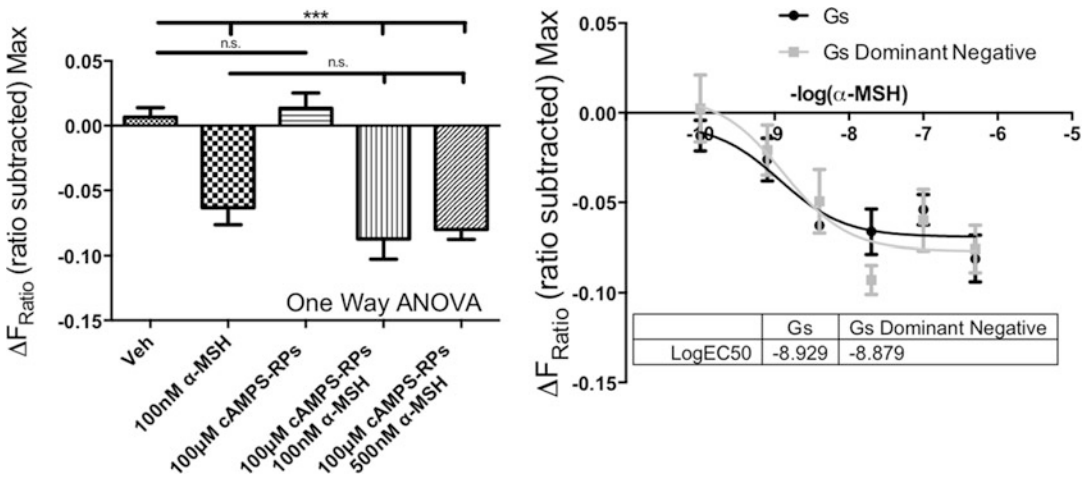

Fig. 6 MC4R-Kir7.1 signaling is not regulated by $G_{s:}$ (**a**) 100 μM Rp-cAMPs does not block the effect of α-MSH on Kir7.1 conductance. $n = 36$ ΔF_{Ratio} measurements/group; Error bars ± SEM; One Way ANOVA $p < 0.001$. (**b**) In this experiment, a dominant negative G_s plasmid or a wild-type G_s plasmid is transfected into HEK293 cells expressing MC4R and Kir7.1. Forty-eight hours later, cells are exposed to a dose response curve of α-MSH. Expression of a dominant negative G_s plasmid in MC4R-Kir7.1 cells does not right shift the α-MSH dose response curve as indicated by the lack of an effect on the EC_{50} of α-MSH. $n = 12$ ΔF_{Ratio} measurements/group; error bars ± SEM; One Way ANOVA $p < 0.001$

Protein Kinase A (PKA) in this signaling pathway. After flicking off the Thallos-AM dye, 10 μL of a 3× Rp-cAMP solution, a potent competitive inhibitor of the activation of cAMP-dependent protein kinases, was added to the cell plate. Following a 2 min incubation, 10 μL of a 4× α-MSH buffer was then added to the assay plate. Using the analysis described in Subheading 3.3, we found that Rp-cAMP was unable to block MC4R-Kir7.1 signaling (Fig. 6a). Examining directly a role of $G_{s\alpha}$ next, we employed a dominant negative G_s construct that has been shown to completely block the canonical $G_{s\alpha}$-AC-cAMP signaling pathway. Co-expression of this construct in HEK293 cells was not able to affect EC_{50} of the α-MSH concentration response curve when compared to transfection with a control $G_{s\alpha}$ plasmid (Fig. 6b). Together, these results support our earlier findings [7] that the MC4R-Kir7.1 signaling is independent of G_s-AC-cAMP signaling pathway. Furthermore, these data suggest that a noncanonical GPCR signaling pathway may be essential for this interaction.

4 Notes

1. Removing the media and assay buffers in a consistent manner is critical for this assay. In the past we have used several expensive plate-washing robots for these purposes. However, the most

consistent and cost-effective manner is the "flick and slam" method:

(a) Using your dominant hand, hold the plate with your palm facing (but not touching) the bottom of the plate.

(b) Next, bend your arm and wrist so that the top of the plate faces your chest.

(c) Finally, rapidly adduct your arm and wrist in a single-fluid movement to expel the buffer contained in the plate into a sink. Wash the media down the drain with 10% bleach.

(d) Finally, invert the plate onto a set of clean laboratory napkins and repeatedly slam the plate down until all of the remaining media is removed.

2. Stable cell lines are critical when performing the thallium assay to characterize GPCR-Kir interactions. Using a tetracycline regulatory system enables the generation of stable cell lines with constructs that may prove toxic when constitutively expressed. Channels that are not toxic when overexpressed may not require this system. However, if you are unfamiliar with the channel you are studying, it is pragmatic to choose this approach.

3. Generation of mono-clones is not necessary when characterizing the presence or absence of a GPCR-Kir interaction. We have successfully employed polyclonal cell lines in this regard. However, when attempting to run this assay in a medium to high-throughput manner, monoclones are essential. Clone selection should be determined empirically using the assay-screening format employed in all future screening.

4. In an attempt to create cell lines more rapidly, our group has used other ways to rapidly generate monoclones. Our more recent studies on MC4R-Kir7.1 signaling were performed on a cell line using the Flp-In/T-REx 293 system (Thermo). This cell line contains a single FRT site that enables FLP recombinase-mediated insertion of the pcDNA5/FRT/TO plasmid. This enables inducible expression of the vector contained in the ORF of the plasmid. Using this plasmid, we designed a bicistronic vector with hMC4R and hKir7.1 (M125R) potassium channel using the cleavable peptide linker p2A. This method required a single round of selection in BH media because recombination and transcription is only possible from the FRT locus.

5. Creating a compound plate is critical because it enables uniform addition to each well. In our experience, a minimum of 12 compound-treated wells and 12 vehicle-treated wells are necessary to observe changes in Tl^+ flux caused by melanocortin agonists. This is largely due to a small signal-to-noise ratio

and intrinsic assay variance. If possible, do not use Row A, B, O, and P as they are subject to an edge effect.

6. It may be necessary to optimize the incubation time for different ligands. This can be accomplished with a time course as depicted in Fig. 5.

Acknowledgments

We thank Dr. Jerod Denton for providing DNA plasmids, compounds, as well as cell lines throughout this project. This work was funded by T32 GM07347, F30DK108476, and RO1DK070332.

References

1. Katz B (1949) Les constantes electriques de la membrane du muscle. Arch Sci Physiol 3:285–299
2. Hibino H, Inanobe A, Furutani K, Murakami S, Findlay I, Kurachi Y (2010) Inwardly rectifying potassium channels: their structure, function, and physiological roles. Physiol Rev 90 (1):291–366
3. Hilgemann DW, Ball R (1996) Regulation of cardiac Na+,Ca2+ exchange and KATP potassium channels by PIP2. Science 273 (5277):956–959
4. Furst O, Mondou B, D'Avanzo N (2014) Phosphoinositide regulation of inward rectifier potassium (Kir) channels. Front Physiol 4:404
5. Pfaffinger PJ, Martin JM, Hunter DD, Nathanson NM, Hille B (1985) GTP-binding proteins couple cardiac muscarinic receptors to a K channel. Nature 317(6037):536–538
6. Tucker SJ, Gribble FM, Proks P, Trapp S, Ryder TJ, Haug T et al (1998) Molecular determinants of KATP channel inhibition by ATP. EMBO J 17 (12):3290–3296
7. Ghamari-Langroudi M, Digby GJ, Sebag JA, Millhauser GL, Palomino R, Matthews R et al (2015) G-Protein-independent coupling of MC4R to Kir7.1 in hypothalamic neurons. Nature 520(7545):94–98
8. Weaver CD, Harden D, Dworetzky SI, Robertson B, Knox RJ (2004) A thallium-sensitive, fluorescence-based assay for detecting and characterizing potassium channel modulators in mammalian cells. J Biomol Screen 9(8):671–677

Chapter 17

Stopped-Flow Fluorometric Ion Flux Assay for Ligand-Gated Ion Channel Studies

David J. Posson, Radda Rusinova, Olaf S. Andersen, and Crina M. Nimigean

Abstract

Quantitative investigations into functional properties of purified ion channel proteins using standard electrophysiological methods are challenging, in particular for the determination of average ion channel behavior following rapid changes in experimental conditions (e.g., ligand concentration). Here, we describe a method for determining the functional activity of liposome-reconstituted K^+ channels using a stopped-flow fluorometric ion flux assay. Channel activity is quantified by measuring the rate of fluorescence decrease of a liposome-encapsulated fluorophore, specifically quenched by thallium ions entering the liposomes via open channels. This method is well suited for studying the lipid bilayer dependence of channel activity, the activation and desensitization kinetics of ligand-dependent K^+ channels, and channel modulation by channel agonists, blockers, or other antagonists.

Key words Ion channel function, Stopped-flow assay, Liposomal ion flux assay, ANTS quenching, Thallium

1 Introduction

Ion channel activity has most commonly been studied in a cellular context using standardized electrophysiological measurements [1, 2]. However, techniques such as patch clamp electrophysiology are technically challenging for purified and lipid-reconstituted ion channel proteins [3, 4]. Such purified systems are not only suitable for structural characterization; they also offer the opportunity to study intrinsic channel properties and lipid-dependent changes in channel function, thereby providing for further studies into fundamental biophysical mechanisms underlying channel function. Electrophysiology, using proteoliposomes fused into artificial lipid bilayers (black lipid membranes), is one solution, but is mostly applicable for systems already characterized in bulk and is difficult to use for non-equilibrium studies, such as detection of the instantaneous channel response to fast ligand application. Here, we

Show-Ling Shyng et al. (eds.), *Potassium Channels: Methods and Protocols*, Methods in Molecular Biology, vol. 1684,
DOI 10.1007/978-1-4939-7362-0_17,

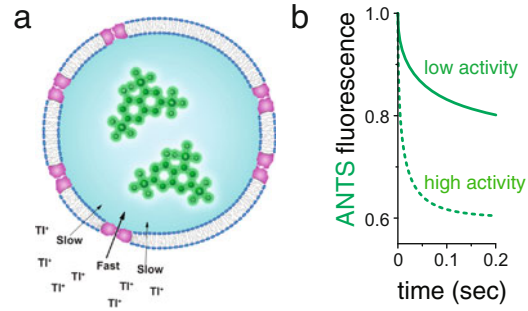

Fig. 1 General principle underlying the detection of K^+ channel activity using Tl^+ flux measurements. (**a**) K^+ channels are reconstituted into liposomes with ANTS fluorophore inside, and rapidly mixed with Tl^+-containing solutions using a stopped-flow mixing device. When channels are open, external Tl^+ ions enter and exchange for K^+ exiting the liposomes. The increasing internal Tl^+ concentration creates a time-dependent quenching of the ANTS fluorescence inside the liposomes. (**b**) Higher K^+ channel activity leads to faster ANTS fluorescence quenching rate than lower K^+ channel activity (*dotted line* compared to *solid line*)

describe a quantitative method to study ligand-gated ion channel activity and kinetics using a spectrofluorometric ion flux assay performed with a stopped-flow instrument. In the protocol below, we describe the channel reconstitution and ion flux assay steps we routinely use to characterize ligand-dependent channel kinetics. Similar procedures can be adapted for the study of channel blockade, the dependence of lipid composition, the influence of temperature, the channel response to agonists and antagonists, etc.

In this flux assay, open K^+ channels reconstituted into large unilamellar vesicles (LUVs) allow the diffusive flux of external thallium ions (Tl^+) into the liposomes, which then quench an encapsulated 8-Aminonaphthalene-1,3,6-Trisulfonic acid (ANTS) fluorophore (Fig. 1a). The flux is rapid because K^+ channels are permeable to Tl^+ ions [2] (*see* **Note 1**). As Tl^+ enters the liposomes, a charge-compensating exchange occurs, resulting in K^+ exiting the liposomes. If the assay conditions favor high channel activity, the Tl^+ influx rate will be high and the fluorescence quenching fast. If conditions favor less channel activity, the Tl^+ flux will be comparably slower, as will the fluorescence quenching rate (Fig. 1b). This assay format was first used for acetylcholine receptors [5, 6] and fragmented sarcoplasmic reticulum membrane preparations [7, 8]. A variant, based on Tl^+ selective fluorescent indicators, later was employed and commercialized for cell-based flux assays [9]. The method also has been adapted for use in gramicidin channel assays [10–12], and more recently was employed using updated methods for biophysical studies on purified, reconstituted K^+ channels

[13–15]. Thus, although we here describe the assay as it was used for K^+ selective channels, the assay will work equally well for any cation-selective ion channel that is permeable to Tl^+.

The first step in studying the function of a purified ion channel is to obtain the channel protein free from a cellular environment. In principle, the protein could derive from an in vitro translation system or extraction and purification from native biological specimens, but in practice this is most often accomplished using cultures of heterologous expression systems. The protocol we describe here typically requires several hundred micrograms of purified protein, a quantity achievable for numerous prokaryotic and eukaryotic ion channels. The protein expression and purification methodologies are not explicitly given here, as many reviews and books are available [16–19].

Once pure ion channel protein is available, it needs to be reconstituted into liposomes for the stopped-flow assay. Numerous methods for membrane protein reconstitution have been described [20]; we used SM-2 Bio-Beads to remove the detergent from mixtures of solubilized, purified protein and synthetic lipids, as this is an efficient way for making protein-reconstituted liposomes (proteoliposomes). The liposomes are next extruded through a 100 nm-pore-size membrane in order to obtain the LUVs. Because the liposomes are formed in the presence of ANTS, the fluorophore initially is both inside and outside the LUVs at equal concentrations. The liposome preparation is finished by passing the sample through a gravity-driven desalting column that exchanges the extra-liposomal solution with ANTS-free buffer, leaving the fluorophore only inside the liposomes. The sample is now ready to be used in channel activity assays [13].

The assay is performed using a sequential mixing stopped flow device, in which the channel is activated in the first mixing reaction and channel activity is assayed in the second reaction. This multistep mixing is crucial for the accurate tracking of kinetic processes, and it allows for varying the time between the application of a particular assay condition such as ligand application (sample mixing #1, syringes L + X, Fig. 2a, b) and testing the channel activity by the application of Tl^+ ions (sample mixing #2, syringe Q, Fig. 2a, b). To accomplish this, we have used the SX20 instrument from Applied Photophysics, due to the high-performance specifications of this instrument, including low mixing dead time (<2 ms) and short minimum delay (~10 ms) between sample mixing #1 and #2. To illustrate the method explicitly, consider an experiment in which a Ca^{2+}-activated K^+ channel (in this case the MthK channel [21–24]) has been reconstituted into proteoliposomes. If the liposomes are mixed first with a Ca^{2+} solution (sample mixing #1, at 17.2 mM Ca^{2+} final concentration), Ca^{2+} will bind to the channels and activate them during incubation in the delay loop (Fig. 2a, b). If this incubation is short (~100 ms), the channels are fully activated

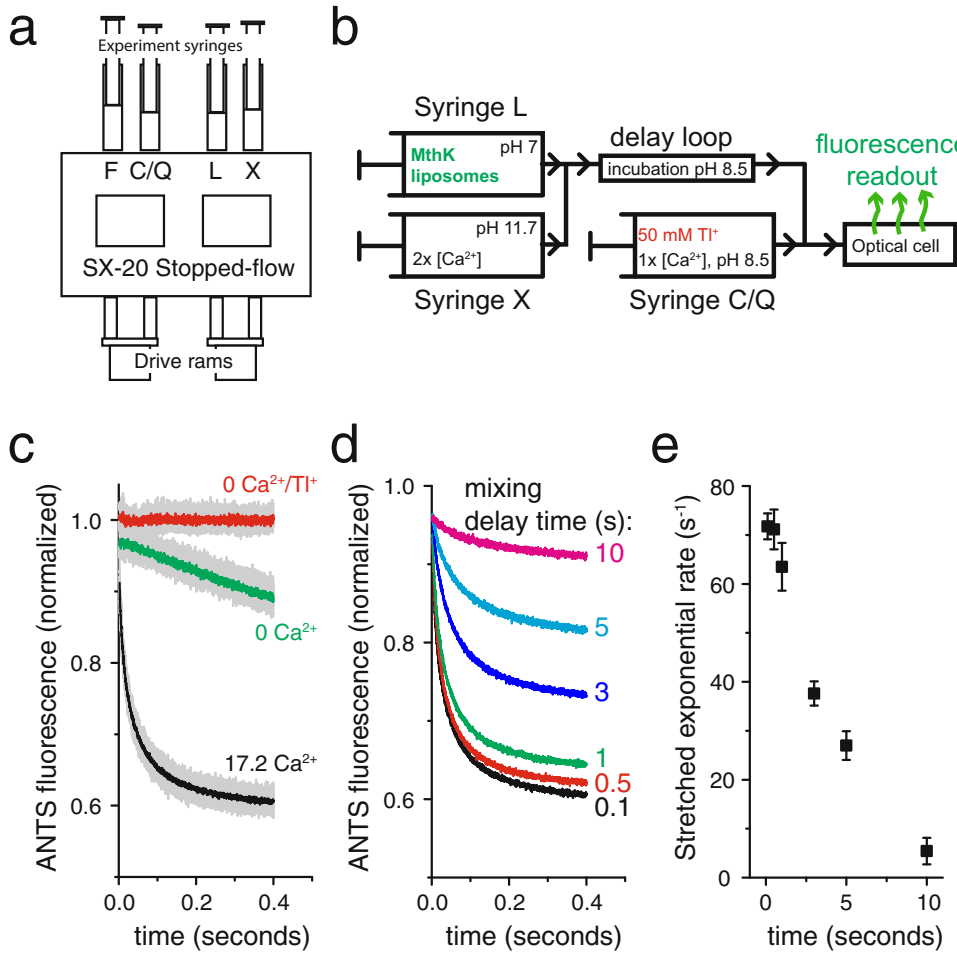

Fig. 2 Kinetic measurements of channel activity are performed using a sequential-mixing stopped-flow spectrofluorometer. (**a**) Cartoon of the sample handling chamber of the SX20 stopped-flow device (Applied Photophysics). Liposomes in syringe L are mixed with experimental test conditions in syringe X. Following a user-defined reaction delay time, the L + X mixture is further mixed with the contents of syringe C/Q; *C* denotes a non-quenching control experiment and *Q* denotes a Tl^+-containing quenching experiment. (**b**) Schematic flow diagram for the sequential mixing steps performed inside the stopped-flow apparatus for an experiment testing the Ca^{2+} activation of the MthK K^+ channel. (**c–e**) Example data obtained with the MthK Ca^{2+}-activated K^+ channel. (**c**) Raw data from repeated mixing reactions (light gray data) with mean signal (dark data overlay) using 100 ms delay between mixing 1 and 2. Red: 0 Ca^{2+} in syringe X and 0 Tl^+ in syringe C, *Green*: 0 Ca^{2+} in syringe X and 50 mM Tl^+ in syringe Q, *Black*: 34.4 mM Ca^{2+} in syringe X and 50 mM Tl^+ in syringe Q. (**d**) Mean ANTS fluorescence quenching time courses from the experiment in **b** with the mixing delay time varied between 0.1 and 10 s, illustrating the loss of MthK activity upon sustained exposure to Ca^{2+}. (**e**) Mean stretched exponential rates from fitting individual mixing repeats from **c–d** to Eq. 1 and calculating the rates using Eq. 2. The error bars are standard deviations from the repeated mixing reactions as in **c**. Experimental replicates on independent samples should also be acquired

when sample mixing #2 occurs, resulting in a relatively fast flux rate (black, Fig. 2c) compared with the slow $TlNO_3$ leak across liposome membranes (green, Fig. 2c). If the experiment is repeated using a longer incubation in the delay loop (up to 10 s), the fluorescence rate displays a gradual decrease over time, indicating that the MthK activity is decreasing; the channels desensitize in the presence of sustained Ca^{2+} (Fig. 2d, e).

To obtain quantitative estimates of flux rates from the raw fluorescence quench time courses (Fig. 2c), we need a measure of the Tl^+ flux into the liposomes immediately following solution mixing, i.e., just after the instrument mixing dead time of ~1.5 ms. This could be done by determining the slope of the fluorescence change at time $t = 2$ ms. However, due to the inevitable noise in the fluorescence signal, such a measurement is not always practical. Instead, a fit to the initial 100 ms of fluorescence data is used to describe the time course of fluorescence quenching. Due to the heterogeneity in liposomal volume and number of channels incorporated in the membrane, the fluorescence time course cannot be described by a single-exponential decay (*see* **Note 2**), and we used a stretched exponential function instead [25] (Eq. 1).

$$F(t) = F_{\text{final}} + (F_{\text{initial}} - F_{\text{final}})e^{(-t/\tau_0)^{\beta}}. \quad (1)$$

$F(t)$ is the normalized fluorescence as a function of time t, F_{initial} the initial fluorescence, F_{final} the final steady-state fluorescence, τ_o a parameter with units of time, and β a parameter that depends on the dispersity of the proteoliposome preparation and describes the deviation from a single-exponential decay. The fluorescence decay rate, and thus Tl^+ influx rate following sample mixing (Eq. 2), is evaluated at 2 ms (*see* **Note 3**):

$$k(2\,\text{ms}) = (\beta/\tau_0)(2\,\text{ms}/\tau_0)^{(\beta-1)}. \quad (2)$$

The stretched exponential function was extensively tested and validated for this purpose during the development of the stopped-flow method for gramicidin activity assays [10] and has worked equally well in the analysis of Tl^+ flux through K^+ channels [13–15]. Given the large number of experiments typically performed, including repeated mixing reactions for a specific sample and experimental condition, multiple experimental conditions of interest, and ultimately, multiple sample preparations to confirm experimental reproducibility, it is convenient to develop a semi-automated analysis procedure using a software package such as Matlab® (Mathworks). However, analysis can similarly be implemented using any robust numerical data fitting routine.

2 Materials

Care should be taken when handling and disposing thallium reagents as they are toxic.

2.1 Preparations for K^+ Channel Reconstitution

1. 1,2-Dioleoyl-sn-glycero-3-phosphocholine (DOPC), in chloroform (Avanti Polar Lipids).
2. 1-palmitoyl-2-oleoyl-sn-glycero-3-phospho-(1′-rac-glycerol) (POPG), in chloroform (Avanti).
3. N_2 gas tank, installed next to a fume hood.
4. 50 mL round-bottom flasks.
5. SM-2 BioBeads (Bio-Rad).
6. Reconstitution buffer (Buffer R) (*see* **Note 4**): 100 mM KNO_3, 10 mM HEPES pH 7.0.

2.2 K^+ Channel Reconstitution

1. Assay buffer (Buffer A): 140 mM KNO_3, 10 mM HEPES pH 7.0.
2. CHAPS detergent.
3. ANTS (8-Aminonaphthalene-1,3,6-Trisulfonic acid, disodium salt, ThermoFisher), prepare a pH-adjusted 75 mM stock solution in reconstitution buffer (Buffer R).
4. 15 mL glass test tubes.
5. Mini-extruder with 100 nm polycarbonate membranes (Avanti).
6. PD-10 columns (GE Healthcare).

2.3 Tl^+ Flux Assay

1. SX20 stopped-flow fluorescence spectrometer (Applied Photophysics) or similar with sequential push capability.
2. Reaction buffer (Buffer X): Buffer A + 2X-concentrated ligands/blockers. For example, if the channel requires 100 μM Ca^{2+} to fully activate, use Buffer A + 200 μM Ca^{2+} to mix 1:1 with liposomes and fully activate the channel (*see* **Note 5**).
3. Control buffer (Buffer C): Buffer A + 1X-concentrated ligands/blockers. For example, if the channel requires 100 μM Ca^{2+} to fully activate, use Buffer A + 100 μM Ca^{2+} to mix 1:1 with the previous solution mixture of liposomes with Buffer X (*see* **Note 5**).
4. Quenching buffer (Buffer Q): 94 mM KNO_3, 50 mM $TlNO_3$, 10 mM HEPES pH 7.0 + 1X-concentrated ligands/blockers. For example, if the channel requires 100 μM Ca^{2+} to fully activate, use 100 μM Ca^{2+}, as in Buffer C (*see* **Note 5**).

3 Methods

All the steps are performed at room temperature. Glassware should be thoroughly cleaned, rinsed, and dried. Make two independent samples with the procedure below. The first sample contains the protein to be studied and the second sample is a protein-free control.

3.1 Preparations for K^+ Channel Reconstitution into Liposomes

1. The day before ion channel reconstitution, mix 11.25 mg of DOPC and 3.75 mg of POPG (15 mg total of 3:1 ratio of DOPC and POPG from chloroform stock solutions) in a 50 mL round-bottom flask for a single batch of liposomes, either made with or without protein (*see* **Note 6**).
2. Evaporate chloroform using a stream of N_2 gas inside a fume hood, rotating the flask by hand so that a thin, opaque film of lipid covers the bottom and sides of the flask.
3. Store the lipid film-containing flask in a vacuum desiccator overnight to eliminate trace chloroform.
4. Degas 5 g of SM-2 BioBeads by combining with 5 mL of reconstitution buffer (Buffer R) in a small vacuum flask and apply vacuum for 2 h (*see* **Note 7**).
5. Sonicate the 50% BioBeads slurry for a couple of minutes in a bath sonicator to ensure the removal of trapped air. Most of the BioBeads should not float (*see* **Note 7**).
6. Remove the 5 mL of Buffer R from the BioBeads slurry carefully by pipetting and replace with a fresh 5 mL of Buffer R. Perform additional washes if the slurry buffer does not appear clear. Store the BioBeads at 4 °C for up to a few weeks.
7. Perform the expression and purification steps required to obtain a high-quality ion channel protein sample for the following day's liposome reconstitution.

3.2 K^+ Channel Reconstitution into Liposomes

1. Finalize preparation of K^+ channel sample. This could be an overnight-dialysis or gel purification step using reconstitution buffer (buffer R) or another compatible buffer (*see* **Note 8**).
2. Rehydrate lipid film in a round-bottom flask by the addition of 1 mL Buffer R and 0.5 mL ANTS fluorophore stock solution.
3. Using a bath sonicator (*see* **Note 9**), sonicate the lipids into solution by the incremental addition of CHAPS detergent to a final concentration of 35 mM (32 mg CHAPS).
4. Transfer lipid-detergent mixture to a glass test tube (~15 mL) with screw cap.

5. Add purified K^+ channel to the lipid solution at a ratio of 20–30 μg protein per mg of lipid (*see* **Note 10**), mix and incubate for 30 min.
6. Add an additional 0.5 mL ANTS fluorophore stock solution and 2 mL 50% Bio-Beads slurry. The liposome batch is formed in ~3 mL final volume of Buffer R (*see* **Note 11**).
7. Incubate for 2 h on a tube rocker. The solution will become turbid as detergent adsorbs to the Bio-Beads and liposomes are formed.
8. Sonicate the newly formed liposomes for 20 s in a bath sonicator.
9. Remove the Bio-Beads from the sample and convert the liposomes into large unilamellar vesicles (LUVs) by passing the sample through a 100 nm-pore-size polycarbonate membrane 42 times using an Avanti mini-extruder.

3.3 Transfer ANTS-Filled Liposomes to ANTS-Free Buffer

1. Equilibrate two PD-10 desalting columns, each with 25 mL assay buffer (Buffer A) for a single 3 mL batch of liposomes. Allow the buffer to completely enter the column.
2. Add 2 mL of buffer A to the 3 mL liposomes sample and mix, bringing the sample volume up to 5 mL total.
3. Load 2.5 mL of sample onto each equilibrated PD-10 column. Allow the sample to completely enter the column.
4. Elute the liposomes by pipetting 3 mL buffer A onto each PD-10 column and combine the 3 mL eluates in a standard plastic conical tube. The liposomes solution should now be a turbid, colorless solution and the yellow ANTS should be visibly trapped inside the PD-10 columns. The 6 mL liposomal eluate has ANTS fluorophore inside but not outside the liposomes.
5. The concentrated, buffer-exchanged liposomes can be stored at 12 °C for several days without loss of intra-vesicular ANTS (*see* **Note 12**).

3.4 Stopped-Flow Tl^+ Flux Assay

1. Dilute the liposomes from a single preparation to 30 mL in assay buffer—buffer A (*see* **Note 6**).
2. Prepare the SX20 (or similar) stopped flow spectrofluorometer by turning on the system, any temperature control systems, light sources, and setting the excitation wavelength for the ANTS fluorophore (~350 nm) (*see* **Note 13**). Ensure that you are using a detection system/emission filter that can record ANTS fluorescence (~520 nm peak). Wash the fluid handling system thoroughly with water. Set the software to record 1 s of data using 5000 recorded points and set the delay time between sequential sample mixing events to a desired value (Fig. 2a). Liposomes in syringe L are first mixed in a 1:1

volume ratio with the reaction buffer (Buffer X) in syringe X and incubated in the delay loop for the specified delay time. At the end of the delay, the L + X mixture is further mixed with the Control/Quench buffer contained in syringe C/Q, again using a 1:1 volume ratio by concurrent loading of the optical cell with the contents of the delay loop (by the flushing action of syringe F) and those of syringe C/Q. Upon mixing L + X with C/Q the fluorescence time course data is recorded.

3. Begin by loading the fluorescent liposomes into syringe L and Assay buffer (Buffer A) into syringes X, C, and F. Ensure that the solutions are equilibrated to the experimental temperature (including room temperature). Wash in the experimental solutions to clear the system of water and filling the detection cell with the final experimental dilution of ANTS-containing liposomes (for the SX20 this requires about four repeated injections). Set the detector gain so that this maximum unquenched fluorescence signal is of appropriate magnitude for data acquisition instrument.
4. Wash the fluid-handling system with water until the fluorescence reading has returned to the water-only baseline value to prepare for the actual experiment. For the SX20, this takes ten to twelve drives/injections from all four syringes to fully wash the system with water.
5. The experiment consists of 8 repeated control dual-mixing reactions (Tl^+-free, Buffer C) and 11 repeated quench measurements (Tl^+ measurements, Buffer Q). Load sufficient proteoliposomes into drive syringe L for 19 measurements; sufficient Reaction buffer (Buffer X) in drive syringe X for 19 measurements; sufficient Flush buffer (Assay Buffer A) in drive syringe F for 19 measurements; sufficient Control buffer (Buffer C) for 8 control fluorescence measurements and, once the control traces have been acquired, sufficient Quench buffer (Buffer Q) for 11 fluorescence quench measurements into drive syringe Q.
6. Acquire the control fluorescence signals using the SX20 control software to collect eight repeated mixing reactions with the desired delay time. For the SX20 spectrofluorometer, the first four to five mixing reactions are necessary to completely wash out the water (or other solutions) in the lines and measuring cell, and should not be used for analysis. The remaining traces are used for the analysis and determination of the control fluorescence.
7. Switch the content of drive syringe C/Q to Buffer Q, and acquire the fluorescence quench measurements by using the software to collect 11 repeated mixing reactions. Again, discard the first four to five mixing reactions, which are necessary to

wash out the control solutions. Following these, assuming that the K^+ channels are active, you should see a time-dependent quenching of the ANTS fluorescence as Tl^+ flows into the proteoliposomes through the active channels (exchanging with K^+ inside the liposomes), as in Fig. 1a.

8. Repeat **steps 4–7** for all experimental conditions of interest. For example, perform titrations of activating ligands and/or channel blockers in Buffers C/Q and X. Alternatively, use a specific set of conditions and vary the delay time between consecutive series of mixing reactions to determine how the channel activity changes as a function of incubation time (*see* Fig. 2) with the Reaction buffer (Buffer X).
9. Examine the data and discard any traces with obvious mixing artifacts. Normalize the fluorescence quench data to the control fluorescence, and fit a stretched exponential function (Eq. 1) to the first 100 ms of the fluorescence quench trace for each experimental repeat. Use these fitted values of τ_0 and β to calculate the relative fluorescence quench (Tl^+ influx) rates at 2 ms (Eq. 2), and use the flux rates from all experimental conditions to analyze ligand dose-response curves and/or ligand kinetics.

4 Notes

1. Tl^+ can also be used for non-selective cation channels. The same fundamental assay principle can also be applied to anion channels, typically using a fluorophore such as N-(ethoxycarbonylmethyl)-6-methoxyquinolinium (MQAE), which can be quenched by chloride ions [26].
2. More precisely, if the liposomes were of uniform size, with the same number of channels per liposome, and the channels were in a perfect steady-state condition (conditions that never occur in practice), the internal $[Tl^+]$ concentration would increase according to a single exponential and the fluorescence would follow a simple Stern-Volmer fluorescence ratio according to that $[Tl^+]_{int}$ time course [10].
3. The rate of the stretched exponential function cannot be extrapolated back to 0 ms, as the rate (according to Eq. 1) goes to infinity as time goes to zero. This non-physical property of the stretched exponential can be side-stepped by using a "modified stretched exponential" function that derives from a simple transformation along the time axis [25]. Generally, this approach has not been necessary in the analysis of these experiments, but has been used to compare "modified" stretched exponential rates at 0 ms in specific cases [15, 27].

4. All the assay solutions employ NO_3^- anion because the chloride salt of thallium has limited water solubility.
5. We prepare our liposomes using pH 7.0 buffer. If, however, a flux experiment is done at another pH, it is necessary for the reaction buffer (Buffer X) to be a "pH-changing" solution and the pH of Buffer X must be set so that a 1:1 volume-ratio mixture with pH 7.0 generates the desired experimental pH. Upon the second mixing with either the control buffer (Buffer C) or the quenching buffer (Buffer Q), the pH should be maintained at the desired pH and thus Buffer C and Buffer Q are "pH-maintaining" buffers and are pH-adjusted to the experimental pH value. This procedure can be scaled up or scaled down as needed. Care should be taken to maintain the specified ratio of components and volumes used with PD-10 desalting columns. The final concentration of liposomes is diluted tenfold from the initial liposome formation step. As written, 15 mg of lipid produce a 3 mL liposome suspension, which is diluted to 30 mL for the assays.
6. This procedure can be scaled up or scaled down as needed. Care should be taken to maintain the specified ratio of components and volumes used with PD-10 desalting columns. The final concentration of liposomes is diluted tenfold from the initial liposome formation step. As written, 15 mg of lipid produce a 3 mL liposome suspension, which is diluted to 30 mL for the assays.
7. Initially washing the Bio-Beads with methanol followed by multiple washes with water before buffer can also be used.
8. We have always used gel filtration as the last step, performed immediately before the reconstitution procedure. If the purified protein can be concentrated to a fairly high concentration, and the buffer thus significantly diluted during reconstitution, a buffer containing chloride salts or other components may be used. If there is difficulty obtaining high-concentration protein, an effort should be made to ensure that the buffer is compatible with the experiment (ideally, identical to the assay buffer) and volumes and concentrations of the lipid components can be adjusted accordingly.
9. Do not allow the lipid-detergent solution get too hot. Both time and sonication will produce a clear solution, but this may take up to 60 min.
10. The protein amount to be added is dependent on the identity of the protein and sample quality. Do not forget to make an identical protein-free control sample.
11. Dry BioBeads may also be added at the ratio of 1 g BioBeads to 35 mg CHAPS. In this case addition of 0.5 mL ANTS to correct for the extra volume when adding BioBeads in 0.5% suspension is not necessary.

12. The liposomes are cooled (12 °C), but remain above the liquid-gel phase transition temperature to keep the ANTS from leaking out. The 12 °C incubator is most conveniently placed close to the stopped-flow device so that liposome samples can be taken out and warmed to room temperature immediately prior to use in the assay.
13. A 360 nm LED light source (Applied Photophysics) may also be used, which provides higher signal intensity and greater stability.

Acknowledgment

This work was supported by NIH grants R01 GM088352 (to C.M.N.) and R01 GM021342 (to O.S.A.), NIH fellowship F32GM087865 (to D.J.P.), and a Kellen Fellowship (R.R.).

References

1. Aidley DJ (1998) The physiology of excitable cells, 4th edn. Cambridge University Press, Cambridge
2. Hille B (2001) Ion channels of excitable membranes, 3rd edn. Sinauer, Sunderland, MA
3. Martinac B, Saimi Y, Kung C (2008) Ion channels in microbes. Physiol Rev 88(4):1449–1490. doi:10.1152/physrev.00005.2008
4. Cordero-Morales JF, Cuello LG, Zhao Y, Jogini V, Cortes DM, Roux B, Perozo E (2006) Molecular determinants of gating at the potassium-channel selectivity filter. Nat Struct Mol Biol 13(4):311–318. doi:10.1038/nsmb1069
5. Moore HP, Raftery MA (1980) Direct spectroscopic studies of cation translocation by Torpedo acetylcholine receptor on a time scale of physiological relevance. Proc Natl Acad Sci U S A 77(8):4509–4513
6. Wu WC, Moore HP, Raftery MA (1981) Quantitation of cation transport by reconstituted membrane vesicles containing purified acetylcholine receptor. Proc Natl Acad Sci U S A 78(2):775–779
7. Garcia AM, Miller C (1984) Channel-mediated monovalent cation fluxes in isolated sarcoplasmic reticulum vesicles. J Gen Physiol 83(6):819–839
8. Garcia AM (1992) Determination of ion permeability by fluorescence quenching. Methods Enzymol 207:501–510
9. Weaver CD, Harden D, Dworetzky SI, Robertson B, Knox RJ (2004) A thallium-sensitive, fluorescence-based assay for detecting and characterizing potassium channel modulators in mammalian cells. J Biomol Screen 9(8):671–677. doi:10.1177/1087057104268749
10. Ingolfsson HI, Andersen OS (2010) Screening for small molecules' bilayer-modifying potential using a gramicidin-based fluorescence assay. Assay Drug Dev Technol 8(4):427–436. doi:10.1089/adt.2009.0250
11. Ingolfsson HI, Andersen OS (2011) Alcohol's effects on lipid bilayer properties. Biophys J 101(4):847–855. doi:10.1016/j.bpj.2011.07.013
12. Ingolfsson HI, Sanford RL, Kapoor R, Andersen OS (2010) Gramicidin-based fluorescence assay; for determining small molecules potential for modifying lipid bilayer properties. J Vis Exp 44. doi:10.3791/2131
13. Rusinova R, Kim DM, Nimigean CM, Andersen OS (2014) Regulation of ion channel function by the host lipid bilayer examined by a stopped-flow spectrofluorometric assay. Biophys J 106(5):1070–1078. doi:10.1016/j.bpj.2014.01.027
14. McCoy JG, Rusinova R, Kim DM, Kowal J, Banerjee S, Jaramillo Cartagena A, Thompson AN, Kolmakova-Partensky L, Stahlberg H, Andersen OS, Nimigean CM (2014) A KcsA/MloK1 chimeric ion channel has lipid-dependent ligand-binding energetics. J Biol Chem 289(14):9535–9546. doi:10.1074/jbc.M113.543389
15. Posson DJ, Rusinova R, Andersen OS, Nimigean CM (2015) Calcium ions open a

selectivity filter gate during activation of the MthK potassium channel. Nat Commun 6:8342. doi:10.1038/ncomms9342

16. Chen H, Shaffer PL, Huang X, Rose PE (2013) Rapid screening of membrane protein expression in transiently transfected insect cells. Protein Expr Purif 88(1):134–142. doi:10.1016/j.pep.2012.12.003
17. Schlegel S, Lofblom J, Lee C, Hjelm A, Klepsch M, Strous M, Drew D, Slotboom DJ, de Gier JW (2012) Optimizing membrane protein overexpression in the Escherichia coli strain Lemo21(DE3). J Mol Biol 423 (4):648–659. doi:10.1016/j.jmb.2012.07.019
18. Hays FA, Roe-Zurz Z, Stroud RM (2010) Overexpression and purification of integral membrane proteins in yeast. Methods Enzymol 470:695–707. doi:10.1016/S0076-6879(10)70029-X
19. Drew D, Newstead S, Sonoda Y, Kim H, von Heijne G, Iwata S (2008) GFP-based optimization scheme for the overexpression and purification of eukaryotic membrane proteins in Saccharomyces cerevisiae. Nat Protoc 3 (5):784–798. doi:10.1038/nprot.2008.44
20. Rigaud JL, Levy D (2003) Reconstitution of membrane proteins into liposomes. Methods Enzymol 372:65–86. doi:10.1016/S0076-6879(03)72004-7
21. Jiang Y, Lee A, Chen J, Cadene M, Chait BT, MacKinnon R (2002) Crystal structure and mechanism of a calcium-gated potassium channel. Nature 417(6888):515–522. doi:10.1038/417515a
22. Zadek B, Nimigean CM (2006) Calcium-dependent gating of MthK, a prokaryotic potassium channel. J Gen Physiol 127 (6):673–685. doi:10.1085/jgp.200609534
23. Li Y, Berke I, Chen L, Jiang Y (2007) Gating and inward rectifying properties of the MthK K+ channel with and without the gating ring. J Gen Physiol 129(2):109–120. doi:10.1085/jgp.200609655
24. Pau VP, Abarca-Heidemann K, Rothberg BS (2010) Allosteric mechanism of Ca2+ activation and H+-inhibited gating of the MthK K+ channel. J Gen Physiol 135(5):509–526. doi:10.1085/jgp.200910387
25. Berberan-Santos MN, Bodunov EN, Valeur B (2005) Mathematical functions for the analysis of luminescence decays with underlying distributions 1. Kohlrausch decay function (stretched exponential). Chem Phys 315(1-2):171–182. doi:10.1016/J.Chemphys.2005.04.006
26. Verkman AS (1990) Development and biological applications of chloride-sensitive fluorescent indicators. Am J Phys 259(3 Pt 1): C375–C388
27. Alejo JL, Blanchard SC, Andersen OS (2013) Small-molecule photostabilizing agents are modifiers of lipid bilayer properties. Biophys J 104(11):2410–2418. doi:10.1016/j.bpj.2013.04.039

Chapter 18

In Vivo Analysis of Potassium Channelopathies: Loose Patch Recording of Purkinje Cell Firing in Living, Awake Zebrafish

Jui-Yi Hsieh and Diane M. Papazian

Abstract

Zebrafish is a lower vertebrate model organism that facilitates integrative analysis of the in vivo effects of potassium and other ion channel mutations at the molecular, cellular, developmental, circuit, systems, and behavioral levels of analysis. Here, we describe a method for extracellular, loose patch electrophysiological recording of electrical activity in cerebellar Purkinje cells in living, awake zebrafish, with the goal of investigating pathological mechanisms underlying channelopathies or other diseases that disrupt cerebellar function. Purkinje cell excitability and a functional cerebellar circuit develop rapidly in zebrafish and show strong conservation with the mammalian cerebellum.

Key words Purkinje cell, Cerebellum, Zebrafish, Patch clamp, Loose patch, Tonic firing, Complex spike, Spinocerebellar ataxia

1 Introduction

We have been using zebrafish to investigate the in vivo effects of mutations in the voltage-gated Kv3.3 potassium channel that cause the autosomal-dominant neurodegenerative disease, spinocerebellar ataxia type 13 (SCA13) [1, 2]. In humans, depending on the mutation, SCA13 is either an infant-onset disease characterized by early cerebellar atrophy, motor delay, persistent motor deficits, and intellectual disability, or an adult-onset disease characterized by progressive ataxia and progressive cerebellar degeneration beginning in the third decade of life or later [3–6]. Because infant- and adult-onset mutations have distinct effects on Kv3.3 function [3, 6–8], we hypothesize that the mutations alter neuronal excitability in differential ways and that these changes in activity underlie the distinct symptoms of the two forms of the disease. In initial studies, we focused on characterizing the effects of infant- and adult-onset mutations on spinal cord motor neurons, which express Kv3.3 in both mammals and zebrafish [1, 9]. However, the most extensive pathology in individuals with SCA13 is found in the cerebellum [3,

Show-Ling Shyng et al. (eds.), *Potassium Channels: Methods and Protocols*, Methods in Molecular Biology, vol. 1684,
DOI 10.1007/978-1-4939-7362-0_18,

10]. To investigate the effects of SCA13 mutations on the excitability of cerebellar neurons, we have developed a method for loose patch, extracellular recording of electrical activity in cerebellar Purkinje cells in awake, live zebrafish [11]. This method is broadly applicable to investigate pathological mechanisms that contribute to other diseases that disrupt cerebellar function.

Characterization of zebrafish Purkinje cells reveals that excitability and synaptic input from parallel fibers and climbing fibers emerge rapidly after Purkinje cells are born on the third day post-fertilization [11]. By 4 days post-fertilization (dpf), zebrafish Purkinje cells are spontaneously active, firing simple spikes in an irregular pattern. At 4 dpf, Purkinje cells are receiving visual input via mossy fibers. By 5 dpf, the frequency and regularity of tonic firing have increased significantly. Complex spiking, indicative of synaptic innervation by climbing fibers, emerges. The winnowing of multiple climbing fiber inputs occurs over the next 1–2 days, so that by 6–7 dpf, Purkinje cells have established a stable pattern of tonic firing and complex spiking. The development of spontaneous firing in zebrafish Purkinje cells is closely correlated with the expression of Nav1.6 and Kv3.3 [11], channels that control pacemaking activity in mammalian Purkinje cells [12–15]. Zebrafish develop entirely outside the body of the mother, so the rapid development of a functional cerebellar circuit likely underlies the early emergence of complex, visually guided behaviors such as prey capture (feeding) that are necessary for survival [16].

This chapter focuses on the technique of making loose patch seals on Purkinje cells in living zebrafish [11]. We assume that the reader is already familiar with patch clamp techniques. If not, the basics of patch clamp electrophysiology have been described previously [17, 18].

2 Materials

Prepare solutions using reagent or analytical grade chemicals and house-distilled water that has been deionized (ddH_2O) using a Milli-Q Advantage A10 water purification system (Millipore) or equivalent. Drugs should be medical or veterinarian grade whenever possible. Store reagents at room temperature unless noted. According to NIH policy, zebrafish become subject to regulations governing the use of vertebrate animals in research upon hatching [19]. Therefore, experiments using zebrafish older than ~3 days post-fertilization (dpf) must be approved by the Institutional Animal Care and Use Committee (IACUC). Hazardous compounds and sharps should be handled and disposed of safely according to institutional regulations.

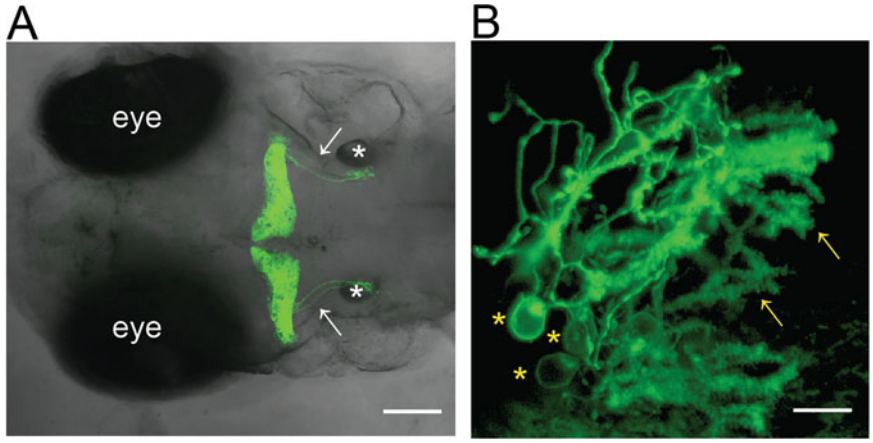

Fig. 1 (**a**) Expression of membrane-bound Venus in a la118Tg:*Tg(aldoca:gap43-Venus)* transgenic zebrafish at 5 dpf [11]. A projected confocal image stack is shown superimposed on a bright field image of the head of the fish, dorsal view. The eyes are labeled. *Arrows* indicate cerebellovestibular axon tracts. *Asterisks* indicate otic vesicles. Scale bar, 100 μm. (**b**) Projection of confocal image stack shows mosaic expression of membrane-bound-EGFP in an F0 (transient) transgenic zebrafish at 8 dpf. *Yellow asterisks* indicate Purkinje cell bodies. *Yellow arrows* indicate dendrites thickly studded with spines. Scale bar, 10 μm. Image courtesy of Ms. Brittany Ulrich

2.1 Zebrafish Transgenic Lines and Husbandry

1. Breeding colony of transgenic zebrafish line that expresses a fluorescent indicator protein specifically in cerebellar Purkinje cells: rk22Tg:*Tg(aldoca:gap-43-Venus)* [20] or la118Tg:*Tg (aldoca:gap43-Venus)* [11] (Fig. 1a). *See* **Notes 1–4**.
2. Aquarium system. Construction of a laboratory aquarium facility for zebrafish has been previously described in detail [21]. *See* **Note 5**.
3. Methylene Blue solution 0.5% (w/v) in H_2O (Sigma-Aldrich cat. no. 50484). Wear lab coat, gloves, and eye protection when working with 0.5% methylene blue solution.
4. 20× E2 mix [21]: Dissolve 17.5 g NaCl, 0.75 g KCl, 2.4 g $MgSO_4$, 0.41 g KH_2PO_4, and 0.12 g Na_2HPO_4 in ddH_2O and bring total volume to 1 L. Autoclave. Refrigerate.
5. 500× $CaCl_2$ [21]: Dissolve 7.5 g $CaCl_2$ in ddH_2O and bring total volume to 100 mL. Autoclave. Refrigerate.
6. 500× $NaHCO_3$ [21]: Dissolve 3 g $NaHCO_3$ in ddH_2O and bring total volume to 100 mL. Autoclave. Refrigerate.
7. 1× E2 embryo medium containing 0.01% Methylene Blue as fungicide (hereafter referred to as E2 medium): Combine 20 mL 20× E2 mix, 2 mL 500× $CaCl_2$, 2 mL 500× $NaHCO_3$, and 60 μL 0.5% Methylene Blue solution and bring total volume to 1 L using ddH_2O. Filter sterilize. Refrigerate. Pre-warm the solution to 28.5 °C before using it with zebrafish. Make fresh weekly.

8. Breeding chambers consisting of outer tank, inner tank with perforated bottom, removable divider, and lid. Aquaneering Inc., cat. no. ZHCT100.
9. Sterile 100 mm × 14 mm polystyrene Petri dishes, Fisher Scientific, cat. no. 0875713.
10. Disposable plastic transfer pipettes, Sigma-Aldrich, cat. no. Z135003.
11. Air incubator set to 28.5 °C, equipped with wide-spectrum LED illumination on a timer to provide a 14/10 h light/dark cycle matched to that of the fish room.
12. Small mesh strainers, stainless steel. Available from kitchen supply stores. The only requirement is that the mesh be fine enough to capture zebrafish embryos immediately after fertilization.
13. GP 100–200 μm larval diet, www.brineshrimpdirect.com, store refrigerated.

2.2 Anesthesia, Paralysis, and Dissection

1. Two pairs Dumont #5SF super fine forceps, Fine Science Tools.
2. Circular, uncoated coverslips, 22 mm, Fisher Scientific, cat. no. S175224.
3. Vaseline®.
4. Krazy Glue®.
5. Polypropylene micro-tubes, 0.5 mL with attached cap, Sarstedt, cat. no. 72.730.100.
6. FDA-approved tricaine methylsulfonate (MS-222), Western Chemical, Tricaine-S. Store at room temperature.
7. MS-222 10× stock solution (0.2%): Dissolve 0.2 g in ddH_2O and bring total volume to 100 mL. Filter sterilize. Store at 4 °C. Prepare fresh weekly. MS-222, which is used to anesthetize fish, may irritate the skin, eyes, and respiratory system. Wear lab coat, gloves, eye protection, and dust mask when weighing the solid. Wash hands thoroughly after handling. In case of exposure to skin or eyes, flush thoroughly with water. In case of inhalation, move to well-ventilated location and seek medical attention.
8. MS-222 1× solution: Just prior to the experiment, mix 1 mL 10× MS-222 stock solution with 9 mL ddH_2O. Transfer the anesthetic solution to a Petri dish.
9. (+)-Tubocurarine hydrochloride pentahydrate (curare), Sigma-Aldrich, cat. no. T2379. Store at −20 °C in a locked, non-frost-free freezer labeled with appropriate hazard signs. Curare is a potent paralytic toxin that inhibits nicotinic acetylcholine receptors at the neuromuscular junction. Wear lab coat,

gloves, eye protection, and dust mask when weighing the solid. Wash hands thoroughly after handling. In case of exposure to skin or eyes, flush thoroughly with water. Seek medical attention. Dispose of curare and contaminated materials as hazardous waste according to institutional regulations.

10. Curare 1000× (10 mM) stock. Dissolve 38.6 mg (+)-tubocurarine hydrochloride pentahydrate in 5 mL ddH_2O. Dispense 100 μL aliquots into 0.5 mL micro-tubes and store at −20 °C in a locked, non-frost-free freezer labeled with appropriate hazard signs.
11. Zeiss Stemi 2000-C stereo microscope on track stand with transmitted light base and adjustable mirror.

2.3 Electrophysiology

1. Disposable 1 L vacuum filter/storage bottle units, 0.22 μm membrane, Corning® Life Sciences, cat. no. 430517.
2. Nalgene® 4 mm syringe filters, 0.2 μm filter, Thermo-Fisher, cat. no. 176-0020.
3. 10× external solution. Dissolve 78.31 g NaCl, 2.16 g KCl, 3.09 g $CaCl_2 \cdot 2H_2O$, 2.44 g $MgCl_2 \cdot 6H_2O$, 23.83 g HEPES, and 18.02 g glucose in ddH_2O. Bring total volume to 1 L with ddH_2O and filter using 1 L 0.22 μm filtration unit attached to the house vacuum. Store at 4 °C.
4. 1× external solution (adapted from ref. 22): 134 mM NaCl, 2.9 mM KCl, 2.1 mM $CaCl_2$, 1.2 mM $MgCl_2$, 10 mM HEPES, 10 mM glucose, pH 7.5. Mix 100 mL 10× external solution with 800 mL ddH_2O. Adjust pH to 7.5. Bring total volume to 1 L with ddH_2O and filter using 1 L 0.22 μm filtration unit attached to the house vacuum. Store at 4 °C. Replace 1× external solution every 2 weeks at a minimum.
5. Borosilicate electrode glass, World Precision, cat. no. 1B150F-4.
6. Flaming Brown micropipette puller, Sutter Instruments, cat. no. P-97.
7. MicroFil® pipette filler, 28 G, 97 mm in length, World Precision Instruments, cat. no. MF28G-5.
8. HSW® Norm-Ject® sterile, disposable syringes, 1 mL, VWR, cat. no. 53548–001.
9. Upright Olympus BX51W1 fluorescence microscope equipped with LUMPlanFL N 40×/0.80 and UMPlanFL N 10×/0.3 water immersion objectives and a monochrome digital camera.
10. Patch clamp rig suitable for slice electrophysiology. Our rig consists of a HEKA Electronik EPC10 patch clamp amplifier, Pulse software running on a Dell desktop computer, TMC 63-533 anti-vibration table, and homemade Faraday cage.

11. Temperature control system (optional, for recording at elevated temperature). In-line solution heater, Warner Instruments, cat. no. SH-27B and automatic temperature controller, Warner Instruments, cat. no. TC-324B.
12. Motorized micromanipulator, Sutter Instruments, cat. no. MP-225.
13. Recording chamber, Siskyou PC-R perfusion chamber, cat. no. 15280000E.
14. Reference electrode, 1.0 mm Ag/AgCl pellet, Warner Instruments, cat. no. E205 64-1309.
15. Electrode holder, Siskiyou Corp., cat. no. ST50-BNC.

3 Methods

3.1 Breeding Zebrafish to Obtain Larvae

1. IUAUC approval must be obtained prior to beginning experiments with zebrafish. Carry out all animal work in a clean, well-organized area.
2. House male and female breeders in separate tanks in the aquarium facility at 28.5 °C using a 14 h/10 h light/dark cycle. *See* **Note 6**.
3. Set up mating crosses in the late afternoon or early evening 3–14 days before the fish are needed for electrophysiological experiments. Use clean breeding tanks containing fresh fish water from the aquarium. Insert the perforated inner tank and removable divider into the outer tank. Transfer one male and one female fish to the separate compartments of each breeding chamber. Cover each chamber with a lid. Leave the tanks overnight at 28.5 °C in a quiet location in the fish facility using a 14 h/10 h light/dark cycle. *See* **Notes 7–9**.
4. Within 30 min after lights on in the morning, remove the divider between the male and female zebrafish in each breeding chamber. Courtship behavior should soon begin. Eggs are laid in the water and fertilized. Embryos fall through the perforations in the inner tank, preventing them from being eaten by their parents. After mating, return the adults to their home tanks in the aquarium. *See* **Note 10**.
5. Collect the embryos by removing the perforated inner tank from the breeding chamber and pouring the fish water in the outer tank through a fine mesh sieve. Immediately transfer the embryos to a 100 mm × 14 mm Petri dish containing 1× E2 medium by gently squirting them out of the sieve using a plastic transfer pipette filled with E2. Treat zebrafish gently and keep them submerged at all times. Typically, embryo

clutches obtained from different breeding pairs are mixed before selecting animals for an experiment.

6. Under the Zeiss stereomicroscope, separate embryos from debris and transfer the embryos to a fresh Petri dish containing 1× E2 medium. Raise embryos at a density of ~50 animals per 100 mm Petri dish and at a reduced density as the zebrafish grow. Mark each Petri dish with the date and time of fertilization. Place the Petri dishes in the 28.5 °C incubator equipped with timed LED illumination to provide a 14 h/10 h light/dark cycle matching that in the fish facility.
7. Late afternoon on the same day, inspect the embryos under the Zeiss stereomicroscope. Remove and euthanize (*see* **step 11**, below) embryos that have not reached 50% epiboly (a smooth layer of cells covering half of the embryo surface [21]), that have protrusions or swellings from the cell layer, or that look in any way abnormal. Most embryos that reach 50% epiboly will survive and develop normally. Remove most of the E2 medium and replace it with pre-warmed, fresh E2.
8. Subsequently, the embryos/larvae should be inspected under the microscope once per day. Remove abnormal, sick, dying, or dead embryos/larvae, and replace E2 medium (pre-warmed to 28.5 °C) at least once per day. Remove chorions from the dish as the animals start to hatch or transfer the larvae to a fresh Petri dish using a disposable plastic transfer pipette.
9. Starting on the fourth day post-fertilization, keep zebrafish larvae in water taken from the aquarium (fish water) rather than E2 medium.
10. Starting on the morning of the fifth day post-fertilization, feed the larvae twice daily with GP 100–200 μm larval diet. Replace fish water after the second feeding of the day.
11. Euthanize unneeded zebrafish. Embryos (prior to hatching) are euthanized by immersion in 1% sodium hypochlorite. Larvae (post-hatching) are euthanized by immersion in 0.2% MS-222. Discard according to institutional regulations. Do not flush live embryos, larvae, or adults down the sink or release them into the environment.

3.2 Anesthesia, Paralysis, and Exposure of the Cerebellum

Because the zebrafish is alive during electrophysiological recordings, animal regulations designate this procedure as survival surgery.

1. Dilute 1 mL 10× (0.2%) MS-222 with 9 mL ddH_2O for a final anesthetic concentration of 0.02%. Transfer the diluted MS-222 to a Petri dish. Using a plastic transfer pipette, transfer a 3–14 dpf zebrafish into the MS-222. The fish should become unresponsive to gentle poking within 10–20 s. Typically, anesthetized fish are unable to maintain an upright posture. Dispose of MS-222-containing solutions as hazardous waste.

2. Thaw 1 vial of 1000× curare (10 mM) and place on ice. Add 200 μL 1000× curare to 199.8 mL 1× external, for a final curare concentration of 10 μM. Dispose of any unused curare or curare-containing solutions as hazardous waste.
3. Place the clean, dry recording chamber on the stage of the Zeiss stereomicroscope. Place a small amount of Vaseline® in the center of the chamber and then place a dry coverslip on the top of it. (The Vaseline® anchors the coverslip in place during the experiment.) Touch the tip of an open tube of Krazy Glue® to the center of cover slip. Using a plastic transfer pipette, place a drop of the anesthetic solution containing an anesthetized fish near the chamber. Gently pick up the anesthetized fish using clean Dumont #5SF forceps. Place the animal's head dorsal side up onto the coverslip outside of the glue and then release the tail onto the glue. Avoid getting glue on the tips of the forceps. *See* **Note 11**.
4. Gently add 1× external solution containing 10 μM curare to the chamber so that the solution flows across the zebrafish from rostral to caudal. This reduces the chance of glue getting on the head. If glue does get on the head, gently scrape it off using the forceps. *See* **Notes 12–14**.
5. Perform the dissection under the stereomicroscope using two pairs Dumont #5SF super fine forceps. To anchor the head, use one pair to pinch the skin immediately caudal to the brain. Then, use the second pair to peel off the skin and skull from caudal to rostral. With practice, one smooth motion should be sufficient to remove both the skin and skull from the brainstem to the forebrain in one piece. Peeling them off in more than one step can damage the preparation. With practice, the dissection takes ~1–2 min. *See* **Notes 15–17**.

3.3 Extracellular Loose Patch Electrophysiology

This protocol focuses on successfully forming loose patches and recording from Purkinje cells in the cerebellum of live, awake zebrafish. It is assumed that the experimenter has previous patch clamp experience. Zebrafish Purkinje cells become electrically active late on day 3 post-fertilization or early on day 4 [11]. We have recorded from zebrafish Purkinje cells at 3–14 dpf. It may be feasible to record at later times, but it may become increasingly difficult to penetrate the dura mater.

1. Pull borosilicate pipette glass using Flaming Brown electrode puller. Check the shape of the micropipette (patch electrode) under a 40× objective (total magnification 400×). In order to penetrate the dura, the taper of the pipette should be narrower and sharper than electrodes used for whole cell patch clamp recording in brain slices. It will be necessary to determine appropriate puller parameters by trial and error to obtain the optimum shape.

2. Fill a 1 mL syringe with a 1× curare-free external solution. Attach a 0.2 μm syringe filter to the syringe and then attach a MicroFil pipette filler to the filter. Use this apparatus to backfill the patch electrode with the 1× curare-free external solution. Filled micropipettes should be free of air bubbles. Electrode resistance should be 7–10 MΩ when filled with the 1× curare-free external solution. *See* **Note 18**.
3. Fix the recording chamber containing the zebrafish with exposed cerebellum to the microscope stage.
4. Set the patch clamp amplifier to voltage clamp mode.
5. Lower the Ag/AgCl reference electrode into the chamber containing 1× external solution with 10 μM curare.
6. Insert the electrode into the patch clamp head stage attached to the Sutter MP-225 motorized micromanipulator. Using a 1 mL syringe attached to the suction port of the pipette holder, apply a small amount of positive pressure before lowering the electrode into the bath solution.
7. Set the voltage on the patch clamp amplifier to 0 mV. Lower the patch pipette into the bath solution. Adjust the baseline to 0 pA. *See* **Notes 19** and **20**.
8. Using the motorized micromanipulator, advance the electrode toward the preparation from the rostral side at an angle of 30° relative to horizontal, aiming for the middle of a Purkinje cell soma (Fig. 2). *See* **Note 21**.
9. After the pipette makes contact with the cell, release the positive pressure and apply gentle negative pressure to make a loose

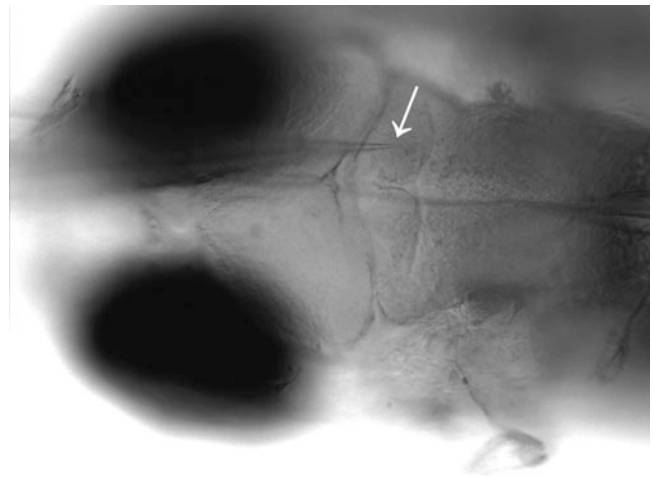

Fig. 2 Bright field image of zebrafish head, dorsal view, showing placement of loose patch electrode (*arrow*) during recording of spontaneous firing in a cerebellar Purkinje cell [11]

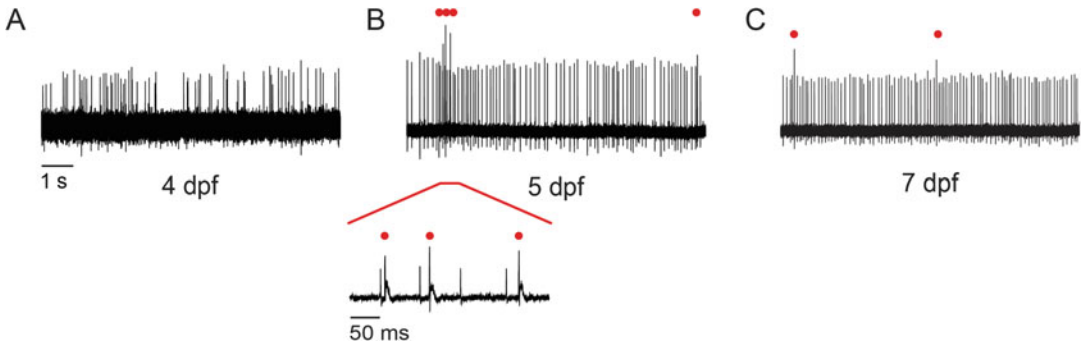

Fig. 3 Representative loose patch recordings taken from Purkinje cells at (**a**) 4 dpf, (**b**) 5 dpf, and (**c**) 7 dpf [11]. *Red dots* indicate complex spikes that result from synaptic input from climbing fibers originating in the inferior olive. In part **b**, complex spikes are shown on an expanded time base

patch onto the surface of the cell. We have used a broad range of seal resistances (20 MΩ to 2 GΩ) in successful experiments. Formation of a seal improves the signal-to-noise ratio and spatial resolution, facilitating the detection of spikes and maximizing the likelihood that the recorded electrical signals arise from a single Purkinje cell. *See* **Notes 22–24**.

10. Turn off ambient and microscope lights while recording. Avoid noise in the rig room. *See* **Note 25**.
11. After forming the loose patch, wait 1–2 min before beginning recording to allow time for the signal to stabilize. During recording, the baseline should be stable. Gap-free recordings are suitable for analyzing Purkinje cell activity. Spontaneous tonic firing, a characteristic activity of Purkinje cells, should be evident (Fig. 3) [11]. The regularity of tonic firing increases between 4 and 5 dpf. Starting at 5 dpf, most Purkinje cells fire complex spikes in response to synaptic input from climbing fibers, which originate in the inferior olive [11]. *See* **Notes 26–30**.

3.4 Euthanasia

1. After the experiment, immerse the fish on its coverslip in 10× MS-222 (0.2%). Due to the coverslip, place the animal in a sharps container that is used specifically for this purpose. Dispose of the container according to institutional regulations.

3.5 Data Analysis

1. To analyze data obtained from single Purkinje cells, discard records that contain simple spikes of different amplitudes or overlapping spikes.
2. To optimize automatic spike detection, post-hoc filtering of the data at 1 kHz using a lowpass Bessel filter is recommended.

4 Notes

1. When learning the technique, a germline transgenic line that expresses membrane-bound Venus, a yellow fluorescent protein, specifically in Purkinje cells under the control of the *aldolaseCa* promoter (*aldoca*) is useful for identifying Purkinje cells [11]. The *aldoca* gene encodes zebrin-II, a Purkinje cell-specific marker in mammals and zebrafish [20, 23]. Unlike in mammals, zebrin-II is apparently expressed in all cerebellar Purkinje cells in zebrafish [24]. The rk22Tg:*Tg(aldoca:gap-43-Venus*) line was generated in the pigmented Oregon AB strain [20], whereas the la118Tg:*Tg(aldoca:gap43-Venus)* line was generated in the unpigmented Tüpfel longfin nacre (TLN) strain to facilitate live imaging, calcium imaging, and optogenetics in the same genetic background used for electrophysiology [11]. TLN lines should be outcrossed to the parental pigmented Tüpfel longfin (TL) strain every three generations to maintain the vigor of the line. Albino progeny that express the *aldoca*-gap43-Venus transgene are selected and raised to be breeders.
2. Mosaic F0 transgenesis in a standard, wild-type laboratory strain such as AB or Tüpfel longfin (TL) or an albino strain such as nacre, TLN, or brass provides an alternative approach for labeling cerebellar Purkinje cells. For F0 transgenesis (sometimes called transient transgenesis [25]), a Tol2 plasmid encoding a fluorescent protein under the control of the *aldoca* promoter is injected into the cell of the zebrafish embryo at the one-cell stage. Injected animals are raised to the desired age and used in experiments. The fluorescent reporter will be expressed in a subset of cerebellar Purkinje cells (Fig. 1b). This method has been previously described [20, 25].
3. F0 transgenesis can be used to express a mutant ion channel in Purkinje cells to determine the effect of the mutation on tonic firing and complex spiking, the characteristic activities of Purkinje cells. Alternatively, germline transgenic lines can be generated by raising injected animals to sexual maturity, breeding them, and identifying founder animals that pass the transgene to their progeny [25].
4. With experience, Purkinje cells can be identified unambiguously in the absence of an indicator protein by their shape and location in the most superficial layer of cell bodies near the dorsal surface of the cerebellum [20, 24].
5. Some institutions, including UCLA, have zebrafish core facilities available on a recharge basis that handle day-to-day maintenance of the water system and routine care and feeding of the animals. The availability of such a facility significantly reduces

the cost and difficulty of establishing zebrafish as a model organism in the laboratory. Basic principles of zebrafish husbandry can be found in refs. 21 and 26.

6. Zebrafish become reproductively mature at ~3 months post-fertilization and are maximally fecund between ~6 months and 1 year of age [27]. To establish a breeding colony, separate 2.5–3 month old males and females for several weeks prior to mating. All breeders in a tank should have the same date of birth. Train the breeders by crossing them as described under **steps 3** and **4** each week for several weeks before zebrafish larvae are needed for experiments. Each tank should be labeled with the date of birth of the breeders and the dates of all crosses.
7. The number of breeding pairs to set up depends on the number of zebrafish needed for the experiment and the average clutch size for the breeding pairs.
8. Individual animals should not be bred more than once per week. Because regular breeding (at least every 2–3 weeks) maintains optimal fecundity and a reliable supply of healthy embryos, we typically cross all male and female breeders from a given tank each week and euthanize unused embryos (*see* **step 11**).
9. Breeding chambers are cleaned by rinsing with hot water and then distilled water, followed by air drying. We do not use detergent on any item into which zebrafish are placed.
10. Some pairs may not produce embryos. Breeding later in the morning or in the afternoon significantly lowers embryo quality and viability.
11. Dumont #5SF forceps must be handled with care because the tips bend very easily. Sharp, straight tips are important for a clean and successful dissection. Clean forceps by wiping them with a Kimwipe wetted with ethanol. To avoid damaging the tips, wipe from the end toward the tips.
12. The external solution with 10 μM curare does not contain MS-222. MS-222 silences electrical activity in zebrafish Purkinje cells and therefore must be removed prior to recording. After transfer to an MS-222-free solution, zebrafish recover from anesthesia in ~5–10 min. Therefore, we transfer the fish to MS-222-free external solution containing curare for the dissection, which with experience takes less than 2 min to perform. Considering the time it takes to mount the chamber onto the microscope, identify a promising cell to patch, fill the electrode, and make the loose patch, the zebrafish will have recovered from the anesthetic before recording begins.
13. Although it is feasible to remove curare after the dissection, the animal may twitch during recordings. To avoid this, we generally record using external solution containing 10 μM curare.

14. At high concentrations (≥100 μM), curare blocks small conductance Ca^{2+}-activated (SK) K^+ channels [28–31], which may affect neuronal excitability. We have confirmed by electrophysiological recording and by calcium imaging that 10 μM curare does not detectably alter Purkinje cell firing (J.-Y. Hsieh, F.A. Issa, and D.M. Papazian, unpublished).
15. After a good dissection, the brain should look clean (no pigment or blood vessels) and fairly transparent. Sometimes, the brain may look good under the Zeiss stereomicroscope but under the upright scope on the rig, yellowish tissue (which may be connective tissue or remaining skin or skull) may be seen on the head. This is a sign of a poor dissection. Patch electrodes will not penetrate this material. In this case, it is best to euthanize the fish and try another.
16. The preparation is delicate. Locate the stereomicroscope within a few feet of the electrophysiology rig to limit the movement and vibration experienced by the fish after dissection.
17. We have used this procedure with zebrafish between 3 and 14 dpf. Clean removal of the skin and skull becomes somewhat more difficult by the end of this period.
18. For extracellular loose patch recording, it is not necessary to fire polish or coat the electrodes.
19. Because the electrode and the bath contain the same solution, no junction potential is generated. Under these conditions, holding at 0 mV provides the most stable recordings.
20. A substantial change in resistance when the pipette is lowered into the bath indicates the tip is clogged. If this cannot be cleared by moderately increasing the positive pressure, replace the patch pipette.
21. The zebrafish cerebellum consists of three lobes. Recordings are made from Purkinje cells in the corpus cerebelli lobe, which is organized in a tri-lamellar structure shared with the mammalian cerebellum [24]. For recording, choose a healthy-looking, superficially-located Purkinje cell. In general, it is easier to patch onto medially located cells. Pipettes approaching laterally located cells tend to distort the tissue, making it more difficult to form a seal.
22. Contact between the electrode and the cell is monitored through the microscope or through the attached camera. Make sure the tip of the electrode is on the target cell before releasing the positive pressure.
23. If seal resistance is high, compensate the fast component of pipette capacitance using the patch clamp amplifier. If seal resistance is low, capacitance compensation is not necessary.

24. We routinely take a picture of each patched cell to record its location in the cerebellar hemisphere.
25. Because the zebrafish is awake with sensory systems intact during the recording, it is important to minimize as much as possible sensory input that might alter firing characteristics. We have found that changes in visual input dramatically alter Purkinje cell firing as early as 4 dpf [11]. Of course, one of the advantages of using zebrafish is that the effect of sensory input on Purkinje cell firing is readily determined.
26. Although we record at room temperature, it should be feasible to record at 28.5 °C, the temperature at which the zebrafish are raised, using an in-line heater and temperature controller.
27. The experimenter should be aware that locomotor activity in zebrafish shows circadian variation by 4 dpf [32]. Purkinje cell firing may vary during the circadian day. Therefore, it may be advantageous to record consistently during the same part of the day.
28. The preparation is stable for ~1 h post-dissection. Individual cells can be held for more than 30 min. We typically limit data collection to 45 min post-dissection. An experienced experimenter may be able to record from as many as four Purkinje cells per animal in this time window. If recording from multiple cells in the same zebrafish, pick cells that are widely separated because inserting an electrode through the dura mater and into the cerebellum may damage the surrounding area.
29. Recordings that show no activity (which may indicate that the cell has been damaged), an unstable baseline, poor signal-to-noise ratio, or evidence that the recorded electrode signals come from more than one cell (*see* Subheading 3.5) are terminated and the data discarded.
30. For pharmacological experiments, the preparation can be perfused using a flow rate of 2–3 mL/min. A minimum of three to five times the volume of the chamber should be perfused to add or remove drugs.

Acknowledgments

We are grateful to Ms. Brittany Ulrich for the image shown in Fig. 1b. This work was supported by NIH grant R01NS058500 and a UCLA Stein-Oppenheimer Seed Grant to Diane M. Papazian. Jui-Yi Hsieh was partially supported by the Jennifer S. Buchwald Graduate Fellowship in Physiology at UCLA.

References

1. Issa FA, Mazzochi C, Mock AF, Papazian DM (2011) Spinocerebellar ataxia type 13 mutant potassium channel alters neuronal excitability and causes locomotor deficits in zebrafish. J Neurosci 31:6831–6841
2. Issa FA, Mock AF, Sagasti A, Papazian DM (2012) Spinocerebellar ataxia type 13 mutation that is associated with disease onset in infancy disrupts neuronal pathfinding during neuronal development. Dis Model Mech 5:921–929
3. Waters MF, Minassian NA, Stevanin G, Figueroa KP, Bannister JPA, Dürr A, Brice A, Papazian DM, Pulst SM (2006) Mutations in voltage-gated potassium channel KCNC3 cause degenerative and developmental central nervous system phenotypes. Nat Genet 38:447–451
4. Figueroa KP, Minassian NA, Stevanin G, Waters M, Garibyan V, Bürk K, Brice A, Dürr A, Papazian DM, Pulst SM (2010) KCNC3: Phenotype, mutations, channel biophysics—a study of 260 familial ataxia patients. Hum Mutat 31:191–196
5. Figueroa KP, Waters M, Garibyan V, Bird TD, Gomez C, Ranum L, Minassian NA, Papazian DM, Pulst SM (2011) Frequency of *KCNC3* DNA variants as causes of spinocerebellar ataxia type 13 (SCA13). PLoS One 6:e17811
6. Duarri A, Nibbeling EA, Fokkens MR, Meijer M, Boerrigter M, Verschuuren-Bemelmans CC, Kremer BP, van de Warrenburg BP, Dooijes D, Boddeke E, Sinke RJ, Verbeek DS (2015) Functional analysis helps to define KCNC3 mutational spectrum in Dutch ataxia cases. PLoS One 10:e0116599
7. Minassian NA, Lin MA, Papazian DM (2012) Altered Kv3.3 channel gating in early-onset spinocerebellar ataxia type 13. J Physiol 590 (7):1599–1614
8. Mock AF, Richardson JL, Hsieh J-Y, Rinetti G, Papazian DM (2010) Functional effects of spinocerebellar ataxia type 13 mutations are conserved in zebrafish Kv3.3. BMC Neurosci 11:99
9. Brooke RE, Moores TS, Morris NP, Parson SH, Deuchars J (2004) Kv3 voltage-gated potassium channels regulate neurotransmitter release from mouse motor nerve terminals. Eur J Neurosci 20:3313–3321
10. Zhang Y, Kaczmarek LK (2016) Kv3.3 potassium channels and spinocerebellar ataxia. J Physiol 594(16):4677–4684
11. Hsieh J-Y, Ulrich B, Wan J, Papazian DM (2014) Rapid development of Purkinje cell excitability, functional cerebellar circuit, and afferent sensory input to cerebellum in zebrafish. Front Neural Circuits 8:147
12. Raman IM, Sprunger LK, Meisler MH, Bean BP (1997) Altered subthreshold sodium currents and disrupted firing patterns in Purkinje neurons of Scn8a mutant mice. Neuron 19:881–891
13. Khaliq ZM, Gouwens NW, Raman IM (2003) The contribution of resurgent sodium current to high-frequency firing in Purkinje neurons: an experimental and modeling study. J Neurosci 23:4899–4912
14. Martina M, Yao GL, Bean BP (2003) Properties and functional role of voltage-dependent potassium channels in dendrites of rat cerebellar Purkinje neurons. J Neurosci 23:5698–5707
15. Akemann W, Knöpfel T (2006) Interaction of Kv3 potassium channels and resurgent sodium current influences the rate of spontaneous firing of Purkinje neurons. J Neurosci 26:4602–4612
16. Westphal RE, O'Malley DM (2013) Fusion of locomotor maneuvers and improving sensory capabilities give rise to the flexible homing strikes of juvenile zebrafish. Front Neural Circuits 7:108
17. Boulton AA, Baker GB, Walz W (eds) (1995) Neuromethods 26: Patch-clamp applications and protocols. Humana, New York, NY
18. Molleman A (2003) Patch clamping: An introductory guide to patch clamp electrophysiology. Wiley, Chichester
19. NIH Office of Animal Care and Use (OACU) (2016) Guidelines for use of zebrafish in the NIH intramural research program. https://oacu.oir.nih.gov/sites/default/files/uploads/arac-guidelines/zebrafish.pdf
20. Tanabe K, Kani S, Shimizu T, Bae Y-K, Abe T, Hibi M (2010) Atypical protein kinase C regulates primary dendrite specification of cerebellar Purkinje cells by localizing Golgi apparatus. J Neurosci 30:16983–16992
21. Nusslein-Volhard C, Dahm R (eds) (2002) Zebrafish: a practical approach. Oxford University Press, Oxford
22. Wen H, Brehm P (2010) Paired patch clamp recordings from motor neuron and target skeletal muscle in zebrafish. J Vis Exp 45:e2351
23. Brochu G, Maler L, Hawkes R (1990) Zebrin II: a polypeptide antigen expressed selectively by Purkinje cells reveals compartments in rat and fish cerebellum. J Comp Neurol 291:538–552

24. Bae Y-K, Kani S, Shimizu T, Tanabe K, Hojima H, Kimura Y, Higashijima S, Hibi M (2009) Anatomy of zebrafish cerebellum and screen for mutations affecting its development. Dev Biol 330:406–426
25. Kikuta H, Kawakami K (2009) Transient and stable transgenesis using Tol2 transposon vectors. Methods Mol Biol 546:69–84
26. Westerfield M (2007) The zebrafish book, 5th edn: a guide for the laboratory use of zebrafish (Danio rerio). University of Oregon Press, Eugene, OR
27. Nasiadka A, Clark MD (2012) Zebrafish breeding in the laboratory environment. ILAR J 53:161–168
28. Ishii TM, Maylie J, Adelman JP (1997) Determinants of apamin and d-tubocurarine block in SK potassium channels. J Biol Chem 272:23195–23200
29. Pedarzani P, McCutcheon JE, Rogge G, Jensen BS, Christophersen P, Hougaard C, Strøbæk D, Stocker M (2005) Specific enhancement of SK channel activity selectively potentiates the afterhyperpolarizing current I_{AHP} and modulates the firing properties of hippocampal pyramidal neurons. J Biol Chem 280:41404–41411
30. Strøbæk D, Jørgensen TD, Christophersen P, Ahring PK, Olesen S-P (2000) Pharmacological characterization of small-conductance Ca^{2+}-activated K^+ channels stably expressed in HEK293 cells. Br J Pharmacol 129:991–999
31. Keating DJ, Rychkov GY, Roberts ML (2001) Oxygen sensitivity in the sheep adrenal medulla: role of SK channels. Am J Physiol Cell Physiol 281:C1434–C1441
32. Hurd MW, Cahill GM (2002) Entraining signals initiate behavioral circadian rhythmicity in larval zebrafish. J Biol Rhythm 17:307–314

Chapter 19

Site-Directed Unnatural Amino Acid Mutagenesis to Investigate Potassium Channel Pharmacology in *Xenopus laevis* Oocytes

Robin Y. Kim and Harley T. Kurata

Abstract

Unnatural amino acid mutagenesis is a useful tool enabling detailed investigation of ion channel structure-function relationships and pharmacology. Methods have been developed to apply this technique to different heterologous systems for electrophysiological studies, with each system offering unique advantages and limitations. Synthesis of aminoacylated-tRNA followed by injection into *Xenopus laevis* oocytes is beneficial because it allows for the incorporation of a wide range of unnatural sidechains, including amino acids with subtle structural differences. Here, we describe a protocol for unnatural amino acid mutagenesis implemented in our lab to study the pharmacology of KCNQ voltage-gated potassium channel opener compounds. This protocol should be applicable to other ion channels and receptor types amenable for functional studies in *Xenopus laevis* oocytes.

Key words Potassium channel, Unnatural amino acid, tRNA synthesis, Electrophysiology, Mutagenesis

1 Introduction

Incorporation of unnatural amino acids (UAA) into membrane receptors is a particularly valuable tool for investigating the detailed chemical interactions underlying protein structures, or receptor: ligand interactions. There are various approaches for the incorporation of unnatural amino acids, which in most cases converge on the generation of aminoacylated-tRNA that is complimentary to a UAG (amber) stop codon introduced at the amino acid position of interest in the target protein [1–4]. A common approach used for electrophysiological recordings in *Xenopus laevis* oocytes has been to co-inject mRNA along with an aminoacyl-tRNA synthesized in vitro. Synthesis of aminoacyl-tRNA involves ligating an amino acid to a modular tRNA molecule that can be used to deliver a wide variety of amino acids [5, 6]. The basic steps and checkpoints that we have used to successfully implement this approach in our lab will be

Show-Ling Shyng et al. (eds.), *Potassium Channels: Methods and Protocols,* Methods in Molecular Biology, vol. 1684,
DOI 10.1007/978-1-4939-7362-0_19,

described here. Alternative approaches have been developed, based on the generation of mutated aminoacyl tRNA synthetases with altered substrate specificity [7]. Plasmids encoding these engineered enzymes can be delivered into mammalian cell lines enabling the generation of the unnatural aminoacylated-tRNA in situ.

Although somewhat challenging, there are many valuable insights to be gained through the application of UAA mutagenesis to the study of voltage-gated ion channels and other membrane proteins. This approach expands the structural and chemical diversity of amino acid side chains that can be incorporated into a protein, enabling very detailed structural perturbations, or the introduction of amino acids with useful functionality. Many recent studies have exploited this approach to describe critical interactions between amino acid sidechains within ion channel architectures [8–13] as well as detailed interactions between ligands/small molecules and their binding sites [14–17]. In our case, we have applied these methods to subtly alter the structure of a conserved Trp sidechain that is essential for the retigabine activation of KCNQ2–5 channels [18, 19]. In this particular drug-binding site, even the substitution of other naturally encoded amino acids (Tyr, Phe) is not sufficient to preserve retigabine activation of KCNQ channels. The UAA mutagenesis method allowed for the incorporation of nearly isosteric Trp analogs including various fluorinated Trp derivatives, and a hydrogen-bond-deficient Trp analog, in order to more precisely define the chemical basis of retigabine interactions in this critical region. At present, there are no engineered aminoacyl tRNA synthetases available with specificity for these subtly altered Trp analogs, and so the in vitro tRNA synthesis approach was the only method available to complete these experiments.

As a final introductory comment, we should point out that the most important step we took toward succeeding with these experiments was establishing a supportive collaborative relationship with individuals that have been successful with the approach in the past. The methods described here utilize knowledge stemming from nearly three decades of pioneering work done in key labs [1, 4, 6]. In our studies, interactions with our colleagues Christopher Ahern and a synthetic chemist Jason Galpin (both located at University of Iowa), along with Stephan Pless (University of Copenhagen) were essential to guide us through the early failures we encountered, and were also extremely helpful in providing validated reagents essential for tRNA synthesis. Both Dr. Ahern and Dr. Pless spent weeks/months in Dr. Dougherty's lab at Caltech, where the unnatural amino acid mutagenesis approach was adapted for ion channel expression in *Xenopus laevis* oocytes [4, 6]. We are grateful that they have been willing to propagate their knowledge and expertise. Throughout the experimental steps described here, we have tried to describe aspects we feel are particularly important for a successful outcome.

2 Materials

Use DEPC (diethyl pyrocarbonate) treated ultra-pure water, and analytical grade reagents for all the procedures. Use RNase inhibitory products (such as RNase Zap) on the workbench, pipettes, and utensils in order to prevent RNA degradation.

2.1 In Vitro Transcription of THG73 tRNA

1. DNA template for THG73 synthesis (*see* **Note 1**).
   (a) Forward oligo: ATTCGTAATACGACTCACTATAGG TTCTATAGTATAGCGGTTAGTACTGGGGACTCT AAATCCCTTGACCTGGGTTCGAATCCCAGTAGGA CCGC.
   (b) Reverse oligo: GCGGTCCTACTGGGATTCGAACCCA GGTCAAGGGATTTAGAGTCCCCAGTACTAACCG CTATACTATAGAACCTATAGTGAGTCGTATTACG AAT.
2. 10× oligo annealing buffer: 100 mM Tris–HCl, pH 7.5, 1 M NaCl and 10 mM EDTA.
3. CellScript T7-Scribe Standard RNA Transcription Kit (CellScript, Cat # C-AS2607).
4. Acid-Phenol:Chloroform, pH 4.5 (Ambion, Cat # AM9720).
5. Chroma Spin-30 + DECP-H_2O columns (Clontech, Cat # 636087).

2.2 Synthesis of UAA-THG73 (Aminoacyl-tRNA)

1. THG73 tRNA (from 2.1).
2. 3 mM of the desired unnatural amino acid, coupled to pdCpA dinucleotide (described later), in DMSO.
3. T4 RNA ligase 1 (NEB, Cat #M0204).
4. 10 mM DEPC HEPES solution at pH 7.4.

2.3 Deprotection and Injection of UAA-tRNA and Template RNA

1. High intensity UV light source for the deprotection of NVOC-protected amino acids (*see* **Note 2**).

3 Methods

Overall, these methods should be considered an adaptation of the initial approach described by Nowak et al. [6], and our goal is that the protocol described here will guide readers to kits, reagents, and specific steps that have been successful in our hands. We have included important quality checkpoints throughout along with some of the practical insights gained as we have used the protocol repeatedly. The general method is described in Fig. 1, illustrating the three components that must be combined to generate a suitable

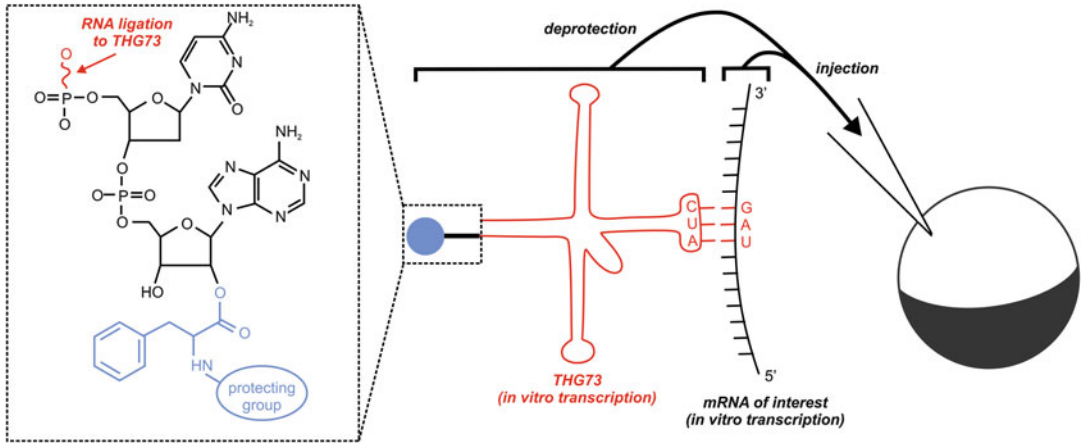

Fig. 1 General experimental scheme for unnatural amino acid mutagenesis in *Xenopus laevis* oocytes. A successful experiment requires generation of a functional aminoacyl-tRNA that is co-injected with mRNA carrying a UAG (amber) stop codon at the position of interest. The UAG stop codon is complimentary to the synthetic tRNA, directing introduction of the unnatural amino acid cargo in the position of the stop codon. Synthesis of aminoacylated-tRNA requires the combination of three components. A dinucleotide (pdCpA) is ligated to the carboxylate group of the desired unnatural amino acid (Phe is shown as an example) in a chemical synthesis. The remainder of the tRNA molecule (THG73) is synthesized by in vitro RNA transcription from a DNA template. THG73 and the coupled amino acid:pdCpA are ligated in an enzymatic reaction (T4 RNA ligase). Following appropriate deprotection steps, the synthetic tRNA can be co-injected with a desired mRNA for downstream ion channel expression and recording

tRNA molecule for injection. The bulk of the tRNA molecule (THG73) is generated by in vitro transcription. A dinucleotide (pdCpA) is synthesized chemically (usually by a commercial provider, unless your lab has particular expertise in chemical synthesis), and coupled to the desired synthetic amino acid. The coupled pdCpA:amino acid is then ligated to THG73 (by T4 RNA ligase) to generate an amino-acylated tRNA molecule. In most instances, the amino acid requires a protecting group (NVOC or BOC) that must be removed in order to generate an aminoacylated-tRNA that can be co-injected with mRNA.

3.1 Generating Template DNA for In Vitro Transcription of THG73 tRNA

The aim of these steps is to generate a concentrated solution of template DNA that will be used in later steps for in vitro transcription of THG73 tRNA (*see* **Note 1**). It is critical to check the DNA concentration at the end of these steps and ensure that you have an adequate amount. High yields of THG73 are important in subsequent steps and require an adequate concentration of template DNA.

1. Dissolve THG73 forward and reverse oligos in water to a final concentration of 4 μg/μL.
2. In a 1.5 mL microcentrifuge tube, combine 20 μL of forward oligo solution, 20 μL of reverse oligo solution, 5 μL of 10× annealing buffer, and 5 μL of water.

3. Heat mixture to 95 °C for 3 min using a heating block. We use a tube cap lock to prevent the lid from popping open. Let the mixture cool to room temperature.
4. Dilute mixture with 200 μL of water and perform ethanol precipitation: add 10 μL of 3 M sodium acetate and 600 μL of ethanol. Place the tube in a − 80 °C freezer for 30 min, centrifuge at maximum speed and 4 °C for 30 min, decant liquid, add 500 μL of 70% ethanol, spin again, decant liquid, and dry the pellet (we air dry the pellet for ~5 min in a RNAse-free box). Dissolve the pellet in 50–100 μL of DEPC-treated water and check DNA concentration. Store in aliquots of 25 μg.

3.2 In Vitro Transcription of THG73 tRNA

For these steps we use the CellScript T7-Scribe standard RNA transcription kit, with some additional steps and quality checks described below. The scale of RNA production is very important. These steps should yield a very large amount of THG73 tRNA (several hundred micrograms). This high yield is important to enable the synthesis of concentrated tRNA in a small volume for later injection steps into individual *Xenopus laevis* oocytes.

1. Mix the following in a microcentrifuge tube (to a total volume of 100 μL with DEPC-treated water): 25 μg of THG73 template DNA (stored in previous steps), 10 μL of 10× transcription buffer, 7.5 μL each of ATP, CTP, GTP, UTP, 10 μL of DTT solution, 2.5 μL of ScriptGuard RNase inhibitor and 10 μL RNA polymerase enzyme (*see* **Note 3**).
2. Incubate for 4–5 h, then add 5 μL DNase for 30–60 min, all at 37 °C.
3. Add 50 μL of water and 150 μL of phenol: chloroform. Vortex for 1 min and centrifuge at maximum RPM for 5 min. Collect the aqueous (upper) fraction into a clean tube, taking care to avoid pipetting organic material at the interface. Add 150 μL of water and repeat the extraction process to increase RNA yield. Combine aqueous fractions to obtain 300 μL of RNA solution.
4. Mix the RNA solution with 5 μL of 3 M sodium acetate and 800 μL ethanol. Precipitate RNA for 1 h in a −80 °C freezer and centrifuge at maximum RPM and 4 °C for 20 min. Decant and discard the supernatant, rinse with 70% ethanol, and centrifuge again. Dry the pellet and dissolve in 100 μL of DEPC water.
5. To purify the RNA, prepare one Clontech chroma-spin column per 50 μL of solution. Remove top and bottom caps from column. Place the provided 2 mL collection tube in the bottom of a 15 mL conical tube, followed by the column. Cap the conical tube and spin at 1800 rpm for 10 min (~700*g, *see* **Note 4**). Discard the flow-through and use the column in subsequent steps.

6. Use a razor blade to remove the lid and hinge from a 1.5 mL Eppendorf tube, so that it can be placed inside a clean 15 mL conical tube and used to collect purified RNA. Carefully transfer the prepared column from the previous step into the new conical tube, on the top of the prepared collection tube, with tweezers. Add 50 μL of RNA solution from **step 4** to the column and spin at 1800 rpm (~700*g) for 10 min. The flow-through from the column should contain the desired THG73 tRNA.
7. Combine purified RNA samples and check the concentration. If tRNA synthesis was successful, the concentration should be between 1 and 3 μg/μL. At this point the tRNA should be aliquoted and stored at −80 °C until use (*see* **Note 5**).

3.3 Ligation of Unnatural Amino Acid to THG73 Using T4 RNA Ligase

These steps describe the ligation of pdCpA-coupled amino acid with THG73 mRNA. Coupling of the pdCpA dinucleotide and the unnatural amino acid is a synthetic step that we have not performed in the lab. We have used reagents supplied by collaborators, although these may also be purchased from a commercial supplier.

1. Use 10 mM HEPES solution to dilute THG73 tRNA to 0.5–1 μg/μL. Unfold the THG73 tRNA by placing the tube in a 94 °C heating block for 3 min, with a tube cap lock on. Meanwhile, prepare 500 μL of boiling water in a 1 L beaker, using a microwave or water heater. Immediately before placing the tubes of tRNA in the hot water bath (use foam floats to suspend the tubes on the top of the water bath), transfer the beaker to a large bucket filled with ice. This helps accelerate cooling and refolding of the tRNA.
2. Meanwhile, mix the rest of the reagents required for unnatural amino acid-THG73 ligation in microcentrifuge tubes: 28 μL of water, 8 μL of 10× T4 RNA ligase buffer, 8 μL of 3 mM unnatural amino acid:pdCpA in DMSO (*see* **Note 6**), 1 μL ATP (10 mM, provided with NEB T4 ligase).
3. When the water bath has cooled to 40 °C, add 30 μL of tRNA to the reaction mixture, and 5 μL of T4 RNA ligase. Incubate at 37 °C for 40 min.
4. Add 220 μL of water, 30 μL of 3 mM sodium acetate and 330 μL of phenol:chloroform (*see* **Note 7**). Vortex 1 min and spin at maximum rpm and 4 °C for 5 min. Carefully collect the aqueous fraction, and add it to 900 μL of cold ethanol. Precipitate at −80 °C for 1 h, spin at maximum rpm in 4 °C for 30 min, decant and discard liquid supernatant, rinse with 70% ethanol, spin again, and dry the pellet (*see* **Note 8**). Store pellet at −80 °C until use. This pellet contains the aminoacylated-

tRNA shown in Fig. 1, with the protecting groups still present on the amino acid. We refer to this as the UAA-THG73 in subsequent steps.

3.4 Deprotection and Injection of UAA-THG73 and Template RNA

Our experiments using unnatural amino acid mutagenesis have primarily used NVOC (6-nitroveratryl oxycarbonyl)-protected derivatives of aromatic amino acids (Phe, Trp). Removal of the NVOC protecting group is done immediately prior to injection, by exposure to UV light as described below. Alternative protecting groups may also be used. The BOC (tert-butoxycarbonyl) protecting group is convenient and can be removed chemically with a variety of procedures. This is useful for research groups that do not have access to a high intensity UV light source. Structures of NVOC and BOC protected Phe amino acids are shown in Fig. 2.

1. Dissolve ligated UAA-THG73 pellet in 1–5 μL of water. Pipette liquid up and down until pellet looks mostly dissolved—insoluble impurities from the previous steps are likely visible.
2. Centrifuge at maximum rpm and 4 °C for 30 min. This will reduce the amount of impurities that can potentially clog oocyte injection tips.
3. Gently transfer the solution to a clean tube for use.
4. For NVOC-protected UAAs, expose UAA-THG73 to 400 W of UV light for 8 min (*see* **Note 9**).
5. Mix deprotected UAA-THG73 solution with template mRNA containing an amber (UAG) codon at the site of interest and inject immediately (*see* **Note 10**).

3.5 Injection and Electrophysiology from *Xenopus laevis* Oocytes

RNA injection and recording techniques using two-microelectrode voltage clamp are quite commonly used and accessible. Rather than exhaustively describing all the steps involved, we have highlighted some of the small adaptations that we believe can contribute to success in these final experimental steps. Many of these specific comments relate to questions we have received from others interested in trying this approach.

1. The quality of harvested *Xenopus laevis* oocytes strongly influences the success of the experiment. Be quite stringent about inspecting and sorting oocytes, and only move ahead with injection of synthesized tRNA when confident that the oocytes are of high quality.
2. Implement several positive control experiments. An important suggestion is to adopt a positive control for general methodology, using a target protein and amino acid that yield a functional channel/receptor (for example, unnatural amino acids have been successfully incorporated into many positions in the

Shaker potassium channel). Second, generate a "wild-type rescue" tRNA, comprising THG73 charged with the native amino acid at the position of interest. This tRNA should restore WT function of the target protein, helping to rule out nonspecific incorporation of amino acids, or unexpected functions of truncated protein. Lastly, it is helpful to include a negative control experiment by co-injecting mRNA along with a pdCpA-coupled tRNA (with no amino acid) as a way to assess the degree of non-specific amino acid incorporation at the introduced stop codon.

3. We have had our best results by injecting oocytes within a few hours of harvesting and collagenase treatment, and no later than 1 day after harvesting. We aim to record as soon as possible after RNA injections. For KCNQ3[A315T] channels, we could typically record currents within 1 day of injection.
4. In our experience and through discussions with colleagues applying similar methods, ion channel types that are most amenable to this approach are those that express large currents, a relatively short time after RNA injection. As an example, while we were evaluating various KCNQ channel subtypes for suitability for nonsense suppression, we found that KCNQ3 [A315T] channels yielded large currents (>30 μA at +20 mV) within 1 day of injection, whereas KCNQ2 required several days to achieve appreciable expression levels (and even then, generated much less current than KCNQ3[A315T], usually <10 μA at +20 mV). If you are attempting this method with channel constructs that do not reliably give large current expression (or take many days to achieve measurable currents), you are likely adding significant complexity to your experiment. You may wish to try alternative vectors, co-expression with auxiliary subunits (that promote channel expression), or codon optimization approaches to maximize channel expression in *Xenopus laevis*.
5. We typically mix the tRNA and mRNA into a single cocktail for injection. It is not necessary to inject separately. One must bear in mind that the injected tRNA cannot regenerate, so at best, one tRNA molecule can be incorporated into one protein subunit. We maximize the amount of tRNA that is injected, and also use concentrated mRNA to maximize expression and the rate of onset of current expression.

4 Notes

1. The oligo sequences contain a T7 promoter sequence followed by the THG73 sequence, minus the last two nucleotides (CA). The missing CA nucleotides are ligated in later steps as

"pdCpA." In earlier iterations of this method, the template was typically generated by a PCR reaction, but with the low cost and easy availability of oligonucleotide synthesis we have found that less troubleshooting is required if we simply order the DNA oligonucleotides and anneal them.

2. For UAA photo-deprotection, we use a Newport UV lamp (Newport, Cat # 66921, including power supply, Cat # 69920). Other light sources capable of delivering >400 W of UV light should suffice. Other protecting groups may also be used if convenient or preferred, and these may be useful if a high intensity UV light is not available. There are a wide variety of commercially available amino acids with a variety of side chains and protecting groups. These should be investigated, as there are many useful tools that can be purchased and obtained immediately with minimal downtime. If the desired reagent is not commercially available, then a custom synthesis is required.
3. This is a scaled-up version of the CellScript T7-Scribe Standard RNA Transcription Kit protocol in order to generate sufficient quantities of THG73 tRNA. Downstream steps, particularly injection of fairly small volumes (50 nL) requires a successful generation of relatively large quantities of tRNA in order to deliver highly concentrated tRNA to maximize ion channel expression.
4. This step is optional but highly recommended. Using the columns not only eliminates impurities in the sample, but ensures that leftover nucleotides are removed so that the end product consists mostly of full-length THG73. This step will also prevent wasting UAAs in subsequent steps if THG73 synthesis is not successful.
5. Typically, we store THG73 tRNA in aliquots of 100 μg, which is sufficient to perform 3–5 ligation reactions. These larger aliquots can be heated and used to perform multiple UAA-tRNA ligations at once, in parallel.
6. To ligate UAAs to THG73, two nucleotides (pdCpA) are attached to the UAAs through chemical synthesis. The chemical reaction for the acylation of pdCpA involves generating a reactive cyanomethyl ester of the backbone carboxylate of the desired amino acid [4, 6]. To make this possible, the desired amino acid should be synthesized or purchased with the free amine group and other reactive side chain functional groups (hydroxyl, carboxylates, amines) protected with an appropriate protecting group (these will be removed immediately prior to injection into *Xenopus laevis* oocytes). The pdCpA dinucleotide starting material is most easily purchased from a commercial supplier (we have purchased from GE-Dharmacon in the

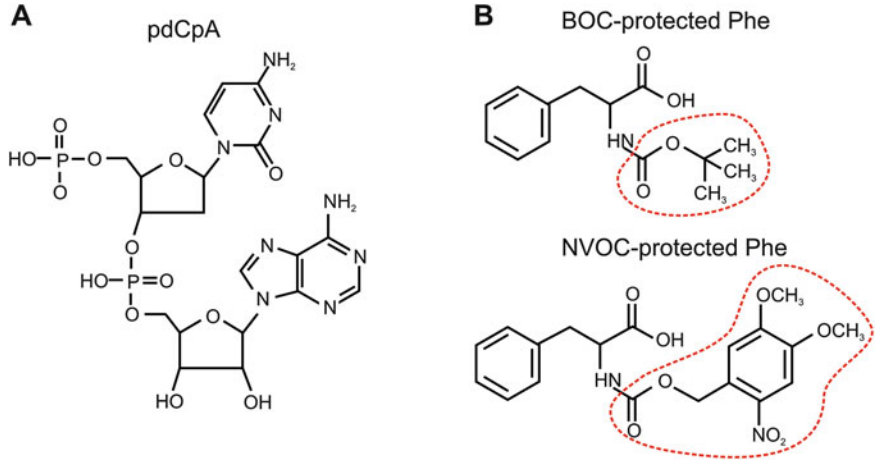

Fig. 2 Specific structures of starting materials required for the generation of coupled amino acid:pdCpA. (**a**) The chemical structure of pdCpA, which can be purchased as a custom chemical synthesis. (**b**) Chemical structures of Phe carrying two commonly used protecting groups on the amino group. The protecting groups are highlighted within the *dashed lines*

past as a custom order). Structures of pdCpA and examples of required amino acid starting materials are shown in Fig. 2.

7. Cold sodium acetate solution should be scaled up and prepared in advance, so that it can be added quickly upon termination of ligation reactions.
8. Centrifuging with the microcentrifuge tubes positioned with the lid hinge facing "up" can help prevent dislodging the precious UAA-tRNA pellet when pipetting the supernatant, as it can be difficult to visualize.
9. To expose UAAs to UV light, place a 1–2 μL droplet in the inner wall of a transparent PCR tube, and use a magnifying lens to focus the light onto the droplet. Heat from the exposure may evaporate a substantial amount of water in the droplet, and adding more water and spinning the tubes afterward may be required to obtain the UAA-THG73 that is ready to inject. We would advise taking the time to optimize this step with a target protein and amino acid previously shown to be amenable to this approach. Depending on the light source and setup, the time of exposure required may vary.
10. The ratio of UAA-THG73 and template mRNA as well as the quantities required for adequate expression will vary depending on the constructs. For the expression of UAAs in KCNQ3 [A315T] channels, we typically dissolve the UAA-THG73 pellets in 1 μL of water, mix with 1 μL of 2 μg/μL of mRNA, and inject 50 nL into each oocyte.

References

1. Dougherty DA, Van Arnam EB (2014) In vivo incorporation of non-canonical amino acids by using the chemical aminoacylation strategy: a broadly applicable mechanistic tool. Chembiochem 15:1710–1720
2. Pless SA, Ahern CA (2013) Unnatural amino acids as probes of ligand-receptor interactions and their conformational consequences. Annu Rev Pharmacol Toxicol 53:211–229
3. Neumann H, Wang K, Davis L, Garcia-Alai M, Chin JW (2010) Encoding multiple unnatural amino acids via evolution of a quadruplet-decoding ribosome. Nature 464:441–444
4. Noren CJ, Anthony-Cahill SJ, Griffith MC, Schultz PG (1989) A general method for site-specific incorporation of unnatural amino acids into proteins. Science 244:182–188
5. Cornish VW, Benson DR, Altenbach CA, Hideg K, Hubbell WL, Schultz PG (1994) Site-specific incorporation of biophysical probes into proteins. Proc Natl Acad Sci U S A 91(8):2910–2914
6. Nowak MW, Gallivan JP, Silverman SK, Labarca CG, Dougherty DA, Lester HA (1998) In vivo incorporation of unnatural amino acids into ion channels in Xenopus oocyte expression system. Methods Enzymol 293:504–529
7. Davis L, Chin JW (2012) Designer proteins: applications of genetic code expansion in cell biology. Nat Rev Mol Cell Biol 13:168–182
8. Pless SA, Niciforovic AP, Galpin JD, Nunez JJ, Kurata HT, Ahern CA (2013) A novel mechanism for fine-tuning open-state stability in a voltage-gated potassium channel. Nat Commun 4:1784
9. Pless SA, Galpin JD, Niciforovic AP, Kurata HT, Ahern CA (2013) Hydrogen bonds as molecular timers for slow inactivation in voltage-gated potassium channels. elife 2: e01289
10. Pless SA, Elstone FD, Niciforovic AP et al (2014) Asymmetric functional contributions of acidic and aromatic side chains in sodium channel voltage-sensor domains. J Gen Physiol 143:645–656
11. Pless SA, Galpin JD, Niciforovic AP, Ahern CA (2011) Contributions of counter-charge in a potassium channel voltage-sensor domain. Nat Chem Biol 7:617–623
12. Tao X, Lee A, Limapichat W, Dougherty DA, MacKinnon R (2010) A gating charge transfer center in voltage sensors. Science 328:67–73
13. Gleitsman KR, Lester HA, Dougherty DA (2009) Probing the role of backbone hydrogen bonding in a critical beta sheet of the extracellular domain of a cys-loop receptor. Chembiochem 10(8):1385–1391
14. Pless SA, Galpin JD, Frankel A, Ahern CA (2011) Molecular basis for class Ib antiarrhythmic inhibition of cardiac sodium channels. Nat Commun 2:351
15. Ahern CA, Eastwood AL, Dougherty DA, Horn R (2008) Electrostatic contributions of aromatic residues in the local anesthetic receptor of voltage-gated sodium channels. Circ Res 102:86–94
16. Lummis SC, McGonigle I, Ashby JA, Dougherty DA (2011) Two amino acid residues contribute to a cation-pi binding interaction in the binding site of an insect GABA receptor. J Neurosci 31(34):12371–12376
17. Xiu X, Puskar NL, Shanata JA, Lester HA, Dougherty DA (2009) Nicotine binding to brain receptors requires a strong cation-pi interaction. Nature 458:534–537
18. Lange W, Geissendorfer J, Schenzer A et al (2009) Refinement of the binding site and mode of action of the anticonvulsant Retigabine on KCNQ K+ channels. Mol Pharmacol 75:272–280
19. Wuttke TV, Seebohm G, Bail S, Maljevic S, Lerche H (2005) The new anticonvulsant retigabine favors voltage-dependent opening of the Kv7.2 (KCNQ2) channel by binding to its activation gate. Mol Pharmacol 67:1009–1017

Chapter 20

Random Spherically Constrained Single-Particle (RSC) Method to Study Voltage-Gated Ion Channels

Liguo Wang

Abstract

To study membrane protein structures using cryo-Electron Microscopy (cryo-EM), membrane proteins are usually extracted from cell membranes and solubilized in detergents. To restore the lipid bilayer environment of membrane proteins, a method called "random spherically constrained" (RSC) single-particle cryo-EM has been developed. The RSC platform establishes the lipid environment for membrane proteins and makes it possible, for the first time, to apply the desired transmembrane potential to trap voltage-gated ion channels in the desired functional states (e.g., deactivated voltage sensor at −120 mV) for structural analysis. No rupture or leakage was observed during the establishment of the transmembrane potential. The spherical geometry of liposomes is used as a constraint to accurately determine the orientation of the inserted membrane protein.

Key words Random spherically constrained (RSC) single-particle cryo-EM, Transmembrane potential, Lipid membrane environment, Voltage-gated ion channel, Membrane protein reconstitution, 2D crystal

1 Introduction

Membrane proteins are essential for cellular life. They are involved in various critical biological processes, thus about a quarter of the genes in most genomes encodes membrane proteins. Membrane proteins account for 70% of all known pharmacological targets and 50% of potential new drug targets due to their intimate involvement in a wide variety of diseases, including diabetes, cancer, and neurological disorders [1]. As shown by both structural and functional studies, lipid membrane environment plays an essential role for the structural integrity and activity of membrane proteins [2–7]. Therefore, it is critical to restore the lipid bilayer environment of membrane proteins. A method, called "random spherically constrained" (RSC) single-particle cryo-EM, where the membrane protein is reconstituted into lipid vesicles (a mimic of an empty cell), was developed and employed to study the large conductance

Show-Ling Shyng et al. (eds.), *Potassium Channels: Methods and Protocols,* Methods in Molecular Biology, vol. 1684,
DOI 10.1007/978-1-4939-7362-0_20,

voltage- and calcium-activated potassium (BK) channels reconstituted into liposomes at 17-Å resolution [8]. Compared with the nanodisc method, where the membrane protein resides in a small patch of lipid bilayer encircled by an amphipathic scaffolding protein [9–11], the major difference is that the RSC method mimics the cell and provides an asymmetric environment (i.e., inside and outside conditions can be varied independently), whereas there is only one environment surrounding the membrane proteins in the nanodisc method. This will be important for membrane proteins where an asymmetric environment is preferred (e.g., applying ligands to only one side of the membrane or applying transmembrane potential for voltage-gated ion channels or voltage-sensitive proteins).

In the RSC method, membrane proteins solubilized in detergents are mixed with detergent-solubilized lipids (Fig. 1a, b). After the removal of the detergents, either by dialysis or gel filtration (for review, *see* ref. 12), membrane proteins are reconstituted into liposomes spontaneously, and functional assay can be carried out to assess the function of the reconstituted membrane proteins. To separate empty liposomes from proteoliposomes, gradient separation can be used, where empty liposomes float up to a higher (i.e., lighter) layer than proteoliposomes. Then proteoliposomes are tethered onto a 2D streptavidin crystal (Fig. 1c), which serves as a concentration step and can be used to assess the image quality and determine contrast transfer function (CTF) parameters [13]. The tethered proteoliposomes are fast frozen in liquid ethane cooled by liquid nitrogen, and imaged in a cryo-electron microscope. The images are processed using Matlab programs. First, periodic 2D streptavidin crystal information is removed computationally as previously described [13], and the liposome contribution is removed with a model based on the average POPC membrane profile (The model was obtained using the Hankel transform as previously described [14]). Protein particle images were manually picked using EMAN boxer [15] and the CTF parameters are estimated using a home-made Matlab (MathWorks, Natick, MA) program [13] from the power spectrum of each micrograph. The picked BK particle images, with crystal and liposome information removed, are used to determine the 3D structure employing constraints based on the spherical geometry of the proteoliposomes as previously described [8] (Fig. 1d). Here, only the sample preparation steps will be illustrated as the image-processing steps are straightforward and the instruction can be obtained with the Matlab programs developed in our laboratory.

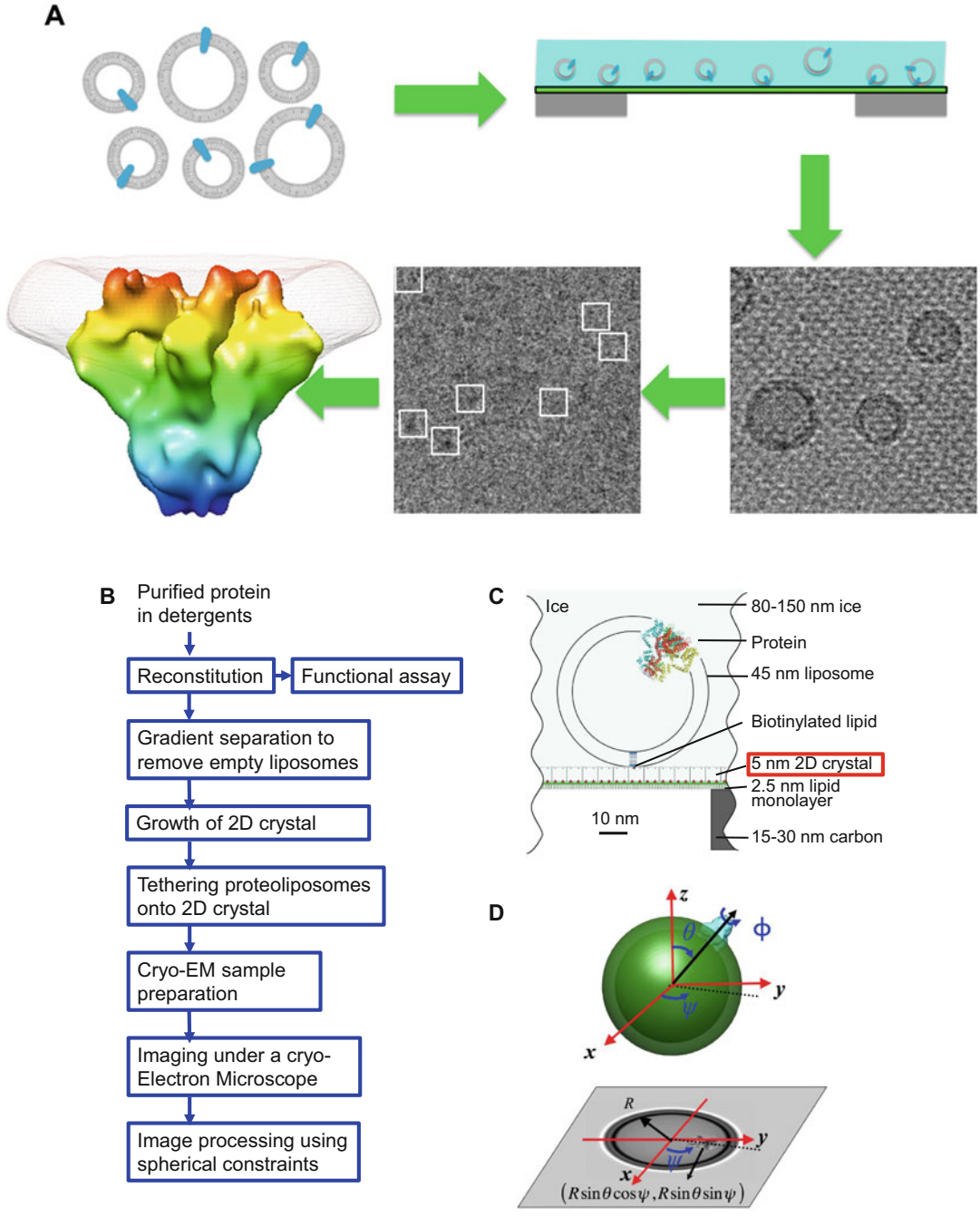

Fig. 1 RSC platform. (**a**) Major steps of the RSC method. Proteoliposomes are tethered onto 2D crystals which spans a hole in the perforated carbon film (*green* region in *top right image*), fast frozen in liquid ethane, and imaged in a cryo-electron microscope (*bottom right image*). Crystal and liposome information is removed (*bottom middle image*), and protein particles are picked (marked by *white boxes*). The selected protein particle images are used to reconstruct the structure of reconstituted membrane protein (*bottom left image*). (**b**) Sample preparation steps. (**c**) Scale drawing of the tethering system. The 2D crystal layer is bound to a lipid monolayer that spans a hole in the perforated carbon film. (**d**) A 3D model of a proteoliposome and its projection image. The geometry can be used to determine the two of the three angles to define the orientation of each individual protein molecule

2 Materials

2.1 Reconstitution of BK Proteins in POPC Liposomes

1. POPC (1-palmitoyl-2-oleoyl-sn-glycero-3-phosphocholine) and biotinylated dipalmitoyl-phosphatidyethanolamine (biotin-DPPE) lipid in chloroform (Avanti Polar Lipids, Inc.).
2. Glass syringe and glass tube ($D = 16$ mm).
3. 1.5 ml Eppendorf tube.
4. 4 and 0.5 ml concentrator tubes with a cutoff of 100 kDa.
5. A small foam box with the internal surface covered by aluminum foil.
6. Nitrogen gas tank with a dispenser, and liquid N_2 tank (Praxair Inc.).
7. Desktop vortexer.
8. Water bath.
9. Orbital shaker or rotator.
10. FPLC with Superdex 200 HR10/30 column or hand-packed column with Sephadex G-50.
11. Hydration buffer: 50 mM Tris, pH 7, 150 mM KCl, 30 mM DM.
12. Gel filtration buffer: 50 mM Tris, pH 7, 150 mM KCl.

2.2 Gradient Separation

1. Nycodenz stock solutions: 40% Nycodenz in water, 30% Nycodenz in water
2. KCl buffer: 150 mM KCl in water.
3. Ultracentrifuge and 2.0 ml centrifuge tube.
4. Round multiFlex gel-loading tips (Fisher Inc.).
5. 4 ml ultrafiltration spin column (Sartorius North America Inc.) with a cutoff of 100 kDa.

2.3 Flux Assay to Assess the Function of Reconstituted Proteins

1. Cationic voltage-sensitive dye: 5P,5P,6,6P–Tetrachloro-1,1,3,3P–tetraethylbenzimadazolyl-carbocyanine iodide (JC-1, Invitrogen Inc.).
2. Dilution buffer: 5 mM KCl, 135 mM NaCl, 1.6 μM of JC-1.
3. KCl solution: 2 M KCl.
4. SpectraMax fluorometer (Molecular Devices).

2.4 Tethering of Proteoliposomes onto Streptavidin 2D Crystals

1. Streptavidin solution: 1 mg/ml (New England Biolabs Inc.).
2. Crystal buffer: 50 mM HEPES, pH 7.2, 150 mM NaCl buffer.
3. Lipid mix: 0.5 mg/ml DOPC, 0.5 mg/ml biotincap-DOPE in chloroform, store at −20 °C.
4. Hexane.

5. Castor oil.
6. C-flat TEM grid: CF-2/2-4C holey Cu grid.
7. Self-locking tweezers: Dumont N4 AC or N5 AC.
8. A 5 μl glass syringe.
9. 35 mm petri dish.
10. Humidity chamber.
11. 1.5 ml Eppendorf tube cap.

2.5 Cryo-Sample Preparation

1. 4 L Dewar filled with fresh liquid N_2.
2. 50 ml falcon tube with string (also termed storage tube) and 1 L sample-transfer dewar.
3. Tweezers sets (>4 sets or the same number of grids to be frozen): self-locking tweezers.
4. Filter paper: 2 cm × 4 cm straps in moisture box (spread the straps on the box, not to pile them together).
5. Pipette and tips, long tweezers, and screw driver.
6. Grid boxes.
7. Liquid N_2 flasks (sample-freezing flask and transfer flask), ethane basket, transfer bucket, and support station.
8. Ethane and N_2 gas.
9. KCl buffer: 50 mM KCl in water.
10. Manual plunger.
11. Safety goggle.

3 Methods

3.1 Reconstitution of BK Proteins in POPC Liposomes

The BK protein was purified from HEK293 cells stably expressing BK proteins as previously described and reconstituted into liposomes [8].

3.1.1 Preparation of Detergent Solubilized Lipid

1. Use a glass syringe to transfer lipid solutions (POPC:biotin-DPPE = 1:3600 molar ratio to yield about 3 biotin-DPPE molecules per 30 nm liposome) into a glass tube.
2. Mix lipids by vortexing for 1 min.
3. Dry the lipid under N_2 air flush in the hood till the lipids turn into a transparent gel-like layer on the glass tube wall. Make sure the N_2 gas dispenser tip posits at the middle of the glass tube to avoid the spill of lipid solution. Rotate the tube gently by hand at the first 5 min to coat the glass wall uniformly. The whole progress takes around 45 min. Check the flow rate every 10 min.

4. Rehydrate lipid mixture in hydration buffer to a final concentration of 10 mM total lipid (*see* **Note 1**).
5. Vortex the lipid solution vigorously for 3 min (use the highest speed of the desktop vortexer).
6. Freeze and thaw the lipid solution. Use a piece of parafilm to seal the tube and dip the tube into a foam box filled with liquid N_2. After the solution is frozen, remove the tube from liquid N_2 and dip the tube into a water bath at 37 °C until melt. Keep moving the tube to avoid breaking the glass tube. Take out the tube from the warm water; wipe off the water outside the tube before dipping it into liquid N_2 again to avoid breaking the glass tube. Repeat ten times (*see* **Note 2**).
7. After freeze-thaw cycle, transfer the milky solution into a 1.5 ml Eppendorf tube.
8. Rotate the lipid-detergent solution at room temperature for overnight or until the solution becomes clear.
9. Transfer the lipid solution into a glass vial and store it at 4 °C.

3.1.2 Reconstitution of Membrane Proteins

1. Mix BK protein with detergent solubilized lipid to a final protein-to-lipid molar ratio of 1:5000 (1–2 copies of BK per 30 nm liposome). Usually, we use 200 μl protein solution and 50 μl lipid-detergent solution (*see* **Note 3**).
2. Rotate the protein lipid mixture for 1 h at 4 °C.
3. Gel filtration is used to remove detergents. Use a 1 ml syringe to inject the 0.25 ml protein-lipid mixture solution into the 0.5 ml loop of FPLC. Using Superdex 200 HR10/30 column with gel filtration buffer at a flow rate of 0.25–0.3 ml/min. Wash pump system, column, and injection loop prior to use. Collect fractions showing lipid signal by measuring phosphate using a colorimetric assay (*see* **Notes 4–6**).
4. Concentrate proteoliposomes at 1000 × *g* to the desired concentration or volume. For example, 0.2 ml is preferred for the subsequent gradient separation.

3.2 Gradient Separation

After the detergent removal, the proteoliposomes, empty (i.e., protein-free) liposomes, and free protein aggregates coexist in the solution. To separate them, gradient separation is used as shown in Fig. 3. After gradient separation, a dilution-concentration method is used to remove Nycodenz.

1. Prepare Nycodenz solutions: mix 30% Nycodenz solution with KCl buffer to get a desired concentration of Nycodenz as shown in Table 1.
2. Add 200 μl BK proteoliposome solution and 600 μl 40% Nycodenz solution into a centrifuge tube, mix with a pipette.

3. Draw 100 μl 40% Nycodenz solution, carefully insert the pipette tip through the sample layer until it touches the bottom of the centrifuge tube. Slowly inject the solution to the bottom of the tube. A 40% Nycodenz layer will form beneath the sample layer.
4. Draw 200 μl 20% Nycodenz solution, touch the tube wall about 5 mm above the liquid level in the tube, slowly inject the solution which will flow down the tube wall and form a layer on the top of the sample layer.
5. Repeat **step 4** to lay 200 μl 15%, 5%, 3%, 1% and 100 μl of KCl buffer on the top of a previously laid layer. The final layers can be seen in Fig. 3a.
6. Carefully put the tube into the ultracentrifuge basket and balance it.
7. Centrifuge at 238,000 × *g* for 18 h at 4 °C.
8. Carefully take out the centrifuge tube, and collect fractions (~200 μl/collection) of the solution from the top to the bottom.
9. Measure lipid concentrations by measuring phosphate using a colorimeter; protein is determined with the BCA (bicinchoninic acid) method, and the relative fraction of BK in each layer is determined by densitometry of a Western blot.
10. The layers containing both liposomes and proteins are collected (e.g., Layers 4 and 5 in Fig. 3b), and load collected proteoliposome solution to an ultrafiltration spin column (*see* **Note 7**).
11. Spin at 1000 × *g* for 5–10 min to 0.2 ml.
12. Add 1.8 ml of KCl buffer, mix by a pipette.
13. Repeat **steps 11** and **12** for 3 more cycles to reach 10,000 times dilution in total.

3.3 Flux Assay to Assess the Function of Reconstituted Proteins

The function of reconstituted BK channels is assessed using the voltage-sensitive dye JC-1 to monitor K^+-induced changes in membrane potential [8, 16, 17].

1. BK proteoliposomes loaded with 150 mM KCl are diluted into dilution buffer giving a total lipid concentration of ~6 μM.
2. 0.8 ml of the solution is added to a cuvette, and the fluorescence signal ($\lambda_{ex} = 480$ nm, $\lambda_{em} = 590$ nm) is recorded.
3. After the signal is stabilized, add 6.0 μl of 2 M KCl solution to increase the external K^+ concentration to 20 mM, and mix it with a pipette.
4. Record the fluorescence signal.

5. After the signal reaches a plateau, add 8.0 μl of 2 M KCl solution to increase the external K^+ concentration to 40 mM, and mix it with a pipette (*see* **Note 8**).
6. Record the fluorescence signal.

3.4 Tethering of Proteoliposomes onto Streptavidin 2D Crystals

In the RSC method, it is essential that the liposomes have a spherical shape. To make proteoliposomes highly spherical, repeated osmotic shocks are applied (*see* **Note 9**).

3.4.1 Swelling of Proteoliposomes

1. Add 0.1 ml BK proteoliposome solution into a 1.5 ml tube.
2. Add 0.011 ml water to BK proteoliposome solution. Vortex for a few seconds at the lightest intensity.
3. Incubate for 30–60 min at 4 °C.
4. Repeat **steps 2** and **3** with the amount of water listed in Table 2.

3.4.2 Streptavidin 2D Crystal Growth and Tethering

1. Dilute 1 mg/ml Streptavidin to 0.5 mg/ml with crystal buffer.
2. Wash C-flat grids with hexane ten times by holding the grid with a pair of tweezers and dipping in hexane solution, and then air dry for 30 min.
3. Store tweezers on ice.
4. Add 5 ml crystal buffer to 35 mm petri dish, use castor oil sticking outside a long pipette tip to cover the water surface, add 0.5–0.8 μl lipid mix to the center using a 5 μl glass syringe. A lipid monolayer will form at the air-water interface. At this point, lipid was applied slowly at the center, taking care that the chloroform should not break through the air-water interface and sink to the bottom of the dish. The lipid immediately breaks through the "puddle" of castor oil. Sufficient lipid is applied so that the monolayer covers ~3/4 of the area of the dish.
5. Pick up lipid monolayer by allowing the carbon side of the holey grid touch the lipid monolayer center briefly ("Dumont" side face top, and the tweezers is cooled down from **step 3**). Put the grid in a humidity chamber with lipid monolayer side facing up, and add 4 μl streptavidin solution to the lipid monolayer side. Cover the humidity chamber, and incubate for 30 min. Make sure the grid is horizontal. Use 10 μl pipette tips, which could drop 4 μl fast as a drop. Also, warming the streptavidin solution to room temperature helps to drop the small amount of liquid.
6. Wash the grids three times in a 1.5 ml-tube-cap filled with 220 μl crystal buffer. The volume of crystal buffer in the cap

can be varied to make sure the water surface is flat (neither concave nor convex) (*see* **Note 10**).

7. Place 8 μl sample on a piece of Parafilm in the humidity chamber. Pick up the grid with the metal-wire loop or a pair of tweezers from the washing tube-cap, gently put it on the top of the sample drop with crystal side facing down. Cover the chamber and incubate for desired time (5–20 min) to have high density of liposomes (not to have many overlapped liposomes) (*see* **Note 11**).

3.5 Cryo-Sample Preparation

To prepare cryo-sample, either a homemade manual plunger or an automated plunger (e.g., FEI Vitrobot) can be used. Here, a homemade plunger as shown in Fig. 2 is used as the 2D crystal is too fragile to survive the blotting process using an automated plunger.

1. Turn on the valves on N_2 gas tank, and check the plunger to confirm it is working smoothly (N_2 pressure: 20 psi).
2. Test the tweezers position to ensure the tips are centered in the ethane bucket and below the ethane bucket top edge (to ensure the grid be immersed in liquid ethane after being plunged).
3. Put the sample storage tube in 1 L sample transfer dewar and then fill the dewar with liquid N_2. Put the lid back on dewar when liquid N_2 quiets down.
4. Unscrew the grid box to ensure that the lid of the grid box is flexible but not too loose, then put the grid box onto the support station in the transfer flask (Fig. 2b).
5. Fill the transfer flask with liquid N_2, use tweezers to turn the lid of the grid box to release the hot gas inside. The liquid N_2 level should be close to the top edge of the flask so no further filling of liquid N_2 is needed.
6. Fill up the sample-freezing flask with fresh liquid N_2, wait for the liquid N_2 to quiet down, and then pour the liquid N_2 to a little bit above the ring level of liquid ethane bucket (Fig. 2c).
7. Wear safety goggles to fill liquid ethane bucket with liquid ethane until the surface is convex. Stop the gas ethane flow before withdrawing the glass tip from the ethane bucket.
8. Use tweezers to pick up one grid with tethered BK proteoliposomes, and mount the tweezers onto the plunger.
9. Add 4 μl KCl buffer onto the grid.
10. Blot the grid with filter paper for several seconds until the diameter of water sign on the filter paper meet your expectation. It is better to wear gloves to reduce heating of the frozen sample during sample transfer to grid boxes.

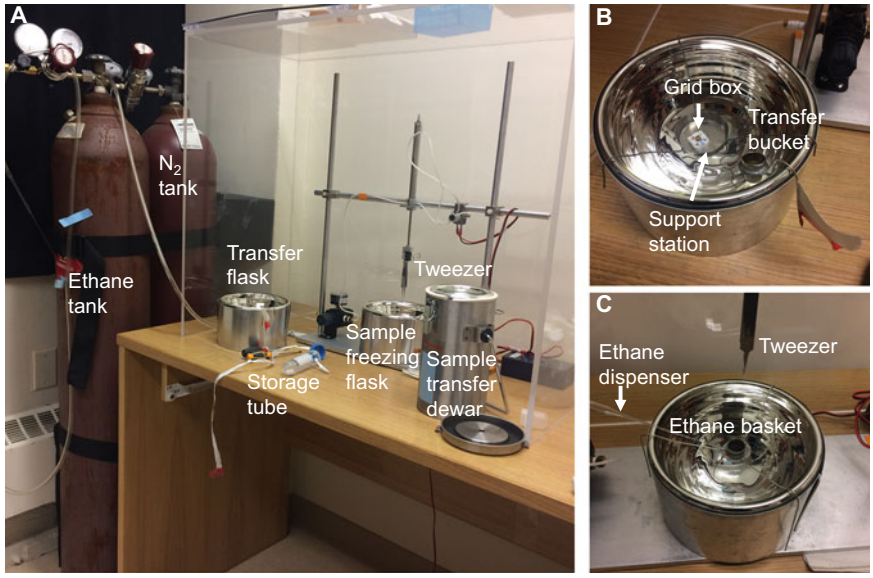

Fig. 2 Cryo-sample preparation equipment. (**a**) An overview of a homemade manual plunger freezing system. (**b**) Zoom-in of the transfer flask and associated tools. (**c**) Zoom-in of the sample freezing flask with associated tools

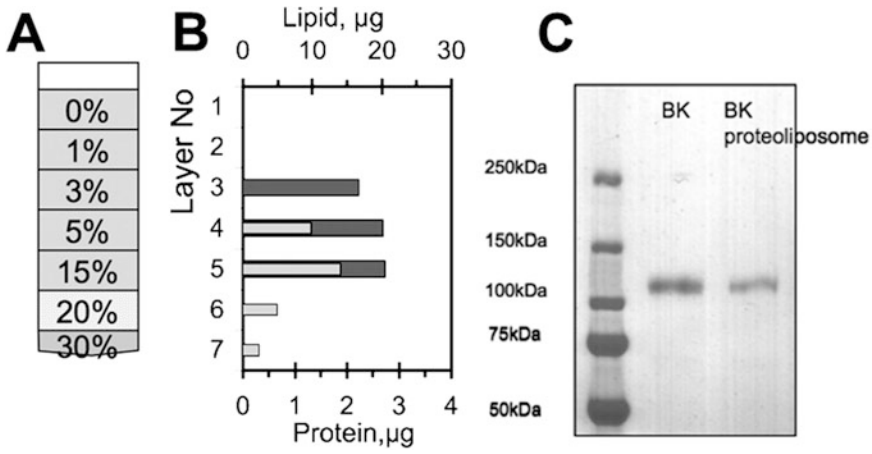

Fig. 3 Separation of BK proteoliposomes. (**a**) Density gradient flotation of proteoliposomes; the percentage concentration (w/v) of Nycodenz is given for each layer. (**b**) Distribution of protein (*gray bars*) and phospholipid (*black bars*) in the gradient layers after flotation (18 h at 238,000 × *g*). Empty liposomes are seen to float to layer 3. (**c**) Coomassie-stained SDS-PAGE gel showing protein extracted from the BK proteoliposomes as compared to the purified, solubilized BK protein before reconstitution

Table 1
Preparation of Nycodenz solutions

30% Nycodenz solution (ml)	1	1	1	1	1
KCl buffer (ml)	0.5	1	5	9	29
Nycodenz concentration (w/v)	0.2	0.15	0.05	0.03	0.01

Table 2
Swelling of 0.1 ml BK proteoliposomes

Fraction of water to be added	11%	14%	18%	24%	33%
Water added (ml)	0.011	0.014	0.018	0.024	0.033
Final volume (ml)	0.111	0.125	0.143	0.167	0.200

11. Plunge freeze sample grid into liquid ethane by stepping on the foot pedal right after removing the filter paper away from the grid.
12. Transfer the frozen grid into a grid box using the small transfer bucket. Make sure no large ice flakes exist in the small transfer bucket.
13. After freezing all the samples, cool down the screwdriver and long tweezers in the freezing flask. Then lock the grid box and transfer it to the precooled storage tube.
14. Tighten the falcon tube lid and transfer the tube to the large liquid N_2 freezer.
15. Clean up all the tweezers and flasks, turn off both N_2 and ethane valves, and put ethane bucket in the hood.

4 Notes

1. To prepare the detergent solubilized lipid, the lipid concentration can be changed, but the detergent concentration should be two to three times the lipid concentration.
2. In protein reconstitution step, a container filled with hot tap water at 37 °C can be used to replace the water bath. Freeze-thaw cycle can be skipped but longer incubation time is needed. The lipid-detergent solution can be stored at 4 °C for 6 months.
3. To calculate the lipid to protein ratio, assume the area of each lipid molecule is around 60 $Å^2$. Each 20 nm sized liposome has ~4,000 lipid molecules.
4. In gel filtration to remove detergents, proteoliposomes elute at 30–45% of the packed volume, and the detergent elutes at about 100% of the packed volume. During the detergent-removal process, the flow rate is critical. If the flow rate is faster than 0.5 ml/min, the detergent will not be removed completely.
5. In the protein reconstitution step, dialysis can also be used to remove detergents. The only drawback is that longer time is needed to remove detergents (a few days vs. a few hours).

6. The reconstitution efficiency (reconstituted membrane protein/total membrane protein) is about 50–70%, and about 50–80% of liposomes are proteoliposomes (fraction of lipid in proteoliposomes/total lipid).
7. In the density gradient, the position of the liposomes depends on the liposome size (smaller liposomes are more dense than larger ones) as well as on the presence of incorporated protein. The clear segregation of empty liposomes and proteoliposomes in the 3% and the 5–15% boundary, respectively, is consistent with an effective separation due to the added density from protein.
8. In the flux assay, the time for the system to reach an equilibrium (i.e., reach a plateau in the fluorescence signal) varied from 20 to 40 min depending on the K^+ concentration gradient across the membrane. The large the concentration gradient, the longer the time to reach an equilibrium.
9. In the swelling step, we found that when we used a single swelling step, many of the liposomes were not spherical. We speculate that the reason is the following: to change from an ellipsoid to a sphere, some of the lipid molecules in the inner leaflet of the liposome membrane have to move to the outer leaflet. The spontaneous flip-flop rate is very slow, but with an osmotic shock the transient formation of a membrane defect allows flip-flop to occur. The multiple osmotic shocks allow equilibration of the two leaflets be achieved to form highly spherical liposomes.
10. The pH value of crystal buffer should be higher than 7.2. Otherwise, the crystal quality will be bad.
11. The tethering time should be varied based on proteoliposome density.

References

1. Weinglass AB, Whitelegge JP, Kaback HR (2004) Integrating mass spectrometry into membrane protein drug discovery. Curr Opin Drug Discov Devel 7(5):589–599
2. Schmidt D, Jiang QX, MacKinnon R (2006) Phospholipids and the origin of cationic gating charges in voltage sensors. Nature 444 (7120):775–779
3. Gonen T et al (2005) Lipid-protein interactions in double-layered two-dimensional AQP0 crystals. Nature 438(7068):633–638
4. Long SB et al (2007) Atomic structure of a voltage-dependent K^+ channel in a lipid membrane-like environment. Nature 450 (7168):376–383
5. Hilgemann DW (2003) Getting ready for the decade of the lipids. Annu Rev Physiol 65:697–700
6. Hille B et al (2015) Phosphoinositides regulate ion channels. Biochim Biophys Acta 1851 (6):844–856
7. Lee AG (2011) Biological membranes: the importance of molecular detail. Trends Biochem Sci 36(9):493–500
8. Wang L, Sigworth FJ (2009) Structure of the BK potassium channel in a lipid membrane from electron cryomicroscopy. Nature 461 (7261):292–295
9. Bayburt TH, Grinkova YV, Sligar SG (2002) Self-assembly of discoidal phospholipid bilayer

nanoparticles with membrane scaffold proteins. Nano Lett 2(8):853–856

10. Katayama H et al (2010) Three-dimensional structure of the anthrax toxin pore inserted into lipid nanodiscs and lipid vesicles. Proc Natl Acad Sci U S A 107(8):3453–3457
11. Gao Y et al (2016) TRPV1 structures in nanodiscs reveal mechanisms of ligand and lipid action. Nature 534(7607):347–351
12. Wang L, Tonggu L (2015) Membrane protein reconstitution for functional and structural studies. Sci China Life Sci 58:66–74
13. Wang L, Ounjai P, Sigworth FJ (2008) Streptavidin crystals as nanostructured supports and image-calibration references for cryo-EM data collection. J Struct Biol 164:190–198
14. Wang L, Bose PS, Sigworth FJ (2006) Using cryo-EM to measure the dipole potential of a lipid membrane. PNAS 103 (49):18528–18533
15. Ludtke SJ, Baldwin PR, Chiu W (1999) EMAN: semiautomated software for high-resolution single-particle reconstructions. J Struct Biol 128(1):82–97
16. Chanda B, Mathew MK (1999) Functional reconstitution of bacterially expressed human potassium channels in proteoliposomes: membrane potential measurements with JC-1 to assay ion channel activity. Biochim Biophys Acta Biomembr 1416(1–2):92–100
17. Reers M (1991) J-aggregate formation of a carbocyanine as a quantitative fluorescent indicator of membrane potential. Biochemistry 30 (18):4480–4486

Chapter 21

CW-EPR Spectroscopy and Site-Directed Spin Labeling to Study the Structural Dynamics of Ion Channels

Cholpon Tilegenova, Benjamin W. Elberson, D. Marien Cortes, and Luis G. Cuello

Abstract

Continuous-wave electron paramagnetic resonance spectroscopy (CW-EPR) and site-directed spin labeling (SDSL) are proven experimental approaches to assess the structural dynamics of proteins in general (Hubbell et al., Curr Opin Struct Biol 8(5):649–656, 1998; Kazmier et al., Curr Opin Struct Biol 45:100–108, 2016; Perozo et al., Science 285(5424):73–78, 1999). These techniques have been particularly effective assessing the structure of integral membrane proteins embedded in a lipid bilayer (Cortes et al., J Gen Physiol 117(2):165–180, 2001; Cuello et al., Science 306(5695):491–495, 2004; Dalmas et al., Structure 18(7):868–878, 2010; Li et al., Proc Natl Acad Sci U S A 112(44):E5926–5935, 2015; Perozo et al., J Gen Physiol 118(2):193–206, 2001), as well as determining the conformational changes associated with their biological function (Kazmier et al., Curr Opin Struct Biol 45:100–108, 2016; Perozo et al., Science 285 (5424):73–78, 1999; Arrigoni et al., Cell 164(5):922–936, 2016; Dalmas et al., Nat Commun 5:3590, 2014; Dong et al., Science 308(5724):1023–1028, 2005; Farrens et al., Science 274(5288):768–770, 1996; Perozo et al., Nat Struct Biol 5(6):459–469, 1998; Perozo et al., Nature 418(6901):942–948, 2002). In this chapter, we described a practical guide for the spin-labeling, liposome reconstitution, and CW-EPR measurements of the prototypical bacterial K^+ channel, KcsA.

Key words Electron paramagnetic resonance spectroscopy, KcsA, Site-directed spin labeling, Liposome reconstitution, Ion channels, Membrane proteins and structural dynamics

1 Introduction

Site-directed spin labeling (SDSL), liposome reconstitution, and continuous-wave electron paramagnetic resonance spectroscopy (CW-EPR spectroscopy) have been invaluable experimental tools for assessing the physiologically relevant conformation(s) of membrane proteins embedded in a lipid bilayer [1–15]. This is particularly true in the case of ion channels, in which the lack of a cell membrane can produce significant changes in the channel's structure or yield a nonfunctional conformation [16]. Moreover, the high-resolution structures of ion channels obtained by

Show-Ling Shyng et al. (eds.), *Potassium Channels: Methods and Protocols*, Methods in Molecular Biology, vol. 1684,
DOI 10.1007/978-1-4939-7362-0_21,

macromolecular crystallography could potentially deviate from a physiological relevant conformation, given the non-physiologically conditions (i.e., pH, precipitant concentration and temperature) used during the crystallization process [4].

CW-EPR spectroscopy has become a powerful methodology to study the structure and dynamic of membrane proteins, particularly with ion channels [17]. This technique relies on the analysis of the properties of a spin label systematically attached to cysteine residues along the primary sequence of a target protein [18]. The spectral line-shape of the spin label is highly sensitive to changes of its conformation and/or surrounding environment. This is very convenient since it can report on highly localized structural changes underlying the biological function of ion channels [18, 19].

We have found that to properly conduct SDSL and CW-EPR studies of ion channels, a systematic optimization of the following steps is necessary: both the expression and purification of the target protein [20], efficiency of the labeling reaction and liposomes reconstitution procedure are crucial to generate the largest amount of structural constraints in the shortest period of time [4, 5].

Here, we present an optimized protocol for: (1) the expression and purification in large scale of the prototypical proton-gated ion channel [21, 22], KcsA (the G116C spin-labeled mutant is a position that faithfully reports on the conformational changes associated with the opening of KcsA's activation gate [2, 12], a process known as activation gating), (2) its highly efficient spin-labeling reaction, and (3) its proper reconstitution in premade liposomes. These properties have allowed us to accurately conduct CW-EPR studies of an ion channel under nearly physiological conditions.

2 Materials

All the solutions used in this protocol were made with analytical grade chemicals and they were stored or made the same day according to our own experience in expressing, purifying, and spin labeling recombinant ion channels. Particular attention should be given to the following steps of this protocol: (1) the *E. coli* competent cells used to express the target protein must be freshly made, since the older is the competent cell, the lower the quality and the yield of the expressed target, (2) the protein concentration for the labeling reaction should be at least 10 mg/mL to maximize the efficiency of labeling, and (3) the amount of the Bio-beads added to the reconstitution mixture should be carefully titrated to ensure protein incorporation into the preformed liposomes.

2.1 Competent Cells

Competent cells are made fresh from glycerol stocks (25% sterile glycerol) stored at −80 °C as follows: transfer 0.5 mL from an overnight *E. coli* preculture to a sterile 250 mL flask containing

50 mL of Luria-Bertani media (LB-media) (add antibiotics as needed). Incubate the cells at 37 °C with continuous shaking at 220 rpm until the optical density (OD) at 600 nm reaches 0.5 (it might take from 2.5 to 3 h, avoid overgrowing the culture since it affects the efficiency of transformation).

Chill the flask on ice for 30 min and transfer the cells to a precooled sterile 50 mL conical tube, then harvest the cells by centrifugation at 1200 RCF for 5 min at 4 °C. Resuspend the cell pellet from a 50 mL conical tube with 2.5 mL of ice-cold transformation and storage solution-TSS solution (TSS solution: 10% Polyethylene Glycol 8000, 5% Dimethyl Sulfoxide (DMSO), 40 mM $MgCl_2$ in LB media, adjust the pH to 6.5) [23] (*see* **Note 1**).

2.2 Detergents and Phospholipids

Triton X-100 and Dodecyl Maltoside (DDM) were purchased from Anatrace. Stock solutions of Triton X-100 (20%) and DDM (200 mM) were prepared, filtered, and kept in the dark at 4 °C. Asolectin polar extract was purchased from Avanti as a 25 mg/mL solution in chloroform.

2.3 Spin Label

Spin label (1-oxyl-2,2,5,5- tetramethyl-D3-pyrroline-3-methyl methanethiosulfonate) was obtained from Toronto Research Chemicals. A 200 mM stock solution is made in DMSO and stored at −20 °C until needed (*see* **Note 2**).

2.4 C.R.A.P Medium for KcsA Expression

CRAP-based medium, $((NH_4)_2SO_4$ 3.57 g/L, Na Citrate · $2H_2O$ 0.71 g/L, KCl 1.07 g/L, Yeast extract 5.36 g/L, HyCase 5.36 g/L pH 7.3 are autoclaved together; next day before starting the cell culture, 100 mM MOPS, 10.5 mM $MgSO_4$, and 0.5% glycerol were added [24] (*see* **Note 3**) supplemented with 0.4 mg/mL ampicillin at 37 °C.

2.5 Lysis Buffer

50 mM Tris-HCl, 150 mM KCl, 170 μg/mL phenylmethylsulfonyl fluoride (PMSF), and 1 mg/mL of egg lysozyme.

3 Methods

3.1 Protein Expression and Purification

1. KcsA-G116C cloned in the bacterial expression vector pQE-70 is transformed in fresh-made C41 cells by heat shock and grown overnight in LB media supplemented with 1% glucose and 0.4 mg/mL ampicillin.
2. Next day, the overnight culture is diluted 100 times in 1 L of C.R.A.P medium (phosphate-limiting media) [24] supplemented with 0.2% glucose, 0.5% glycerol, and 0.4 mg/mL ampicillin [20].
3. Once the cell culture reaches an O.D. of 0.6, it is cooled down to 29 °C for 1 h. Next, KcsA expression is achieved by the

addition of 0.1 mM IPTG and 10 mM $BaCl_2$ (*see* **Note 4**) at 29 °C overnight with constant agitation (250 rpm).

4. Next day, KcsA-expressing cells are harvested, resuspended in lysis buffer, and incubated for 1 h at room temperature. Afterward, cells are broken on an Emulsiflex C3 and spin down at 100,000 × *g* for 1 h.
5. The membrane pellet is resuspended in Buffer A (150 mM KCl, 50 mM Tris-Cl, pH 8.0) + 170 μg/mL PMSF and stored at −80 °C.
6. KcsA-G116C is extracted from the *E. coli* membrane preparation in a buffer containing 1 M KCl, 50 mM Tris-Cl, pH 8.0 and 1.5% Triton X-100 for 1 h at room temperature.
7. The insoluble material is spin down at 100,000 × *g* for 1 h at 4 °C [20].
8. The supernatant is loaded onto a cobalt resin column and washed with Buffer A, 10 mM imidazole, and 1 mM DDM. Finally, KcsA is eluted in BufferA, 1 mM DDM, and 400 mM imidazole (*see* **Note 5**).

3.2 KcsA-G116C Spin-Labeling Reaction

1. KcsA-G116C (Fig. 1) purified as described in Subheading 3.1 is concentrated ~10 mg/mL and reduced by adding 5 mM tris (2-carboxyethyl) phosphine (TCEP) for 30 min (*see* **Note 6**).

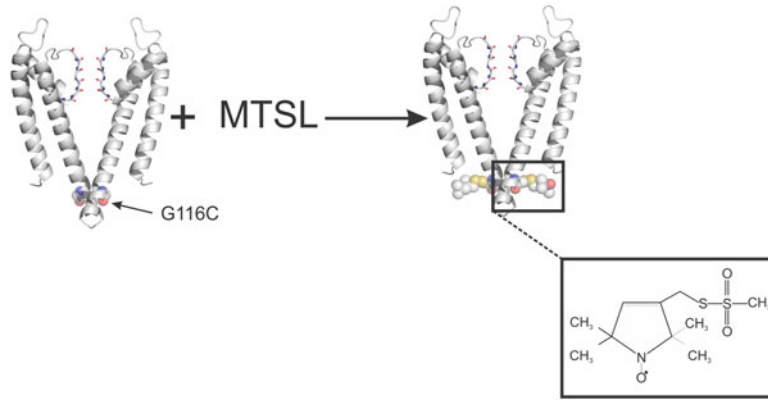

Fig. 1 A schematic representation of the KcsA's spin labeling reaction. Reduced KcsA-G116C mutant (only two subunits are shown for clarity) is reacted with the thiol-specific spin-label (1-oxyl-2,2,5,5- tetramethyl-D3-pyrroline-3-methyl methanethiosulfonate) in a 1 to 10 molar ratio. This reaction yields a channel with four spin labels covalently attached at the activation gate. The diameter of KcsA's activation gate changes as a function of pH, since it is activated by protons, and this process can be tracked with high-sensitivity by measuring the changes in the spectral line-shape of spin labels attached to the activation gate. The *inset* shows in detail the structure of the spin label

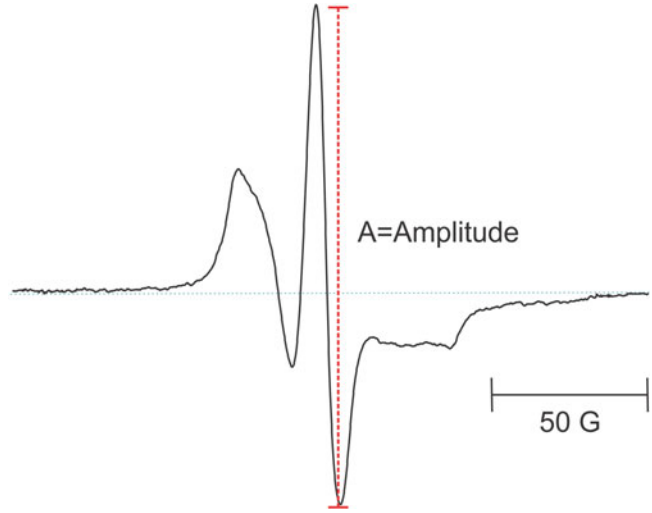

Fig. 2 A typical CW-EPR spectrum of KcsA-G116C spin labeled at pH 3. Since at this pH the channel activation gate is open, the spin-spin interaction is minimal and as a consequence the amplitude of the central resonance line of the normalized CW-EPR spectrum reaches a maximum

2. Then a desalting PD-10 column, pre-equilibrated with a degassed (*see* **Note 7**) Buffer A + 1 mM DDM (*see* **Note 8**), is used to eliminate the excess of reducing agent.
3. Reduced KcsA-G116C (~1 mg) is concentrated to 10 mg/mL (*see* **Note 9**) and incubated with a tenfold molar excess of the highly reactive thiol-specific spin-label (1-oxyl-2,2,5,5-tetramethyl-Δ3-pyrroline-3-methyl methanethiosulfonate) (Fig. 2) for 30 min on ice (*see* **Notes 10**).
4. After 30 min add another pulse of spin label to the reaction, fivefold molar excess, which is half of the volume added before (*see* **Notes 11**) and keep it on ice for another 30 min.
5. Once the labeling reaction is completed, remove the excess of spin label by using a desalting PD column equilibrated with buffer A + 1 mM DDM [20].

3.3 KcsA Reconstitution in Preformed Asolectin Liposomes

1. A desired quantity of Asolectin dissolved in Chloroform (25 mg/mL) is placed on a rotary-evaporator for 2 h to dry and remove any residual organic solvent.
2. The resultant dried lipid film is hydrated by adding Buffer A such that the final concentration of lipid is 10 mg/mL.
3. Next, sonicate the Asolectin suspension on a bath sonicator for ~10 min or until the liposome suspension becomes translucent.
4. KcsA-G116C-spin labeled is concentrated to ~5 mg/mL and then reconstituted by mixing it with the preformed Asolectin liposomes suspension at a 1:1500 molar ratio.

5. For detergent removal and channel reconstitution, add 15 mg of Biobeads SM-2 per 250 μL of reconstitution mixture volume and rotate for 1 h (*see* **Notes 12** and **13**).
6. Add a second pulse of BioBeads SM-2 in the same amount, and rotate for 1 h.
7. Add a third and final pulse of BioBeads SM-2 in the same amount and rotate for 1 h (*see* **Note 11**).
8. Separate the proteoliposome suspension from Biobeads SM-2 by passing it through a disposable screening column.
9. Next, harvest the liposomes by centrifugation at 100,000 × *g* for 1 h (*see* **Note 13**).
10. Resuspend the liposomes pellet with 50 μL of buffer A and split it equally between two small Eppendorf tubes, then dilute each sample tenfold with a high-capacity buffer at pH 4 or 7.
11. Warm the samples for 10 min at 42 °C to equilibrate the internal and external proteoliposome spaces and centrifugate the sample at 100,000 × *g* and 4 °C for 1 h [2].
12. Resuspend the liposome pellet in the smallest possible volume, ~5 μL or less of the high-capacity buffer at pH 4 or 7, to be able to load them into the TPX capillary for EPR measurements.

3.4 CW-EPR Measurements of KcsA-G116C-SL

1. Load the samples into the TPX capillary (*see* **Note 14**). Place them inside the ER 4123D cavity and proceed to fine tune the sample inside the cavity (refer to the manual of the spectrometer to perform this step).
2. Generally, to record a CW-EPR spectrum with a high signal-to-noise ratio for KcsA-G116C, a good starting set of parameters for the EPR spectrometer are as follows: 2 mW incident power, 100 kHz modulation frequency, 1 G field modulation amplitude, 200 G scan width, and 10–12 scans (*see* **Note 15**).
3. Once acquired, the baseline of the CW-EPR spectrum is corrected (refer to the manual of the spectrometer to perform this step).
4. The resultant CW-EPR spectrum is normalized by the number of spin labels to correct by the differences in the amount of protein loaded into the TPX capillary.
5. To quantify the opening of KcsA's activation gate (KcsA is a proton-gated K^+ channel), a set of CW-EPR spectrum at different pH values (pH 3, 4, 5, 6, and 7) are acquired (*see* **Note 16**).
6. KcsA's activation pKa is determined by plotting the amplitude of the central resonance line of the normalized CW-EPR spectrum (Fig. 3) (normalized by the number of spins) versus the pH or $[H^+]$ and the Hill equation was fitted to the data. (Fig. 4).

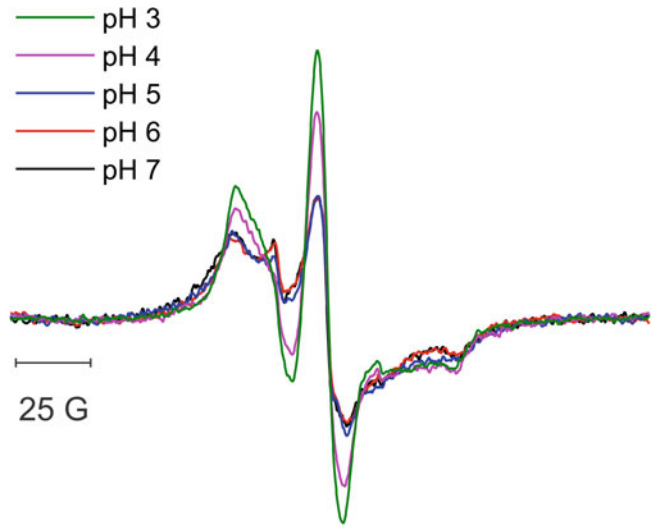

Fig. 3 pH-dependent spectral line changes of the KcsA G116C spin labeled. Upon increasing the proton concentration, KcsA's activation gate opens and spin labels attached at position G116C move away from each other lessening their spin-spin interaction. At pH 7 KcsA's activation gate is closed and the spin labels at position 116 experience a very strong spin-spin interaction due to their spatial proximity

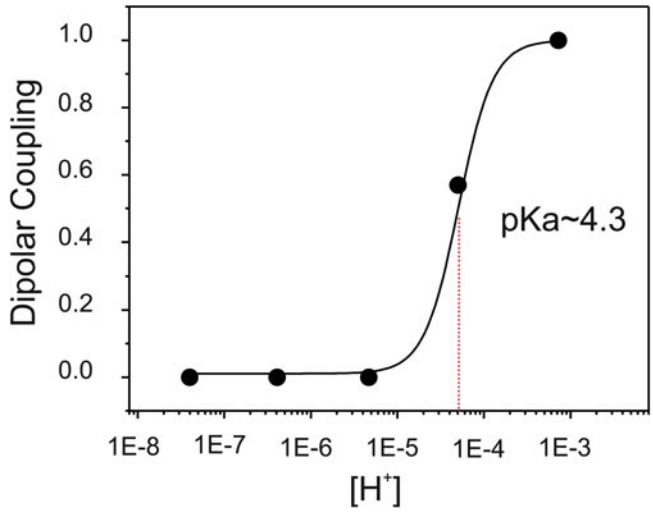

Fig. 4 KcsA pH-dependent activation gating assessed by CW-EPR spectroscopy. Changes in spin-spin interaction or dipolar coupling of the spin labels attached at the position 116 were plotted versus the proton concentration [H^+] and the Hill equation was fitted to the data

4 Notes

1. This is a highly convenient method to make competent cells (from any *E. coli* strain) suitable for molecular biology and/or protein expression. The protocol can be down-sized for few samples and since it is not time consuming it facilitates the use of fresh-made competent cells when needed.
2. The spin label stock solution can be made in at least three different organic solvents: Dimethyl sulfoxide, Dimethylformamide, or Acetonitrile. It is recommended to test the solubility of the target protein in not more than 10% of each of the solvents, to avoid protein precipitation during the labeling procedure.
3. We have determined that when expressing KcsA using C.R.A.P. medium supplemented with glycerol improves the expression and maximizes the final cell culture biomass.
4. The addition of 10 mM $BaCl_2$ (a known K^+ channel blocker) and the use of low IPTG concentration (0.1 mM) resulted in a significant increment of KcsA expression levels.
5. We have found that Triton X-100 or Anzergent 3–12 are more affordable alternative detergents for the extraction of KcsA from *E. coli* membranes. When using Triton X-100 or Anzergent 3–12 the final yield of fully functional and crystallizable KcsA was ~40 mg and ~80 mg per liter of culture, respectively [20].
6. When working with a new protein, it is recommended to test different reducing agents, i.e., TCEP, Dithiothreitol (DTT), or β-Mercaptoethanol, since they can trigger protein precipitation and/or display different reducing efficiencies.
7. Degas Buffer A by bubbling nitrogen gas for 30 min. The concentration of dissolved oxygen is significantly decreased by this procedure as measured by oxygen electrodes. The low concentration of dissolved oxygen in the buffer prevents oxidation of the cysteine residues and hence increases the efficiency of spin labeling [2, 4, 12].
8. Add 1 mM DDM after Buffer A has been degassed to avoid the formation of foam.
9. KcsA-G116C concentrated to 10 mg/mL in a final volume of ~100 μL consistently allows us to achieve maximal efficiency of labeling.
10. Placing on ice the KcsA's spin labeling reaction effectively prevents protein precipitation with negligible effect on the labeling efficiency.

11. The spin label reacts with itself in aqueous solutions, hence its effective concentration decreases rapidly displaying a half-life of ~30 min. The reaction is easily monitored by measuring the broadening of the CW-EPR spectrum as a function of time. Broadening of the EPR spectrum happens as a consequence of the spin-spin interaction between spin labels in close proximity [2, 12].
12. It is recommended that 60 mg of Biobeads SM-2 should be used for 1 mL of reconstitution mixture. The final amount of BioBeads SM-2 added to 1 mL of reconstitution mixture would be 60 mg × 3 = 180 mg.
13. If an insufficient amount of BioBeads SM-2 are added to the reconstitution mixture, the protein will not reconstitute into the liposomes and will remain in the solution (because too much detergent is still present in the solution). Alternatively, if an excess of Bio-Beads is added to the mixture, it could induce protein aggregation and precipitation (due to removing detergent to rapidly).
14. TPX capillaries are gas-permeable capillaries that allow full equilibration of the sample with either oxygen or nitrogen for accessibilities studies.
15. The number of scans, receiver gain, and sweep time are parameters that very often should be adjusted to correct for reconstituted samples with very poor signal-to-noise ratio, e.g., low amount of protein or poor efficiency of labeling.
16. The CW-EPR spectral line shape of the spin labels is very sensitive to their spatial proximity, the closest they are, the largest the changes. The CW-EPR spectrum displays a reduction in the amplitude of central resonance line as the spin labels proximity increases. In the proton-activated K^+ channel, KcsA, an increment of the intracellular proton concentration activates the channel by opening its activation gate. Spin labels attached at the position G116C faithfully track this activation process exhibiting a clear reduction of the central resonance line amplitude of the CW-EPR spectrum [2] (Fig. 4).

Acknowledgments

This work was supported in part by CMPR-TTUHSC seeding grant, American Heart Association [11SDG5440003], National Institute of Health [1RO1GM097159-01A1], and Welch Foundation [BI-1757].

References

1. Kazmier K, Claxton DP, McHaourab HS (2016) Alternating access mechanisms of LeuT-fold transporters: trailblazing towards the promised energy landscapes. Curr Opin Struct Biol 45:100–108
2. Perozo E, Cortes DM, Cuello LG (1999) Structural rearrangements underlying K+-channel activation gating. Science 285 (5424):73–78
3. Cortes DM, Cuello LG, Perozo E (2001) Molecular architecture of full-length KcsA: role of cytoplasmic domains in ion permeation and activation gating. J Gen Physiol 117 (2):165–180
4. Cuello LG, Cortes DM, Perozo E (2004) Molecular architecture of the KvAP voltage-dependent K+ channel in a lipid bilayer. Science 306(5695):491–495
5. Dalmas O et al (2010) Structural dynamics of the magnesium-bound conformation of CorA in a lipid bilayer. Structure 18(7):868–878
6. Li Q et al (2015) Resting state of the human proton channel dimer in a lipid bilayer. Proc Natl Acad Sci U S A 112(44):E5926–E5935
7. Perozo E, Kloda A, Cortes DM, Martinac B (2001) Site-directed spin-labeling analysis of reconstituted Mscl in the closed state. J Gen Physiol 118(2):193–206
8. Arrigoni C et al (2016) Unfolding of a temperature-sensitive domain controls voltage-gated channel activation. Cell 164(5):922–936
9. Dalmas O, Sompornpisut P, Bezanilla F, Perozo E (2014) Molecular mechanism of Mg2+-dependent gating in CorA. Nat Commun 5:3590
10. Dong J, Yang G, McHaourab HS (2005) Structural basis of energy transduction in the transport cycle of MsbA. Science 308 (5724):1023–1028
11. Farrens DL, Altenbach C, Yang K, Hubbell WL, Khorana HG (1996) Requirement of rigid-body motion of transmembrane helices for light activation of rhodopsin. Science 274 (5288):768–770
12. Perozo E, Cortes DM, Cuello LG (1998) Three-dimensional architecture and gating mechanism of a K+ channel studied by EPR spectroscopy. Nat Struct Biol 5(6):459–469
13. Perozo E, Cortes DM, Sompornpisut P, Kloda A, Martinac B (2002) Open channel structure of MscL and the gating mechanism of mechanosensitive channels. Nature 418 (6901):942–948
14. Perozo E, Kloda A, Cortes DM, Martinac B (2002) Physical principles underlying the transduction of bilayer deformation forces during mechanosensitive channel gating. Nat Struct Biol 9(9):696–703
15. Zhu S et al (2016) Mechanism of NMDA receptor inhibition and activation. Cell 165 (3):704–714
16. Jiang Y et al (2003) X-ray structure of a voltage-dependent K+ channel. Nature 423 (6935):33–41
17. Mchaourab HS, Steed PR, Kazmier K (2011) Toward the fourth dimension of membrane protein structure: insight into dynamics from spin-labeling EPR spectroscopy. Structure 19 (11):1549–1561
18. Hubbell WL, Gross A, Langen R, Lietzow MA (1998) Recent advances in site-directed spin labeling of proteins. Curr Opin Struct Biol 8 (5):649–656
19. Mchaourab HS, Lietzow MA, Hideg K, Hubbell WL (1996) Motion of spin-labeled side chains in T4 lysozyme, correlation with protein structure and dynamics. Biochemistry 35 (24):7692–7704
20. Tilegenova C, Vemulapally S, Cortes DM, Cuello LG (2016) An improved method for the cost-effective expression and purification of large quantities of KcsA. Protein Expr Purif 127:53–60
21. Cuello LG, Romero JG, Cortes DM, Perozo E (1998) pH-dependent gating in the Streptomyces lividans K+ channel. Biochemistry 37 (10):3229–3236
22. Heginbotham L, Lu Z, Abramson T, MacKinnon R (1994) Mutations in the K+ channel signature sequence. Biophys J 66 (4):1061–1067
23. Chung CT, Niemela SL, Miller RH (1989) One-step preparation of competent Escherichia coli: transformation and storage of bacterial cells in the same solution. Proc Natl Acad Sci U S A 86(7):2172–2175
24. Huber R, Roth S, Rahmen N, Buchs J (2011) Utilizing high-throughput experimentation to enhance specific productivity of an E.coli T7 expression system by phosphate limitation. BMC Biotechnol 11:22

Chapter 22

Ion Binding to Transport Proteins using Isothermal Titration Calorimetry

Shian Liu and Steve W. Lockless

Abstract

Isothermal titration calorimetry (ITC) is an emerging, label-free technology used to measure ligand binding to membrane proteins. This technology utilizes a titration calorimeter to measure the heat exchange upon ligands binding to proteins, the magnitude of which is based on the overall enthalpy of the reaction. In this protocol, the steps we and others use to measure ion binding to ion transport proteins are described.

Key words Isothermal titration calorimetry, Channel, Transporter, Ion binding, Equilibrium

1 Introduction

Ion transport proteins, including channels and transporters, allow the passage of specific ions (and sometimes cargo) across hydrophobic lipid membranes to perform signaling and metabolic processes. Several methods have been used to quantify the equilibrium ion preferences of these transport proteins, including X-ray crystallography [1–4], nuclear magnetic resonance (NMR) spectroscopy [5, 6], thermostability assays [7, 8], electrophysiology [9], and isothermal titration calorimetry (ITC) (see references below). Choosing an appropriate method depends on the particular properties of the protein and the availability of facilities with the appropriate equipment [10]. The advantages of ITC are that: (1) it requires no labeling of the protein since the binding signal is the enthalpy (or heat) change of the reaction, and (2) the resulting isotherm can be fit using the same chemical reaction equations that have been developed for other equilibrium assays, i.e., the fitting algorithm uses a change in signal to estimate the fraction of bound protein

Electronic supplementary material: The online version of this chapter (doi: 10.1007/978-1-4939-7362-0_22) contains supplementary material, which is available to authorized users.

Show-Ling Shyng et al. (eds.), *Potassium Channels: Methods and Protocols,* Methods in Molecular Biology, vol. 1684,
DOI 10.1007/978-1-4939-7362-0_22,

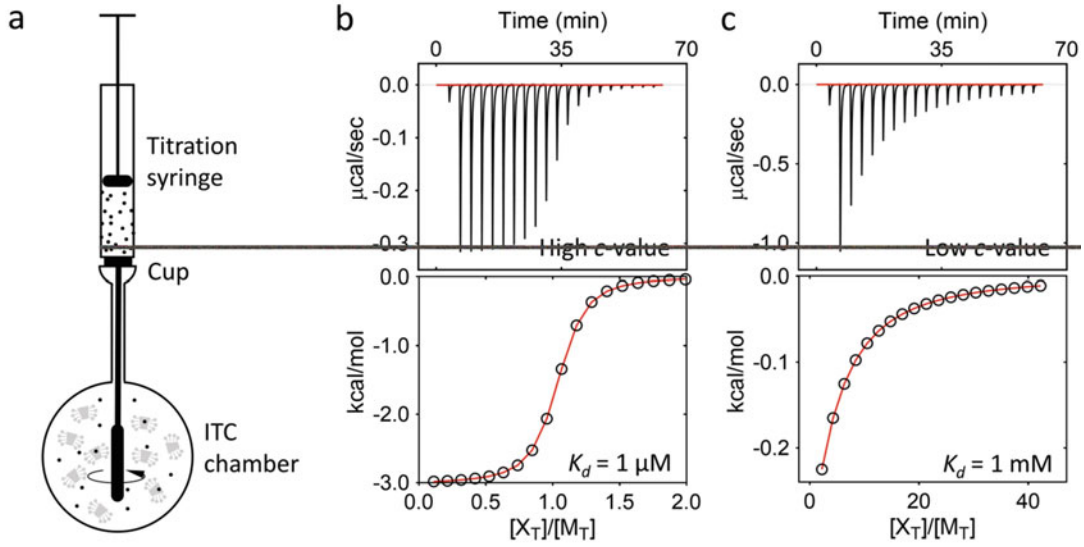

Fig. 1 Schematic of the ITC instrument and two binding regimes. (**a**) The relevant portion of the ITC instrument includes two parts, a calorimetry titration syringe filled with ligand and a thermally controlled chamber filled with the ion transport protein. During the injection, the ligand is rapidly mixed with the protein and the heat exchange is recorded in thermograms (**b**, **c**) (*top*). Integrating the heat exchange from each injection yields binding isotherms (**b**, **c**) (*bottom*) that are fit to one set-of-sites functions (Eq. 1). The two isotherms are simulated with $[M_T]$ = [protein] = 100 µM, $[X_T]$ = [ligand] = 1 mM (**b**) or 20 mM (**c**), $\Delta H = -3$ kcal/mol and $n = 1$ with the affinities indicated in the panels

given the total protein and ligand concentrations [11]. Because of these advantages, ITC has been used to measure ion binding to transport proteins in several cases, including tetrameric cation channels [12–14], Cl^-/F^- channels/transporters [15–18], and various small molecule and metal ion transporters [19–21].

The protein sample is contained within the ITC chamber that is connected to a cup that captures overflow solution during protein loading and the titration (Fig. 1a). A syringe filled with the ligand is inserted into the chamber that both injects the ligand solution and mixes the contents of the chamber during the experiment. During each injection, a small amount of ligand is rapidly mixed with the protein, from which heat is exchanged (either absorbed or released) and recorded in the resulting thermogram (Fig. 1b, c—top). The heat exchange is usually from two processes—ion binding to the protein and dilution of the concentrated ions (called the heat of dilution). Ideally, the heat of dilution is small and constant so that any change of the integrated heat between injections is the result of the desired ion binding reaction.

The integrated heat from each injection is used to generate a binding isotherm (Fig. 1b, c—bottom), that is fit, in this case, to a quadratic equation for a one set-of-sites function,

$$Q = \frac{nM_t \Delta H V_0}{2}\left[1 + \frac{X_t}{nM_t} + \frac{1}{nKM_t} - \sqrt{\left(1 + \frac{X_t}{nM_t} + \frac{1}{nKM_t}\right)^2 - \frac{4X_t}{nM_t}}\right] \quad (1)$$

where Q is the total heat, V_0 is the chamber volume, X_t is the total ligand concentration, and M_t is the total protein concentration [22]. The three fit variables are the stoichiometry of identical sites n, the association constant K, and the enthalpy ΔH. The association constant K is typically used when fitting a binding isotherm instead of its related dissociation constant K_d ($K = 1/K_d$). Both will be referred to throughout this protocol. Other functions could be applied or developed to fit more complex binding isotherms, but will not be discussed in this protocol [23–27].

When fitting a binding isotherm, the K_d falls into two regimes based on the shape of the isotherm and the variables that can be fit independently. These two regimes can be roughly differentiated by a parameter called the c-value ($c = nKM_t$). With a c-value = 5–500, a resulting sigmoidal isotherm (Fig. 1b) is sufficient to determine all three variables (n, K, and ΔH), and typically has a K_d in the low micromolar to nanomolar range. Transport proteins, especially channels, tend to fall into the second regime with a c-value <5, which produces a hyperbolic curve (Fig. 1c) and K_ds in the milli- to high micro-molar range. In this regime, there are too few constraints to fit both n and ΔH independently, so n is fixed to unity or its known value so that ΔH and K can be extracted [28, 29]. Although n and ΔH cannot be obtained from a single binding isotherm in this c-value range, they may be determined through a global, multi-temperature ITC-based fitting approach [30].

Outlined here are steps we and others use to measure ions binding to ion transport proteins, with an emphasis on low affinity interactions (the second c-value regime).

2 Materials

Base solution is the common solution that protein and ligand (ions) are solubilized in for the ITC experiments. It typically consists of 25–50 mM buffer to maintain pH (note that buffer ionization of H^+ may alter the enthalpy if H^+ are exchanged during a reaction), 100–300 mM salt for ionic strength, and detergent to solubilize the transport protein.

The machine parameters and volumes described here are for the Malvern MicroCal iTC200 machine, but the overall approach can be used with other microcalorimeters (such as the NanoITC) with similar sensitivities.

3 Methods

The first objective is to obtain evidence of ion binding to the transport protein. From this initial thermogram, the affinity and enthalpy are estimated, which is used to identify conditions (with the help of simulations) that will yield high-quality data. The sections below describe this process.

3.1 Sample Preparation for the Initial Experiment

The initial experiment is designed with an assumptive low affinity (nearly worst case) reaction,

$K_d = 0.5$ mM (or $K = 2000$ M^{-1})	lower affinities than this are extremely hard to measure unless the background signal is very small
$\Delta H = -1.0$ kcal/mol	with protein concentrations limited by solubility, this is close to the limit of detection for a binding reaction
$n = 1$	low affinity reactions cannot yield the stoichiometry, so it is set to unity

to capture evidence of binding, i.e., the heat exchange attributable to ions associating with the transport protein. Therefore, the protein and ligand concentrations suggested in this section enable the detection of binding reactions with a wide range of affinities and enthalpies.

1. The titrated ion is often used to purify and stabilize transport proteins during purification, but must be removed prior to the titration experiment. To remove these ions, purify the protein through size-exclusion chromatography (SEC) in a base solution (*see* Subheading 2) excluding the ions that will be titrated. Alternatively, dialyze the purified protein against the base solution. Exchange with base solution three to five times until the ligand concentration has dropped to sufficiently low levels.
2. The concentration of the functional protein should be near 100 μM; higher protein concentrations increase the chance of observing a signal but may reduce the overall stability of the protein. Carefully choose the filter size of the concentrator to minimize the detergent accumulation. Prepare the protein sample in a final volume of 300 μL, slightly exceeding the volume of the iTC200 chamber (~200 μL).
3. Incubate the protein sample at 25 °C for several hours to test its stability; it is critical that the protein is stable over the course of the experiment. Visually check for precipitate, and run a sample through SEC to examine its retention volume and whether it is mono-dispersed. If an ion transport protein is slowly losing its integrity when deprived of its preferred ligand, the addition of glycerol or NMG^+ may help increase its stability (*see* **Note 1**).

One could also try to stabilize the protein using a lower affinity ligand that can be displaced in a competition reaction, such as K^+ displacing Na^+ in the K^+ channel reaction (*see* Subheading 3.5) [12, 13]. Due to the small volumes, degassing protein and ligand solutions should be avoided. Instead, use the supernatant after spinning down the sample at 15,000 rcf for 10 min; this removes tiny air bubbles from the solution and any particulates.

4. Add the ion/ligand to the base solution to a final concentration of 20 mM in a volume of 200 μL. The recommended minimum volume is 100 μL for each titration, assuming a titration syringe volume of 40 μL (*see* **Note 2**).

3.2 Setup for the Initial ITC Experiment

This section describes the standard ITC setup for the initial experiment using an iTC200 machine [24]. The same overall procedure is followed during subsequent experiments, but the values of some of the user-entered parameters will be different.

1. Wash the chamber thoroughly, either manually or using the automated program that is part of the iTC200 software package. To use the automatic program, choose "Instrument Controls" tab, then select "Cell and Syringe Wash" on the right panel and follow the on-screen instructions. After the chamber is washed, remove any residual solution inside the chamber with the loading syringe. Rinse the cell three times with the base solution.
2. Fill the chamber with the protein solution, taking care not to trap air bubbles, which can generate a very noisy baseline and obscure binding signals; solutions with detergents are prone to create air bubbles (*see* **Note 3**).
3. Transfer 200 μL of the ligand solution into a PCR tube, and place the tube into the calorimeter stage.
4. Choose the "Syringe Fill" on the right panel of the "Instrument Controls" tab. Follow the instructions to complete loading of the ligand solution. After loading, select the "Purge → ReFill" function in the middle panel. Then, enter 0.2 μL in the "Distance" box and click "Dn" to shift the direction of the drive screw to prevent backlash error during the first injection [31] (*see* **Notes 4** and **5**).
5. Set the "Jacket Temperature" on the left panel of the "Instrument Controls" to 25 °C, slightly higher than the room temperature.
6. Click the "Advanced Experimental Design" tab. On the left panel, enter 20 for the "Number of injections," 25 °C for the "Cell Temperature," 10 μcal/s for the "Reference Power," 180 s for the "Initial Delay," and 1000 RPM for the "Stirring Speed." Set the "Syringe Concentration" and "Cell Concentration" according to the user's need. Set high for the

"Feedback Mode/Gain." In the "Date File Comments..." section, include the contents of the chamber and the syringe, and any other relevant experimental information to be saved in the .itc results file.

7. On the right panel labeled "Injection Parameters," click the first row of the table, which corresponds to the parameters of the first injection. Enter 0.2 μL in the "Volume" box, 180 s in the "Spacing" box and 5 s in the "Filter" box. Select the second row of the table, and then enter 2.0 μL in the "Volume" box, 180 s in the "Spacing" box and 5 s "Filter." Click "Apply To Rest" to set the parameters of subsequent injections identical to the second one. Click "Unique" to complete the setup (*see* **Note 6**).
8. Click "Start" to initiate the titration. It is advisable to observe the run to make appropriate real-time adjustments. For example, the initial 180 s spacing is typically sufficient for ligand mixing and for the calorimetric signal to relax back to the baseline before the next injection, but if not, the user can increase the spacing to a larger value and then select "Update Run Param." Many parameters can be updated this way during the experiment. The titration also can be terminated during the run if there is a noisy baseline.
9. Upon completion of the titration, examine the saturated protein through SEC to ensure that minimal changes have occurred to its retention volume and mono-dispersity.
10. Perform a ligand-into-base solution titration using identical conditions as above for the protein titration. This step is to determine whether the signal in the initial trial is primarily from the ion association rather than ion dilution/solvation.

3.3 Experimental Design: Optimization

Once evidence of ion binding is observed, it is necessary to optimize the experimental design based on newly acquired thermograms. In this section, we highlight potential issues from the initial experiment and outline some approaches to overcome them in subsequent experiments.

1. Summarized below are a few issues with the quality of the thermogram that may be encountered. It might be necessary to perform multiple rounds of optimization, because adjusting one parameter may uncover previously hidden issues in the thermogram.
   (a) The heat of dilution is large, obscuring any potential ion-binding signal. This is apparent when the peaks from the second and the last injections have similar, large magnitudes (Fig. 2a) and the ligand-into-base buffer titrations have a similarly large signal (Subheading 3.2, **step 10**).

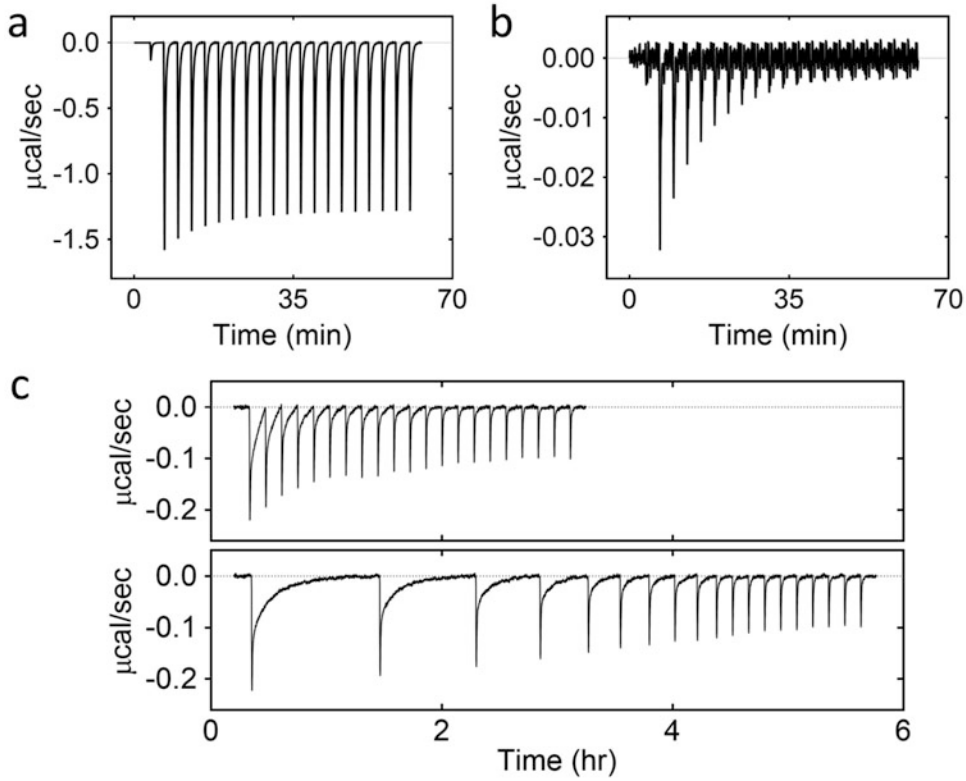

Fig. 2 Examples of problems that may be apparent from the initial experiment. The simulated thermograms assume a 1:1 stoichiometric-binding reaction. (**a**) A simulated thermogram with $K_d = 0.5$ mM and $\Delta H = -1$ kcal/mol where the heat exchange due to binding is obscured by the heat from ion dilution; note that the reaction is nearly saturated but still has a large signal. (**b**) A simulated thermogram with $K_d = 0.5$ mM and $\Delta H = -0.3$ kcal/mol to highlight the low signal-to-noise. (**c**) The thermogram of KcsA K^+ channel binding to K^+ is shown with insufficient time for the signal to return to baseline between injections (*top*) and sufficient spacing between injections (*bottom*)

Solutions: (1) Increase the protein concentration, which will increase the binding signal proportionally. (2) Use lower ligand concentrations in the syringe. If the ligands are interacting with themselves in the syringe, the large background signal could be from the enthalpy associated with breaking the ligand quasi-structure upon injecting it into the chamber. (3) Supplementing the base solution with molecules that are similar to the desired ligand but will not associate strongly with the protein. For example, use a lower affinity Na^+ ion in the base solution when measuring K^+ ion channels, or use a phosphate ion when measuring Cl^- ion channels. This approach may help suppress the solvation energy from injecting highly concentrated ligands into dilute solutions.

(b) The heat of dilution is small and the binding signal is weak (Fig. 2b).

Solutions: (1) The heat exchanged (ΔQ) is proportional to the number of protein-ion complexes formed in solution following ligand injection. Better signal-to-noise can be obtained through increasing the protein concentration, increasing the ligand concentration and/or increasing each injection volume. (2) Lowering the reference power to 5 μcal/s may help reduce noise of the baseline. (3) If ion binding is coupled with H^+ exchange, the signal could be enhanced by using a pH buffer with a different H^+-ionization enthalpy. (4) Depending on the heat capacity of the system, the enthalpy of a reaction could be increased by changing the temperature of the experiment by ±10 °C.

(c) The system is not fully re-equilibrated following an injection (Fig. 2c—top).

Solution: The spacing between injections needs to be extended if 180 s is not sufficient for the binding signal to return to the baseline. The long re-equilibration time could be from either a large heat exchange signal (requiring more time for the machine to re-equilibrate) or a slow conformational change associated with ligand binding (requiring more time for the protein conformations to re-equilibrate). In the latter case, it might be possible to also determine kinetic parameters associated with ligand binding and the coupled conformational change [32, 33] (*see* **Note 7**).

(d) The enthalpy associated with ligand binding is large such that the power during an injection drops below 0.

Solutions: (1) If the large signal is from ligand binding (and not a large heat of dilution), then the protein concentration should be lowered (two to tenfold). (2) The reference power could be increased.

(e) There is significant background noise or random spikes in the thermogram.
Solution: This is indicative of unstable protein, trapped air bubbles or a dirty chamber or syringe. Solutions to the first two potential sources are discussed in Subheading 3.1, **step 3** and 3.2, **step 2**, respectively. A base solution-base solution (or water-water) control is suggested before each new set of experiments to ensure that the ITC chamber and syringe are clean.

2. Integrate the thermogram and perform an analysis of the binding isotherm to estimate K and ΔH (*see* Subheading 3.4). Even when the issues described above exist in the thermogram, the estimates of K and ΔH could help constrain the parameters for the next experiments.

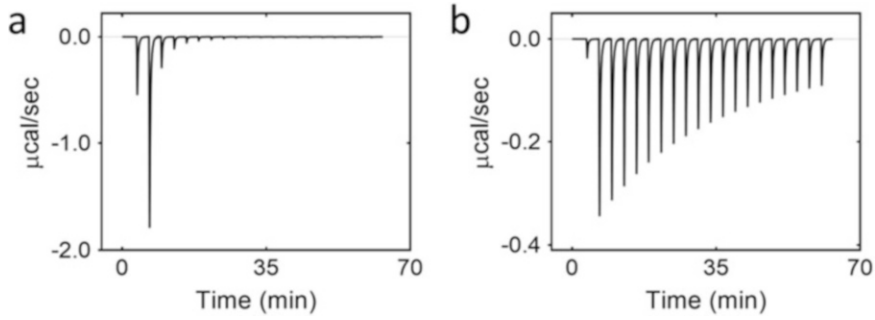

Fig. 3 Simulated thermograms with a 1:1 stoichiometry, the same $\Delta H = -1$ kcal/mol but different affinities. The higher affinity reaction ($K_d = 0.1$ mM) saturates within the first few injections (**a**), while a lower affinity reaction ($K_d = 2.5$ mM) does not saturate in the thermogram (**b**)

3. Optimize the operational parameters—protein and ligand concentrations, injection volume and spacing between injections. The goal of this step is to design an experiment where the protein is >90% saturated by the last injection. Assume K and ΔH from the fit binding isotherm of the non-optimized data are near the true values, and then design the subsequent experiment to acquire an ideal thermogram to obtain the more accurate values. Use a numeric simulation (provided in the iTC200 program or the SI Excel file) to help determine the parameters for the next experiment (*see* **Note 8**).
   Based on the initial experiment, consider the following approaches to optimize the operational parameters:
   (a) The transport protein saturates too early in the experiment, indicative of high affinity binding (Fig. 3a).
   Solution: Lower the ligand concentration and/or injection size based on the estimated K and ΔH.
   (b) The transport protein is not saturated (or nearly saturated) at the end of the experiment, indicative of low affinity binding (Fig. 3b).
   Solution: Increase the ligand concentration, taking care that the heat of dilution is not so large that it obscures the signal from ion binding.

3.4 Data Analysis

The assumption in this section is that the data can be fit to a single set-of-sites binding isotherm, where either one or multiple ions bind with the same affinities and enthalpies. In the case of more complicated binding isotherms, a different binding function would be used in **step 5** [23–27]. (See the User Manual for additional information on using Origin to fit binding isotherms, or export the data for use in other programs such as Matlab, IgorPro, or Prism.)

1. Open the Origin ITC program and click "Read Data. . ." on the left panel to select the .itc file of interest. A binding isotherm is

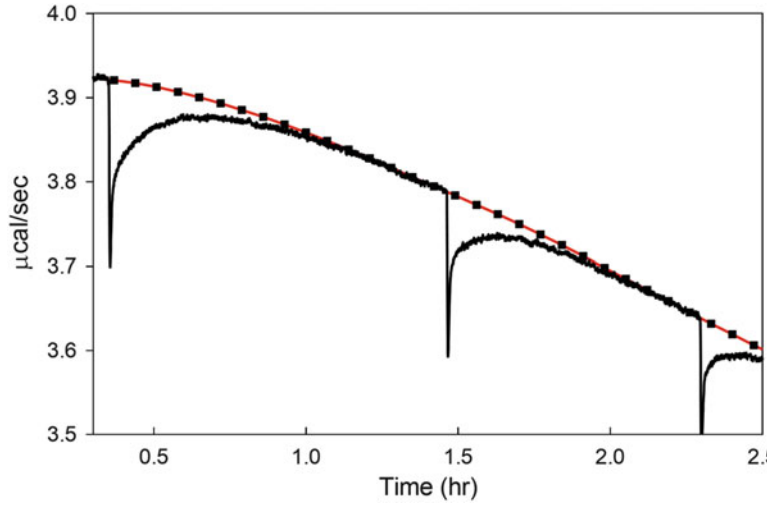

Fig. 4 A portion of the raw thermogram from KcsA channel binding to K^+ (from Fig. 2c). The DP (µcal/s) measurement of the system is shown in the *black trace*, and the curvi-linear baseline is shown as connected *red lines*

automatically calculated and displayed. Examine the isotherm and locate outlier data points for closer examination.

Open the thermogram by choosing "Window" from the top panel of the program and navigating to "RawITC" in the list. The baseline trend might be linear (with positive, negative, or zero slope) or curvilinear depending on the external temperature fluctuations in and around the machine during the ITC experiment. The Origin program automatically estimates the baseline (in red) by positioning it through the middle of the noise. However, the estimates are not always correct, which can affect the final binding isotherm. To adjust the baseline manually, select "Adjust Integrations. . ." on the left panel, and then click on the first injection of the thermogram. In the popped-out window, click the "Move Baseline Points" button to enable the adjustment. Select "Quit" to return to the full thermogram. The goal of this step is to estimate the baseline as if no injections of ligand were made into the chamber (Fig. 4).

2. Once the baseline has been adjusted, generate a new isotherm by clicking "Integrate All Peaks."
3. Click "Remove Bad Data. . ." and double-click on the first data point to delete it from the isotherm (*see* **Note 9**).
4. Click "One Set of Sites. . ." on the left panel to select the simplest binding mode. A "NonLinear Curve Fitting" window will appear where you can change the fitting parameters. Fix parameter N (n in Eq. 1) to 1 by deselecting the "Vary?" box next to it. Provide an initial estimate of K (K in Eq. 1) and H (ΔH in Eq. 1) by entering 1000 into the "K" box and −5000 into the "H"

box; once better estimates of K and H are known, those new values can be used as initial parameters. Repeatedly click the iteration buttons until the parameters converge the lowest Chi^2 value. If you find that the affinity is sufficiently high that the estimated c-value >5, then N should be fit with K and H simultaneously (*see* **Note 10**).

5. The experimental data will likely not fit the curve well near saturation because the heat of dilution is often nonzero, which is not accounted for in Eq. 1. To subtract a constant heat of dilution, choose "Math" from the top panel of the program and navigate to "SimpleMath" in the list. Enter a value in the "Y2" box, and enter either "+" or "−" for the operator to decide the direction of the subtraction. Click the "OK" button and refit the isotherm data. Repeat this procedure to search for a value that minimizes Chi^2 (*see* **Note 11**).
6. Choose "Analysis" from the top panel of the program and navigate to create a "Final Figure." The iTC200 manual provides detailed instructions to format the graph (*see* **Note 12**).

3.5 Using Competition to Shift the Measurable Range of Ion-Binding Affinities

A limitation of ITC is the narrow range of ion-binding affinities that can be obtained directly. This results from the need for enough protein in the chamber that the heat exchanged is measurable (limiting the ability to measure low nanomolar affinities) and the need to have concentrated ligands in the syringe (limiting the ability to measure millimolar affinities). A general strategy to measure a wide range of affinities with ITC is to utilize competing ligand to shift the apparent affinities of the titrated ligand [23]. For example, to measure high-affinity (e.g., nanomolar) interactions, one can shift the apparent affinity of the titrated ligand into a desirable range with a lower-affinity competing ligand [34]. The same approach can be used to measure low affinity (e.g., millimolar) interactions by calculating the shift in the apparent affinity of a measurable higher affinity ligand in the presence of the competing lower-affinity ligand in the base solution.

In cases where neither ligand's affinity (either the titrated or competing) can be measured without the presence of the other, the apparent affinity of the titrated ligand must be determined at multiple concentrations of the competing ligand; this approach was necessary to measure the K^+ affinities for tetrameric ion channels, since the channels became unstable in the absence of Na^+ or K^+ ions [13, 14]. The two affinities then can be extracted from the following relationship:

$$K_d^{app} = \frac{K_d^X\left(K_d^Y + [Y]\right)}{K_d^Y} \tag{2}$$

where X and Y are the titrated ligand and the competing ligand in the base solution, respectively, K_d^{app} is the apparent affinity of X determined from ITC, and K_d^X and K_d^Y are the dissociation constants of the higher affinity ligand X and the lower affinity competitor ligand X. This approach is also relevant when measuring two very high-affinity ligands, since the competing ligand in the base solution could be used to shift the titrated ligand into a measurable range.

3.6 Conclusion

The use of ITC to measure ion binding to transport proteins is relatively new and is rapidly developing based on the needs of the community. Advances in membrane protein purification and stabilization in different membrane mimics should lead to increased use of this technique to measure binding of ligands with a variety of chemical properties. The recognition that the heat change measured from an ITC machine is simply a proxy for ligand binding (and/or a conformational change) is leading to the import of approaches from other technologies to obtain both equilibrium and kinetic parameters from ITC thermograms.

4 Notes

1. The sample will become more viscous with glycerol or NMG^+, so the sample should be pipetted slowly.
2. It is critical to match as closely as possible the contents of the base solutions between the protein and the ligand so that the heat of dilution is minimized and constant throughout the entire titration. If the base solution ingredients are difficult to control, such as in the case of proteins in bicelles, the ligand stock can be directly diluted into the protein solution; this procedure also requires an altered data analysis that is outlined elsewhere [35].
3. To reduce the chance of trapping air bubbles, load 250–300 μL of the protein solution into the chamber, which causes a slight overflow into the cup. Slowly lift the loading syringe outward without dropping the solution level lower than the bottom of the cup, and then release the loading syringe back into the chamber. Repeat this procedure until air bubbles no longer emerge from the chamber. Gently swirling the loading syringe inside the chamber may also facilitate the removal of bubbles. Finally, remove the excess protein solution from the cup, leaving just enough protein solution to cover the entrance to the chamber.
4. One large air bubble sometimes is trapped at the top of the syringe, which can be circumvented by loading the ligand solution manually. The procedure is similar to the automatic

loading except that a 1 mL syringe and an adaptor will be used (see User's Manual).

5. The white plunger tip of the syringe gradually wears, and it can be difficult to estimate the degree of damage. Consider replacing it if the integrated heat of the second injection systematically deviates from the fit binding isotherm curve.
6. The first injection is typically not used for data analysis [31].
7. It becomes more difficult to fit the baseline when re-equilibration times exceed 10 min, so a very stable baseline throughout the experiment is critical.
8. Click the "Experimental Design" tab in the iTC200 program, and apply estimated K and ΔH to obtain an optimized experimental setup (the protein and the ligand concentrations). A sigmoidal thermogram is generated and displayed on the screen. It should be noted that the iTC200 program treats the c-value as a primary constraint to search for the optimization setup. As a result, the program will state that the reaction requires millimolar concentrations of protein, which is incompatible with reality. Instead, fix the c-value to 1. Check the new concentrations displayed on the screen. The iTC200 program may highlight the low signal strength in red as a warning, which can be ignored. Alternatively, enter K and ΔH in the attached Excel file to simulate an experiment by manually varying the protein concentration, ligand concentration, and injection size to obtain an optimal thermogram.
9. If large noise or spikes in the thermogram cause outlier data points, they probably originated from air bubbles trapped in the cell. These data points should also be discarded from the isotherm.
10. The parameter n used in the one set-of-sites binding equation is the ion-to-protein stoichiometry, assuming identical affinities and enthalpies for all sites, and is not a Hill coefficient. Cooperative ion binding, which the Hill coefficient represents, cannot be obtained from a one set-of-sites binding equation.
11. It is necessary to perform a titration to check the signal from the heat of diluting the ion ligand (called a reference titration) in the absence of the protein. If the heat of dilution signal varies in size from the first injection to the end of the titration, the user may consider performing a reference subtraction analysis. A detailed procedure can be found in the iTC200 manual that corresponds to a specific version of the Origin program. There is debate on the most appropriate way to subtract the background from ligand alone. In "ideal solutions," where protein is dilute and base solutions are identical in the chamber and syringe, one can simply subtract the ligand-into-base solution control. However, we have found that most ITC experiments

with membrane protein in detergents are far from ideal, so it is important to suppress the reference titration's magnitude and ensure the resulting injections are as constant in size as possible.

12. The values of the final thermogram and binding isotherm can be downloaded to a spreadsheet/matrix. These data can then be analyzed or graphed in other programs if desired.

Acknowledgment

This work was supported by The Welch Foundation grant A-1742 and Texas A&M Startup Funds to S.W.L.

References

1. Zhou Y, MacKinnon R (2003) The occupancy of ions in the K+ selectivity filter: charge balance and coupling of ion binding to a protein conformational change underlie high conduction rates. J Mol Biol 333(5):965–975
2. Alam A, Jiang Y (2009) Structural analysis of ion selectivity in the NaK channel. Nat Struct Mol Biol 16(1):35–41
3. Ye S, Li Y, Jiang Y (2010) Novel insights into K+ selectivity from high-resolution structures of an open K+ channel pore. Nat Struct Mol Biol 17(8):1019–1023
4. Sauer DB et al (2013) Sodium and potassium competition in potassium-selective and non-selective channels. Nat Commun 4:2721
5. Bhate MP et al (2010) Conformational dynamics in the selectivity filter of KcsA in response to potassium ion concentration. J Mol Biol 401 (2):155–166
6. Ader C et al (2009) Coupling of activation and inactivation gate in a K+-channel: potassium and ligand sensitivity. EMBO J 28 (18):2825–2834
7. Krishnan MN et al (2005) Functional role and affinity of inorganic cations in stabilizing the tetrameric structure of the KcsA K+ channel. J Gen Physiol 126(3):271–283
8. Renart ML et al (2006) Effects of conducting and blocking ions on the structure and stability of the potassium channel KcsA. J Biol Chem 281(40):29905–29915
9. Neyton J, Miller C (1988) Potassium blocks barium permeation through a calcium-activated potassium channel. J Gen Physiol 92 (5):549–567
10. Williams M, Daviter T (eds) (2013) Protein-ligand interactions. Humana Press, Totowa, NJ
11. Cantor CR, Schimmel PR (1980) Biophysical chemistry. W.H. Freeman and Company, New York, NY
12. Lockless SW, Zhou M, MacKinnon R (2007) Structural and thermodynamic properties of selective ion binding in a K+ channel. PLoS Biol 5(5):e121
13. Liu S, Bian X, Lockless SW (2012) Preferential binding of K+ ions in the selectivity filter at equilibrium explains high selectivity of K+ channels. J Gen Physiol 140(6):671–679
14. Liu S, Lockless SW (2013) Equilibrium selectivity alone does not create K+-selective ion conduction in K+ channels. Nat Commun 4:2746
15. Picollo A et al (2009) Basis of substrate binding and conservation of selectivity in the CLC family of channels and transporters. Nat Struct Mol Biol 16(12):1294–1301
16. Lim HH, Stockbridge RB, Miller C (2013) Fluoride-dependent interruption of the transport cycle of a CLC Cl-/H+ antiporter. Nat Chem Biol 9(11):721–725
17. Picollo A et al (2012) Synergistic substrate binding determines the stoichiometry of transport of a prokaryotic H(+)/Cl(-) exchanger. Nat Struct Mol Biol 19(5):525–531. S1
18. Brammer AE, Stockbridge RB, Miller C (2014) F-/Cl- selectivity in CLCF-type F-/H+ antiporters. J Gen Physiol 144 (2):129–136
19. Reyes N, Oh S, Boudker O (2013) Binding thermodynamics of a glutamate transporter homolog. Nat Struct Mol Biol 20(5):634–640
20. Ehrnstorfer IA et al (2014) Crystal structure of a SLC11 (NRAMP) transporter reveals the

basis for transition-metal ion transport. Nat Struct Mol Biol 21(11):990–996

21. Piscitelli CL, Krishnamurthy H, Gouaux E (2010) Neurotransmitter/sodium symporter orthologue LeuT has a single high-affinity substrate site. Nature 468(7327):1129–1132
22. Wiseman T et al (1989) Rapid measurement of binding constants and heats of binding using a new titration calorimeter. Anal Biochem 179 (1):131–137
23. Sigurskjold BW (2000) Exact analysis of competition ligand binding by displacement isothermal titration calorimetry. Anal Biochem 277(2):260–266
24. Malvern (2014) MicroCal iTC200 system user manual. Malvern, Malvern
25. Freiburger LA, Auclair K, Mittermaier AK (2009) Elucidating protein binding mechanisms by variable-c ITC. ChemBioChem 10 (18):2871–2873
26. Freire E, Schon A, Velazquez-Campoy A (2009) Isothermal titration calorimetry: general formalism using binding polynomials. Methods Enzymol 455:127–155
27. Heerklotz HH, Binder H, Epand RM (1999) A "release" protocol for isothermal titration calorimetry. Biophys J 76(5):2606–2613
28. Turnbull WB, Daranas AH (2003) On the value of c: can low affinity systems be studied by isothermal titration calorimetry? J Am Chem Soc 125(48):14859–14866
29. Tellinghuisen J (2008) Isothermal titration calorimetry at very low c. Anal Biochem 373 (2):395–397
30. Tellinghuisen J (2016) Analysis of multitemperature isothermal titration calorimetry data at very low c: global beats van't Hoff. Anal Biochem 513:43–46
31. Mizoue LS, Tellinghuisen J (2004) The role of backlash in the "first injection anomaly" in isothermal titration calorimetry. Anal Biochem 326(1):125–127
32. Egawa T et al (2007) Method for determination of association and dissociation rate constants of reversible bimolecular reactions by isothermal titration calorimeters. Anal Chem 79(7):2972–2978
33. Burnouf D et al (2012) kinITC: a new method for obtaining joint thermodynamic and kinetic data by isothermal titration calorimetry. J Am Chem Soc 134(1):559–565
34. Velazquez-Campoy A, Freire E (2006) Isothermal titration calorimetry to determine association constants for high-affinity ligands. Nat Protoc 1(1):186–191
35. Bian X, Lockless SW (2016) Preparation to minimize buffer mismatch in isothermal titration calorimetry experiments. Anal Chem 88 (10):5549–5553

Chapter 23

Building Atomic Models of the Ion Channels Based on Low Resolution Electron Microscopy Maps and Homology Modeling

Valery Novoseletsky, Olfat A. Malak, Gildas Loussouarn, and Olga S. Sokolova

Abstract

Voltage-gated potassium channels play pivotal roles in excitable and non-excitable cells. For many decades, structural properties and molecular mechanisms of these channels were inferred from functional observations. At the turn of the twenty-first century, structural biology revealed major aspects in the structural basis of ion channel organization, permeation, and gating. Among the available tools, homology modeling associated with low resolution microscopy helps in delineating the different structural elements of voltage-gated channels. Here, we describe in detail the methodology of homology modeling, using the 3D structure of the Kv2.1ΔCTA ion channel as a reference.

Key words Kv2.1 ion channel, Structure, Single-particle electron microscopy, Modeling, Homology

1 Introduction

Voltage-gated potassium channels (Kv) are ubiquitous proteins and, in excitable cells, they are responsible for the repolarization phases of the action potential [1]. They are synthesized on the rough endoplasmic reticulum and targeted to appropriate sites in the plasma membrane where they allow passage of potassium ions regulated by membrane voltage [2]. Kv channels encoded by ~40 genes belong to the largest and most complex potassium channel superfamily [3], which is divided into 12 subfamilies (Kv1-Kv12) [4, 5]. These channels perform a prominent function in cardiac muscle contraction by controlling repolarization duration and frequency of the action potential (e.g., in human, Kv4.3, Kv7.1, and Kv11.1) [6, 7]. They also play a major role in neuronal excitability (e.g., Kv2.1) [8, 9], insulin secretion (Kv2.1) [10, 11], neurotransmitter release, epithelial K^+ transport (Kv7.1 and associated auxiliary subunits) [12–14]. In addition, some Kv channels are essential

Show-Ling Shyng et al. (eds.), *Potassium Channels: Methods and Protocols,* Methods in Molecular Biology, vol. 1684,
DOI 10.1007/978-1-4939-7362-0_23,

to control cell proliferation (e.g., Kv1.1 and Kv11.1) [15, 16], differentiation (Kv3.3 and Kv2.1) [17], and apoptosis (Kv1.3 and Kv1.5) [18–20]. Of note, several Kv channels are targets of therapeutic agents, for instance the antiarrhythmic agent dofetilide is a blocker of Kv11.1 [21].

Prior to any 3D structural data of voltage-gated ion channels by X-ray crystallography or cryo-electron microscopy (cryo-EM) techniques, functional approaches already suggested fundamental molecular properties of voltage-gated channels. In 1952, the two biophysicists Alan Hodgkin and Andrew Huxley were awarded the Nobel Prize for their studies on the conductance properties of voltage-gated ion channels and the role of these channels in action potential generation. In these studies, they proposed that Kv and Nav channels contain charged particles within the bilayer membrane, which allow the channel to switch between activated and deactivated/inactivated states in response to changes in the membrane voltage. Thereafter, the advent of DNA sequencing gave the first glimpse of channel organization, through the amino-acids sequence and secondary structure prediction [22]. Kv channels are tetramers of α-subunits, each of them consisting of six transmembrane segments, S1–S6. The voltage-sensing domain (VSD) contains the S1–S4 segments, while the pore domain (PD), also named the ion-selective pore, is formed by the S5–S6 segments. The S4 segment carries positively charged amino-acids (Arginine and Lysine), which underlie its voltage sensitivity allowing for the opening of the Kv channel activation gate upon depolarization, as hypothesized by Hodgkin and Huxley [1, 23, 24].

Furthermore, early knowledge of the relationship between voltage-gated ion channel structure and function was obtained through many studies named “structure-function,” which could have been named more properly as “mutation-function” studies. In these studies, a huge number of mutations (some of them identified in patients) were characterized by electrophysiological methods in Kv and other channels [25, 26]. The mutations identified in patients cause ion-channel-related diseases named channelopathies and target skeletal muscles (e.g., hypokalemic and hyperkalemic periodic paralysis), the brain (e.g., epilepsy, ataxia, and migraine), and the heart (e.g., Long QT syndrome) [26, 27]. Thus, the methods used in “structure-function” studies, such as directed mutagenesis, patch-clamp (Erwin Neher and Bert Sakmann, Nobel Prize 1991) [28], and cell biology methods (Western blot, biotinylation, and immunofluorescence assays), were crucial to shed light on many functions and molecular mechanisms of Kv channels. Therefore, the deduced molecular bases of conductance, potassium selectivity, activation/inactivation gating, and channel block gave us a framework for the physiological organization of Kv channels, but without a precise structure.

The conversion from hypothetical schemes to a more precise structure was started with the first crystal structure of the bacterial potassium channel "KcsA," determined by Roderick Mackinnon and his team in 1998 (Nobel Prize in Chemistry 2003) [29]. The structure of KcsA channels, whose sequence was homologous to the pore domain of Kv channels, gave valuable insights into this structure, and in particular the selectivity filter. A few years later, the same team determined the crystal structure of another bacterial potassium channel, MthK, in the open conformation [30]. The comparison between the KcsA crystal structure in the closed conformation and the MthK crystal structure in the open conformation leds to a molecular mechanism underlying Kv channel gating [31]. Despite the technical difficulties, the first structure of the eukaryotic voltage-gated channel structure, rat Kv1.2, was determined by the X-ray crystallography approach in 2005 [32, 33].

X-ray crystal structures clarified the processes underlying potassium selectivity and voltage-dependent gating of Kv channels at atomic resolution. However, they present the structure of the channel only in one conformation, they do not show dynamic views of Kv channel gating. Furthermore, for other voltage-gated channels, such as Nav and Cav, which present a very long amino-acid sequence and also heavy glycosylation, structural elucidation by X-ray crystallography was not amenable [34]. Of note, the isolation and purification of the channel samples in large enough quantities was the main impediment for X-ray crystallography, which needs a large amount of materials to optimize the crystallization condition.

A few years after the X-ray crystallography revolution, the cryo-electron microscopy (cryo-EM) technique became crucial in high-resolution structure determination of macromolecules, such as voltage-gated channels and other proteins. In contrast to X-ray crystallography, only a small amount of materials is required to yield a high-resolution structure by cryo-EM method. Noteworthy, the biological samples used in cryo-EM are made directly by fast freezing in liquid nitrogen, which keeps the macromolecules in their soluble state. By contrast, X-ray crystallography specimens are packed in the crystal lattice. Therefore, this difference between samples preparation methods gives cryo-EM the advantage of revealing the high-resolution structure in a more close-to-native state, than X-ray crystallography [35, 36]. Furthermore, by cryo-EM, up to hundreds of thousands of single-particle cryo-EM images can be obtained from one type of macromolecule. Thereafter, using advanced software to analyze all these single-particle cryo-EM images enables the generation of 3D structures (3D cryo-EM maps) [36]. Moreover, these images can be regrouped in different classes corresponding to different conformations, allowing a first glimpse of the channel dynamics [37].

In 2008, using single-particle electron microscopy, the 3D structure of one of the Kv channels, Kv2.1, which is widely

expressed in the central nervous system, was determined at 25 Å resolution [38]. The closest channel crystal structure(Kv1.2) [32] has been fitted to the 3D EM map of Kv2.1 for interpretation. It suggested that Kv2.1 channel structure presents a closed conformation, the same as KcsA [38]. Using single-particle EM on Kv2.1 channels lacking various parts of the C-terminus, we later showed that the C-terminus is formed by two distinct domains. In addition, using homology modeling with Kv1.2 channels as a template, and subsequent molecular dynamics simulation (MDS) we obtained data suggesting that C-terminal truncation favors the open-state of the channel [39]. Here, we aim to describe in detail the methodology of homology modeling, using the abovementioned Kv2.1 3D structure as a reference [39]. We are going to start with a general approach, and at the end of each paragraph we will illustrate it using our own data.

2 Materials

2.1 EM Maps

The EM map for this study was obtained by single-particle reconstruction of the recombinant rat Kv2.1 channel, lacking residues 741 through 853 (Kv2.1ΔCTA), as we described previously [39]. The residues removed were predicted to form the cytoplasmic domain (CTA) [40].

Briefly, the Kv2.1ΔCTA channel was expressed in COS7 cells, purified to homogeneity using affinity chromatography, and the purified channel protein was applied to a carbon-coated glow-discharged copper grid. Images were taken in an electron microscope Tecnai G12 (FEI) at low dose conditions (10–20 e/Å^2), single-channel images were selected manually and combined with each other to obtain one large image stack, which contains more than 5000 single-channel images in random orientations. Images were then band-pass filtered, aligned to each other, and classified into several classes, each of which contains images in one orientation. Several iterations of image processing revealed strong classes, which were used to obtain a 3D reconstruction (Fig. 1a, b). The threshold for visualization of the reconstruction was chosen based on an average protein density of 810 Da/nm^3 [41] and volume corresponding to ~420 kDa for Kv2.1ΔCTA (Fig. 1a).

Alternative reconstruction strategies are also possible, based on the nature of the sample of interest (e.g., crystalline or a homogeneous preparation of isolated macromolecules). Depending on the software used for reconstruction, the user will obtain maps in a variety of different formats [e.g., SPIDER [42], MRC [43], IMAGIC [44], or RELION [45]]. These formats may be interconverted using em2em, which is a free component of the IMAGIC software [44]. We have used the MRC format in our study.

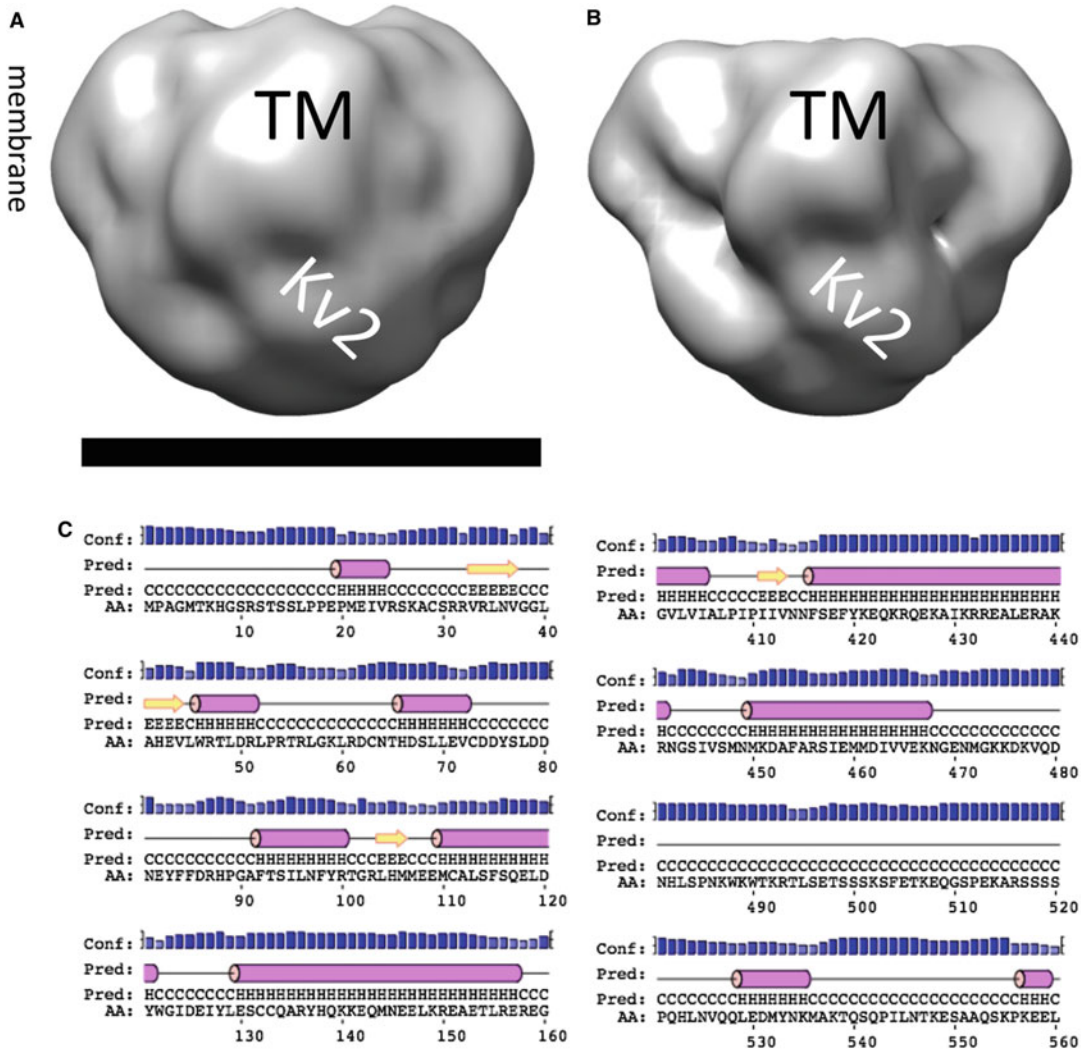

Fig. 1 Kv2.1 ion channel structure. (**a**) 3D structure of Kv2.1ΔCTA tetramer, obtained by single-particle EM, and visualized with UCSF Chimera. The threshold of the reconstruction is set to the volume corresponding to ~420 kDa. (**b**) The same reconstruction, with a larger threshold imposed, making the domain structure of the channel tetramer clearly visible. This threshold corresponds to ~300 kDa. *TM* transmembrane domain, *Kv2* predictable location of the cytoplasmic Kv2 domain. Bar—10 nm. (**c**) Secondary elements prediction for Kv2.1 in *PSIPRED*. *Left*—N-terminal residues (1–160). *Right*—residues 401–560 that include part of the C-terminus. *Blue bars*—confidence of prediction; *magenta cylinder*—helix prediction, *yellow arrow*—strand prediction

2.2 Atomic Structures

Crystallographic or NMR structures of homologous proteins and/or fragments may be obtained in the PDB format from the *Protein Data Bank* (http://www.rcsb.org) [46], which is maintained by the Research Consortium for Structural Bioinformatics (RCSB). For the structures used in this study, the reader may refer to Subheading 3.1, **step b**.

2.3 Sequence Analysis Software

In this study, search of homologous ion channels and fragments has been performed using the *Uniprot* database [47] and PDB, as well as the *FASTA* web-service [48]. Multiple alignment was performed with the help of the *Clustal-Omega* web-service [49]. One must pay close attention to available parameters of implemented algorithms (substitution matrices, number of iterations, etc.) to get the most reliable results. Other web or local software with similar functionality could be used, including BLAST [50] for search and T-Coffee [51] or UGENE [52] for sequence alignment. It should be borne in mind that various software may produce different alignments, which is especially important in case of low identity of target and template sequences.

2.4 Modeling Software

Structural models can be generated in *Modeller* [53]. This program input requires the X-ray or NMR structure (the template) and a sequence alignment of the target molecule with template. The output of this program will be our new model. Several templates could be used simultaneously for improved model quality in overlapping regions, allowing assembly of the final model from complementary templates. In this case, templates should be superimposed.

Any other software with a similar functionality could be used. Web-services such as SWISS MODEL [54], I-TASSER [55], and *Modweb* (http://modbase.compbio.ucsf.edu/modweb/) are also available.

2.5 Visualization Software

To display EM maps and the atomic models, we have used UCSF Chimera [56], but PyMol (Schrödinger, LLC), Coot [57], or O [58] may be used for this purpose as well.

2.6 Computer Workstations

Modeling and fitting were carried out on Linux workstations running 4 Intel Core i5-3340 cpus (3 GHz) with 16 Gb RAM. Using this hardware, homology modeling of Kv2.1ΔCTA (residues 30–470) took ~2 min.

3 Methods

The process of fitting an atomic model into an electron density map was discussed elsewhere [59–61]. Generally, if there is at least one structure with significant homology to the target protein, it can be used as a template for homology modeling. As for Kv ion channels, there is sometimes no structure with significant homology to the entire target channel amino acid sequence, so one needs to use several templates for different regions of the amino acid chain. The potassium channel's pore domain is the most conservative region in the sequence and thus can be modeled rather easily. In some cases, the structure of cytoplasmic domains has already been determined by X-ray crystallography [62–64], yet it remains unclear how to

combine several domains to build the whole channel. Moreover, for some regions (mainly N- and C-termini) neither templates nor any other hints for guessing the structure can be found. Modeling of such regions could employ various methods (e.g., ab initio modeling) that are beyond the scope of this chapter. For the structured part of the channel protein the recommended steps are: (1) First, the domain organization of the channel must be clarified and possible template structures for every domain must be chosen. (2) Next, the sequence alignment must be constructed for the template structures and, if possible, for every domain of the target channel. In the case of weak homology, it is strongly recommended to use multiple alignment and to also add several homologous sequences for better identification of conservative regions (e.g., helices). (3) Based on this sequence alignment, a structural model for the target protein can then be built. This model should fit into the corresponding EM density and/or other experimentally derived data.

3.1 How to Choose the Structures as Templates for Constructing a Homology Model

(a) First, the target channel sequence should be analyzed to clarify its domain organization and to perform secondary structure prediction (Fig. 1c). Domain organization could be obtained from the *Uniprot* protein page, which lists all the available links on it [CATH [65], *Pfam* [66] etc.]. In addition, the structural information from recent publications should be retrieved. Secondary structure prediction could be performed using special web-services like *PSIPRED* (http://bioinf.cs.ucl.ac.uk/psipred/) [67] or *HHpred* (https://toolkit.tuebingen.mpg.de/hhpred) [68]. Such predictions allow for discovering faintly related templates, thus facilitating further homology modeling.

Next, the target protein sequence is used to search for homologs using FASTA or BLAST with default parameters over the proteins deposited in PDB. If the structures of the closely homologous proteins are absent, as was the case for the cytoplasmic domain of Kv2.1, it is recommended to use proteins with less homology as templates for modeling. The main parameter for this choice is the similarity between the template sequence and the corresponding region of the target sequence. Normally, several templates of sufficient similarity are enough for further processing. Conformation of templates is also important, but could be considered later.

(b) In this study, to build a model of Kv2.1ΔCTA, we chose the following templates (Fig. 2): Kv1.2-2.1 chimera channel [pdb-code 2R9R [33]] for residues 30–424, for the N-terminal fragment (30–140)—tetramerization (T1) domain from Kv4.3 channel [pdb-code 2I2R [63]] and homologous tetramerization domain from Kv3.1 channel [pdb-code 3KVT

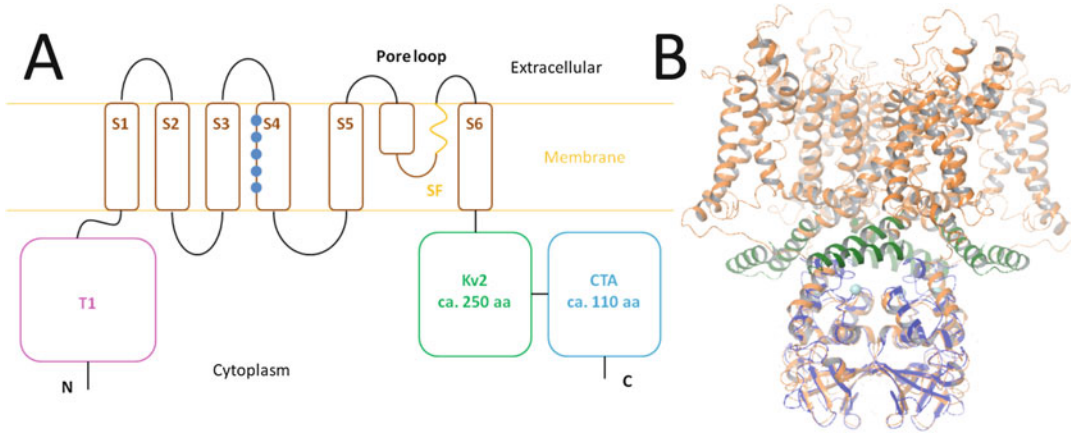

Fig. 2 Building the model of the Kv2.1ΔCTA channel. (**a**) Membrane topology of the Kv2.1 channel with predictable domain composition. (**b**) Template structures of the Kv1.2-2.1 channel (pdb-codes 2R9R) (*orange*), a homologous tetramerization domain from the Kv3.1 channel (pdb-code 3KVT), and a segment of cyclic nucleotide-gated channel 2 (pdb-code 1Q5O) (*green*) superposed with 2R9R. Templates 2I2R and 3UKV are not shown for clarity. Zinc atoms are shown in *cyan*

[64]]. For cytoplasmic residues (425–470)—a segment of cyclic nucleotide-gated channel 2 [pdb-code 1Q5O [69]] and carboxy-terminal region of a KCNH channel [pdb-code 3UKV [70]] were used. The resolution of these structural templates was acceptable (2.0–3.35 Å). N- and C-termini (1–30, 471–858) were analyzed with *PSIPRED*, predicted to be disordered, and thus impossible to model. This does not mean that the C-terminal region is truly disordered, since other methods (single particle EM) demonstrated the existence of extra-densities on the sides and underneath the N-terminal T1 domain [38, 39]. Our lack of success only means that the Kv2.1 cytoplasmic termini structure is unpredictable with the software used in this study.

3.2 Aligning of Template Sequences with the Target Protein

(a) Template sequences should be obtained from PDB. Of note, correct alignment is a key requirement for accurate model building. To obtain such alignment it is recommended to use additional related sequences and perform accurate detection of conservative residues and patterns. They may be downloaded from the protein sequence *UniProt* database. Various programs, such as *Clustal* or *T-coffee*, could be used to prepare the alignment. In general, the default parameters could be used, but, in case of low homology, the number of iterations (if applicable) should be increased.

(b) In this study we used the Kv1.2-Kv2.1 chimera channel structure (2R9R) as a master template. Overall, the identity between the Kv2.1ΔCTA sequence and this template is about 50%, but it varies, with 20% in T1 cytoplasmic domain,

Fig. 3 Multiple sequence alignment of segments of target Kv2.1 channel (sequence in *black*) with templates. Identities with target sequence are marked with *stars*. Secondary structure (prediction with *PSIPRED* for target and actual data for templates) denoted as background: *pink* for helices and *yellow* for beta-strands. H. . .CC zinc-binding motif is marked with *diamonds*. The part of the predictable Kv2 cytoplasmic domain is marked with a *frame*

30% in the beginning of voltage sensing domain (helices S1–S3a), near 100% in the S3b and S4 helices of VSD (due to chimeric nature of the template) and near 60% in the pore domain (helices S5-P-S6). Templates 2I2R and 3KVT with a 30% identity to Kv2.1 T1 domain were added for this reason. In addition, both templates possess a zinc atom coordinated with a conservative H. . .CC motif (Fig. 3a, b). The same motif is present in the Kv1.2 sequence, but absent from the 2R9R template. Despite its structural and functional similarity, the VSD is a highly variable region in voltage-gated channels [71] and, in some cases, correct sequence alignment cannot be obtained automatically, but only manually with the aid of preliminary structural alignment of several templates. This is not the case for Kv2.1, but is true for other Kv channels, like Kv10.2.

Meanwhile, there is low identity between the last segment (425–470 aa) of the Kv2.1 target sequence and the corresponding templates 1Q5O and 3UKV (near 15%). Nevertheless, it is possible to use these templates, because *PSIPRED* predicts two α-helices in this segment and all relative templates have the same secondary and tertiary structure (Fig. 3c).

3.3 Building of the Homology Model

(a) To build a homology model, the *Modeller* software [53] can be used. For Kv ion channels it is important that the C4 symmetry should be imposed on the template structures; otherwise, steric clashes between monomers could arise. When *Modeller* completes the task, we will obtain a pseudo-atomic model of the target protein with a corresponding sequence and fold-like template(s). Using several slightly different models is highly recommended to explore the conformational flexibility of loops between secondary structure elements. Additionally, software such as *Maestro* [72], *UCSF Chimera* etc. allow manual sculpturing of the loops. The alternative is to use the *Modeller Web server* (MODWEB) (https://modbase.compbio.ucsf.edu/modweb/), I-Tasser (http://zhanglab.ccmb.med.umich.edu/I-TASSER/), or SWISS-MODEL (https://swissmodel.expasy.org), which only require the target channel sequence, while the alignment, template search, and model building are performed automatically.

The final model needs to be verified. First, it should be visualized using suitable software (e.g., UCSF Chimera) and visually inspected. Special attention should be paid to regions of low homology to the template molecule. It is very likely that further changing of their local orientation or conformation will be necessary.

(b) In this study we used a composite template, which consists mainly of the 2R9R structure, but also of 2I2R, 3KVT, 1Q5O, and 3UKV (Fig. 2b). Note that in the intracellular helix-turn-helix motives (green helices) are oriented approximately parallel to the membrane plane.

3.4 Fitting the Final Model to the EM Map

(a) The obtained model needs to be fitted into a low-resolution EM density map. This may be performed automatically (e.g., using rigid body fitting software, like *Situs* [73]). This software allows modeling of atomic domain structures into low-resolution density maps obtained by electron microscopy, tomography, or small-angle X-ray scattering. The maximum of the correlation function between the EM map and the atomic structure demonstrates the best fit.

The fastest way to estimate the correct position of the model inside the EM map is to do it manually. In this case, one should visualize both the model and the EM map in the same software

(*UCSF Chimera* is the perfect choice), rotate and translate the first relative to the latter. Since one can shift the model only in the plane of display, it is necessary to rotate the view to obtain the correct fit. This process is rather simple. A detailed description of such operations can be found in the software manual (https://www.cgl.ucsf.edu/chimera/tutorials.html). Sometimes, it is useful to slightly vary volume threshold level of the model to reveal more or less dense regions. To facilitate or to refine manual fitting, one can use the "*Fit in Map*" function in Chimera.

In some cases, optimization of the fitting could be performed. To do this, the model can be divided into separate domains and each domain can be moved independently to obtain the best fit to the density map. Domain separation can be done either by editing the structural file in a text editor or interactively through the graphical user interface of Chimera or any similar software. Molecular dynamics could suggest possible orientations of domains relative to each other [39]. Details on the molecular dynamics flexible fitting (MDFF) method can be found elsewhere [74].

(b) After fitting our final model to the Kv2.1ΔCTA density map we found a general mismatch between the helix-turn-helix cytoplasmic motif (green in Fig. 2b) and the corresponding EM map density. To eliminate this mismatch we relocated the motif in the template and remodeled the channel. In the final model, the cytoplasmic helix-turn-helix motif is now tilted at approximately 45° relative to the membrane plane (triangles in Fig. 4b), and now fit to the extra-densities on the sides of the T1 domain, that we interpreted earlier to be parts of C-terminal Kv2 domains [39].

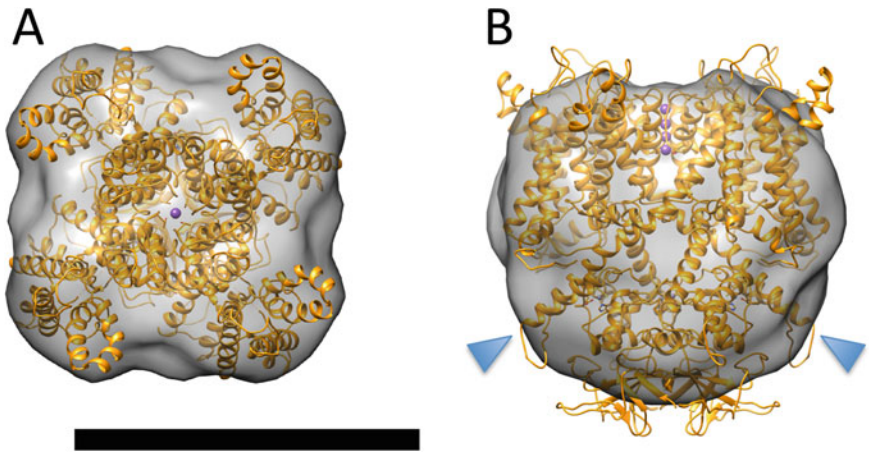

Fig. 4 Fitting of model (*golden* helixes) into the Kv2.1 ΔCTA EM map. (**a**) Top view of the channel; (**b**) Side view of the channel. *Blue arrowheads* are pointing to the cytoplasmic helix-turn-helix motif. Potassium ions shown as *purple balls*. Bar—10 nm

As a result of our interpretation, some EM densities at the bottom of the full-length channel structure [38] still remained unoccupied, because we did not find any homologous template to model the remaining C-terminal part. Further work is necessary to resolve this issue, and to build the full-length channel homology model.

4 Conclusions

Here, we described the method of obtaining a pseudo-atomic map of a Kv channel using homology modeling and subsequent fitting to the low-resolution EM maps. Another possibility of obtaining membrane proteins structures is now moving at a fast pace: solving the high-resolution structure of an ion channel using cryo-EM and direct electron detectors [75, 76]. In this case, the atomic structure may be determined directly from electron density. Recently, cryo-EM has enabled the determination of the complex structure of the calcium voltage-gated channel Cav1.1 with its auxiliary subunits at 4.2 Å resolution. The Cav1.1 complex was purified from rabbit skeletal muscle membranes, and single-particle cryo-EM was used along with other techniques, such as homology modeling, to achieve the detailed complex structure of Cav1.1 with its auxiliary subunits [34]. However, molecular mechanisms such as voltage gating and ion selectivity of Cav1.1 could not be resolved at 4.2 Å, and also many parts of the complex structure were almost invisible. One year later, the same team has improved the resolution of EM maps to 3.6 Å, showing a potential inactivated state and also allowing for more molecular details to be determined such as 16 glycosylation sites in the pore-forming and auxiliary subunits of the Cav1.1 channel [37].

This approach however strongly relies on the biochemical and molecular biology achievements in membrane protein purification, which are still under development.

In conclusion, the association between mutagenesis, electrophysiological studies, X-ray crystallography, homology modeling, molecular dynamics simulation, and single-particle cryo-EM approaches is instrumental to shed light on the underlying molecular mechanisms of potassium selectivity, gating, functions, and physio-pathological mechanisms related to Kv channels.

Acknowledgment

Olfat Malak wishes to personally thank Mrs. Line Pomaret for her generous support. The authors would like to thank Ms. Lisa Trifonova for proofreading the manuscript. This work was funded by the Kolmogorov program of the Partenariat Hubert Curien

(35503SC) for Gildas Loussouarn and Olfat Malak. Olfat Malak is a laureate of the Line Pomaret-Delalande prize of the Fondation pour la Recherche Médicale (PLP20141031304; FRM). Molecular modeling experiments were supported by the Ministry of science and education of the Russian Federation (RFMEFI61615X0044).

References

1. Hille B (2001) Ion channels of excitable membranes, 3rd edn. Great Britain, Sinauer, Sunderland, MA
2. Brueggemann LI, Gentile S, Byron KL (2013) Social networking among voltage-activated potassium channels. Prog Mol Biol Transl Sci 117:269–302
3. Jin HW, Wang XL (2002) Voltage-gated potassium channels and human neurological diseases. Sheng Li Ke Xue Jin Zhan 33(1):21–25
4. Gutman GA et al (2003) International union of pharmacology. XLI. Compendium of voltage-gated ion channels: potassium channels. Pharmacol Rev 55:583–586
5. Pischalnikova AV, Sokolova OS (2009) The domain and conformational organization in potassium voltage-gated ion channels. J Neuroimmune Pharmacol 4:71–82
6. Huo R, Sheng Y, Guo WT, Dong DL (2014) The potential role of Kv4.3 K^+ channel in heart hypertrophy. Channels (Austin) 8 (3):203–209. doi:10.4161/chan.28972
7. Charpentier F, Mérot J, Loussouarn G, Baró I (2010) Delayed rectifier K^+ currents and cardiac repolarization. J Mol Cell Cardiol 48:37–44. doi:10.1016/j.yjmcc.2009.08.005
8. Murakoshi H, Trimmer JS (1999) Identification of the Kv2.1 K^+ channel as a major component of the delayed rectifier K^+ current in rat hippocampal neurons. J Neurosci 19:1728–1735
9. Malin SA, Nerbonne JM (2002) Delayed rectifier K+ currents, I K, are encoded by Kv2 α-subunits and regulate tonic firing in mammalian sympathetic neurons. J Neurosci 22:10094–10105
10. Jacobson DA, Kuznetsov A, Lopez JP, Kash S, Ammala CE, Philipson LH (2007) Kv2.1 ablation alters glucose-induced islet electrical activity, enhancing insulin secretion. Cell Metab 6:229–235
11. MacDonald PE, Sewing S, Wang J et al (2002) Inhibition of Kv2.1 voltage-dependent K+ channels in pancreatic beta-cells enhances glucose-dependent insulin secretion. J Biol Chem 277:44938–44945
12. Preston P, Wartosch L, Günzel D, Fromm M, Kongsuphol P, Ousingsawat J, Kunzelmann K, Barhanin J, Warth R, Jentsch TJ (2010) Disruption of the K^+ channel β-subunit KCNE3 reveals an important role in intestinal and tracheal Cl^- transport. J Biol Chem 285:7165–7175
13. Abbott GW (2016) KCNE1 and KCNE3: The yin and yang of voltage-gated K^+ channel regulation. Gene 576:1–13
14. Al-Hazza A, Linley J, Aziz Q, Hunter M, Sandle G (2016) Upregulation of basolateral small conductance potassium channels (KCNQ1/KCNE3) in ulcerative colitis. Biochem Biophys Res Commun 470:473–478
15. Wu WK, Li GR, Wong HP et al (2006) Involvement of Kv1.1 and Nav1.5 in proliferation of gastric epithelial cells. J Cell Physiol 207:437–444. doi:10.1002/jcp.20576
16. Suzuki T, Takimoto K (2004) Selective expression of HERG and Kv2 channels influences proliferation of uterine cancer cells. Int J Oncol 25:153–159
17. Song MS, Choi SY, Ryu PD, Lee SY (2016) Voltage-gated K+ channel, Kv3.3 is involved in hemin-induced K562 differentiation. PLoS One 11(2):e0148633. doi:10.1371/journal.pone.0148633
18. Leanza L, Zoratti M, Gulbins E, Szabò I (2012) Induction of apoptosis in macrophages via Kv1.3 and Kv1.5 potassium channels. Curr Med Chem 19:5394–5404. doi:10.2174/092986712803833281
19. Villalonga N, Escalada A, Vicente R et al (2007) Kv1.3/Kv1.5 heteromeric channels compromise pharmacological responses in macrophages. Biochem Biophys Res Commun 352(4):913–918
20. Villalonga N, David M, Bielanska J et al (2010) Immunomodulation of voltage-dependent K+ channels in macrophages: molecular and biophysical consequences. J Gen Physiol 135 (2):135–147
21. Shenasa F, Shenasa M (2016) Dofetilide: electrophysiologic effect, efficacy, and safety in patients with cardiac arrhythmias. Card Electrophysiol Clin 8(2):423–436
22. Tempel BL, Papazian DM, Schwarz TL, Jan YN, Jan LY (1987) Sequence of a probable potassium channel component encoded at

Shaker locus of Drosophila. Science 237:770–775
23. Yellen G (1998) The moving parts of voltage-gated ion channels. Q Rev Biophys 31 (3):239–295
24. Bezanilla F (2000) The voltage sensor in voltage-dependent ion channels. Physiol Rev 80(2):555–592
25. Jentsch TJ, Hubner CA, Fuhrmann JC (2004) Ion channels: function unravelled by dysfunction. Nat Cell Biol 6:1039–1047
26. Lehmann-Horn F, Jurkat-Rott K (1999) Voltage-gated ion channels and hereditary disease. Physiol Rev 79(4):1317–1372
27. Loussouarn G, Baró I, Escande D (2006) KCNQ1 K+ channel-mediated cardiac channelopathies. Methods Mol Biol 337:167–183
28. Neher E, Sakmann B (1976) Single-channel currents recorded from membrane of denervated frog muscle fibres. Nature 260:799–802
29. Doyle DA et al (1998) The structure of the potassium channel: molecular basis of K+ conduction and selectivity. Science 280:69–77
30. Jiang Y et al (2002) Crystal structure and mechanism of a calcium-gated potassium channel. Nature 417:515–522
31. Jiang Y et al (2002) The open pore conformation of potassium channels. Nature 417:523–526
32. Long SB, Campbell EB, Mackinnon R (2005) Crystal structure of a mammalian voltage-dependent Shaker family K+ channel. Science 309:897–903
33. Long SB, Tao X, Campbell EB, MacKinnon R (2007) Atomic structure of a voltage-dependent K+ channel in a lipid membrane-like environment. Nature 450:376–382
34. Wu J et al (2015) Structure of the voltage-gated calcium channel Cav1.1 complex. Science 350:aad2395
35. Wang HW, Wang JW (2017) How cryo-electron microscopy and X-ray crystallography complement each other. Protein Sci 26 (1):32–39. doi:10.1002/pro.3022
36. Kuhlbrandt W (2014) Biochemistry. The resolution revolution. Science 343:1443–1444
37. Wu J, Yan Z, Li Z, Qian X, Lu S, Dong M et al (2016) Structure of the voltage-gated calcium channel $Ca_v1.1$ at 3.6 Å resolution. Nature 537:191–196
38. Adair B, Nunn R, Lewis S, Dukes I, Philipson L, Yeager M (2008) Single particle image reconstruction of the human, recombinant Kv2.1 channel. Biophys J 4:2106–2114
39. Grizel A, Popinako A, Kasimova MA, Stevens L, Karlova M, Moisenovich MM et al (2014) Domain structure and conformational changes in rat KV2.1 ion channel. J Neuroimmune Pharmacol 9(5):727–739
40. Ju M, Stevens L, Leadbitter E, Wray D (2003) The Roles of N- and C-terminal determinants in the activation of the Kv2.1 potassium channel. J Biol Chem 278(15):12769–12778
41. Matthews BW (1968) Solvent content of protein crystals. J Mol Biol 33:491–497
42. Frank J, Radermacher M, Penczek P, Zhu J, Li Y, Ladjadj M, Leith A (1996) SPIDER and WEB: processing and visualization of images in 3D electron microscopy and related fi elds. J Struct Biol 116:190–199
43. Crowther RA, Henderson R, Smith JM (1996) MRC image processing programs. J Struct Biol 116:9–16
44. van Heel M, Harauz G, Orlova EV, Schmidt R, Schatz M (1996) A new generation of the IMAGIC image processing system. J Struct Biol 116:17–24
45. Scheres SH (2012) RELION: implementation of a Bayesian approach to cryo-EM structure determination. J Struct Biol 180(3):519–530
46. Berman HM, Westbrook J, Feng Z, Gilliland G, Bhat TN, Weissig H, Shindyalov IN, Bourne PE (2000) The protein data bank. Nucleic Acids Res 28:235–242
47. UniProt Consortium (2015) UniProt: a hub for protein information. Nucleic Acids Res 43 (Database issue):D204–D212
48. Pearson WR (2016) Finding protein and nucleotide similarities with FASTA. Curr Protoc Bioinformatics 53:3.9.1–3.925
49. Sievers F, Wilm A, Dineen DG, Gibson TJ, Karplus K, Li W, Lopez R, McWilliam H, Remmert M, Söding J, Thompson JD, Higgins DG (2011) Fast, scalable generation of high-quality protein multiple sequence alignments using Clustal Omega. Mol Syst Biol 7:539
50. Altschul SF, Madden TL, Schaffer AA, Zhang J, Zhang Z, Miller W, Lipman DJ (1997) Gapped BLAST and PSI-BLAST: A new generation of protein database search programs. Nucleic Acids Res 25:3389–3402
51. Notredame C, Higgins DG, Heringa J (2000) T-Coffee: A novel method for fast and accurate multiple sequence alignment. J Mol Biol 302 (1):205–217
52. Okonechnikov K, Golosova O, Fursov M (2012) UGENE team. Unipro UGENE: a unified bioinformatics toolkit. Bioinformatics 28 (8):1166–1167
53. Fiser A, Sali A (2003) Modeller: generation and refinement of homology-based protein structure models. Methods Enzymol 374:461–491
54. Schwede T, Kopp J, Guex N, Peitsch MC (2003) SWISS-MODEL: an automated

protein homology-modeling server. Nucleic Acids Res 31(13):3381–3385

55. Roy A, Kucukural A, Zhang Y (2010) I-TASSER: a unified platform for automated protein structure and function prediction. Nat Protoc 5:725–738
56. Pettersen EF, Goddard TD, Huang CC, Couch GS, Greenblatt DM, Meng EC, Ferrin TE (2004) UCSF Chimera–a visualization system for exploratory research and analysis. J Comput Chem 25:1605–1612
57. Emsley P, Lohkamp B, Scott W, Cowtan K (2010) Features and development of Coot. Acta Crystallogr D Biol Crystallogr 66:486–501
58. Jones TA, Zou JY, Cowan SW, Kjeldgaard M (1991) Improved methods for building protein models in electron density maps and the location of errors in these models. Acta Crystallogr A 47:110–119
59. Fabiola F, Chapman MS (2005) Fitting of high-resolution structures into electron microscopy reconstruction images. Structure 13(3):389–400
60. Topf M, Sali A (2005) Combining electron microscopy and comparative protein structure modeling. Curr Opin Struct Biol 15 (5):578–585
61. Allen GS, Stokes DL (2013) Modeling, docking, and fitting of atomic structures to 3D maps from cryo-electron microscopy. Methods Mol Biol 955:229–241
62. Kreusch A, Pfaffinger PJ, Stevens CF, Choe S (1998) Crystal structure of the tetramerization domain of the Shaker potassium channel. Nature 392(6679):945–948
63. Pioletti M, Findeisen F, Hura GL, Minor DL Jr (2006) Three-dimensional structure of the KChIP1-Kv4.3 T1 complex reveals a cross-shaped octamer. Nat Struct Mol Biol 13:987–995
64. Bixby KA, Nanao MH, Shen NV, Kreusch A, Bellamy H, Pfaffinger PJ, Choe S (1999) Zn2+-binding and molecular determinants of tetramerization in voltage-gated K+ channels. Nat Struct Biol 6:38–43
65. Sillitoe I, Lewis TE, Cuff A, Das S, Ashford P, Dawson NL, Furnham N, Laskowski RA, Lee D, Lees JG, Lehtinen S, Studer RA, Thornton J, Orengo CA (2015) CATH: comprehensive structural and functional annotations for genome sequences. Nucleic Acids Res 43 (Database issue):D376–D381
66. Finn RD, Coggill P, Eberhardt RY, Eddy SR, Mistry J, Mitchell AL, Potter SC, Punta M, Qureshi M, Sangrador-Vegas A, Salazar GA, Tate J, Bateman A (2016) The Pfam protein families database: towards a more sustainable future: The Pfam protein families database: towards a more sustainable future. Nucleic Acids Res 44(Database Issue):D279–D285
67. Buchan DWA, Minneci F, Nugent TCO, Bryson K, Jones DT (2013) Scalable web services for the PSIPRED Protein Analysis Workbench. Nucleic Acids Res 41(W1):W340–W348
68. Söding J, Biegert A, Lupas AN (2005) The HHpred interactive server for protein homology detection and structure prediction. Nucleic Acids Res 33(Web Server issue):W244–W248
69. Zagotta WN, Olivier NB, Black KD, Young EC, Olson R, Gouaux JE (2003) Structural basis for modulation and agonist specificity of HCN pacemaker channels. Nature 425:200–205
70. Brelidze TI, Carlson AE, Sankaran B, Zagotta WN (2012) Structure of the carboxy-terminal region of a KCNH channel. Nature 481:530–533
71. Guda P, Bourne PE, Guda C (2007) Conserved motifs in voltage-sensing and pore-forming modules of voltage-gated ion channel proteins. Biochem Biophys Res Commun 352 (2):292–298
72. Laimer J, Hofer H, Fritz M, Wegenkittl S, Lackner P (2015) MAESTRO–multi agent stability prediction upon point mutations. BMC Bioinformatics 16:116. doi:10.1186/s12859-015-0548-6
73. Wriggers W (2012) Conventions and workflows for using situs. Acta Cryst D 68:344–351
74. Xu X, Yan C, Wohlhueter R, Ivanov I (2015) Integrative modeling of macromolecular assemblies from low to near-atomic resolution. Comput Struct Biotechnol J 13:492–503
75. Liao M, Cao E, Julius D, Cheng Y (2013) Structure of the TRPV1 ion channel determined by electron cryo-microscopy. Nature 504(7478):107–112
76. Tao X, Hite RK, MacKinnon R (2016) Cryo-EM structure of the open high-conductance Ca^{2+}-activated K^+ channel. Nature 541:46

Chapter 24

Studying Kv Channels Function using Computational Methods

Audrey Deyawe, Marina A. Kasimova, Lucie Delemotte, Gildas Loussouarn, and Mounir Tarek

Abstract

In recent years, molecular modeling techniques, combined with MD simulations, provided significant insights on voltage-gated (Kv) potassium channels intrinsic properties. Among the success stories are the highlight of molecular level details of the effects of mutations, the unraveling of several metastable intermediate states, and the influence of a particular lipid, PIP_2, in the stability and the modulation of Kv channel function. These computational studies offered a detailed view that could not have been reached through experimental studies alone. With the increase of cross disciplinary studies, numerous experiments provided validation of these computational results, which endows an increase in the reliability of molecular modeling for the study of Kv channels. This chapter offers a description of the main techniques used to model Kv channels at the atomistic level.

Key words Voltage-gated ion channels, Homology modeling, Molecular dynamics simulations, Transmembrane potential, Gating charge, Lipid membranes

1 Introduction

Voltage-gated ion channels play major roles in excitable tissues [1]. Consistent with that, rare diseases are directly caused by mutations in voltage-dependent ion channels expressed in the heart, skeletal muscles, and neurons, referred to as channelopathies [2–6]. Several frequent diseases, such as heart failure or myocardial infarction, may be due to the remodeling of ionic currents [7]. Both rare and frequent cardiac diseases are associated with sudden death. Thus, a better understanding of the molecular mechanisms of voltage-gated ion channels and the development of molecules that modulate their activity with high specificity and high potency may pave the way for new therapeutic strategies.

Among voltage-gated ion channels, the potassium selective ones, regrouped in the superfamily of voltage-gated K^+ (Kv) channels, are essential for membrane repolarization in excitable cells

Show-Ling Shyng et al. (eds.), *Potassium Channels: Methods and Protocols,* Methods in Molecular Biology, vol. 1684,
DOI 10.1007/978-1-4939-7362-0_24,

such as neurons and cardiomyocytes [8]. Intriguingly, one of the Kv channels, KCNQ1, is highly modulated by single-transmembrane proteins KCNEx. In cardiomyocytes, KCNE1 slows KCNQ1 activation and right-shifts the activation curve [8]. In epithelial cells, KCNE3 renders KCNQ1 voltage-independent allowing it to maintain the driving force necessary for transepithelial transport [9, 10]. These observations are among many others that illustrate the complexity of ion channel proteins and their auxiliary subunits. In face of such complexity, structural data and molecular modeling will help in understanding the impact of genetic mutations on channels function at the molecular level, and possibly designing new drugs, as pointed out by the Nobel Prize Laureate Roderick MacKinnon [11].

2 Main Discoveries Drawn from Experimental Results

2.1 Ionic Currents

One advantage that ion channel proteins display as compared to other proteins is that some of their conformations, namely Closed/Inactivated and Open conformations, can be tracked in "real time" at the timescale of milliseconds. A direct observation of such states was made possible in the 1970s by the development of the patch-clamp method by Erwin Neher and Bert Sakmann [12]. By realizing a tight seal between a glass pipette and a membrane patch from a frog muscle fiber, they could record the transitions of ion channels between conducting and nonconducting states through discrete deflections in the recorded current. At physiological range of membrane potentials, currents deflections were in the 10-picoAmpere (pA) range, amplified with an operational amplifier and observed on an oscilloscope.

2.2 Gating Currents

In the same decade, another type of current could be observed in isolated squid giant axons [13]. Such a current is not linked to the passage of ions though the conducting pore, but to conformational changes of the channel protein itself, confirming the prediction of Allan Hodgkin and Andrew Huxley that a part of the protein acts as a voltage sensor. These transient currents, named gating currents, are triggered by a change in membrane potential, and mostly linked to the movement of the positive charges of the voltage sensors (fourth transmembrane segment, S4) through the electric field [14, 15].

Gating currents, associated with all the "macroscopic" measurements of the current generated by the entire population of channels of one cell, their biophysical characteristics (kinetics, steady-state voltage dependence), as well as their single-channel characteristics (mean open time, mean closed time) provide a whole set of observable parameters. Such constraints allow one to establish mathematical models (Kinetic models) describing channel

activity through voltage- and time-dependent transitions between a small number of states such as open, closed, and inactivated [16]. Such models may be useful to better understand the effect of specific regulators/mutations/toxins on the channel conformation [17].

2.3 DNA Sequencing of Kv Channel-Related Genes

Starting from the premise that voltage-gated ion channels are evolutionarily related [1], the Shaker gene of Drosophila Melanogaster, known to code for a voltage-gated potassium channel, was first sequenced [18]. This gene appeared to code for a protein sequence containing seven predicted membrane-spanning sequences, including the fourth one that contained numerous arginine residues positioned every three amino acids. These sequences are relatively similar to the ones determined in a previously studied voltage-gated sodium channel of electric eel [19]. Particularly, the fourth sequence of Shaker gene carrying the arginines was highly similar to the S4 segments revealed in the sodium channel. However, these results, while being very promising, were not able to offer an accurate insight into potassium channels structures.

2.4 Details of Kv1.2 Channel Crystal Structure

Although it is very difficult to obtain good diffraction data from crystals of transmembrane proteins, in the early 2000s, the first 3D structure of a mammalian Kv channel, the rat Kv1.2, was resolved by X-ray crystallography [20]. The channel is composed of four identical subunits, each of them presenting six transmembrane segments (from S1 to S6). The first four segments constitute the voltage sensor domain (VSD), while the last two (S5, S6) constitute the pore domain (PD). The pore domain, homologous to the bacterial potassium channel KcsA [21], is composed of two major regions: at the extracellular side, the P-loops that bind S5 and S6 segments join each other to form the selectivity filter, which favors the permeation of K^+ ions over other cations and is defined by a strongly conserved motif, TTVGYG; at the cytosolic side, the gate is formed by the S6 segments, and endows open or closed state of the pore. Among S6 residues, a particular motif sequence, PVP, forms a slight kink on S6 helices. This motif, well conserved among few Kv channels, is essential for channel gating [22–24]. Since the diameter of the pore at the level of the tangle formed by S6 segments in the resolved Kv1.2 structure is about 12 Å, the channel has been crystallized in an open state.

The intracellular N-terminus from each subunit, that precede S1 segments, gather in an I_4 symmetry, whose center is located right under the main pore axis to form the tetramerization (T1) domain in the cytosol. Concerning the VSD, the S1–S4 segments are tightly packed together and oriented roughly perpendicular to the membrane plane. This VSD spatial organization is in agreement with previous experimental results [25, 26]: each VSD of one subunit faces the PD of an adjoining subunit. VSD and PD of

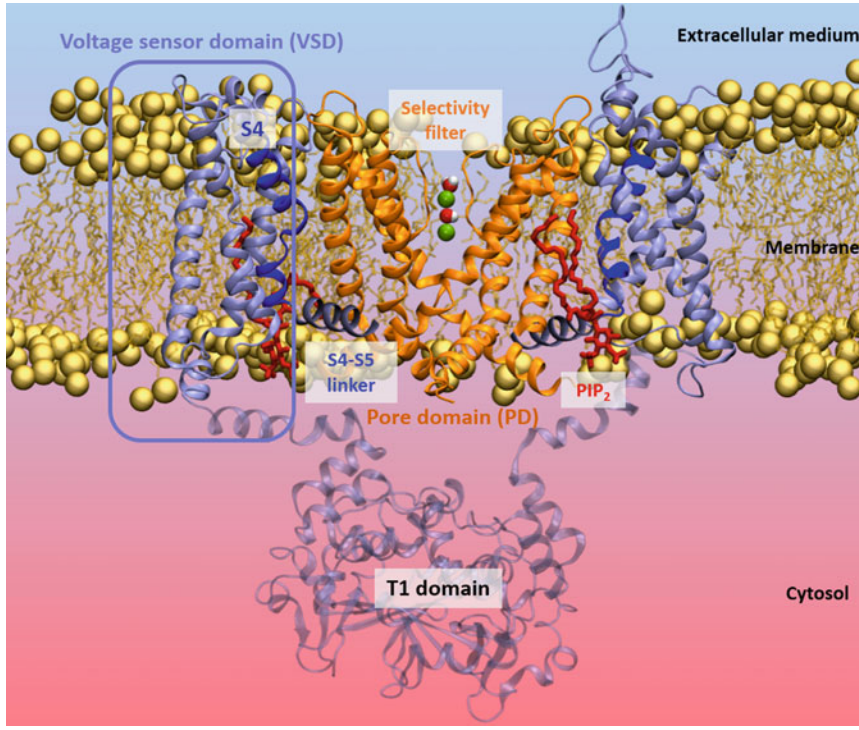

Fig. 1 X-ray structure of activated Kv1.2 channel embedded in POPC membrane. Only two subunits are shown for clarity. The domains taken into account for the model building are represented in *solid colors*. The T1 domain, generally not considered in Kv molecular models, is represented in *transparent colors*. Within the selectivity filter, potassium ions are represented by *green spheres* and water molecules are represented by *red* and *white spheres*. The solvent (extra- and intra-cellular media is not shown for clarity)

one subunit are attached by a helical amphipathic S4-S5 linker (Fig. 1).

As seen in numerous voltage-gated ion channels, the S4 segment in Kv1.2 bears six positively charged residues (R294, R297, R300, R303, K306, and R309, referred to hereafter as R1, R2, R3, R4, K5, and R6). Four negative charges, acting as countercharges for S4 positive gating charges, are distributed in the interior of the VSD (E183 on S1, E226 and E236 on S2 and D259 on S3). In the refined structure, four salt-bridges are present within the VSD: R3 interacts with E183, R4 with E226, K5 with D259, and R6 with E236. R1 and R2 both interact with lipid head groups from the upper part of the membrane. This conformation was identified as an activated state of the VSD, in agreement with the fact that the pore of the channel is open. In the Kv1.2 crystal structure, electron density is quite weak in the VSD region. The backbone was however fully resolved as TM helices while the side chains in S1 and S3 were only partially resolved. The loops connecting each segment to another are absent as well. Later, two crystal structures, the first one being a chimera of Kv1.2 structure in which the S3b/S4 paddle was

replaced by its equivalent in Kv2.1 [27], the second one being a refined structure [28], offered a better resolution of the channel structure, since conformations of missing side chains and loops were eventually resolved. In addition, these models also enabled a more precise characterization of the VSD and its salt-bridge network, allowing a stabilization of S4 helix orientation in relation to the membrane plane.

2.5 Coupling Between the Voltage Sensor Domain and the Pore Domain

In voltage-gated potassium channels, the VSD and the pore PD are coupled, and the nature of the coupling seems to vary from one channel to another. Crystallization and X-ray diffraction of a voltage-gated potassium Kv1.2 showed that "domain swapped" voltage sensors are facing the S6 helix of the neighboring subunits. This position allows the S4-S5 linker to perform mechanical work on the pore gate, and suggested a mechanical lever mechanism to explain the direct coupling between VSD and PD movements [20]. However, a recent structure of Kv10.1 channel shows that S4-S5 linkers in this channel are not domain swapped, suggesting another mechanism of voltage dependence [11]. An allosteric rather than obligatory mechanism of coupling was already suggested from functional studies on the closely related Kv11.1 channel (65% of homology in the transmembrane region) [29, 30]. Allosteric coupling may be realized through a ligand/receptor mechanism in which S4-S5 linker acts as an inhibitor, stabilizing the gate in a closed state. Upon membrane depolarization, S4 pulls S4-S5 out of its binding pocket, and the channel open probability increases. This allosteric model has been suggested for Kv7.1 [31, 32]. Noteworthy, phosphatidyl-inositol-4,5-bisphosphate (PIP_2) may also modulate the coupling between the voltage sensor and the gate [33, 34].

3 Molecular Modeling Techniques to Obtain Kv Channels 3D Structure

The availability of the Kv1.2 structure makes it feasible to construct three-dimensional (3D) models of related Kv channels previously characterized as therapeutic targets and for which high-resolution crystal structures are not available. In building atomistic structural models of Kv channels, the goal is to make the models as reliable as possible with respect to experimental results. Two main approaches that belong to the field of molecular modeling that can be used to obtain relevant Kv models will be presented in the next section.

3.1 Homology Modeling

3.1.1 Principle

Homology modeling, also known as comparative modeling, aims to build a protein structure from its primary sequence. This method starts from the premise that two proteins with similar primary sequences will display similar folds (3D structures). Since functional regions of Kv channels, including the VSD with its S4 transmembrane segment, and the PD with its selectivity filter, are

relatively well conserved, this method is particularly interesting if one wants to build a model of a Kv channel for which the structure has not yet been resolved. Hence, several 3D models of Kv7.1 channel, involved in cardiac arrhythmias, were built using homology modeling [35, 36]. Here, we will use the example of the Kv7.1 model to describe this method [37]. It is important to note that several on-line servers [38–40] allow one to perform all of the homology modeling steps automatically, using the protein sequence of interest as a query.

3.1.2 Template Selection

In order to select a template structure for a known protein sequence, one can launch search algorithms on protein sequences from the PDB, such as BLAST, or its protein-specific version, PSI-BLAST [41] in order to find the best template for a sequence of interest. Yet, if available, several templates can be used, in order to maximize the robustness of the model. In the case of Kv7.1, the refined X-ray structure of Kv1.2 [28] was directly selected as a template from the PDB, without using any of these algorithms.

3.1.3 Sequence Alignment

This step is by far the most important of the homology modeling method since the quality of the resulting model depends on that of the sequence alignment. Thus, it is necessary to evaluate the similarity between the template sequence and the query sequence. This similarity is called sequence identity, and is expressed in percentage values. Generally, the minimum sequence identity required to obtain a model of sufficient quality is ≈30%. The alignment of Kv7.1 and Kv1.2 was first conducted automatically, using ClustalW2 [42]. To obtain a multiple sequence alignment, which strengthens the confidence of the procedure, Kv7.1 sequence was aligned to Kv1.2 along with protein sequences of the four other channels from Kv7 family. For the PD, the percentage of sequence identity between Kv7.1 and Kv1.2 is 36%. For the VSD, the percentage is 19.5%. This lower sequence identity is mainly due to the S2-S3 loop, which is longer in Kv7.1 than in Kv1.2. In order to overcome this kind of discrepancy, one can refine this alignment manually and locally. Indeed, in order to maximize the sequence identity for the VSD, important residues in Kv7.1 (conserved phenylalanine residue of S2, conserved acidic residues of S2 and S3, S4 conserved basic residues) were specifically aligned with similar Kv1.2 ones, and insertions and deletions were concentrated in the loop regions. Eventually, without the S2-S3 loop, the percentage of identity was increased to 25% for the VSD.

3.1.4 Model Building and Optimization

There are several programs that are dedicated to this task, including SCRWL [43] and MODELLER [44]. The latter was used to build 50 Kv7.1 models. This software performs constrained modeling, a technique defined by the use of template coordinates and sequence alignment information as constraints for the 3D model building.

Thus, bond and non-bonded lengths, as well as angle and dihedral values of the Kv1.2 structure, are used as stereochemical constraints to build the required Kv7.1 model. S2-S3 loop has been modeled from a template 3D structure extracted from NMR data [45], which suggests a helical structure for this connecting loop. In addition, MODELLER allows one to add specific geometric restraints. For the Kv7.1 model, several constraints were applied according to site-mutagenesis results to increase its reliability with respect to experimental data. In order to adjust Kv7.1 salt-bridges patterns of the VSD with respect to experimental results [46, 47], E1 charged groups were constrained toward R1 and E2 toward R2 in resting/closed state, whereas in activated/open state, E1 was constrained toward R4. Among these 50 obtained models, the best ten were selected according to their potential energy values, calculated using the DOPE (*D*iscrete *O*ptimizing *P*rotein *E*nergy) [48] knowledge-based scoring function, implemented in MODELLER.

3.1.5 Evaluation of the Obtained Molecular Model

The most common way to evaluate the stereochemical quality of a 3D model is to verify for each residue whether its backbone torsion angle values, defined as Phi and Psi, fall in the favored areas of the Ramachandran plot. To do this on the ten best models that were previously selected, the software PROCHECK [49] was used. The models that present the highest number of torsion angles in Ramachandran's plot well favored areas (>95%), as well as the lowest number of torsion angles in the disfavored areas (<5%), were chosen to perform molecular dynamics simulations in order to study Kv7.1 function.

3.2 Ab Initio Methods

This approach aims to accurately model structurally variable regions of proteins whose sequences are still related, like the S2-S3 loop in Kv1.2 and Kv7.1 channels, in order to overcome the discrepancies arising from homology modeling. Starting with a query sequence, the 3D model is built with the combination of both secondary structure predictions and peptide fragments. These peptides are coming from a knowledge-based fragment library composed of stereochemical descriptors of structural loops extracted from protein structure databases like the PDB, with the help of specific algorithms.

The Rosetta algorithm [50] runs by browsing the query sequence and sequentially picking similar fragments of 3 or 9 amino acids, whose torsion angles of both the backbone and side chains are then corrected with the help of a Monte Carlo conformational search algorithm, prior to being energetically minimized and assembled to model the entire structure. In the online servers like ROBETTA [51], or TASSER [52], ab initio methods are combined with comparative modeling methods, which happened to create models with a stronger accuracy than models built by comparative modeling alone. The principal drawback of this

method resides in the fact that it can take a significant amount of time to build a model such as a Kv channel subunit. Nevertheless, ab initio models of activated/open and resting/closed states of Kv1.2 were built with Rosetta [53] and turned out to be in significant agreement with Kv1.2 X-ray structure.

4 Following the Evolution of Kv Channels Structure In Silico

4.1 Principle

Molecular dynamics (MD) refers to a family of computational methods aimed at simulating a macroscopic behavior through the numerical integration of the classical equations of motion of a microscopic many-body system. Macroscopic properties are expressed as functions of particle coordinates (r_1, r_2, …, r_N) and/or momenta, which are computed along a phase space trajectory generated by classical dynamics [54–56]. MD simulations require the choice of a potential energy function $U_{ri}(r_1, r_2, \ldots, r_N)$, usually referred to as a Force Field, by which the N particles interact. Those most commonly used FFs in chemistry and biophysics, e.g., GROMOS [57], CHARMM [58], and AMBER [59] and OPLS [60] are based on molecular mechanics and a classical treatment of particle-particle interactions that precludes bond dissociation and therefore the simulation of chemical reactions. They comprise a summation of bonded forces associated with chemical bonds stretching, bond angles and bond dihedrals deformation, and non-bonded forces associated with van der Waals and electrostatic interactions. The parameters associated with each term are optimized to reproduce structural and conformational changes of the macromolecular system.

The MD simulations use information (positions, velocities or momenta, and forces) at a given instant in time, t, to predict the positions and momenta at a later time, $t + \delta t$ where δt is the time step, of the order of a femtosecond, taken to be constant throughout the simulation. Numerical solutions to the equations of motion $F_i = m_i d^2 r_i / \mathrm{d}t^2 = \nabla U_{ri}(r_1, r_2, \ldots, r_N)$ are thus obtained by the iteration of this elementary step. Computer simulations are usually performed on a small number of molecules (a few tens to a few hundred thousand atoms), the system size being limited of course by the speed of execution of the programs, and the availability of computer power. In order to eliminate edge effects and to mimic a macroscopic system, simulations of condensed phase systems consider a small patch of molecules confined in a central simulation cell, and replicate the latter using periodic boundary conditions (PBCs) in the three directions of Cartesian space. For membranes hosting ion channels for instance the simulated system would correspond to a small fragment of a liposome incorporating the channel.

4.2 Modeling Kv Channels in Their Membrane Environment

In order to reproduce the behavior of Kv channels in their membrane environment, they are usually embedded in lipid bilayers (Fig. 1). To do this, two strategies are generally used. The first one consists in modeling a very large patch of lipids, prior to placing the channel structure in the middle of the patch and then removing all the lipids that are in direct contact with the protein. A second method, available in the input generator of the CHARMM-GUI interface [61], consists in aggregating lipid molecules around the protein structure [62]. Most studies use phosphatidylcholine (PC) lipids (e.g., Palmitoyl-oleylPC- or POPC) which are the most abundant lipids found in cell membranes. To describe lipids alkyl chains, the representation commonly adopted is the "united atom" one in which the methylene ($-CH_2-$) and methyl groups ($-CH_3$) are represented by a single-interaction bead.

However, if necessary, it is possible to model multi-components and more adequate lipid membranes. For instance, one might consider symmetrical or asymmetrical bilayers composed of several types of lipids, e.g., sphingomyelin (SPGM) a lipid present only in the outer leaflet of the membrane [63]. PIP_2, a phospholipid that only comprises 1% of the inner leaflet of the membrane but required for the Kv7s activation mechanism [64] has, for instance, been considered an important molecule in modeling such channels. The specificity of its binding to Kv channels being unknown, two strategies have been used so far to determine its binding sites: the first one consists of flooding the bilayer with an excess of PIP_2 lipids [37], while the second relies on experimental data to place PIP_2 lipids in proximity of the Kv channel side chains identified as potential binding sites [65].

4.3 MD Simulations

MD simulations solve differential equations by numerically integrating the equation of motions in an iterative manner with a time step δt in the order of a femtosecond ($1\ \text{fs} = 10^{-15}\ \text{s}$), to satisfy the principle of energy conservation. Ideally, as Kv channels activate on the millisecond time scale, this time range should be reached by MD simulations in order to provide a molecular insight of this mechanism. Nowadays, the time range that can be commonly reached by this technique is rather on the order of microseconds, with the exception of a few extremely rare cases [66] using for instance special purpose machines.

Generally, in MD simulations one studies the time evolution of a classical system composed of a constant number of particle N, evolving in a constant volume V. Using Newton's equations of motion, the total energy is kept constant, which enables the system to sample a micro-canonical ensemble (NVE) along the MD trajectory. Two other ensembles can be used in order to mimic the laboratory conditions, namely the isothermal-isobaric (NPT) ensemble where both temperature and pressure are controlled, or canonical ensemble (NVT) where the volume and the temperature

are kept constant [67]. An important number of programs are dedicated to perform MD simulations, including CHARMM [68], AMBER [69], GROMACS [70], NAMD [71], and Desmond [72].

In the following section, we will describe the step-by-step protocols used by us in modeling the Kv1.2 and Kv7.1 channels: The simulations are carried out at a fixed temperature of 300°K, and a fixed pressure of 1 atm. Note here that the lipid used is POPC, which has a transition temperature above 300°K, i.e., it is in its liquid crystal phase. Chemical bond lengths between hydrogens and heavy atoms were all constrained at their equilibrium values so that a time-step of 2.0 fs could be used. The system (lipid + channel) was embedded in a 150 mM KCl electrolyte bath. In our specific runs we used the CHARMM22 force-field [58], along with CMAP correction [73] and the NAMD code [71].

4.3.1 Equilibration Phase

As the lipid bilayer around the channel and water needs to equilibrate and fully solvate the protein, it is necessary to proceed with careful equilibration of the system. Starting from either a channel crystal structure or a homology model, a first MD run should be performed with all protein atoms fixed, until a constant density of the system is reached. This normally takes a few tens of nanoseconds. The constraints on the protein might then be gradually released, for instance, by a second run (of few tens of ns) with constraints on the motion of the protein backbone atoms, while allowing for the side chains to relax.

4.3.2 Production Phase

This phase constitutes strictly speaking the MD simulation. It is performed normally without constraints unless for a specific aim. For instance, the motion of the backbone atoms of the selectivity filter can be prevented, by fixing their position to avoid ion conduction. One expects the length to be in the 100 ns range to make sure the behavior of the channel is fine.

4.3.3 Applying a Transmembrane (TM) Voltage Using Local Electrostatic Potential (EP)

Kv channels are mainly present in the membranes of excitable cells and are subject to a TM voltage (defined as a difference between the electrostatic potential (EP) of the cytosol, and that of the extracellular medium). This difference is generated by a concentration gradient of several ions (Na^+, K^+, Ca^{2+}, and Cl^-) on both the sides of the membrane. In MD simulations, it is conventional to assume that the bottom bath represents the cytosol, while the top bath represents the extracellular medium. Accordingly, two water baths with appropriate (selected) ion concentrations are added to both the sides of the lipid/channel construct. In such a way, the MD simulations are carried out in an explicit solvent. The estimation of the TM potential calls for the evaluation of the difference between the EP of these two water baths. Using Poisson's equation, the EP can be estimated from the (atomic) charge density

distribution, ignoring electronic polarization. At a given position r throughout the MD trajectory of the system, the EP, denoted by φ, can be computed by solving the Poisson's equation $\nabla^2\varphi(r) = -4\pi\sum_i \rho_i(r)$ where the sum runs over all of the atoms i that bear a partial charge $p(r)$. The local electric field at a position r may be obtained as the derivative of the EP.

So far, two methods (protocols) were proposed to impose a TM voltage to a model membrane in MD simulations. The electric field method starts from the premise that a TM potential, in experiments, leads to an electric field that propagates along the axis z perpendicular to the membrane plan. In MD simulations, the implementation of this method consists in applying directly a constant normal force $F = q_i \cdot E$ [74–77] to all the atoms carrying a charge q_i, mimicking therefore the effect of the electric field E. This constant force, applied perpendicular to the membrane, induces a rearrangement of the molecules (polarizes mainly water molecules) which in turn creates a transmembrane voltage. Note that in experiments, a voltage difference driven by an electric field is equal to $\Delta V = E \cdot d$, d being the thickness of the membrane. Using Periodic Boundary conditions in membranes simulations modifies the expression of ΔV. Indeed, in such setups, the latter depends on L_z, the simulation box length along z [78–80] and expresses as $\Delta V = E \cdot L_z$. The electric field method was applied to polarize or depolarize membranes embedding Kv channels [81–83], and to study ion conduction [84].

The second protocol, using a charge imbalance, aims to mimic the conditions of patch clamp experiments in MD simulations. Indeed, the experimental technique consists in inserting electrodes on both the sides of the membrane to deliver a voltage pulse sufficiently long (milliseconds) over the membrane charging time to generate a charge imbalance. In order to induce this charge imbalance in the MD system, a method that consists of using a single bilayer, surrounded by two independent electrolyte baths, each delineated by an air/water interface was developed [86]. These interfaces prevent any ion migration from one PBC image to another [87], and therefore maintain the imposed charge imbalance between the electrolyte baths. If these baths are large enough (>30 Å), the lipid bilayer acts as if it was in contact with an infinite solution. The protocol gives rise to a TM potential $\Delta V = Q_s/C$, when a charge imbalance per surface area Q_s is imposed, C being the capacitance of the membrane. This method might present a drawback. Indeed, reorganization of the charges within the membrane in response to an applied voltage (ion conduction, reorganization of charged residues of a protein, etc.) leads to a drop in ΔV. Whereas this may be a desired effect in some applications (see the next paragraph for the computation of gating charges), a method that enables one to maintain ΔV roughly constant was recently proposed [88].

4.3.4 Analysis of the Obtained MD Trajectory

The most common program used to visualize MD trajectories generated by a variety of MD codes is VMD [89]. Most other MD codes have their own analyses programs that allow one to perform the most frequent type of analyses. As in any MD simulation performed in the NPT ensemble, the total energy fluctuates. The first and foremost analysis consists in verifying that the system's total energy E converges toward a certain value. Several other measures can be conducted, such as the root-mean-square-deviation (RMSD) of the atoms coordinates with respect to the starting structure for checking, for instance, the protein stability. A Ramachandran plot can be drawn to verify if the structure still adopts favored torsion angles in the MD trajectory.

All available experimental constraints, e.g., those obtained through site-mutagenesis can also be assessed to increase the reliability of the simulations. Hence, residue proximity and salt bridges between charged moieties and their stabilities need to be monitored throughout the MD simulation.

4.4 Gating Charge Calculation Methods Used on Kv1.2 Model

In the case of voltage-gated cation channels such as Kv channels, gating currents arise from the movements of the charges tethered to the VSD within the lipid dielectric in response to the change in TM voltage. The time integral of the gating current, Q, corresponds to the amount of electric charge translocated across the membrane capacitor, and is characteristic of a specific conformational change.

In voltage-clamp experiments, the gating current can be measured by blocking the current through the main pore (using for instance a nonconductive mutant such as W434F Shaker [90]). The gating charge Q may also be formally related to the excess free energy induced by the applied TM voltage. It is then expressed as a product of the channel's charges by the fraction of the electric field that they traverse throughout conformational changes induced by the TM voltage [91]. Accordingly, in MD simulations, two independent routes that mimic the aforementioned experimental techniques can be used to estimate Q.

4.4.1 Direct Measurement

With the charge imbalance method, if ionic conduction through the channel's pore is prevented, the movement of protein charges across the membrane capacitor is reflected directly by a change in the measured TM potential ΔV [92]. The TM voltage is related to the charge imbalance q_0 between the electrolyte baths through: $\Delta V = q_0/AC$, in which q_0 arises from the contribution of both ions q_0^{ions} and of the protein q_0^{prot}, A is the membrane area and C the membrane capacitance. As the latter is constant for a channel/membrane system in the considered TM voltage range [16, 92], one can write the former equation for every channel conformation

λ_i as $q_0^{\text{prot}}(\lambda_i) = q_0^{\text{ions}}(\lambda_i) + AC\Delta V$. As $q_0^{\text{ions}}(\lambda_i)$ is constant (ion conduction is blocked), variations in ΔV are then directly linked to the expression of the protein gating charge.

In practice, the gating charge Q associated with the conformational change from λ_1 to λ_2 can be estimated from $\Delta V_{\lambda 1}$ and $\Delta V_{\lambda 2}$ the two measures of the transmembrane potential imposed by a charge imbalance q_0^{ions} as: $Q = 0.5\left[q_0^{\text{ions}}(1 - \Delta V_{\lambda_1}/\Delta V_{\lambda_2})\right]$. The direct measurement method turned out to be the most appropriate one to extract the total gating charge from simulations of a model channel in its membrane environment and to compare with electrophysiology measurements.

4.4.2 Energetic Formalism

In general, the total free energy of a system includes an intrinsic contribution arising from the molecular environment, and another reflecting the coupling of the system with the applied TM potential ΔV. This second contribution may be linked to the gating charge, Q, through the relation $Q\Delta V = [\Delta G(\lambda_2,\Delta V) - \Delta G(\lambda_1,\Delta V)]$ where $\Delta G(\lambda_i,\Delta V)$ is the excess free energy of the channel (in its conformation λ_i due to ΔV). This free energy may be evaluated directly as the difference between two free energy perturbation calculations performed at two different transmembrane voltages [93].

$\Delta G(\lambda,\Delta V)$ can also be directly linked to the "electrical distance" δ_i^λ [94–96] and expressed as $\Delta G(\lambda, \Delta V) = G(\lambda, \Delta V) - G(\lambda, 0) = \Delta V \sum_i q_i \delta_i^\lambda$, where the sum runs over all charges q_i of the channel. δ_i^λ accounts for the coupling between the TM potential and the variations of the local electrostatic potential felt by the charge q_i located at the position r_i [97–99] ***and is expressed as*** $\delta_i^\lambda = \frac{\partial}{\partial V}\phi_i^\lambda(r_i)$. Hence, it corresponds to the fraction of the electric field at the charge position.

In practice, for a given channel conformation λ, one needs to perform two independent MD simulations (~1 ns each) under different TM potentials. For each simulation we estimate first the local electrostatic potential $\phi_i^\lambda(r_i)$ as the average over $n \sim 100$ configurations sampled over the trajectories by computing the 3D electrostatic potential maps $\Phi_j(r, \Delta V)$ (using for instance the plugin PMEpot in VMD): $\phi_i^\lambda(r_i, \Delta V) = \frac{1}{2}\sum_{j=1}^{n} \Phi_j(r, \Delta V)$. Note here that this quantity must be computed without consideration of the contribution of charges belonging to the proteins. The electrical distance for every charge q_i of the channel located at the position r_i might then be estimated as $\delta_i^\lambda = \left[\phi_i^\lambda(r_i, \Delta V_2) - \phi_i^\lambda(r_i, \Delta V_2)\right]/(\Delta V_2 - \Delta V_1)$. This hints already to the fact that charges that are located in regions where the electrostatic potential does not vary (e.g., loops located in the extra and intra cellular regions) do not contribute to the gating charge.

Note that in contrast to the direct measure, and to experiments, the contributions of individual residues of the protein (such as the

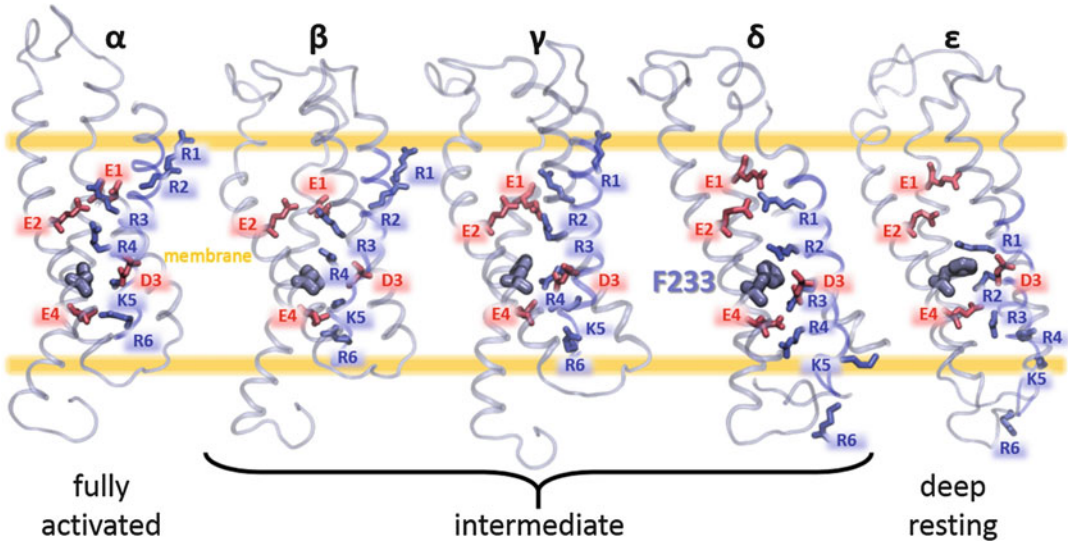

Fig. 2 Kv1.2 metastable states obtained with MD simulations. Conformations of the Kv1.2 VSD obtained from MD simulations (adapted from [85]). The β and γ states were generated via an unbiased 2.2 μs MD simulation of VSD submitted to a hyperpolarized TM voltage of −600 mV. For each state, the VSD backbone is represented in *transparent colors*, with the S4 segment in *blue*. S4 basic charges (R1: R294, R2: R297, R3: R300, R4: R303, K5: K306, R6: R309) and their acidic countercharges (E1: E183, E2: E226, D3: D259, E4: E236) are represented in *light blue* and *light red sticks*, respectively. The hydrophobic plug, F233, is represented in *mauve sticks*

S4 amino-acids) to the total gating charge, and therefore their role in the voltage-sensing mechanism may be directly evaluated.

The gating charge calculations are often used to assess the validity of an unknown structure, e.g., that of the closed stated channel model given that of the open state structure or to follow the conformational change during in silico activation/inactivation when submitting the channel to a transmembrane potential [85, 92] (Fig. 2).

4.5 Computational Studies of Kv Mutants

Kv channels are mostly dedicated to reset the resting potential in the membranes of excitable tissues. Thus, inherited or acquired genetic mutations on Kv channel family will generally disrupt the action potential leading to mild or severe pathologic phenotypes [100–102]. The effects of a known Kv mutation can be assessed in silico, by simply modifying the residue side chain using VMD for example. Afterward, one can perform a MD simulation of a few hundreds of nanoseconds to let the mutant structure equilibrate in the membrane and, if possible, to determine its behavior with respect to the native structure.

Among the most studied mutations in voltage-gated channels are those concerning amino acids of the VSD. They turned out to be related to the emergence of a current component called "omega" or gating-pore current that is different from the pore

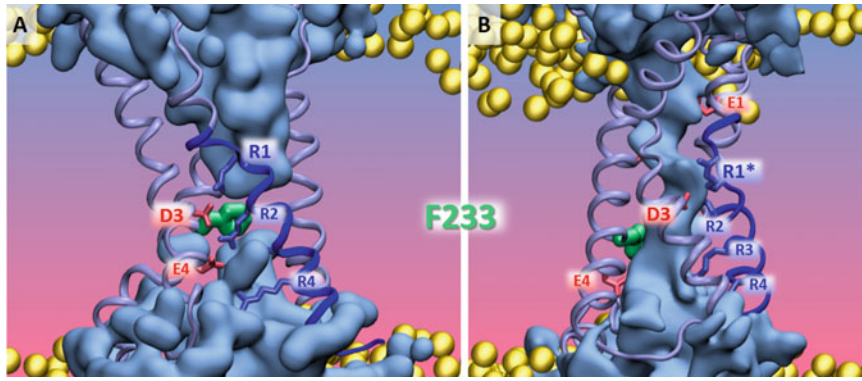

Fig. 3 Effects of R1 neutralizing mutation on Kv1.2 resting state model at hyperpolarized TM voltages. The pictures represent the VSD of Kv1.2. S4 segment is colored in *blue*, while the other VSD segments are colored in *mauve*. The polar heads of the lipid bilayer are colored in *yellow*. (**a**) The solvent-accessible surface (in *light blue*) of wild-type Kv1.2 has an hour-glass shape and is constricted at the level of F233 (in *green*). This aromatic residue shelters the salt bridge between R1 and D3 from the solvent. (**b**) When R1 is neutralized (R1*) the R1-D3 salt bridge is broken. Thereby, the solvent-accessible surface of Kv1.2 mutant can completely span the membrane, which favors a leak current of ions. Adapted from [107]

conduction. This current is characterized by a leak of ions through a conduction pathway in the VSD induced by mutations on S4 basic residues [103]. Hence, for instance, the substitution of R1 by a small and uncharged residue yields a mutant able to generate voltage-independent and unselective "omega" currents, which indicates that R1 constitute a steric hindrance for the ion conduction through the gating pore [104]. In addition, the Shaker mutants R1H and R4H lead to voltage-dependent leak currents of protons at hyperpolarized [105] and depolarized TM voltages [106], respectively. Interestingly, many mutations related to genetic diseases such as epilepsy, hypokalemic periodic paralysis, or long QT syndrome are characterized by the presence of these "omega" currents that affect Kv channel function at hyperpolarized voltages, where the Kv channel is supposed to be closed.

Despite the fact that no S4 basic residue mutations in Kv1.2 have been associated with channelopathies, Kv1.2 was used as a prototype to study the effects of these mutations [107]. Using both open and closed state models, residues R1 and K5 were subsequently neutralized and submitted to MD simulations under various TM voltages to monitor a possible appearance of a gating pore current. The S4 hydrophilic pathways of the resulting Kv1.2 mutants turned out to be able to generate voltage-dependent "omega" currents of K^+ ions at hyperpolarized voltages for R1 neutral mutants (Fig. 3), and at depolarized voltages for K5 neutral mutants. These results are in agreement with similar computational studies [108, 109], and with the experimental results obtained for the Shaker channel.

5 Conclusion

An overview of computational methods aimed at studying the structure and the function of Kv channels has been presented in this chapter. As examples, we have briefly described studies of both Kv1.2 and Kv7.1 channels that yielded a large amount of important results. This information offered a molecular insight of Kv channels function that could not have been reached through experimental studies alone. Nevertheless, we would like to stress the fact that integrative approaches including both experimental and computational methods allow an exchange of knowledge, which endows an improvement in the reliability of the molecular models and molecular modeling techniques, as well as an enhancement of the quality of the results.

Acknowledgment

Results of the MD simulations were obtained thanks to generous allocation of computer time from GENCI France.

References

1. Hille B (2001) Ion channels of excitable membranes, 3rd edn. Sinauer, Sunderland, MA
2. Jouni M, Si-Tayeb K, Es-Salah-Lamoureux Z, Latypova X, Champon B, Caillaud A, Rungoat A, Charpentier F, Loussouarn G, Baró I, Zibara K, Lemarchand P, Gaborit N (2015) Toward personalized medicine: using cardiomyocytes differentiated from urine-derived pluripotent stem cells to recapitulate electrophysiological characteristics of Type 2 long QT syndrome. J Am Heart Assoc 4: e002159. doi:10.1161/JAHA.115.002159
3. Laurent G, Saal S, Amarouch MY, Béziau DM, Marsman RFJ, Faivre L, Barc J, Dina C, Bertaux G, Barthez O, Thauvin-Robinet C, Charron P, Fressart V, Maltret A, Villain E, Baron E, Mérot J, Turpault R, Coudière Y, Charpentier F, Schott J-J, Loussouarn G, Wilde AAM, Wolf J-E, Baró I, Kyndt F, Probst V (2012) Multifocal ectopic purkinje-related premature contractions. J Am Coll Cardiol 60:144–156. doi:10.1016/j.jacc.2012.02.052
4. Loussouarn G, Sternberg D, Nicole S, Marionneau C, Le Bouffant F, Toumaniantz G, Barc J, Malak OA, Fressart V, Péréon Y, Baró I, Charpentier F (2016) Physiological and pathophysiological insights of Nav1.4 and Nav1.5 comparison. Front Pharmacol 6:314. doi:10.3389/fphar.2015.00314
5. Park K-H, Piron J, Dahimene S, Mérot J, Baró I, Escande D, Loussouarn G (2005) Impaired KCNQ1-KCNE1 and phosphatidylinositol-4,5-bisphosphate interaction underlies the long QT syndrome. Circ Res 96:730–739. doi:10.1161/01.RES.0000161451.04649.a8
6. Yang Y, Vasylyev DV, Dib-Hajj F, Veeramah KR, Hammer MF, Dib-Hajj SD, Waxman SG (2013) Multistate structural modeling and voltage-clamp analysis of epilepsy/autism mutation Kv10.2-R327H demonstrate the role of this residue in stabilizing the channel closed state. J Neurosci 33:16586–16593. doi:10.1523/JNEUROSCI.2307-13.2013
7. Nattel S, Maguy A, Le Bouter S, Yeh Y-H (2007) Arrhythmogenic ion-channel remodeling in the heart: heart failure, myocardial infarction, and atrial fibrillation. Physiol Rev 87:425–456. doi:10.1152/physrev.00014.2006
8. Charpentier F, Mérot J, Loussouarn G, Baró I (2010) Delayed rectifier K+ currents and cardiac repolarization. J Mol Cell Cardiol 48:37–44. doi:10.1016/j.yjmcc.2009.08.005

9. Schroeder BC, Waldegger S, Fehr S, Bleich M, Warth R, Greger R, Jentsch TJ (2000) A constitutively open potassium channel formed by KCNQ1 and KCNE3. Nature 403:196–199. doi:10.1038/35003200
10. Vallon V, Grahammer F, Volkl H, Sandu CD, Richter K, Rexhepaj R, Gerlach U, Rong Q, Pfeifer K, Lang F (2005) KCNQ1-dependent transport in renal and gastrointestinal epithelia. Proc Natl Acad Sci 102:17864–17869. doi:10.1073/pnas.0505860102
11. Whicher JR, MacKinnon R (2016) Structure of the voltage-gated K+ channel Eag1 reveals an alternative voltage sensing mechanism. Science 353:664–669. doi:10.1126/science.aaf8070
12. Neher E, Sakmann B (1976) Single-channel currents recorded from membrane of denervated frog muscle fibres. Nature 260:799–802
13. Armstrong CM, Bezanilla F (1973) Currents related to movement of the gating particles of the sodium channels. Nature 242:459–461
14. Aggarwal SK, MacKinnon R (1996) Contribution of the S4 segment to gating charge in the Shaker K+ channel. Neuron 16:1169–1177. doi:10.1016/S0896-6273(00)80143-9
15. Seoh S-A, Sigg D, Papazian DM, Bezanilla F (1996) Voltage-sensing residues in the S2 and S4 segments of the shaker K+ channel. Neuron 16:1159–1167. doi:10.1016/S0896-6273(00)80142-7
16. Stefani E, Toro L, Perozo E, Bezanilla F (1994) Gating of shaker K+ channels: I. Ionic and gating currents. Biophys J 66:996–1010. doi:10.1016/S0006-3495(94)80881-1
17. Loussouarn G (2003) Phosphatidylinositol-4,5-bisphosphate, PIP2, controls KCNQ1/KCNE1 voltage-gated potassium channels: a functional homology between voltage-gated and inward rectifier K+ channels. EMBO J 22:5412–5421. doi:10.1093/emboj/cdg526
18. Tempel BL, Papazian DM, Schwarz TL, Jan YN, Jan LY (1987) Sequence of a probable potassium channel component encoded at Shaker locus of Drosophila. Science 237:770–775. doi:10.1126/science.2441471
19. Noda M, Shimizu S, Tanabe T, Takai T, Kayano T, Ikeda T, Takahashi H, Nakayama H, Kanaoka Y, Minamino N (1984) Primary structure of Electrophorus electricus sodium channel deduced from cDNA sequence. Nature 312:121–127
20. Long SB (2005) Voltage sensor of Kv1.2: structural basis of electromechanical coupling. Science 309:903–908. doi:10.1126/science.1116270
21. Doyle DA, Morais Cabral J, Pfuetzner RA, Kuo A, Gulbis JM, Cohen SL, Chait BT, MacKinnon R (1998) The structure of the potassium channel: molecular basis of K+ conduction and selectivity. Science 280:69–77
22. del Camino D, Holmgren M, Liu Y, Yellen G (2000) Blocker protection in the pore of a voltage-gated K+ channel and its structural implications. Nature 403:321–325. doi:10.1038/35002099
23. Beckstein O, Biggin PC, Bond P, Bright JN, Domene C, Grottesi A, Holyoake J, Sansom MS (2003) Ion channel gating: insights via molecular simulations. FEBS Lett 555:85–90. doi:10.1016/S0014-5793(03)01151-7
24. Domene C, Haider S, Sansom MSP (2003) Ion channel structures: a review of recent progress. Curr Opin Drug Discov Devel 6:611–619
25. Broomand A, Männikkö R, Larsson HP, Elinder F (2003) Molecular movement of the voltage sensor in a K channel. J Gen Physiol 122:741–748. doi:10.1085/jgp.200308927
26. Neale EJ, Elliott DJS, Hunter M, Sivaprasadarao A (2003) Evidence for intersubunit interactions between S4 and S5 transmembrane segments of the shaker potassium channel. J Biol Chem 278:29079–29085. doi:10.1074/jbc.M301991200/6493
27. Long SB, Tao X, Campbell EB, MacKinnon R (2007) Atomic structure of a voltage-dependent K+ channel in a lipid membrane-like environment. Nature 450:376–382. doi:10.1038/nature06265
28. Chen X, Wang Q, Ni F, Ma J (2010) Structure of the full-length Shaker potassium channel Kv1.2 by normal-mode-based X-ray crystallographic refinement. Proc Natl Acad Sci U S A 107:11352–11357. doi:10.1073/pnas.1000142107
29. Vardanyan V, Pongs O (2012) Coupling of voltage-sensors to the channel pore: a comparative view. Front Pharmacol 3:145. doi:10.3389/fphar.2012.00145
30. Ferrer T, Rupp J, Piper DR, Tristani-Firouzi M (2006) The S4-S5 linker directly couples voltage sensor movement to the activation gate in the human ether-a-go-go-related gene (hERG) K+ channel. J Biol Chem 281:12858–12864. doi:10.1074/jbc.M513518200

31. Choveau FS, Rodriguez N, Ali FA, Labro AJ, Rose T, Dahimene S, Boudin H, Le Henaff C, Escande D, Snyders DJ, Charpentier F, Merot J, Baro I, Loussouarn G (2011) KCNQ1 channels voltage dependence through a voltage-dependent binding of the S4-S5 linker to the pore domain. J Biol Chem 286:707–716. doi:10.1074/jbc.M110.146324
32. Choveau FS, Abderemane-Ali F, Coyan FC, Es-Salah-Lamoureux Z, Baró I, Loussouarn G (2012) Opposite effects of the S4–S5 linker and PIP2 on voltage-gated channel function: KCNQ1/KCNE1 and other channels. Front Pharmacol 3:125. doi:10.3389/fphar.2012.00125
33. Zaydman MA, Silva JR, Delaloye K, Li Y, Liang H, Larsson HP, Shi J, Cui J (2013) Kv7.1 ion channels require a lipid to couple voltage sensing to pore opening. Proc Natl Acad Sci 110:13180–13185. doi:10.1073/pnas.1305167110
34. Zaydman MA, Kasimova MA, McFarland K, Beller Z, Hou P, Kinser HE, Liang H, Zhang G, Shi J, Tarek M et al (2014) Domain–domain interactions determine the gating, permeation, pharmacology, and subunit modulation of the IKs ion channel. Elife 3:e03606
35. Smith JA, Vanoye CG, George AL, Meiler J, Sanders CR (2007) Structural models for the KCNQ1 voltage-gated potassium channel †. Biochemistry (Mosc) 46:14141–14152. doi:10.1021/bi701597s
36. Xu Y, Wang Y, Meng X-Y, Zhang M, Jiang M, Cui M, Tseng G-N (2013) Building KCNQ1/KCNE1 channel models and probing their interactions by molecular-dynamics simulations. Biophys J 105:2461–2473. doi:10.1016/j.bpj.2013.09.058
37. Kasimova MA, Zaydman MA, Cui J, Tarek M (2015) PIP2-dependent coupling is prominent in Kv7.1 due to weakened interactions between S4-S5 and S6. Sci Rep 5:7474. doi:10.1038/srep07474
38. Pons J-L, Labesse G (2009) @TOME-2: a new pipeline for comparative modeling of protein-ligand complexes. Nucleic Acids Res 37:W485–W491. doi:10.1093/nar/gkp368
39. Biasini M, Bienert S, Waterhouse A, Arnold K, Studer G, Schmidt T, Kiefer F, Cassarino TG, Bertoni M, Bordoli L, Schwede T (2014) SWISS-MODEL: modelling protein tertiary and quaternary structure using evolutionary information. Nucleic Acids Res 42:W252–W258. doi:10.1093/nar/gku340
40. Yu J, Picord G, Tuffery P, Guerois R (2015) HHalign-Kbest: exploring sub-optimal alignments for remote homology comparative modeling: Fig. 1. Bioinformatics 31:3850. doi:10.1093/bioinformatics/btv441
41. Altschul SF, Madden TL, Schäffer AA, Zhang J, Zhang Z, Miller W, Lipman DJ (1997) Gapped BLAST and PSI-BLAST: a new generation of protein database search programs. Nucleic Acids Res 25:3389–3402
42. Larkin MA, Blackshields G, Brown NP, Chenna R, McGettigan PA, McWilliam H, Valentin F, Wallace IM, Wilm A, Lopez R, Thompson JD, Gibson TJ, Higgins DG (2007) Clustal W and Clustal X version 2.0. Bioinformatics 23:2947–2948. doi:10.1093/bioinformatics/btm404
43. Krivov GG, Shapovalov MV, Dunbrack RL (2009) Improved prediction of protein side-chain conformations with SCWRL4. Proteins Struct Funct Bioinforma 77:778–795. doi:10.1002/prot.22488
44. Webb B, Sali A (2014) Comparative protein structure modeling using MODELLER: comparative protein structure modeling using MODELLER. In: Bateman A, Pearson WR, Stein LD, Stormo GD, Yates JR (eds) Current protocal bioinformatics. John Wiley & Sons, Inc., Hoboken, NJ, pp 5.6.1–5.6.32
45. Peng D, Kim J-H, Kroncke BM, Law CL, Xia Y, Droege KD, Van Horn WD, Vanoye CG, Sanders CR (2014) Purification and structural study of the voltage-sensor domain of the human KCNQ1 potassium ion channel. Biochemistry (Mosc) 53:2032–2042. doi:10.1021/bi500102w
46. Wu D, Delaloye K, Zaydman MA, Nekouzadeh A, Rudy Y, Cui J (2010) State-dependent electrostatic interactions of S4 arginines with E1 in S2 during Kv7.1 activation. J Gen Physiol 135:595–606. doi:10.1085/jgp.201010408
47. Wu D, Pan H, Delaloye K, Cui J (2010) KCNE1 remodels the voltage sensor of Kv7.1 to modulate channel function. Biophys J 99:3599–3608. doi:10.1016/j.bpj.2010.10.018
48. Shen M, Sali A (2006) Statistical potential for assessment and prediction of protein structures. Protein Sci 15:2507–2524. doi:10.1110/ps.062416606
49. Morris AL, MacArthur MW, Hutchinson EG, Thornton JM (1992) Stereochemical quality of protein structure coordinates. Proteins Struct Funct Genet 12:345–364. doi:10.1002/prot.340120407
50. Rohl CA, Strauss CEM, Chivian D, Baker D (2004) Modeling structurally variable regions in homologous proteins with rosetta. Proteins

Struct Funct Bioinforma 55:656–677. doi:10.1002/prot.10629

51. Raman S, Vernon R, Thompson J, Tyka M, Sadreyev R, Pei J, Kim D, Kellogg E, DiMaio F, Lange O, Kinch L, Sheffler W, Kim B-H, Das R, Grishin NV, Baker D (2009) Structure prediction for CASP8 with all-atom refinement using Rosetta. Proteins Struct Funct Bioinforma 77:89–99. doi:10.1002/prot.22540
52. Yang J, Yan R, Roy A, Xu D, Poisson J, Zhang Y (2015) The I-TASSER Suite: protein structure and function prediction. Nat Methods 12:7–8
53. Yarov-Yarovoy V, Baker D, Catterall WA (2006) Voltage sensor conformations in the open and closed states in ROSETTA structural models of K(+) channels. Proc Natl Acad Sci U S A 103:7292–7297. doi:10.1073/pnas.0602350103
54. Allen MP, Tildesley DJ (1987) Computer simulation of liquids. Clarendon Press, Oxford
55. Leach AR (2001) Molecular modelling: principles and applications, 2nd edn. Prentice Hall, Harlow
56. Frenkel D, Smit B (2002) Understanding molecular simulation: from algorithms to applications, 2nd edn. Academic Press, San Diego, CA
57. Schuler LD, Daura X, van Gunsteren WF (2001) An improved GROMOS96 force field for aliphatic hydrocarbons in the condensed phase. J Comput Chem 22:1205–1218. doi:10.1002/jcc.1078
58. MacKerell AD, Bashford D, Bellott M, Dunbrack RL, Evanseck JD, Field MJ, Fischer S, Gao J, Guo H, Ha S, Joseph-McCarthy D, Kuchnir L, Kuczera K, Lau FTK, Mattos C, Michnick S, Ngo T, Nguyen DT, Prodhom B, Reiher WE, Roux B, Schlenkrich M, Smith JC, Stote R, Straub J, Watanabe M, Wiórkiewicz-Kuczera J, Yin D, Karplus M (1998) All-atom empirical potential for molecular modeling and dynamics studies of proteins †. J Phys Chem B 102:3586–3616. doi:10.1021/jp973084f
59. Ponder JW, Case DA (2003) Force fields for protein simulations. Adv Protein Chem 66:27–85
60. Jorgensen WL, Maxwell DS, Tirado-Rives J (1996) Development and testing of the OPLS all-atom force field on conformational energetics and properties of organic liquids. J Am Chem Soc 118:11225–11236. doi:10.1021/ja9621760
61. Jo S, Kim T, Iyer VG, Im W (2008) CHARMM-GUI: a web-based graphical user interface for CHARMM. J Comput Chem 29:1859–1865. doi:10.1002/jcc.20945
62. Wu EL, Cheng X, Jo S, Rui H, Song KC, Dávila-Contreras EM, Qi Y, Lee J, Monje-Galvan V, Venable RM, Klauda JB, Im W (2014) CHARMM-GUI Membrane Builder toward realistic biological membrane simulations. J Comput Chem 35:1997–2004. doi:10.1002/jcc.23702
63. Xu Y, Ramu Y, Lu Z (2008) Removal of phospho-head groups of membrane lipids immobilizes voltage sensors of K+ channels. Nature 451:826–829. doi:10.1038/nature06618
64. Zhang H, Craciun LC, Mirshahi T, Rohács T, Lopes CMB, Jin T, Logothetis DE (2003) PIP2 activates KCNQ channels, and its hydrolysis underlies receptor-mediated inhibition of M currents. Neuron 37:963–975. doi:10.1016/S0896-6273(03)00125-9
65. Eckey K, Wrobel E, Strutz-Seebohm N, Pott L, Schmitt N, Seebohm G (2014) Novel Kv7.1-phosphatidylinositol 4,5-bisphosphate interaction sites uncovered by charge neutralization scanning. J Biol Chem 289:22749–22758. doi:10.1074/jbc.M114.589796
66. Shaw DE, Dror RO, Salmon JK, Grossman JP, Mackenzie KM, Bank JA, Young C, Deneroff MM, Batson B, Bowers KJ, Chow E, Eastwood MP, Ierardi DJ, Klepeis JL, Kuskin JS, Larson RH, Lindorff-Larsen K, Maragakis P, Moraes MA, Piana S, Shan Y, Towles B (2009) Millisecond-scale molecular dynamics simulations on anton. In: Proc. Conf. High Perform. Comput. Netw. Storage Anal. ACM, New York, NY, pp 39.1–39.11
67. Martyna GJ, Klein ML, Tuckerman M (1992) Nosé–Hoover chains: the canonical ensemble via continuous dynamics. J Chem Phys 97:2635–2643. doi:10.1063/1.463940
68. Brooks BR, Brooks CL, Mackerell AD, Nilsson L, Petrella RJ, Roux B, Won Y, Archontis G, Bartels C, Boresch S, Caflisch A, Caves L, Cui Q, Dinner AR, Feig M, Fischer S, Gao J, Hodoscek M, Im W, Kuczera K, Lazaridis T, Ma J, Ovchinnikov V, Paci E, Pastor RW, Post CB, Pu JZ, Schaefer M, Tidor B, Venable RM, Woodcock HL, Wu X, Yang W, York DM, Karplus M (2009) CHARMM: the biomolecular simulation program. J Comput Chem 30:1545–1614. doi:10.1002/jcc.21287
69. Case DA, Cheatham TE, Darden T, Gohlke H, Luo R, Merz KM, Onufriev A, Simmerling C, Wang B, Woods RJ (2005) The Amber

biomolecular simulation programs. J Comput Chem 26:1668–1688. doi:10.1002/jcc.20290

70. Van Der Spoel D, Lindahl E, Hess B, Groenhof G, Mark AE, Berendsen HJC (2005) GROMACS: fast, flexible, and free. J Comput Chem 26:1701–1718. doi:10.1002/jcc.20291
71. Phillips JC, Braun R, Wang W, Gumbart J, Tajkhorshid E, Villa E, Chipot C, Skeel RD, Kalé L, Schulten K (2005) Scalable molecular dynamics with NAMD. J Comput Chem 26:1781–1802. doi:10.1002/jcc.20289
72. Bowers KJ, Chow E, Xu H, Dror RO, Eastwood MP, Gregersen BA, Klepeis JL, Kolossvary I, Moraes MA, Sacerdoti FD et al (2006) Scalable algorithms for molecular dynamics simulations on commodity clusters. In: Proc. 2006 ACMIEEE Conf. Supercomput. ACM, New York, NY, p 84
73. Buck M, Bouguet-Bonnet S, Pastor RW, MacKerell AD (2006) Importance of the CMAP correction to the CHARMM22 protein force field: dynamics of hen lysozyme. Biophys J 90:L36–L38. doi:10.1529/biophysj.105.078154
74. Suenaga A, Komeiji Y, Uebayasi M, Meguro T, Saito M, Yamato I (1998) Computational observation of an ion permeation through a channel protein. Biosci Rep 18:39–48. doi:10.1023/A:1022292801256
75. Zhong Q, Jiang Q, Moore PB, Newns DM, Klein ML (1998) Molecular dynamics simulation of a synthetic ion channel. Biophys J 74:3–10. doi:10.1016/S0006-3495(98)77761-6
76. Tieleman DP, Biggin PC, Smith GR, Sansom MSP (2001) Simulation approaches to ion channel structure–function relationships. Q Rev Biophys 34:473–561. doi:10.1017/S0033583501003729
77. Crozier PS, Henderson D, Rowley RL, Busath DD (2001) Model channel ion currents in NaCl-extended simple point charge water solution with applied-field molecular dynamics. Biophys J 81:3077–3089. doi:10.1016/S0006-3495(01)75946-2
78. Tarek M (2005) Membrane electroporation: a molecular dynamics simulation. Biophys J 88:4045–4053. doi:10.1529/biophysj.104.050617
79. Tieleman DP (2004) The molecular basis of electroporation. BMC Biochem 5:10. doi:10.1186/1471-2091-5-10
80. Gumbart J, Khalili-Araghi F, Sotomayor M, Roux B (2012) Constant electric field simulations of the membrane potential illustrated with simple systems. Biochim Biophys Acta 1818:294–302. doi:10.1016/j.bbamem.2011.09.030
81. Bjelkmar P, Niemelä PS, Vattulainen I, Lindahl E (2009) Conformational changes and slow dynamics through microsecond polarized atomistic molecular simulation of an integral Kv1.2 ion channel. PLoS Comput Biol 5:e1000289. doi:10.1371/journal.pcbi.1000289
82. Schow EV, Nizkorodov A, Freites JA, White SH, Tobias DJ (2010) Down-state model of the KvAP full channel. Biophys J 98:315a. doi:10.1016/j.bpj.2009.12.1709
83. Jensen MØ, Jogini V, Borhani DW, Leffler AE, Dror RO, Shaw DE (2012) Mechanism of voltage gating in potassium channels. Science 336:229–233. doi:10.1126/science.1216533
84. Köpfer DA, Song C, Gruene T, Sheldrick GM, Zachariae U, de Groot BL (2014) Ion permeation in K+ channels occurs by direct Coulomb knock-on. Science 346:352–355. doi:10.1126/science.1254840
85. Delemotte L, Tarek M, Klein ML, Amaral C, Treptow W (2011) Intermediate states of the Kv1. 2 voltage sensor from atomistic molecular dynamics simulations. Proc Natl Acad Sci 108:6109–6114
86. Delemotte L, Dehez F, Treptow W, Tarek M (2008) Modeling membranes under a transmembrane potential. J Phys Chem B 112:5547–5550. doi:10.1021/jp710846y
87. Bostick D, Berkowitz ML (2003) The implementation of slab geometry for membrane-channel molecular dynamics simulations. Biophys J 85:97–107. doi:10.1016/S0006-3495(03)74458-0
88. Kutzner C, Grubmüller H, de Groot BL, Zachariae U (2011) Computational electrophysiology: the molecular dynamics of ion channel permeation and selectivity in atomistic detail. Biophys J 101:809–817. doi:10.1016/j.bpj.2011.06.010
89. Humphrey W, Dalke A, Schulten K (1996) VMD: visual molecular dynamics. J Mol Graph 14(33–38):27–28
90. Perozo E, MacKinnon R, Bezanilla F, Stefani E (1993) Gating currents from a nonconducting mutant reveal open-closed conformations in Shaker K+ channels. Neuron 11:353–358
91. Nonner W, Peyser A, Gillespie D, Eisenberg B (2004) Relating microscopic charge movement to macroscopic currents: the Ramo-Schockley theorem applied to ion channels. Biophys J 87:3716–3722
92. Treptow W, Tarek M, Klein ML (2009) Initial response of the potassium channel voltage

sensor to a transmembrane potential. J Am Chem Soc 131:2107–2109. doi:10.1021/ja807330g

93. Roux B (2008) The membrane potential and its representation by a constant electric field in computer simulations. Biophys J 95:4205–4216
94. Sigworth FJ (1994) Voltage gating of ion channels. Q Rev Biophys 27:1–40
95. Lecar H, Larsson HP, Grabe M (2003) Electrostatic model of S4 motion in voltage-gated ion channels. Biophys J 85:2854–2864
96. Jogini V, Roux B (2007) Dynamics of the Kv1. 2 voltage-gated K+ channel in a membrane environment. Biophys J 93:3070–3082
97. Islas LD, Sigworth FJ (2001) Electrostatic and the gating pore of Shaker potassium channels. J Gen Physiol 117:69–89
98. Roux BT (1997) Influence of the membrane potential on the free energy of an intrinsic protein. Biophys J 73:2980–2989
99. Grabe M, Lecar H, Jan YN, Jan LY (2004) A quantitative assessment of models for voltage-dependent gating ion channels. Proc Natl Acad Sci U S A 101:17640–17645
100. Dedek K, Kunath B, Kananura C, Reuner U, Jentsch TJ, Steinlein OK (2001) Myokymia and neonatal epilepsy caused by a mutation in the voltage sensor of the KCNQ2 K+ channel. Proc Natl Acad Sci 98:12272–12277. doi:10.1073/pnas.211431298
101. Lupoglazoff J-M, Denjoy I, Villain E, Fressart V, Simon F, Bozio A, Berthet M, Benammar N, Hainque B, Guicheney P (2004) Long QT syndrome in neonates. J Am Coll Cardiol 43:826–830. doi:10.1016/j.jacc.2003.09.049
102. Millat G, Chevalier P, Restier-Miron L, Da Costa A, Bouvagnet P, Kugener B, Fayol L, Gonzàlez Armengod C, Oddou B, Chanavat V, Froidefond E, Perraudin R, Rousson R, Rodriguez-Lafrasse C (2006) Spectrum of pathogenic mutations and associated polymorphisms in a cohort of 44 unrelated patients with long QT syndrome. Clin Genet 70:214–227. doi:10.1111/j.1399-0004.2006.00671.x
103. Tombola F, Pathak MM, Gorostiza P, Isacoff EY (2006) The twisted ion-permeation pathway of a resting voltage-sensing domain. Nature 445:546–549. doi:10.1038/nature05396
104. Tombola F, Pathak MM, Isacoff EY (2005) Voltage-sensing arginines in a potassium channel permeate and occlude cation-selective pores. Neuron 45:379–388
105. Starace DM, Bezanilla F (2004) A proton pore in a potassium channel voltage sensor reveals a focused electric field. Nature 427:548–553. doi:10.1038/nature02270
106. Starace DM, Bezanilla F (2001) Histidine scanning mutagenesis of basic residues of the S4 segment of the shaker potassium channel. J Gen Physiol 117:469–490
107. Delemotte L, Treptow W, Klein ML, Tarek M (2010) Effect of sensor domain mutations on the properties of voltage-gated ion channels: molecular dynamics studies of the potassium channel Kv1.2. Biophys J 99:L72–L74. doi:10.1016/j.bpj.2010.08.069
108. Gamal El-Din TM, Heldstab H, Lehmann C, Greeff NG (2010) Double gaps along Shaker S4 demonstrate omega currents at three different closed states. Channels Austin TX 4:93–100
109. Khalili-Araghi F, Tajkhorshid E, Roux B, Schulten K (2012) Molecular dynamics investigation of the ω-current in the Kv1.2 voltage sensor domains. Biophys J 102:258–267. doi:10.1016/j.bpj.2011.10.057

INDEX

Show-Ling Shyng et al. (eds.), *Potassium Channels: Methods and Protocols,* Methods in Molecular Biology, vol. 1684,
DOI 10.1007/978-1-4939-7362-0, © Springer Science+Business Media LLC 2018

L

M

N

O

P

R

S

T

U

V

Z